PB81-168015

Seminar/Workshop Proceedings: Persistent Elevated Pollution Episodes, March 1979
Durham, North Carolina

Research Triangle Inst.
Research Triangle Park, NC

Prepared for

Environmental Sciences Research Lab.
Research Triangle Park, NC

Mar 81

U.S. Department of Commerce
National Technical Information Service
NTIS

TECHNICAL REPORT DATA
(Please read Instructions on the reverse before completing)

1. REPORT NO. EPA-600/9-81-016	2.	3. RECIPIENT'S ACCESSION NO. PB81 168015
4. TITLE AND SUBTITLE SEMINAR/WORKSHOP PROCEEDINGS: PERSISTENT ELEVATED POLLUTION EPISODES		5. REPORT DATE MARCH 1981 ISSUING DATE. 6. PERFORMING ORGANIZATION CODE
7. AUTHOR(S) Harry L. Hamilton, Jr. and N. Stuart Jones		8. PERFORMING ORGANIZATION REPORT NO.
9. PERFORMING ORGANIZATION NAME AND ADDRESS Research Triangle Institute P.O. Box 12194 Research Triangle Park, NC 27709		10. PROGRAM ELEMENT NO. C05A1A/16-0225 (FY-80) 11. CONTRACT/GRANT NO. 68-02-3000
12. SPONSORING AGENCY NAME AND ADDRESS Environmental Sciences Research Laboratory - RTP, NC Office of Research and Development U.S. Environmental Protection Agency Research Triangle Park, N.C. 27711		13. TYPE OF REPORT AND PERIOD COVERED 14. SPONSORING AGENCY CODE EPA/600/09

15. SUPPLEMENTARY NOTES

16. ABSTRACT

A Seminar/Workshop was convened by the Regional Field Studies Office of the Environmental Protection Agency's Environmental Sciences Research Laboratory to provide for the exchange of research results and to discuss the state-of-the-art of instrumentation and investigative techniques applicable to studies of regional scale persistent elevated pollution episodes (PEPE's). This report comprises the results of four workshops conducted after 2 1/2 days of formal presentations of scientific papers. The workshops, held concurrently, were charged with the responsibility of providing definitive recommendations on the conduct of future field studies of PEPE's. The subjects covered by the workshops were: experiment design, measurement strategy and tactics and communication requirements; meteorology, transport and validation; and instrumentation. The instrumentation workshop was divided into two sessions: instrumentation for the study of transformation of pollutants and instrumentation for remote sensing of pollutants. Separate reports are included for each of these sessions.

17. KEY WORDS AND DOCUMENT ANALYSIS

a. DESCRIPTORS	b. IDENTIFIERS/OPEN ENDED TERMS	c. COSATI Field/Group

18. DISTRIBUTION STATEMENT RELEASE TO PUBLIC	19. SECURITY CLASS *(This Report)* UNCLASSIFIED	21. NO. OF PAGES 602
	20. SECURITY CLASS *(This page)* UNCLASSIFIED	22. PRICE

EPA Form 2220-1 (Rev. 4-77) PREVIOUS EDITION IS OBSOLETE

TYPING GUIDE SHEET

PB81-168015

EPA-600/9-81-016
MARCH 1981

SEMINAR/WORKSHOP PROCEEDINGS: PERSISTENT ELEVATED POLLUTION EPISODES

by

Harry L. Hamilton, Jr.
N. Stuart Jones
Research Triangle Institute
P.O. Box 12194
Research Triangle Park, North Carolina 27709

Contract No. 68-02-3000

Project Officer

William E. Wilson
Regional Field Studies Office
Environmental Sciences Research Laboratory
Research Triangle Park, North Carolina 27711

ENVIRONMENTAL SCIENCES RESEARCH LABORATORY
OFFICE OF RESEARCH AND DEVELOPMENT
U.S. ENVIRONMENTAL PROTECTION AGENCY
RESEARCH TRIANGLE PARK, NORTH CAROLINA 27711

EPA-287 (Cin.)
(4-78)

REPRODUCED BY
NATIONAL TECHNICAL
INFORMATION SERVICE
U.S. DEPARTMENT OF COMMERCE
SPRINGFIELD, VA 22161

TYPING GUIDE SHEET
BEGIN FIRST LINE OF TEXT HERE
CENTER OF PAGE
TOP OF IMAGE AREA
DROPPED HEAD; BEGIN SECTIONS HERE

DISCLAIMER

This report has been reviewed by the Environmental Sciences Research Laboratory, U.S. Environmental Protection Agency, and approved for publication. Approval does not signify that the contents necessarily reflect the views and policies of the U.S. Environmental Protection Agency, nor does mention of trade names or commercial products constitute endorsement or recommendation for use.

6-1/2"
9-1/8"
BEGIN LAST LINE OF TEXT
BOTTOM OF IMAGE AREA; OUTSIDE DIMENSION FOR TABLES AND ILLUSTRATIONS
3/8"

PAGE NUMBER
EPA-287 (Cin.)
(4-76)

PREFACE

The Seminar/Workshop on Persistent Elevated Pollution Episodes (PEPE's) was sponsored by the Regional Field Studies Office, Environmental Sciences Research Laboratories (ESRL), Environmental Protection Agency (EPA) to provide for the exchange of information among scientists and to generate, from the Workshop, a set of recommendations for the conduct of future regional scale field investigations. These investigations will be directed toward obtaining the data base required to elucidate the atmospheric chemical and physical processes involved in the development of persistent regional scale areas of high concentrations of pollutants, particularly aerosols that can cause degradation of visibility.

This PEPE seminar/workshop is the second to be sponsored by EPA/ESRL to provide guidance for field studies. The first, a Workshop on Regional Air Pollution Studies, was held at Boone, North Carolina, in June 1976. The results of that workshop led to the development of a program to investigate Sulfur Transport and Transformation in the Environment (STATE).

The PEPE seminar/workshop is directed toward the continuation of the STATE Program through the exchange of information acquired from recently completed observation and measurement programs, reviews of the present state-of-the-art measurement techniques applicable to the detection and delineation of PEPE's, and discussions of methods for identifying and tracking air parcels in dynamic flow fields.

The papers presented at the seminar appear in this volume in the order in which they were presented. All of the speakers were invited and asked to speak on subjects germane to the objectives of the subsequent workshops.

After 2½ days of formal presentations, four concurrent workshops were held to provide definitive recommendations on experiment design, measurement strategy and tactics, and communications requirements; meteorology, transport, and multiday parcel tracking; model development and validation--measurement needs; and instrumentation. The instrumentation workshop was divided into two sessions: instrumentation for study transformation and instrumentation for remote sensing.

The reports of the workshop chairmen were made to a final plenary session. These reports were also distributed at the close of that plenary session to all recipients of the Environmental Protection Agency Request for Proposal DU 78-B246, "Conduct Research Program Designed to Study Transport of Pollutants in Power Plant Plumes, Urban and Industrial Plumes, and Persistent Elevated Pollution Episodes." Representatives of each recipient firm had been invited to attend and participate in all sessions of the seminar/workshop.

Dr. William E. Wilson, Director, Regional Field Studies Office, EPA/ESRL, was the Project Officer for contract 68-02-3000 under which the seminar/workshop was conducted, and served as General Chairman of the sessions; Mr. James J. B. Worth of the Research Triangle Institute was the Technical Chairman. Mr. Harry L. Hamilton, Jr., also of RTI, planned and coordinated the seminar/workshop.

BEGIN FIRST LINE OF TEXT HERE
TYPING GUIDE SHEET
CENTER OF PAGE
TOP OF IMAGE AREA
DROPPED HEAD BEGIN SECTIONS HERE

ABSTRACT

A Seminar/Workshop was convened by the Regional Field Studies Office of the Environmental Protection Agency's Environmental Sciences Research Laboratory to provide for the exchange of research results and to discuss the state-of-the-art of instrumentation and investigative techniques applicable to studies of regional scale persistent elevated pollution episodes (PEPE's). This report comprises the results of four workshops conducted after 2 1/2 days of formal presentations of scientific papers. The workshops, held concurrently, were charged with the responsibility of providing definitive recommendations on the conduct of future field studies of PEPE's. The subjects covered by the workshops were: experiment design, measurement strategy and tactics and communication requirements; meteorology, transport and multiday air parcel tracking; measurement needs for model development and validation; and instrumentation. The instrumentation workshop was divided into two sessions: instrumentation for the study of transformation of pollutants and instrumentation for remote sensing of pollutants. Separate reports are included for each of these sessions.

BEGIN LAST LINE OF TEXT
BOTTOM OF IMAGE AREA OUTSIDE DIMENSION FOR TABLES AND ILLUSTRATIONS
3/8"

PAGE NUMBER
EPA-287 (Cin.)
(4-76)

Contents

Page

19 March 1979

Identification of PEPE's By Visibility Isopleths 1
R. B. Husar and D. E. Patterson

Evidence of Transport of Hazy Air Masses From Satellite Imagery 19
Walter A. Lyons

Remote Sensing of Regional Air Pollution From Satellites 46
E. J. Friedman and E. L. Keitz

Characterization of Regional Sulfate/Oxidant Episodes in the Eastern United States 95
E. Y. Tong, M. T. Mills, B. L. Niemann, and L. F. Smith

Statistics of Elevated Pollution Episodes 123
Gerald F. Watson and Walter J. Saucier

Some Dynamic Aspects of Extended Pollution Episodes 152
William J. King and Fred M. Vukovich

Application of Numerical Models to Prolonged Elevated Pollution Episodes 178
C. Shepherd Burton and Mei-Kao Liu

EPRI's Air Quality Studies 195
Glenn R. Hilst

Ensemble Trajectory Analysis of Summertime Sulfate Concentrations in the Eastern United States 202
Perry J. Samson

20 March 1979

Some Results of the Sulfate Regional Experiment and the PEPE Experiment Design 214
G. M. Hidy, P. K. Mueller, and T. F. Lavery

Fluorocarbon Tracer System for Atmospheric Transport and Dispersion Studies 228
Gilbert J. Ferber

Contents (continued)

Page

20 March 1979 (continued)

MAP3S Programs Applicable to PEPE's 236
Michael C. MacCracken

Regional Scale Aircraft Mapping of Hazy Air Masses During Project MISTT, 1975 and 1976 243
D. E. Patterson, J. M. Holloway, and R. B. Husar

Ground Measurements of Regional Haze 341
Kenneth T. Whitby and Peter H. McMurray

Comparison of Air Quality Within the Mixed Layer With That at the Surface 367
James J. B. Worth

Passive Remote Sensing of SO_2 406
Millán M. Millán

Summary of the NASA Remote Sensing Program 425
S. H. Melfi

Validity of Balloons for Air Parcel Tracking 450
Frank B. Tatom and George H. Fichtl

Navigational Aids for Air Parcel Tracking 469
James G. Haidt

Satellite Positioning of Tracers 480
James J. B. Worth

Radar Tracking 489
C. Raymond Dickson

Light-Weight, Low-Cost Radar, Transponder Systems 500
Earl F. Pound

Miniaturized Laser Doppler Velocimeter 504
David H. Dickson

21 and 22 March 1979—Workshops

I. **Experiment Design, Measurement Strategy and Tactics, Communications Requirements** 529
Roy Evans, Chairman

II. **Meteorology, Transport, and Multiday Tracking** 545
Harry L. Hamilton, Jr., Chairman

Contents (continued)

Page

21 and 22 March 1979 (continued)

III. Model Development and Validation—Measurement Needs 551
George M. Hidy, Chairman

IV. Part 1. Instrumentation for Study of Transformation 560
Robert K. Stevens, Chairman

IV. Part 2. Instrumentation for Remote Sensing 567
Frank Allario, Chairman

PARTICIPANTS

Abdul J. Alkezweeny
Battelle Pacific Northwest Laboratories--Area Office
Muskegon MI

Frank Allario
Langley Research Center
National Aeronautics and Space Administration
Hampton VA

A. Paul Altshuller
Environmental Sciences Research Laboratory
U.S. Environmental Protection Agency
Research Triangle Park NC

Kurt Anlauf
Atmospheric Environment Service
Downsville, Ontario

Wendell Ayers
Langley Research Center
National Aeronautics and Space Administration
Hampton VA

John D. Bachman
Strategies and Air Standards Division
U.S. Environmental Protection Agency
Research Triangle Park NC

W. D. Balfour
Radian Corporation
Austin TX

Francis Binkowski
Environmental Sciences Research Laboratory
U.S. Environmental Protection Agency
Research Triangle Park NC

Donald L. Blumenthal
Meteorology Research, Inc.
Santa Rosa CA

C. Shepherd Burton
Systems Applications, Inc.
San Rafael CA

Michael Chan
Aerovironment, Inc.
Pasadena CA

Jason Ching
Environmental Sciences Research Laboratory
U.S. Environmental Protection Agency
Research Triangle Park NC

Robert Chunn
Contracts Management Division
U.S. Environmental Protection Agency
Research Triangle Park NC

John F. Clarke
Environmental Sciences Research Laboratory
U.S. Environmental Protection Agency
Research Triangle Park NC

Samual C. Coroniti
Dynatrend, Inc.
Burlington MA

Richard Coulter
Argonne National Laboratory
Argonne IL

Dagmar Cronn
Washington State University
Pullman WA

Walter F. Dabberdt
SRI International
Menlo Park CA

Kenneth L. Demerjian
Environmental Sciences Research Laboratory
U.S. Environmental Protection Agency
Research Triangle Park NC

Rosa de Pena
Department of Meteorology
Pennsylvania State University
State College PA

C. Raymond Dickson
Idaho National Engineering Research Laboratory
National Oceanic and Atmospheric Administration
Idaho Falls ID

Allen C. Dittenhoefer
Department of Meteorology
Pennsylvania State University
State College PA

Ron Drake
Battelle Pacific Northwest Laboratories
Richland WA

Jack L. Durham
Environmental Sciences Research Laboratory
U.S. Environmental Protection Agency
Research Triangle Park NC

Thomas G. Dzubay
Environmental Sciences Research Laboratory
U.S. Environmental Protection Agency
Research Triangle Park NC

Cary Eaton
Research Triangle Institute
Research Triangle Park NC

John Eckert
Environmental Monitoring and Support Laboratory
U.S. Environmental Protection Agency
Las Vegas NV

James G. Edinger
Atmospheric Sciences Department
University of California at Los Angeles
Los Angeles CA

Roy Evans
Environmental Sciences Research Laboratory
U.S. Environmental Protection Agency
Research Triangle Park NC

Gilbert J. Ferber
Air Resources Laboratory
National Oceanic and Atmospheric Administration
Silver Spring MD

Edward Friedman
The MITRE Corporation
McLean VA

G. T. Gay
Sandia Laboratories
Albuquerque NM

Noor Gillani
Department of Mechanical Engineering
Washington University
St. Louis MO

Dan Golomb
Office of Energy, Minerals and Industry
U.S. Environmental Protection Agency
Washington DC

James G. Haidt
Research Triangle Institute
Research Triangle Park NC

Harry L. Hamilton, Jr.
Research Triangle Institute
Research Triangle Park NC

George M. Hidy
Environmental Research and Technology, Inc.
West Lake Village CA

Glenn R. Hilst
Electric Power Research Institute
Palo Alto CA

George C. Holzworth
Environmental Sciences Research Laboratory
U.S. Environmental Protection Agency
Research Triangle Park NC

Rudolf B. Husar
Department of Mechanical Engineering
Washington University
St. Louis MO

N. Stuart Jones
Research Triangle Institute
Research Triangle Park NC

Edwin Keitz
The MITRE Corporation
McLean VA

William King
Research Triangle Institute
Research Triangle Park NC

Robert G. Lamb
Environmental Sciences Research Laboratory
U.S. Environmental Protection Agency
Research Triangle Park NC

Bryan W. Lambeth
Radian Corporation
Austin TX

Lee Langan
Environmental Measurements, Inc.
San Francisco CA

Paul Lioy
Institute for Environmental Medicine
New York University Medical Center
New York NY

Mei-Kao Liu
Systems Applications, Inc.
San Rafael CA

Maris Lusis
Air Resources Branch
Toronto, Ontario

Walter A. Lyons
MESOMET, Inc.
Chicago IL

Michael MacCracken
Lawrence Livermore Laboratory
Department of Energy
Livermore CA

David Mage
Environmental Monitoring and Support Laboratory
U.S. Environmental Protection Agency
Research Triangle Park NC

Ronald J. Massa
Dynatrend, Inc.
Burlington MA

Peter H. McMurray
Department of Mechanical Engineering
University of Minnesota
Minneapolis MN

S. Harvey Melfi
Office of Space and Terrestrial Applications
National Aeronautics and Space Administration
Washington DC

Edwin L. Meyer
Monitoring and Data Analysis Division
U.S. Environmental Protection Agency
Research Triangle Park NC

Ron Meyers
Brookhaven National Laboratory
Upton NY

Millán M. Millán
Atmospheric Environment Service
Downsview, Ontario

Dave Miller
Battelle Columbus Laboratories
Columbus OH

R. L. Myers
Rockwell International
Creve Coeur MO

Larry E. Neimeyer
Environmental Sciences Research Laboratory
U.S. Environmental Protection Agency
Research Triangle Park NC

Leonard Newman
Brookhaven National Laboratory
Upton NY

Brand L. Niemann
Teknekron, Inc.
Berkeley CA

A. F. Oberta
Environmental Resources Group, Inc.
Danville VA

Brynjulf Ottar
Norwegian Institute for Air Research
Royal Norwegian Council for
  Scientific & Industrial Research
Lillestrom, Norway

T. G. Pace
Monitoring and Data Analysis Division
U.S. Environmental Protection Agency
Research Triangle Park NC

Robert A. Papetti
Office of Air, Land and Water Use
U.S. Environmental Protection Agency
Washington DC

David Patterson
Department of Mechanical Engineering
Washington University
St. Louis MO

Francis Pooler
Environmental Sciences Research Laboratory
U.S. Environmental Protection Agency
Research Triangle Park NC

Earl Pound
Utah State University
Logan UT

Rudolf Pueschel
Environmental Research Laboratory
National Oceanic and Atmospheric Administration
Boulder CO

Madhav Ranade
Research Triangle Institute
Research Triangle Park NC

J. C. Romanovsky
Environmental Sciences Research Laboratory
U.S. Environmental Protection Agency
Research Triangle Park NC

Perry Samson
N.Y. State Department of Environmental Conservation
Albany NY

Dave Sanchez
Control Programs Development Division
U.S. Environmental Protection Agency
Research Triangle Park NC

Walter J. Saucier
Department of Geosciences
North Carolina State University
Raleigh NC

Frank A. Schiermeier
Environmental Sciences Research Laboratory
U.S. Environmental Protection Agency
St. Louis MO

Joseph Sickles, II
Research Triangle Institute
Research Triangle Park NC

Lowell Smith
Office of Energy, Minerals and Industry
U.S. Environmental Protection Agency
Washington DC

Chester W. Spicer
Battelle Columbus Laboratories
Columbus OH

Lester L. Spiller
Environmental Sciences Research Laboratory
U.S. Environmental Protection Agency
Research Triangle Park NC

Gene E. Start
Idaho National Engineering Research Laboratory
National Oceanic and Atmospheric Administration
Idaho Falls ID

Gary Stensland
Illinois State Water Survey
Urbana IL

Robert K. Stevens
Environmental Sciences Research Laboratory
U.S. Environmental Protection Agency
Research Triangle Park NC

George Sverdrup
Battelle Columbus Laboratories
Columbus OH

Gary Tannahill
Radian Corporation
Austin TX

Frank B. Tatom
Engineering Analysis, Inc.
Huntsville AL

Prekimi U. Tawath
The MITRE Corporation
McLean VA

James Tommerdahl
Research Triangle Institute
Research Triangle Park NC

Eugene Tong
Teknekron, Inc.
Berkeley CA

Edward Uthe
SRI International
Menlo Park CA

William M. Vaughan
EMI, Inc.
University City MO

Fred Vukovich
Research Triangle Institute
Research Triangle Park NC

Scott Wagner
Office of Space and Terrestrial Applications
National Aeronautics and Space Administration
Washington DC

T. L. Waldron
Rockwell International
Creve Coeur MO

Gerald Watson
Department of Geosciences
North Carolina State University
Raleigh NC

Marvin L. Wesely
Argonne National Laboratory
Argonne IL

Kenneth T. Whitby
Department of Mechanical Engineering
University of Minnesota
Minneapolis MN

William E. Wilson
Regional Field Studies Office
Environmental Sciences Research Laboratory
Research Triangle Park NC

George Wolff
General Motors Research Laboratories
Warren MI

James J. B. Worth
Research Triangle Institute
Research Triangle Park NC

Bernard Zak
Sandia Laboratories
Albuquerque NM

ABBREVIATIONS

AES	Atmospheric Environment Services
APT	automatic picture transmission
ATS	Applications Technology Satellite
AVHRR	advanced very high resolution radiometer
BNL	Brookhaven National Laboratory
BOR	Biggs Optical Range
b_{scat}	light scattering due to aerosols
CBM	carbon-bond mechanism
CIMATS	correlation interferometer for measuring atmospheric trace species
CNC	condensation nuclei count
COG	center of gravity
COPE	Carbon Monoxide Pollution Experiment
COSPEC	correlation spectrometer
CVB	constant-volume balloon
DARS	differential absorption remote tensing
DIAL	differential absorption lidar
EAA	electrical aerosol analyzer
EML	Environmental Measurements Laboratory (DOE)
EPE	elevated pollution episode
EPRI	Electric Power Research Institute
ERAQS	Eastern Regional Air Quality Studies
ESRL	Environmental Systems Research Laboratory

FAA	Federal Aviation Administration
FPD	flame photometric detection
GCMS	gas chromatography-mass spectrometry
GFC	gas filter correlation
HK	haze and/or smoke
HRWS	helicopter remote wind sensor
HSI	high-speed interferometer
HSRL	high spectral resolution lidar
IHR	infrared heterodyne radiometer
IHS	infrared heterodyne spectrometer
IPM	inhalable particulate matter
IPMN	Inhaled Particulate Monitor Network
LAS	laser absorption spectrometer
LCS	laser crosswind sensor
LDV	laser doppler velocimeter
LHS	laser heterodyne spectrometer
LPI	low-pressure impactor
LRC	Langley Research Center
MAPS	measuring air pollution from satellites
MAP3S	Multistate Atmospheric Power Production Pollution Study
McIDAS	Man/Computer Interactive Data Access System
MISTT	Midwest Interstate Sulfur Transformation and Transport
MOPS	multispectral observation of pollutants
MSS	multispectral scanner
NASN	National Air Sampling Network
NBS	National Bureau of Standards

NESS	National Environmental Satellite Service
NMHC	nonmethane hydrocarbon
NOAA	National Oceanic and Atmospheric Administration
NWS	National Weather Service
OFT MAPS	oribital flight test MAPS
OPC	optical particle counter
ORBS	Ohio River Basin Study
PEPE	persistent elevated pollution episode
PMR	pressure-modulated radiometer
PMV	Plume Model Validation
PSD	prevention of significant deterioration
RAMS	Regional Air Monitoring System Random Access Measurement System
RAPS	Regional Air Pollution Study
RAQS	Regional Air Quality Study
RBV	return beam vidicon
RF	radio frequency
RH	relative humidity
SAGE	Stratospheric Aerosol and Gas Experiment
SAM	Stratospheric Aerosol Measurement
SAROAD	Storage and Retrieval of Aerometric Data
SBUV-TOMS	solar backscatter ultraviolet-total ozone measurement system
SMS/GOES	Synchronous Meteorological Satellite/Geostationary Operational Environmental Satellite
STATE	Sulfur Transport and Transformation Experiment
SURE	Sulfate Regional Experiment
TDMA	tandem differential mobility analyzer

TSP	total suspended particulate
TVA	Tennessee Valley Authority
UMML	University of Minnesota Mobile Laboratory
UV DIAL	ultraviolet differential absorption lidar
VAS	VISSR atmospheric sounder
VCO	voltage-controlled oscillator
VISSR	visual infrared spin-scan radiometer
XRF	x-ray fluorescence

IDENTIFICATION OF PEPE'S BY VISIBILITY ISOPLETHS

R. B. Husar* and D. E. Patterson

Washington University, St. Louis, Missouri

Abstract

Persistent elevated pollution episodes (PEPE's) may be identified by regional scale high concentrations of secondary sulfate and ozone. Sulfate aerosol causes visibility reduction, for which fine spatial and temporal resolution is available. Visibility appears to be a suitable surrogate for sulfate concentrations, so that the spatial distribution and trends of visibility offer information about the frequency of occurrence of PEPE's.

INTRODUCTION

The past several decades have seen a shift in the spatial scale of visibility-reducing particulates, expanding from areas immediately surrounding each factory to entire metropolitan areas to multistate regions covered by haze. The control of smokestack particulate concentrations in the atmosphere has reduced the occurrence of locally visible "hot spots". However, the emissions of precursor gases such as SO_2, hydrocarbons, and NO_x have increased greatly over this period. As will be discussed below, the average haziness has increased over most of the United States in the past three decades, due to the production in the atmosphere of secondary aerosols such as sulfate.

The atmospheric transmission of tall stack point source and urban area source effluents has been studied extensively during the past decade, most recently in the Midwest Interstate Sulfur Transformation and Transport (MISTT) project and in the Sulfur Transport and Transformation in the Environment (STATE) project, where the transport, chemical transformations, removal, and process interactions in determining the sulfur budget of large plumes were assessed.

---

*Speaker.

URBAN PLUMES

Urban plumes constitute an aggregate plume originating from various sources within a metropolitan area. One thoroughly studied urban plume is that of the metropolitan St. Louis area, a major urban industrial center including coal-fired power plants with a combined capacity of 4,600 MW, oil refineries with a combined capacity of 4.4×10^5 bbl/d (1 bbl = 160 L), various other industries, and a population of about two million (White et al., 1976). Because St. Louis is remote from other major metropolitan areas, its impact on the surrounding ambient air quality is relatively easy to identify; air that has been modified by the aggregate emissions of the metropolitan area form an "urban plume" downwind.

As part of project MISTT, the three-dimensional flow of aerosols and trace gases in the St. Louis urban plume was studied (Wilson, 1978). The plume was successfully tracked up to 240 km, and it was mapped quantitatively up to 160 km (Figure 1). At these distances, the plume was still defined and on the order of 50 km wide.

An increased concentration of light-scattering aerosols is a key characteristic of the St. Louis urban plume. The primary contribution of project MISTT was to quantify the flow of material at increasing downwind distances so as to study the transformations that pollutants undergo in the atmosphere.

The flow rate of ozone, b_{scat}, and particulate sulfur, S_p, all increased with distance downwind of St. Louis on July 18, 1975, reflecting the secondary origin of ozone and most of the light-scattering aerosols (White et al., 1976). Most of the increase in the b_{scat} flow rate was observed downwind of the major increase in ozone flow rate, consistent with the finding of the laboratory studies that aerosol production lags behind ozone production in a photochemical system (Wilson et al., 1973). The ratio of the flow rate of b_{scat} to the flow rate of S_p indicates that sulfate compounds accounted for most of the newly formed aerosol in the urban plume. This case study illustrates that emissions from a metropolitan area such as St. Louis cause reduced visibility and elevated ozone concentrations in urban plumes, long after their primary precursors have been diluted to low concentrations.

From extrapolation of measured plume transport, it is clear that the urban plume of one metropolitan area may become a "background haziness" for another. It is therefore reasonable to assume that the pollutant background in nonurban regions of the eastern United States is likely due to the combined emissions of metropolitan and industrial areas, as well as to emissions from power plants far upwind. Regrettably, direct observations of plume impacts have only been carried out up to a few hundred kilometers from their sources. Beyond those distances, single or even urban plumes tend to elude convenient aircraft mapping; also, they are likely to be superimposed on a plume of another major source. It has been proposed that the observed large-scale haziness of a large part of the eastern United States during stagnation is in fact the result of the superposition of numerous urban and industrial power plant plumes, as discussed in the next section.

Regional Scale PEPE Episodes

Early works on air pollution episode potential focused on local inversion situations rather than stagnation of a regional scale air mass. Hosler (1961) found that the southeast coast of the United States and the Smoky Mountain region had the highest incidence of surface inversions nationally. Holzworth (1967) evaluated the pollution potential of several U.S. urban areas based on mean mixing heights and wind speeds. Korshover (1967) constructed a climatology of stagnating anticyclones in the Eastern United States from 1936-1965 and found the highest potential for large-scale stagnation east of the Rocky Mountains to be in the Southern Appalachian and Smoky Mountain regions.

One of the earliest examinations of regional scale air pollution detailed the evolution and impact of the Thanksgiving 1966 episode over the eastern U.S. seaboard, in which a stagnating high-pressure system caused prolonged elevated regional concentrations of primary pollutants and total suspended particulates.

Formation of secondary pollutants (such as sulfate) in the atmosphere is believed to be the major problem of regional air pollution today. The residence time of secondary particles is the sum of the time required to create them and the subsequent time for removal from the atmosphere. The flow diagram of sulfur transmission through the atmosphere (Figure 3) illustrates, for example, that most of the SO_2 emission is removed or transformed to sulfate within the first day of atmospheric residence, but the atmospheric burden of the secondary sulfate may remain relatively high for several days of residence time.

Mean winds of 500 km per day are not uncommon in the eastern United States (Blumenthal et al., 1978), so a reasonable scale of sulfate impact from an individual SO_2 source is on the order of 1,000 to 2,000 km. The implication, as seen in Figure 4, is that ambient light-scattering sulfate aerosol can result from the additive effects of tens or even hundreds of SO_2 plumes of different atmospheric ages. Long-range transport of fine aerosol sulfate within a stagnating regional scale air mass can create a PEPE.

In the past decade, several researchers have presented evidence of long-range transport of visibility-reducing fine aerosol. Rodhe (1972), Brosset et al. (1975), Eliassen and Saltbones (1975), Smith and Jeffrey (1975), and Szepesi (1978) are among those who have established the reality of long-range transport of sulfates in Europe. Chung (1978) found evidence of transport of sulfate from the northeastern Midwest of tne United States into southeast Canada.

In the United States, Altshuller (1976) noted the anomaly of decreasing urban SO_2 concentrations with increasing rural sulfate trends and proposed long-range transport as the cause of regional sulfate levels. Wilson et al. (1976) also proposed long-range transport as the explanation for regional sulfate concentrations, based on field studies of plume transmission. Gage et al. (1977) demonstrated the sulfate episode potential when multiple SO_2 sources are aligned along the wind direction.

One of the earliest case studies of transport of large-scale hazy air masses was that of Hall et al. (1973). Since about 1975, the evolution and transport of regional scale hazy air masses have been receiving increasing attention from numerous research groups. Detailed case studies of such episodes have been reported by Tong et al. (1976), Husar et al. (1976), Lyons and Husar (1976), Wolff et al. (1977), Samson and Ragland (1977), Vukovich et al. (1977), Calvin et al. (1978), Hidy et al. (1978), and Chung (1978), among others.

A common finding in recent studies is that formation of regional scale haziness is usually associated with the presence of slow-moving high-pressure systems. Because precipitation is relatively infrequent in anticyclonic systems, the residence time of sulfate aerosol may be as long as a week or more.

An example of one such episode over a 2-week period in June-July 1975 is presented in Figure 5 as visibility isopleths. Inspection of the sequence of contour maps reveals that multistate regions are covered by a haze layer in which noon visibility is less than 10 km ($b_{ext} > 4 \times 10^{-4} m^{-1}$, outer contours).

The apparent movement of the areas of haze was confirmed by geostationary satellite photographs. The region of haziness on July 30 may be clearly seen in Lyons and Husar (1976), where the turbid air mass is visible over the States of Arkansas, Missouri, Kansas, Iowa, and Minnesota.

The air mass of June 25, 1975 (defined by the shaded region of visibility 6.5-10 km) was of maritime origin in the Gulf of Mexico and had followed a trajectory through Louisiana northward into Illinois and Indiana. Between June 25 and 27, relative stagnation prevailed in the Great Lakes region, leading to increasing haziness in this high emission density area. The tropical storm "Amy" moving northward off the northeast coast blocked the eastern motion of the hazy air mass as a front approached the Great Lakes from the northwest. Between June 28 and 30 an easterly flow developed, causing the hazy air mass to drift slowly westward, passing over St. Louis, MO, on June 28-29 and continuing across Missouri and Kansas by June 30. From June 30 to July 2 the haze moved in a clockwise pattern to the southern Great Lakes. By July 3, the advancing Canadian front formed the northern border of an extensive hazy air mass occupying most of the midwestern and northeastern United States. The hazy air mass again passed over St. Louis at this time. During July 3-5 the cold front advanced rapidly to the south, pushing the heavily polluted air mass across the southeastern States and out to sea.

The two passages of the hazy air mass over St. Louis, MO, resulted in sharp increases of b_{scat} over the entire metropolitan region (Figure 6a). Sulfate concentration also increased during the haze episode, from about 9 to 33 $\mu g/m^3$. The spatial coherency of haziness is seen in the correspondence of the extinction coefficient at St. Louis, MO, and Springfield, IL (Figure 6b), again confirming that the observed haziness was primarily due to inflow of the polluted "background" material of the hazy air mass rather than local contributions.

Sufficient sulfate data were available from the National Aerometric Data Bank for comparison with visibility on two days during the episode period.

Figure 7 indicates the substantial correspondence of sulfate and visibility: sulfate concentrations in excess of 30 μg/m^3 are seen to coincide with regions of lowest visibility.

In order to examine the correlation between ozone and visibility reduction on a synoptic scale, contour plots of SAROAD daily maximum ozone were also prepared (by hand) for the period June 25 through July 5, 1975 (Figure 8).

The plots show that the former U.S. standard for ozone (0.08 ppm) was exceeded over large areas of the eastern United States on all days of the air pollution episode. Comparison of the maps for visibility and ozone (Figures 5 and 8, respectively) reveals that the geographical location of high ozone concentrations roughly corresponds to the areas of low visibility (and high sulfate). As may be anticipated, however, the correlation with haziness (low visibility) is much better for sulfates than for ozone.

During this period, the visual air quality was beyond the control of any local jurisdiction. The Alabama Air Pollution Control Commission (AAPCC) reported the following (Bulletin of the AAPCC, 1975):

> During the weekend of July 5, 1975, a heavy haze layer enveloped the state of Alabama and much of the Southeastern U.S. At that time, the AAPCC technical staff received many comments from the public concerning the origin and composition of the haze.
>
> The National Weather Service in Birmingham did issue an air stagnation advisory (ASA) for Alabama for this same time period; however, the traditional pollutant measurements made by the AAPCC and local programs did not show excessive levels. In fact, the measured local levels were lower than had been measured under previous ASA's, making the dramatic decrease in visibility more intriguing.

Husar et al. (1976) reported that in June-August 1975 there were at least six episodes similar to the above. The work of other investigators confirms that episodes of regional scale hazy air masses are not rare in the eastern United States. Yet at present only the qualitative features of such episodes are understood, i.e., the observed effect on visibility, the composition in terms of secondary sulfate and ozone, and the apparent motion of the haze.

Important questions remain to be answered about regional scale episodes of haziness, including the following:

- To what degree do the hazy air mass and the meteorologically defined anticyclone coincide?
- Are the effects of superimposing multiple SO_2 plumes and urban reactive plumes simply additive?
- What are the roles and possible feedback mechanisms of high pollutant concentrations on dry and wet deposition, cloudiness, etc?
- What is the actual residence time of the particulates in the atmosphere during such episodes?

TRENDS AND SPATIAL DISTRIBUTION OF HAZINESS

The upcoming Prolonged Elevated Pollution Episode (PEPE) project of STATE will be specifically designed to sample such regional scale episodes of haziness from their inception throughout their residence over the eastern United States. PEPEs are important factors in determining the mean extinction coefficient (or haziness). Therefore, historical information on visibility trends and spatial distribution may be useful. Figures 9 and 10, with their associated captions, summarize the seasonal and spatial trends of haziness over the eastern United States since 1948.

SUMMARY

This report and the companion paper, "Regional Scale Aircraft Mapping of Hazy Air Masses During Project MISTT, 1975 and 1976," present direct evidence of long-range (200-300 km) transport of urban and power plant plumes. Regional scale polluted air masses, defined by elevated concentrations of sulfate and ozone, may be followed by the examination of visibility isopleths. The region of most severe average summertime haziness includes the Ohio River Valley and the Smoky Mountain States; therefore, the upcoming PEPE field study probably should be located within this area.

ACKNOWLEDGMENT

This research has been supported by the Federal Interagency Energy/Environment Research and Development Program through U.S. Environmental Protection Agency Grant No. R803896. The work was conducted as part of projects MISTT (Midwest Interstate Sulfur Transformation and Transport) and STATE (Sulfur Transformation and Transport in the Environment) with the close cooperation of Dr. William E. Wilson, Jr., Project Officer.

REFERENCES

Altshuller, A. P. 1976. Regional Transport and Transformation of Sulfur Dioxide to Sulfates in the U.S. *J. Air Pollut. Control Ass.*, 26:318-324.

Blumenthal, D. L., J. A. Ogren, and J. A. Anderson. 1978. Airborne Sampling System for Plume Monitoring. *Atmospheric Environment*, 12:613-620.

Brosset, C., K. Andreasson, and M. Ferm. 1975. The Nature and Possible Origin of Acid Particles Observed at the Swedish West Coast. *Atmospheric Environment*, 9:631-642.

Chung, Y. S. 1978. The Distribution of Atmospheric Sulfates in Canada and its Relationships to Longe-Range Transport of Air Pollutants. *Atmospheric Environment*, 12:1471-1480.

Eliassen, A., and J. Saltbones. 1975. Decay and Transformation Rates SO , as Estimated From Emission Data, Trajectories, and Measured Air Concentrations. *Atmospheric Environment*, 9:425-429.

Gage, S. J., L. F. Smith, P. M. Cukor, and B. L. Nieman. 1977. Long-Range Transport of SO_x/MSO_4 From the U.S. EPA/Teknekron Integrated Technology Assessment of Electric Utility Energy Systems. *Proceedings International Symposium on Sulfur in the Atmosphere* (ISSA), Dubrovnik, Yugoslavia.

Galvin, P. J., P. J. Samson, E. C. Peter, and D. Romano. 1978. Transport of Sulfate to New York State. *Atmospheric Environment*, 9:643-659.

Hall, F. P., Jr., C. E. Duchon, L. G. Lee, and R. R. Hagan. 1973. Long Range Transport of Air Pollution: A Case Study, August 1970. *Mon. Weather Rev.*, 101:404-411.

Hidy, G. M., P. K. Mueller, and E. Y. Tong. 1978. Spatial and Temporal Distributions of Airborne Sulfate in Parts of the United States. *Atmospheric Environment*, 12:735-752.

Hosler, C. R. 1961. Low Level Inversion Frequency in the Contiguous United States. *Monthly Weather Rev.*, 89:319-339.

Holzworth, G. C. 1967. Mixing Depths, Wind Speeds and Air Pollution Potential for Selected Locations in the United States. *JAM*, 6:1039-1044.

Husar, R. B., D. E. Patterson, C. C. Paley, and N. V. Gillani. 1976. Ozone in Hazy Air Masses. Paper presented at the International Conference on Photochemical Oxidant and its Control, Raleigh, NC, September 12-17, 10 pp.

Korshover, J. 1967. Climatology of Stagnating Anticyclones East of the Rocky Mountains, 1936-1965. *NAPCA*.

Lyons, W. A., and R. B. Husar. 1976. SMS/GOES Visible Images Detect a Synoptic-Scale Air Pollution Episode. *Mon. Weather Rev.*, 104:1623-1626.

Rodhe, H., C. Persson, and O. Akesson. 1972. An Investigation Into Regional Transport of Soot and Sulfate Aerosols. Atmospheric Environment, 6:675-693.

Samson, P. J., and K. W. Ragland. 1977. Ozone and Visibility Reduction in the Midwest: Evidence for Large-Scale Transport. J. Appl. Meteorol., 16:1101-1106.

Smith, F. B., and G. H. Jeffrey. 1975. Airborne Transport of Sulfur Dioxide From the United Kingdom. Atmospheric Environment, 9:643-659.

Szepesi, D. J. 1978. Transmission of Sulfur Dioxide on Local, Regional and Continental Scale. Atmospheric Environment, 12:529-535.

Thanksgiving 1966 Air Pollution Episode in the Eastern United States, NAPCA, AP-45, 1968.

Tong, E. Y., G. M. Hidy, T. F. Lavery, and F. Berlandi. 1976. Regional and Local Aspects of Atmospheric Sulfates in the Northeast Quadrant of the U.S. Proceedings Third Symposium of Turbulence Diffusion and Air Quality, AMS.

Vukovich, F. M., W. D. Bach, Jr., B. W. Crissman, and W. J. King. 1977. On the Relationship Between High Ozone in the Rural Surface Layer and High Pressure Systems. Atmospheric Environment, 11:967-983.

White, W. H., J. A. Anderson, D. L. Blumenthal, R. B. Husar, N. V. Gillani, J. D. Husar, and W. E. Wilson. 1976. Formation and Transport of Secondary Air Pollutants: Ozone One Aerosols in the St. Louis Urban Plume. Science, 194:187-189.

Wilson, W. E., Jr., D. F. Miller, A. Levy, and R. K. Stone. 1973. J. Air Pollut. Control Assoc., 23:949.

Wilson, W. E., R. J. Charlson, R. B. Husar, K. T. Whitby, and D. L. Blumenthal. 1976. 69th Annual Meeting of Air Pollution Control Assoc., Portland, OR, June 27-July 1, 76-30-06.

Wilson, W. E., Jr. 1978. Sulfates in the Atmosphere: A Progress Report on Project MISTT. Atmospheric Environment, 12:537-547.

Wolff, G. T., P. J. Lioy, R. E. Meyers, and R. T. Cederwall. 1977. An Investigation of Long-Range Transport of Ozone Across the Midwestern and Eastern United States. Atmospheric Environment, 11:797-802.

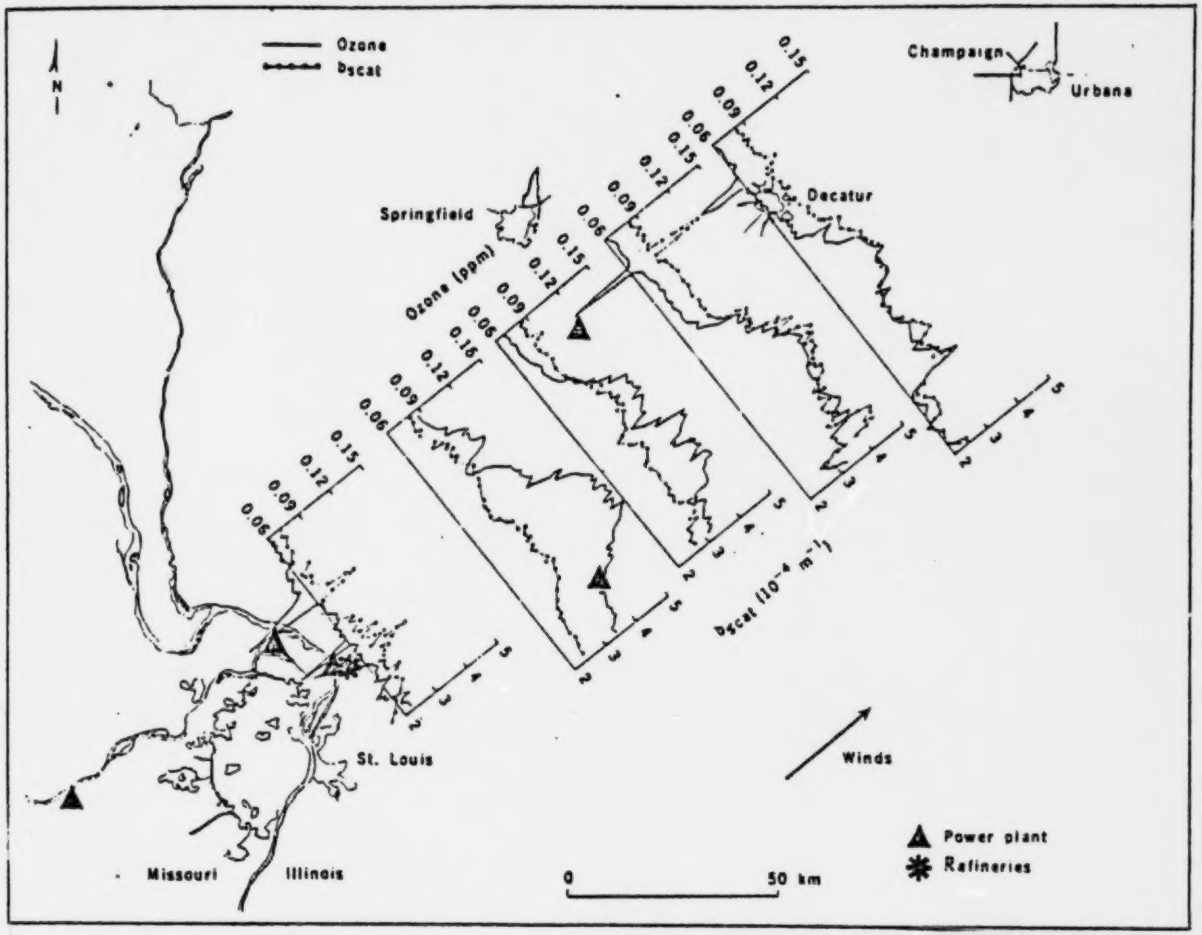

Figure 1. Concentrations of O_3 and b_{scat} values downwind of St. Louis on 18 July 1975. Data are taken from horizontal traverses by instrumented aircraft, at altitudes indicated in Figure 2A. Graph baselines show sampling paths; baseline concentrations are not zero (White et al.).

© 1976 by the American Association for the Advancement of Science. This figure originally appeared in an article by W. H. White et al. in volume 194 of *Science*, pp. 187-189.

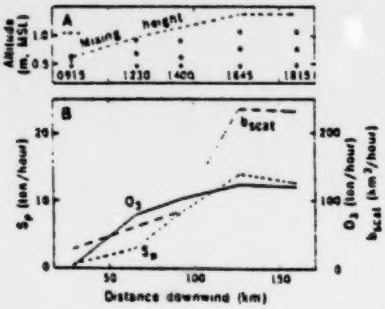

Figure 2. Traverse altitudes and pollutant flow rates in the St. Louis urban plume on 18 July 1975. Data are plotted against distance downwind of the St. Louis Gateway Arch. (A) Location of horizontal traverses; closed circles correspond to traverses shown in Figure 1. Mixing heights were determined from aircraft soundings. Approximate time (CDT) of sampling is shown at the bottom. (B) Flow rates (in excess of background) of O_3, b_{scat}, and S_p (White et al.).

© 1976 by the American Association for the Advancement of Science. This figure originally appeared in an article by W. H. White et al. in volume 194 of *Science*, pp. 187-189.

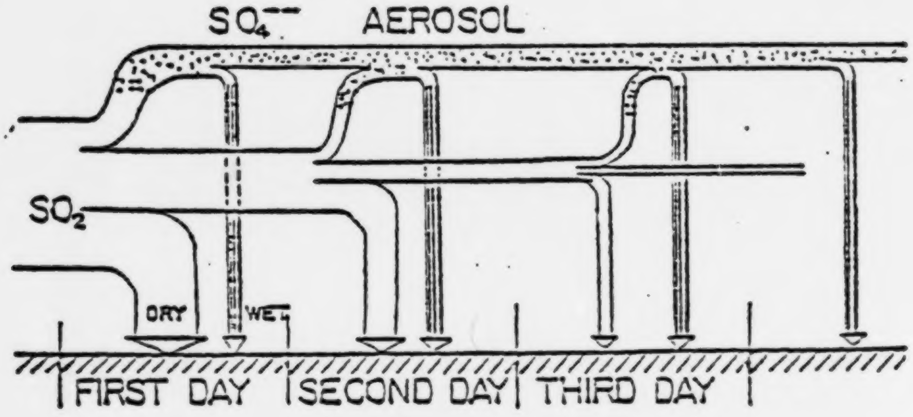

Figure 3. Flow diagram of sulfur transmission through the atmosphere.

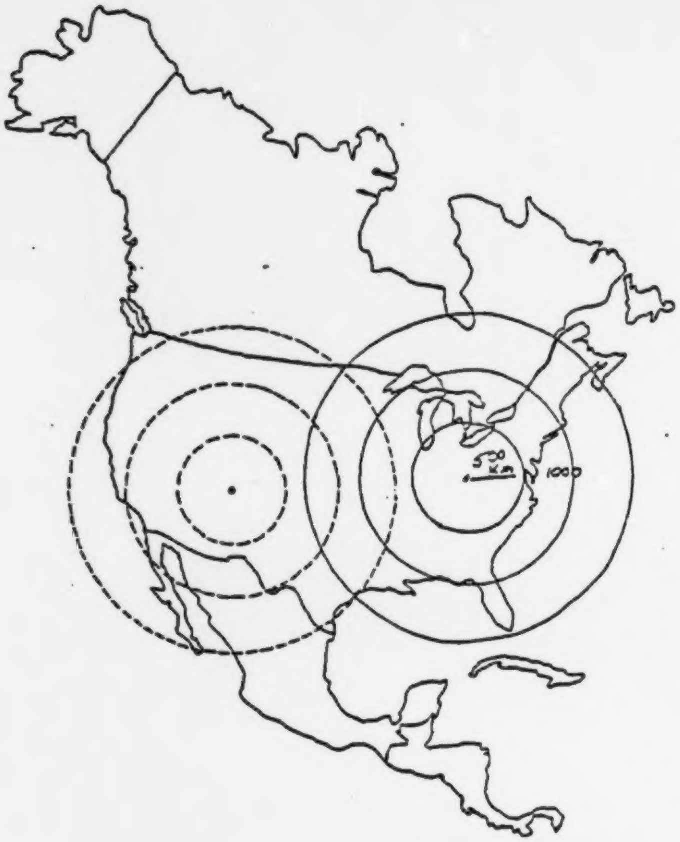

Figure 4. Schematic illustration for the range of transport of fine particles. A reasonable mean transport distance is considered to be 1,500 km. The actual transport depends on the synoptic-scale wind field.

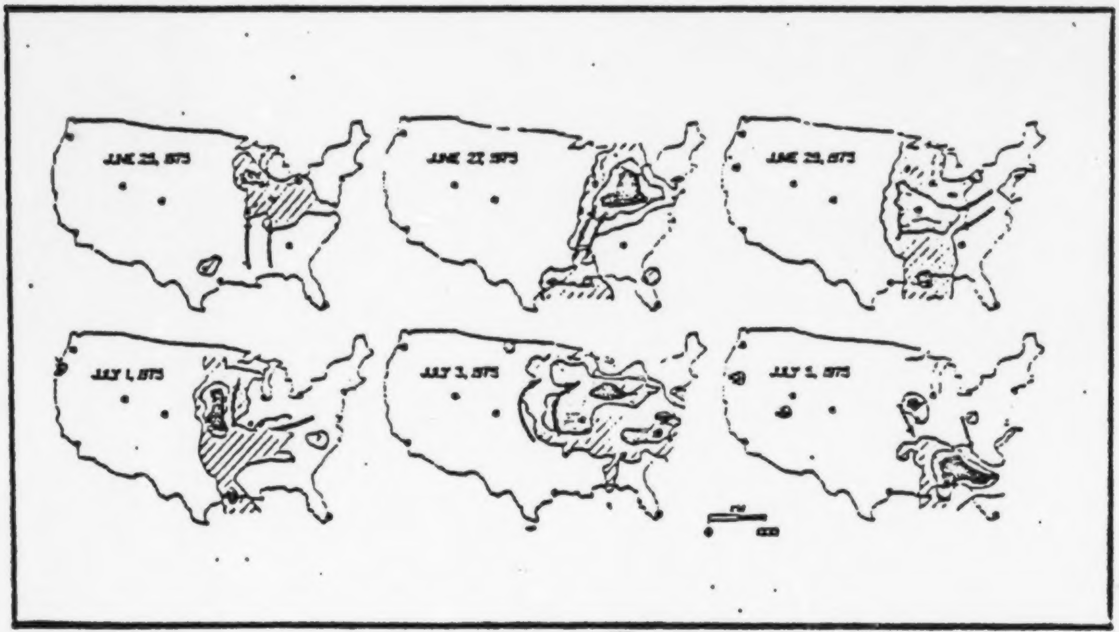

Figure 5. Sequential contour maps of noon visibility for June 25–July 5, 1975, illustrates the evolution and transport of a large-scale hazy air mass. Contours correspond to visual range 6.5–10 km (light shade), 5–6.5 km (medium shade), and <5 km (black).

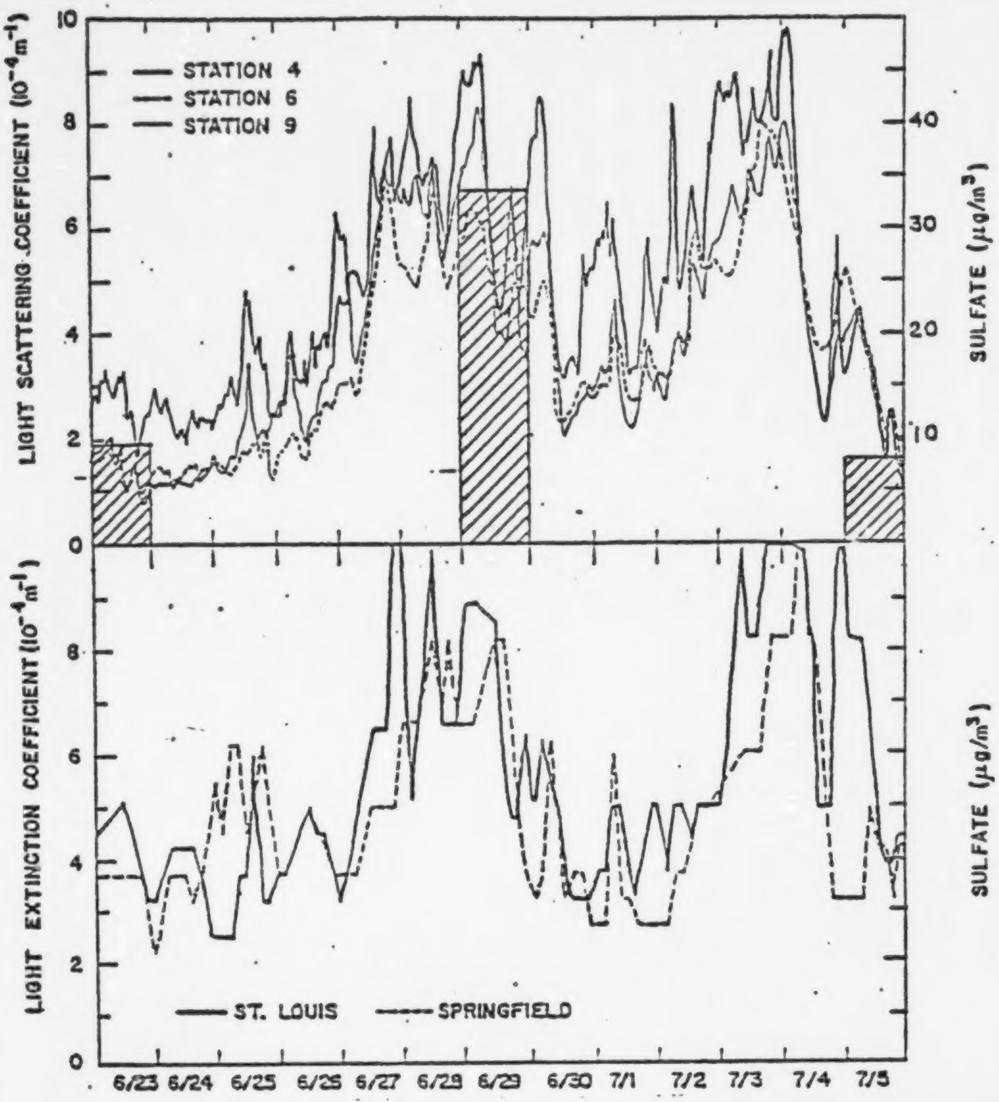

Figure 6. Local monitoring data in the St. Louis, MO, area during the June–July 1975 haziness episode. (a) Light-scattering coefficient (b_{scat}) recorded at three widely spaced locations in the St. Louis metropolitan area and daily average sulfate concentrations; (b) extinction coefficients (b_{ext}) obtained from visibility observations at St. Louis, MO, and Springfield, IL, 150 km apart.

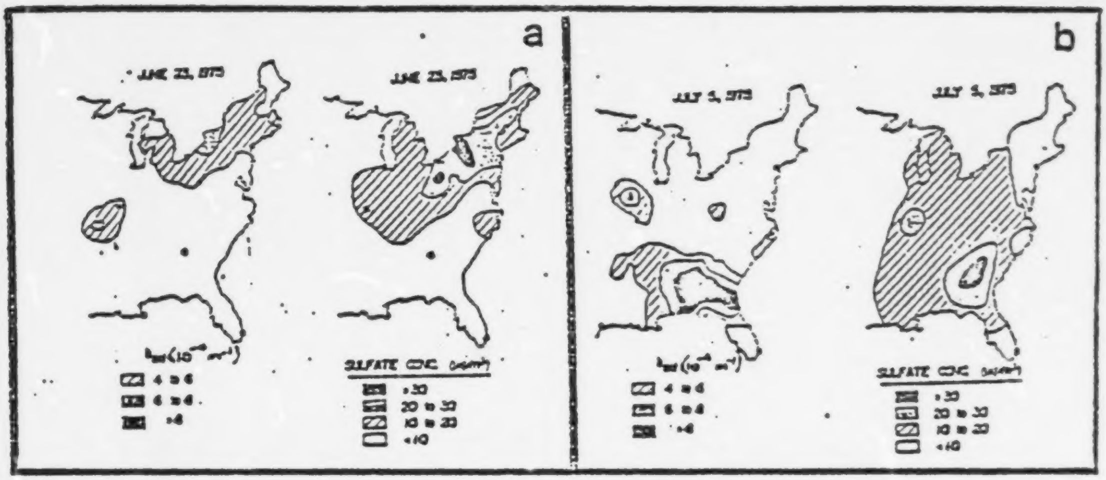

Figure 7. Comparison of noon extinction coefficient and daily mean sulfate concentration on June 23 and July 25, 1975. The regions of highest sulfate concentrations coincide with areas of lowest visibility.

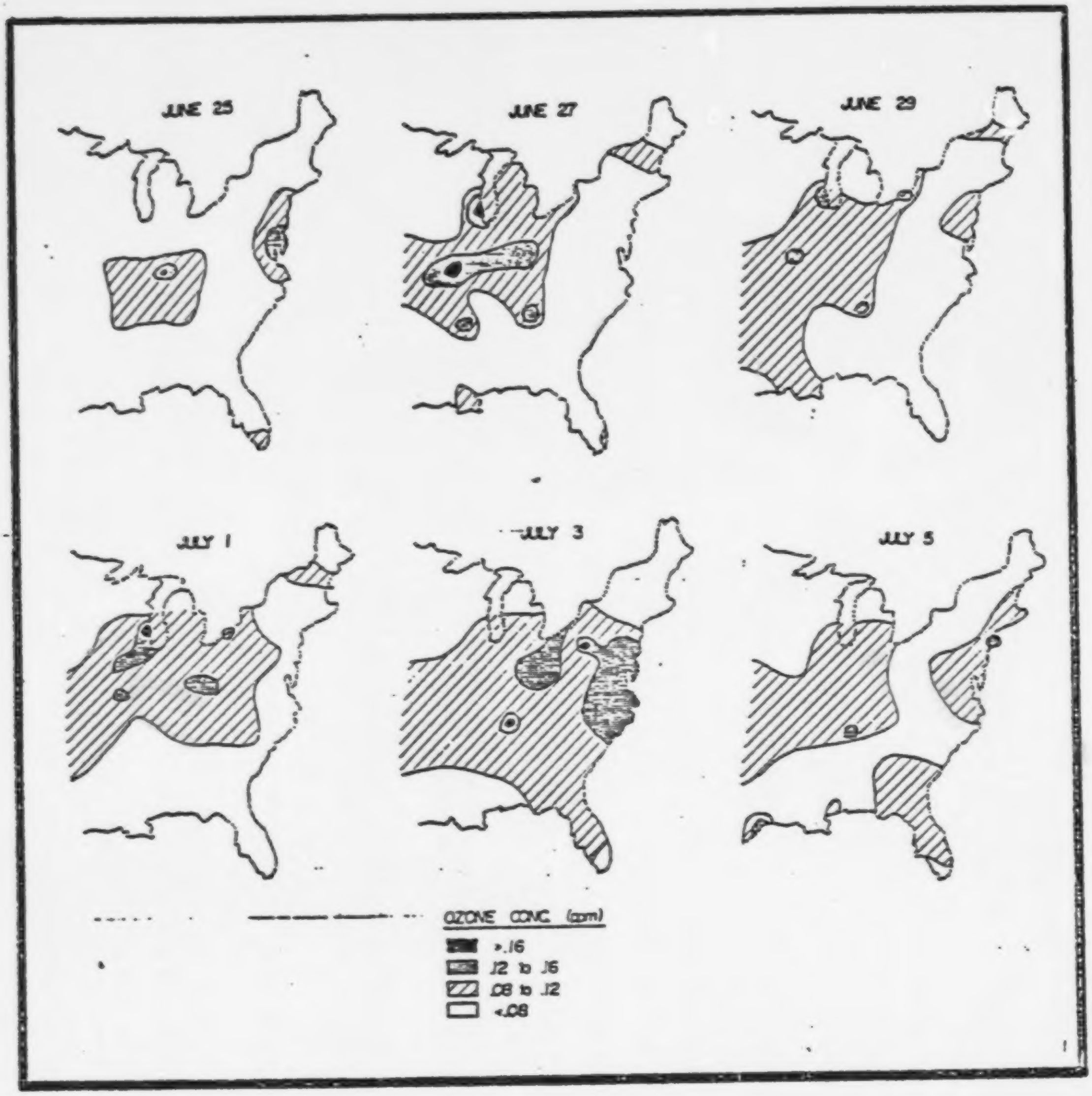

Figure 8. Sequential contour plots of daily peak ozone concentration.

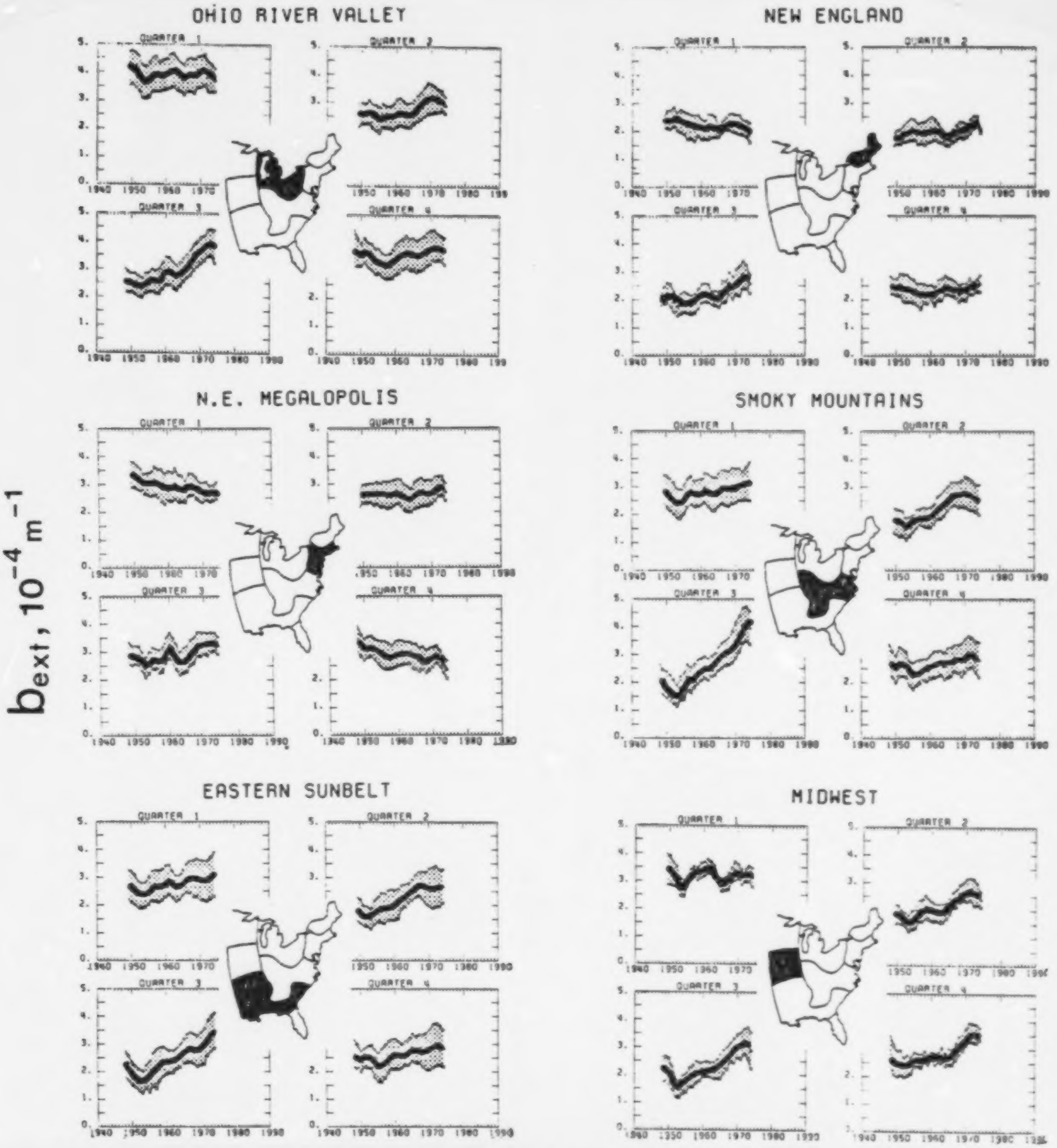

Figure 9. In the Ohio River Valley region, the winter (quarter 1) average extinction decreased slightly while the spring (quarter 2) average increased. The summer (quarter 3) haziness increased from roughly 2.5 in the 1950's (a visibility of 10 miles) to about 4 in the 1970's (a visibility of less than 6 miles). Fall (quarter 4) haziness remained essentially constant. New England haziness declined in the winter and increased in the spring and summer quarters while the fall average remained essentially unchanged. The summer average increase was from about 2 to 3 corresponding to a reduction in visibility from 12 to 8 miles. The N. E. Megalopolis region shows a general decline in haziness during quarters 1 and 4, while quarters 2 and 3 display a slight increase from b = 2.7 (9 miles) to 3 (8 miles). The Smoky Mountain region displays a strong increase in the average summer quarter extinction coefficient from about 1.6 to 4, corresponding to visibility deterioration from 15 to 6 miles. Smaller but still pronounced increases are noted for quarters 2 and 4. Evidently the Smoky Mountains have become appreciably "smokier" over the past 20 summers. The Eastern Sunbelt region has an increased haziness for all quarters, most pronounced being the summer quarter with an increase from 2 (12 miles) to 3.5 (7 miles). Midwest quarter 1 extinction fluctuated slightly with no discernible trend. The spring and fall quarters have increased appreciably but summer values nearly doubled, from 1.5 to 3 (16 to 8 miles).

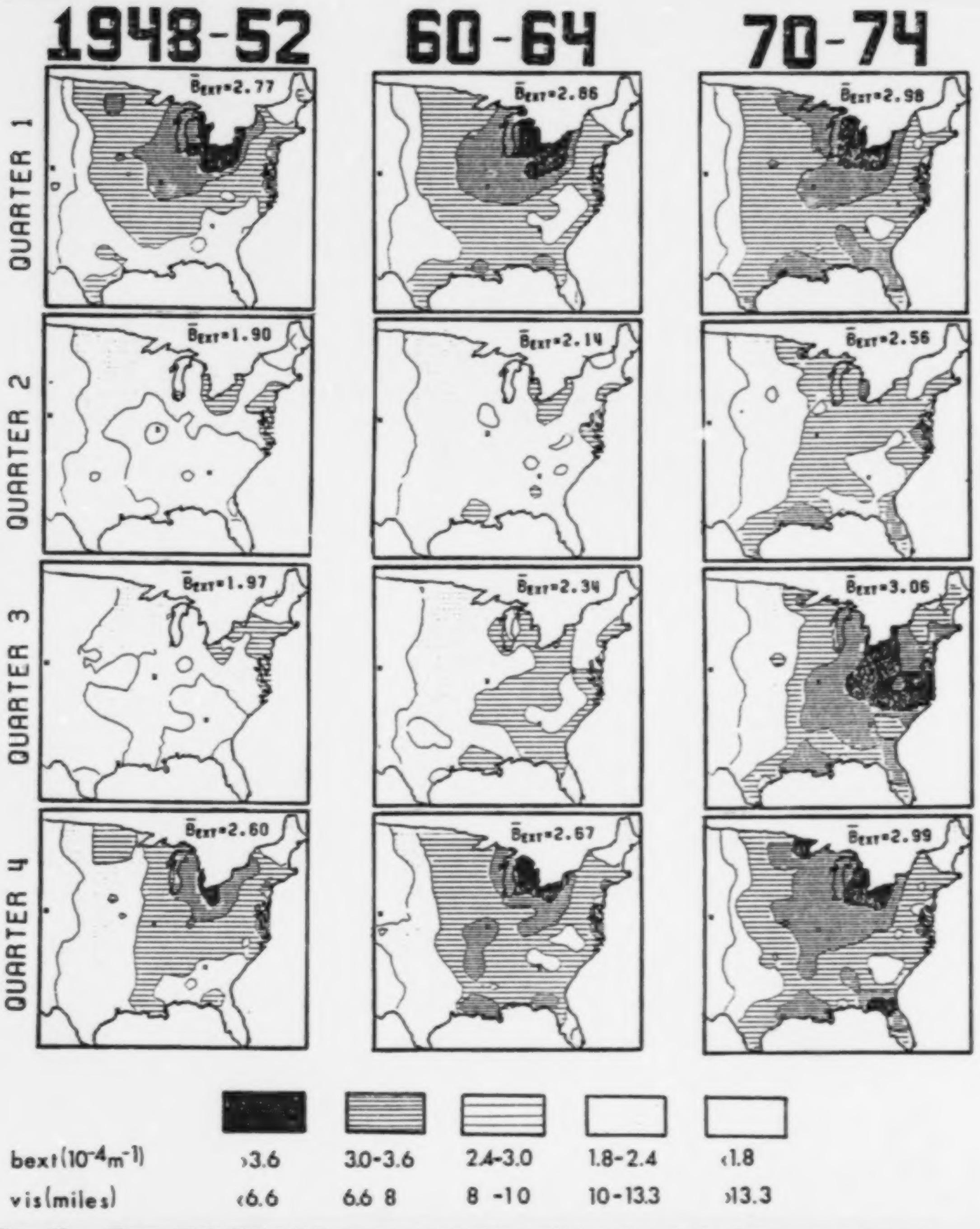

Figure 10. The spatial distribution of 5-year average extinction coefficients show the drastic increases of quarter 3 extinction coefficients in the Carolinas, Ohio River Valley, and Tennessee-Kentucky area. In the summers of 1948-1952, a 1,000-km size multi-State region centered around Atlanta, Georgia, had visibility greater than 15 mi, which has declined to less than 8 mi by the 1970's. The spatial trend of winter (quarter 1) visibility shows improvements in the N.E. Megalopolis region and some worsening in the Sunbelt region. Both spring and fall quarters exhibit moderate but detectable increase over the entire eastern United States.

EVIDENCE OF TRANSPORT OF HAZY AIR MASSES FROM SATELLITE IMAGERY

Walter A. Lyons

Mesomet, Inc., Chicago, Illinois

INTRODUCTION

Often, a new way of visualizing natural phenomena helps us crystallize our understanding of basic physical processes. The ability of conventional meteorological satellites to routinely observe massive areas of turbidity in the atmosphere produced by both natural and anthropogenic sources has shed new light on long-range pollution transport. This paper briefly summarizes some of the observations of major aerosol events in the atmosphere and suggests that routine detection and tracking of synoptic scale pollution episodes, along with quantitative measurements of their intensity, is entirely feasible with existing spacecraft and data analysis systems.

Long-range transport of certain long-lived atmospheric pollutants was graphically demonstrated three decades ago by the tracking of nuclear bomb debris, in some cases, for several circuits of the globe. The Clean Air Act of 1967 and 1970, however, had as an underlying assumption the notion that the concentrations of various primary pollutants at some unspecified, but not too great, distance downwind from the source would become indistinguishable from the "natural background" due to dilution, wet and dry deposition, and perhaps chemical transformation. During the 1970's, we have gradually come to realize that these chemical transformations produce secondary pollutants of significant concentrations, which become of greater concern at distances typically greater than 100 km.

Blumenthal et al.[1] measured photochemical oxidants being exported out of the Los Angeles Basin at the rate of 100 tons/hr. Lyons and Cole[2] noted that high ozone values recorded in both urban and rural sections of Wisconsin were the combined results of local emissions, mesoscale transport, and synoptic transport, all comingled in a manner making it most difficult to separate the fraction resulting from each mechanism. Coffey and Stasiuk,[3] Wolff et al.,[4] and Ott and Lyons[5] were among many suggesting that ozone-laden air masses could easily travel hundreds or even thousands of kilometers over several days. Periods of elevated ozone in air masses undergoing long-range transport were also found to be associated with reduced visibility by Samson and Ragland.[6] As research continued (e.g., project MISTT), it became clear that important secondary aerosol-producing mechanisms were being found. The conversion of SO_2 gas into aerosols within individual power plant or urban plumes was documented by many, including White et al.[7] The progressive deterioration of regional summer visibility, correlated with increased SO_2 emissions into the upper portion of the boundary layer by the greater use of coal and higher stacks, is reported by Husar.[8]

Reduced visibility, or visual range, is the result of decreasing contrast of a distant object against a background by the scattering of light into the intervening volume of air. It is reasonable, then, to assume that measurements of visible wavelength radiation from an orbital platform would reveal both increased atmospheric brightness and reduced contrast of ground targets, if the aerosol were of appropriate size and concentration, and the remote sensing device were of required sensitivity, resolution, and spectral response.

As early as 1971, Mohr[9] noted anomalous areas of turbid air in ESSA satellite APT images over Europe and suggested the possibility of using conventional weather satellites to monitor regional air pollution events. In the same year, McLellan[10] had some success in using the digital brightness readings from the geosynchronous ATS satellite to detect the smog buildup in the Los Angeles Basin by its enhanced upward light scatter.

The prime contributor to widespread areas of turbidity appears to be the conversion of SO_2 gas to sulfate aerosols, with transformation rates somewhere around one to several percent per hour, according to Wilson et al.[11] Figure 1 maps the region with the highest SO_2 emission densities in the United States. The contributions of the coal-burning power plants, especially in the Ohio River Valley and surrounding areas, are significant. The isopleths of maximum recorded sulfate levels (Figure 2) show the pattern centered near the major source regions, but with values exceeding 20 $\mu g/m^3$ possible almost anywhere in the eastern United States. It is in this area that our search for satellite images revealing large-scale pollution episodes will be focused.

SATELLITE DETECTION OF AEROSOLS

Various meteorological satellites have shown themselves capable of detecting a wide variety of aerosol episodes in the atmosphere. Landsat images were analyzed by Lyons,[12] revealing point source smoke plumes of 100 km plus length over Lake Michigan. Also, Lyons et al.[13] noted apparent indications of high turbidity within entire air masses. Unfortunately, the small areal and infrequent temporal coverage of Landsat makes synoptic monitoring impractical. The same could be said of 35-mm photography from manned spacecraft missions, although some individual scenes of note were described by Randerson.[14]

The operational meteorological satellite, while designed to detect bright, high-contrast clouds, has proven itself suitable for mapping large-scale areas of atmospheric dust, haze, and smoke. The Synchronous Meteorological Satellite/Geostationary Operational Environmental Satellite (SMS/GOES) series has been used for this research.[15] Two systems observe the United States from 36,000 km above the equator, one centered at 75° W, the second at 135° W longitude. Every 30 min, 4-km resolution (subpoint) infrared (10.5-12.5 μm) scans of the earth are made from pole to pole. During daylight hours, visible images at 1.0-km subpoint resolution are obtained at the same interval. The visual infrared spin-scan radiometer (VISSR) responds to visible light in the 0.54- to 0.70-μm band. Data are transmitted from the satellite at 8-bit resolution. The enormous data volume is managed in many ways, but primarily by conversion to photographic form. However, special computer-based systems do allow investigations to access and manipulate the data quantitatively.

Figure 3 is an example of a major aerosol event in the atmosphere--a massive plume of smoke from the Hawaiian volcanic eruption of September 1977. On subsequent days, the plume drifted in a cohesive manner in the trade winds for many hundreds of miles. Shenk et al.[16] were among the first to note the cross-Atlantic transport of large clouds of Saharan dust. In Figure 4, a dust cloud reached Cuba after having left the African coast less than 5 days before, all the while visible in the SMS/GOES visible imagery. During the U.S. drought of 1977, several major dust storms occurred in the central United States. One such storm raged from 23 to 25 February 1977. On 24 February the satellite detected a "plume" of dust stretching from the Oklahoma

Panhandle to Georgia (Figure 5). It was subsequently seen to spread over the Atlantic as far east as Bermuda. During the passage, local visibilities dropped as low as 1 to 3 miles. Hi-vol aerosol measurements taken by the Texas Air Resources Board found 24-hr averages ranging from around 600 μg/m^3 near Houston to as high as 2,450 μg/m^3 in northeast Texas.

An often overlooked source of manmade pollution is smoke from agricultural burning. As noted by Parmenter,[17] massive areas of slash burning in southern Mexico, Yucatan, and Guatemala during the late winter dry season generate massive smoke palls over much of the Gulf of Mexico. Figure 6 shows one of the many such incidents noted in recent years. These smoke-filled air masses frequently reach the southern United States.

Smoke from giant forest fires in the western United States can routinely be monitored on SMS/GOES imagery. However, the plume of smoke from a small northern Minnesota forest fire is shown in its seventh hour (Figure 7) after having been tracked at 30-min intervals from its inception that morning.

DETECTION OF SULFATE AEROSOL HAZES

Lyons and Husar[18] presented an SMS/GOES picture showing a large area of "haze" covering the midwest. Comparisons with other data showed the area to be associated with reduced visibility (6 nmi or less), high sulfate concentrations, and generally elevated ozone levels. The photograph showed a "typical" episode: on the scale of 1,000 km, lasting for several days to nearly 2 weeks, associated with a warm moist air mass that had significant injections of SO_2 from major source regions. That particular image first needed a certain degree of photographic darkroom enhancement to make the "smog blob" or "hazy blob" or "elevated pollution episode" clearly recognizable.

SMS/GOES image processing is generally geared to highlight high-contrast cloud systems. Haze is not always easily apparent. A technique has been developed by NOAA's National Environmental Satellite Service (NESS), as reported by Parmenter and Anderson,[19] to better delineate the subtly different radiances of polluted versus "clean" air masses. A digital enhancement curve, similar to that applied to infrared imagery, was found very useful. Figure 8 shows an example of the NESS technique. The top panel is a segment of a 2-km resolution image over Florida, as would be seen on a standard weather office satellite receiver. Application of the digital enhancement makes the band of turbid air across the central part of the peninsula and surrounding waters highly visible (middle panel). Reported surface visibilities were under 7 miles within the haze band. Sufficient solar insolation was reflected to result in significant differential ground heating, as evidenced by the supression of afternoon convection beneath the haze band (lower panel). Another example of the technique was produced on 14 May 1977, when a "clean" polar air mass descended into the northeast United States, displacing a stagnant, polluted anticyclone southward (Figure 9). The enhanced image at 1230 GMT (Figure 10) shows a clear demarcation of the two air masses, especially over the ocean areas. This effective digital technique, however, is not routinely available from NESS. Thus, researchers studying such phenomena must rely on darkroom enhancement of prints made from negatives, or special processing of "live" or recorded digital satellite data on special image analysis systems. The problem in sulfate haze detection is therefore not one of satellite sensor capabilities, but one of ground image processing techniques.

CASE STUDIES

The image described by Lyons and Husar[18] was taken on 30 June 1975, the midpoint of an episode lasting from before 25 June until after 5 July. It was clearly visible on the prints made from SMS/GOES negatives. Figure 11 is a photographically enhanced picture, 2 km resolution, 29 June 1975. A persistent high-pressure cell over the northeast had caused an accumulation of secondary pollutants over the lower Ohio River Valley and from Louisiana to Minnesota. Trajectories made from 600-m winds confirm this overall flow pattern.[20] Of note in Figure 11, in addition to widespread obscuration of ground features in cloud-free areas, are pockets of "reduced turbidity," as suggested by lowered image brightness. Film animation shows that these pockets travel with the general low-level winds, and retain continuity for a day or more. There is considerable circumstantial evidence relating the pockets to areas of "wash out" by prior thunderstorms. Knowledge of such regions from satellite images would greatly aid in analyzing surface and aircraft aerosol measurements. The volume of air undergoing significant wet removal can also be calculated from such "convective footprints" if correlated to radar data.

Figure 12 summarizes some of the measurements made on 29-30 June 1975. The visibility contours show that noontime readings (6, 4, 3, and 2.7 nmi) closely correlate to the haze area seen on the satellite image. Those ozone monitoring sites reporting 1-hr averages of 160 ppb or higher were located in or near the "blob." Scattered sulfate measurements showed values as high as 80 μg/m^3 within the haze boundary, and generally 15 μg/m^3 or less outside.

A major episode occurred from 16 to 28 August 1976. This was discussed in detail by Lyons et al.[21] Figure 13 shows the "blob" on 26 August 1976. It was particularly "bright" over the Chesapeake Bay area, and extended far eastward into the Atlantic.

Figure 14 is a map of the 18 GMT, 22 August 1976 weather conditions, with contours of the 5- and 3-nmi visibilities (corrected for precipitation), and the boundary of the hazy area seen on the satellite picture. This analysis was performed for each 13 days of the episode. In virtually all cases, the 5-nmi visibility contour lay inside the visible boundary of the "haze blob." It appears that as regional visual ranges drop below 6 or 7 nmi, the haze becomes "visible" in properly printed SMS/GOES images, especially over water and other low-albedo targets.

Figure 15 shows the various parameters for 28 August 1976, overlain with isopleths of National Air Sampling Network (NASN) sulfate data. The areas of Pennsylvania and New York State, where the visibilities were generally lowest and the image appeared haziest, were associated with 24-hr sulfate levels between 30 and 50 μg/m^3. All sulfate readings made within the hazy area seen on the 28 August, 2230 GMT image averaged 22.7 μg/m^3, but outside the haze area readings averaged only 5.7 μg/m^3. Similarly, a series of sulfate measurements were made in New York City by Brookhaven National Lab during this period. When the blob, as seen on the satellite prints, covered the area, sulfates averaged 23.7 μg/m^3, but were only 7.5 μg/m^3 when clean air covered the area. This suggests overall enhancements of sulfate within satellite-detected hazy blobs of 3.98 and 3.16 times for these two cases. Similarly, for each of the 13 episode days, the highest hourly ozone measured at all stations reported in the National Aerometric Data Bank were plotted. The average for those sites outside the visible blob was 69.4 ppb; inside the average rose to 90.8 ppb, or 30 percent higher. This suggests that the correlation of hazy, low visibility air to sulfates is stronger than to ozone levels. This is partly due to the apparently greater spatial variability of ozone, as a result of local NO_x sources, etc.

As discussed in an earlier paper,[21] the SMS/GOES data can be analyzed quantitatively using such systems as the Man-Computer Interactive Data Access System (McIDAS) developed by the University of Wisconsin's Space Science Engineering Center. Digital data tapes from the August 1976 episode were archived. McIDAS allows total pixel-by-pixel manipulations of the imagery. All scenes are navigated and gridded, with animation of sequential images easily accomplished via rapid access from video analog disk. A cursor allows the operator to select any number of image pixels and measure the digital brightness counts (DBC, Range 1-256), which can, by application of calibration procedures, be converted into radiances. Over water, with apparently clean air masses present (and confirmed by nearby land visibility of 7 mi or more), DBC's typically ranged from 40 to 45 units. In hazy but otherwise cloud-free areas, values would usually range from 70 to 85 DBC's. Thus the "signal" of a hazy air mass in the SMS/GOES data was clearly well out of the noise level. Over land, typical values in high-visibility polar air masses during August would be around 60 to 80 DBC's, but could be as much as 50 percent higher when apparent haze covered the target. By careful selection and calibration of ground targets, it appears totally plausible to use digital satellite data to routinely obtain a measure of "atmospheric brightness," and thus of turbidity, visual range, and to a lesser degree, sulfates. What the technique lacks in precision it would appear to compensate for in terms of spatial and temporal coverage--particularly over water where virtually no routine air quality measurements exist.

CONCLUSION

The current generation of meteorological satellite data in pictorial, and especially digital, form, is capable of synoptic monitoring of the formation, growth, and movement of large-scale hazy blobs known to be correlated with elevated sulfate episodes. Details of the long-range transport and removal process can also be studied. Figure 17 shows a "front" of haze moving southwestward along the Atlantic coast on 25 August 1976. This feature was tracked for 3 days; it finally disappeared on 26 August, after being advected into a line of thunderstorms along the Florida peninsula where its aerosols presumably underwent washout.

The satellite data allow for rational extrapolation of surface visibility and sulfate measurements and provide a context for the analysis of aircraft data. Tracking well-defined structural haze features provides a possible means for verifying trajectory and transport models. The export of polluted air masses into, and possibly across, the Atlantic can be studied. (The European METEOSAT satellite provides a similar capability in the eastern Atlantic.) Actual digital processing of the SMS/GOES data allows for the testing of statistical and physical models relating atmospheric turbidity, visual range, and sulfate aerosol content.

ACKNOWLEDGMENTS

This research was primarily funded by the Regional Field Studies Office, U.S. Environmental Protection Agency (Dr. William E. Wilson, Director), under subcontract No. 68-02-3000, "Conduct Seminar/Workshop on Elevated Pollution Episodes and Furnish Background Reports to Assist EPA Management in Planning Future STATE Intensive Field Studies and Related Activities."

REFERENCES

1. Blumenthal, D. L., W. H. White, R. L. Peace, and T. B. Smith. Determination of the feasibility of the long range transport of ozone or ozone precursors. Meteorology Research Inc. Report, EPA Contract 68-02-1462, 1974. 92 pp. [NTIS No. EPA-450/3-74-061].

2. Lyons, W. A., and H. S. Cole. Photochemical oxidant transport: Mesoscale lake breeze and synoptic-scale aspects. Journal of Applied Meteorology, 15:733-743, 1976.

3. Coffey, P. E., and W. N. Stasiuk. Evidence of atmospheric transport of ozone into urban areas. Environmental Science and Technology, 9:59-62, 1975.

4. Wolff, G. T., P. J. Lioy, G. D. Wright, R. E. Meyers, and R. Cederwall. An investigation of long-range transport of ozone across the midwestern and eastern United States. Atmospheric Environment, 11:797-802.

5. Ott, S., and W. A. Lyons. Further evidence of long-range photochemical oxidant transport inferred from acoustic sounder data. AMS/APCA Joint Conference on Applications of Air Pollution Meteorology, Boston, 1977. pp. 33-38.

6. Sampson, P. J., and K. W. Ragland. Ozone and visibility reduction in the Midwest: Evidence of large-scale transport. Journal of Applied Meteorology, 16:1101-1106, 1977.

7. White, W. H., J. A. Anderson, D. L. Blumenthal, R. B. Husar, N. V. Gillani, J. D. Husar, and W. E. Wilson, Jr. Formation and transport of secondary air pollutants: Ozone and aerosols in the St. Louis urban plume. Science, 194:187-189, 1976.

8. Husar, R. B.. Man's impact on the troposphere: Lectures in tropospheric chemistry. NASA Reference Publication, No. 1022, 1978. pp. 319-348.

9. Mohr, T. Picture of the month: Air pollution photographed by satellite. Monthly Weather Review, 99 (8):653, 1971.

10. McLellan, A. Satellite remote sensing of large scale local atmospheric pollution. Proceedings, Second International Clean Air Congress, H. M. Englund and W. T. Beery, eds., Academic Press, New York, 1971. pp. 570-574.

11. Wilson, W. E., R. J. Charlson, R. B. Husar, K. T. Whitby, and D. Blumenthal. Sulfates in the atmosphere. Preprints, 69th Annual Meeting of Air Pollution Control Association, Paper 76-30-06, 1976. 20 pp.

12. Lyons, W. A., and S. R. Pease. Detection of particulate air pollution plumes from major point sources using ERTS-1 imagery. Bulletin of the American Meteorological Society, 54:1163-1170, 1976.

13. Lyons, W. A., C. S. Keen, and R. Northhouse. ERTS-1 satellite observations of mesoscale air pollution dispersion around the Great Lakes. Proceeding, AMS/WMO Symposium on Atmospheric Diffusion and Turbulence, Boston, 1974. pp. 273-280.

14. Randerson, D. Quantitative analysis of atmospheric pollution phenomena. Skylab Explores the Earth, NASA, SP 380, Available Government Printing Office, 1978. pp. 381-400.

15. Ensor, G. J. User's guide to the NOAA geostationary satellite system. U.S. Department of Commerce, NOAA, NESS, Washington, D.C., 1978. 101 pp.

16. Shenk, W. E., and R. J. Curran. The detection of dust storms over land and water with visible and infrared measurements. Monthly Weather Review, 102 (12):830-837, 1974.

17. Parmenter, F. C. Monitoring air quality from satellites. Proceedings, 4th Joint Conference on Sensing of Environmental Pollutants. American Chemical Society, Washington, D.C., 1978. pp. 254-257.

18. Lyons, W. A., and R. B. Husar. SMS/GOES visible images detect a synoptic-scale air pollution episode. Monthly Weather Review, 104 (12):1623-1626, 1976.

19. Parmenter, F. C., and R. K. Anderson. A satellite overview of inadvertent weather modification. Preprints, Sixth Conference on Inadvertent Weather Modification. American Meteorological Society, Boston, 1977. pp. 83-86.

20. Teknekron, Brand Niemann, personal communications.

21. Lyons, W. A., J. C. Dooley, Jr., and K. T. Whitby. Satellite detection of long range pollution transport and sulfate aerosol hazes. Atmospheric Environment, 12:621-631, 1978.

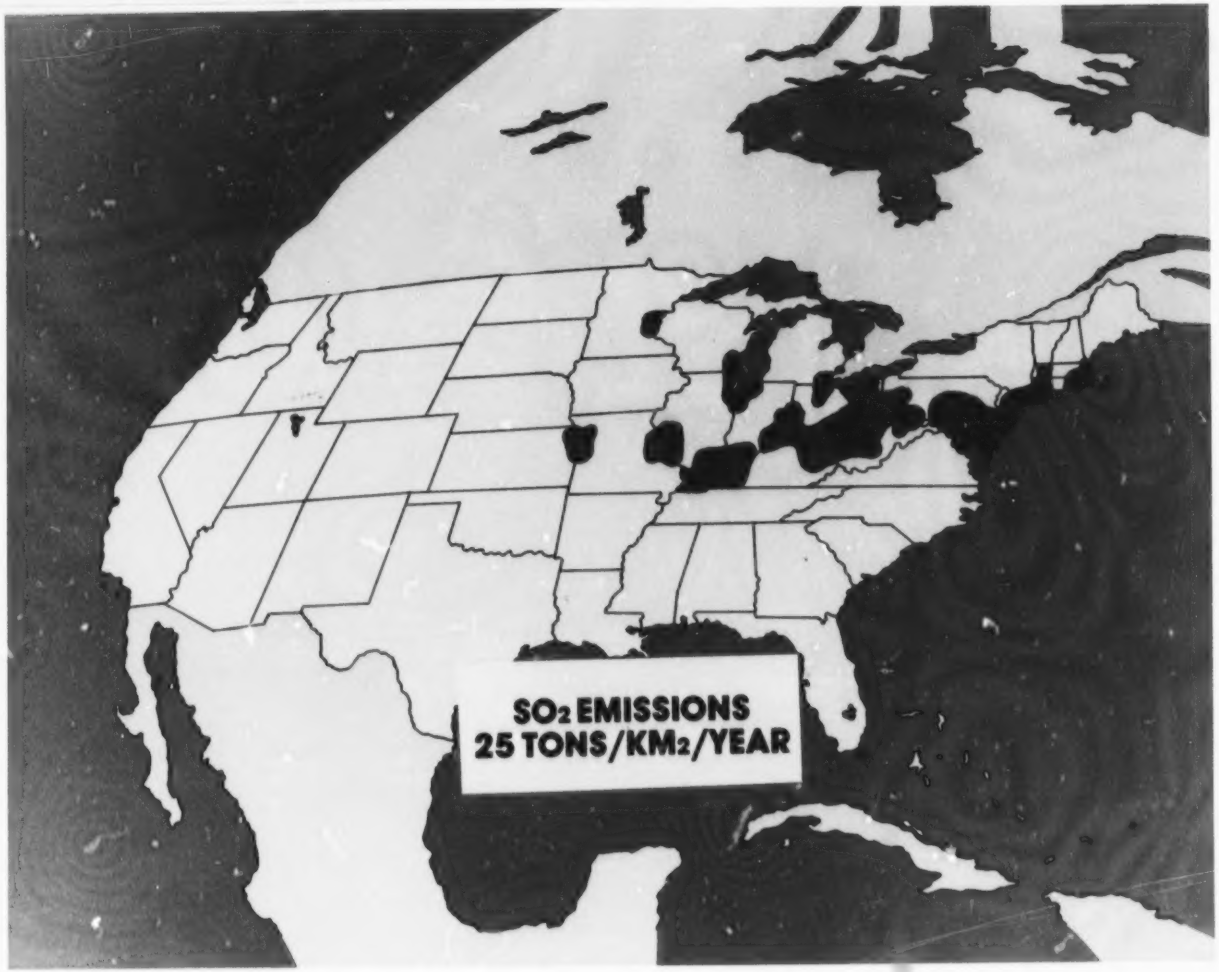

Figure 1. Map of regions where SO_2 emission density exceeds 25 tons/km^2/yr.

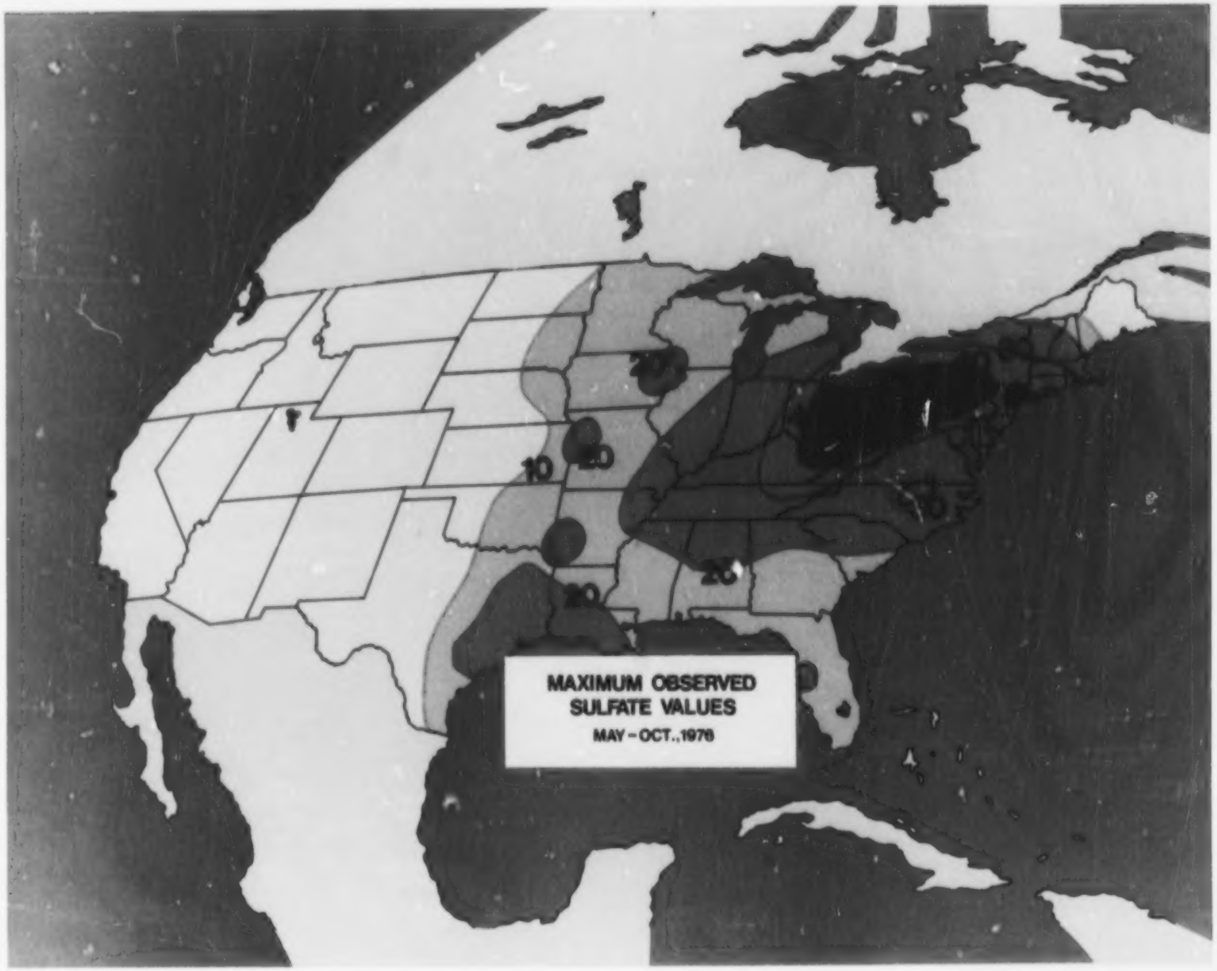

Figure 2. Plot of observed maximum sulfate values ($\mu g/m^3$) at NASN sites during the period May through October 1976.

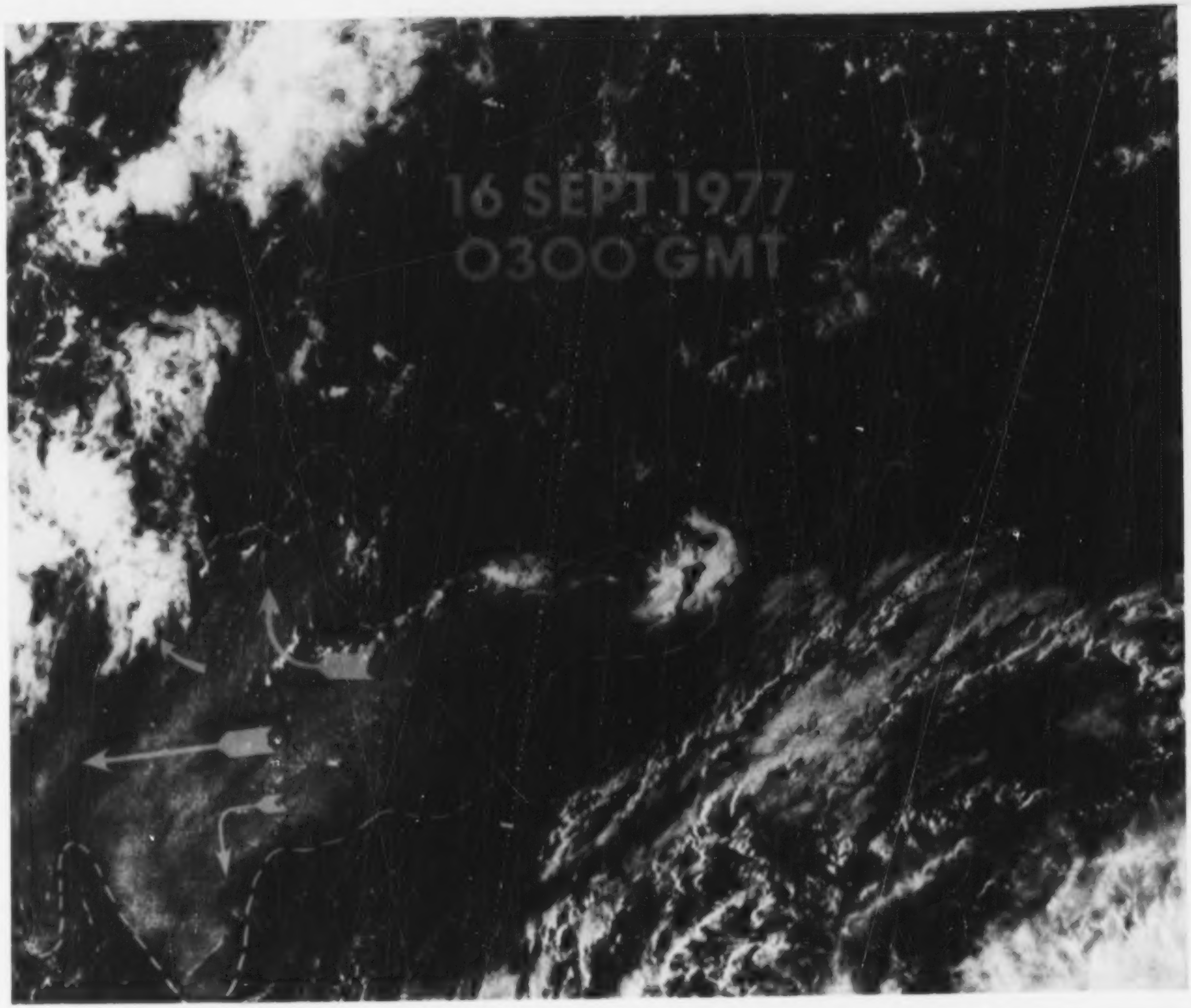

Figure 3. SMS/GOES 1.0-km resolution visible image, showing plume of smoke from Hawaiian volcanic eruption drifting several hundred kilometers southwestward, at 0300 GMT, 16 September 1977.

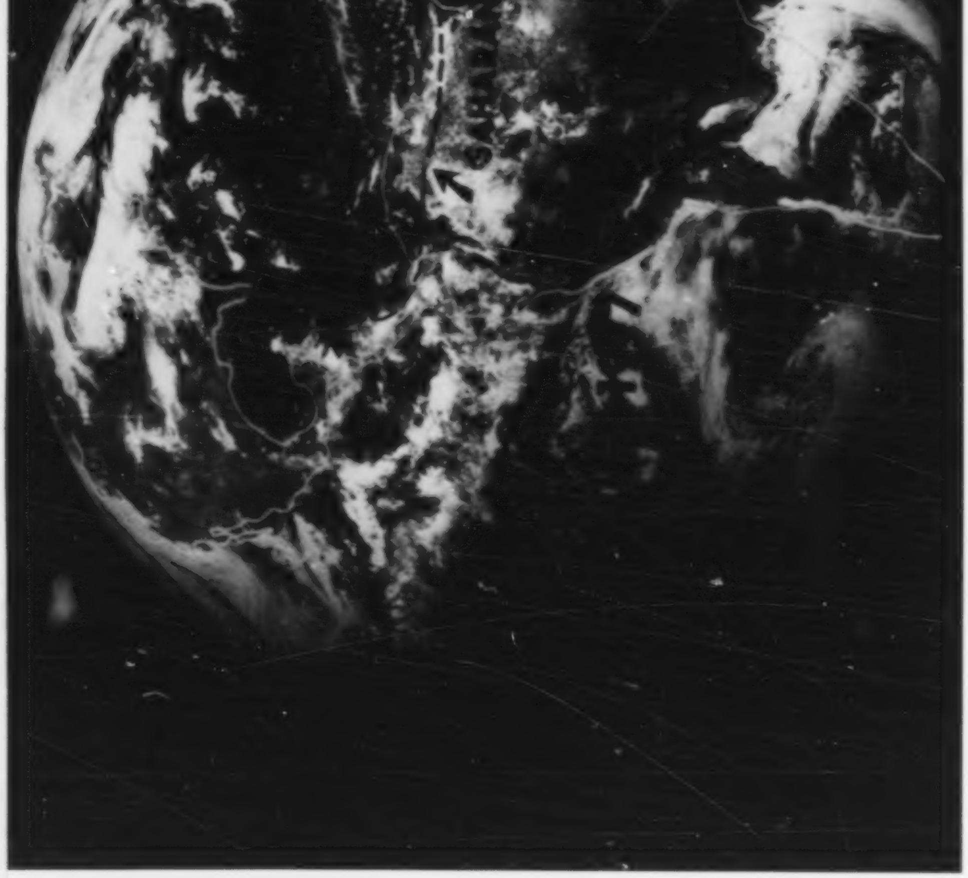

Figure 4. Full disk SMS/GOES 4.0-km resolution visible image, 1500 GMT, 18 June 1977. Saharan dust cloud had crossed the Atlantic in 4 days. The position of the leading edge of the dust on 14 June is indicated by an arrow.

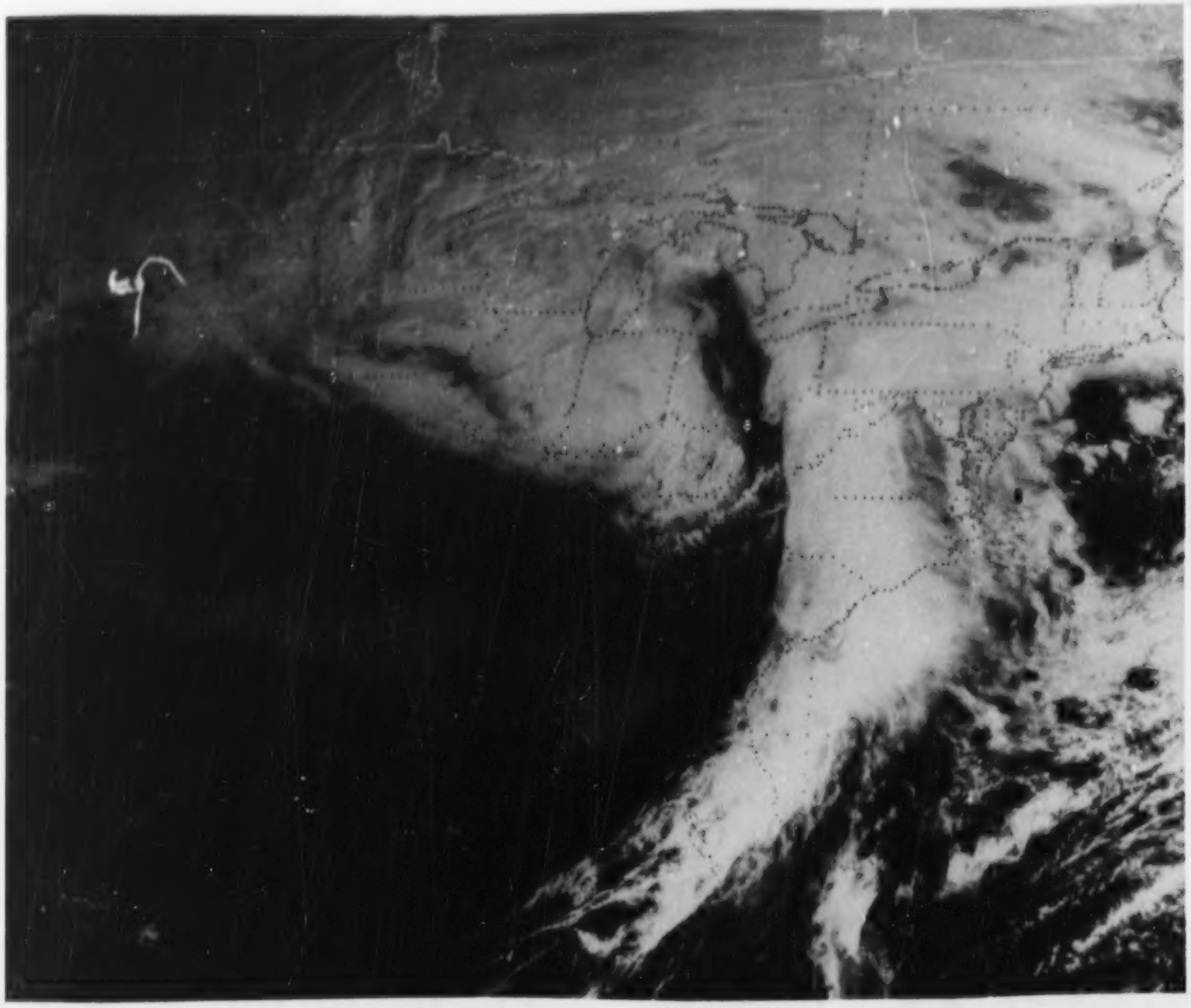

Figure 5. SMS/GOES 2.0-km resolution visible image, 1530 GMT, 24 February 1977, shows cloud of dust stretching from Oklahoma Panhandle to Georgia. Dust cloud followed cold front many hundreds of miles into the Atlantic.

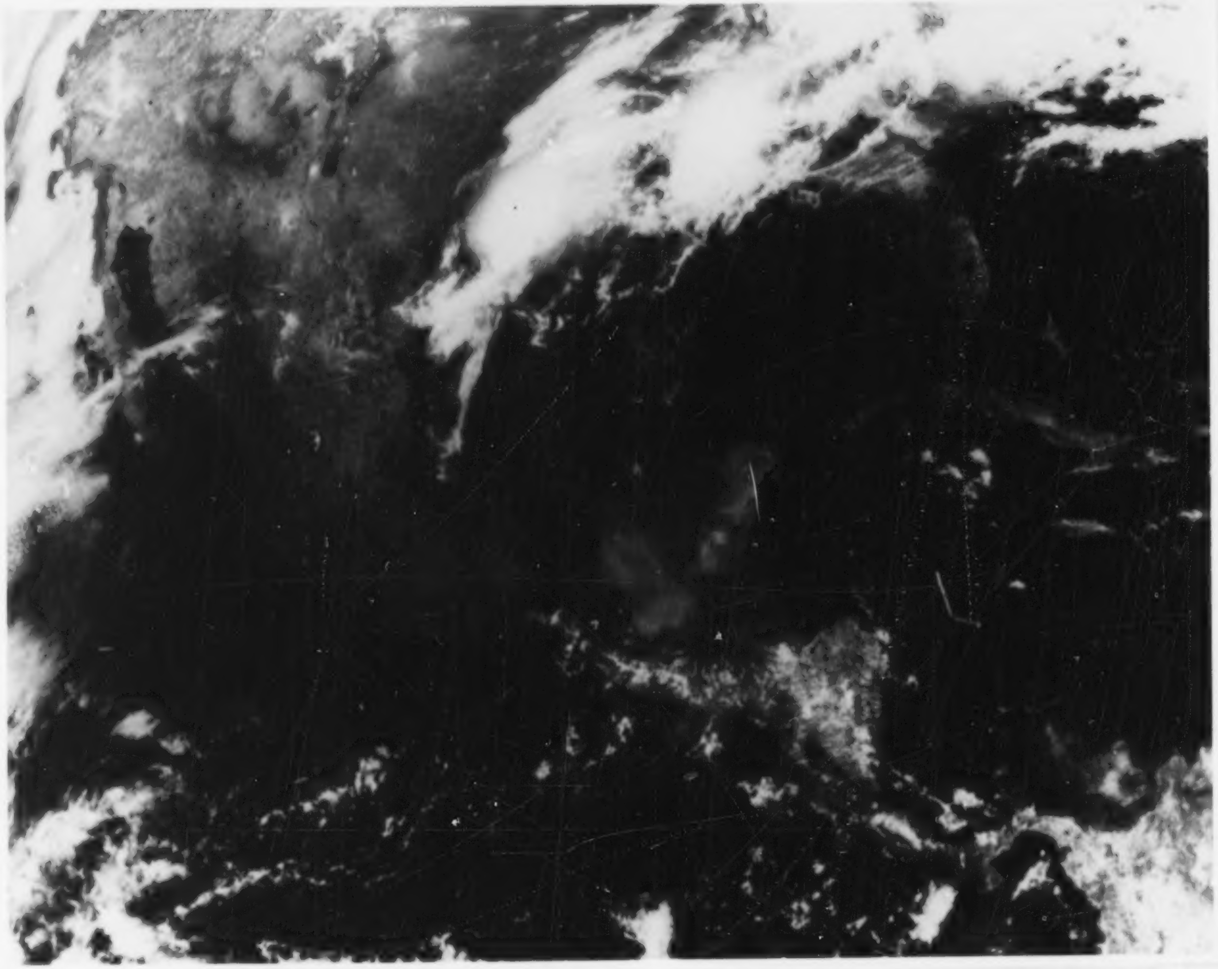

Figure 6. SMS/GOES 2.0-km resolution visible image, 1700 GMT, 30 April 1975, showing large area of smoke over Yucatan and the Western Gulf of Mexico, the result of widespread agricultural slash burning.

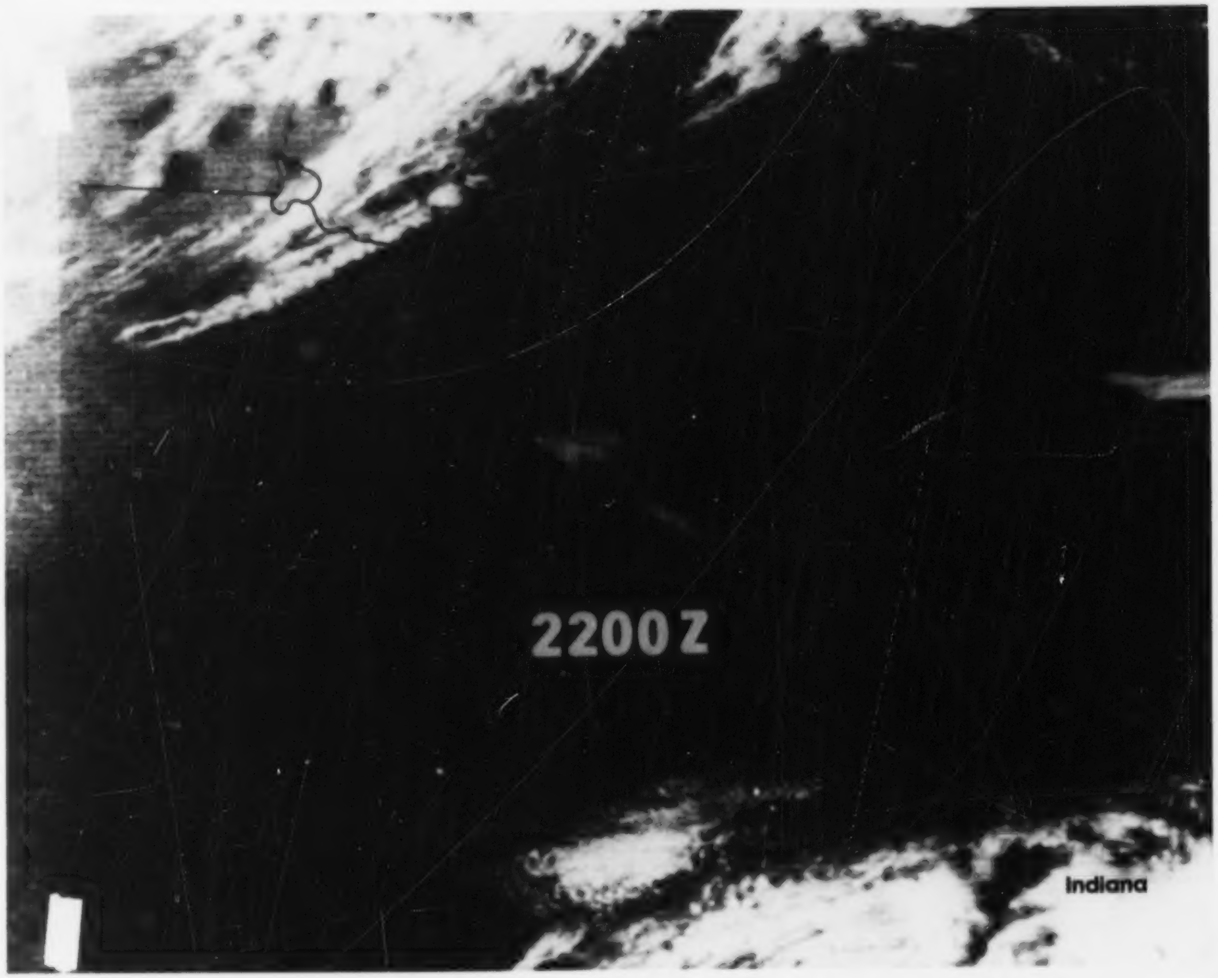

Figure 7. Blowup of SMS/GOES 1.0-km resolution visible image, 2200 GMT, 29 September 1976, showing plume of smoke from a small forest fire in northern Minnesota, having drifted about 100 km southeast after about 7 hr.

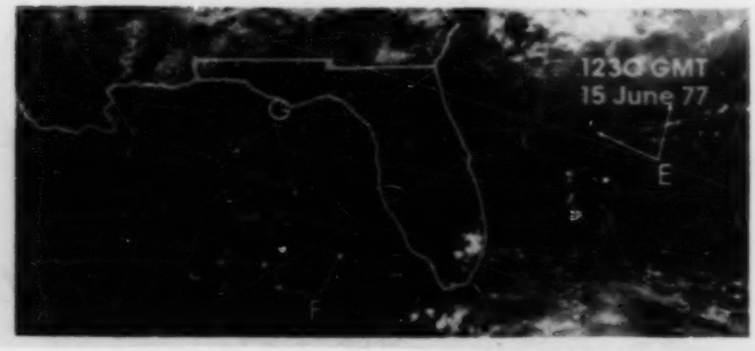

Figure 8(a). Portion of SMS/GOES 2.0-km resolution visible image over Florida, 1230 GMT, 15 June 1977.

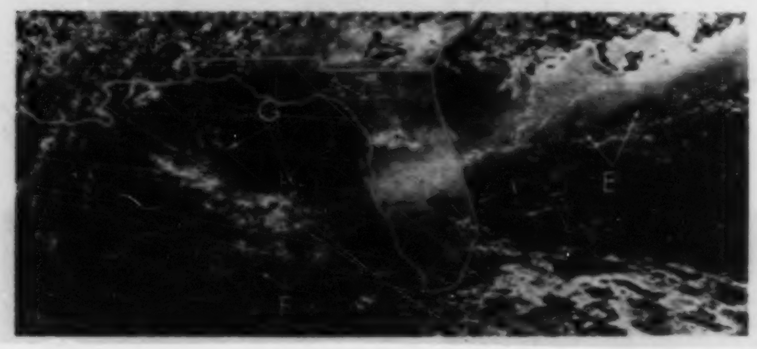

Figure 8(b). Same scene, but with imagery digitally enhanced using experimental technique developed by National Environmental Satellite Service. Band of hazy air now distinct.

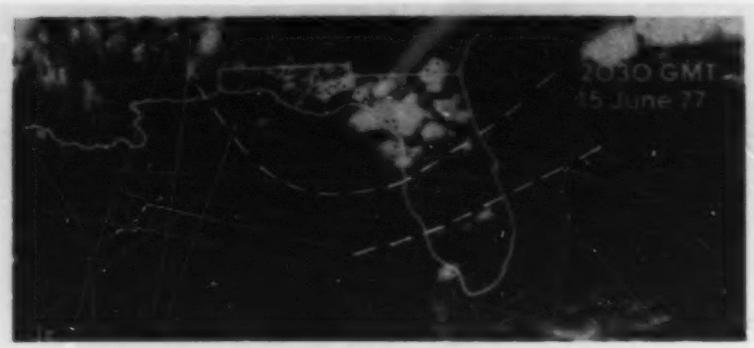

Figure 8(c). Same region, but at 2030 GMT, 15 June 1977. Haze was sufficiently dense to apparently suppress afternoon convection, present both north and south of haze band.

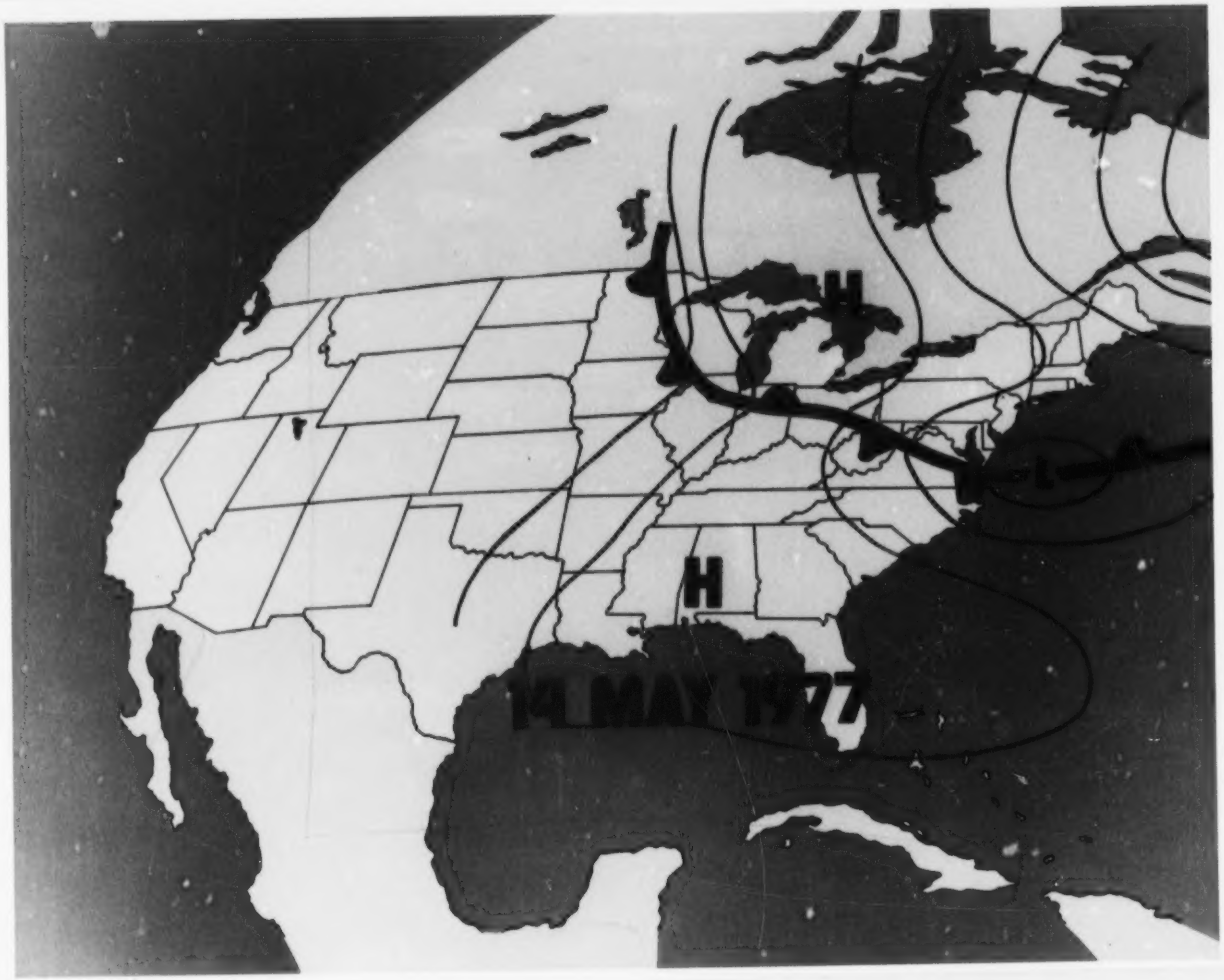

Figure 9. Surface weather map, 1200 GMT, 14 May 1977.

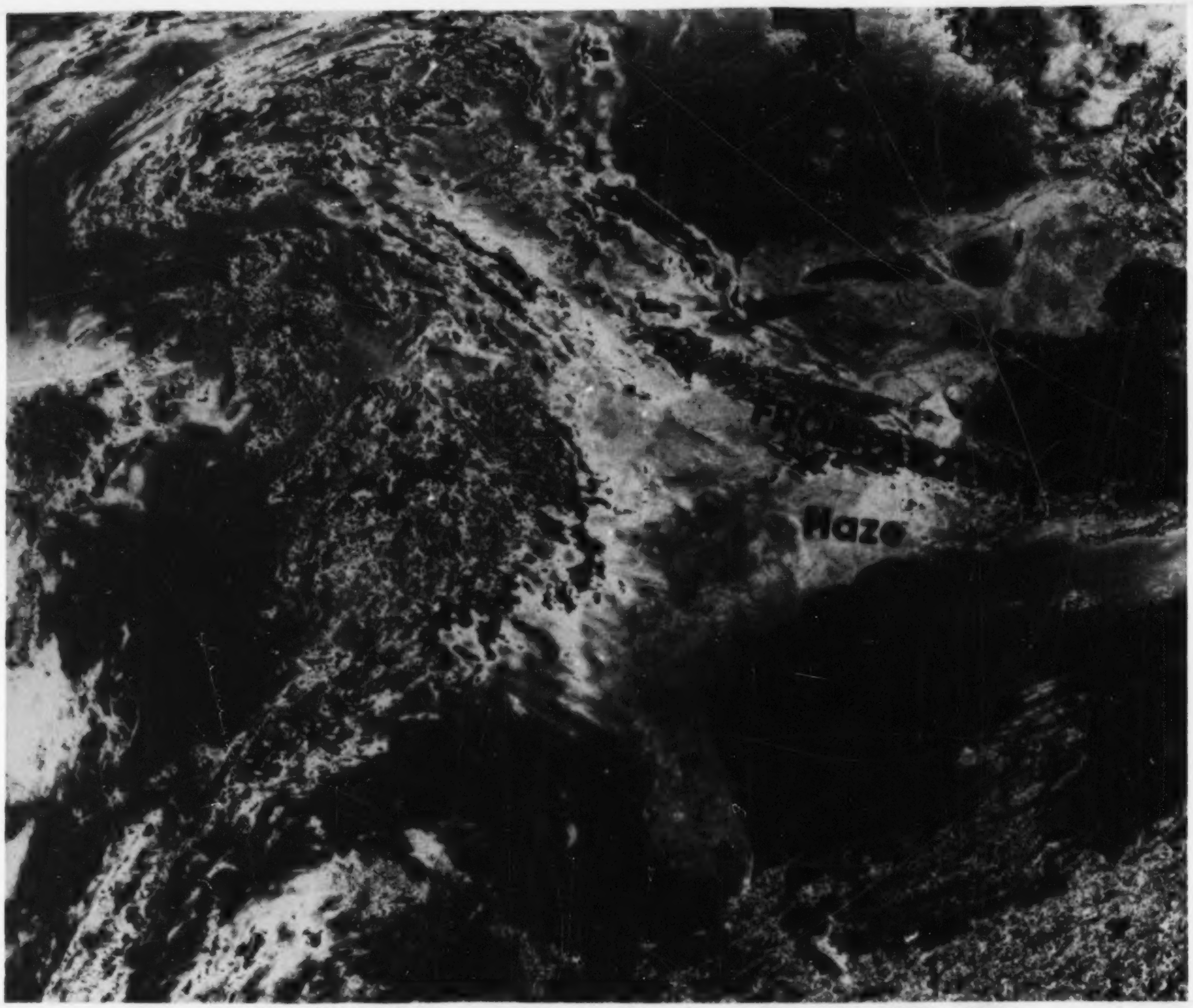

Figure 10. SME/GOES 2.0-km resolution visible image, 1230 GMT, 14 May 1977, specially enhanced by computer processing at NESS. A sharp discontinuity in atmospheric turbidity is clearly found at the front separating the two anticyclones.

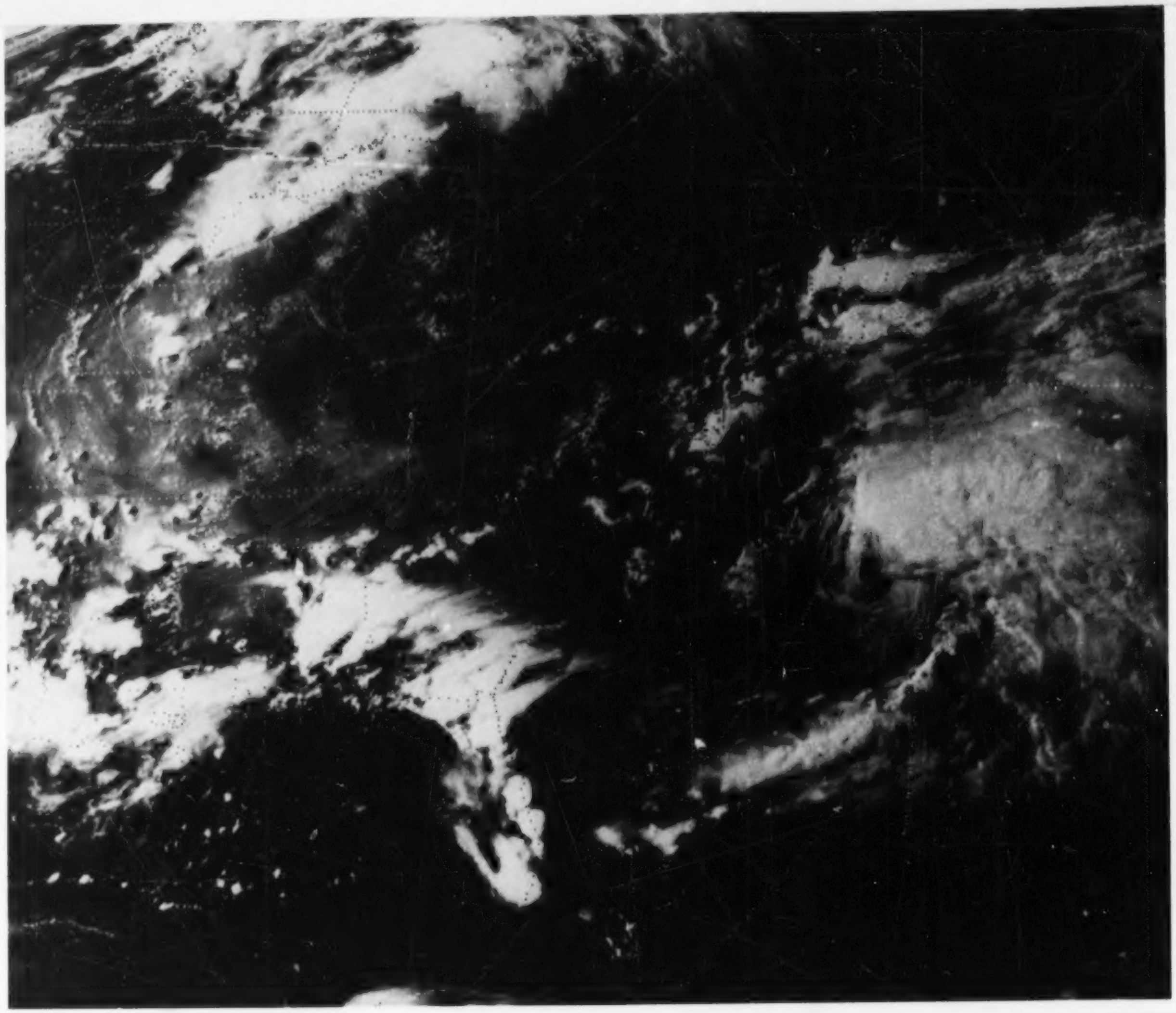

Figure 11. SMS/GOES 2.0-km resolution visible image, 2200 GMT, 29 June 1975, showing massive "smog blob" west of Appalachians to Kansas and from the Gulf Coast to the upper Great Lakes.

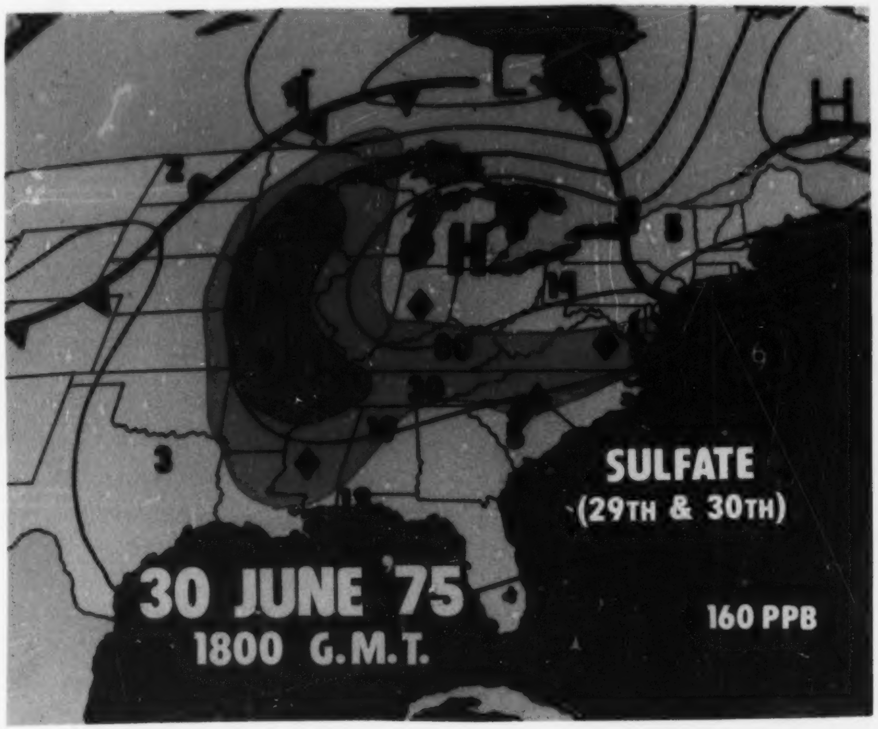

Figure 12. Synoptic map, 1800 GMT, 30 June 1975. Shaded areas represent visibility contours of 6, 4, 3, and 2.7 nmi. NASN sulfate values ($\mu g/m^3$) recorded during June 29 and 30 are shown, and triangles mark oxidant monitors that recorded maximum hourly values in excess of 160 ppb.

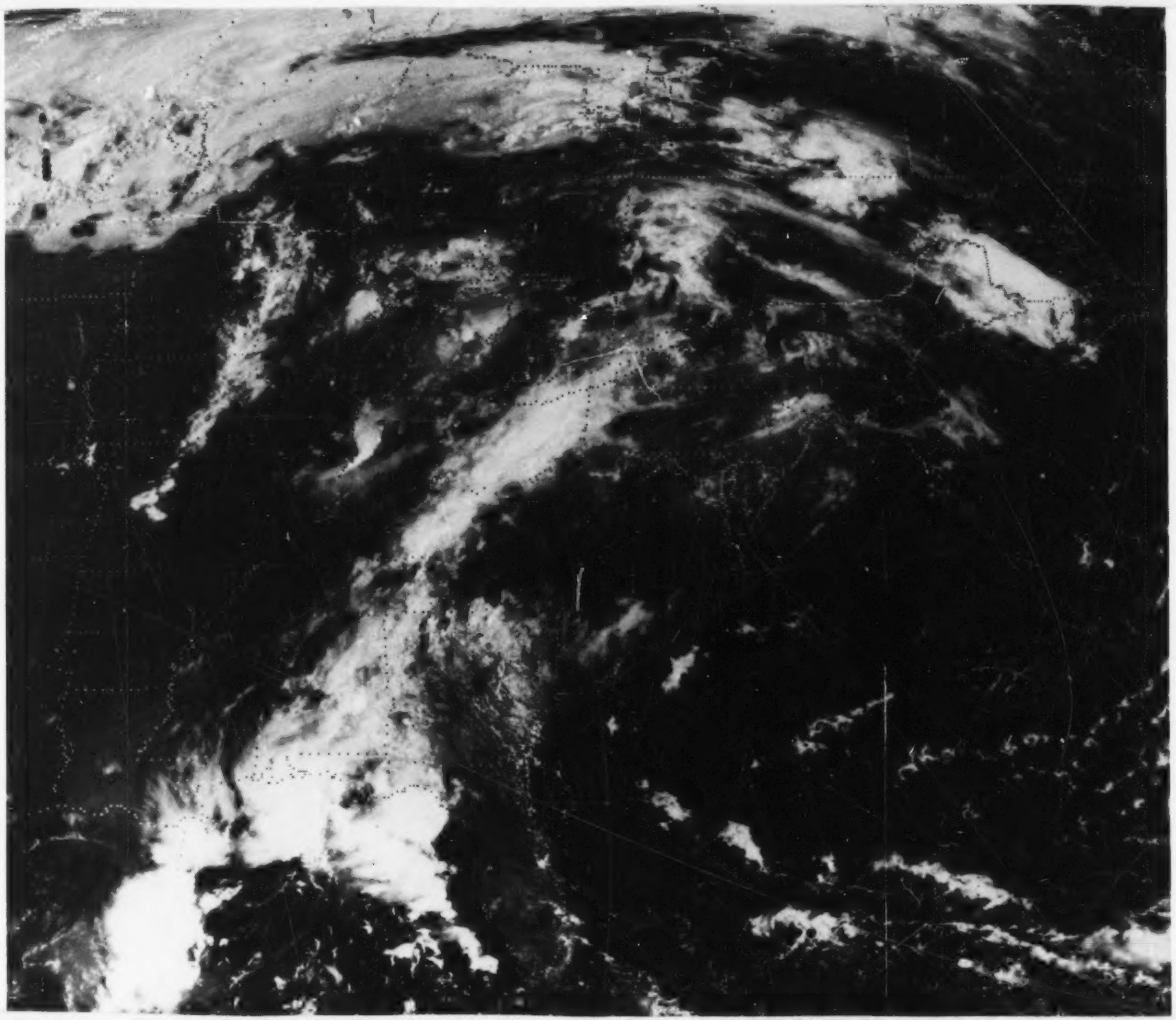

Figure 13. SMS/GOES 2.0-km resolution visible image, 1430 GMT, 26 August 1976, showing widespread "smog blob" stretching from the Mississippi River eastward into the Atlantic Ocean.

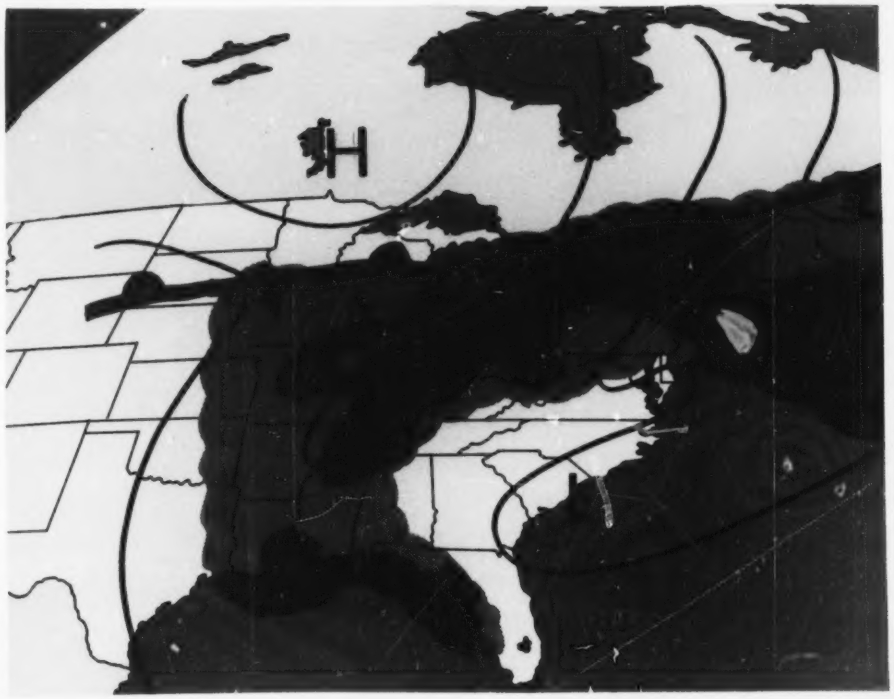

Figure 14. Synoptic map, 1800 GMT, 22 August 1976. Stipple represents hazy area as observed on satellite image. Contours of 5- and 3-nmi visibility are also plotted.

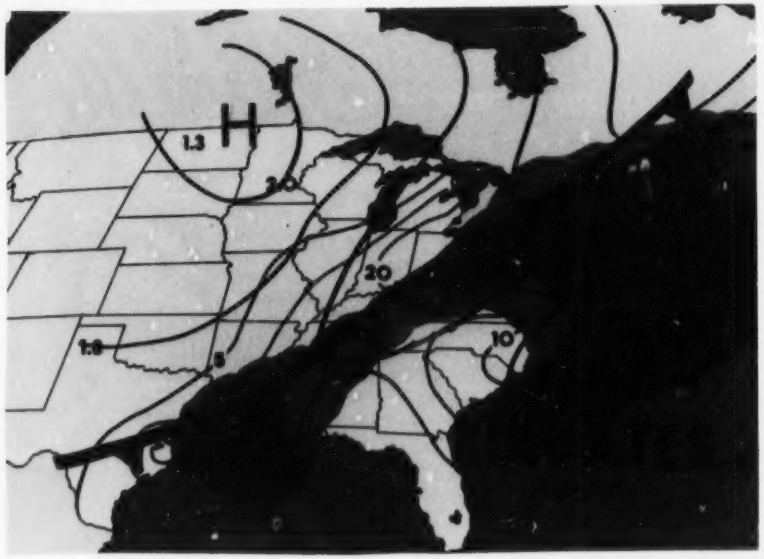

Figure 15. Synoptic map, 1800 GMT, 28 August 1976. Overlain on the hazy area outline and 3- and 5-nmi visibility contours are the observed NASN sulfate readings ($\mu g/m^3$). Readings in excess of 40 $\mu g/m^3$ were found in low visibility air in Pennsylvania and New York.

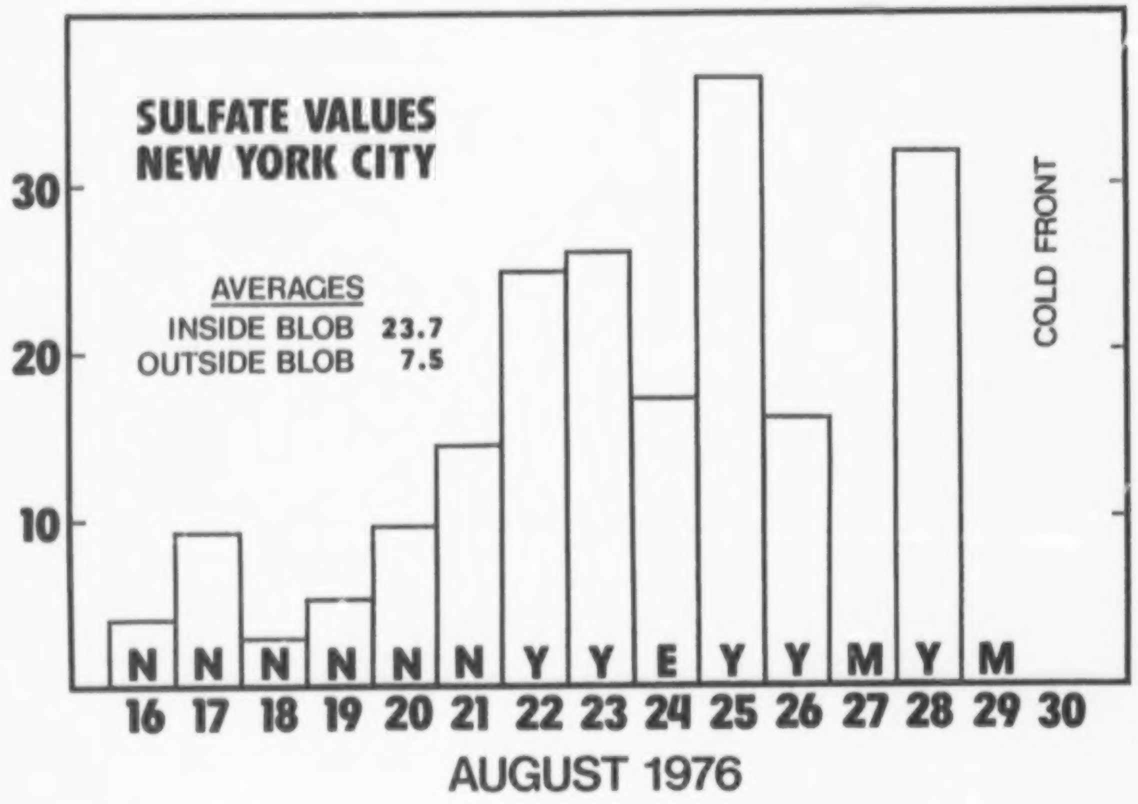

Figure 16. Sulfate values, 24-hr averages, recorded in New York City by Brookhaven National Laboratory from 16 to 28 August 1976. N indicates smog blob, as seen on the satellite, was not over the area. Y or E indicates the monitor was in or on the edge of the smog blob.

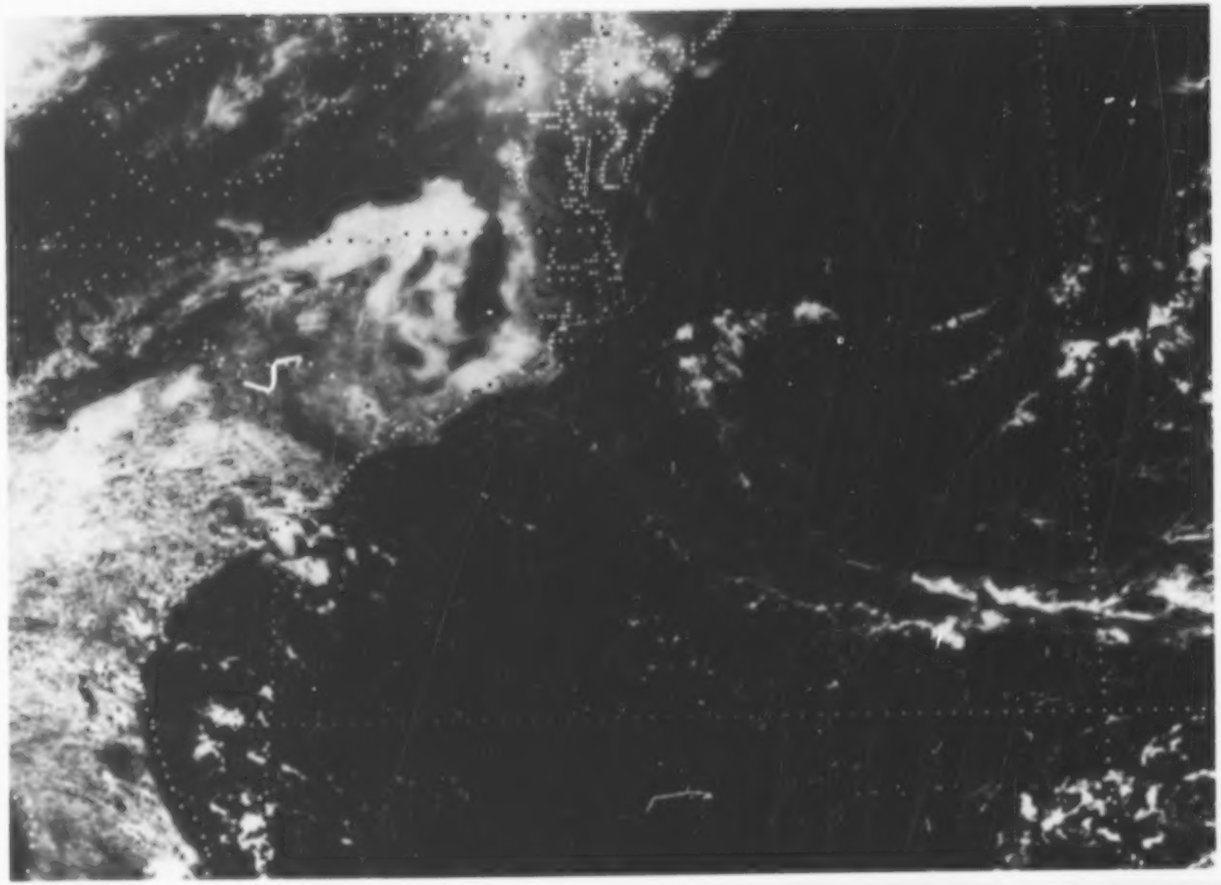

Figure 17. Portion of 2.0-km resolution visible image, 2230 GMT, 25 August 1976, showing a front of turbid air moving south and west off the U.S. Atlantic Coast.

REMOTE SENSING OF REGIONAL AIR POLLUTION FROM SATELLITES

E. J. Friedman* and E. L. Keitz

The Mitre Corporation, McLean, Virginia

Abstract

The potential for regional measurement of gaseous pollutants by use of remote sensing from orbiting satellites is analyzed. Based on a study of the capabilities of a wide variety of remote sensors to measure and monitor air pollution over regional areas, two sensors were selected for possible satellite application. These sensors are assumed to be orbiting in a typical Space Shuttle orbit. A number of aspects of the problem are considered including the data requirements of users, a model for statistical interpretation of the observations, the influence of orbit parameters on the spatial and temporal sampling and an example of application of the model over the eastern United States.

INTRODUCTION

This paper is based primarily on the results of two studies completed recently. In the first of these an analysis was made of the potential for remote sensing techniques to measure and monitor air pollution over regional areas.[1] The performance of such instruments was contrasted with that expected from both ground-based monitors and airborne contact sensors. Included in the study were evaluations of measurement strategies for the long-range transport of both an urban oxidant plume and a fossil-fueled power plant sulfur dioxide/sulfate plume. The study also addressed regional measurement requirements and the current status of specific remote sensors, which have a theoretical capability for regional measurement or monitoring.

The second study investigated the role that might be played by the Space Shuttle in obtaining data that describe the air quality of the eastern

---

*Speaker.

United States.[2] A number of aspects of the problem were considered including a model for statistical interpretation of the observations, the influence of orbit parameters on the spatial and temporal sampling and an example of application of the model. This study was limited to the measurement of gaseous species.

The present paper discusses appropriate parts of these two studies and focuses on the potential for regional measurement of gaseous pollutants from orbiting satellites. The overall conclusion is that although the potential for regional measurement of pollutant gases from satellites is clearly evident, this potential is unlikely to be realized in sufficient time to be of assistance in the experiments being discussed at this workshop. Although one remote sensor (TRW/MAPS) is scheduled to fly on the second Space Shuttle mission, the mission is experimental only and the characteristics of the pollution monitoring will be constrained by the overall Shuttle flight schedule.

MEASUREMENT REQUIREMENTS

A wide variety of scientific and regulatory groups have needs for measurement of air quality on a regional scale. Not all of these groups, however, have requirements for measurement of the same species or over the same four-dimensional network. An extensive study of the users and needs for local and regional air quality monitoring in the troposphere has been completed by the National Academy of Sciences.[3] This study provides a comprehensive treatment of the topic. Table 1 presents a summary of the results showing which of the various users have interests in four basic categories of needs.

A summary of the air pollutants either recommended for measurement or actually measured in various regional studies is presented in Table 2. Care must be exercised not to precisely compare the various species lists shown in the tables since each study focuses on either slightly or markedly different objectives. These various objectives are summarized below.

1. National Academy of Sciences[3]--generalized tropospheric monitoring.
2. Sulfate Regional Experiment[4]--investigation of sulfate formulation from power plant emissions.

3. Stanford Research Institute[5]--remote sensing of regional pollutants.
4. Regional Air Monitoring System/Regional Air Pollution Study[6]--generalized urban and regional air quality.
5. Los Angeles Reactive Pollutant Program[7]--validation of mathematical models of air pollution photochemistry.
6. Environmental Protection Agency/Oxidant Study[8]--investigation of rural oxidant levels as related to urban hydrocarbons.
7. Battelle Columbus Laboratories[9]--formation and transport of ozone in nonurban areas.

Inspection of the table shows that the power-plant-oriented study is not concerned with measurements of CO or hydrocarbons because these are not generally emitted from efficient combustion processes. On the other hand, studies concerned primarily with rural oxidants have not measured SO_2 or related pollutants.

Based on the foregoing information and experience with similar programs, a set of measurement requirements was developed for monitoring of both the urban and power plant plumes. Table 3 presents a listing of the major pollutants and meteorological parameters that should be measured in any generalized monitoring program. Also shown are estimates of the accuracies that should be required. Obviously, programs with specific scientific or regulatory objectives may have requirements for additional or different parameters.

Tracking of the urban plume oxidant chain primarily requires the measurement of ozone, oxides of nitrogen, and hydrocarbons. Other gases such as carbon monoxide and acetylene may be monitored as good tracers of the urban plume's position and extent. Acetylene is particularly attractive since there are no known natural sources of this substance. Tracking of the single power plant plume principally requires measurement of those species directly involved in the sulfur dioxide/sulfur chain. These are sulfur dioxide, sulfates, and ammonia. Other species having a probably synergistic effect in the sulfate chain are ozone and nitrogen oxides.

Table 4 presents recommended horizontal grid spacings for typical types of regional monitoring. As in the case of the pollutants to be measured, special regulatory or scientific objectives may indicate the need for finer or coarser grids.

Vertical grid spacing may vary from a single surface measurement for some regulatory situations to as many as 10 or 20 levels for certain pollutants or meteorological parameters in a scientific study. In general the vertical spacing of measurements should be nonlinear because concentrations generally change in shorter distances near the surface than at higher levels. Table 5 presents recommended vertical grid spacings for various types of regional monitoring.

The time scale required for regional pollutant measurements should depend on the time scales of the major factors that influence regional pollution. For urban plume studies, the principal factor influencing temporal changes in concentrations is the variation in mobile source emissions throughout the day. Thus changes occurring over a time span of 1 to 2 hr could be important, particularly in scientific studies. Although the emission patterns from power plants are not as readily identifiable, a temporal measurement span of 1 to 2 hr also seems reasonable for regional scientific studies. For regulatory use, the frequency of measurements should be much less, particularly in those situations where scientific studies have developed good correlations between concentrations measured at one specific time and the overall diurnal pattern. In some cases, a measurement frequency as low as one per day may suffice. Table 6 presents a summary of recommended time intervals for typical regional situations.

REMOTE SENSING INSTRUMENT SURVEY

The performance characteristics of six categories of remote sensors were reviewed to judge their ability to be used in a regional system whether ground-based, airborne, or satellite-borne. These categories were:

1. Gas filter correlation,
2. Correlation interferometry,
3. LIDAR,
4. Laser heterodyne radiometry,
5. Laser absorption spectrometry,
6. Solar absorption spectrometry.

Specific instruments were analyzed and the outlook for the performance capability of each over the next 5 years was estimated.

In this report, emphasis will be placed on the TRW/MAPS and the CIMATS instruments because they were the instruments whose characteristics were used in the satellite modeling study to be discussed later.

Gas Filter Correlation (TRW/MAPS)

The MAPS instrument uses gas filter correlation in order to obtain high radiation throughput and resolution. The present instrument is the third gas filter correlator developed under the project (preceded by SR&T/MAPS and SAI/AAFE/MAPS). A sample of the gas of interest, CO, is placed in a gas cell located in an optical path carrying radiation from the scene to the detector. Another, otherwise identical, path traverses an evacuated cell. The difference provides an indication of the amount of gas of interest between the infrared radiation source (normally the Earth and its atmosphere) and the instrument. A further refinement in the MAPS instrument involves the inclusion of a gas cell at a different partial pressure of the gas of interest than is contained in the first gas cell. By comparing the different signals derived from each gas cell and the evacuated cell, the measurement is less subject to errors caused by the presence of interfering species in the atmosphere.[10] An added potential advantage in the use of two gas cells of different pressures is the ability to obtain some coarse information on several vertical layers of the atmospheric path.

Figure 1 shows general features of the MAPS instrument. The reference blackbody is sampled alternately with the scene radiation to provide a baseline reference level. The hot and cold blackbodies are adjusted to span the anticipated temperature range of the scene. They are sampled at a higher frequency than the scene energy and reference blackbody in order to allow electronic separation of the signals for subsequent processing. Gain controls on the electronics are driven by the balance sources so as to keep the gain of the gas cell paths equal to that of the vacuum path for both temperature extremes. This procedure effectively balances the system and reduces the effects of variations of radiance reaching the two detectors.[11] For the optical path through the evacuated cell, the modulated energy from the balance sources is used for radiometric calibration, while that from the scene and reference is used to determine scene brightness.

In the nadir-viewing (or vertically down-looking) mode, MAPS will provide data on the total column burden of CO in cloud-free areas of the Earth. Planned refinements in the choice of gas partial pressures and data processing may result in data representative of two broad vertical bands in the atmosphere.

Extensive field tests of this instrument were conducted during the summer of 1977 over Lake Michigan using a Cessna 402 as the platform. Results of these tests have been given in detail elsewhere.[12] [13] These tests demonstrated the ability of the instrument to measure the carbon monoxide urban plume from Chicago as it progressed over the lake.

Since that time efforts have concentrated on developing an on-board microprocessor capability for the instrument in an attempt to provide real-time data. Although the work is not yet completed, progress has been significant and this capability should be achieved shortly.

In April of this year the instrument will begin field tests on board the NASA Convair 990 in the Indian Ocean. Testing will continue for a few months. Future plans include a firm commitment to fly a satellite-hardened version of the instrument on board the second Space Shuttle flight for the measurement of global and regional CO patterns. The earliest launch date for this mission is March 1980. The flight would be of 4 days' duration with all MAPS data tape recorded on board rather than telemetered to ground stations. This will be the first attempt to measure tropospheric gaseous pollution from a spacecraft.

Correlation Interferometry (CIMATS)

The CIMATS instrument is a two-channel infrared (IR) interferometer, which uses the same general principles of operation as its predecessor, the Carbon Monoxide Pollution Experiment (COPE).[14] [15] [16] The instrument is a variant of a normal Michelson interferometer. A time-varying path difference is introduced into one of the optical paths by the rotation of a phase plate. The other optical path is of constant length (phase). Recombination of the two paths results in an alternating reinforcement and cancellation, depending upon the phase difference of the two rays. The result is analogous to a Fourier transform of the incident radiation. The effect of this design is to transform the electromagnetic variation at optical frequencies to electrical signals that can be conveniently processed. The basic components of the instrument are illustrated in Figure 2. The range of scan (phase delay) is chosen to optimize the signal-to-noise ratio for a particular species of pollutant in the atmosphere.

In the presence of interfering species, the interferogram does not provide a unique indication of the species of interest. Table 7 lists the major interferents and the expected signal-to-noise ratio for each measurable species for both the reflected solar (Channel A) and the IR (Channel B) ranges. To reduce interference effects, use must be made of weighting functions that are chosen to minimize the contribution made by constituents other than those of interest, while maximizing the signal-to-noise ratio of the desired species. The weighting functions are determined both theoretically and experimentally. The best available atmospheric models and spectral absorption properties are used to construct a "base interferogram." Variation of the concentrations of various constituents results in a set of different interferograms. Since each interferogram consists of a set of data points, the set of interferograms may be considered a set of simultaneous linear equations which, in turn, may be solved for the appropriate weighting functions. Laboratory experiments are then performed to generate interferograms based upon actual gas concentrations at a range of partial pressures.

In operation, interference filters limit the range of the radiation incoming to the instrument to a very narrow band, selected to coincide with the region where the effects of absorption by the species of interest are greatest. Interferograms are generated while observing the area of interest in a nadir-viewing (vertical down-looking) mode; one complete scan requiring 1 to 3 seconds. These interferograms are compared to the stored weighting functions to determine the best fit of the data. Scale factors may be applied to the weighting functions in order to facilitate this matching process. When the correct weighting function is applied to the data, the result gives the column burden of the specie of interest. In some cases, CIMATS will require vertical profiles of temperature, pressure, and humidity to perform calibrations.

The instrument was delivered to NASA/Langley in December 1978 by the General Electric Company, the prime contractor. Channel A has been partially tested against laboratory samples of pollutant gases. No testing of channel B has been done to date. In the near future both channels will undergo additional laboratory testing and channel A will be ground tested using reflected sunlight as the source. Further plans are uncertain owing to economic constraints.

Fixed Wavelength LIDAR

Remote sensing instruments that use laser energy in some form generally fit into three categories. The first of these, in which a fixed wavelength pulse is transmitted through the atmosphere and the reflected or backscattered signal is detected, is one type of LIDAR. The second, in which a laser(s) is used as the local oscillator in a passive tunable remote system, falls under the generic term of laser heterodyne radiometry. The third, in which a tunable laser(s) is used in an active remote system, is called laser absorption spectrometry.

Laser and lidar-type instruments have been used for many years in the measurement of particulates, aerosols, and clouds. Since the first lidar measurement of backscattering from tropospheric aerosols in 1963, similar observations have been made by many investigators and by now are considered to be routine.[5] This discussion is limited to the ruby laser operated by the LIDAR Applications Section of the Environmental and Space Sciences Division at the NASA/Langley Research Center.

The NASA/LRC Ruby Laser is a ground-based semimobile instrument mounted on a truck bed. The operating wavelength is 0.6943 μm in the red portion of the visible spectrum. The laser operates at 1 pps with a field of view of 2 milliradians and an angular resolution of about 1 milliradian. The data are digitized at 5 to 100 MHz, which provides a range resolution of about 1.5 m. Elevation resolution is 1/15 degree. A PDP-11/10 minicomputer controls the optical scanning and data collection. A "quick look" capability is provided by a continually refreshed CRT, which provides 16 gray scales for the range-height indicator display. Polaroid photography is used for hard copy of the display.

The typical use of the instrument is in monitoring of power plant plumes through aerosol backscatter. It is estimated that a typical power plant plume would show the following particulate concentrations at a 10-km range.

Wind speed	Concentration
3 mps	35 μg/m^3
10 mps	78 μg/m^3

The 10-km range represents the probable greatest range for meaningful measurements of σ_y or σ_z with the instrument and 15 km is probably the maximum range for detecting anything at all under typical conditions. The maximum detectable concentration is not known because it is in part a function of the background concentration. In order to get any response, concentrations on the order of 1-1/2 to 2 times the background are needed.

Laser Heterodyne Radiometry

This section discusses the present status and outlook for the future of passive tunable remote sensing systems that use a laser(s) as the local oscillator. Two versions of the instrument are under development by the Laser and Molecular Physics Branch at the NASA/Langley Research Center. The first version of the instrument is called the Infrared Heterodyne Spectrometer (IHS). This instrument is completed and has been undergoing testing.[17] Another version of the instrument is planned for Shuttle application. This version is called the Laser Heterodyne Spectrometer (LHS). Since the LHS program is similar to the IHS program, only the latter will be discussed here.

The IHS is a 2-GHz bandwidth multichannel spectrometer being developed for ground-based and airborne measurements of the concentration and altitude distribution of tropospheric NH_3 and O_3 in both the atmospheric emission and solar occultation modes. The instrument utilizes discretely tunable $C^{13}O_2^{16}$ laser local oscillators operating in the 9- to 11-μm spectral region.

A number of gases of interest have spectral signature lines in the 9- to 11-μm region of the infrared. These include NH_3, O_3, D_2H_4, NHO_3, H_2O, and several of the chlorofluoromethanes. However, after initial studies of the calculated and measured spectra of the various gases, it was decided to select ammonia and ozone for initial applications. NH_3 is measured in the 10.78-μm wavelength while O_3 is measured at two wavelengths, 9.75 μm for solar absorption and 9.66 μm for nadir radiance.

In a Shuttle application, this type of instrument may be capable of measuring HNO_3, ClO, NH_3, and CCl_2F_2 (Freon 12) in a solar occultation mode. Calculations based on stratospheric simulations have shown sensitivities as low as 0.01 ppb for NH_3 and 0.005 ppb for Freon 12.

Laser Absorption Spectrometry

Three active tunable remote instruments were reviewed. They are:

1. Differential Absorption Remote Sensing (DARS),
2. UV Differential Absorption LIDAR (DIAL),
3. Westinghouse IR LIDAR.

The DARS instrument has been under development by the NASA/Langley Research Center for a number of years and the basic theory and operating principles are well known.[18] [19] The current version of the instrument is under fabrication at the Jet Propulsion Laboratory. This version uses CO_2 lasers as both the energy source and the local oscillator. The operating wavelengths will be in the 9- to 12-μm band and should be runable over a 600- to 800-MHz range. From an altitude of 10 km, surface horizontal resolution would be a couple of kilometers. The data gathered should provide the total burden of O_3 (at 9.45 μm) and possibly any other species in the 9- to 12-μm band.

The DIAL system utilizes a commercial flashlamp-pumped frequency doubled dye laser, a 0.25-m diameter receiver telescope, and a minicomputer for controlling data acquisition and processing. The output of the laser is typically 100 millijoules per pulse at 15 pps for wavelengths coincident with the peaks and valleys in the sulfur dioxide absorption spectrum from 0.2960 to 0.3001 μm. The difference in absorption coefficient for each pair of transmitted wavelengths is monitored using an auxiliary beam from the laser. Results obtained from the calibration show the linearity of the system with respect to the measurement of the total burden of sulfur dioxide. The instrument should be capable of measuring the average concentration of sulfur dioxide out to a range of 1 km with sensitivities less than 15 ppb.

Quantitative measurements of the average sulfur dioxide were obtained around a NASA/Langley steam plant. The measurements were made at night at ranges from 0.8 km to 1.9 km. Sensitivities varied from 10 ppb (at 0.8 km) to 20 ppb (at 1.9 km), with the maximum observed concentration being 150 ppb over a 1.2-km range. The maximum range achievable is estimated to be 7 km.[20]

Another LIDAR system with potential urban and regional application is being built for NASA by Westinghouse Research Labs.[21] Development is also being supported by the Environmental Protection Agency, U.S. Air Force, and U.S. Army. The instrument utilizes an optical parametric oscillator.[5] [22] Development of this type of oscillator began in 1961[23] and the first tunable system was demonstrated in 1965.[24] At the present time it is possible to obtain tunable energy through the visible region, over a portion of the near-UV and over most of the IR between 1 and 20 μm.

The instrument is expected to be delivered to NASA/Langley in the Spring of 1979 and will undergo laboratory spectroscopy studies.[21] The ranging capability anticipated for the instrument during design and development will not be fully achieved. This is due to the discovery that a significantly greater amount of energy per pulse than previously calculated is required for an adequate return signal. The optical parametric oscillator is limited in the amount of energy attainable. Thus, initial field measurement will probably be limited to column content to a maximum altitude of 3 to 4 km. Pollutants currently expected to be measured are HCl, CH_4, and a broad spectrum measurement of hydrocarbons in the 3.5-μm region. If any ranging capability is eventually achieved it will probably be limited to a few broad ranges over a distance of several kilometers.

Solar Absorption Spectrometry

The Radiometry Section of the Measurement Physics Branch at NASA/Langley Research Center has developed two solar absorption type instruments for close monitoring of pollution plumes.[22] [23] In the solar occultation mode (Videcon), a conventional TV-type camera is used to monitor particulates, NO_2, and total opacity. In the sky background mode, a UV videcon is used to monitor SO_2. Each of these systems is described below.

In the solar occultation mode, a conventional TV camera is used with appropriate filters to monitor particulates, NO_2, and total opacity. The operational wavelengths are as follows:

Wavelength (μm)	Species measured
0.800	Opacity
0.600	Opacity
0.694	Particulates
0.400	Particulates plus NO_2

Measurements made on clean stacks have shown opacities of around 3 to 4 percent with efficient precipitators in operation. Little or no NO_2 has been found in these plumes.

The UV videcon is used to measure SO_2 in power plant plumes by monitoring the sky background in the 0.310-μm wavelength band. This measurement is made on the wing of the 0.280-μm SO_2 peak due to stratospheric ozone interference. Readings are made on the plume at 0.310 μm and off to the sides at 0.340 μm to establish zero background levels and eliminate interference from background particulates. Data are recorded on tape and also displayed in real time on a TV screen. SO_2 areas show on the screen in varying shades of gray, depending on concentration.

Measurements to date have shown that SO_2 bubbles out of the stack rather than emerging in a smooth steady flow. This allows tracking of identifiable features in the plume yielding velocity measurements. In actual practice, these features are tracked by cross correlation techniques using two instruments with a small vertical separation. The practical lower limit for SO_2 measurements is in the 50 to 100 ppm range with an estimated accuracy of +50 ppm or approximately +10 percent. Velocity measurements are estimated to be accurate to +20 percent. Measurements have been made at distances up to 1 mile from the plume.

During the course of this study various other remote sensing instruments were considered briefly and judged to be unsuitable for regional monitoring either from aircraft or spacecraft.[1] These will not be discussed here.

Instrument Performance Characteristics

Based on the information gathered during the instrument survey it is apparent that not all of the remote sensors are will suited for regional monitoring applications. Table 8 presents a summary of the basic information in this regard. The basic suitability assumes that any instrument that only measures CO and/or NO_x is not suited to power plant plume monitoring. Also shown on the table is the expected operational mode of the instrument (i.e., airborne or ground-based) and the limitation of the period of operation (i.e., day and/or night). Obviously passive instruments operating in the visible or UV are restricted to daylight operation and in some cases require full sunlight.

The various air pollution remote sensors encounter a series of limitations on their operation. Some of these limitations apply to all instruments while others apply to individual categories of IR, UV, visible, passive, or active sensors. In addition, each of the instruments has certain limitations on its capability to measure the surface value of the pollutant or provide vertical profile data. These topics are discussed below and summarized in Table 9.

All of the instruments under study require a cloudless line of sight between the detector and the ground surface background (or sky background for upward looking instruments). Thus any significant occurrence of clouds, rain, or fog in the field of view prevents operation of all of the sensors with the possible exception of the Videcon, which may have a limited capability in light rain or light fog. In addition, the passive instruments operating in the visible or UV require strong sunlight for reflection or scattering from the ground surface or sky background. Thus, high sun angles are generally required, which precludes operation during early morning or late evening periods. Most of the instruments are affected to some degree by aerosols such as smoke, dust, haze, and the like. The effect may range from negligible to important as in the case of DARS and the ruby laser. For many of the instruments the effect of aerosols has not been completely analyzed and remains unknown.

The passive nadir-looking instruments in both IR and visible wavelength bands are generally affected by rapid changes in the surface background reflectivity or emission characteristics. This problem can be minimized by use of techniques such as automatic gain control, signal integration over a longer time or ground path, and/or auxiliary measurements. However, all of the instruments involved perform better when operated with uniform background reflectivity or background emissions.

In the thermal region, the signal received by a nadir-looking passive instrument depends strongly on the temperature difference between the pollutant and the underlying surface.[24] Thus little if any signal will be received from the layers of the atmosphere nearest the surface where the surface and air temperature are similar. In general, the difference in temperature must be on the order of a few degrees Celsius in order for an instrument such as

MAPS to receive an acceptable signal. This effect is sometimes referred to as the vertical sensitivity of the instrument. A schematic representation of this effect is shown in Figure 3. The lowest levels show little contribution due to the small temperature difference while the upper levels have only a small effect due to low pollutant density. Thus, large variations in the near-surface profiles or pollutant concentrations have only a small effect on the total signal received. In order to incorporate this effect into the data processing, weighting functions must be produced for each pollutant, preferably over a range of atmospheric conditions. The inability to accurately compute this weighting function would cause serious errors in pollutant concentration calculations particularly in the critical near surface layers.

Many of the remote sensors, particularly the passive ones, require auxiliary measurements in order to perform the data reduction or for proper interpretation of the data. Usually it is some form of meteorological data that is required. The data reduction programs generally require knowledge of the temperature and/or water vapor profiles in the atmosphere. These profiles are usually obtained from the nearest National Weather Service station and this, of course, may introduce significant errors in the resulting data. In more precise usage, it may be necessary to require specialized temperature or water vapor profile measurement at the exact time and location of the remote measurement.

Other types of auxiliary data are sometimes also required. For example, in the measurement of CO and CH_4 with the COPE instrument, CO_2 is an interfering gas whose effect must be calculated and adjusted. This is accomplished by means of a CO_2 detector built into the instrument.

All of the passive remote sensors receive incoming signals that have interacted with the atmosphere throughout the entire path from the radiation source to the sensor. Since there is no way to obtain ranging information on these signals without the aid of auxiliary measurements, the received signal provides only a column content measurements. Thus, it is not possible to directly measure either the surface value of the pollutant or the value for any specific altitude or vertical layer. There are two basic approaches that can be used for obtaining vertical profiles or surface data with such instruments. The first involves the obvious technique of physically moving the sensor through different altitudes to measure the differences in column content corresponding to such movement. This technique will provide adequate vertical information but does not justify the conclusion that the instrument can provide vertical profiles of the data. Furthermore, its use is restricted to airborne platforms.

The second method involves the postulation or assumption of certain information about the vertical distribution of the pollutant such as an assumed vertical mixing ratio profile. This profile can be used to differentiate the column content data into individual vertical layers. The accuracy of this method is highly dependent on the accuracy of the assumed auxiliary information. Up to the present time, attempts to apply this method to actual remote measurements have only been marginally successful. This method is applicable to both airborne and satellite platforms.

Vertical or range information from active systems are much more practical. The accuracy and resolution of such systems depends to a great extent on ability of the instrument to precisely control the pulse length and time of the transmitted signal and to precisely measure the arrival time of the return signal. In the case of pulsed laser systems, range resolution on the order of a few meters is easily obtainable.

ORBITS

The characteristics of the orbit(s) chosen for the spacecraft observations of the polluted toposphere will exhibit a considerable influence on data quality. The altitude is directly related to the spatial resolution of the observations and determines, along with the orbit inclination, the spatial and temporal coverage and sampling. Orbit parameters, along with the launch date, control the solar elevation along the orbit track, which is important for the proper operation of instruments working in the visible spectrum. The orbit parameters also determine the repeat cycle of the orbit, expressed as the number of orbits (or equivalently, the number of days) between ground tracks that exactly coincide. The repeat cycle controls the frequency with which observations are made of a particular site.

Orbits of particular interest in the near future are those associated with the Space Shuttle. The orbits that might be expected for Shuttle missions will range from approximately 250 to 450 km in altitude and from 28.5° to 57° in inclination. Appropriate selection of values from each of these ranges will result in orbits whose repeat cycles are an integral number of days. Examples of such orbits are shown in Figures 4 and 5 and Table 10. The figures illustrate the ground track that will occur for 1- and 7-day repeat cycles. Repeat cycles of 2, 3, 4, 5, and 6 days exhibit similar coverage patterns that increase in density as the repeat cycle grows. Conversely, the frequency of temporal sampling drops as the spatial sampling increases.

One of the orbits (Figure 4) has an altitude higher than one might expect for Shuttle but is included both because it shows the control of orbit inclination on latitudinal coverage (no observations above 45° occur in the example) and because it has a 1-day repeat cycle. In effect, this example orbit illustrates one extreme in the trade-off between spatial sampling density and frequency of sampling. The other extreme, for the proposed 7-day mission duration, is shown in Figure 5. The orbit has a 7-day repeat cycle, about four times as much spatial sampling density as the 1-day repeat cycle case but only one-seventh the frequency of sampling (since it takes 7 days to complete the sampling pattern). There are two factors that, along with the orbit parameters, determine the solar elevation history along the ground track of the orbit: the local time of the various observations and the declination of the sun as it varies with the seasons. The solar elevation is primarily of importance in determining the occasions in which the sensors using the visible spectrum can be used effectively.

Variation from measurement to measurement of the local sun time is of significance because it indicates the amount of diurnal sampling that can be achieved during the mission. If the mission is sufficiently long that each hour of the day and night is sampled many times, the diurnal sampling is better than in the case of a sun-synchronous or nearly sun-synchronous orbit for which all observations at a particular point are made at the same local time.

Seasonal variations in the declination of the sun and the movement of the orbit plane with respect to the Earth-Sun line determine the range of latitudes for which observations can be made at various times of the year. Figure 6 illustrates these limits for a 56° inclination orbit if 30° solar elevation is to be achieved. The figure shows that missions as long as approximately 20 days can enjoy the maximum possible latitude coverage in one hemisphere or the other, as long as the launch date is chosen with care. The time of day of the launch is also important (in this case it was assumed that the first orbit crossed the equator at 12:00 noon). The figure also shows that winter conditions limit the latitudes that can be covered. From November to March only latitudes up to 30° can be covered in the northern hemisphere.

MODEL FOR DATA INTERPRETATION

Characterization of the uncertainty in spacecraft observations of air quality requires information on three factors: (1) the uncertainty in individual observations as determined by the performance of the instrument and data reduction methods; (2) the uncertainty associated with incomplete sampling of the scene in space and time; and (3) uncertainty associated with instrument response to spatial and temporal variability in the scene. Identification of instrument uncertainty (both bias and random) is relatively straightforward as a result of laboratory calibration and field testing. Sampling uncertainties are somewhat more complex, however, since they involve both the sampling characteristics provided by the orbit, as well as the natural spatial and temporal variability of the pollutants and interfering clouds. Models of the spatial and temporal response of the instrument are presented first. From these models, a total response function is developed and used to compute response errors. The next stage in the analysis is computation of uncertainties associated with limited sampling. Finally, the three contributors to the total uncertainty are used to calculate the results that might be expected in observational programs.

Spatial Impulse Response Function

A number of parameters characterize the capability of a remote sensor to respond to the variations in the pollution it is attempting to detect.

These include:

velocity of the ground track - V (km/seconds)
time constant of the instrument* - τ_1(seconds)
full angle field-of-view - Ω (radians)
altitude of the spacecraft - A (kilometers)
footprint of the field-of-view - $D = \Omega A$

Each element that enters the field-of-view acts like a unit step function whose amplitude indicates the absolute amount of pollution in that element region. During its time in the field-of-view (D/V), that element produces a response of the form

$$1-e^{-t/\tau_1}$$

After the element has moved outside the field-of-view, the response approaches zero according to

$$e^{-t/\tau_1}$$

As the footprint progresses along the orbit path, each successive small area interacts with the changed concentration and alters the output of the sensor.

If the pollution level is described as g(x), then the contribution from elements in the field-of-view at any place x is given by

$$f_1(x) = \frac{1}{D} \int_{x-D}^{x} g(x') \left[1- \exp\left(- \frac{x-x'}{V\tau_1}\right)\right] dx' \qquad (1)$$

Similarly, the contribution of the elements that have moved out of the field-of-view is given by

$$f_2(x) = \frac{1}{D} \left[\exp\left(\frac{D}{V\tau_1}\right)-1\right] \int_{0}^{x-D} g(x')\exp\left(\frac{x'-x}{V\tau_1}\right) dx'. \qquad (2)$$

---

*Assumes the instrument response to a step function grows a $1-e^{-t/\tau_1}$.

The total response of the sensor thus becomes

$$f\ (x) = \frac{1}{D} \int_{x-D}^{x} g(x')\left[1-\exp\left(-\frac{x-x'}{V\tau_1}\right)\right] dx'$$

$$+\frac{1}{D}\left[\exp\left(\frac{D}{V\tau_1}\right)-1\right] \int_{0}^{x-D} g(x')\ \exp\ \frac{x'-x}{V\tau_1}\quad dx' . \tag{3}$$

Equation 3 is a convolution of two functions and can be rewritten as

$$f\ (x) = \int g(x')\ \ h_1\ (x-x')\ \ dx'$$

where h_1 (x) is the spatial impulse response function and is given by

$$\begin{aligned} h_1\ (x) &= \frac{1}{D}\left[1-\exp\ \left(-\frac{x}{V\tau_1}\right)\right]U(x) \\ &- \frac{1}{D}\left[1-\exp\ \left(-\frac{x-D}{V\tau_1}\right)\right]U(x-D). \end{aligned} \tag{4}$$

U(x-D) here is a unit step function defined as

$$U(x-D) = \begin{cases} 0 & x<D \\ 1 & x>D \end{cases} \tag{5}$$

Equation 4 is simplified further when expressed in terms of spatial frequencies. The frequency spectrum H_1 $(j\omega_1)$ is the Fourier Transform of $h_1(x)$:

$$\begin{aligned} H_1\ (j\omega_1) &= \int_{-\infty}^{\infty} h(x)\ e^{-j\omega_1 x}\quad dx \\ &= \frac{1-e^{-j\omega_1 D}}{j\omega_1 D(1+j\omega_1 V\tau_1)} \end{aligned} \tag{6}$$

Temporal Impulse Response Function

To determine the temporal impulse response function, the instruments can be represented by the block diagram below.

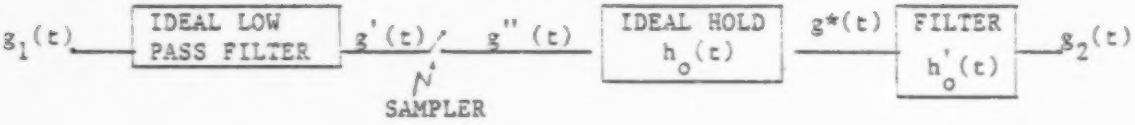

The ideal low pass filter in the front end of the sensor limits the maximum frequency content in the pollution distribution to be observed by the sensor and aids in determining the optimum sampling rate. The bandwidth Δf of this filter is approximately given by

$$\Delta f \approx \frac{1}{4\tau_1} .$$

where

τ_1 is the electronic time constant of the instrument.

The output signal $g'(t)$, which is limited to the frequency band 0 to Δf, is sampled at a constant frequency of $f_0 = \frac{1}{T_0}$, where $f_0 \geq 2\Delta f$. This sampling rate is required because to transmit a band-limited signal of duration T_1 and maximum frequency f_m, it suffices to send a finite set of $2f_mT_1$ independent amplitude samples obtained by sampling the instantaneous amplitude of the signal at a regular rate of $2f_m$ samples/second. This is a statement of the so-called Nyquist criterion.

$g''(t)$ is a train of impulses given by

$$g''(t) = \sum_{n=o}^{T_1/T_o} g(nT_o)\,\delta(t-nT_o) \quad (7)$$

where δ is the Dirac delta function.

T_0 is the sampling interval and as discussed above is related to Δf and the electronic time constant by

$$T_o = \frac{1}{2\Delta f} = 2\tau_1 . \qquad (8)$$

$g^*(t)$ is a sampled function consisting of short pulses, F_1, F_2,.... F_n, of equal duration τ_3 at equal intervals T_0. Thus, the impulse response function of the hold circuit is given by

$$h_o(t) = U(t) - U(t-\tau_2) \text{ for all } \tau_2 < T . \qquad (9)$$

The last filter of the system gives a real time response and reflects the time constant (τ_1) of the system. Its impulse response function is given by

$$h'_o(t) = e^{-t/\tau_1} . \qquad (10)$$

Finally, the convolution of $h_0(t)$ with $h'_0(t)$ determines the temporal impulse response function. The temporal impulse response function $h_2(t)$ is given by

$$\begin{aligned} h_2(t) &= h_o(t) * h'_o(t) \\ &= \tau_1 \left[1-\exp\left(-\frac{t}{\tau_1}\right)\right]U(t) \qquad (11) \\ &+ \tau_1 \left[1-\exp -\left(\frac{t-t_2}{\tau_1}\right)\right]U(t-\tau_2) \text{ for all } \tau_2 < T . \end{aligned}$$

The temporal frequency response function is the Fourier Transform of $h_2(t)$ and is presented by $H_2\ (j\omega_2)$:

$$\begin{aligned} H_2\ (j\omega_2) &= \int_{-\infty}^{\infty} h_2(t)\, e^{-j\omega_2 t}\, dt \\ &= \tau_1 \cdot \frac{1-e^{-j\omega_2 \tau_2}}{j\omega_2\ (1+j\omega_2 \tau_1)} \quad \text{for all } \tau_2 < T \qquad (12) \end{aligned}$$

Total System Impulse Response Function

The pollution distribution is a function of time as well as spatial variations. In general, because of meteorology, the pollution distribution at any point x_2, at time t_2, may be influenced by the pollution distribution of point x_1 at time t_1 ($t_1 < t_2$). The instrument responses in space and time, as derived above, can be considered as independent of one another.

Thus, the total system impulse response function represented as h(x,t) is given by

$$\begin{aligned} h(x,t) &= h_1(x) \cdot h_2(t) \\ &= \left[\frac{1}{D}\left(1-e^{-x/V\tau_1}\right) U(x) - \frac{1}{D}\left(1-e^{-(x-D)/V\tau_1}\right) U(x-D)\right] \\ &\quad \cdot \left[\tau_1\left(1-e^{-t/\tau_1}\right) U(t) - \tau_1\left(1-e^{-(t-\tau_2)/\tau_1}\right) U(t-\tau_2)\right] \end{aligned} \tag{13}$$

Taking the double Fourier Transform of Equation 13, we obtain the system bi-frequency impulse response function as

$$\begin{aligned} H(j\omega_1, j\omega_2) &= \int_{-\infty}^{\infty}\int_{-\infty}^{\infty} h(x,t)\, e^{-j\omega_1 x} \cdot e^{-j\omega_2 t}\, dx\, dt \\ &= \frac{1-e^{-j\omega_1 D}}{j\omega_1 D(1+j\omega_1 V\tau_1)} \cdot \tau_1 \cdot \frac{1-e^{-j\omega_2\tau_2}}{j\omega_2(1+j\omega_2\tau_1)} . \end{aligned} \tag{14}$$

This formulation is applied to instrument performance evaluation in the next section.

Instrument Performance Evaluation

Let $g_1(x,t)$ be the input pollution distribution at any x, and t and $g_2(x,t)$ be the instrument response to this input. To determine how accurately the original distribution is reproduced, a criterion relating the average power in the input and output pollution distributions may be used. The average power of a random process x(t) is given by

$$E\left\{x^2(t)\right\}$$

where E is the expectation operator. The difference between the average power of $g_1(x,t)$ and $g_2(x,t)$ will be given by

$$\varepsilon = E\left\{g_1^2(x,t)\right\} - E\left\{g_2^2(x,t)\right\} . \tag{15}$$

The power spectrum or a spectral density $S_{g1}(\omega_1,\omega_2)$ of the process $g_1(x,t)$ is the Fourier Transform of its autocorrelation:

$$S_{g_1}(\omega_1,\omega_2) = \int_{-\infty}^{\infty}\int_{-\infty}^{\infty} R_{g_1}(\xi_1,\xi_2)\, e^{-j\omega_1\xi_1} \cdot e^{-j\omega_2\xi_2}\, d\xi_1\, d\xi_2 \tag{16}$$

where

$$R_{g_1}(\xi_1,\xi_2) = E\left\{g_1(x,t)g_1(x+\xi_1,\ t+\xi_2)\right\}. \tag{17}$$

From Equation 16, using the Fourier inversion formula, it follows that

$$R_{g_1}(\xi_1,\xi_2) = \frac{1}{4\pi^2}\int_{-\infty}^{\infty}\int_{-\infty}^{\infty} S_{g_1}(\omega_1,\omega_2)\, e^{j\omega_1\xi_1}\, e^{j\omega_2\xi_2}\, d\omega_1\, d\omega_2. \tag{18}$$

With $\xi_1 = 0$, and $\xi_2 = 0$, the above yields an expression for the average power of the input distribution

$$E\left\{g_1^2(x,t)\right\} = \frac{1}{4\pi^2}\int_{-\infty}^{\infty}\int_{-\infty}^{\infty} S_{g_1}(\omega_1,\omega_2)\, d\omega_1\, d\omega_2. \tag{19}$$

Then the difference ε becomes

$$\varepsilon = \frac{1}{4\pi^2}\int_{-\infty}^{\infty}\int_{-\infty}^{\infty} S_{g_1}(\omega_1,\omega_2)d\omega_1 d\omega_2 - \frac{1}{4\pi^2}\int_{-\infty}^{\infty}\int_{-\infty}^{\infty} S_{g_2}(\omega_1,\omega_2)d\omega_1 d\omega_2 \tag{20}$$

The spectral density $S_{g^2}(\omega_1,\omega_2)$ of the output $g_2(x,t)$ is dependent upon the system impulse response function and the spectral density of the input. It is given by

$$S_{g_2}(\omega_1,\omega_2) = \left| H(j\omega_1,j\omega_2)\right|^2 \quad S_{g_1}(\omega_1,\omega_2) . \tag{21}$$

So that

$$\varepsilon = \frac{1}{4\pi^2}\int_{-\infty}^{\infty}\int_{-\infty}^{\infty} S_{g_1}(\omega_1,\omega_2)\, d\omega_1\, d\omega_2$$

$$- \frac{1}{4\pi^2}\int_{-\infty}^{\infty}\int_{-\infty}^{\infty} H(j\omega_1,j\omega_2)^{2} \quad S_{g_1}(\omega_1,\omega_2)\, d\omega_1\, d\omega_2 \tag{22}$$

and the percent difference is given by

$$\%\ \varepsilon = 100 \cdot \left(1 - \frac{\displaystyle\int_{-\infty}^{\infty}\int_{-\infty}^{\infty} \left| H(j\omega_1,j\omega_2)\right|^2 \ S_{g_1}(\omega_1,\omega_2)\, d\omega_1\, d\omega_2}{\displaystyle\int_{-\infty}^{\infty}\int_{-\infty}^{\infty} S_{g_1}(\omega_1,\omega_2)\, d\omega_1\, d\omega_2} \ . \right) \tag{23}$$

The difference of Equation 23 can be used as a part of the uncertainty analysis.

Uncertainty Due to Sampling Strategies

One of the key issues in determining the performance of remote sensors in space is the determination of the uncertainty in assessing pollution distributions because of the sampling distribution in space and time.

The sampling problem arises because the selection of the orbit and the inhibiting influence of clouds may make the spatial and temporal sampling less than adequate for the purpose of characterizing the spatial and temporal variability of the pollution.

For a scene with little spatial variability, a few observations at different points may be adequate to obtain statistically meaningful averages. The problem at hand, unfortunately, is characterized by a high spatial and temporal variability so that sampling limitations become important. It is the purpose of this subsection to quantify the sampling by considering both that which can be achieved as well as the spatial and temporal variability in the pollution distribution.

The pollutants of interest may exhibit considerable spatial and temporal variability. In fact, different pollutants may exhibit different patterns of diurnal, seasonal, and spatial variability. The pollution can therefore be regarded as a stochastic variable, with the pollution variations through each day being a record from the ensemble of all possible records. Let $\mu(t)$ represent the ensemble mean of $P_i(t)$, the pollution at time of the day, t on the i^{th} day. Then, the average pollution for N days at time t is

$$\mu(t) = \frac{1}{N} \sum_{i=1}^{N} P_i(t) \tag{24}$$

Note that $\mu(t)$ is not independent of time because of the diurnal variations and, therefore, the process is a nonstationary stochastic process.

Integrating Equation 24 over the times of the day that instruments are capable of taking measurements, we obtain the time average pollution for N days. This is given by

$$\mu = \frac{1}{T} \int_{\text{time of the day}} \mu(t)dt \quad . \tag{25}$$

Since Shuttle will be visiting one place only a finite number of times in N days, Equation 25 is rewritten as a sum:

$$\mu = \frac{1}{n} \sum_{j=1}^{n} \overline{P(t_j)} \tag{26}$$

where

t_j is the j^{th} hour

$$n = \frac{24N}{\Delta t} \quad ,$$

$$\Delta t = t_{j+1} - t_j$$

Δt will be determined by the orbit parameters since they control the time between passes over the same place. Ideally, one would like to keep Δt as close as possible to the sampling interval given by Nyquist criterion, which may be impossible to achieve considering large variations in pollution diurnal cycles. For example, if the temporal variability of the scene is on the order of a day, which is not uncommon, the Nyquist criterion requires that samples be made on a scale of fractions of a day. It is unlikely that samples can be made with this temporal density. Therefore, the estimate of the average pollution at time t_j, $\hat{\mu}(t_j)$ may only be available from a single measurement taken at the j^{th} hour of the i^{th} day, $P_i(t_j)$. Let the variance of this single estimate be σ, defined as

$$\mathrm{Var}\left[\hat{\mu}(t_j)\right] = \sigma^2(t_j) \tag{27}$$

then the estimate of the ensemble average over N days will be given by

$$\hat{\mu} = \frac{1}{n} \sum_{j=1}^{n} \mu(t_j) \tag{28}$$

and the variance of this pollution estimate, $\hat{\mu}$, will be

$$\mathrm{Var}\;[\hat{\mu}] = \frac{1}{n^2} \sum_{j=1}^{n} \sigma^2(t_j) + \frac{1}{n^2} \sum_{\substack{i=j \\ i=1,\; j=1}}^{n} \sigma(t_i)\,\sigma(t_j)\;\rho(i-j) \tag{29}$$

where $\rho(i-j)$ is the correlation between the pollution estimates $\mu(t_j)$ and $\mu(t_i)$ made at different times.

This analysis can be carried further using the following assumptions:

1. The samples over the period are uniformly distributed over the time of the day,

2. The variance in any pollution estimate is $\sigma 2$ and,

3. The correlation between pollution estimates can be assumed to be of exponential form, i.e.,

$$\rho(i-j) = e^{-k\alpha'} \tag{30}$$

where

k is the index representing the k^{th} repeat cycle, and takes values between 0 and n.

n is the number of repeat cycles in a time period of interest and equals the number of samples of a place in that time period.

α' is the correlation coefficient/repeat cycle.

If M represents the number of days/repeat cycle, and α is assumed to be the correlation coefficient for one day, then

$\alpha' = M\alpha$.

Under these conditions, Equation 29 becomes:

$$\begin{aligned} \text{Var}(\hat{\mu}) &= \frac{\sigma^2}{n} + \frac{2\sigma^2}{n^2} \sum_{k=1}^{n-1} (n-k)\, e^{-k\alpha'} \\ &= \frac{\sigma^2}{n} + \frac{2\sigma^2}{n^2} \; \frac{(n-1)e^{\alpha'} - n + e^{-(n-1)\alpha'}}{(e^{\alpha'}-1)^2} \end{aligned} \tag{31}$$

Equation 31 can also be used to generate a set of curves for different values of n, M, and α', which illustrate the variance in estimates (in units of σ) for various mission durations, repeat cycles, and pollution correlations. Curves developed from this equation are shown in Figures 7, 8, and 9. The mission durations considered in the examples are 7, 15, and 30 days. The data pertaining to 15- and 30-day missions are included for comparison to illustrate the value of missions longer than the expected 7-day Shuttle missions. The correlation of pollution on 2 successive days is indicated by ρ. The correlation coefficient, ρ, for 1 day is determined from using Equation 30, and is given by

$$\alpha = -\ln(\rho) \tag{32}$$

Upon examination of the figures it is clear that for a very high correlation of pollution of 2 successive days, the uncertainty in the estimate of pollution in units of σ is not significantly reduced by making a large number of samples. On the other hand, for a highly varying pollution scene, the correlation of pollution on 2 successive days is low, and the potential reduction in the uncertainty in the estimate of pollution provided by a single observation is more pronounced.

Application of The Analytical Methods

The statistical tools developed in the previous sections can now be used collectively to determine the data quality that might result from a real mission. For example, a typical Shuttle orbit might have a 5-day repeat cycle. This information, along with data on the correlation of pollution and the probability of cloud cover, can be used to estimate the sampling uncertainty. The inability of certain instruments to operate under conditions other than relatively high solar elevation angles can also be included.

Pollution Statistics--

An extensive listing of air quality statistics for New York City were obtained from the Environmental Protection Agency. The data were provided in the form of hourly and daily averages of pollution levels for July and August 1974. From these data, weekly, biweekly and monthly means and standard deviations were computed using conventional statistical methods. In addition, the correlations were also computed. Data for one monitoring site appear in Table 11. The correlation computation was carried out using the method normally used in regression analysis. That is,

$$\rho = \frac{n\sum x_{i+i}x_i - \sum x_{i+i}\sum x_i}{\left\{\left[n\sum x_{i+i}^2 - \left(\sum x_{i+i}\right)^2\right]\left[n\sum x_i^2 - \left(\sum x_i\right)^2\right]\right\}^{1/2}} \tag{33}$$

where all sums range from 1 to n, the number of entries (for example, for a 30-day mission the number of entries will be 30). Thus, the coefficient ρ represents the correlation between each measurement and the next successive one.

Use of the Data--

The standard deviation and correlation data of Table 11 have been used to compute the sampling uncertainty as a function of days per repeat cycle. The uncertainty due to sampling is

$$\frac{\mathrm{Var}\ (\hat{\mu})}{\hat{\mu}} \times 100 \tag{34}$$

Use of Equation 34 and Table 11 results in Table 12, which is an example of the magnitude of sampling uncertainty that might occur in attempting to make estimates of the pollution in the New York City area, assuming that an IR sensor, unaffected by solar limitations, is used. A 50 percent chance of cloudiness was assumed. The sampling uncertainty for a mission of the expected duration (7 days) ranges from 20 to 36 percent, depending on the number of days in the repeat cycle of the orbits. However, for a mission of a month, the sampling uncertainty is reduced to the range of 10 to 22 percent, depending on the number of days per repeat cycle. As expected, the 1-day repeat cycle provides the smallest sampling error. However, the orbit that produces a 1-day repeat cycle is also the one that results in the poorest areal coverage (as illustrated in Figure 4).

Total System Performance--

Three major elements make up the total uncertainty in estimates of pollution. They are the radiometric uncertainty imposed by the instrument performance, uncertainties dictated by the spatial and temporal response functions of the instrument, and the sampling uncertainty. Under the assumption that these uncertainties are independent, and they appear to be, then the data quality is defined by a root sum of squares calculation. The total uncertainty is given by

$$\%\ \text{uncertainty} = \left\{ \frac{\sigma_1^2}{L} + \frac{\sigma_2^2}{L} + \sigma_3^2 \right\}^{1/2} \tag{35}$$

where L is the number of observations during the mission

σ_1: uncertainty in individual estimates.

σ_2: uncertainty associated with response.

σ_3: sampling uncertainty (derived from Table 12).

Table 13 illustrates the total system uncertainty for various mission lengths and repeat cycles. As in the data of Table 12, 50 percent cloud cover is assumed. Other assumptions used in the analysis are that each pollution estimate has an uncertainty of 50 percent and that response uncertainties may be as high as 10 percent, based on the use of Equation 23 and typical pollution distributions.

An expected result appears immediately; mission duration has a significant impact on the uncertainties, the shorter repeat cycle orbits exhibiting the best data quality. Conversely, these short repeat cycle orbits have the poorest density of sampling of the region of interest. The mission designer has the choice, then, of attempting to achieve the best possible data but for limited locations. Alternatively, he may choose to gain the best possible spatial sampling of the region at the expense of data quality at individual locations.

Clearly, a considerable number of assumptions have been included in the analysis above (frequency of cloudiness, uncertainty of individual pollution estimates, etc.). It was the object of this analysis to illustrate the methods to be used in analyzing sensor/orbit performance. Additional analysis would be required if the assumptions were to be modified.

REFERENCES

1. E. L. Keitz et al. The Capability of Remote Sensing for Regional Atmospheric Pollution Studies. The MITRE Corporation, MTR-7267, January 1977.

2. E. Friedman et al. Shuttle Applications in Tropospheric Air Quality Observations. The MITRE Corporation, MTR-7628, August 1978.

3. ________. Practical Applications of Space Systems, Supporting Paper 7, Environmental Quality. The Report of the Panel on Environmental Quality to the Space Applications Board of the Assembly of Engineering. National Research Council, National Academy of Sciences, Washington, 1975.

4. G. M. Hidy et al. Design of the Sulfate Regional Experiment (SURE), Volumes I-IV. Environmental Research and Technology, Westlake Village, California, February 1976.

5. M. L. Wright et al. A Preliminary Study of Air-Pollution Measurement by Active Remote-Sensing Techniques. Stanford Research Institute, NASA CR-132724, June 1975.

6. R. L. Myers and J. A. Reagen. The Regional Air Monitoring System, St. Louis, Missouri, USA. International Conference on Environmental Sensing and Assessment, September 1975, Las Vegas, Nevada, Institute of Electrical and Electronics Engineers, New York, 1976.

7. R. B. Evans. Aerial Air Pollution Sensing Techniques. *Proceedings, Second Conference on Environmental Quality Sensors*. National Environmental Research Center, Las Vegas, Nevada, October 1973.

8. ________. Investigation of Rural Oxidant Levels as Related to Urban Hydrocarbon Control Strategies. Prepared by the Research Triangle Institute for the U.S. Environmental Protection Agency, March 1975.

9. C. W. Spicer et al. Final Data Report on the Transport of Oxidant Beyond Urban Areas. EPA Contract No. 68-02-2241, January 16, 1976.

10. TRW, Inc. Monitoring Air Pollution from Satellites (MAPS). NASA CR-145137, Final Report, 1 March 1977.

11. T. W. Ward and H. H. Zwick. Gas Cell Correlation Spectrometer: GASPEC. *Applied Optics*, XIV:2896, December 1975.

12. S. M. Beck et al. Aircraft Instrumentation System for the Remote Sensing of Carbon Monoxide. *Proceedings, Fourth Joint Conference on Sensing of Environmental Pollutants*. November 1977, New Orleans, LA, American Chemical Society, Washington, D.C.

13. J. C. Casas et al. Procedures Utilized for Obtaining Direct and Remote Atmospheric Carbon Monoxide Measurements Over the Lower Lake Michigan Basin in August of 1976. *Proceedings, Fourth Joint Conference on Sensing of Environmental Pollutants*. November 1977, New Orleans, LA, American Chemical Society, Washington, D.C.

14. M. H. Bortner et al. Analysis of the Feasibility of an Experiment to Measure Carbon Dioxide in the Atmosphere. NASA CR-2303, October 1973.

15. R. Dick et al. Development of an Engineering Model Correlation Interferometer for the Carbon Monoxide Pollution Experiment. General Electric Company, Philadelphia, Pennsylvania, November 1974.

16. M. H. Bortner et al. Carbon Monoxide Pollution Experiment: Final Report. NASA CR-132717, January 1975.

17. R. K. Seals, Jr., and B. J. Peyton. Remote Sensing of Atmospheric Pollutant Gases Using an Infrared Heterodyne Spectrometer. Presented at the International Conference on Environmental Sensing and Assessment, Las Vegas, Nevada, September 14-19, 1975.

18. L. J. Duncan et al. Airborne Remote Sensing System for Urban Air Quality. The MITRE Corporation, MTR-6601, February 1974.

19. R. K. Seals and C. Bair. Analysis of Laser Differential Absorption Remote Sensing Using Diffuse Reflection from Earth. Presented at the Second Joint Conference on Sensing of Environmental Pollutants, December 10-12, 1973, Washington, D.C.

20. J. M. Hoell, Jr., et al. Remote Sensing of Atmospheric SO_2 using the Differential Absorption LIDAR Techniques. Presented at the International Conference on Environmental Sensing and Assessment, September 14-19, 1975, Las Vegas, Nevada.

21. E. Browell, private communication, NASA/Langley Research Center, March 1979.

22. R. J. Exton, private communication, NASA/Langley Research Center, April 1976.

23. R. J. Exton and R. W. Gregory. A Four Channel Portable Solar Radiometer for Measuring Particulates and/or Aerosol Opacity and Concentration of NO_2 and SO_2 in Stack Plumes. NASA-TN-D 8182, June 1976.

24. H. G. Reichle. MAPS (Measurement of Air Pollution for Satellites). NASA Langley Research Center, April 1973.

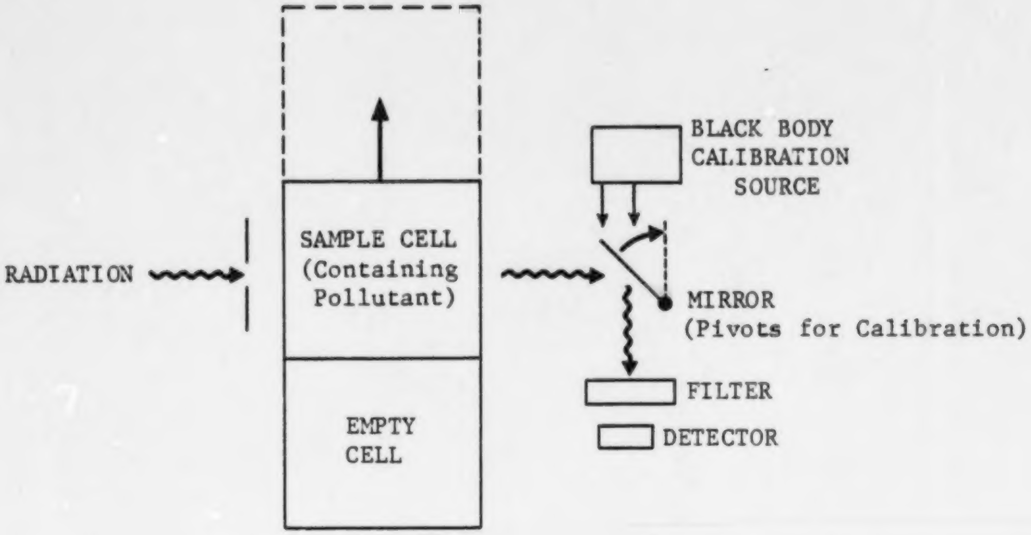

Figure 1. Gas cell correlation analyzer.

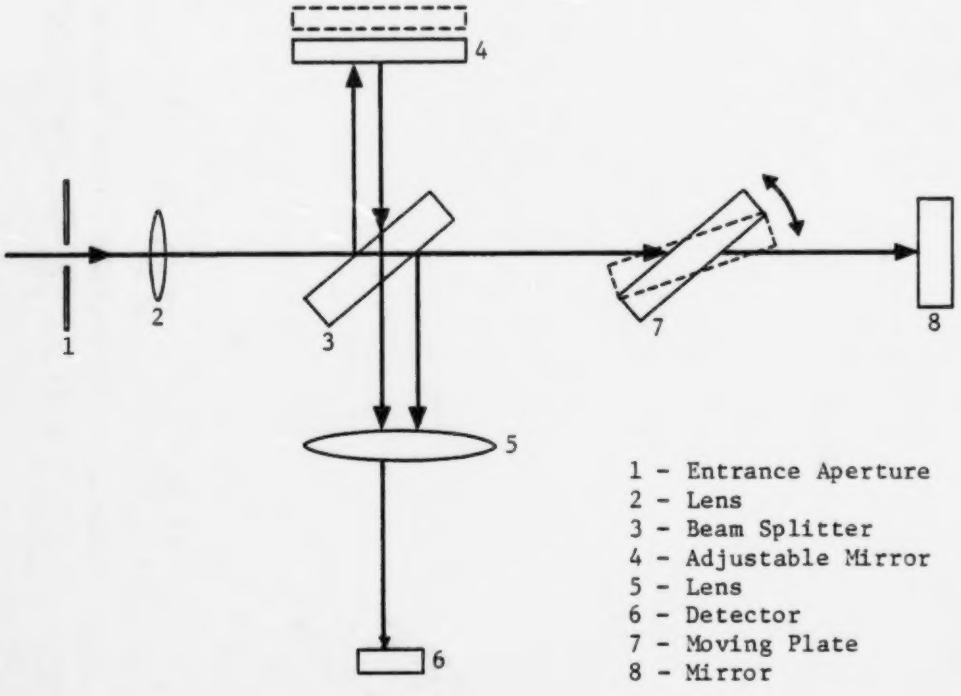

Figure 2. Correlation interferometer.

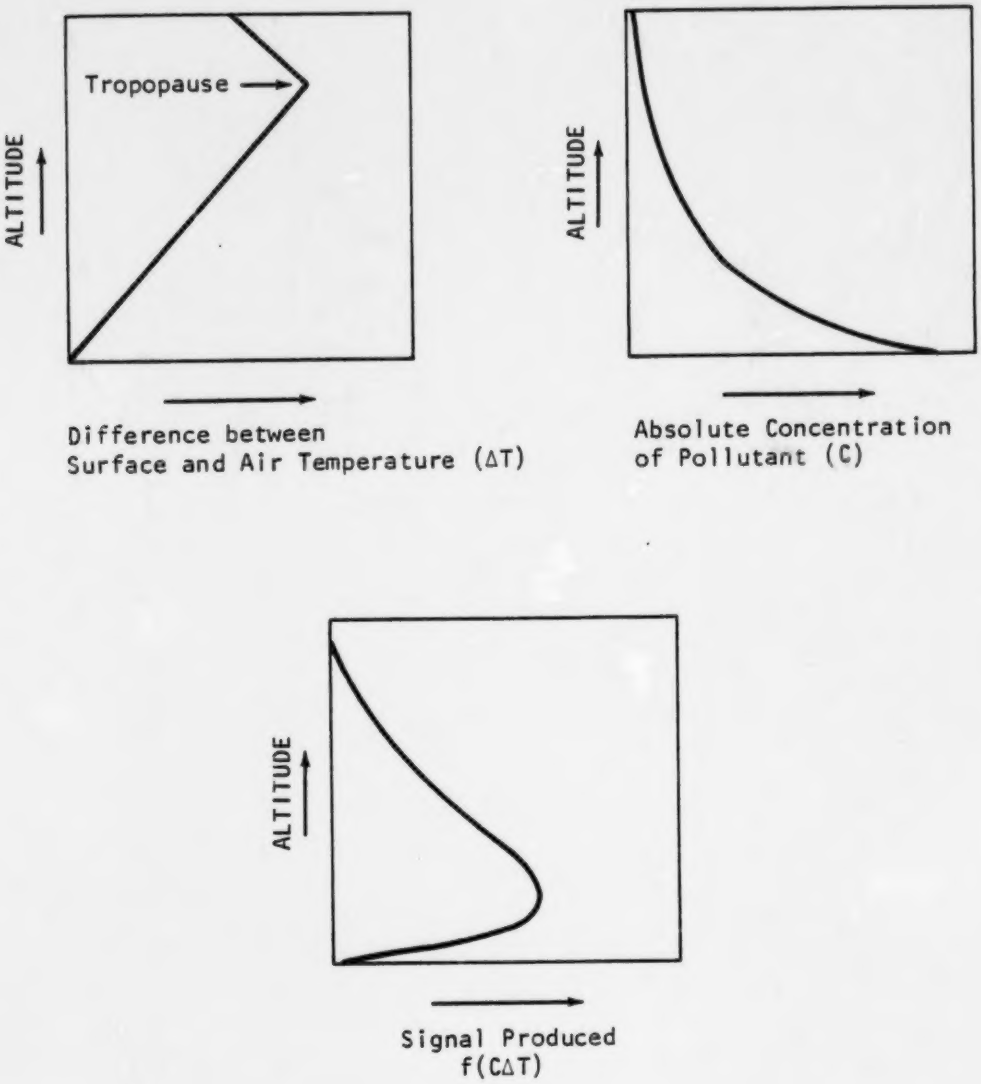

Figure 3. Schematic of effect of the difference between surface and air temperatures on the instrument signal.

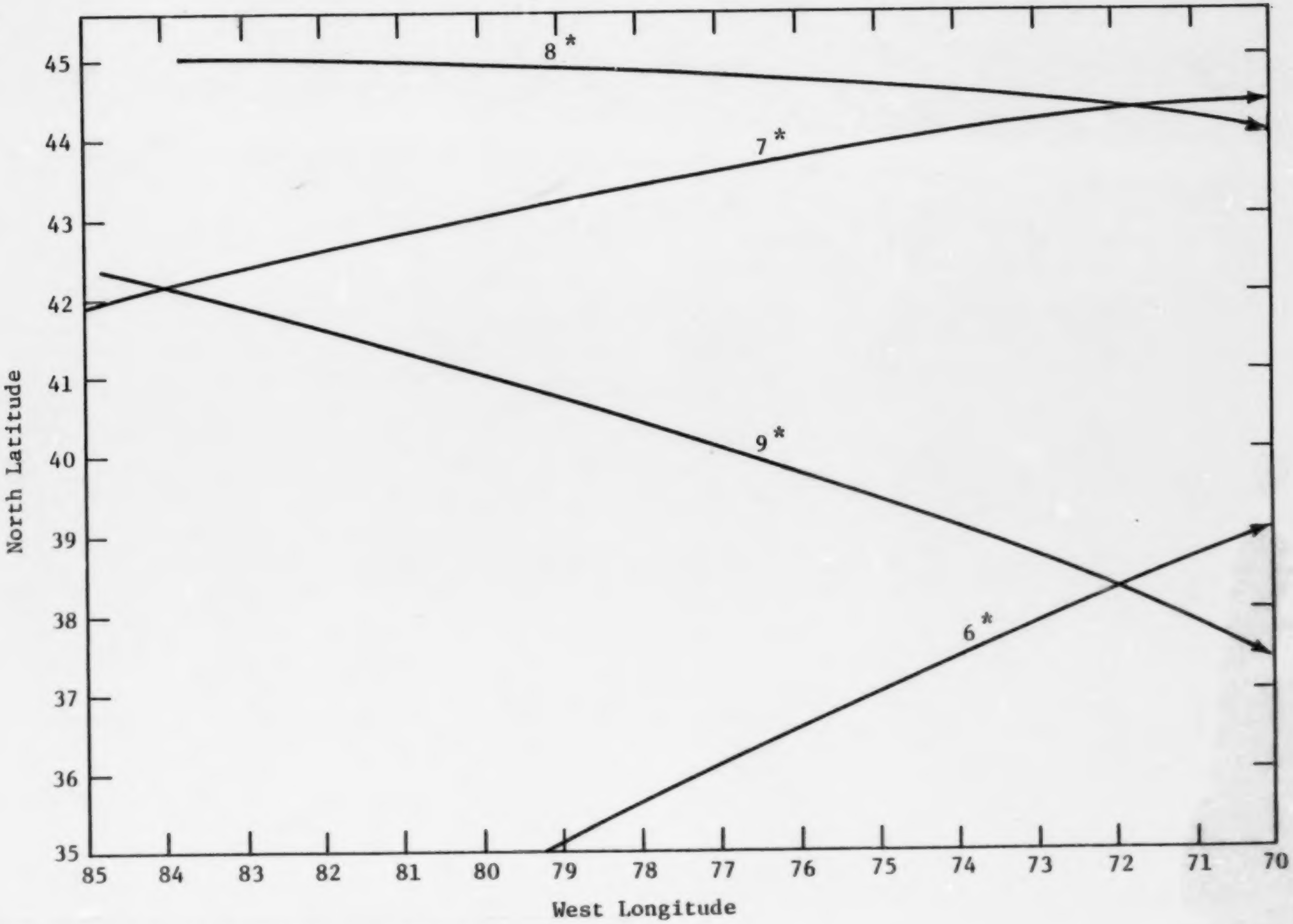

*Indicate which orbit of the cycle is responsible for each ground track.

Figure 4. Ground track for orbit with 1-day repeat cycle (altitude = 492 km, inclination = 45°).

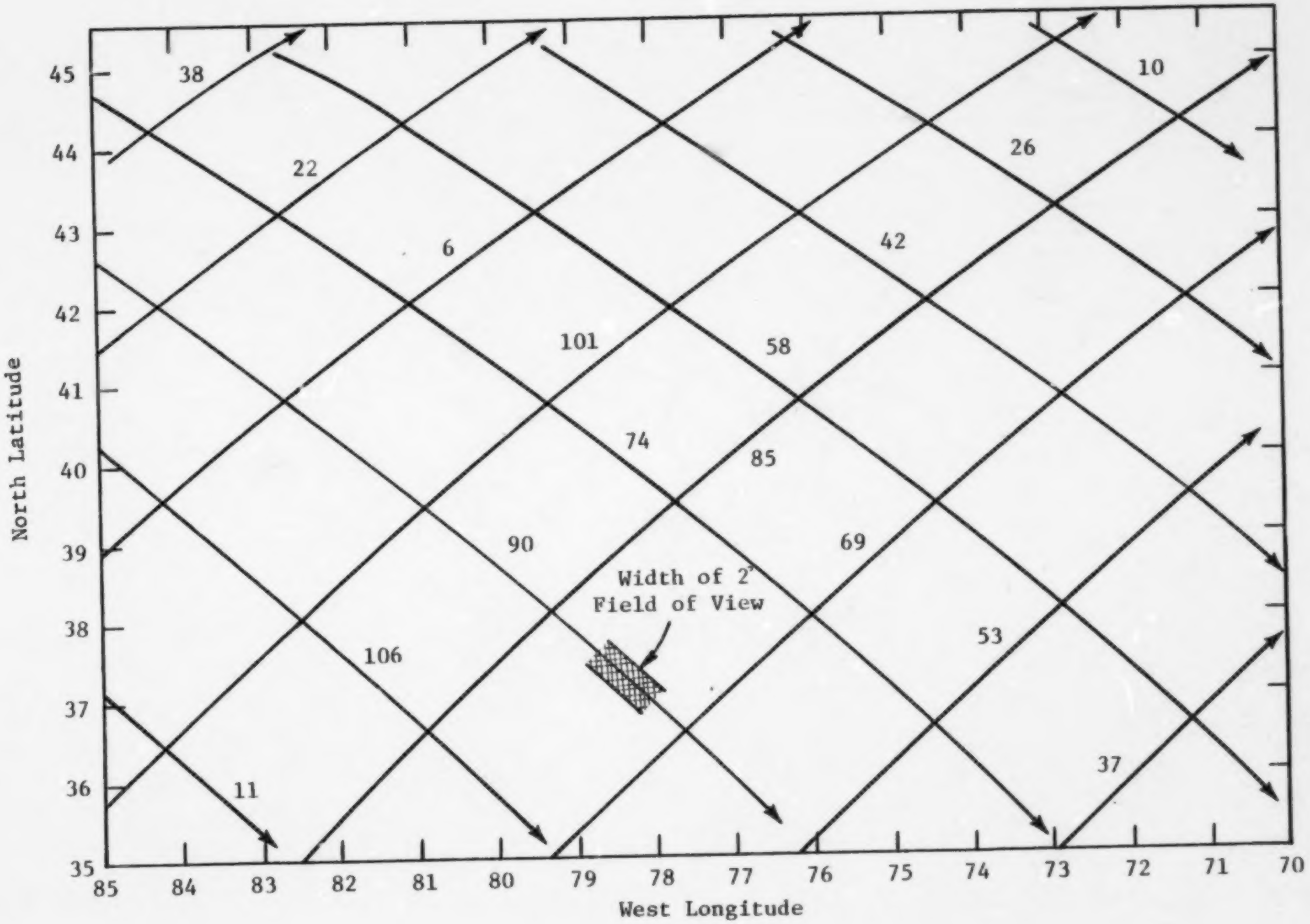

Figure 5. Ground track of typical shuttle orbit (altitude = 245 km, inclination = 57°). Each track is associated with the number of orbits since the start of the mission.

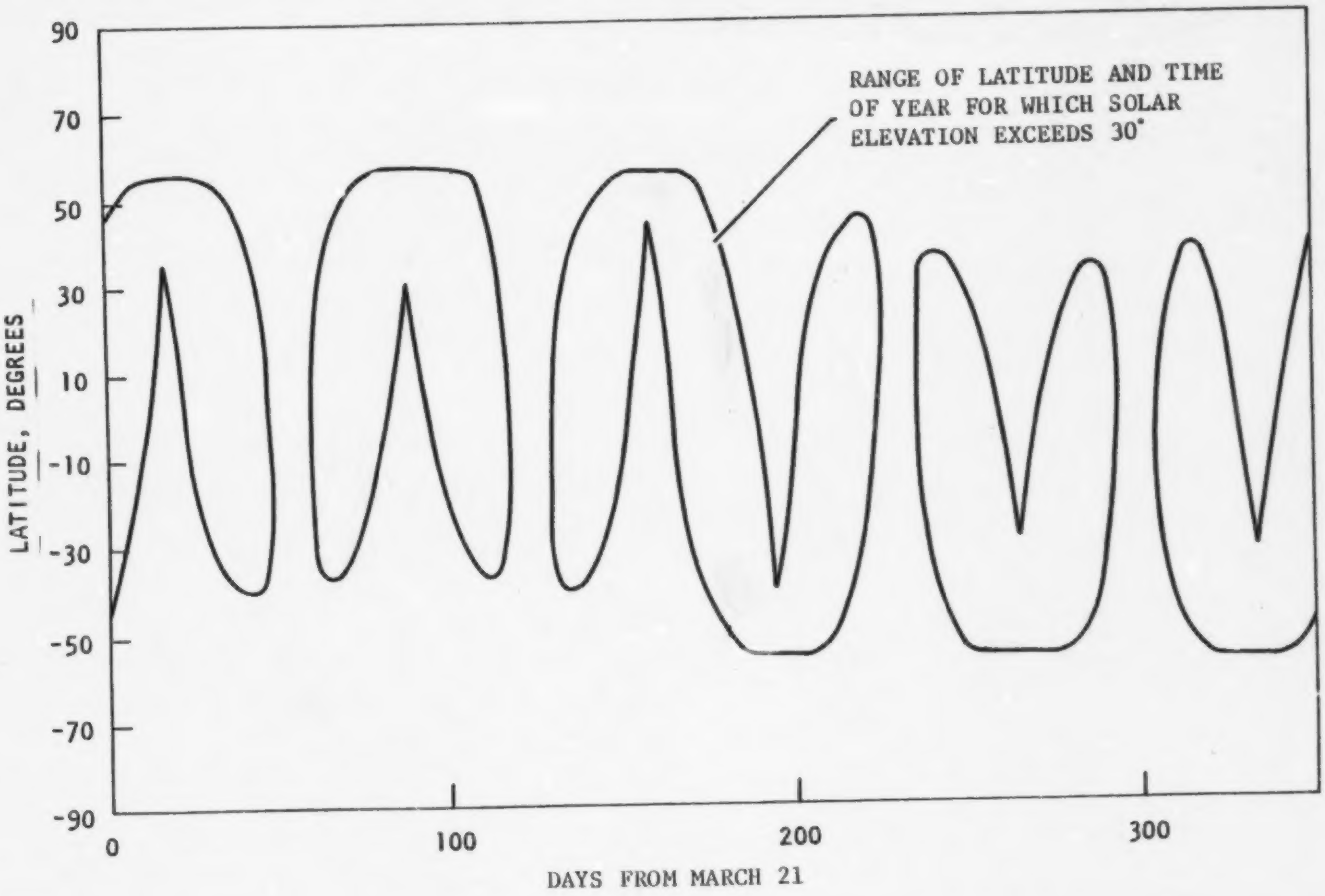

Figure 6. Latitudes covered by a typical 56° orbit with the requirement that the solar elevation exceeds 30°.

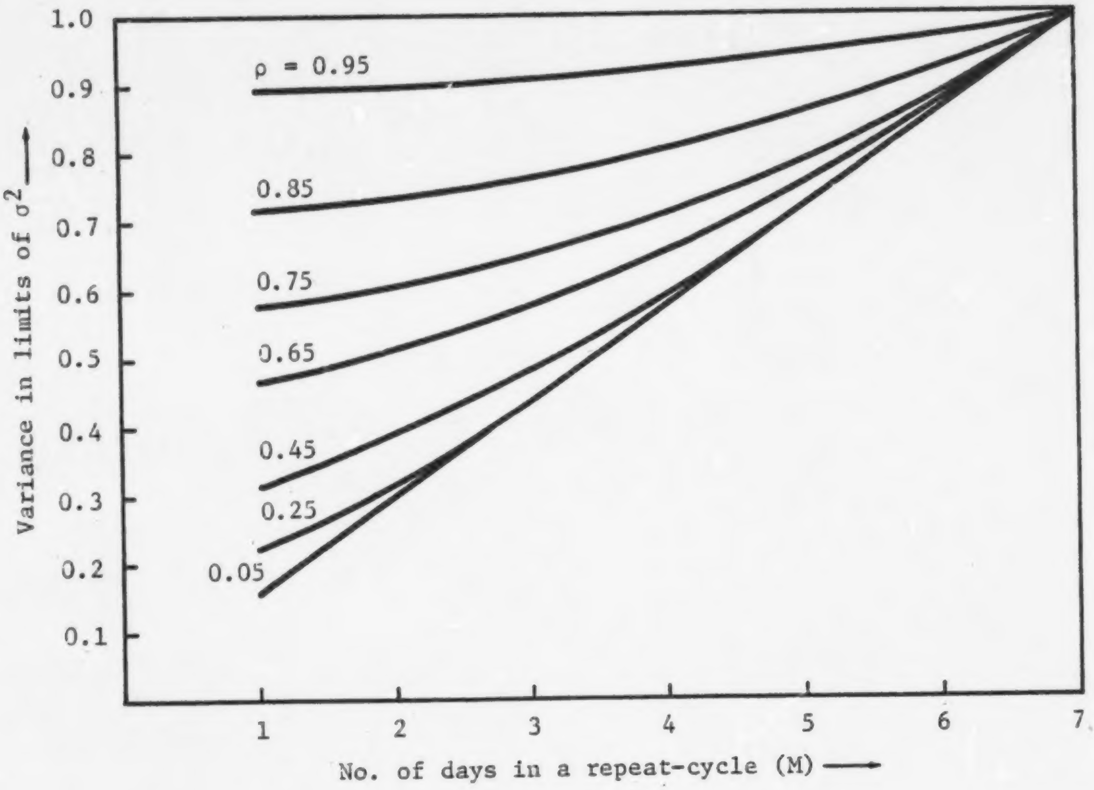

Figure 7. Errors due to sampling in a 7-day mission.

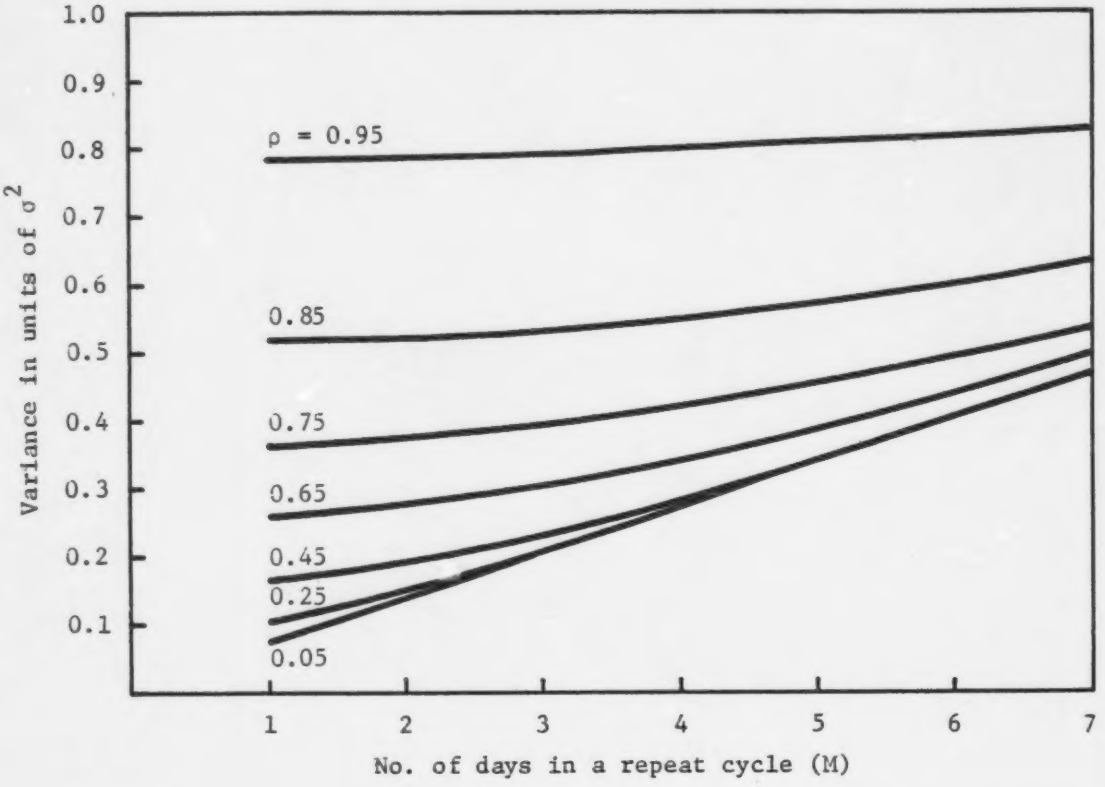

Figure 8. Errors due to sampling in a 15-day mission.

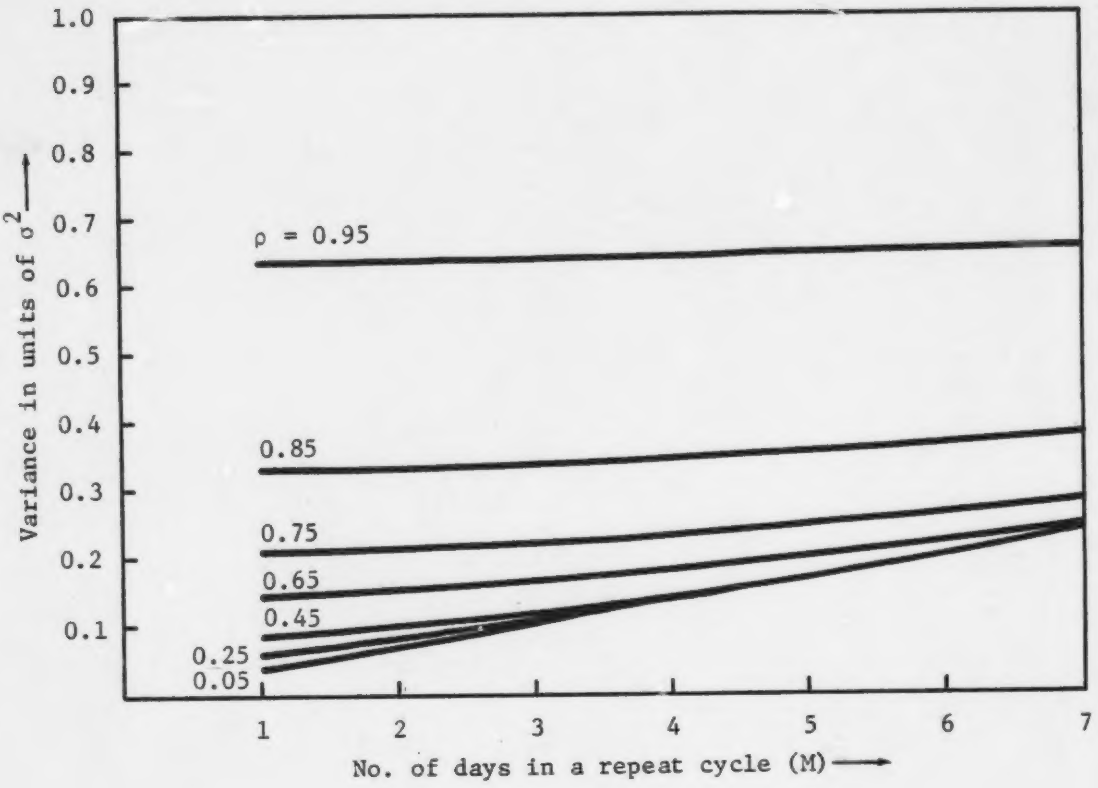

Figure 9. Errors due to sampling in a 30-day mission.

TABLE 1. USERS AND NEEDS FOR LOCAL AND REGIONAL AIR QUALITY MONITORING IN TROPOSPHERE

	BASIC NEEDS			
Principal users	Near surface sensing (local)	Regional air quality data	Predictive model inputs	Major point source emissions
U.N. organizations	X	X	X	X
Federal agencies				
EPA	X	X	X	X
AEC			X	
NOAA			X	
DOT		X	X	
HEW	X	X		
NSF		X	X	
State and local agencies				
Regulatory	X	X	X	X
Planning	X	X		
Resource	X	X	X	X
Regional air pollution control boards	X	X	X	X
Environmental consultants	X	X	X	X
Engineers and architects	X	X	X	X
Research and scientific investigators	X	X	X	X
Medical and nursing professions	X	X		X
Public-interest groups	X	X		X
Industrials	X	X	X	X
News media	X	X	X	X

TABLE 2. SPECIES RECOMMENDED OR ACTUALLY MEASURED IN VARIOUS REGIONAL STUDIES

Species	NAS		SURE		SRI		RAMS/RAPS		LARPP		EPA/OXIDANT		BATTELLE	
	Recommended	Accuracy	Recommended	Accuracy	Recommended	Accuracy	Measured	Accuracy	Measured	Accuracy	Measured	Accuracy	Measured	Accuracy
Carbon monoxide (CO)	X	10 ppb			X	10 ppb	X	NS	X	NS			X	NS
Formaldehyde (H_2CO)	X	1 ppb			X	1 ppb								
Halogens	X	1 ppb												
Ammonia (NH_3)	X	10 ppb	X	NS*	X	10 ppb								
Sulfur dioxide (SO_2)	X	10 ppb	X	NS	X	10 ppb	X	NS	X	NS				
Hydrogen sulfide (H_2S)	X	0.1 ppb	X	NS			X	NS						
Nitrogen oxides (NO_x)	X	10 ppb							X	NS	X	NS	X	NS
Peroxyacetyl nitrates (PAN)	X	10 ppb												
Hydrocarbons	X	1 ppb			X	est 1 ppb	X	NS	X	NS	X	NS		
Ozone (O_3)	X	10 ppb	X	NS	X	10 ppb	X	NS	X	NS	X	NS	X	NS
Mercury (Hg)	X	10^{2} ppb												
Nitric oxide (NO)			X	NS			X	NS	X	NS	X	NS	X	NS
Nitrogen dioxide (NO_2)			X	NS							X	NS	X	NS
Aerosols or particulates			X	NS			X	NS	X	NS				
Methane (CH_4)					X	0.5 ppm	X	NS			X	NS	X	NS
Hydrogen chloride (HCl)					X	0.5-1 ppm								
Nonmethane hydrocarbon (NMHC)									X	NS	X	NS	X	NS
Total sulfur (S)							X	NS						
Acetylene (C_2H_2)											X	NS	X	NS
Ethylene (C_2H_4)													X	NS
Ethane (C_2H_6)													X	NS
Fluorocarbon-11 (CC_3F)													X	NS
Carbon tetrachloride (CCl_4)													X	NS

*NS: Not stated.

TABLE 3. REGIONAL MEASUREMENTS REQUIRED

	Estimated accuracy	Urban plume*	Power plant plume
Carbon monoxide	10 ppb	x	
Ammonia	10 ppb	x	x
Sulfur dioxide	10 ppb	x	x
Hydrogen sulfide	0.1 ppb	x	x
Nitrogen oxides	10 ppb	x	x
Nitric oxide	10 ppb	x	x
Nitrogen dioxide	10 ppb	x	x
Total hydrocarbon	1 ppb	x	
Methane	0.5 ppm	x	
Acetylene	0.05 ppb	x	
Ozone	10 ppb	x	x
Aerosols or particulates	25 $\mu g/m^3$	x	x
Sulfates	0.5 $\mu g/m^3$	x	x
Surface and vertical temperature	2° C	x	x
Surface and vertical humidity	10%	x	x
Surface wind velocity	10°; 2 mps	x	x
Vertical profile of wind	10°; 2 mps	x	x

*It is assumed that the urban plume contains one or more power plant plumes.

TABLE 4. RECOMMENDED HORIZONTAL GRID SPACING

Distance from source	Type of monitoring		
	General regulatory	Urban plume scientific	Power plant scientific
25 m	25-100 km	5-10 km	1-5 km
25-50 km	25-100 km	10-25 km	5-10 km
50 km	50-100 km	25-50 km	10-25 km

TABLE 5. RECOMMENDED VERTICAL GRID SPACING

Parameters	General regulatory	Urban plume scientific	Power plant scientific
Pollutants only	1-4 levels*	5-10 levels*	5-10 levels†
Nonsurface weather	Use NWS data	15-25 levels, surface to 1 km above mixing layer	15-25 levels, surface to 2 km

*Decreasing logarithmically to 1 km above mixing layer.
†Poisson distribution starting at surface with maximum at plume level.

TABLE 6. REGIONAL TEMPORAL MEASUREMENT REQUIREMENTS

	Type of monitoring	
Parameters	General regulatory	Urban plume or power plant scientific
Pollutants and surface meteorology	1 to 4 per day	6 to 24 per day
Upper air meteorology	Use NWS data	4 to 12 per day

TABLE 7. INTERFERENTS AND ANTICIPATED SIGNAL-TO-NOISE RATIOS [S/N] FOR CIMATS MEASUREMENTS [10]

Channel	Species	Assumed background	Center wavelength (μm)	Interferents	S/N
A	CO	0.1 ppm	2.33	CH^4, H^2O	20:1
A	CH_4	1.5 ppm	2.33	CO_2, H_2O	40:1
A	N_2O	0.2 ppm	2.27	CH_4, NH_3 CO_2, H_2O	10:1
A	NH_3	1.0 ppb	2.23	CH_4, H_2O	2:1
B*	CO	0.1 ppm	4.62	CO_2, H_2O	2:1
B*	N_2O	0.2 ppm	4.62	CO_2, H_2O	2:1
B*	SO_2	2.0 ppb	8.70	CH_4, N_2O O_3, H_2O	Not available

*S/N ratios of thermal channel are based on the assumption of no independent measurement of temperature profile of the atmosphere. Availability of such measurements will increase S/N ratios.

TABLE 8. SUITABILITY OF REMOTE SENSORS FOR REGIONAL MONITORING

Instrument	Typical regional use				Species monitored	Operational mode			Period of operation	
	Urban plume	Power plant plume	Power plant close in	Not suited		Airborne	Ground-based	Satellite	Day	Night
SR&T/MAPS	X				CO	X		X	X	X
TRW/MAPS	X				CO, CH_4	X		X	X	X
TRW/MAPS		X			NH_3	X		X	X	X
COPE	X				CO, CH_4	X			X	
CIMATS (visible)	X 	 X			CO, N_2O, CH_4 NH_3	X X		X X	X X	
CIMATS (IR)	X				CO, N_2O	X		X	X	X
CIMATS (IR)	X	X			SO_2	X		X	X	X
DARS	X				O_3	X			X	X
DIAL			X		SO_2		X		X	X
Westinghouse IR LIDAR	X	X			HCl, CH_4, HC	X	X		X	X
IHS (solar)				X	O_3, NH_3		X		X	
IHS (nadir)	X				O_3	X			X	X
IHS (nadir)		X			NH_3	X			X	X
Ruby Laser			X		Particulate		X		X	X
UV Videcon			X		SO_2		X		X	
Videcon			X		Particulate, NO_2		X		X	

*The current version of the instrument is not engineered for this measurement.

TABLE 9. SUMMARY OF SPECIFIC INSTRUMENT LIMITATIONS AND CAPABILITIES

	Sensor limitations					Auxiliary data		Vertical measurement capability			Surface measurement capability		
	High sun angle required	Cloudless line of sight required	Minimum of aerosols required	Uniform background desirable	Vertical sensitivity important	Temperature profile required	Water vapor profile required	Column content only	Limited ranging or profile	Precise ranging or profile	No practical capability	Requires assumed mixing ratio profile	Measures layer near surface
SR&T/MAPS		X		X	X	X	X	X				X	
TRW/MAPS		X		X	X	X	X	X				X	
COPE	X	X		X	X			X				X	
CIMATS (visible)	X	X		X	X			X				X	
CIMATS (IR)		X		X	X	X	X	X				X	
DARS		X	X			X			X				X
DIAL		X								X	X		
Westinghouse IR LIDAR		X							X				X
IHS (nadir)		X		X	X	X		X			X		
Ruby Laser		X	X							X	X		
UV Videcon	X	X						X			X		
Videcon		X						X			X		

TABLE 10. ORBIT DATA

Altitude (km)	Inclination (°)	Repetition factor	Repeat cycle (days)	Nodal movement per orbit	Orbits per repeat cycle
492	45	15.00	1	24	15
349	56	15.50	2	23.23	31
399	56	15.33	3	23.48	46
277	57	15.75	4	22.86	63
245	57	15.86	7	22.70	111

TABLE 11. CARBON MONOXIDE POLLUTION DATA FOR A TYPICAL URBAN LOCATION (FOR AUGUST 1974 AT GREENPOINT AVENUE, NEW YORK, NEW YORK)

Averaging period (days)	Mean* (ppm)	Standard deviation (ppm)	Correlation
7	3.36	1.20	0.46
15	3.34	1.19	0.45
30	3.35	1.20	0.45

TABLE 12. PERCENT SAMPLING UNCERTAINTY IN NEW YORK AS A FUNCTION OF DAYS PER REPEAT CYCLE (INCLUDING 50 PERCENT CHANCE OF CLOUDINESS)

	Percent error*		
	Mission duration (days)		
Repeat cycle (days)	7	15	30
1	20.14	14.25	10.22
2	25.16	17.41	12.38
3	30.32	20.79	14.73
4	35.77	23.91	16.92
5	35.77	26.72	18.89
6	35.77	29.26	20.69
7	35.77	31.61	22.35

*Equal to $\sqrt{\frac{\text{VAR}(\hat{\mu})}{\hat{\mu}} \times 100}$

TABLE 13. TOTAL UNCERTAINTY (IN PERCENT) IN POLLUTION ESTIMATES ASSUMING 50 PERCENT CHANCE OF CLOUD COVER AND 50 PERCENT UNCERTAINTY IN INDIVIDUAL POLLUTION ESTIMATES

	Mission duration (days)		
Repeat cycle (days)	7	15	30
1	27.9	19.4	13.8
2	37.1	25.5	18.1
3	45.1	30.9	21.8
4	52.6	35.6	25.2
5	56.0	39.8	28.1
6	59.2	43.5	30.8
7	62.3	47.0	33.3

CHARACTERIZATION OF REGIONAL SULFATE/OXIDANT EPISODES IN THE EASTERN UNITED STATES AND CANADA

E. Y. Tong*, M. T. Mills, B. L. Niemann*
Teknekron, Inc., Waltham, Massachusetts

L. F. Smith

Office of Energy, Minerals and Industry, U.S. Environmental
Protection Agency, Washington, DC

Abstract

Current national interests in developing air quality modeling and predictive procedures have resulted in several analyses and measurement programs. The test of these predictive techniques must ultimately be based on their ability to simulate field measurements. This paper contains results of synoptic sulfate/oxidant analysis to provide a regional characterization of the air quality and aerometric features over the eastern United States and Canada. This regional analysis shows evidence to support the co-occurrence of elevated concentrations of atmospheric particulate sulfates and ground-level ozone. Furthermore, it was found that these "warm episodes" are not only related to the trajectories of the polluted air parcels, but also to certain easily identifiable synoptic features at the surface and aloft. The most outstanding episode is related to the eastward movement of occluded frontal systems and the circulation around the Bermuda High. Within this warm and humid sector, recirculation may occur, resulting in high sulfate/ozone concentrations within a relatively small region. This circulation may be a subsynoptic system embedded in a subcontinental polluted air mass.

INTRODUCTION

A meaningful assessment of the extent and magnitude of regionally elevated concentrations of particulate sulfate and oxidant calls for the collection and analysis of large volumes of data from public and private sources. Under the aegis of the EPA Office of Research and Development, Teknekron, Inc., has compiled a relatively large aerometric data archive, on which this report is based. The primary objective is to characterize the synoptic and aerometric features of the interstate and regional occurrence of elevated ground-level concentration of particulate sulfate ($SO_4^=$) and ambient ozone (O_3). The results of the analysis should provide a basis for the development and evaluation of regional air quality models and other predictive methods.

---

*Speakers.

The fact that under certain meteorological conditions $SO_4^=$ and O_3 are co-occurring aerometric parameters in the industrial eastern United States and Canada has been demonstrated by several investigators. Vukovich et al.[1] showed the relationship between elevated O_3 concentrations and the presence and movement of anticyclones. They identified the back side of high-pressure systems as a region most conducive to the occurrence of high O_3 levels (i.e., contravention of the 0.08 ppm standard), particularly for those air masses that have a relatively long residence time over the industrialized source regions. These synoptic conditions are nearly identical to the intrusion of warm and moist maritime tropical air from the Gulf of Mexico, conditions found by Tong et al.[2] to be most conducive for the occurrence of $SO_4^=$ levels exceeding, say, 20 $\mu g/m^3$. Tong and Niemann,[3] in their examination of regional transport over the Ohio River Valley, have shown the close correspondence between regional $SO_4^=$ and O_3 episodes that were often related to an occluded system moving from west to east over the Great Lakes. The presence of a more or less stagnant west-east front located along the Canadian border area and the westward intrusion of the Bermuda High is another configuration that gives rise to regional excursions of $SO_4^=$ levels in the Midwest and Northeast. Chung[4] and Chung and Melo[5] have largely confirmed these findings over Ontario, Canada. In addition, Wolff et al.,[6] Samson,[7] Lioy and Samson,[8] and others have demonstrated, using the Moodus[8] data, the eastward and north-eastward transport of O_3 from the source or accumulation regions following the movement of a generally eastward-moving anticyclone.

The analysis presented in this paper is directed at an examination of data covering a period of 3 years--1975, 1976, and 1977--over the entire eastern United States and the industrialized portions of eastern Canada. The approach involves scanning both the $SO_4^=$ and O_3 data by means of an episode retrieval program and then selecting suitable (in terms of data coverage) cases for detailed aerometric analysis. Supplemental data such as the routine radiosonde soundings and an enhanced satellite photograph were used whenever possible.

EPISODE TALLY AND CASE SELECTION

The episode retrieval program is designed to scan the air quality data archive and tally the number of monitoring stations that reported a concentration greater than a designated threshold for each day of the month. The program also gives the percentage of stations reporting on a given day to facilitate case selection. Tables I, II, and III present the O_3 episode tallies for each of the 3 years. In this analysis, the 1:00 p.m. EST O_3 concentrations were used. The entries in these tables show the number of stations that exceeded the indicated threshold values, and the percentage of stations reporting on that day. For example, on July 16, 1977, a total of 114 out of 238 stations reported O_3 concentrations exceeding 0.08 ppm. A similar episode retrieval was performed for the $SO_4^=$ data from the National Aerometric Sampling Network (NASN).

Examination of the O_3 episode selection results for the 3 years shows the well-known photochemical phenomenon of a summer O_3 peak. During the period from April through September of 1977 (Table III), area-wide contravention of the 0.08-ppm level was almost a daily occurrence. The July 16, 1977, episode, for example, was quite extensive spatially with 30 stations exceeding 0.14 ppm. In fact, this episode lasted for 6 days from July 16 through July 21. Regional sulfate data for case analysis are available for July 18, 1977. Unfortunately, the 6-day and 12-day $SO_4^=$ sampling frequency makes it impossible to examine the regional distribution of $SO_4^=$ concentrations corresponding to the peak O_3 day (July 16).

The retrieval exercise for the $SO_4^=$ data used a threshold value of 25 $\mu g/m^3$, 24-hr average. This screening resulted in the identification of nine regional episodes that are candidates for case analysis. These cases are summarized in Table IV with a brief description of the synoptic situation. An additional O_3 case, which was analyzed by Wolff et al.[6] and reanalyzed by Tong and Niemann,[3] will also be examined to show the influence of the occluded system. Presented below are three cases selected on the basis of the co-occurrence of $SO_4^=/O_3$ episodes: April 12-24, 1976; August 20-22, 1976; and July 16-21, 1977.

TIME SERIES ANALYSIS

It is of interest to show the regional characteristics of O_3 episodes and their day-to-day development by means of a modified time-series plot. Figures 1, 2, and 3 are the time/regionality plots for April 1976, August 1976, and July 1977, respectively. The number of stations exceeding the threshold value has been normalized by the ratio of the percentage of the total reporting stations to the average percentage of stations reporting during the period of interest.

Examination of Figures 1, 2, and 3 and Tables I, II, and III shows that the variation of regional O_3 levels was more or less cyclic during the warm months of the year. This cyclic characteristic is most likely a response to the changes of synoptic systems as they migrate across the eastern United States and Canada. This has been demonstrated to some extent by Lioy and Samson[8] in their tracking of anticyclones in conjunction with the analysis of the Moodus O_3 data. Also given in Figures 1, 2, and 3 are the daily air mass classifications for the Ohio Valley. These provide a rough indication of the degree of moisture and heat intrusion. In addition, periods of stagnation based on Korshover's classification scheme are also indicated in Figures 1, 2, and 3 by horizontal arrows.

It is seen from the monthly plots in the figures that the synoptic meteorological features exhibited certain identifiable macroscale characteristics. First, days with regionally elevated O_3 levels were, almost without exception, associated with the back side of anticyclonic circulations over the study region. These anticyclones originated in the interior of Canada and moved eastward or southeastward into the eastern United States. An example of this type of activity is the April 1976 case. During the summer months, the advance and retreat of the semipermanent Bermuda High became the dominant factor. In either case, the southerly and southwesterly flow on the western side of the anticyclone was frequently the same in terms of the direction of pollutant or precursor transport. In all cases, as shown in the figures, the peak O_3 days were largely associated with maritime tropical air masses originating over tropical or subtropical waters.

Second, the correspondence of stagnation periods over the source region (the Midwest) with the regional O_3 peaks strongly supports the findings of

Vukovich,[1] Lioy and Samson,[8] and others, that the onset of O_3 episodes is often preceded by a day or more of accumulation of O_3 precursors. Presumably the presence of the fair weather anticyclone would promote photochemical generation of O_3 leading to peak O_3 levels toward the end of the stagnation period. The decline of the O_3 episodes is often the result of frontal passage, which is followed by the replacement of the polluted air mass by a fresh polar continental air mass.

CASE STUDIES

The analysis presented above leads naturally to a review of the regional sulfate distributions analyzed by Hidy et al.[10] and Tong and Batchelder[11] during the past year. The cases selected are:

Case 1--April 18, 1976, corresponding to the peak O_3 day;

Case 2--August 22, 1976, one day after the peak O_3 day; and

Case 3--July 18, 1977, two days after the peak O_3 day.

What is of interest, in addition to the "indirect" analysis discussed above, is to examine the spatial distribution of all relevant parameters in the traditional synoptic manner. This direct analysis for the actual episodes of interest may be performed by mapping both the O_3 and $SO_4^=$ data, along with other relevant variables. The case analyses presented below provide this detailed spatial examination.

Case 1--April 12-24, 1976

The O_3 episode in Case 1 was originally presented by Wolff et al.[12] who showed the eastward movement of the O_3 isopleth pattern. The tracking began on April 12 when a small closed area of O_3 >0.08 ppm was observed over Ohio. This high O_3 area expanded progressively as it moved eastward within the warm sector of the occluded frontal system. Its size reached a peak on April 18, covering a large region on the Atlantic seaboard. On that day (see Figure 4), the area of O_3 >0.08 ppm extended from southern New Hampshire and Vermont to the southern Virginia border, then westward to cover West Virginia, Pennsylvania, and part of New York State. Partial dissipation of this regional pattern occurred when a cold front advanced southeastward, became occluded, and then moved northward again. O_3 levels in the warm sector remained high; e.g., O_3 was greater than 0.06 ppm in the warm sector, but was less than half that value north of the warm front. During the peak day on April 18, the backward trajectories (see Wolff et al.[12]) showed directions generally from the west and southwest, in accordance with the systematic macroscale translation of the occluded system.

On April 18, the $SO_4^=$ pattern was almost identical to the O_3 pattern in that the area of maximum $SO_4^=$ coincided with that for O_3 (see Figure 4). The 50-$\mu g/m^3$ $SO_4^=$ isopleth encompassed almost exactly the same region of O_3 >0.08 ppm. The relative magnitudes of $SO_4^=$ concentration, with respect to the position of the warm sector, showed the same variation as for O_3, as shown in Tong and Niemann[3]. Sulfate concentrations were available from five stations around Boston on April 12, 18, and 24. The five-station averages for each of the 3 days show that, before the onset and after the decline of the episode, the $SO_4^=$ levels are generally around 10 $\mu g/m^3$. During the peak day of this episode, the $SO_4^=$ level exceeded 25 $\mu g/m^3$ in Boston.

Case 2--August 18-23, 1976

The August 1976 case is an interesting episode in that it represents a stagnation situation in which there is strong evidence of recirculation of the pollutants within a relatively small region in eastern Ohio and western Pennsylvania. In addition, it shows evidence of long-distance transport of pollutants into western Tennessee and Arkansas from areas to the east. For these reasons, this case is examined in considerable detail. The analysis focuses on the day before, during, and after the date for which the $SO_4^=$ map has been constructed on the basis of AQCR averages. Unfortunately, $SO_4^=$ data for August 22 were available only for the midwestern States, southern Ontario and some of the northeastern States.

The synoptic patterns during August 21, 22, and 23 are summarized in Figure 5, showing positions of fronts and pressure centers, with the dates indicated. During the several days preceding and during this episode, the synoptic meteorology may be characterized by air stagnation with passage of minor weak fronts. There was no significant movement of the high-pressure center just south of Lake Erie during August 21 and 22. The entire eastern United States was dominated by high pressure with a weak gradient. A weak low-pressure center was present on the southern Atlantic Coast from August 19 through August 24.

The O_3 episode began on August 18 with 38 of the monitoring stations exceeding the 0.08 ppm level. This number grew and reached a peak of 117 on August 21 and then declined to 99 on the following day. The region (see Figure 6) encompassing the western half of Lake Erie, northern Ohio, the northeastern corner of Indiana, southeastern Michigan, and southwestern Ontario reported O_3 levels consistently greater than 0.14 ppm on August 21, 22, and 23. Most of the northeastern quadrant of the United States and southern Ontario was within the region of contravention (>0.08 ppm) during these 3 days. The decline of the regional peak came on August 23 and 24 with the passage of a weak cold front that advanced from the northwest. The region of high O_3 began to diminish in size as the stagnation dissipated with the frontal passage. The regional pattern did not disappear entirely because on August 25 the eastern United States was again dominated by an anticyclone centered over eastern Pennsylvania. Light but persistent moisture and heat advection from the south and southwest continued through August 28.

As shown in Figure 6, the $SO_4^=$ distribution for August 22 is a typical prefrontal pattern with the cold front situated in the northeast-southwest direction over the Great Lakes. Highest $SO_4^=$ was observed over the Detroit-Windsor-Cleveland-Toledo region coinciding almost exactly with the persistent regional O_3 peak mentioned above but not shown in Figure 6. Again the area within the 20-$\mu g/m^3$ $SO_4^=$ isopleth is also coincident with the O_3 pattern as shown by the large shaded area in Figure 6. This area extended roughly from the eastern half of Indiana to the New England coast.

The persistence of the O_3 pattern and the stagnation of the high-pressure center during this episode led to an examination of visibility patterns and air parcel trajectories. These patterns are shown in Figure 7 for August 22. Two visual range isopleths are plotted, one enclosing airport visibility values between 3 and 4 miles; and another for the interval of 4 to 6 miles. The general correspondence between the latter isopleth and the $SO_4^=/O_3$ pattern described above is quite evident. Of interest is the small closed area of visibility less than 4 miles over the regional $SO_4^=/O_3$ peak (Detroit-Windsor-Cleveland-Toledo) on this day. Furthermore, an enhanced satellite photograph was made available by Lyons[13] who was able to delineate the boundary of the haze layer adjacent to the ground surface. The location of this boundary is roughly shown in Figure 5, showing the possible subcontinental extent of the polluted air mass on this day. In view of the persistence of the O_3 pattern, it may be speculated that this subcontinental haze layer may also have persisted for at least 3 days.

In an attempt to infer the source-receptor relationships for this day, selected air parcel trajectories were constructed and shown in Figure 7. Two interesting results should be noted. First, around the anticyclone that persisted for 2 days just south of Lake Erie, there was a recirculation of the polluted air for 3 days beginning on August 20. Pollutants emitted in the vicinity of the Ohio-Pennsylvania border moved slowly westward into Ohio, curved northward into southeastern Michigan, and then returned to Pennsylvania via southwestern parts of Ontario. This case is somewhat extraordinary due to the long-distance circular transport that resulted in equally persistent high $SO_4^=/O_3$ levels in the western Lake Erie multi-city complex.

The second point of interest is the trajectories originating in south-central Tennessee. In their previous analysis, the authors had observed occasional $SO_4^=$ "hot spots" over western Tennessee and Arkansas. Perhaps because that region is only in the periphery of major source regions, namely the Ohio Valley and the Tennessee Valley, no detailed analysis was made of these excursions. On the basis of Figure 7, however, it appears that the westerly transport of pollutants emitted in Tennessee and northern Alabama contributed to the high O_3 observed along the Tennessee-Arkansas border (see Figure 6). Reisinger and Crawford,[14] in their detailed analysis of three August 1976 episodes, reported a peak $SO_4^=$ concentration of 32 $\mu g/m^3$ at Blytherville, Arkansas, confirming the consistency of these observations and the correspondence between regionally elevated $SO_4^=$ and O_3 concentrations.

Case 3--July 12-21, 1977

Case 3 is a regional O_3 episode that was first analyzed by Wolff and Lioy.[12] This episode was associated with a prolonged stagnant air mass covering the entire eastern half of the United States, with persistent hot and humid conditions lasting for more than 9 days. This period was termed by Wolff and Lioy[12] a heat wave; and the transport was said to take place in an "ozone river" that ran from the Texas Coast to the Washington-Boston corridor. While the existence of this idealized "river" remains to be verified, the transport of pollutant toward the northeast from the mid-South region appears to be a macroscale feature of the general flow. It is of interest at this point to focus on the aerometric conditions during the 3-day period, July 16, 17, and 18.

The synoptic conditions during this period, aside from the presence of the generally stagnant air mass, are a broad pressure gradient throughout the region, and the presence of a stationary front over the midwestern States as shown in Figure 8. This stationary front delineated the two contrasting air masses: maritime tropical to the south and polar air to the north. There was a fairly broad transitional zone along the front that fluctuated somewhat in the north-south direction. These conditions were not broken until 4 days later on July 22.

The peak O_3 day was July 16, on which a broad band extended from eastern Arkansas eastward to the Carolinas, thence to southern Maine as shown in Figure 9. Areas in which O_3 exceeded 0.14 ppm were situated over the junction of Tennessee, Alabama, and Georgia; over the northern Delmarva Pennisula; and over southern New England. The fact that this broad band was deflected southward was due primarily to the position of the stationary front. On the next day, July 17, the pattern had diminished in size and O_3 concentrations were generally lower. The area of O_3 greater than 0.14 ppm remained in only southern Connecticut.

On July 18 (see Figure 10), a day when regional $SO_4^=$ data were available, the stationary front became somewhat less defined. The O_3 pattern moved northward into the Midwest, with two areas exceeding 0.10 ppm, one located in Indiana and Ohio, and another over central Tennessee and Kentucky. The $SO_4^=$ pattern over the Midwest is nearly identical to the O_3 pattern. Sulfate concentrations of 40 and 50 $\mu g/m^3$ coincided with the O_3 peak in Indiana and Ohio. Southern Ontario showed relatively low levels of $SO_4^=$ (and probably O_3, also) during these days due primarily to the frontal barrier along the border.

DISCUSSION

The compilation and analysis of $SO_4^=/O_3$ episodes are continuing to further characterize the corresponding regional aerometric features. Examination of these case studies and others not yet published (see Table IV) leads to the following conclusions:

1. The co-occurrence of $SO_4^=/O_3$ episodes is primarily a warm and fair weather phenomenon, in which photochemical activities are thought to be much enhanced.
2. Pollutants such as $SO_4^=$ and O_3 and/or their precursors are transported by the eastward translation of an occluded system, circulations around the backside of an anticyclone, and circular advection around small and persistent high-pressure centers.
3. Episodes in western Tennessee and Arkansas may occasionally be due to advection of pollutants and/or precursors from sources in the Tennessee Valley.
4. Frontal positions are good macroscale markers delineating the boundaries of $SO_4^=$ and O_3 episodes.
5. Since regional $SO_4^=/O_3$ episodes are primarily a fair-weather occurrence, the haze layer formed by these pollutants can be detected by satellite imagery.
6. The spatial extent of $SO_4^=/O_3$ episodes may on occasion be subcontinental in scale, which would require interstate and international action for control.

ACKNOWLEDGMENT

The authors acknowledge with thanks the data processing and technical assistance provided by Mr. David Hergert, Dr. Alan Hirata, and Ms. Anne Mazzarelli of Teknekron. This work was sponsored by the U.S. Environmental Protection Agency under Contract Number 68-01-1921.

REFERENCES

1. Vukovich, F. M., et al. On the Relationship Between High Ozone in the Rural Surface Layer and High Pressure Systems. Atmos. Environ., 11:967, 1977.

2. Tong, E. Y., et al. Regional and Local Aspects of Atmospheric Sulfates in the Northeast Quadrant of the United States. Proceedings, Third Symposium on Atmospheric Turbulence, Diffusion and Air Quality, American Meteorological Society, October 1976.

3. Tong, E. Y., and B. L. Niemann. Meteorological Similarities Between the Occurrence of Ambient Ozone and Particulate Sulfate Episodes. Teknekron Staff Research Memorandum, unpublished, April 1978.

4. Chung, Y. S. Ground-Level Ozone, Sulphates and Total Suspended Particulates in Canada. Proceedings, International Clean Air Conference, Brisbane, Australia, May 15-19, 1978.

5. Melo, O. T., and Y. S. Chung. Regional Air Pollution-Sulphates. Meeting of the Chemical Institute of Canada, Winnipeg, Canada, June 4-7, 1978.

6. Wolff, G. T., et al. Transport of Ozone Associated With an Air Mass. Paper presented at 70th Annual Meeting, APCA, Toronto, Canada, June 20-24, 1977.

7. Samson, P. J., and K. W. Ragland. Ozone and Visibility Reduction in the Midwest: Evidence for Large-Scale Transport. Jour. Appl. Met., 1101-1106, 1977.

8. Lioy, P. J., and P. J. Samson. Ozone Concentration Patterns Observed During the 1976-1977 Long-Range Transport Study. Paper submitted to Environment International, 1979.

9. Korshover, J. Climatology of Stagnating Anticyclones East of the Rocky Mountains, 1936-1975. NOAA Tech. Memo. ERL-ARL-55, Air Resources Laboratory, Silver Spring, Maryland, March 1976.

10. Hidy, G. M., P. K. Mueller, and E. Y. Tong. Spatial and Temporal Distributions of Airborne Sulfate in Parts of the United States. Atmos. Environment, 12:735-752, 1978.

11. Tong, E. Y., and R. B. Batchelder. Aerometric Data Compilation and Analysis for Regional Sulfate Modeling. Technical Report, Teknekron, Inc., under EPA Contract Number 68-01-1921, Berkeley, California, 1978.

12. Wolff, G. T., and P. J. Lioy. Ozone Concentration Patterns Associated With the July 1977 Eastern U.S. Heat Wave. Paper presented at 71st Meeting of APCA, Houston, Texas, June 25-30, 1978.

13. W. Lyons, Mesomet, Inc., Chicago, Illinois, private communication, 1979.

14. Reisinger, L. M., and T. L. Crawford. August 1976 Sulfate Episodes in the Tennessee Valley Region. TVA Technical Report, TVA/EP-79/04, 1979.

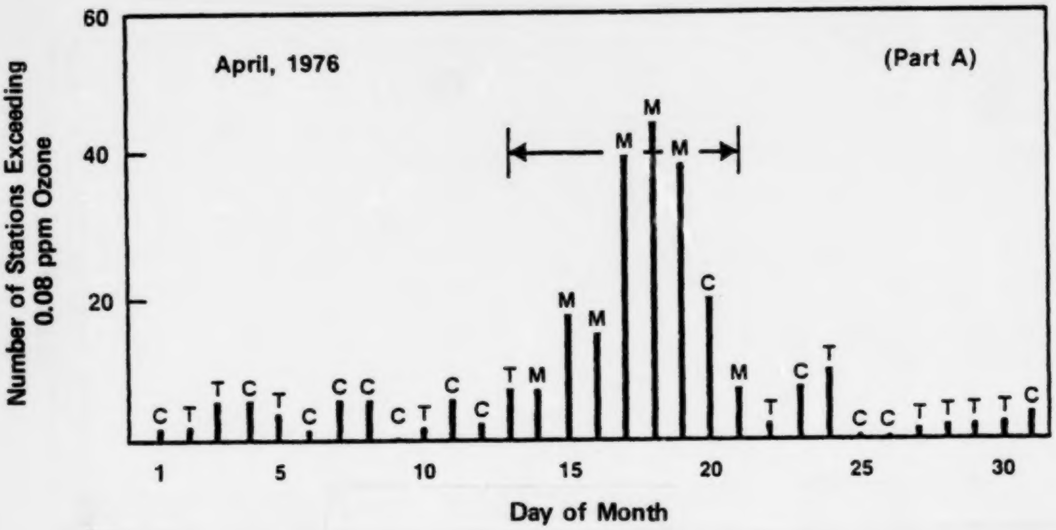

NOTE: Letters indicate the predominant air mass over the Midwest (M = maritime tropical; C = polar continental; T = transitional). Arrows indicate the periods of air stagnation based on Korshover's criteria.

Figure 1. Time-series regionality plots of ozone showing the normalized number of stations that exceeded 0.08 ppm for April 1976.

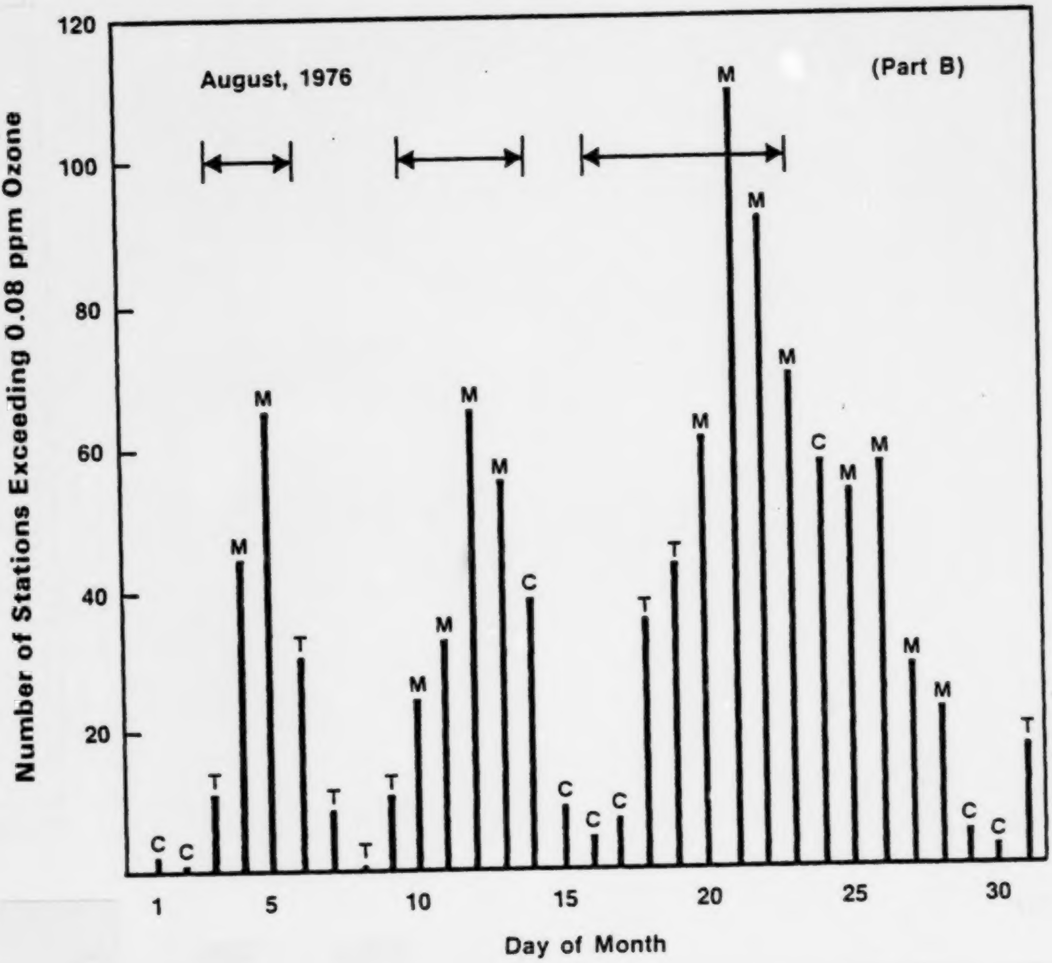

NOTE: Letters indicate the predominant air mass over the Midwest (M = maritime tropical; C = polar continental; T = transitional). Arrows indicate the periods of air stagnation based on Korshover's criteria.

Figure 2. Time-series regionality plots of ozone showing the normalized number of stations that exceeded 0.08 ppm for August 1976.

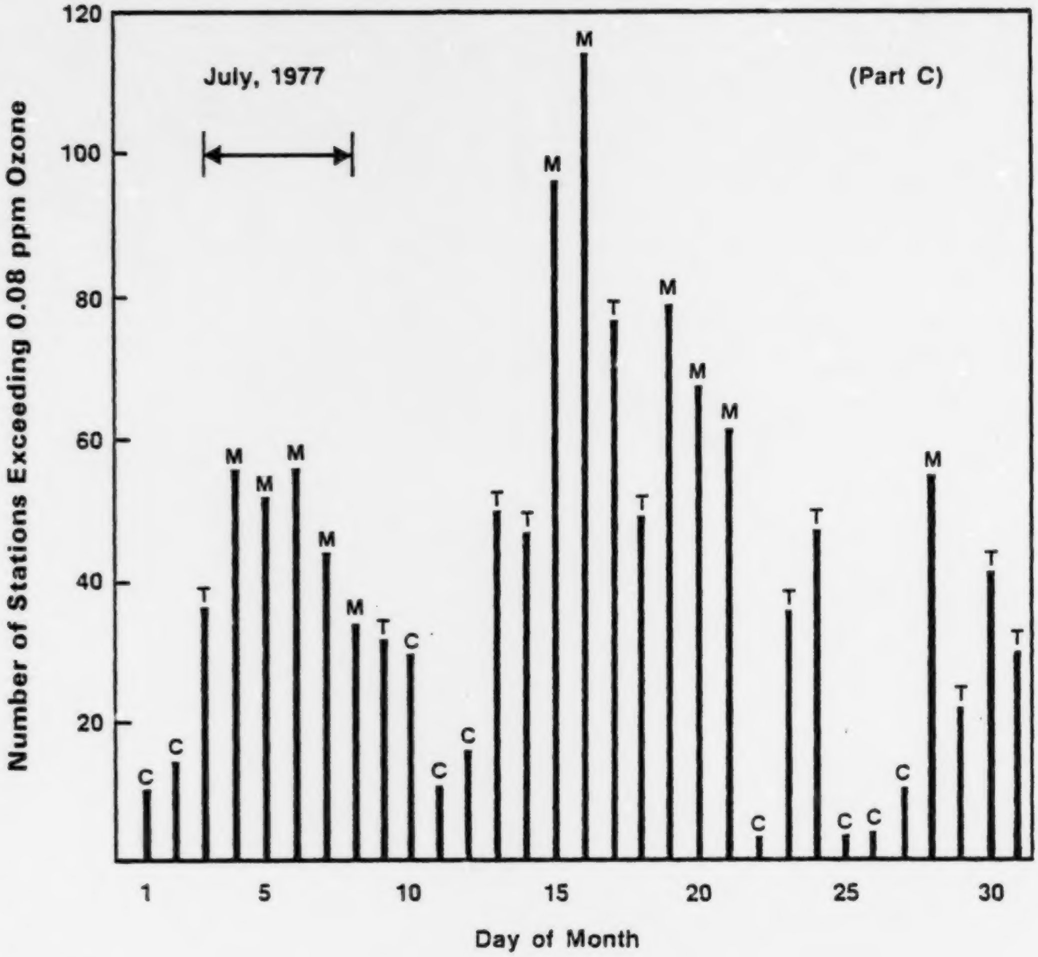

NOTE: Letters indicate the predominant air mass over the Midwest (M = maritime tropical; C = polar continental; T = transitional). Arrows indicate the periods of air stagnation based on Korshover's criteria.

Figure 3. Time-series regionality plots of ozone showing the normalized number of stations that exceeded 0.08 ppm for July 1977.

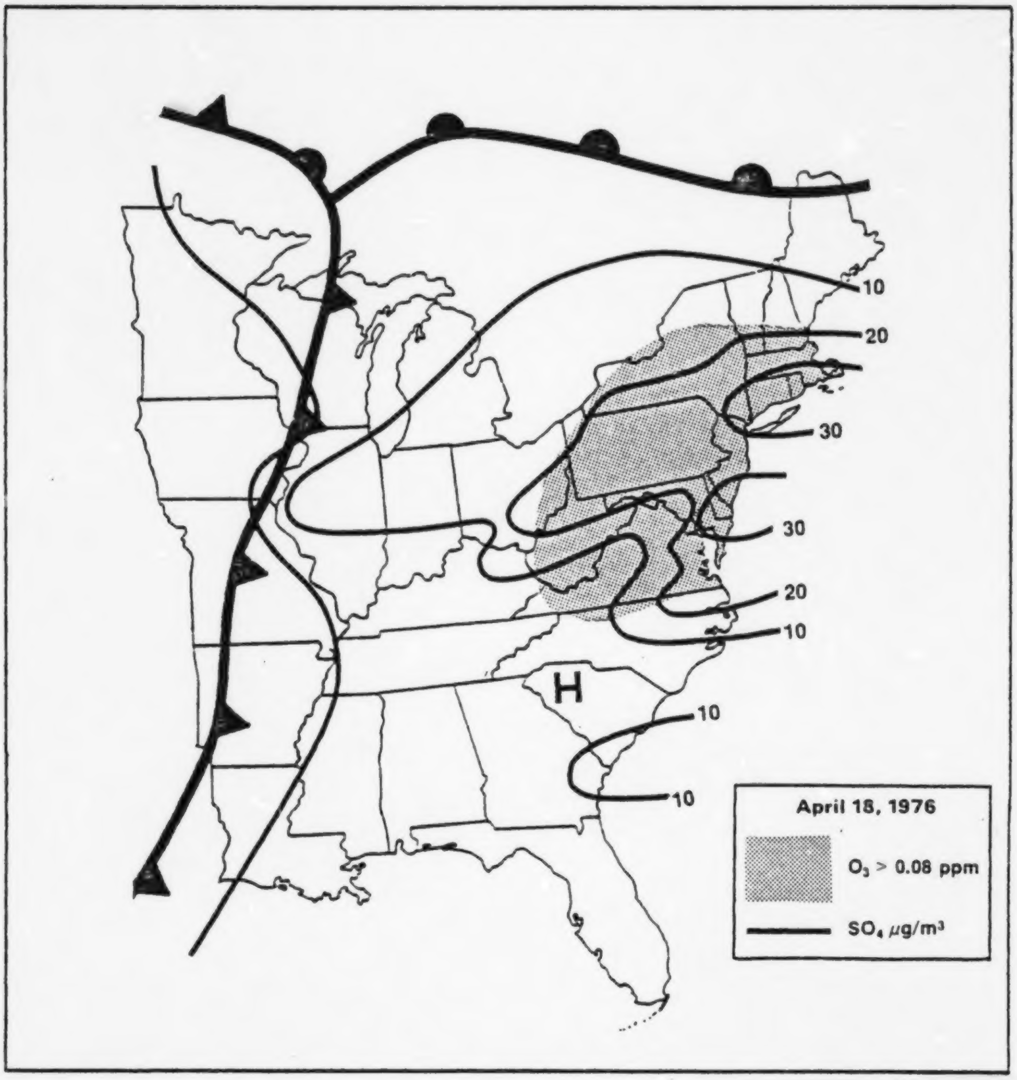

Figure 4. Aerometric summary of Case 1, April 18, 1976, showing the relationship of ozone and sulfate and pollutant confinement in an occlusion.

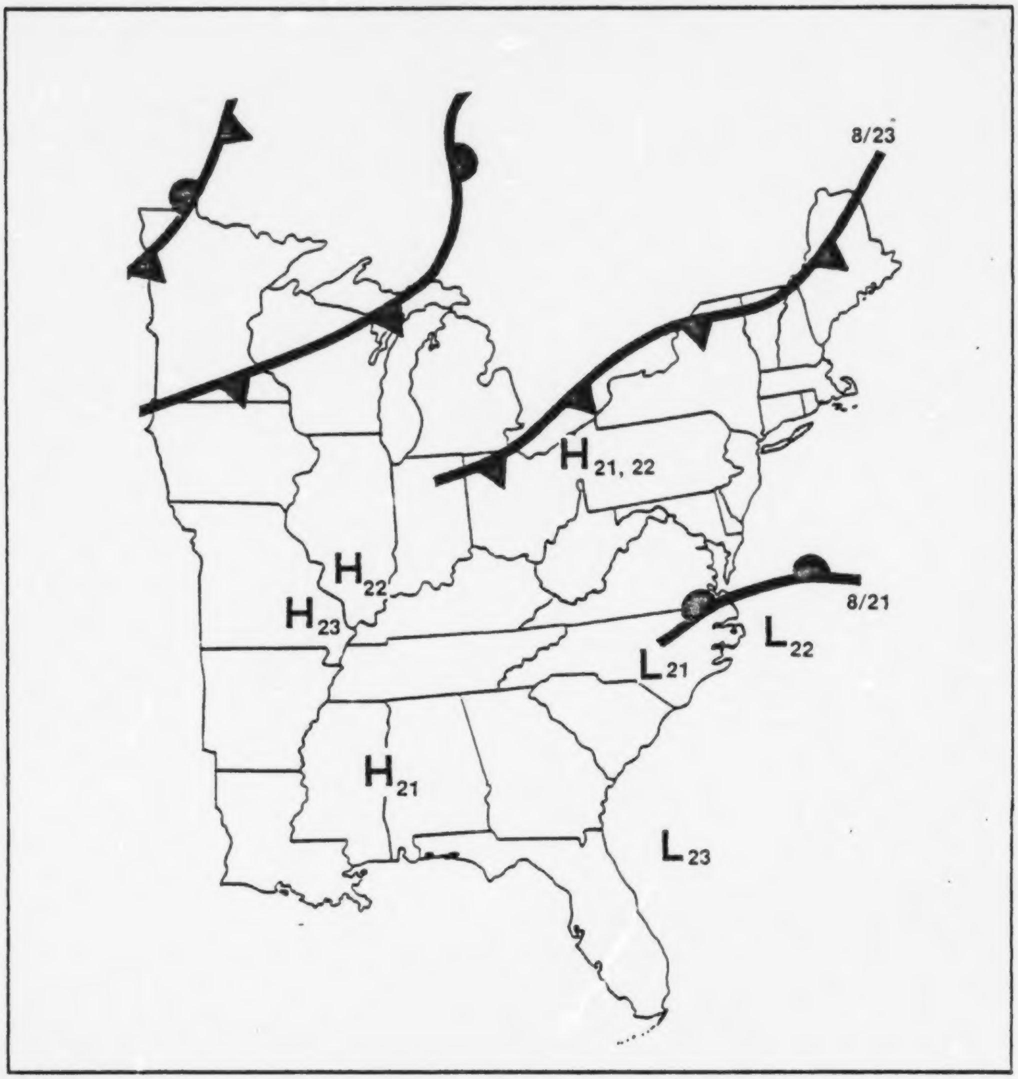

Note the persistent anticyclone just south of Lake Erie, the presence and advancement of a weak cold front, and the presence of a low-pressure center on the southern Atlantic Coast.

Figure 5. Summary of synoptic events for Case 2, August 21, 22, and 23, 1976.

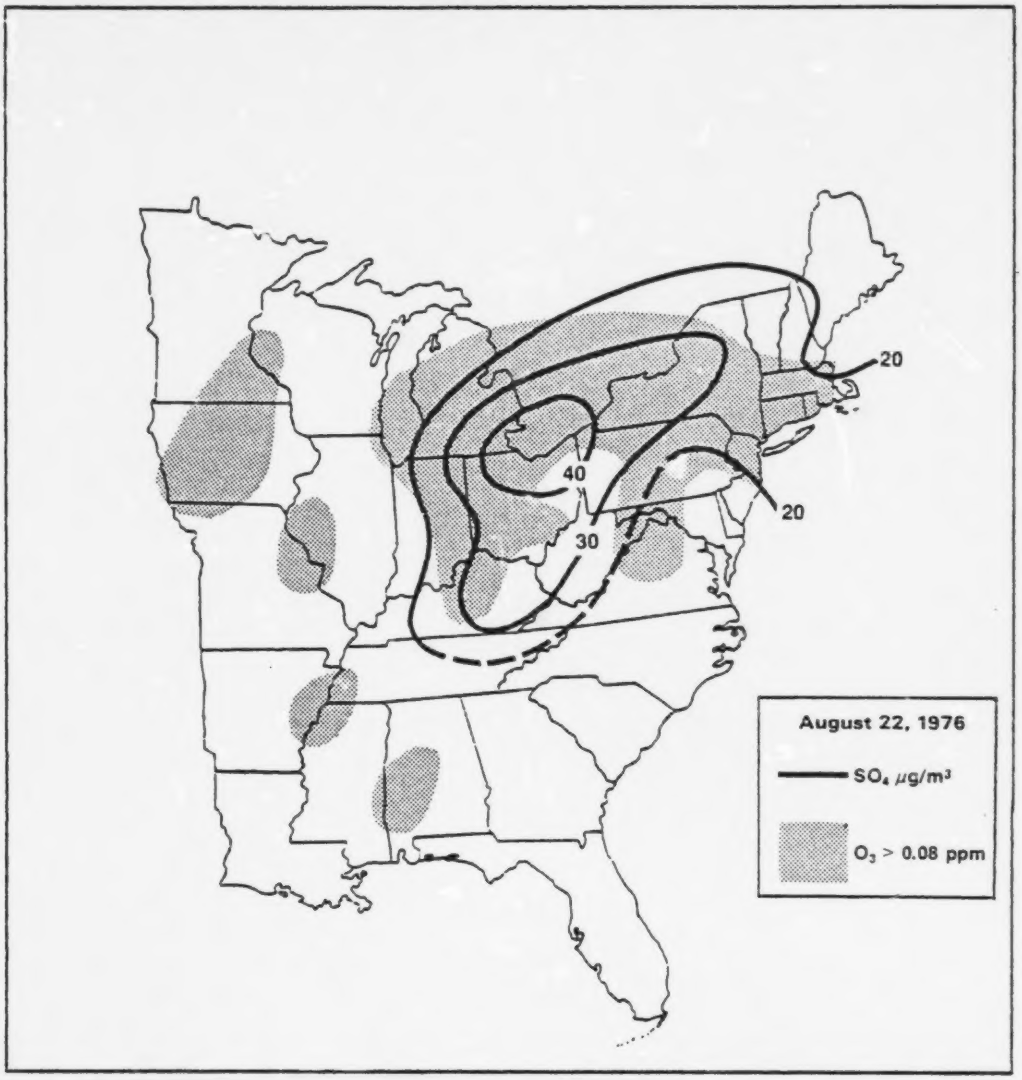

Note the correspondence of the two pollutant patterns and the area enclosed by the 40-μg/m^3 $SO_4^=$ isopleth in which O_3 concentrations exceeded 0.14 ppm.

Figure 6. Spatial distribution of sulfate and ozone for August 22, 1976.

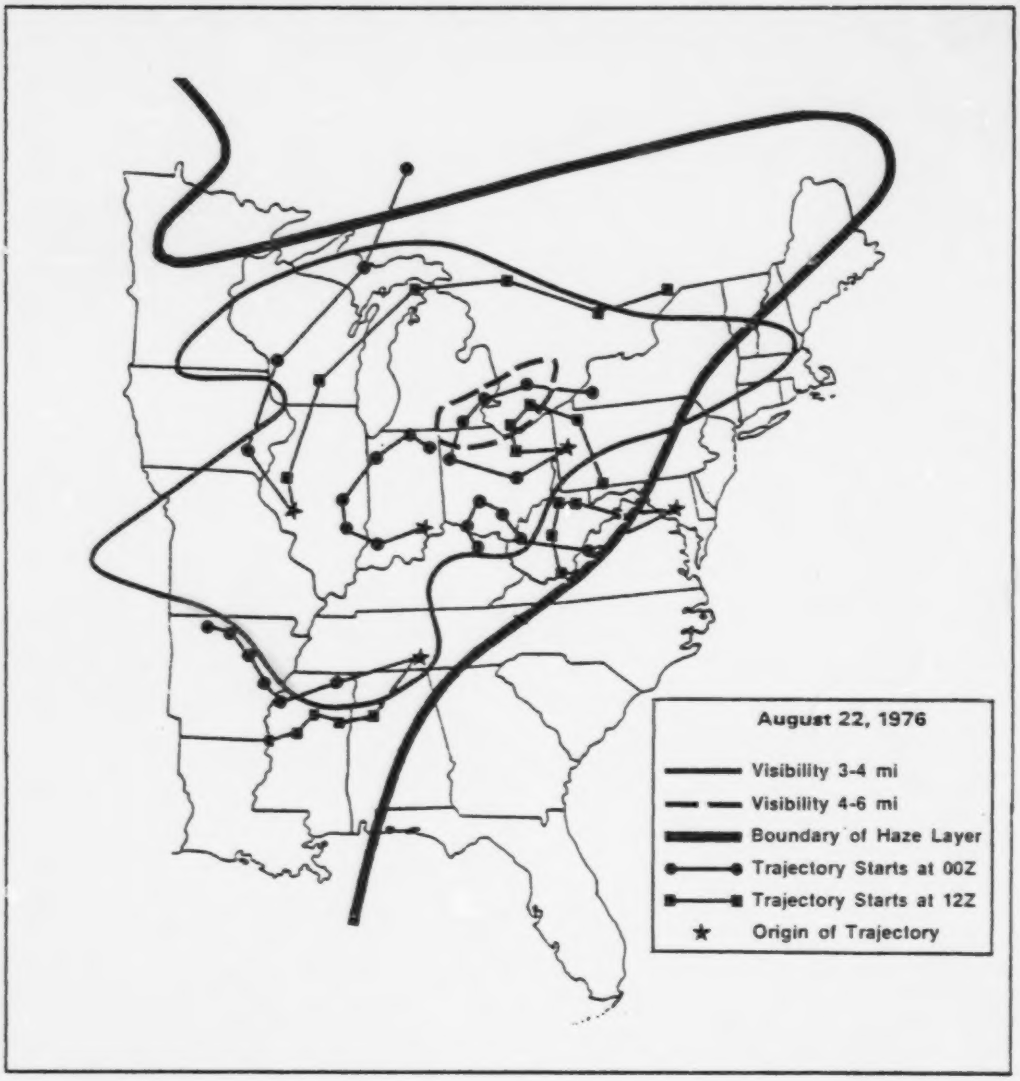

Note the recirculation around the northeast corner of Ohio and the likely regional transport of pollutants into western Tennessee and Arkansas.

Figure 7. Spatial distribution of visual range, the satellite-observed haze layer, and the forward trajectories (beginning on August 20) of air parcels.

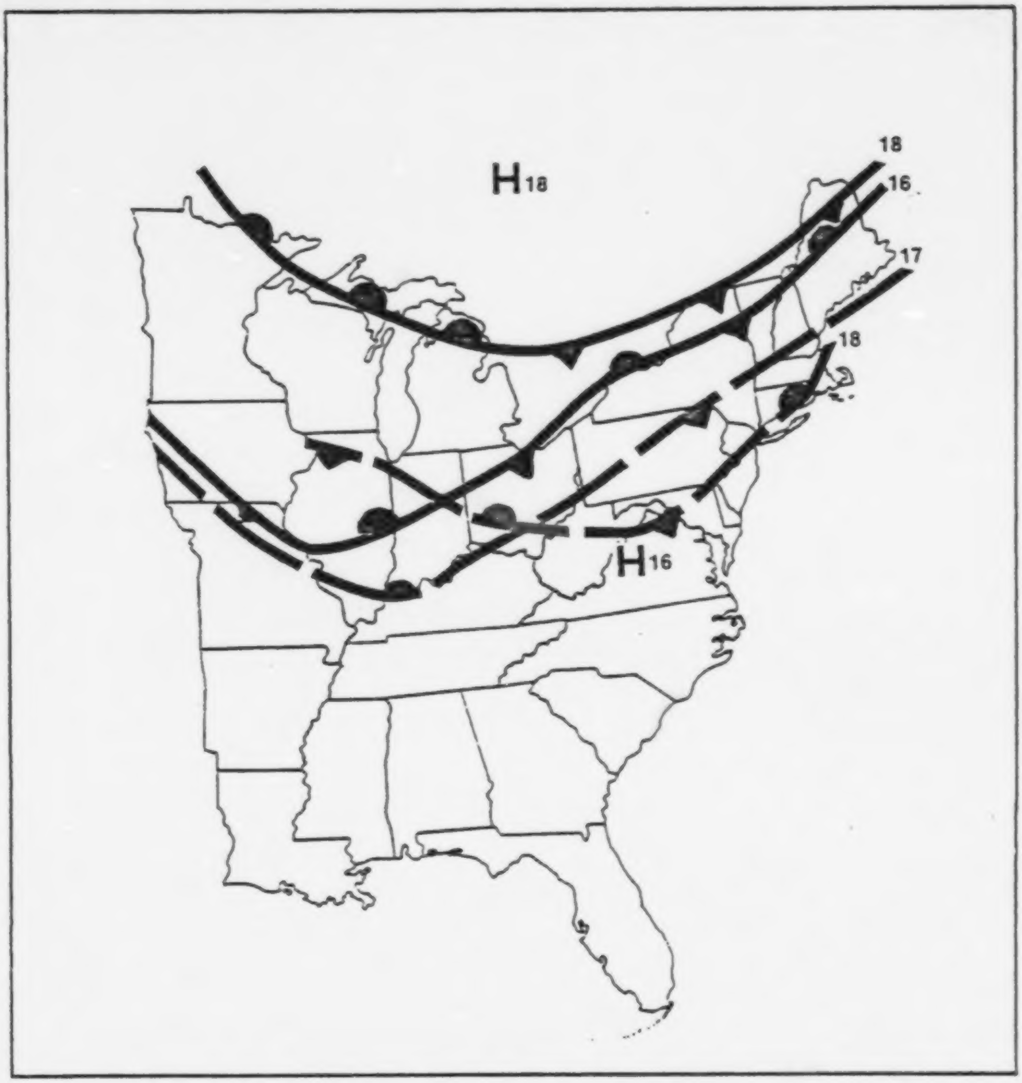

Note the washing out and stationary nature of the frontal zone.

Figure 8. Summary of synoptic events for Case 3, July 16, 17 and 18, 1977.

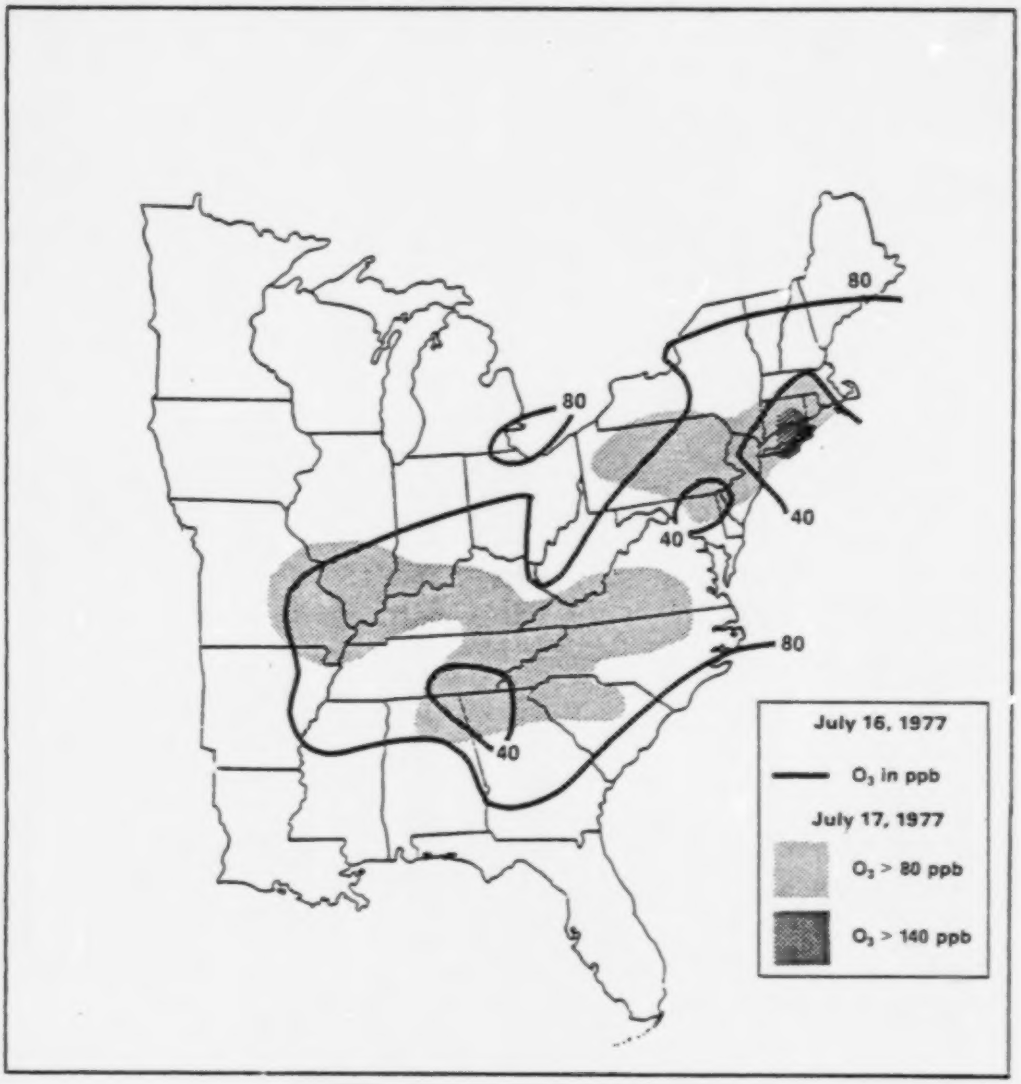

Note the reduction in size of the pattern and the persistent high O_3 area in Connecticut.

Figure 9. Spatial distribution of ozone for July 16 and 17, 1977, during the peak of the ozone episode.

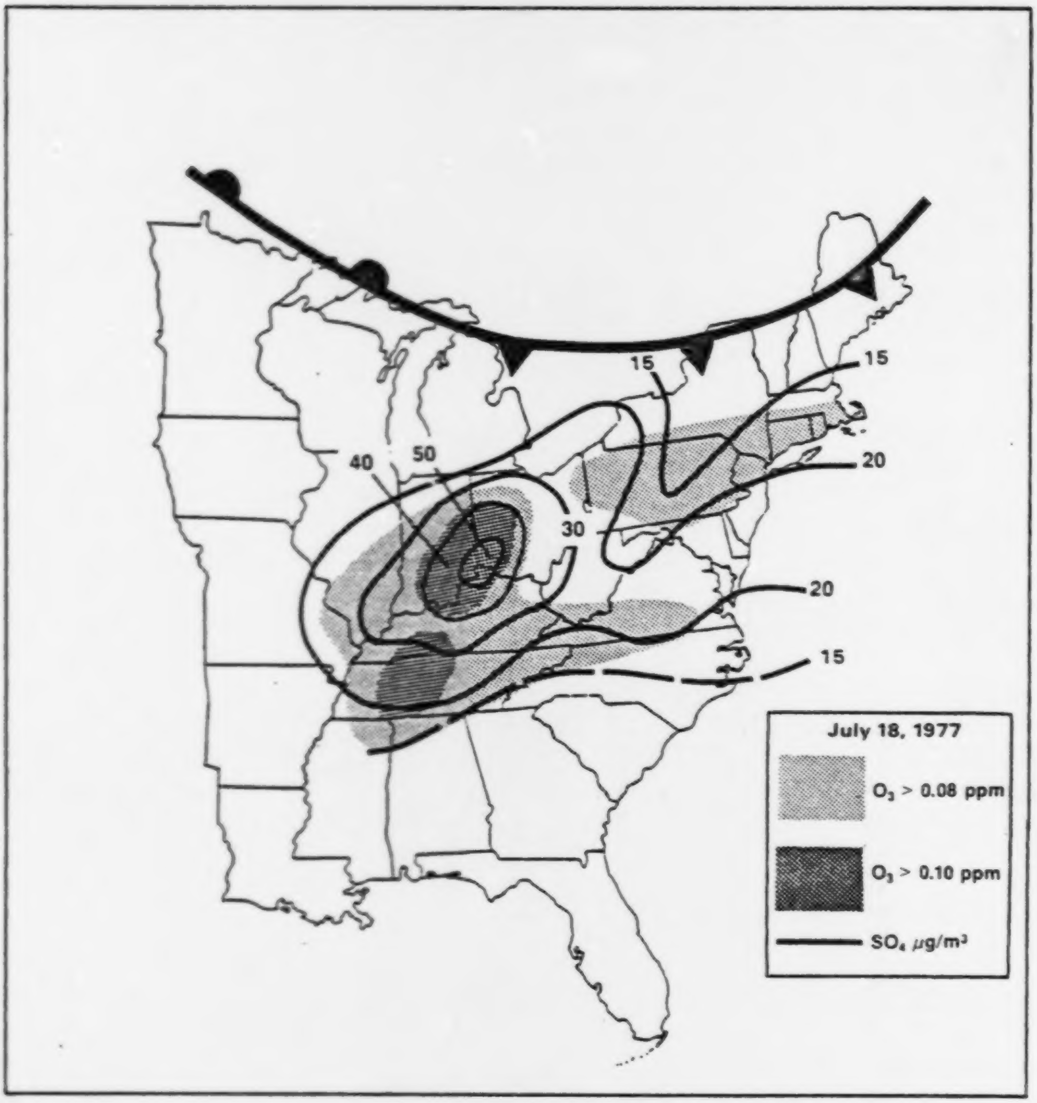

Note the correspondence of O_3 and $SO_4^=$ over the region, particularly over Indiana and Ohio.

Figure 10. Spatial distribution of sulfate and ozone concentrations for July 18, 1977.

TABLE I. RESULTS OF EPISODE RETRIEVAL FOR 1975*

Threshold Value 0.08 ppm

Day	January	February	March	April	May	June	July	August	September	October	November	December
1			1-32			1-33	37-40	96-44	6-44	3-41		
2	1-31			1-32		4-36	66-40	72-42	9-46			
3					9-32	10-36	67-40	48-41	16-45			
4				1-31	1-31	11-35	27-39	29-44	12-45			
5				1-30	3-33	11-36	32-39	20-44	9-46	5-37		
6				1-30	3-33	1-35	36-38	1-44	1-46	3-39		
7					4-32		16-40	3-44	4-45	1-39		
8					6-32	1-36	40-39	10-44	7-46	2-38		
9					11-32		33-40	32-44	4-45	3-39	1-29	
10				1-31	14-32	8-36	41-41	62-44	4-45	6-37		
11					19-32	9-36	13-42	33-44	4-45	6-38		
12				2-31	7-32	2-36	9-40	41-45		5-38		
13				3-30	4-32	11-36	8-39	39-46	1-45	4-39		
14			1-31	2-31	6-32	26-35	1-42	14-46	1-41	4-39		
15			1-31		29-33	13-34	11-42	9-45		3-39		
16			1-31	2-32		1-35	28-43	14-44			1-30	
17			4-32	3-32	13-31	13-36	26-43	5-44	3-44			
18					20-31	13-36	41-43	34-45			1-36	
19					22-32	19-31	22-42	9-46				
20			1-30	1-30	44-33	13-34	14-43	17-45	1-44	2-38	1-35	
21			1-33	2-30	33-33	23-33	26-44	24-45		5-38		
22		1-32	1-27	1-32	25-34	46-32	26-44	14-46		10-38		
23				5-33	45-32	34-36	75-43	10-46	1-45	11-39		
24			1-30		29-32	41-36	43-44	6-44		2-38		
25				4-32	5-30	33-38	2-44	16-45			1-35	
26				4-31	3-30	20-38	11-43	26-45				
27				1-26	5-31	28-38	46-41	7-45	2-44			
28				1-32	9-30	30-37	56-44	27-46	4-41			
29					18-33	31-35	29-44	47-46	4-44			
30				2-32	14-33	25-37	74-45	16-45	15-46			
31					1-34		97-44	4-45				

*See footnote at the end of table.

(continued)

TABLE I (continued)

Threshold Value 0.14 ppm

Day	January	February	March	April	May	June	July	August	September	October	November	December
1			1-32				2-40	25-44				
2				1-32			9-40	16-42				
3							10-40	5-41	2-45			
4								10-44	1-45			
5												
6							3-38					
7												
8							1-39					
9					1-32			3-44				
10					1-32			1-44		1-37		
11								1-44		1-38		
12							1-40	1-45				
13								3-46				
14												
15					1-33							
16							2-43					
17							3-43					
18							3-43					
19					1-32		2-42					
20					3-33							
21						3-33						
22					5-34	1-32	2-44					
23					6-32	3-36	11-43	1-46				
24					5-32	7-35	1-44	1-44				
25						1-38						
26						1-38	2-43	2-45				
27						2-38						
28						3-37	3-44					
29					1-33	1-35		3-46				
30							9-45		1-46			
31							27-44	1-45				

*First number of each entry is the total number of stations exceeding the threshold value, and the second number is the percentage of stations reporting for that day. The total number of reporting stations is 466.

TABLE II. RESULTS OF EPISODE RETRIEVAL FOR 1976*

Threshold Value 0.08 ppm

Day	January	February	March	April	May	June	July	August	September	October	November	December
1			2-39	1-42			19-44	3-43	41-49	6-50		
2				2-41	10-44	1-45	25-45		2-50	34-48		
3				7-40	6-45	7-46	35-45	14-45	9-51	41-48		
4				7-40	2-44	20-45	21-45	50-46	6-51	21-50		1-41
5				4-41	8-42	30-45	29-44	71-46	4-51		1-44	
6			1-41	3-41	19-42	52-44	59-45	35-45	5-50			
7			1-40	6-41	1-42	68-45	20-47	11-45	11-51		4-42	
8			1-41	6-42	1-42	116-45	55-47		52-52			
9					7-42	100-45	41-47	13-45	47-51		1-42	
10		1-36		3-42	24-42	107-46	41-47	29-45	4-51	6-45		
11			1-40	7-42	12-43	108-46	41-44	37-46	7-51	14-48		
12				3-43	9-42	71-46	3-47	70-47	27-51	13-48		1-40
13				9-43	7-43	40-45	18-45	58-48	46-50	12-49		
14		1-39		9-43	3-43	22-45	28-47	44-46	61-49	11-50		
15				20-43	2-44	49-45	33-47	11-45	27-50	17-50		
16			1-41	18-42	1-44	20-45	27-45	6-47	5-50			
17				48-41	1-45	12-46	12-45	9-47	16-51			
18			1-42	55-40		39-46	30-43	38-47	29-50			2-39
19			1-42	47-41	1-44	1-44	59-47	45-48	34-48		1-43	1-39
20			7-41	23-42	20-44	4-44	67-47	66-47	18-50		1-41	1-39
21				9-44	30-44	6-44	27-47	117-47				1-39
22				2-44	14-44	10-45	11-47	99-46	1-50	1-46		1-39
23				9-43	5-44	20-45	27-48	74-47	9-51	1-45		1-40
24			2-41	12-43	3-45	17-46	38-47	60-48	8-52			1-39
25		2-39	1-41		6-44	9-47	18-47	56-49	7-52		1-41	1-38
26			2-41		5-44	27-45	26-47	61-48	4-51	1-45	1-41	
27		2-40	3-41	2-44	10-44	57-43	59-48	31-48				
28		3-39	1-40	3-45	13-44	48-46	39-46	25-47	1-50	1-45		
29		6-32		3-45	11-43	29-46	15-46	6-47	2-50			
30				5-45	3-42	5-45	26-46	5-48	1-50	1-42		
31					7-41		26-45	18-47				

(continued)

*See footnote at the end of table.

TABLE II (continued)

Threshold Value 0.14 ppm

Day	January	February	March	April	May	June	July	August	September	October	November	December
1						3-44				2-50		
2										3-48		
3					1-45		1-45			1-48		
4							3-45					
5				1-41			2-44	6-46				
6							9-45	1-45				
7						1-45	2-47					
8						2-45	1-47		2-52			
9						8-45	1-45		4-51			
10						13-46	1-47					
11						7-46	5-44	2-46				
12						9-45		7-47				
13							1-45	12-48	1-50	1-49		
14							1-47	6-46	7-49			
15						2-45	1-47					
16						3-45	2-45	1-47				
17				1-41								
18				6-40		4-46		5-47	1-50			
19				5-41		1-44		3-45				
20				1-42			7-47	3-47				
21								10-47				
22								2-46				
23								2-47				
24						3-46	3-47	1-48				
25							3-47	2-49				
26						1-45		7-48		1-45	1-41	
27						3-43	3-48					
28						7-46	8-46					
29						3-46						
30							1-46					
31												

*First number of each entry is the total number of stations exceeding the threshold value, and the second number is the percentage of stations reporting for that day. The total number of reporting stations is 466.

TABLE III. RESULTS OF EPISODE FOR 1977*

Threshold Value 0.08 ppm

Day	January	February	March	April	May	June	July	August	September	October	November	December
1				3-46	19-45	9-50	10-50	19-50	18-50	3-45		
2			4-42		1-49	25-50	14-48	18-51	40-50			
3		1-39	1-41		1-49	14-49	38-47	37-51	17-48			
4				1-45		71-50	59-47	56-51	23-48			
5			1-41	1-47	3-49	73-49	53-49	41-51	10-47			
6				1-47	21-48	14-48	55-50	22-50	13-49	1-48		
7	1-42			2-48	1-47	1-51	44-51	10-48	10-49		1-42	
8				1-47	4-47	10-52	34-51	9-50	21-50			
9			1-41	8-47	2-49	9-52	31-50	8-51	10-50			
10			1-42	8-46		22-54	30-50	14-51	3-49			
11	1-40		4-42	20-48	14-51	41-52	9-51	20-51	1-48	1-49		
12			4-42	60-48	39-51	48-51	15-50	11-50	3-49			
13				39-48	63-53	33-53	50-50	1-49	6-51			
14				11-50	62-50	44-51	49-49	12-48				
15			3-42	22-50	50-50	66-53	94-52	8-50	1-49	5-48		
16				28-48	57-52	56-54	114-51	7-50		1-47	1-40	
17			1-43	31-47	109-52	50-53	78-50		1-48			
18				27-48	72-52	34-51	51-49	3-51	10-47			
19				17-47	57-53	6-50	78-51	18-52	6-48	1-48		
20				17-48	74-53	22-51	70-49	17-50	1-49	1-48		
21				20-49	61-51	4-52	61-51	18-50		1-47		
22	1-41	1-42	1-43	22-49	37-50	5-52	2-51	9-51	2-49	11-47		
23		1-41		1-48	30-51	14-52	36-49	10-50	7-49	3-46		
24	1-42				67-51	29-53	51-48	2-50	1-49	2-45		
25	1-41	1-42			64-51	9-51	1-51	3-50	3-48			
26			2-42		38-50	19-50	4-50	11-50				
27			1-41	3-49	60-52	51-51	10-51	23-50				
28	1-42		2-42	8-49	117-51	40-51	55-51	26-48		1-46		
29			2-43	4-50	52-50	15-51	21-52	28-49	1-48	3-46		
30	1-41		5-42	6-49	41-46	25-52	41-51	15-47	3-49	1-45		
31			1-42		38-51		30-50	21-48				

*See footnote at the end of table.

(continued)

TABLE III (continued)

Threshold Value 0.14 ppm

Day	January	February	March	April	May	June	July	August	September	October	November	December
1									2-50			
2						1-50			5-50			
3								1-51				
4						1-50	3-47	1-51				
5						1-49	2-49	8-51				
6							3-50	4-50				
7							2-51					
8							3-51					
9					1-49		3-50					
10						1-54	1-50					
11								1-51				
12						1-51						
13				1-48	1-53		2-50					
14					1-50		3-49	1-48				
15					2-50	5-53	4-52					
16					3-52	3-54	30-51					
17					2-52	3-53	4-50					
18					5-52	5-51	2-49					
19					3-63		11-51	1-52				
20							8-49					
21				1-49	1-51		6-51					
22												
23							1-49					
24					3-51		1-48					
25					5-51							
26					2-50	1-50						
27					2-52	3-51						
28					9-51	2-51	2-51	6-48				
29					3-50			4-49				
30							1-51	2-47				
31							1-50					

*First number of each entry is the total number of stations exceeding the threshold value, and the second number is the percentage of stations reporting for that day. The total number of reporting stations is 466.

TABLE IV. SUMMARY OF SULFATE EPISODES DURING 1975, 1976, and 1977

DATE	DESCRIPTION
1975	
June 23	High-pressure center on Atlantic Coast dominating eastern half of United States for several days. Sulfate advection from midwest and southcentral States to as far as northern New York and New England.
July 17	Identical synoptic situation as June 23, except Bermuda High is farther inland on the Atlantic Coast. This situation resulted in high sulfate concentrations in Wisconsin, Illinois, Indiana, and Michigan, as well as pollutant advection into Ontario, New York State, and New England.
August 10	Bermuda High dominating eastern United States. High-pressure center persisted for several days on the southern Atlantic Coast. Pollutant transport is similar to that on July 17, with high sulfate levels also being advected into the mid-Atlantic and northern Atlantic States.
1976	
June 11	Data available for only a few of the States in the northeast quadrant of the United States. Sulfate levels exceeding 40 μg/m^3 in Ohio and West Virginia. Stationary front just north of Great Lakes. Persistent high-pressure center situated in northern Georgia-western Carolinas for several days.
August 22	A persistently stagnant situation with high-pressure center just south of Lake Erie. Sulfate levels exceeded 50 μg/m^3 in the northern Ohio-southern Michigan region. Recirculation is evident over several States. Westward advection from western Pennsylvania, northerly and northeasterly transport into Michigan, Ontario, and recurvature southward to New York State and Pennsylvania. Westerly transport is also evident in the TVA region, resulting in episodic concentrations in western Tennessee and Arkansas.
September 9	Typical case of pollutant confinement in the warm sector of an occluded system. High sulfate concentration in Ohio, Pennsylvania, New York, and States abutting them to the south.
1977	
May 31	Another example of the occluded confinement. The warm sector is farther south than the previous case.
June 24	Nearly identical to May 31 case.
July 18	A persistent Bermuda High situation with a west-east stationary front along the Canadian border. Eastern half of United States experienced hot and humid conditions for many days. High sulfate levels in a tier of States from Missouri to New Jersey, excluding northern parts of New York and New England.
August 5	Poor data coverage but high sulfate levels in Pennsylvania and New York. A typical Bermuda High situation.
August 11	Moderate sulfate levels in Ohio, West Virginia, and western Pennsylvania. A peripheral occlusion situation.
August 23	Similar to August 11 case.
October 22	Similar to August 11 and 23 cases.

STATISTICS OF ELEVATED POLLUTION EPISODES

Gerald F. Watson* and Walter J. Saucier*

North Carolina State University, Raleigh, North Carolina

INTRODUCTION

Climatological studies of pollution episodes are few and have mainly been indirect in that the meteorological conditions often associated with pollution are studied rather than the pollutants themselves. Thus, Holzworth (1972, 1974) compiled statistics on air pollution potential by means of a mixing depth/boundary-layer mean-wind index. Korshover's (1975) 40-year climatology of stagnating anticyclones is well known. One of the few studies directly concerned with pollutants is Altshuller's (1978) 10-year climatology of high oxidant levels at four observation sites in the eastern United States.

The present study will report on some of the statistical characteristics of elevated pollution episodes (EPE's) based on the evolution of haze and/or smoke (HK) areas east of the Rocky Mountains. This study, too, is an indirect approach to the climatology of pollutants. However, many investigators (e.g., Altshuller, 1978; Wolff et al., 1977; Hall et al., 1973) have established that persistent HK areas (blobs) are often, if not always, associated with increased oxidant concentrations. Related light-scattering aerosols produce the low visibilities accompanying the hazy conditions. In so far as this relationship holds, the following results based on haze may be interpreted as indicative of the statistical behavior of atmospheric pollutants--natural and manmade.

PROJECT DESCRIPTION AND GOALS

A recent 5-year period, June 1973-May 1978, was selected, and daily NMC Weather Depiction Charts were obtained from the National Climatic Center. The primary chart time was 1900 GMT (2 p.m. EST), chosen to minimize the interference of morning radiation fogs. Also, sufficient convective mixing should have occurred by this time so that transient high concentrations of early morning HK would not be mistaken for day-long persistence of interest here.

---

*Speakers.

The major goals of the project were to:

1. Identify and track prominent HK blobs.
2. Determine the geographical distribution of monthly HK occurrence and persistence, and to relate these characteristics to the synoptic-scale weather and flow patterns.
3. Compile statistics on the dimensions, trajectories, visibilities and other associated weather parameters (e.g., humidity, cloud cover, etc.).
4. Relate HK episodes to actual pollutant concentrations via EPA SAROADS data.

In the 3 months since formal work on the project began, some of these goals have been attained and other at least explored. The progress thus far achieved is in large measure due to the enthusiastic help of seven of our meteorology students--three graduate students and four seniors. I would like to acknowledge their help at this time.

IDENTIFICATION OF HK EPISODES

The identification of HK episodes involved a day-by-day scan of the Weather Depiction Charts looking for hazy areas that exhibited continuity over a few days. Obvious mesoscale and/or transient situations were eliminated; more substantial cases were outlined on tracing paper for their duration. These daily isochrones of blob outline would include limited areas of fog and precipitation if associations were clear. Otherwise, only stations reporting haze or smoke were included.

Incidentally, it is somewhat regrettable--from the point of view of this project--that NMC changed the Weather Depiction Chart symbology for weather and obscurations in about the middle of the 5-year period (July 1976). In the earlier part of the period, aviation code symbology was used; synoptic code symbology was adopted in the latter half. The aviation code permitted the observer to report, for example, the occurrence of haze with other kinds of weather as fog or rain. The computer-printed synoptic symbology displays only one type, the dominant weather, thus making decisions about the incorporation of weather areas in close proximity to a hazy area somewhat more subjective.

In any case, the daily HK isochrones for each of the episodes were to serve many purposes in this project, and much effort went into their construction. One of the uses of the HK isochrones was to determine the geographical distribution of HK persistence. Persistence is certainly of importance in the determination of the possible adverse health effects. Also, these charts helped to formalize the definition of an HK episode for purposes of this project.

EXAMPLES OF HK EPISODES

Figure 1 shows isopleths of persistence (i.e., the number of consecutive days with haze or smoke) for two episodes. Persistence values were determined by superimposing the daily isochrones on a 1° latitude/1° longitude grid and marking all grid squares with at least 50 percent of the area included within the isochrone.

The first example in Figure 1 is a mini-episode, June 22-25, 1976. The dashed line is the episode "envelope," or the area within which haze/smoke was reported on at least one day. During its brief 4-day lifetime the blob affected some 350,000 km^2 over the eastern Great Lakes.

The isopleths of 2, 3, and 4 consecutive days of haze/smoke are drawn. Though the episode was of short duration, it was sufficiently stationary so that an area of more than 50,000 km^2 experienced the maximum HK persistence of 4 days.

The other HK episode shown in Figure 1 lasted for 21 days (July 4-24, 1977), and during this time affected an area of at least 2.8 million km^2. How far the HK area may extend into the Atlantic is unknown. Maximum persistence of 9 days occurred along the Ohio Valley and coastal regions of Virginia and North Carolina.

Examination of many such cases from the 5 years of data led to what is believed to be a reasonable working definition of a "haze/smoke episode." An episode is one in which the region of 3 or more days' persistence covers an area of at least 10^5 km^2. Such an area is a box about 3° latitude square, or about the area of North Carolina.

Application of HK episode criterion to those cases originally obtained resulted in the neglect of some and in the addition of a few. The brief and localized June 1976 case shown in Figure 1 would be readily accepted as an episode under the criterion.

TABULATION OF HK EPISODES

Table 1 lists dates of the 42 episodes identified during the 5-year period June 1973-May 1978. Episodes that only marginally satisfied the above criterion are indicated by asterisks. The arrows indicate episodes that are continuous across months.

The remarkable 3-month eposide extending from July 1 to October 4, 1973, is to be noted. This is one episode because a 3-month continuity of HK areas can be traced, although the areal extent varied from occupying the eastern one-third of the United States to near disappearance for a day or so. As a matter of fact, except for what appear to be clean breaks on June 30 and October 5, the episode may have been 4 months long--June 9 to October 13! Nothing quite like this occurred in the other years, although there were a few episodes approaching a month in length.

For purposes of counting episodes, July, August, and September (including the first 4 days of October) 1973 are each assigned one episode of a full month's duration. The number of episodes in each month, and their minimum and maximum duration, are given at the bottom of the table. The total number of monthly episodes (46) differs from that of the actual total (42) because episodes that spanned 2 months were credited to both if at least one-third of the episode duration occurred in one or the other month. Table 1 shows a broad maximum in episode number and duration centered on July.

The table also gives (below the dates) the general geographical region(s) of persistence ≥ 3 days. None of the episodes extended west of 100° longitude; the six geographical regions in the eastern United States are defined in Figure 2. The abbreviations are as follows: central region (C), north central (NC), northeast (NE), east central (EC), southeast (SE), and south central (SC). Episodes concentrated primarily along the boundaries between regions are indicated by underscoring.

The percentages shown in Figure 2 represent the number of times each geographical region appears in Table 1 divided by the total number of episodes (42). Thus, for example, ≥ 3 days' persistence occurred in the northeast region in 74 percent of the 42 episodes. This region was most frequently visited by persistent HK episodes, the south central region least frequently.

SPATIAL AND TEMPORAL VARIABILITY OF HK EPISODES

Tabulations of frequency of occurrence of HK in 1° latitude/1° longitude grid squares for each episode were partitioned into the respective months involved. Monthly statistics over the 5-year period of HK spatial and temporal variability represent the major completed work of the project. Some examples will now be presented.

The distribution of the frequency of occurrence of haze/smoke during July (1973-1977) is shown in Figure 3. The outer long-dashed curve represents the extremity of haziness composited over the 5 years; the western boundary along the 100° meridian is to be noted.

The isopleths are lines of constant probability (percent) and were obtained by dividing the number of days of HK by the total number of July days in 5 years. For practical purposes the total days is taken to be 150 for all months; then 3 days of HK out of 150 days is 2 percent. In general, the actual number of days with HK can be obtained by multiplying the isopleth values by 1.5.

The proper interpretation of Figure 3 is that it shows the probability of the occurrence of HK on any individual day in July. This is HK associated with episodes and is not necessarily the same as that obtained if all HK events were included. One notes in the figure that HK is most likely along the Virginia-North Carolina border where the probability exceeds 40 percent (or more than 60 days of HK during July over the 5 years). Norfolk, VA, is located in the region of maximum probability.

The chance of one day of haze in every three (32 percent) encompasses most of North Carolina, the Great Smoky Mountains, and a secondary maximum (36 percent) along the Ohio River in southern Ohio. This pattern, including the prominent minimum (<24 percent) on the Virginia-West Virginia boundary, is recognizable in other months, June-September.

Of greater concern from the point of view of the impact of episodes on human health is the persistence of polluted conditions over a given locale. Monthly statistics on the likelihood of ≥ 2, ≥ 3, ≥ 4, and ≥ 5 consecutive days of HK are provided in the final report. An example is shown in Figure 4 in which the isopleths represent the probability (percent) of ≥ 4 consecutive days of HK occurring at least once during July. The 20 percent value corresponds to such an occurrence observed once in the 5-year period, 40 percent to twice in 5 years, and 100 percent to an occurrence in each of the 5 years.

Figure 4 suggests that EPA could maximize its chances ($\geq$80 percent) of encountering an extended pollution episode by situating the STATE field experiments in the upper Ohio River Valley; the Washington, DC-Baltimore, MD, area; and/or along the Virginia-North Carolina border.

The charts provided in the final report can be combined in a variety of ways to show other aspects of HK variability. For example, Figure 5 depicts regions in which the probability is 60 percent that 2, 3, 4, 5, and 6 consecutive days of HK will occur. The hatched areas indicate that persistence is of shorter duration than the isopleth value. The figure shows a better than even chance of $\geq$2 successive days of HK during July over the eastern one-third of the country. Such a probability for at least 4 days in a row is restricted to the mid-Atlantic States and the Ohio River Valley.

Figure 6 is similar to the previous figure except that the probability is 100 percent. A nearly certain chance of 3 successive days of HK sometime during July is limited to North Carolina and a few other locales. Regions in which stagnant conditions lasted a week or more, and which occurred at least once in the 5-year period, are shown in Figure 7.

Some idea of interannual variability is illustrated in Figure 8. Isochrones of 4 or more consecutive days of haze in July 1973, 1975, and 1977 are shown, and differences are evident. The southern extent of the haze areas along the east coast is found farther northward as time progresses, and the east coast areal coverage in 1977 is much smaller than in the other 2 years. Another 1977 area is centered over the Ohio River; this region was free of persistent haze in 1973 and 1975.

Monthly variability is demonstrated by Figure 9. The isopleths show regions in which there is a 60 percent probability of $\geq$4 days of haze for all months between May and October. However, only 3 of the months--June (JN), July (JL), and August (AU)--exhibited such areas. Along the east coast the areal coverage in July is much larger than 1 month earlier or later. August appears to have the larger and better organized region over the Ohio Valley.

HK EPISODE DIMENSIONS AND VISIBILITIES

Figure 10 shows the variability in areal and linear extent of the HK area during one of the major episodes (June 18-July 13, 1975), as well as associated visibilities. Areal extent is the total overland area encompassed by isochrones, which sometimes imply continuation over adjacent water. This episode commences along coastal Virginia with a typical 10^5-km^2 area, and expands as it moves westward. The areal coverage increased by an order of magnitude to 10^6 km^2 during the first 10 days. At the time of maximum size (July 3, 1.5×10^6 km^2), the blob extended from the coast of the mid-Atlantic States west-northwestward to the eastern Dakotas. The general pattern of decline in areal extent was similar to that of the rise. One should note the occasional rapid fluctuations in size that verify one's impressions of day-to-day expansions-contractions, separations-recombinations of haze areas.

Maximum and minimum linear dimensions of overland HK areas have also been tabulated. No matter what the actual blob shape, some measure of length (major axis) and width (minor axis) was attempted for the largest blob. When the blob extended out to sea, the major axis would often be the distance along the coast and the minor axis the inland extent.

Figure 10 plots of major and minor axes show a more or less steady increase from 10^2 km to 10^3 km during the first half of the period. Axis ratios vary from about 1:1 (nearly circular) to 2:1, with 3:2 being most frequent. The long and narrow shape at the time of maximum areal extent and near the episode end (July 8-10) are to be noted. The latter result because large haze areas extend into the Atlantic.

Areal mean and absolute minimum visibilities over the episode duration are also shown in Figure 10. The mean visibility for each day is a subjectively determined, weighted mean of visibilities inside isochrones. The minimum visibility is the lowest reported value associated with haze/smoke. One should keep in mind that haze/smoke cannot be reported unless the visibility is 6 miles or less.

The inverse relationship between visibility and areal extent is notable--as the haze area grows it also becomes more "intense." Lowest mean visibilities are 3 miles; the overall mean for this case is close to 4 miles. Minimum visibilities are usually confined to small regions and the absolute minimum most often reported by one station. During the "mature state" in episode development, local minima are frequently 2 miles or less and occasionally as low as 1 mile.

Some statistical characteristics of HK blob dimensions and visibilities are presented in Figures 11 and 12. Here September 1973-77 is used as an example. The histogram in the former figure is percent frequency of haze area in categories of 10^5 km^2 centered on the value indicated. Total haze days in September was 85. The 50 percentile value is around 4.5×10^5 km^2 (about 6° latitude square). There appears to be only a 1 in 10 chance of the HK area equaling or exceeding 10^6 km^2 (about 9° latitude square). The significance of the trimodal character of the frequency distribution is not clear.

Major and minor axis measurements (° latitude) are represented as a scatter diagram in Figure 11. The average major axis is 9.8° latitude (1,088 km) long, the average minor axis about 4.5° latitude (500 km) long. An eye-estimated line of best fit passing through the mean (solid line) represents the most probable minor axis length given the major axis. This would be a crude estimate at best because of the large scatter about the line.

The relative frequency (percent) of lowest visibilities during September is shown in Figure 12. Visibility categories are at 1-mile intervals centered on the values shown. The mean, median, and mode are, respectively, 2.6, 2.5, and 2.0 miles.

HK BLOB TRAJECTORIES

The evolution of HK blobs, as controlled by synoptic-scale flow patterns and weather distributions, is recognized as an important problem whose solution could lead to better forecasts of the onset, migration, duration, and intensity of EPE's. One aspect of the problem has received attention in recent years, namely, the following of well-defined pollution and/or HK blobs by means of trajectories--the "long-range transport" problem.

Case studies of long-range transport have, on occasion, provided insight into the association of HK blobs and the synoptic situation. Hall et al. (1973) and Wolff et al. (1977) have noted that pollution blobs, usually formed in association with an anticyclone, will persist as the initiating circulation system moves on. Wilson (1978) emphasizes the special challenge of studying chemical transformations and pollution concentration variability within migrating hazy air masses.

It is hoped that a continuation of the present project will produce statistical relationships among HK areas and synoptic-scale pressure and weather distributions. At the moment, an interesting case study of a blob trajectory and the interacting pressure systems that produced it, will be presented. First, however, a comment about HK blob trajectories.

RTI studies, among others, point out that many factors contribute to the formation, maintenance, and dissipation of large, hazy air masses. The factors include available source regions, chemical transformations related to sunshine and humidity (perhaps temperature also), the wind field with associated small-scale mixing and large-scale convergence, and the vertical mixing depth, itself dependent on several processes.

Parts of a large HK blob may be translated by the local wind, but the area as a whole is more likely a propagation phenomena resulting from the interaction of many processes. Thus, blob trajectories and air trajectories originating in the same general area may not be the same. What feature of a large polluted air mass, then, can be identified and tracked? It was decided to try to construct the trajectory of the "center of mass" or "centroid."

The centroid of an HK blob was determined subjectively, but carefully, from its outline by attempting to balance areas within the blob. If multiple blobs existed on a particular day, the centroid of each was determined, and the area-weighted mean center of the entire system determined. It was satisfying to find that the individual daily centroids did fit together in a reasonably continuous manner. The centroid trajectory for the June 18-July 13, 1975, case is shown in Figure 13. This is the same case described in the previous section, some aspects of which were presented in Figure 10.

Daily centroid positions are plotted in Figure 13. There was a general westward movement from June 18-July 1, complicated by a series of anticyclonic loops. The last such loop lasted for about 6 days, June 28-July 4. The centroid then executed a cyclonic U-turn across the southeastern States and headed northward along the Atlantic coast. It dawdled for about a week (July 7-13) around the Virginia-Maryland-Delaware region before dissappearing at almost the same location where it had begun nearly a month earlier!

What produced such an interesting trajectory? Indeed, does it make sense? The episode began in the climatologically hazy area of coastal Virginia (see Figure 4). The initial HK area was associated with a weak anticyclone (1,022 mb) located over eastern Tennessee. The relationship of the centroid trajectory to this circulation system and others is shown in Figure 14.

The initiating or "parent" anticylcone (the abbreviation PA is appropriate) moves westward over the next few days, essentially disappearing as a 1,019-mb high over western Kentucky on the 21st. The haze area during this time performed a small anticyclonic loop so that it eventually headed in the same direction as the PA.

Anticyclogenesis occurred over Lake Ontario on the 20th-21st and this system became the second dominant anticylone (A2) in the life of the migrating HK blob. In response to A2's southeastward movement and circulation pattern, the blob centroid moved northward as far as Lake Erie. As A2 moved out to sea, a new high formed in eastern Tennessee (A3), and the HK area responded to this system's movement and circulation by heading southward and completing a second anticyclonic loop.

As A3 weakened, a moderate polar high (A4) moved rapidly eastward north of the Great Lakes and took control of the HK blob. In the easterly and southeasterly flow south of A4, the blob moved westward. Around the 26th, yet another anticyclone (A5) took over. Third and fourth anticyclonic loops were completed before A5 relinquished control to a developing high on the Texas-Oklahoma border (A6).

A6 dropped south and then eastward into the central Gulf. The HK centroid dutifully followed until July 6. For the next week, until the episode ended, a nearly stationary pressure pattern formed along the east coast--a north-south trough along the Appalachians and a high pressure ridge extending from the Gulf northeastward into the Atlantic. The general southerly flow along the coast stretched the haze area northward beginning on the 6th. A combination of large-scale ascent in the vicinity of the trough and the convective mixing and precipitation scavenging associated with rain showers eroded the haze area until it finally disappeared.

Thus, a succession of six anticylones influenced the movement of the haze area in this case. Perhaps the story should be presented in terms of cyclones and fronts in order to clarify their large-scale interaction with haze areas. Also, the role of other processes, such as those mentioned above, should be examined to determine why the anticylonic environment seemed to be favorable to the formation and long-term maintenance of hazy air masses.

ASSOCIATION OF HK EPISODES AND STAGNATING ANTICYLONES

The association of the HK episodes with the large-scale weather patterns--lows, highs, and fronts--remains to be investigated. However, Korshover's (1975) listing of stagnation periods (4 or more days' duration) accompanying warm anticyclones was available, and included a 2½-year overlap (June 1973-December 1975) with the present project. The HK episode decisions (Table 1) were made independently of any considerations of weather pattern associations. It thus appeared to be of interest to examine the association between the two sets of data.

To do so, the 2½-year period was divided into weekly intervals starting with June 3, 1973. Each week was assigned a "yes" (y) or "no" (n) depending on the presence of a stagnating anticyclone, and HK episodes were treated similarly. When either situation spanned 2 consecutive weeks, both weeks were credited with a "yes" if the condition existed for at least 2 days of that week.

The results for the warm seasons of each year (June-October, 1973; May-October 1974 and 1975) are presented as two-way contingency tables in Figure 15, Case A. The numbers in the table are the numbers of weeks of the association indicated for the box. The smaller printed numerals are row and column totals and the grand total. Thus, in Case A there is a total of 76 weeks, 46 of which included HK episodes and 26, stagnating highs. Perfect correspondence between the two phenomena would find numbers only in the boxes y-y and n-n.

Following standard statistical procedures (Panofsky and Brier, 1958) a "No Relation" table was constructed. In this case, the "No Relation" table is the same as the "Observed"! If Chi-Squared is used to test the significance in any difference between the two tables, $\chi^2 = 0$. Thus the null hypothesis of no relationship could not be rejected at any level of confidence. This would imply that stagnating anticyclones are not sufficient--not even necessary--for the occurrence of HK episodes.

It was thought, however, that some of the lack of association may be due to the inclusion of 1973, which, as mentioned previously, contained nearly 4 months of continuous haze. Thus, there are many consecutive weeks of "yes" for HK occurrence, but few for stagnating anticyclones. Case B in Figure 15 is similar to Case A except that only May-October 1974 and 1975 are considered. This time there is some difference between the "Observed" and "No Relation" tables and $\chi^2 = 1.3$. For 1 degree of freedom, this χ^2 value occurs at the 25 percent confidence level. Thus, one would take considerable risk in rejecting the null hypothesis in this case also.

The problem in this surprising result may lie in incompatible definitions of stagnating anticyclones and/or in HK episodes. Indeed, Altshuller (1978) found that in associating elevated oxidant levels with Korshover's stagnating highs over a 10-year period, there were many instances of the former occurring at times when the stagnation criteria were not satisfied. Perhaps, then, what is being indicated is that other meteorological factors must also be considered.

CONCLUDING REMARKS

In the brief 3 months of work on this project, some headway has been made in compiling 5-year statistics on the evolution of haze/smoke episodes and their meteorological context. Identification of episodes and the compositing of monthly statistics on the geographical distribution of HK occurrence and persistence and of dimensions and associated visibilities has occupied most of the time. These materials are available in the final report to RTI.

Studies of the interaction of hazy air masses with the synoptic-scale flow and weather distributions have been initiated. The development of statistical models would seem to require detailed case studies and thoughtful consideration to means of compositing individual results. The statistical association of haze episodes with elevated oxidant and other pollutant levels should be determined. This may shed further light on the relative contributions of natural and manmade sources to haze production.

The speaker, for one, looks forward to pursuing these problems.

REFERENCES

Altshuller, A. P. 1978. Association of Oxidant Episodes with Warm Stagnating Anticyclones. Journ. Air Pollu. Control Assoc., 28:152-155.

Hall, F. P., C. E. Duchan, L. G. Lee, and R. R. Hagen. 1973. Long-Range Transport of Air Pollution: A Case Study, August 1970. Mon. Wea. Review 101:404-411.

Holzworth, G. C. 1974. Meteorological Episodes of Slowest Dilution in Contiguous United States. Environmental Monitoring Series (EPA-650/4-74-002), NERC-Environmental Protection Agency, Research Triangle Park, N.C., p. 80.

______________. 1972. Mixing Heights, Wind Speeds, and Potential for Urban Air Pollution Throughout the Contiguous United States. Office of Air Programs Publication No. AP-101, Environmental Protection Agency, Research Triangle Park, N.C., p. 118.

Korshover, J. 1975. Climatology of Stagnating Anticyclones East of the Rocky Mountains, 1936-1975. NOAA Tech. Memorandum ERL ARL-55, Air Resources Laboratory, Silver Spring, MD, p. 26.

Panofsky, H. A., and G. W. Brier. 1958. Some Applications of Statistics to Meteorology. The Pennsylvania State University, University Park, PA, p. 224.

Robinson, E., F. M. Vukovich, and D. H. Pack. 1978. The Issue of Oxidant Transport. Journ. Air Pollu. Control Assoc., 28:209-210.

Wilson, W. E. 1978. Sulfates in the Atmosphere: A Progress Report on Project MISTT. Atmospheric Environment, 12:537-547.

Wolff, G. T. 1977. An Investigation of Long-Range Transport of Ozone Across the Midwestern and Eastern United States, Atmospheric Environment, 11: p. 797-802.

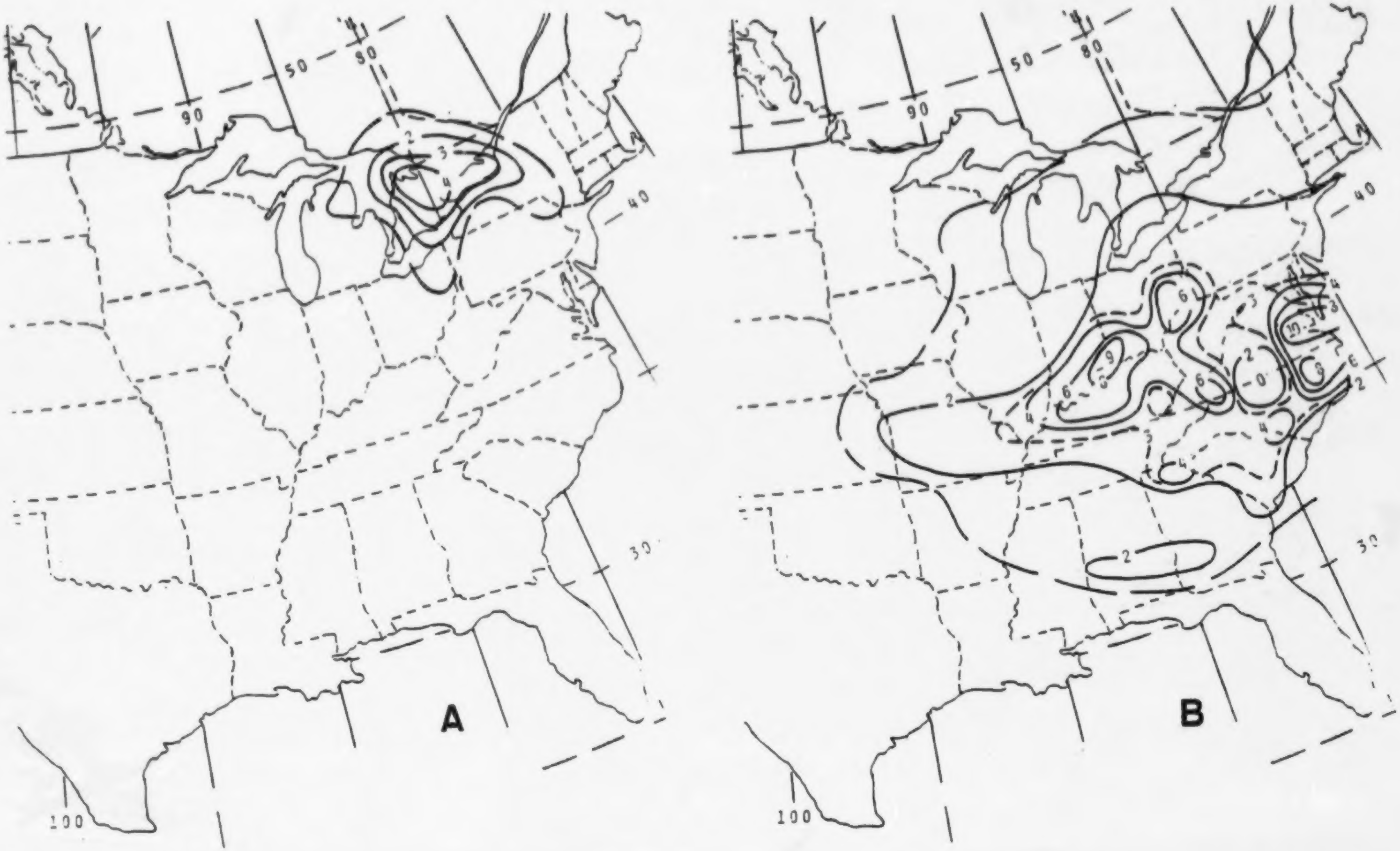

Figure 1. Examples of haze/smoke episodes. Chart A: minor episode June 22-25, 1976. Chart B: major episode July 4-24, 1977. The outer dashed curve is the episode envelope. Number of successive days (persistence) of haze/smoke is shown.

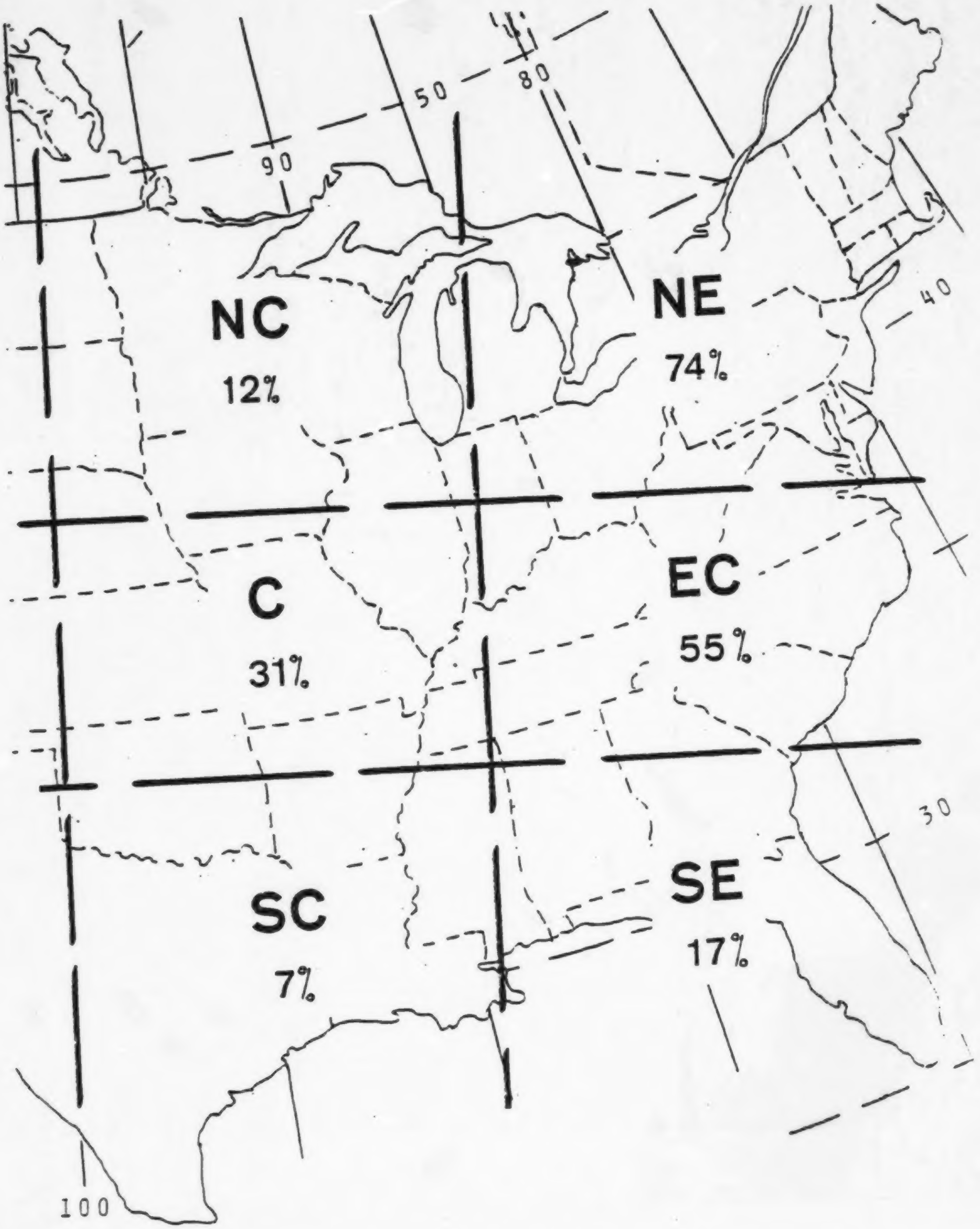

Figure 2. Geographical regions (defined in the text) with the percentage of all episodes (total 42) in which the region experienced ⩾3 successive days of haze/smoke.

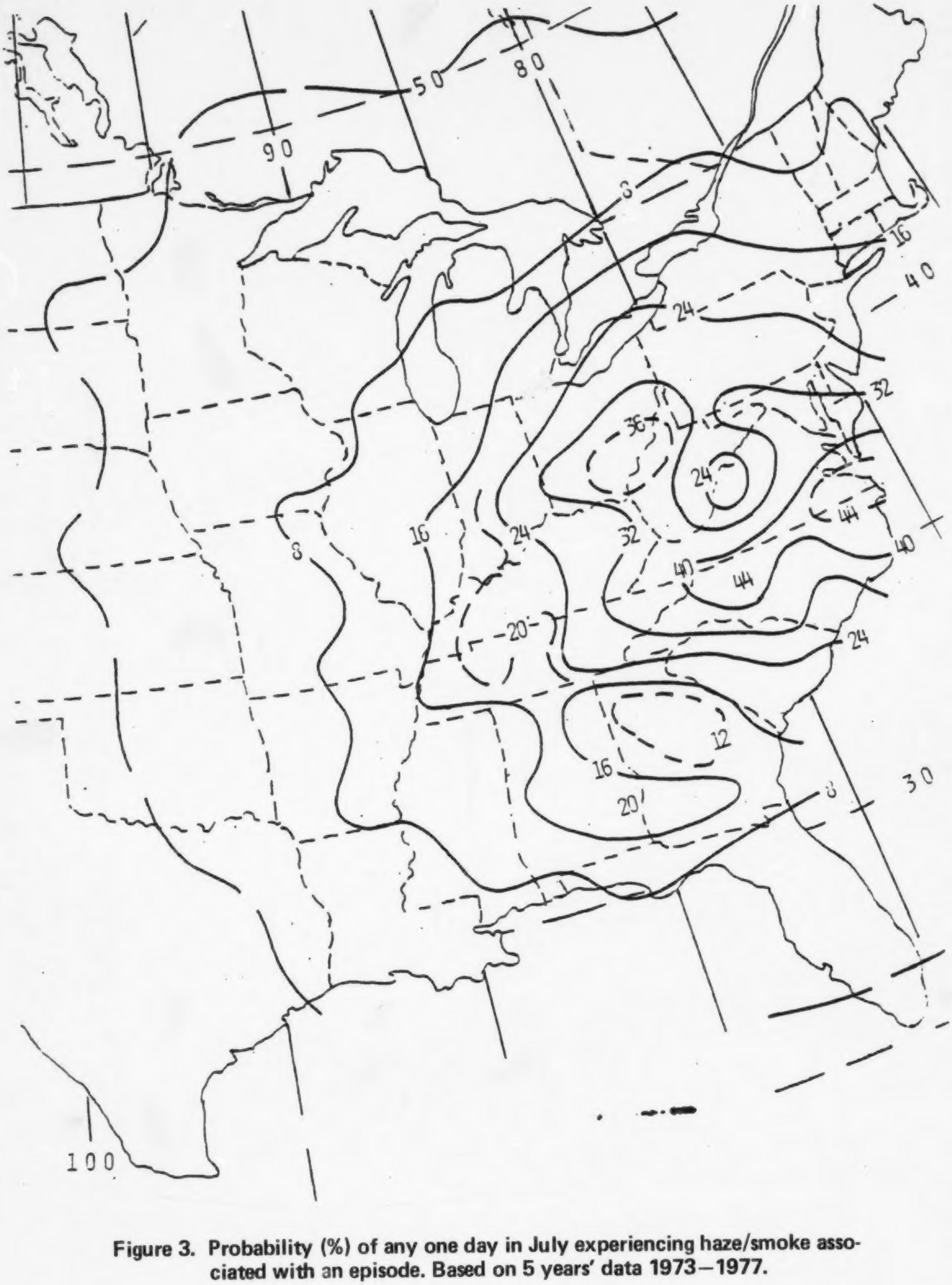

Figure 3. Probability (%) of any one day in July experiencing haze/smoke associated with an episode. Based on 5 years' data 1973–1977.

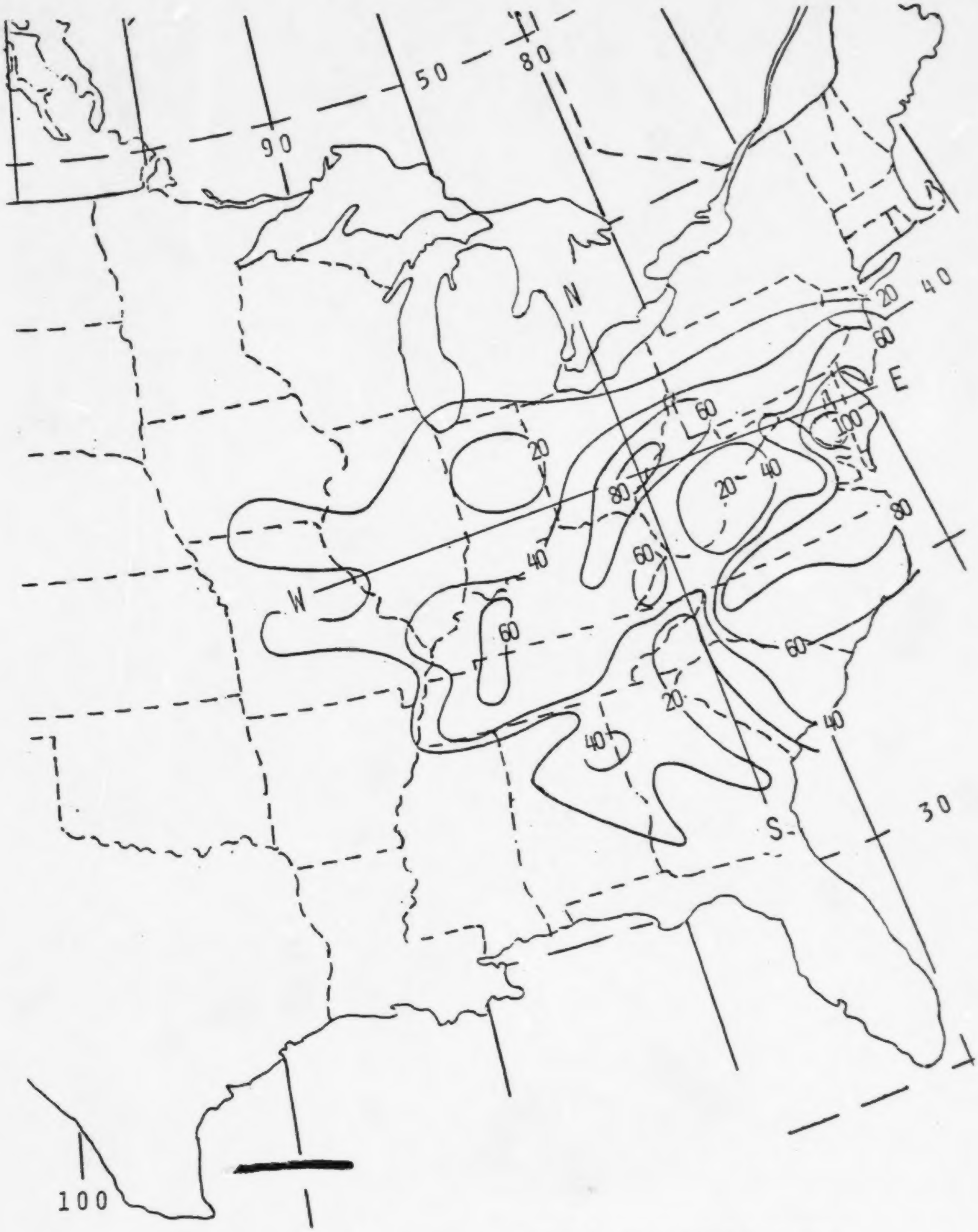

Figure 4. Probability (%) of ⩾4 consecutive days of haze/smoke occurring at least once in July.

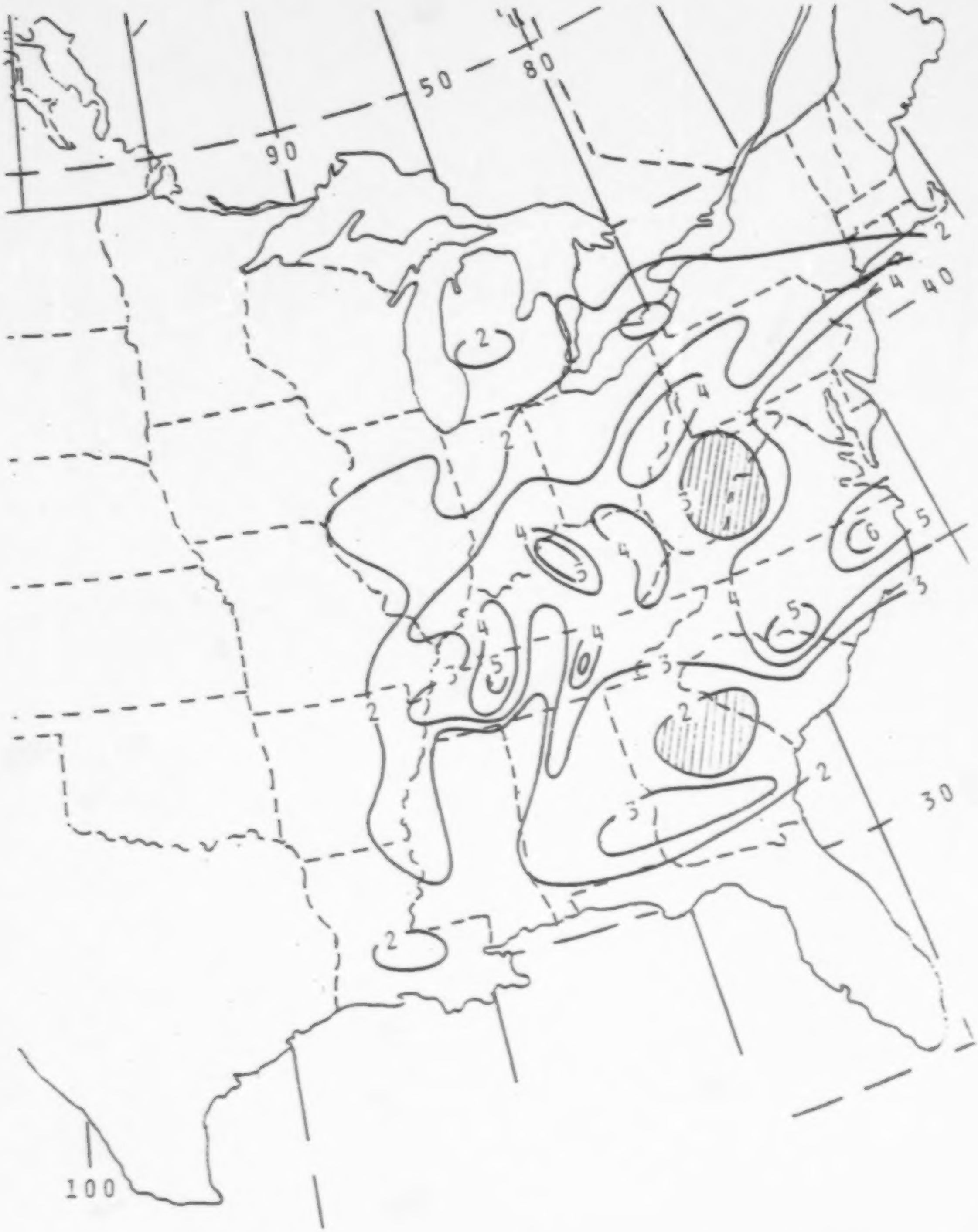

Figure 5. Number of consecutive days of haze/smoke in July with a probability of 60 percent.

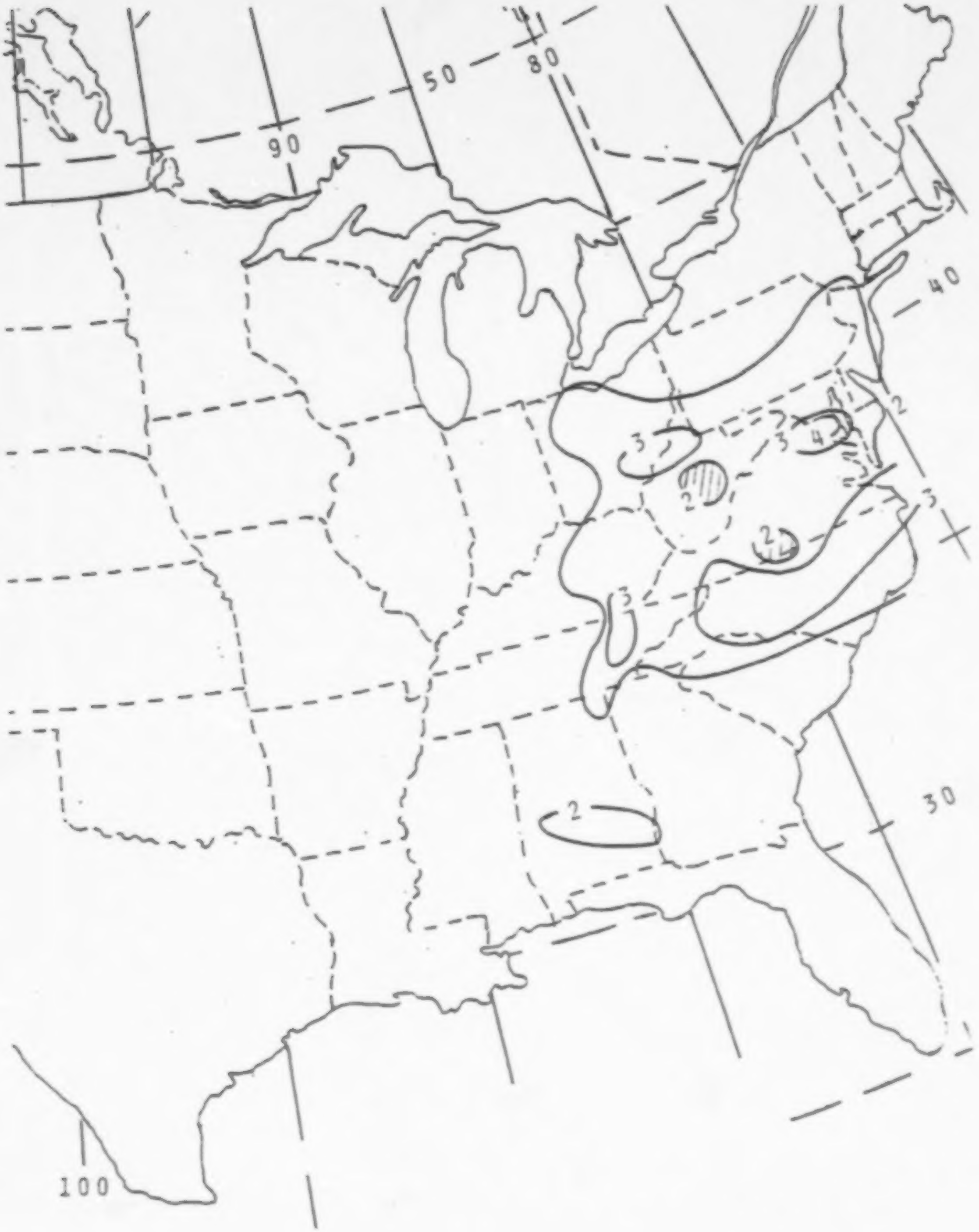

Figure 6. Number of consecutive days of haze/smoke in July with a probability of 100 percent.

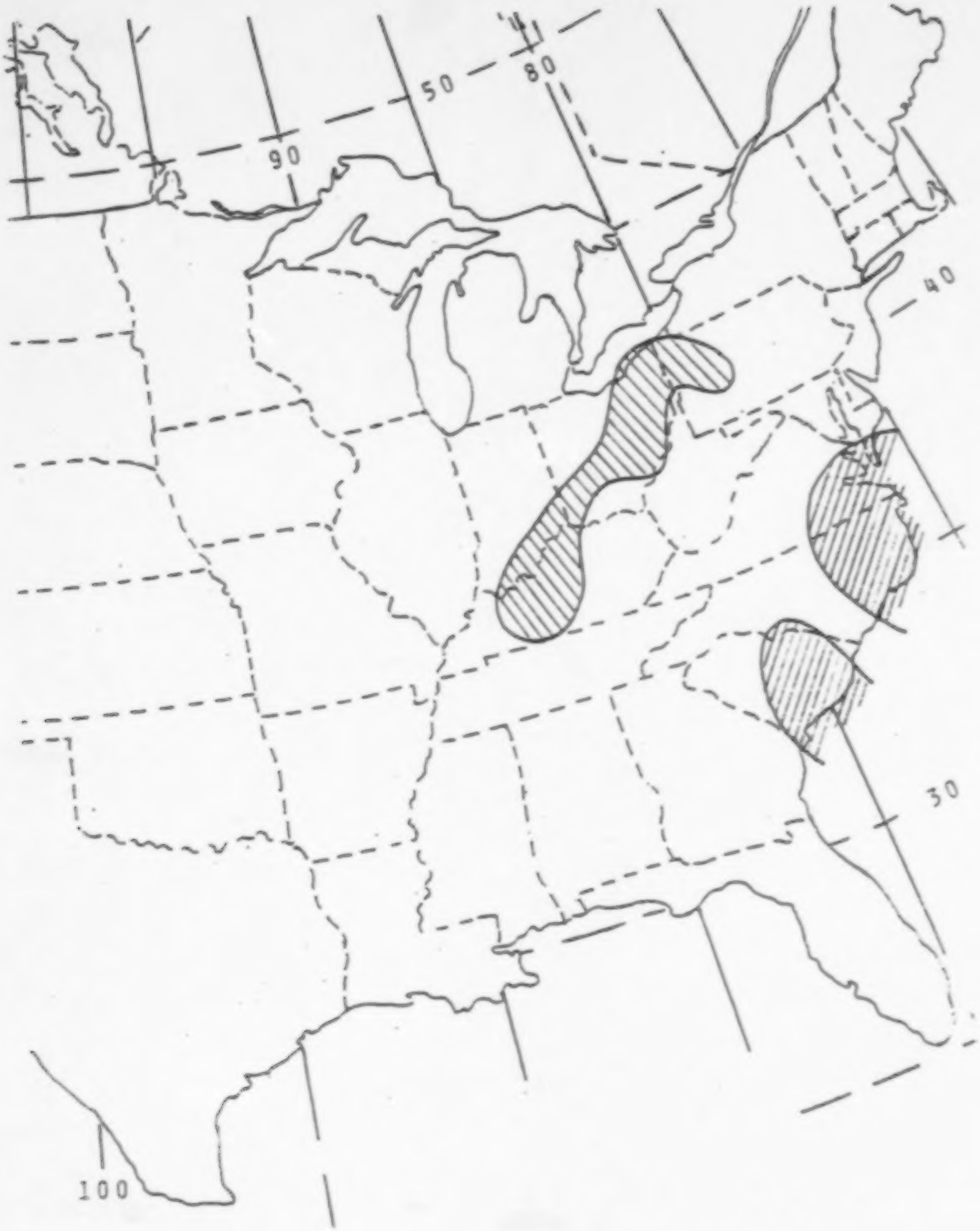

Figure 7. General areas in which persistent haze/smoke lasts for a week or more at least once in 5 years.

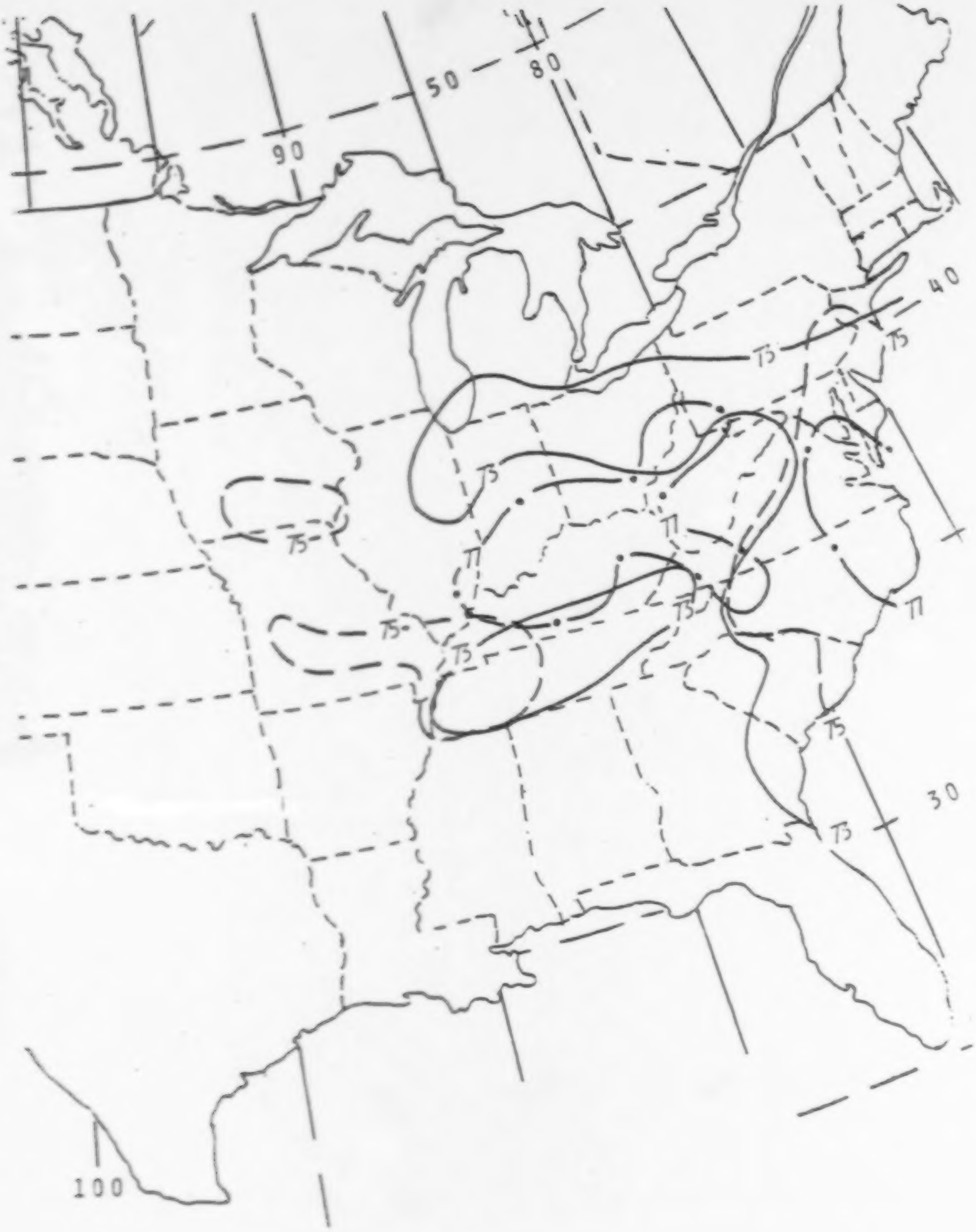

Figure 8. Illustrating interannual variability. Isopleths of >4 consecutive days of haze/smoke for the years 1973, 1975, and 1977.

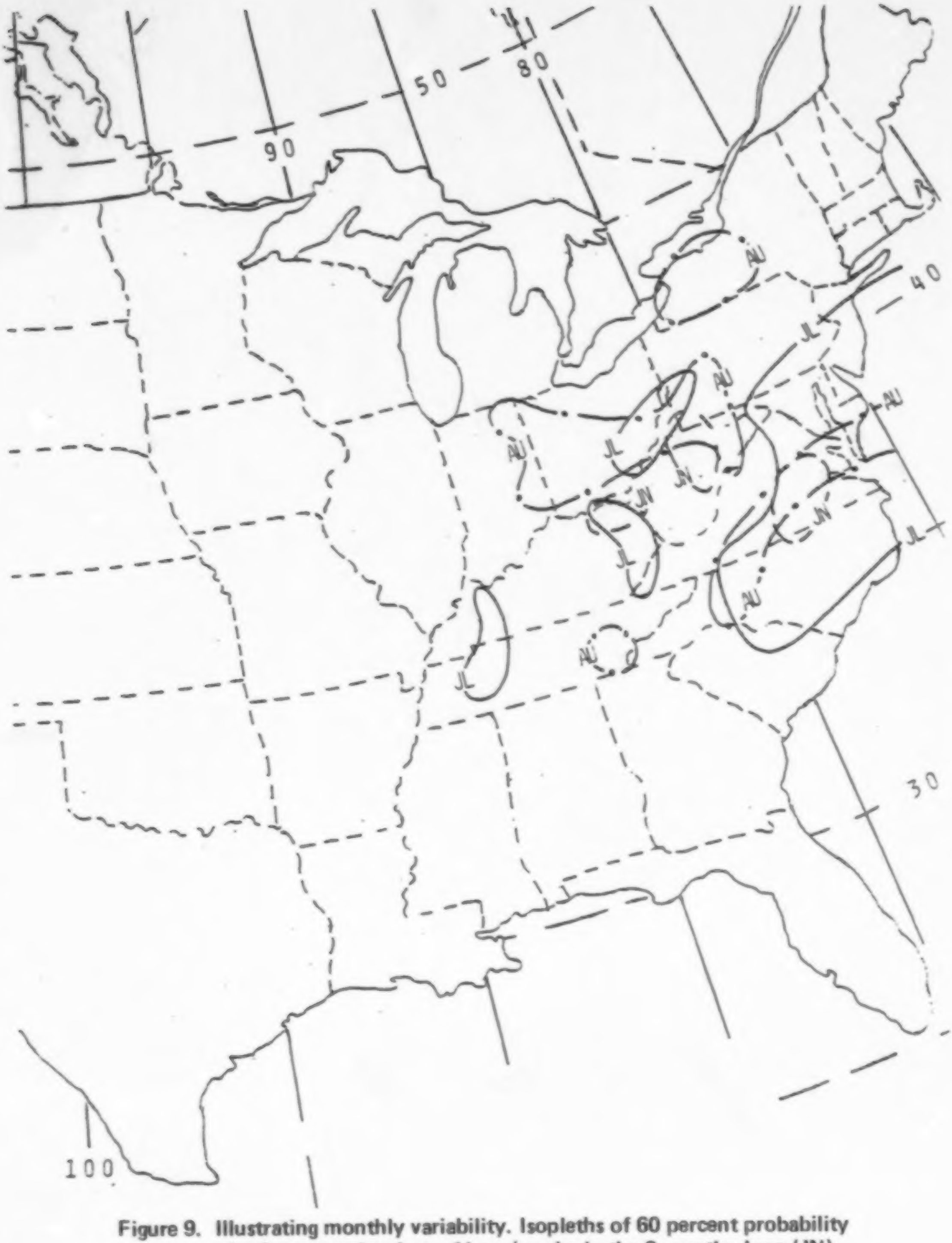

Figure 9. Illustrating monthly variability. Isopleths of 60 percent probability of >4 consecutive days of haze/smoke in the 3 months June (JN), July (JL), and August (AU).

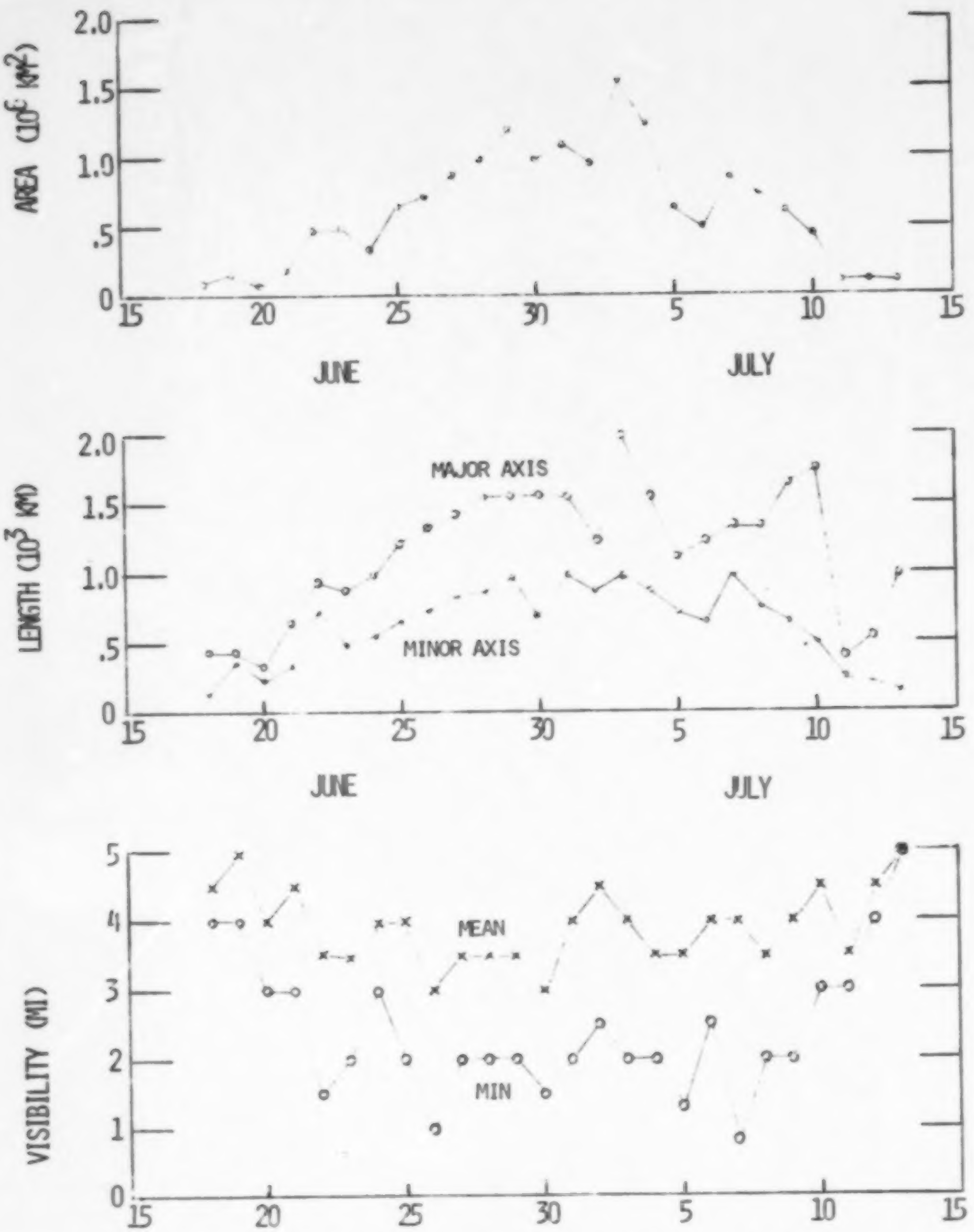

Figure 10. Evolution of areal and linear dimensions of HK areas during the major episode June 18–July 13, 1975. Associated mean and minimum visibilities are also shown.

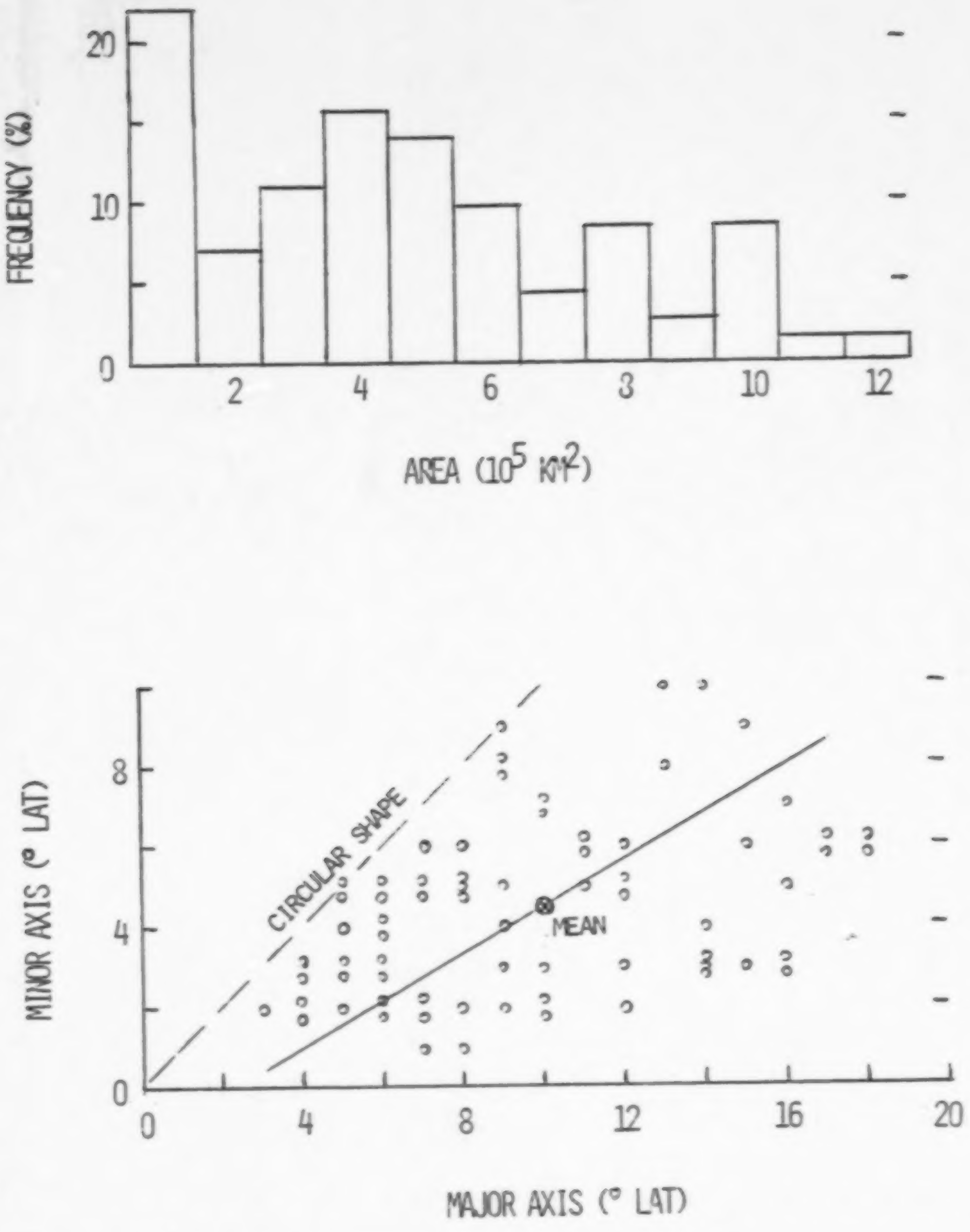

Figure 11. Upper chart: histogram of relative frequency of overland areal coverage of haze/smoke blobs for all episodes, September 1973–1977. Lower chart: scatter diagram of major versus minor axes of haze/smoke blobs for the same 5-year period. The solid line is an eye-estimated line of best fit.

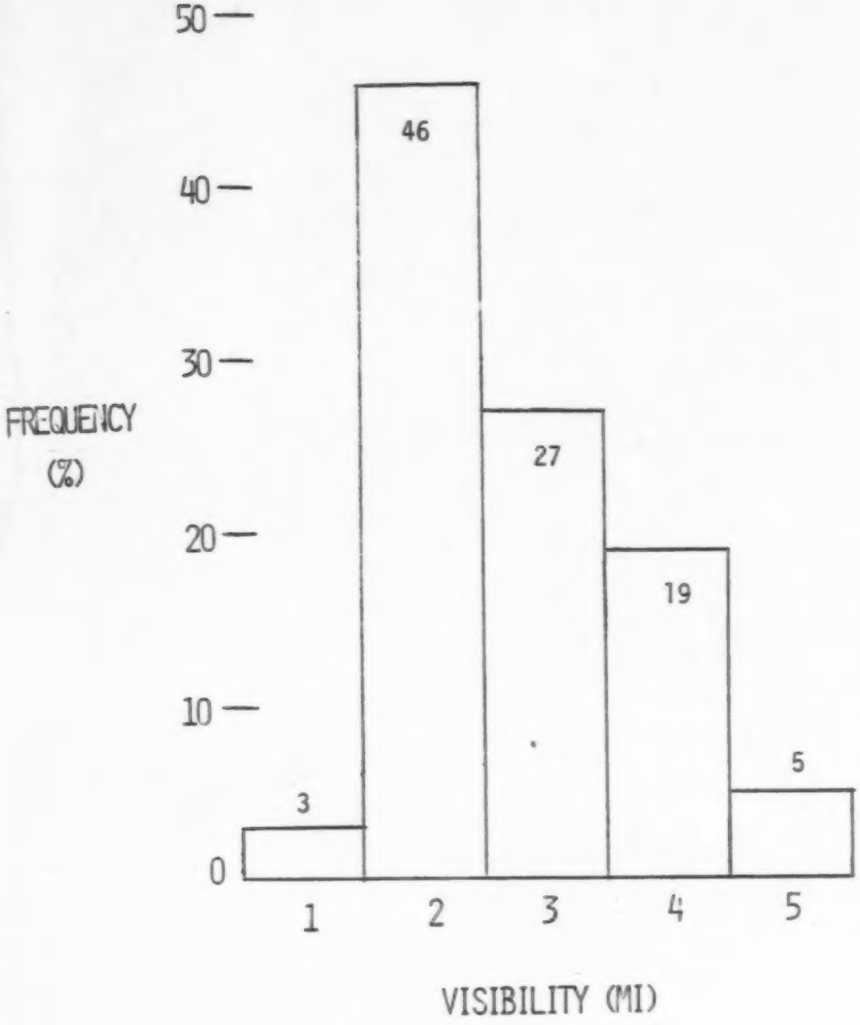

Figure 12. A relative frequency histogram of minimum visibilities during haze/smoke episodes, September 1973–1977.

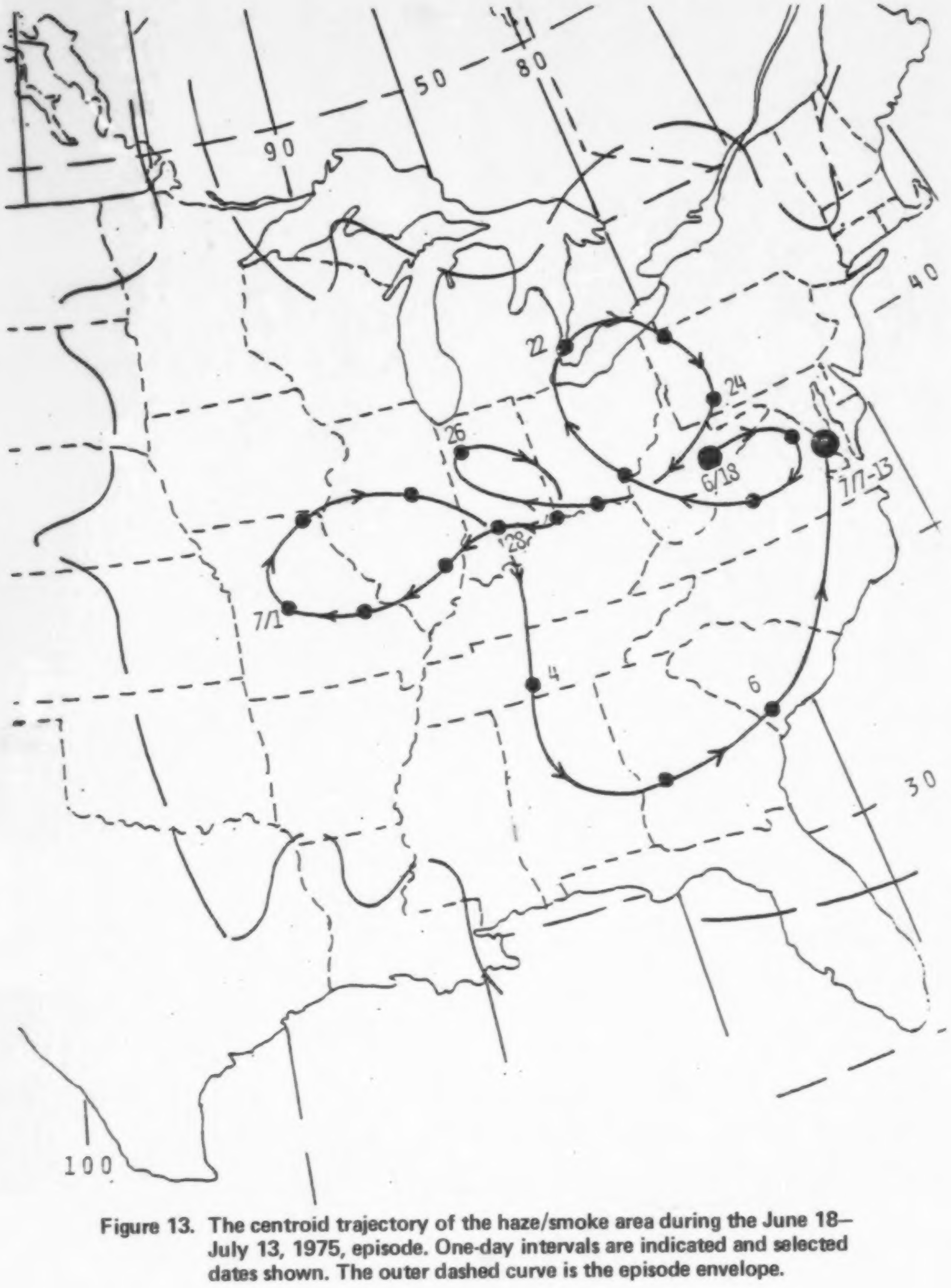

Figure 13. The centroid trajectory of the haze/smoke area during the June 18–July 13, 1975, episode. One-day intervals are indicated and selected dates shown. The outer dashed curve is the episode envelope.

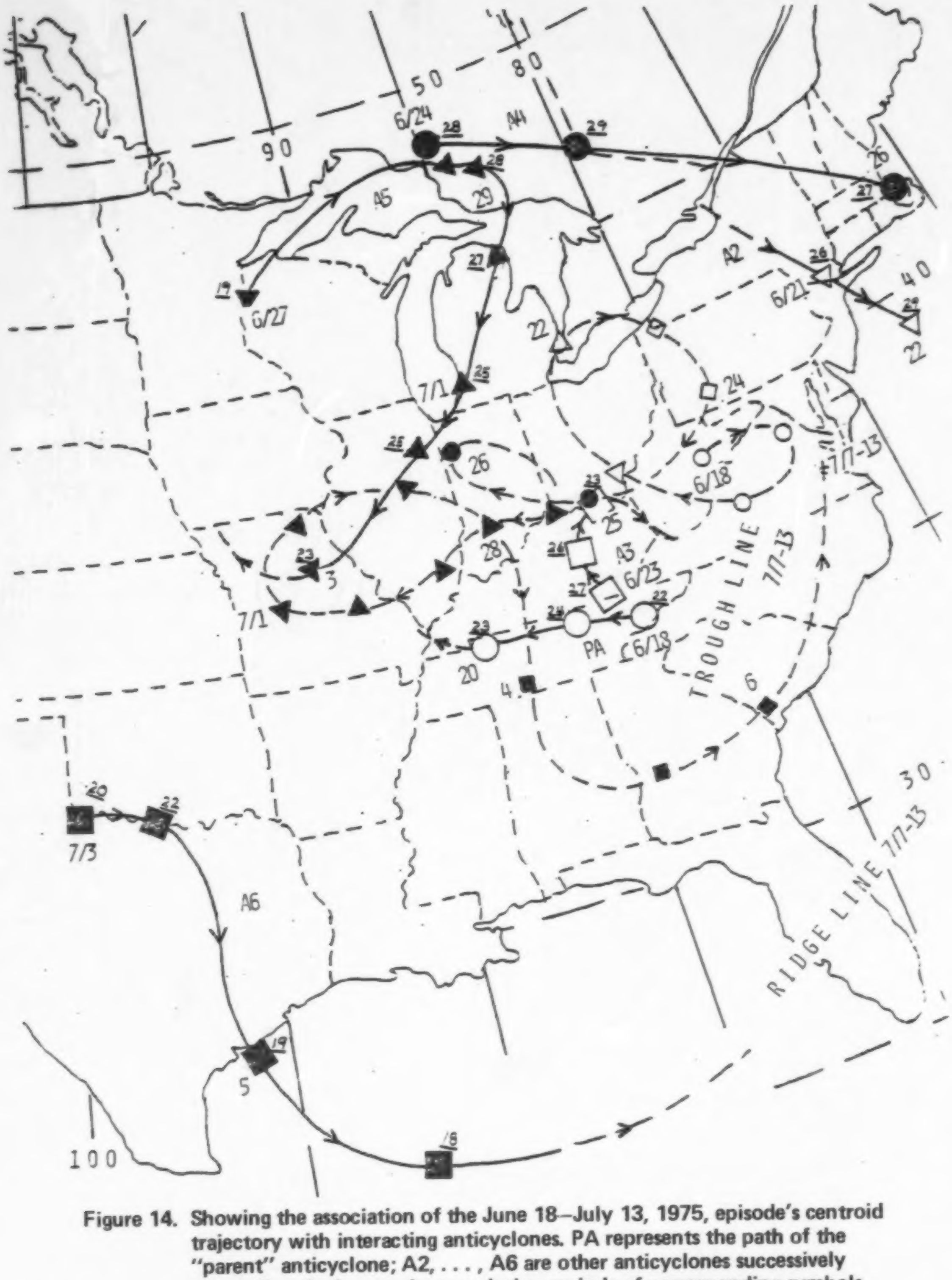

Figure 14. Showing the association of the June 18–July 13, 1975, episode's centroid trajectory with interacting anticyclones. PA represents the path of the "parent" anticyclone; A2, . . . , A6 are other anticyclones successively controlling the haze trajectory during periods of corresponding symbols. Selected dates are indicated, and central pressures are underscored.

		OBSERVED			NO RELATION	
		STAGNATING HIGH			STAGNATING HIGH	
		y	n		y	n
HK	y	16	30	46	16	30
	n	10	20	30	10	20
		26	50	76	26	50

$\chi^2 = 0$

A

HK	y	12	16	28	10	18
	n	7	19	26	9	17
		19	35	54	19	35

$\chi^2 = 1.3$

B

Figure 15. "Observed" relationship between the occurrence of warm stagnating high pressure systems and haze/smoke (HK) episodes. The "No Relation" table results from assumed random association. Case A: June–October 1973 plus May–October 1974 and 1975. Case B: same as A excluding 1973. See the text for further discussion.

TABLE 1. HAZE/SMOKE EPISODES EAST OF THE ROCKY MOUNTAINS IN THE 5-YEAR PERIOD JUNE 1973–MAY 1978 (see the text for explanation)

Month / Year	Jan	Feb	Mar	Apr	May	Jun	Jul	Aug	Sep	Oct	Nov	Dec
1973						9 — 29 NE EC	1 → 1 NE EC SE	1 → 1 NC NE EC SE	1 → 4 NE EC SE SC C	6-13 NE		
1974						28 → 15 * NE EC	14 - 31 NE EC C	7-12 NE 20-28 NE EC	4-13 NE 14-22 SC	11-15 * NE 29 → 3 * NE		
1975		11-15 C			4-9 SC 17-26 NE EC	18 → 13 C NC NE EC SE	16-25 * NE 27 → 26 NE EC	28 → 11 * C EC				
1976						8-16 NE EC SE C 22-25 NE	5-12 EC SE 20-31 NE EC	10-16 NE 20-28 C NE	2-5 EC 15-21 EC SE			
1977				15-21 NE	16-24 EC 30 → 1 * NE EC	11-18 NE EC C	4-24 NE EC 27 → 1 * NE EC	11-16 * C NE 20-28 EC 31 → 14 C NE		24 → 1 NC C		
1978		1-5 C NC 9-12 * C NE 15-22 * NE EC			22 → 6 NC NE							
# Episodes/ Duration Range (days)	0	4/4-7	0	1/7	5/3-16	7/3-21	9/6-31	8/6-31	7/4-30	4/5-9	1/6	0

SOME DYNAMIC ASPECTS OF EXTENDED POLLUTION EPISODES

William J. King and Fred M. Vukovich*

Research Triangle Institute
Research Triangle Park, North Carolina

Abstract

A boundary layer trajectory model was used to compute the residence time of air parcels within transient high-pressure systems of Canadian origin traversing the eastern Ohio River Valley. A strong correlation was noted among the presence of a transient anticyclone, elevated pollution levels, deteriorating horizontal visibility, and the length of time an air parcel had been entrained in the boundary layer of the high-pressure system.

INTRODUCTION

A large body of research over the past decade has been devoted to the "elevated pollution episode" (EPE) and the "persistent elevated pollution episode" (PEPE). One phase of this work, as performed by the Research Triangle Institute, has revolved around the investigation of nonurban ozone buildups, particularly as they relate to high-pressure systems and their movement (Bach et al., 1976; Vukovich et al., 1977; Decker et al., 1976; EPA Report No. 450/3-74-034; and EPA Report No. 450/3-75-036.) This extended research effort has suggested the following major conclusions:

1. Atmospheric conditions in a high-pressure system lend themselves to the rapid synthesis of ozone, providing sufficient ozone precursors have been injected into the system.
2. High ozone during the summer months is associated with high-pressure systems.
3. The concentration of ozone within an air parcel in a high-pressure system correlates with the residence time of the air parcel within the system.

---

*Speaker.

4. Air parcels on the "back side" of a moving high-pressure system have had the longest residence time and contain the highest ozone concentrations in the system.
5. Maximum residence times within a moving high-pressure system vary inversely with the speed at which the system is moving.
6. Maximum ozone concentrations in transient high-pressure systems on the continental United States are higher the farther east (where the population density is greatest) the system moves, suggesting the importance of anthropogenic sources of ozone precursor material to the synthesis of ozone within the high.

There has been limited evidence that pollutants other than ozone reach high levels in high-pressure systems (Husar et al., 1976, and Vukovich, 1979). Restricted horizontal visibility due to lithometeor obstructions to vision (smoke and/or haze) has been suggested as a possible indicator and method of monitoring the progress of an EPE. This paper presents a preliminary evaluation of the dynamic meteorological conditions in a restricted visibility state utilizing the same basic research techniques that were developed during the course of the RTI summer ozone field programs. Comparisons have been made among the various data components to determine the relative coincidence of peaks in air pollution levels and minimum visibility readings in the area of the Ohio River Valley. Then the dynamics of several transient anticyclones are examined to see just how well system residence times compare with in situ visibility and pollution concentration data.

Several surface analyses were performed over a macroscale study area centered along the Ohio River Valley and including most of the northeast and north central United States from approximately 36° to 46° north and from 73° to 92° west. This region was selected because, in the summer of 1974, a number of transient anticyclones traversed the area during periods when two major air pollution monitoring programs were operating. The Research Triangle Institute's Summer Ozone Study field network stations were operating at Wilmington, McConnellsville, and Wooster, Ohio; DuBois, Pennsylvania; and McHenry, Maryland. At the same time, the Electric Power Research Institute's SURE network was taking 24-hr average measurements of sulfate, sulfur dioxide, and total suspended particulate. The SURE stations were located at Rockport, Madison, and Lawrenceburg, Indiana; Collins, Illinois; Huntington and Wheeling, West Virginia; Scranton, Pennsylvania; and Albany, New York.

Weather data for the period including visibility, present weather, station pressure, dry bulb and dew point temperatures, surface analyses, and anticyclone movement were obtained from U.S. Department of Commerce publications such as Daily Weather Maps; Climatological Data, National Summary; and Local Climatological Data summaries for 61 National Weather Service (NWS) first-order stations over an 18-State area.

In addition to the primary study area, a 500 × 500 km square mesoscale study area centered around Columbus, Ohio, was used for certain detailed analyses including the effects of system residence time upon pollution levels and horizontal visibility.

PEAKS IN STATION PRESSURE, AIR POLLUTION, AND RESTRICTED VISIBILITY

A simple test was devised for comparing the relative coincidence of occurrence of maximum values of station pressure, various pollutant concentrations and restricted visibility. The data for this test were taken from the mesoscale study area previously described and were compiled as follows:

1. Station pressure--the area-averaged, daily average station pressure (inches of mercury) computed from the following cluster of NWS stations in northern Ohio: Akron, Cleveland, Columbus, and Youngstown;
2. Restricted visibility--the area-averaged, 1700 EDT visibility reported at the following cluster of NWS stations: Akron, Cleveland, Mansfield, and Youngstown. The 1700 EDT visibility was used in order to remove the effects of morning fog.
3. Ozone--the area-averaged, 8-hr average (1200-2000 EDT) ozone concentration ($\mu g\ m^{-3}$) computed from the following RTI ozone monitoring sites in Ohio: Wilmington, McConnellsville, and Wooster.
4. Sulfate, sulfur dioxide, and total suspended particulate (TSP)--the area-averaged, 24-hr average concentration ($\mu g\ m^{-3}$) computed from the following EPRI SURE stations: Lawrenceburg, Indiana; Huntington and Wheeling, West Virginia.

Numbering the days consecutively beginning with 16 June 1974 (day 1) and running through 31 August 1974 (day 77), the day relative to day 1 when peaks were reached in each of the above listed parameters are given in Table 1.

From these data, station pressure seems to peak generally before the other parameters, particularly restricted visibility. This is precisely the predicted relationship: the high-pressure system moves through an area; the pressure rises and peaks as the center passes the monitoring station; during this time, pollution levels rise and visibility deteriorates with peaks being reached in the air on the "back side" of the high. In order to determine which of these parameters most closely follows the trend in restricted visibility, the data in Table 1 are used to compare the date of occurrence of maximum restricted visibility relative to the date of occurrence of peaks in the other parameters (Table 2).

These 14 cases suggest that maximum restricted visibility correlates best with peaks in sulfate, ozone, and total suspended particulate. Also, the primary pollutant, sulfur dioxide, appears to reach a maximum concentration in advance of the other pollutants and then tapers off, most probably because of its reactive nature. This contrasts with the results of Vukovich (1979), which suggest that the SO_2, SO_4, and TSP peaks occur simultaneously. Noteworthy is the fact that, with only three exceptions, minimum visibility was reached at the same time or after each of the selected pollutants peaked.

FOUR CASE STUDIES

In order to examine the relationships of visibility to air pollution in more detail, the following case study periods were defined:

July 9-15, 1974	(days 24-30)
July 15-19, 1974	(days 30-34)
July 19-23, 1974	(days 34-38)
August 4-8, 1974	(days 50-54)

Each case study covers a period between major frontal passages when a transient anticyclone of Canadian origin traversed the Ohio River Valley including the 500 × 500 km mesoscale study area. It has been found that west to east moving Canadian high-pressure systems remain relatively free of pollution buildups until they penetrate the industrialized north central United States (Bach et al., 1976; Vukovich et al., 1977). In every case, the center of the anticyclone passed to the north of Columbus, Ohio; three times within 200 km and once within 400 km.

As suggested earlier, as long as an air parcel remains in the domain of a moving high-pressure system, potential exists to develop higher concentrations of certain pollutants. This is particularly true of secondary pollutants such as ozone and sulfate. Figure 1 shows the residence time of air parcels within a circular symmetric anticyclone relative to the speed at which the system is moving. These residence time representations evolved from a boundary layer trajectory model (Vukovich et al., 1977). This same model was used to calculate the residence time isopleths within the 500 × 500 km study area for each day of each case study period. There follows a discussion of the results of this modeling effort and the general meteorological conditions for each case study.

July 9-15 Case Study

A rather intense anticyclone developed on July 9 to the northwest of Hudson Bay and began immediately moving to the south. An idealized representation of the system's location and direction of movement each day at 1700 EDT is given in Figure 2. For simplification, the anticyclone is represented by a circle with a 1,000-km radius. System speed and approximate central pressure are also indicated.

On day 29, the high-pressure system had stalled and was beginning to exhibit the first signs of anticyclolysis. The approximate position of the system on day 29 is indicated by the dashed circle centered in the extreme southeast corner of the Columbus study area. The system had totally dissipated by the following morning.

Figure 3 shows the 500 × 500 km study area centered on Columbus, Ohio. The isopleths indicate the residence time of air in the high-pressure system. Pollutant and meteorological milestones are noted. As the high-pressure system advanced, it slowed steadily, the center traversing the northern portion of the study area on day 27 (Figure 2). On days 28 and 29, the air over the study area was on the "back side" of the system in the region of longest residence times (Figure 3). The total suspended particulate concentration peaked out on day 28, with visibility and each of the other pollutants following suit on day 29 (Figure 4).

On day 30, a weak cold front traversed the study area. The frontal zone showed little temperature variation but could be identified by an elevated dew point temperature and a 180° wind shift across the frontal zone. However, surface winds remained relatively light both behind and ahead of the front. As the front passed, the pollutant concentrations decreased. The visibility increased, except in an isolated region around Lake Erie extending south into West Virginia where smoke and haze continued to restrict visibility after the front had passed and well into the evening of day 30 before clearing. Why this anomaly occurred is not readily apparent from the available data.

July 15-19 Case Study

On July 15 (day 30), a ridge of high pressure developed over the north central United States and central Canada with its center northwest of Lake Superior. Figure 5 documents the progress of this large anticyclone, the center of which traversed the northern portion of the Columbus study area on the evening of day 31, picking up speed as it progressed. By the afternoon of day 33, the center was off the coast of Virginia. Although this idealized representation indicates the system had passed out of the Columbus area, the actual synoptic picture shows the system to be considerably larger with the study area still on the "back side" of the high. Figure 6 shows the residence time modeling analysis.

Of the four case studies, this July 15-19 anticyclone best exhibits the relationships suggested by the research in the previous section about visibility deterioration, anticyclone movement and system residence time. The reactive primary pollutant, sulfur dioxide, peaks early (day 31), followed the next day by the pressure peak as the anticyclone center traverses the study area. On day 33, the study area is on the "back side" of the high where air has reached maximum residence time within the system. On this day, visibility reached a minimum and the sulfates, total suspended particulate, and the secondary pollutant ozone, which is normally associated with photochemical smog, reached a maximum. Figure 7 shows the pattern of restricted visibility on day 33 on the "back side" of the high. By day 34, the strong cold front shown in Figure 7 had moved through the study area. The passage of this front, which was accompanied by rain showers and a pronounced wind shift, resulted in a dramatic reduction in air pollution levels and a corresponding increase in visibility.

July 19-23 Case Study

An anticyclone formed in the Beaufort Sea off the north shore of Alaska on July 13. It then took 6 days to make its way southeastward across Canada, entering our study area (Figure 8) on July 19 (day 34). At this point, partially blocked by a low off Nova Scotia, the high slowed and turned eastward, the center passing just north of the study area. Upon reaching the New England coast, the anticyclone again accelerated and continued up the coastline finally dissipating south of Labrador.

The residence time modeling analysis (Figure 9) exhibits some rather interesting milestones. Although total suspended particulate peaked early (day 35), TSP levels remained near that peak through day 38. This EPE did not terminate due to a frontal passage, but rather due to anticyclolysis on day 38. On day 37, the "back side" of the high was still quite well defined. Both the fairly reactive pollutants, ozone and sulfur dioxide, reached peaks. As dissipation set in on day 38, the system became disorganized with pressure dropping rapidly in the study area and some rain shower activity noted. Ozone and sulfur dioxide concentrations decreased sharply while sulfate reached a peak. Visibility dropped again significantly and the sulfates increased on day 38.

August 4-8 Case Study

This broad anticyclone formed just south of Victoria Island the evening of July 31 moving south and southeast until it was centered over northern Nebraska the morning of August 4. It then turned 90 degrees and headed almost due east, dissipating off the New England coast on August 8 (Figure 10). The residence time analysis is shown in Figure 11. The sulfur dioxide peaked on day 52, and the other parameters on day 53 (Figure 12).

AIR MOTION DYNAMICS, RESIDENCE TIME, AND ELEVATED POLLUTION EPISODES

Figure 13 shows idealized trajectories of air parcels in the boundary layer in high-pressure systems. Two out of the three trajectories show air parcels that leave the boundaries of the high-pressure system very quickly. One of the air parcels, that which originates in the northeastern quadrant of the high-pressure system, travels hundreds of miles in the domain of the high-pressure system due to the circulation within that system. It is interesting to note that though that air parcel has traveled hundreds of miles, it passes over its own trajectory only a few tens of miles away from its origination point. It is this air parcel that has the large residence time within the high-pressure system and is most likely to be associated with elevated pollution episodes within the high-pressure system.

The northeastern quadrant of a high-pressure system is generally characterized by northwesterly flow (Figure 14) and is the region of the high-pressure system that characterizes post-cold-frontal conditions. Generally low levels of pollutants are found in this air mass for two reasons: there is rainout of the pollutants and deep mixing associated with the front. The air mass behind the front is generally cold, dry Canadian air, which is relatively free of air pollutants. Shenfeld (1977) has shown relatively low concentrations of oxidants to exist in the forest lands of Canada where this air mass originates. As this air moves southward, it is modified through the injection of heat and moisture at the surface. Furthermore, the concentration of primary air pollutants increases in the air mass due to injection from each city and town, which act as isolated point sources. Chemical reactions take place and some primary pollutants are gradually transformed, creating secondary pollutants within the air mass. As these reactions continue, the concentrations of the secondary air pollutants increase.

However, as the high-pressure system continues to move eastward, the region comes under the influence of the air on the "backside" of the high, which is generally flowing from the south (Figure 15). This southerly flow is warm and moist and, depending upon its trajectory, may be relatively free of air pollutants. Decker et al. (1976) has shown that air parcels that have a long fetch over water are generally free of air contaminants. Their study was in the Gulf of Mexico where the warm, moist air on the "back side" of the high generally originates. As this air mass moves northward, it is modified by two processes. First there is a transport of heat and moisture at the surface; and also there is entrainment of the cooler, dryer, generally more polluted air ahead of this air mass. The entrainment of the polluted air and the injection of pollutants into the air mass at the surface from population centers in the region increases the potential for producing an elevated pollution episode. It is important to note that elevated pollution episodes generally occur in the warm, moist air mass (see Bach (1975) for a correlation among moisture, temperature, and high levels of ozone). Water vapor appears in chemical reactions associated with the production of ozone and certain sulfur compounds. It is also an important factor in producing larger aerosols that might impede visibility.

Because residence time in high-pressure systems is a function of system speed (Figure 1), it is expected that the persistent pollution episodes occur in relatively slow moving highs or stationary high-pressure systems. In a stationary high-pressure system, there is generally very little exchange between the air within the high-pressure system and that outside the high-pressure system. Under these circumstances, the injection of primary air pollutants and the production of secondary air pollutants would continue unabated, particularly since a high-pressure system is relatively free of cloud cover that would interfere with solar radiation reaching the surface.

REFERENCES

Bach, W. D., W. J. King, and F. M. Vukovich. 1976. Nonurban Ozone Concentrations in Transient High Pressure Systems. Presented at the Symposium on the Non-Urban Troposphere, Hollywood, Florida, November 14.

Decker, C. E., L. A. Ripperton, J. J. B. Worth, F. M. Vukovich, W. D. Bach, J. B. Tommerdahl, F. Smith, and D. E. Wagoner. 1976. Formation and Transport of Oxidants Along the Gulf Coast and in the Northern United States. Environmental Protection Agency, Report No. EPA-450/3-76-033, Research Triangle Park, NC.

Husar, R. B., D. E. Patterson, C. C. Paley, and N. V. Gillani. 1976. Ozone in Hazy Air Masses. Presented at the International Conference on Photochemical Oxidant Pollution and Its Control, Raleigh, NC, September 12-17.

Environmental Protection Agency. 1974. Investigation of Ozone and Ozone Precursor Concentrations at Non-Urban Locations in the Eastern United States. Report No. EPA-450/3-74-034, Research Triangle Park, NC.

Environmental Protection Agency. 1975. Investigation of Rural Oxidant Levels as Related to Urban Hydrocarbon Control Strategies. Report No. EPA-450/3-75-036, Research Triangle Park, NC.

Shenfeld, L. 1977. Report on Oxidants and Their Precursors in Canada. Proc. Int. Conf. on Photochemical Oxidant Pollution and its Control. EPA-600/3-77-001A, Research Triangle Park, NC, pp. 917-927.

Vukovich, F. M., W. D. Bach, B. W. Crissman, and W. J. King. 1977. On the Relationship Between High Ozone in the Rural Surface Layer and High Pressure Systems. Atmospheric Environment, 11:967-983.

Vukovich, F. M. 1979. A Note on Air Quality in High Pressure Systems. Atmospheric Environment, 13:255-265.

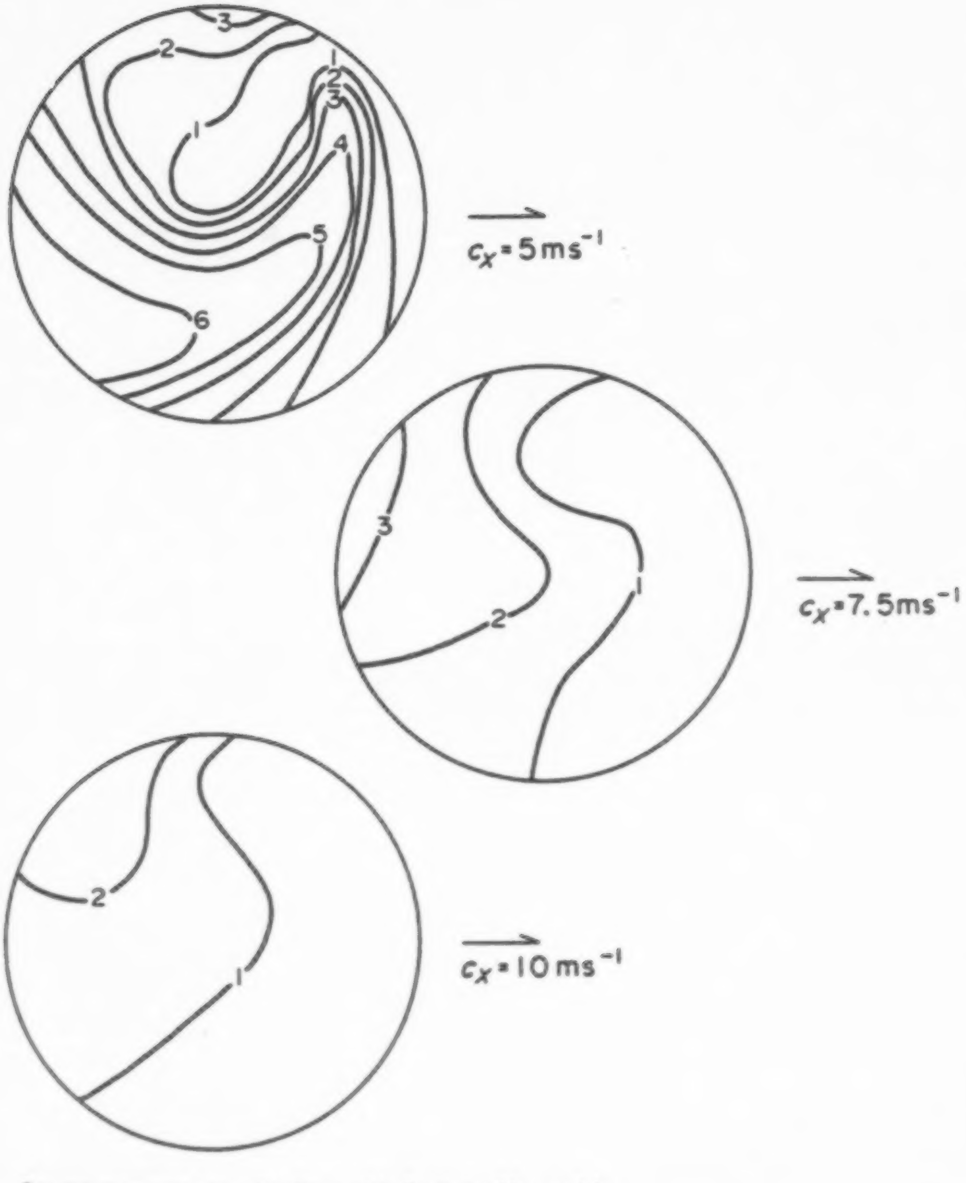

©1977 by Pergamon Press. This figure originally appeared in an article by F. M. Vukovich in volume 11 of *Atmospheric Environment*, p. 973.

Figure 1. The number of days air parcels in high-pressure systems have spent (residence time) within the system versus the speed of the system, for a circular symmetric high-pressure system with a radius of 1,000 km.

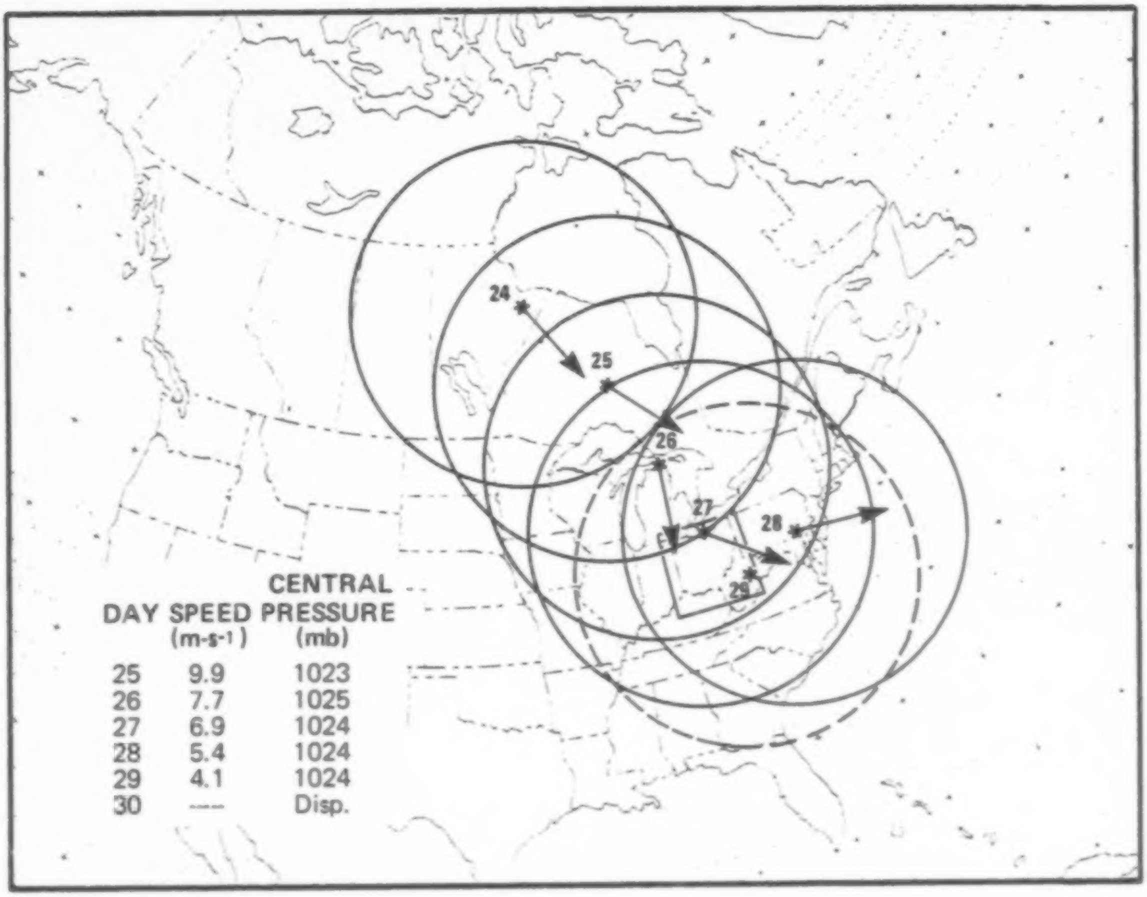

DAY	SPEED (m-s-1)	CENTRAL PRESSURE (mb)
25	9.9	1023
26	7.7	1025
27	6.9	1024
28	5.4	1024
29	4.1	1024
30	---	Disp.

Figure 2. Location and speed of movement at 1700 EDT each day for the July 9-15 case study. Also tabulated are 24-hr average speed for the system and central pressure at 1700 EDT.

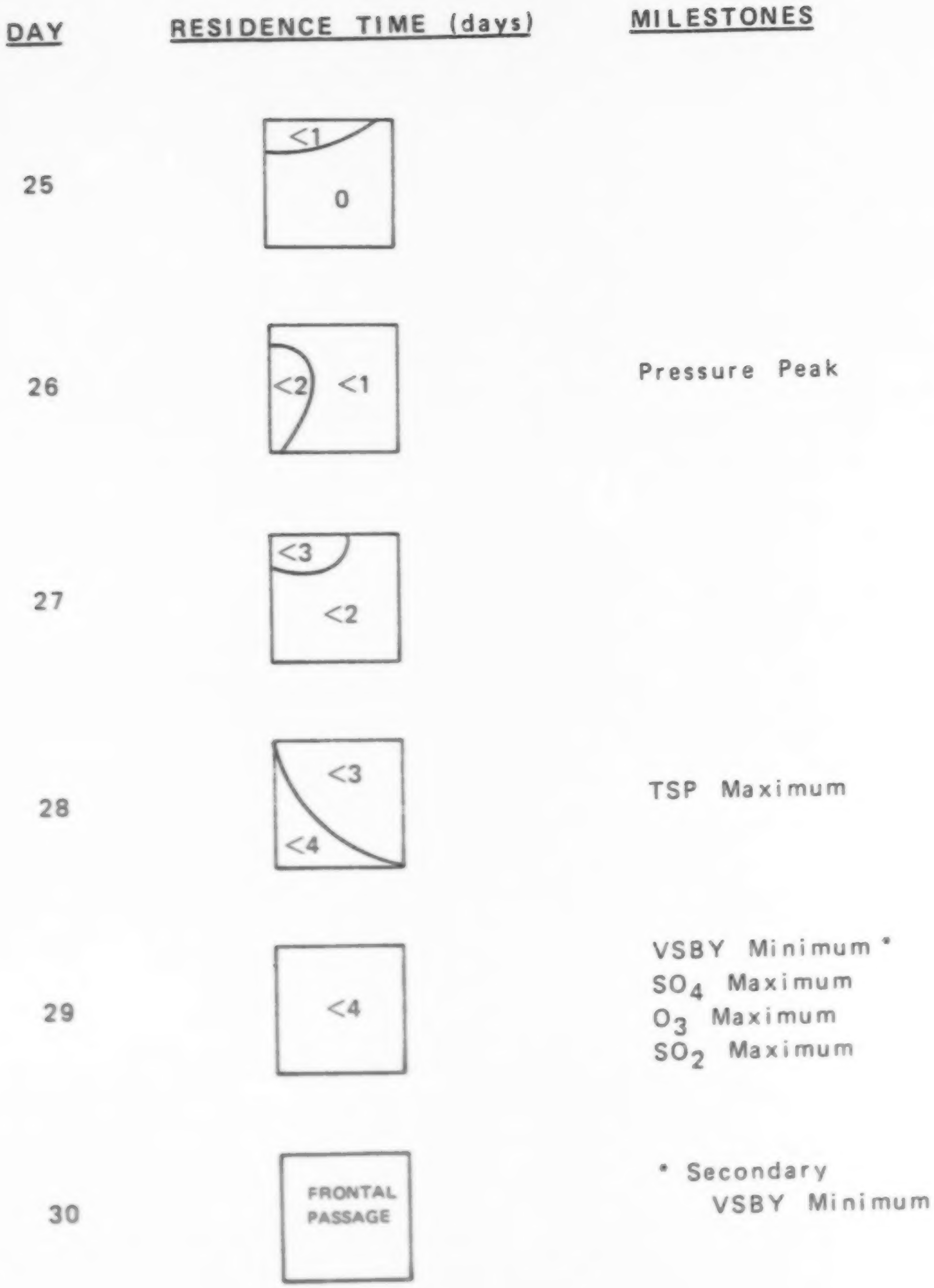

Figure 3. Residence time (days) for each day of the July 9-15 case study in the 500 × 500 km Columbus study area.

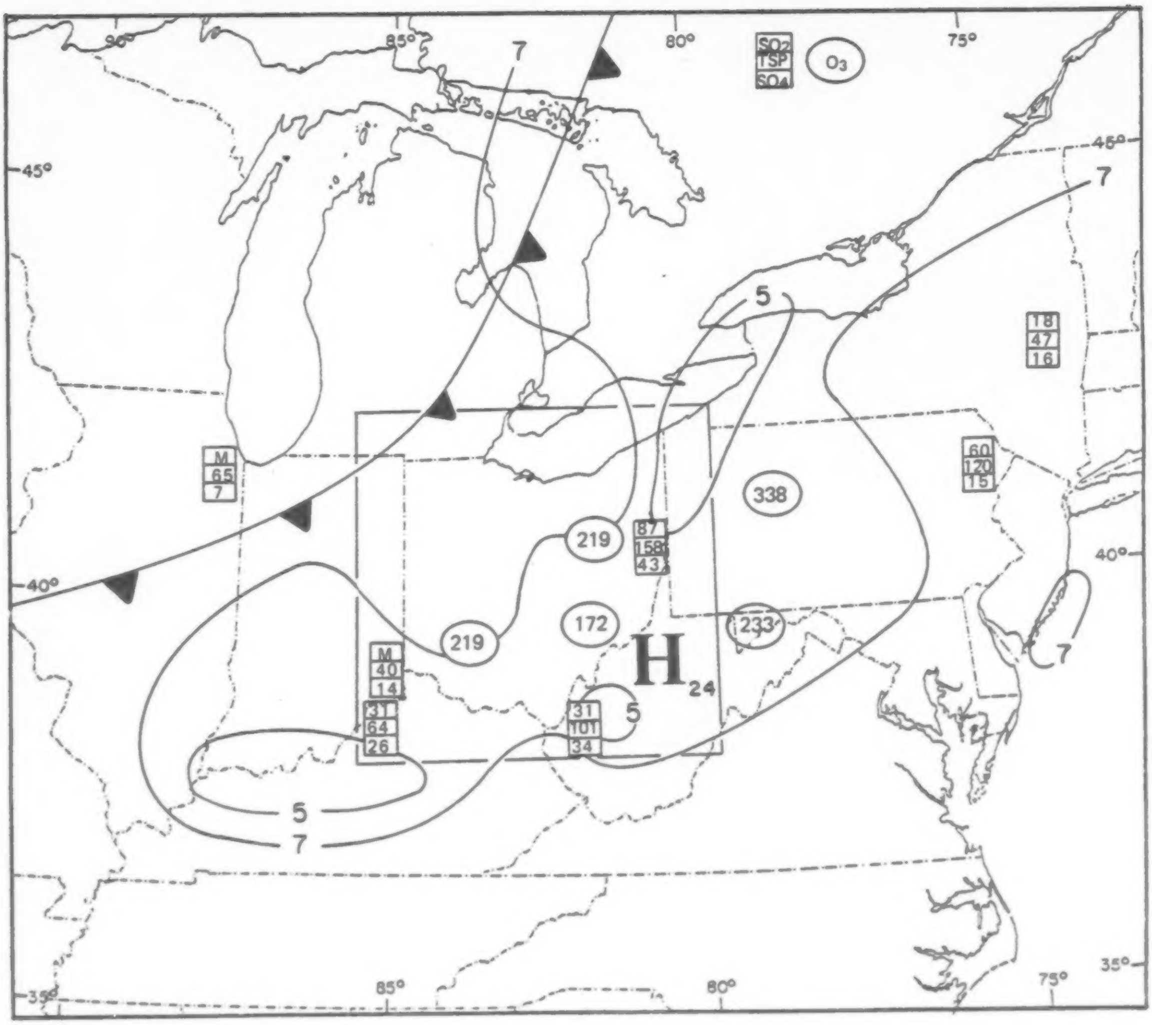

Figure 4. July 14 (day 29) surface weather analysis showing visibility isopleths (miles) and the location of pressure centers and fronts. Also shown are 8-hr average ozone values ($\mu g\text{-}m^{-3}$) from the RTI network and 24-hr average values for SO_2, TSP, and SO_4 ($\mu g\text{-}m^{-3}$) from the EPRI SURE network.

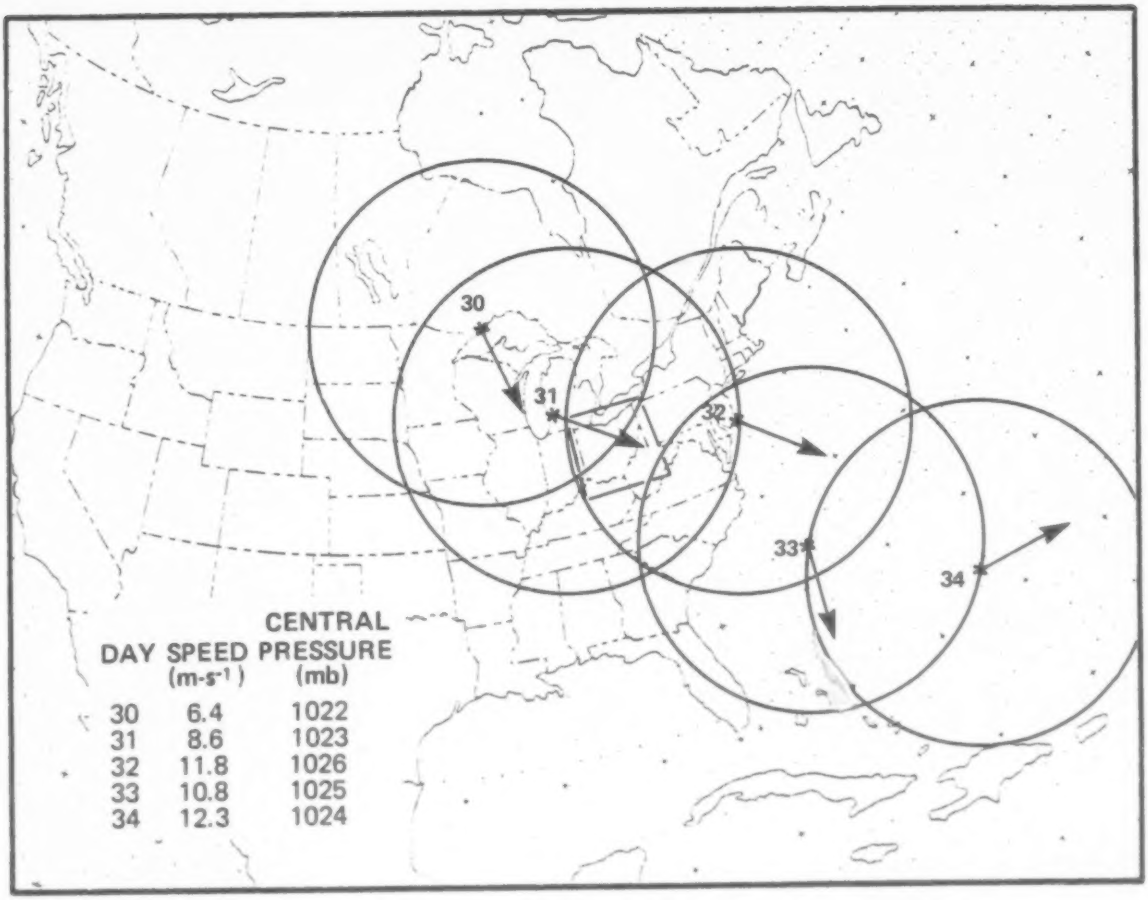

DAY	SPEED $(m\text{-}s^{-1})$	CENTRAL PRESSURE (mb)
30	6.4	1022
31	8.6	1023
32	11.8	1026
33	10.8	1025
34	12.3	1024

Figure 5. Location and speed of movement at 1700 EDT each day for the July 15-19 case study. Also tabulated are 24-hr average speed for the system and central pressure at 1700 EDT.

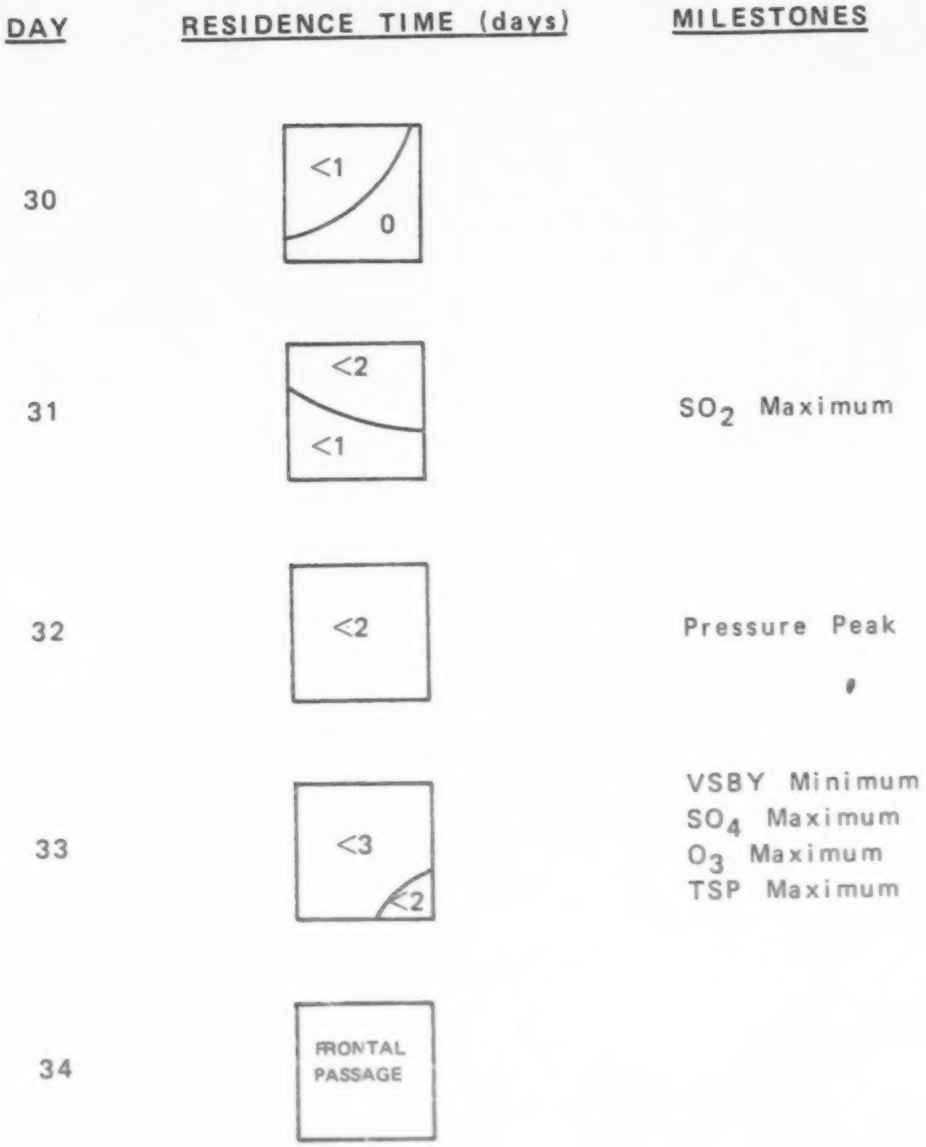

Figure 6. Residence time (days) for each day of the July 15-19 case study in the 500 × 500 km Columbus study area.

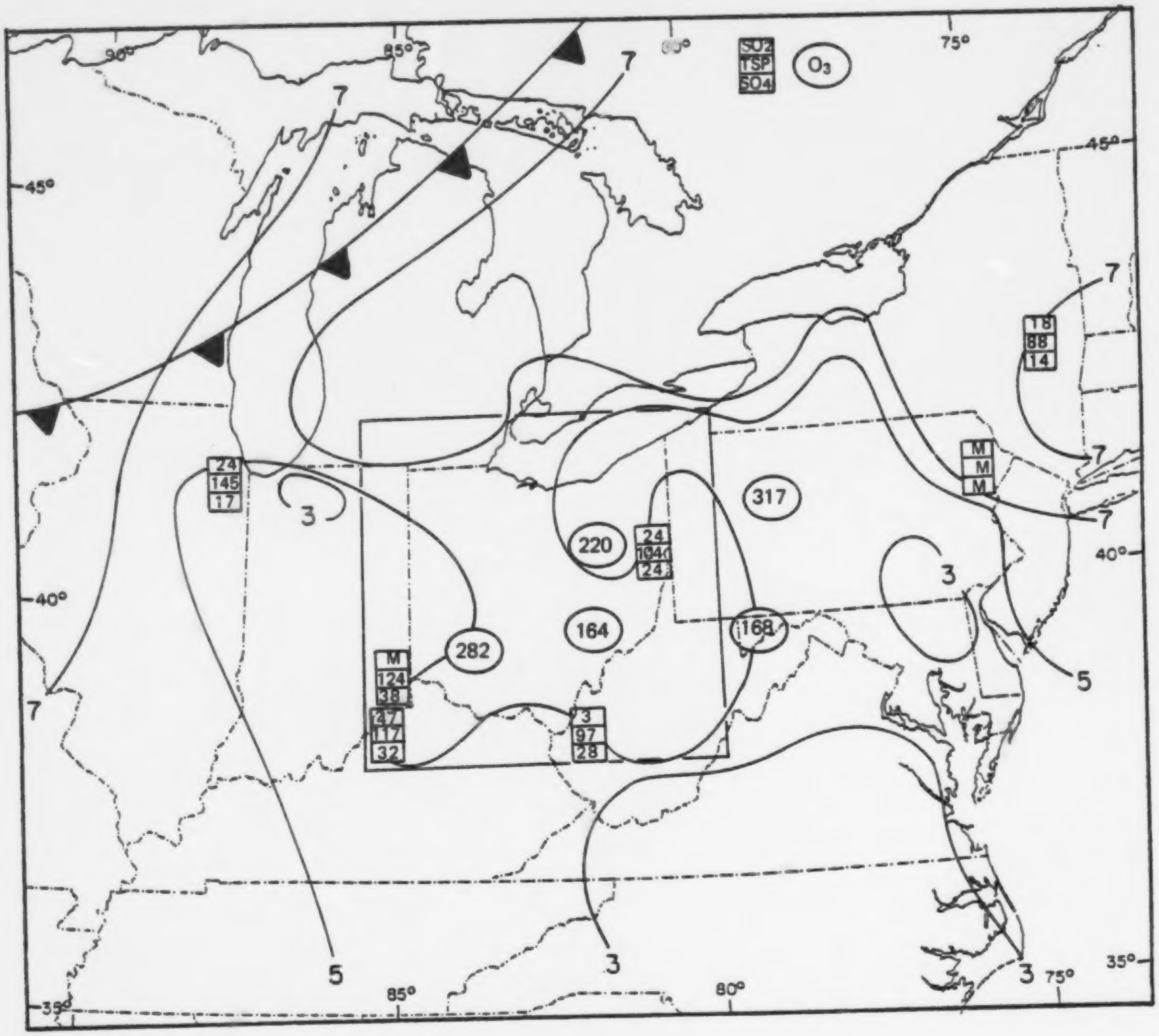

Figure 7. July 18 (day 33) surface weather analysis showing visibility isopleths (miles) and the location of pressure centers and fronts. Also shown are 8-hr average ozone values ($\mu g\text{-}m^{-3}$) from the RTI network and 24-hr average values for SO_2, TSP, and SO_4 ($\mu g\text{-}m^{-3}$) from the EPRI SURE network.

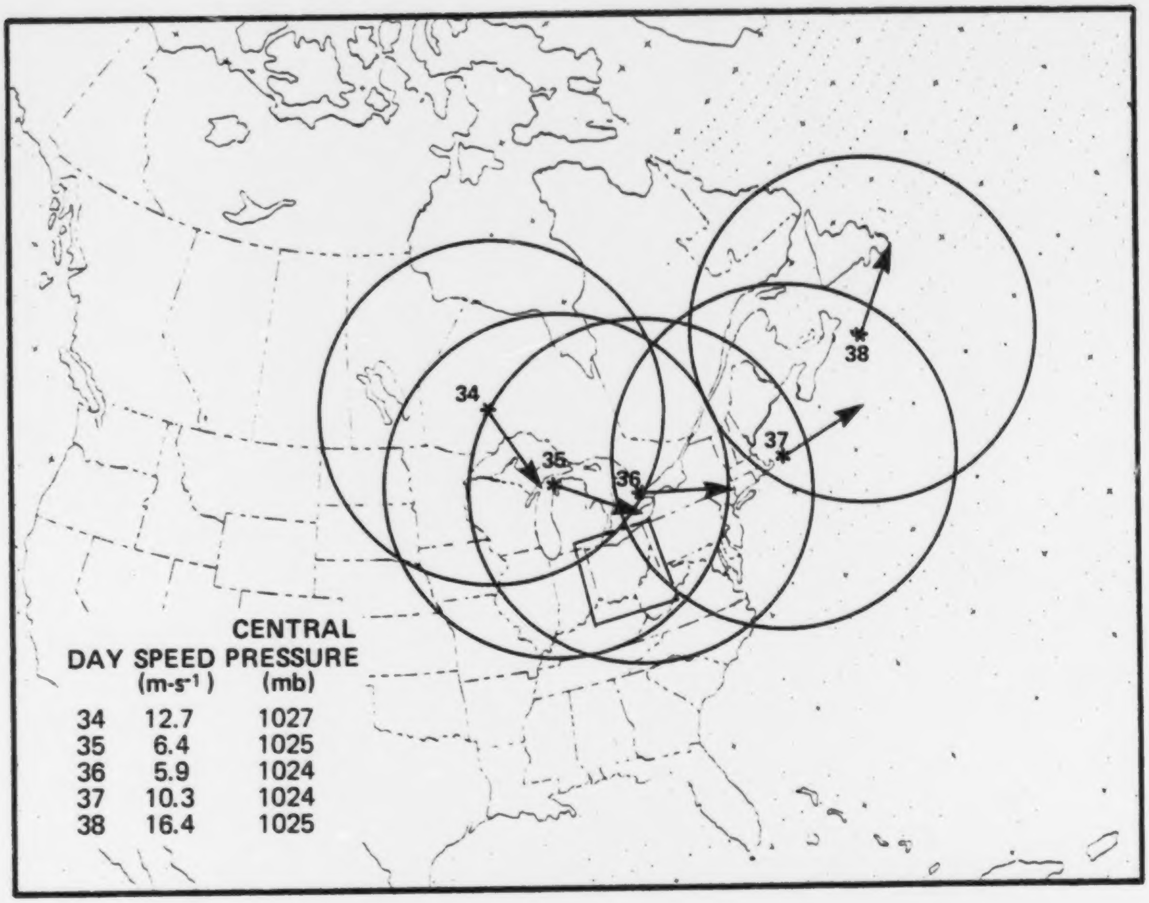

DAY	SPEED ($m \cdot s^{-1}$)	CENTRAL PRESSURE (mb)
34	12.7	1027
35	6.4	1025
36	5.9	1024
37	10.3	1024
38	16.4	1025

Figure 8. Location and speed of movement at 1700 EDT each day for the July 19-23 case study. Also tabulated are 24-hr average speed for the system and central pressure at 1700 EDT.

DAY	RESIDENCE TIME (days)	MILESTONES
34	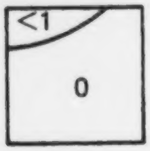	
35	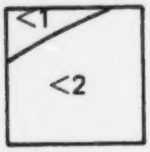	Pressure Peak TSP Maximum
36	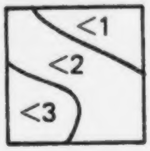	
37	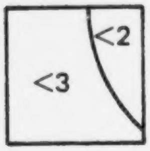	SO_2 Maximum O_3 Maximum
38	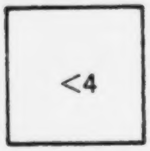	VSBY Minimum SO_4 Maximum

Figure 9. Residence time (days) for each day of the July 19-23 case study in the 500 × 500 km Columbus study area.

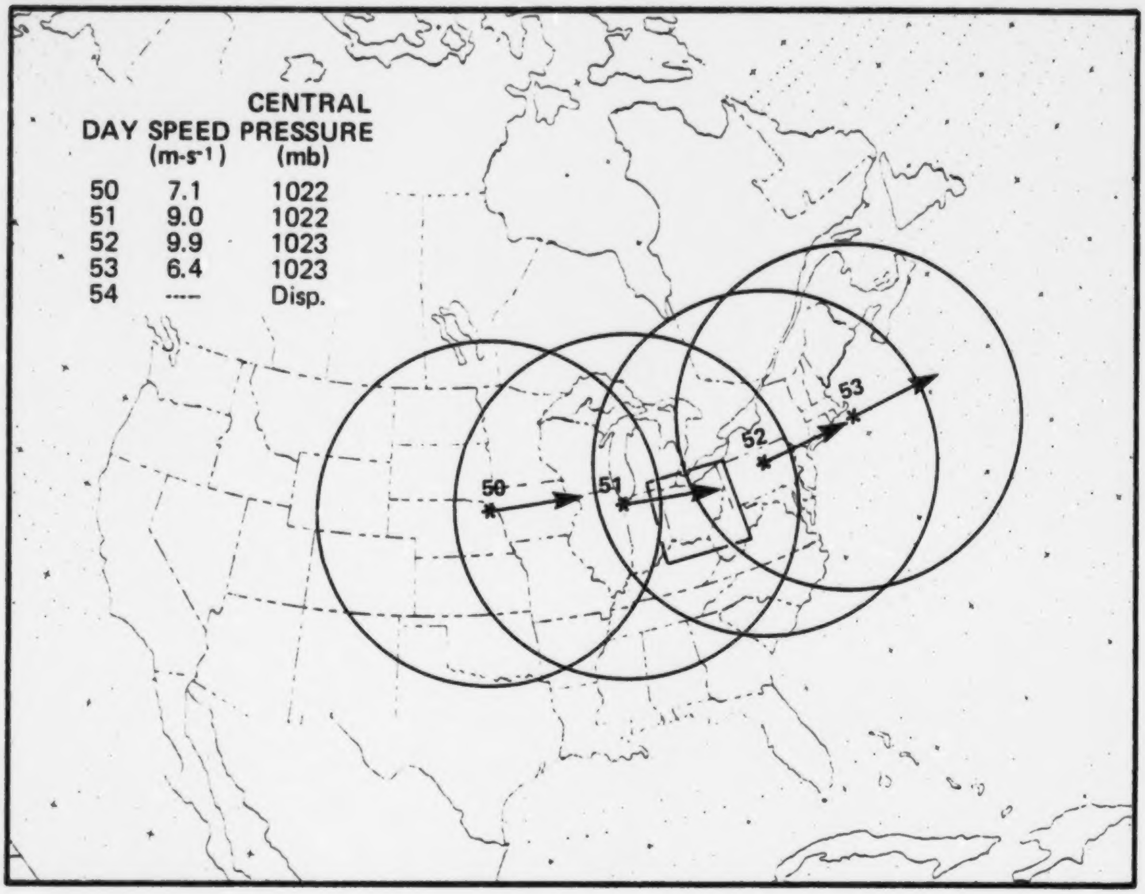

DAY	SPEED (m-s⁻¹)	CENTRAL PRESSURE (mb)
50	7.1	1022
51	9.0	1022
52	9.9	1023
53	6.4	1023
54	----	Disp.

Figure 10. Location and speed of movement at 1700 EDT each day for the August 4-8 case study. Also tabulated are 24-hr average speed for the system and central pressure at 1700 EDT.

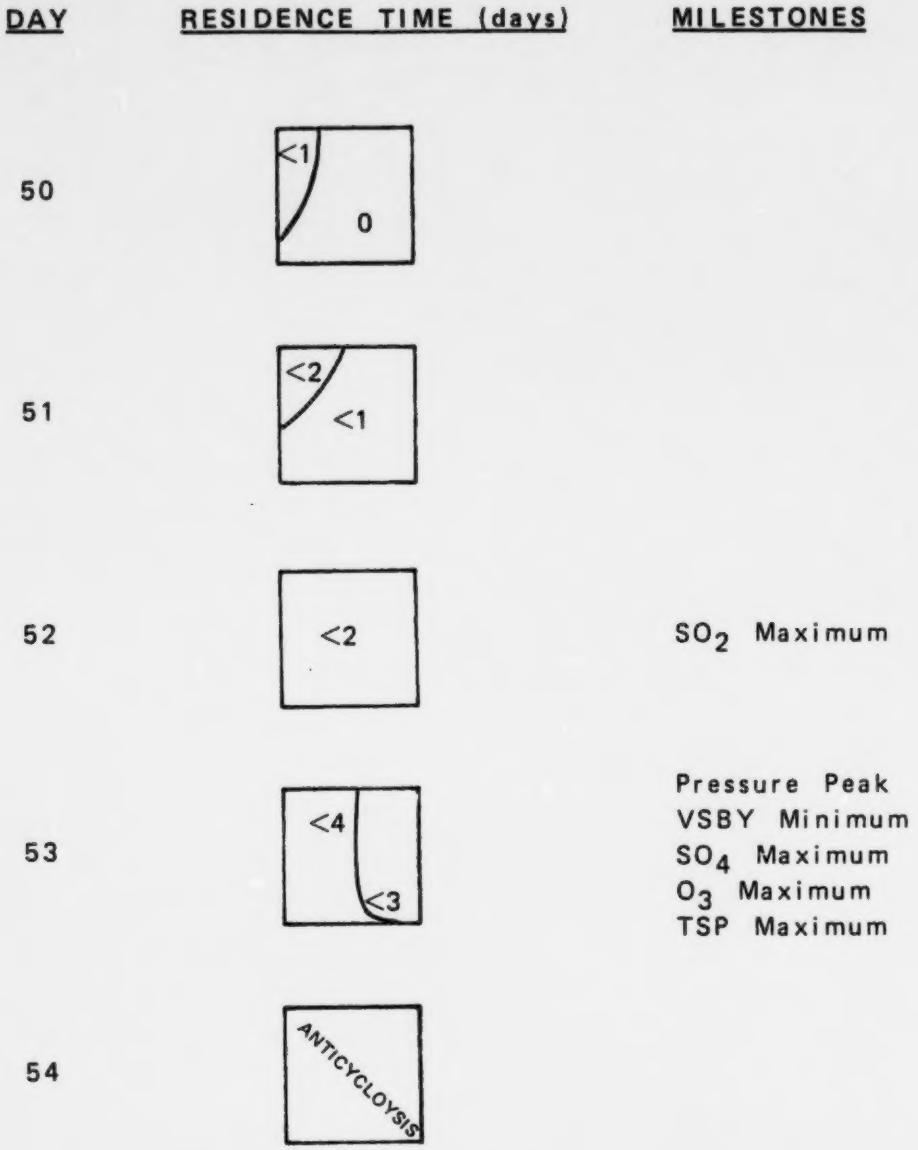

Figure 11. Residence time (days) for each day of the August 4-8 case study in the 500 × 500 km Columbus study area.

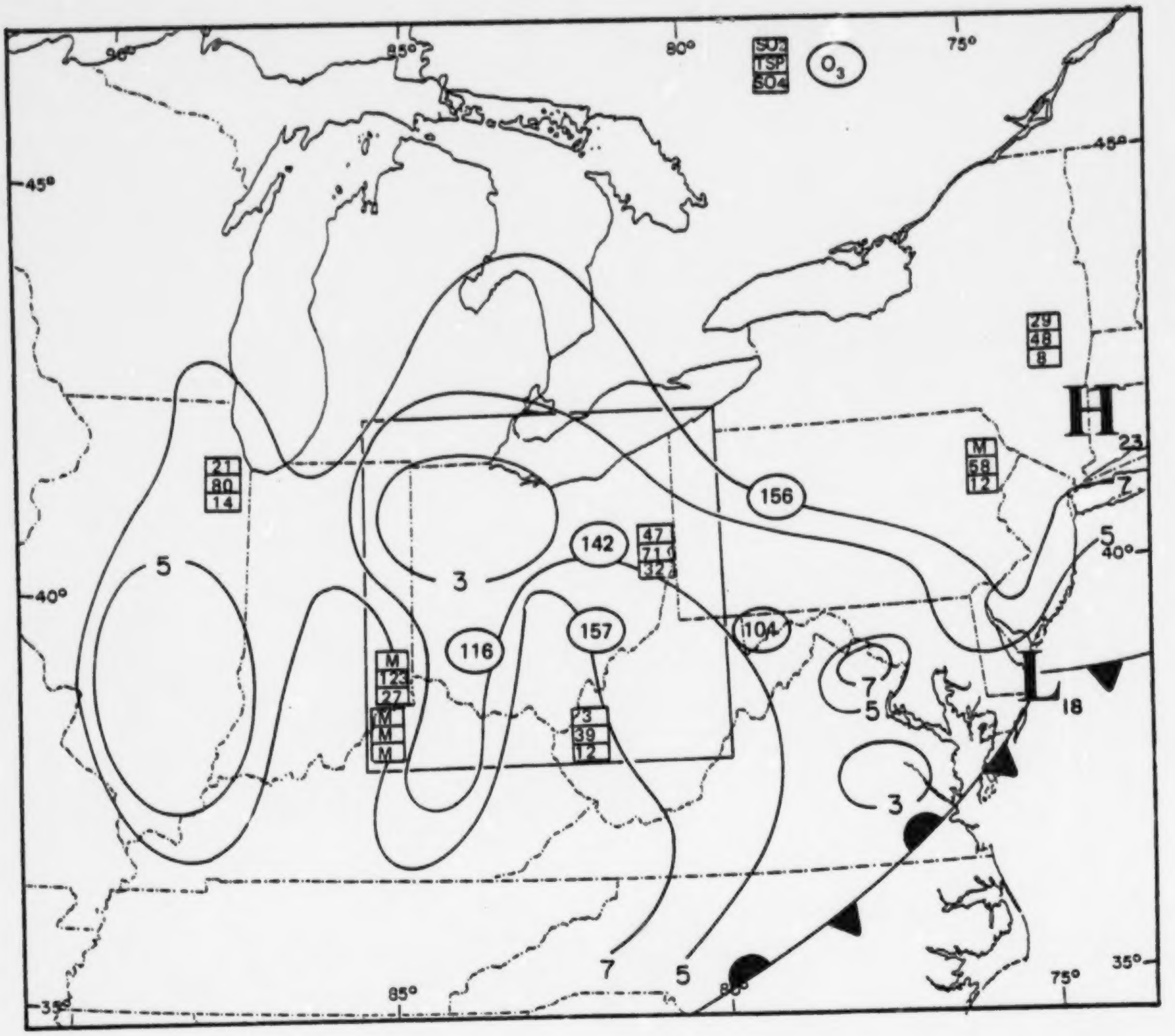

Figure 12. August 7 (day 53) surface weather analysis showing visibility isopleths (miles) and the location of pressure centers and fronts. Also shown are 8-hr average ozone values ($\mu g-m^{-3}$) from the RTI network and 24-hr average values for SO_2, TSP, and SO_4 ($\mu g-m^{-3}$) from the EPRI SURE network.

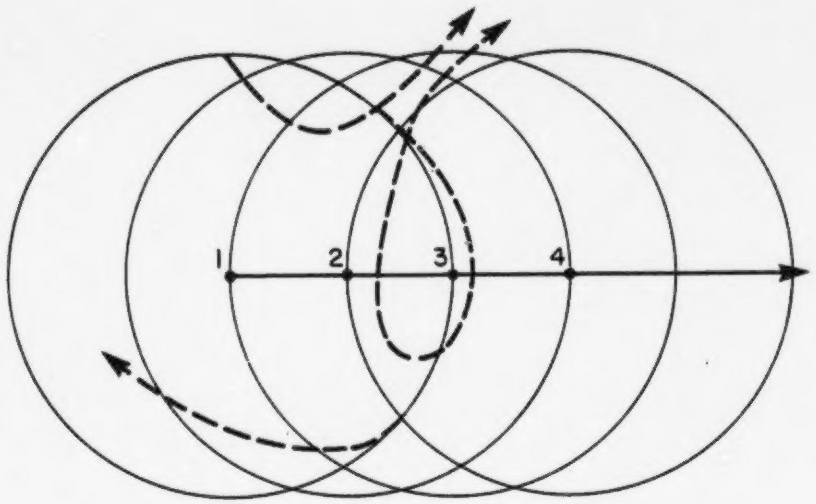

Figure 13. Three idealized trajectories of air parcels in the boundary layer of a moving high-pressure system.

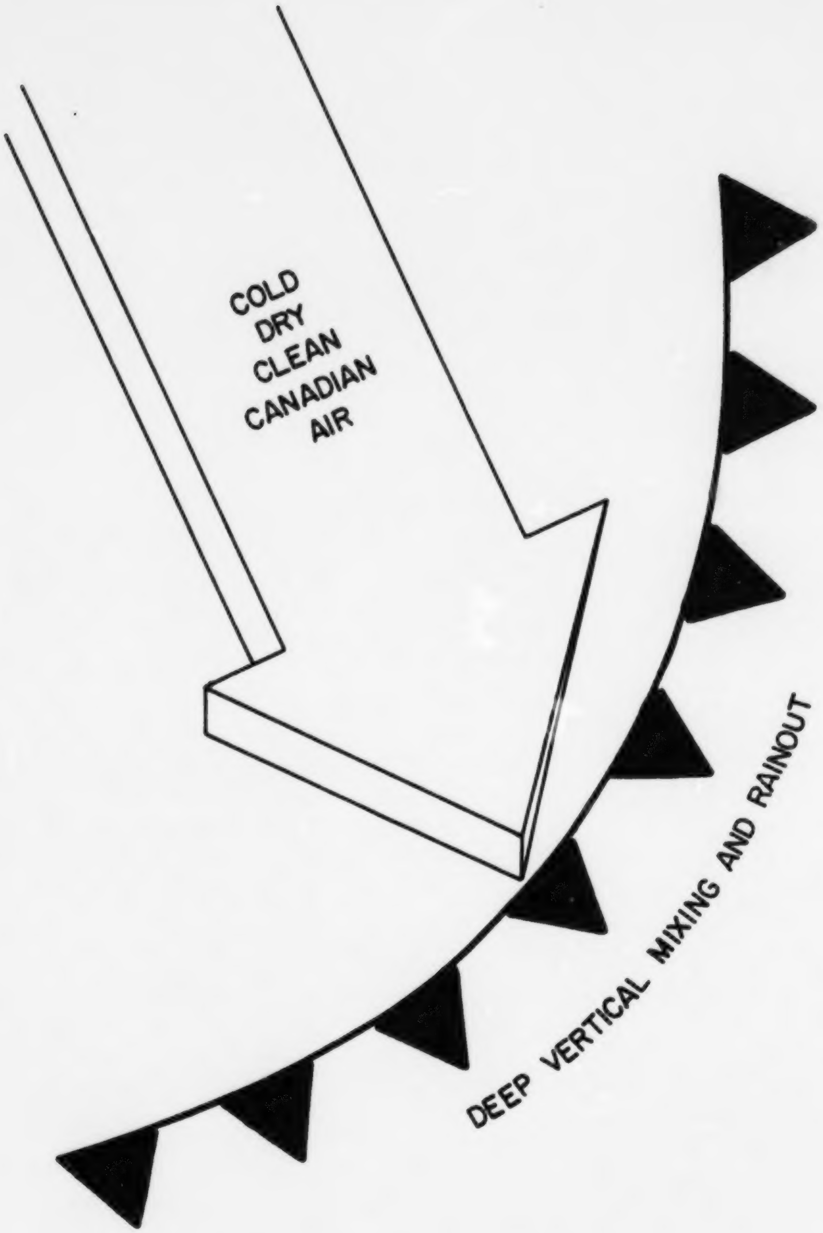

Figure 14. Leading edge of a high-pressure system.

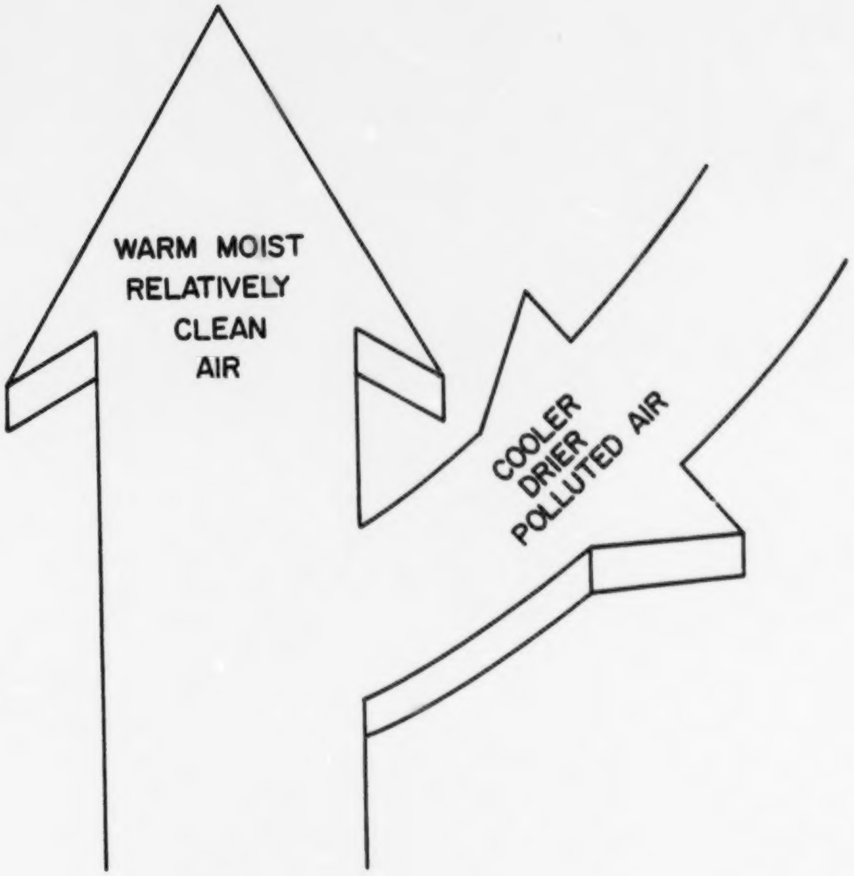

Figure 15. Trailing edge of a high-pressure system.

TABLE 1. THE DAYS VARIOUS PARAMETERS REACHED PEAKS (JUNE 16 = DAY 1)

Station pressure	Restricted visibility	Sulfate	Ozone	TSP	SO_2
4	5	5	5	5	7
18	18	18	18	18	18
22	24	24	25	24	24
26	30	29	29	28	29
32	33	33	33	33	31
35	38	38	37	35	37
40	42	42	41	42	41
47	48	47	48	47	-
53	53	53	53	53	52
56	56	56	56	56	55
61	62	61	61	61	61
66	67	66	66	66	66
67	69	69	70	69	69
71	73	72	73	72	72

TABLE 2. COMPARISON OF THE DATE MAXIMUM RESTRICTED VISIBILITY OCCURRED WITH THE DATE OF OCCURRENCE OF PEAKS IN SULFATE, OZONE, TOTAL SUSPENDED PARTICULATE, SULFUR DIOXIDE, AND STATION PRESSURE

	Number of times maximum restricted visibility occurred						
Peaks	2 days before	1 day before	Same day	1 day after	2 days after	3 days after	4 days after
Sulfate			9	5			
Ozone		2	7	5			
TSP			8	4	1	1	
SO_2	1		3	8	1		
Pressure			3	5	4	1	1

APPLICATION OF NUMERICAL MODELS TO PROLONGED ELEVATED POLLUTION EPISODES

C. Shepherd Burton* and Mei-Kao Liu

Systems Applications, Inc., San Rafael, California

Abstract

Many field experiments have been carried out recently to study the problem of pollutant transport over long distances under prolonged pollution episode conditions. The use of a numerical model designed to examine this problem is discussed in this paper. This model is composed of a plume module for treating the transport, dispersion, and chemical transformations of a limited number of plumes near major point sources, and a grid module for accommodating the advection, diffusion, chemical reactions, and surface deposition of pollutants from upwind boundaries as well as urban, and other widely scattered, sources. This model can be employed as a tool in designing a monitoring network, or it can be used to analyze and interpret data collected in the field measurement program.

INTRODUCTION

During the past few years, considerable effort has been devoted to the understanding of the problem of long distance transport of air pollutants from either major point sources or urban areas under prolonged pollution episode conditions. Several comprehensive field measurement programs have been carried out to characterize the problem. For example, the 1975 Northeast Oxidant Experiment was conducted to examine the role played by ozone and its precursors from upwind sources on many high oxidant concentrations observed in rural areas in the Northeast Corridor (Dimitriades and Altshuller, 1977). Another example is the Sulfate Regional Experiment, which was deployed to assess the relationships between sulfur oxide emissions and ambient air quality on regional scales (Hidy et al., 1976). More recently, the Midwest Interstate Sulfur Transformation and Transport (MISTT) study was performed to study the detailed distribution of sulfur oxides downwind of a large coal-fired power plant (Wilson, 1978).

---

*Speaker.

The MISTT study has provided a rich data base to aid in the understanding of the various atmospheric processes that dictate the transformations and distributions of sulfur oxides emitted from a coal-fired power plant. For example, Husar et al. (1978) have found that transport of pollutants is governed during daytime hours by the wind field in the mixed layer and by the nocturnal jet during nighttime. They have also found that the SO_2/sulfate conversion rates are higher during daytime hours. In addition, they have observed that plumes from elevated sources begin to mix downward early in the morning. Apparently, to analyze these phenomena, one must take into consideration diffuse sources from upwind urban areas.

In this paper, the use of a numerical model that is designed to simulate transport, diffusion, chemical reactions, and surface deposition is discussed. In the first section, the various components of the model are described. Next, the application of this model is delineated. In the last section, potential use of this model to the prolonged elevated pollution episodes (PEPE) is discussed.

DESCRIPTION OF THE MODEL

As stated earlier, the distribution of air pollutants to distances far downwind of sources is a result of the interplay between emissions from major point sources and the upwind background. Because of the differing characteristics that govern the transport and diffusion processes for point and diffuse sources, a hybrid modeling approach is proposed. This model consists of a plume module for treating a limited number of point sources in their initial phases, and a grid module for accommodating areal and diffuse sources. The major components of this model are briefly described in the next section.

The Grid Module

One of the intrinsic difficulties of regional scale modeling of the interaction between emissions from a major point source and those from diffuse sources emanating from upwind cities is the problem of spatial resolution. Obviously, grid spacings that are large enough to cover the region of interest are not sufficient for resolving the evolution of a point-source plume. Furthermore, according to classical diffusion theory, the spread of a pollutant cloud, as measured by the horizontal dispersion coefficient σ_y, initially grows as the first power of time and eventually approaches the square root of time. The short time limit, a valid description of the dispersion of a point source, is the basis for the Gaussian formulation; the large-time asymptotics, adequate for describing areal or diffuse sources, is the basis for the gradient transfer approach used in the grid model. For these reasons, separate approaches, as shown in Figure 1, have been adopted for modeling the plume and upwind diffuse sources.

The grid module, with the horizontal region of interest being divided into an equal-spaced grid, has two full vertical layers with which to handle advection, diffusion, and chemical reactions in the inversion layer and the mixed layer, and a surface layer embedded in the mixed layer for treating vertical diffusion and dry deposition.

The time-dependent multiple-species atmospheric diffusion equation in two dimensions is used as the model equation for the inversion layer and the mixed layer:

$$\frac{\partial c_i^\ell}{\partial t} + u^\ell \frac{\partial c_i^\ell}{\partial x} + v^\ell \frac{\partial c_i^\ell}{\partial y} = \frac{\partial}{\partial x}\left(K_x^\ell \frac{\partial c_i^\ell}{\partial x}\right) + \frac{\partial}{\partial y}\left(K_y^\ell \frac{\partial c_i^\ell}{\partial y}\right) + D^\ell \cdot f(D^\ell) + R_i^\ell + S_i^\ell , \quad (1)$$

$$i = 1, 2, \ldots, N ,$$

$$\ell = \begin{cases} \text{I: Inversion Layer;} \\ \text{II: Mixed Layer} \end{cases} ,$$

where c_i^ℓ is the vertically averaged concentration of species i; u^ℓ, v^ℓ, and k_x^ℓ, k_y^ℓ are wind velocities and turbulent diffusivities in the x- and y-directions, D^ℓ is the two-dimensional divergence (= $du^\ell/dx + dv^\ell/dy$), R_i^ℓ and S_i^ℓ are chemical reaction and volumetric source terms in the ℓ-th layer, respectively. The value of $f(D^\ell)$ denotes the corresponding concentration from influxes and outfluxes.

The major feature of this model equation is that the pollutant distribution is assumed to be uniform in the vertical direction for both layers. With this assumption, the model equation can be shown to be formally derived from the more general atmospheric diffusion equation. The compelling reason for using this assumption is that, for the scale of interest, the vertical diffusion term has been found to be one or two orders of magnitude greater than the transport term and the horizontal diffusion term (Durran et al., 1979). Because of the relatively large spatial scale employed, however, the pseudo-diffusion associated with the numerical solution of Eq. (1) can be overwhelming. Consequently, an accurate scheme must be used for the simulation of the transport term. On the basis of consideration of both predictive accuracy and computational speed, the SHASTA method (Boris and Book, 1973) was chosen for use in this study. This method consists of two computational stages: a transport stage that is conservative and nonnegative, and an antidiffusion stage designed to cancel, in part, the pseudo-diffusion generated in the transport stage. A comprehensive testing of this and other numerical methods indicates that, for the present application, the SHASTA method yields realistic results with a reasonable computational burden (Durran et al., 1979).

The Plume Module

To resolve the spatial-resolution problem, a multiple-box reactive plume model has been used to track the first phase of the plumes emanating from major point sources. At a sufficiently downwind location, pollutants contained in the plume module will be released into the appropriate grid in the grid module. The multiple-box reactive plume model (Liu, Stewart, and Roth, 1978) assumes that the width and height of cell j can be described by two parameters:

$$w^j = w^j (s) \quad , \qquad (2)$$

$$h^j = h^j (s) \quad , \qquad (3)$$

where w^j denotes the width of cell j, h^j is the vertical thickness of the plume, and s represents the distance downwind of a point source measured along the plume axis. On the basis of a mass balance, the governing equation along a wind trajectory, s, can then be expressed in the following manner:

$$\frac{dc_i^j}{dt} = \left(\frac{dc_i^j}{dt}\right)_{chem} - \left(\frac{1}{w^j} \cdot \frac{dw^j}{ds}\right) uc_i^j - \left(\frac{1}{h^j} \cdot \frac{dh^j}{ds}\right) uc_i^j \; , \qquad (4)$$

$$i = 1,2,\ldots, N, \; j = 1,2,\ldots, M,$$

where c_i^j denotes the concentration of chemical species i in cell j, u is the wind speed along the plume trajectory, and t is time since emission. Thus, the model can be envisioned as a series of temporally varying, expanding puffs released at fixed time intervals.

As envisioned in this model, the total mass of each primary pollutant is divided equally among M cells. By allowing the volume of each cell to expand as dictated by atmospheric dispersion, cell boundaries can be viewed as being impermeable for unreactive pollutants. Thus, only the diffusion of reactive and entrained pollutants must be parameterized. For example, within the framework of a Gaussian formulation and for an elliptically shaped plume, the radii (in transformed polar coordinates) of concentric rings containing equal pollutant masses can be shown (Freiberg, 1976) to be represented by the following equation:

$$r_j = \sqrt{2\ln\left(\frac{M}{M-j}\right)} \; , \qquad (5)$$

where r_j is the radius of the j-th concentric ring, and σ_y and σ_z represent the horizontal and vertical dispersion coefficients for the plume in transformed polar coordinates given by $r^2 = y^2/\sigma_y^2 + z^2/\sigma_z^2$. Plume distributions other than Gaussian can also be incorporated into this model.

A unique feature of this model is the manner in which the plume dispersion is treated. For an inert species emitted from the source, the rates of expansion of these cells are determined by horizontal dispersion such that there is no net mass flux across cell boundaries. For a background or a reactive pollutant, the Fickian diffusion approach is adopted: the flux across the interface between cells j and j+1 is assumed to be equal to the product of an equivalent diffusion coefficient, K_j, and the concentration gradient of the background or reactive species relative to that of an inert species. That is,

$$F_j = -K_j\left(\frac{c}{y}\bigg|_j - \frac{\tilde{c}}{y}\bigg|_j\right) , \tag{6}$$

where c and $\tilde{c}$ denote the concentration distributions of the background or reactive pollutant and the inert species, respectively. The equivalent diffusion coefficient can be determined by considering the case of a constant background concentration, c_B. Since, after each time step, c_B should be unchanged, a simple balance of mass fluxes for cell j yields

$$c_B\left(\frac{dy_j}{dt}\right) - c_B\left(\frac{dy_{j-1}}{dt}\right) = K_j\left(\frac{\partial\tilde{c}}{\partial y}\bigg|_j\right) - K_{j-1}\left(\frac{\partial\tilde{c}}{\partial y}\bigg|_{j-1}\right) . \tag{7}$$

Assuming local symmetry at the centerline of the plume, one may impose

$$K_0 = 0 \quad . \tag{8}$$

Then the equivalent diffusion coefficient K_j can be solved by using the recurrence formula, Eq. (7), and appropriate finite difference approximations (Figure 2).

The Chemical Kinetics Module

The application of both the grid module and the plume module requires a kinetic mechanism describing pertinent chemical reactions. This mechanism must include a specification of the elementary kinetic steps and their associated rate constants.

Extensive efforts have been made in the past to develop a valid kinetic mechanism for photochemical smog, focusing primarily on systems of hydrocarbons and nitrogen oxides. One recent result of these studies is carbon-bond mechanism. When the carbon-bond mechanism (CBM) was first formulated, it represented a condensation of existing explicit mechanisms, mainly for propylene and butane. The original carbon-bond mechanism has been recently updated (Whitten et al., 1978) for the following reasons:

1. Changes in one reaction may require compensating changes in other reactions to maintain the overall predictive accuracy of simulations using the mechanism.

2. Testing of the CBM on a large set of smog chamber data should be carried out subsequent to any changes to ensure that no special problems have been created.
3. Documentation of changes is necessary to keep all users of the CBM informed.

The formulation of the new version of the CBM reflects the following changes to the original CBM:

1. Inclusion of the reactions of the intermediate Criegee species formed from the ozone-olefin reactions, and surrogate species for the hydroxyperoxyalkyl products.
2. Inclusion of a new formulation for carbonyl photolysis and oxidation.
3. Treatment of alkyl radicals in long-chain paraffins, and internal olefins as carbonyls.
4. Explicit treatment of ethylene, and incorporation of a new aromatic chemical reactions scheme.

Each of these changes to the CBM is discussed in detail by Whitten et al. (1978). The full version of this updated carbon-bond mechanism is implemented in the plume module, and a simplified version is incorporated in the grid module.

The Surface Module

The importance of dry deposition of SO_2 and sulfate in long-range transport problems necessitates treatment of this process in the model. For pollutants originating from either elevated or distant ground-level sources, most of the pollutant mass is contained in the mixing layer. The removal processes consist of the diffusion of the pollutants through the surface layer to the ground, followed by absorption or adsorption at the atmosphere-ground interface. A unique feature of the surface layer is its diurnal variation in temperature, which is a result of daytime heating and nighttime cooling of the surface. This variation affects the vertical pollutant distribution through atmospheric stabilities and, consequently, the rate of surface uptake of pollutants.

The surface layer can be viewed as being composed of two layers: the turbulent layer and the viscous sublayer. With this simplification, the pollutant flux to the ground surface due to dry deposition, F, can be obtained through the following equation:

$$I \cdot F + \gamma^{-1/a} \cdot F^{1/a} - c = 0 \ , \qquad (9)$$

where

$$I \equiv \frac{1}{\beta u_\star} + \int_{z_0}^{h} \frac{\phi(z)}{k u_\star z} \cdot dz \ , \qquad (10)$$

and where k is the von Karman constant, $u_\star$ is the frictional velocity, β is the Stanton number, ϕ is the dimensionless wind shear (Thom, 1972), and z_0 and h are the surface roughness and the height of the surface layer, respectively. The parameters γ and a represent the reaction rate and reaction order, respectively, for the uptake of air pollutants by chemical reaction or catalytic decomposition at the ground surface. For a = 1, 2, and 3, closed-form solutions can be found for F:

$$F = \begin{cases} \dfrac{c}{I + \dfrac{1}{\gamma}} \ , & a = 1 \ , \\[2ex] \dfrac{\dfrac{1}{\sqrt{\gamma}} + \left(\dfrac{1}{\gamma} + 4Ic\right)^{1/2}}{2I} \ , & a = 2 \ , \\[2ex] (A_+ + A_-)^3 \ , & a = 3 \ , \end{cases} \qquad (11)$$

where

$$A_\pm = 3\left\{ \frac{c}{I} \pm \left[\frac{c}{2I}^{2} + \frac{1}{27\gamma I^3} \right]^{1/2} \right\}^{1/2} . \qquad (12)$$

These formulas reduce to that of Thom (1972) for the special case of a first-order surface reaction and a neutrally stratified atmosphere.

PRIOR APPLICATIONS OF THE MESOSCALE MODEL

The first exercise of the mesoscale model was its application to the Northern Great Plains. An early version of this model, without the cloud layer and using only an inert plume module, was used to assess the regional air quality impact of emissions from local coal development (Durran et al., 1979). Figure 3 shows the computed SO_2 and sulfate concentrations. It is interesting to note that the surface deposition predicted by this model does exhibit strong diurnal patterns, shown in Figure 4, as was observed by Husar et al. (1978).

The development of the reactive plume module has also been completed. As shown in Figure 5, a preliminary test run (without the grid module) demonstrated that this model appears to retrieve qualitatively many features of the observed concentration profiles, namely, the Gaussian distribution for an inert species and the depletion of ozone near the source.

A more recent application of one version of the mesoscale model was in the simulation of the 1975 Northeast Oxidant Experiment (Lamb et al., 1977). Although preliminary results (Figure 6) appear to be encouraging, problems such as the prescription of the background concentrations upwind of the modeling region remain to be resolved.

APPLICATION OF THE MESOSCALE MODEL TO PEPE

The Mesoscale Air Quality Model described earlier can be used in one or more of the following three modes in the PEPE experiments:

1. Planning mode. In the initial phase the Mesoscale Model can be used as a planning tool for designing and scheduling the field measurement program. Meteorological scenarios leading to prolonged elevated pollution episodes in the area of interest would first be identified using climatological data. The Mesoscale Model can then be exercised to determine the temporal and spatial distribution of high pollutant concentrations as a result of transport of precursors, typically at the trailing edge of a high-pressure system. These predictions should be useful for (a) the siting of ground-level monitoring stations and the specification of location and density of concentrations; and (b) the development of airborne measurements protocols.
2. Analysis mode. The Mesoscale Model can also be used to analyze and interpret data collected in the field measurement program. For example, by comparing the HC/NO_x ratios, as computed by the model, with the corresponding measured values, one may be able

to unravel the differences between smog chamber experiments and secondary pollutants. One may also be able to examine the adequacy of emissions inventories. Through a series of well-designed sensitivity studies, one could also employ the mesoscale model to examine the interaction of large point-source plumes with upwind urban emissions under prolonged elevated pollution episodes as well as to determine the role played by different meteorological scenarios (pressure contours, wind trajectories, SO_2/sulfate conversion rate, relative humidities, and so on) in the formation of sulfate, ozone, and other secondary pollutants.

3. Prediction. After the Mesoscale Model has been subjected to a careful and thorough verification exercise, it can be used to predict prolonged elevated pollution episodes. It can be utilized in forecasting the worst conditions under prolonged elevated pollution episodes and in formulating control strategies on a regional basis.

ACKNOWLEDGMENT

Support for portions of this work from the U.S. Environmental Protection Agency is gratefully acknowledged. In particular, we acknowledge the guidance and assistance provided by D. Henderson (currently with the National Park Service), and K. Demerjian, M. Dodge, and R. Lamb of ESRL.

REFERENCES

Boris, J. P., and D. L. Book. 1973. Flux-Corrected Transport--I: SHASTA, A Fluid Transport Algorithm That Works. J. Computational Phys., 11:38-69.

Dimitriades, B., and A. P. Altshuller. 1977. International Conference on Oxidant Problems: Analysis of the Evidence/Viewpoints Presented, Part I: Definition of Key Issues. J. Air Poll. Contr. Assoc., 27, No. 4:299-307.

Durran, D., et al. 1979. A Study of Long Range Air Pollution Problems Related to Coal Development in the Northern Great Plains. To be published in Atmos. Environ.

Freiberg, J. 1976. The Iron Catalyzed Oxidation of SO_2 to Acid Sulfate in Dispersion Plumes. Atmos. Environ., 10:121-130.

Hidy, G. M., et al. 1976. Design of the Sulfate Regional Experiment (SURE), Vol. I: Supporting Data and Analysis. EC-125, Environmental Research & Technology, Incorporated, Westlake Village, California.

Husar, R. B., et al. 1978. Sulfur Budget of a Power Plant Plume. Atmos. Environ., 12:549-568.

Lamb, R. G., et al. 1977. Development and Evaluation of a Mesoscale Photochemical Air Quality Simulation Model. EI77-69, Systems Applications, Incorporated, San Rafael, California.

Liu, M. K., D. A. Stewart, and P. M. Roth. 1978. An Improved Version of the Reactive Plume Model (RPM-II). 9th International Technical Meeting on Air Pollution Modeling and Its Application, 28-31 August 1978, Toronto, Canada.

Miller, D. F., et al. 1978. Ozone Formation Related to Power Plant Emissions. Science, 202:1186-1188.

Thom, A. S. 1972. Momentum, Mass and Heat Exchange of Vegetation. Quart. J. Roy. Met. Soc., 98:124-134.

Whitten, G. A., et al. 1978. Modeling of Simulated Photochemical Smog with Kinetic Mechanisms. EF78-121, Systems Applications, Incorporated, San Rafael, California.

Wilson, W. E. 1978. Sulfates in the Atmosphere: A Progress Report on Project MISTT. Atmos. Environ., 12:537-547.

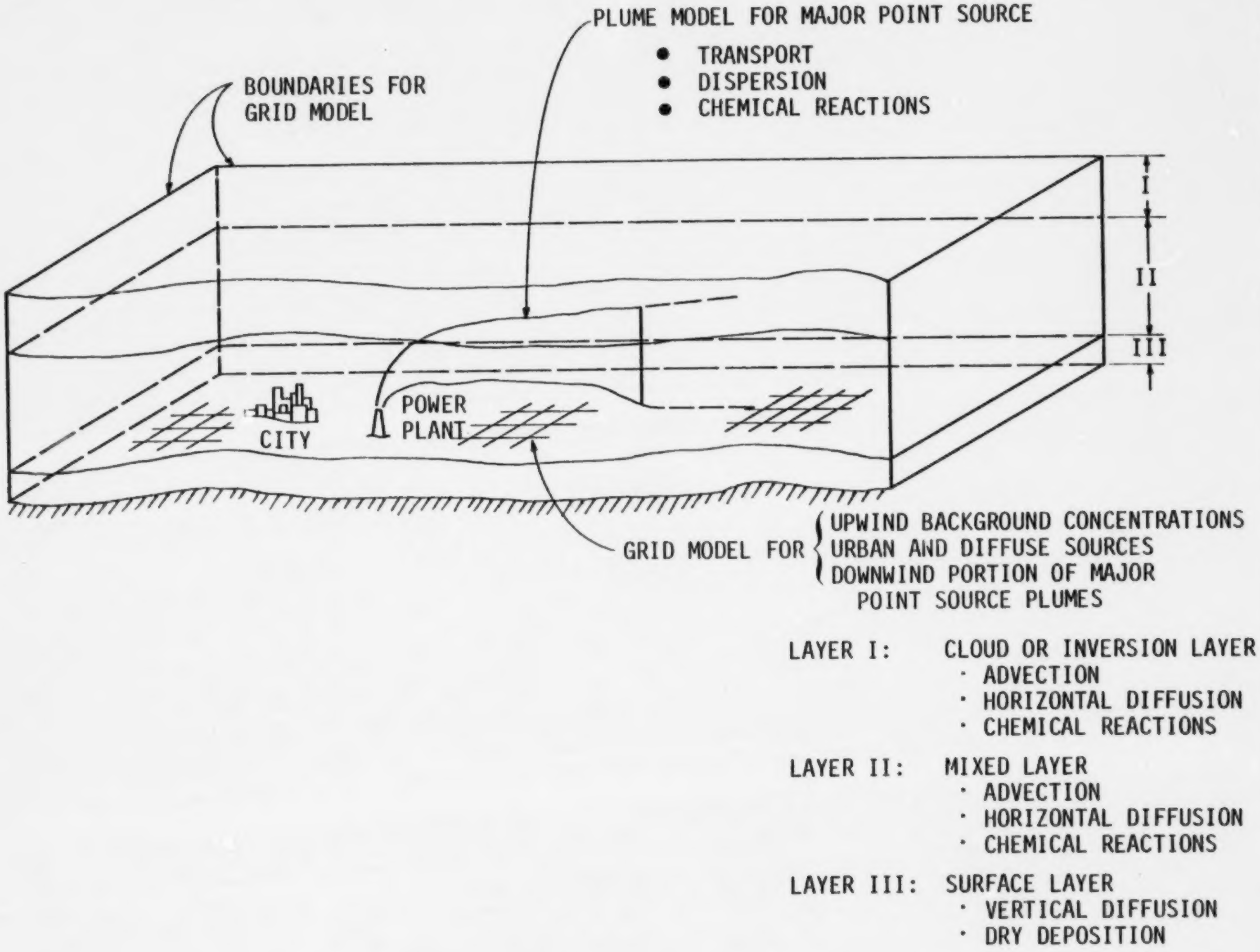

Figure 1. Schematic for the SAI mesoscale air pollution model.

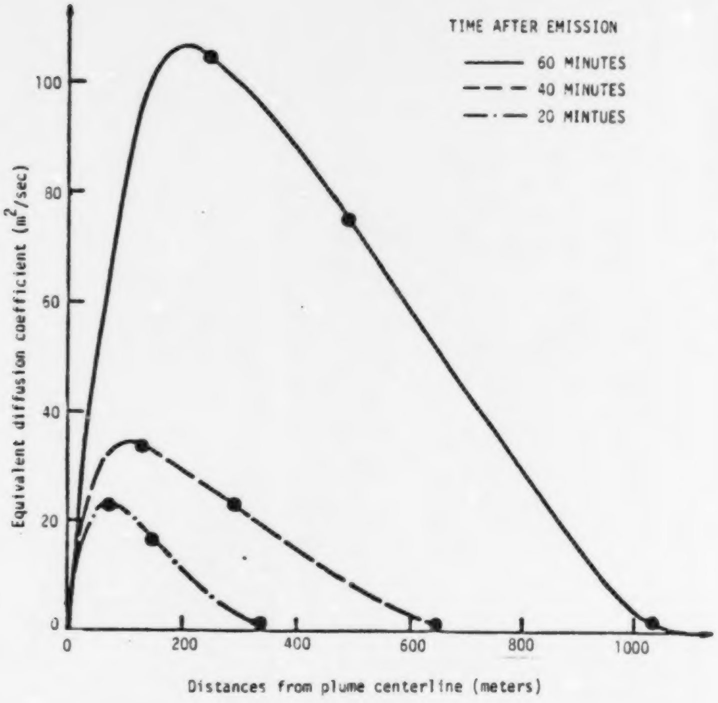

Figure 2. Equivalent diffusion coefficients as a function of time after emission and location.

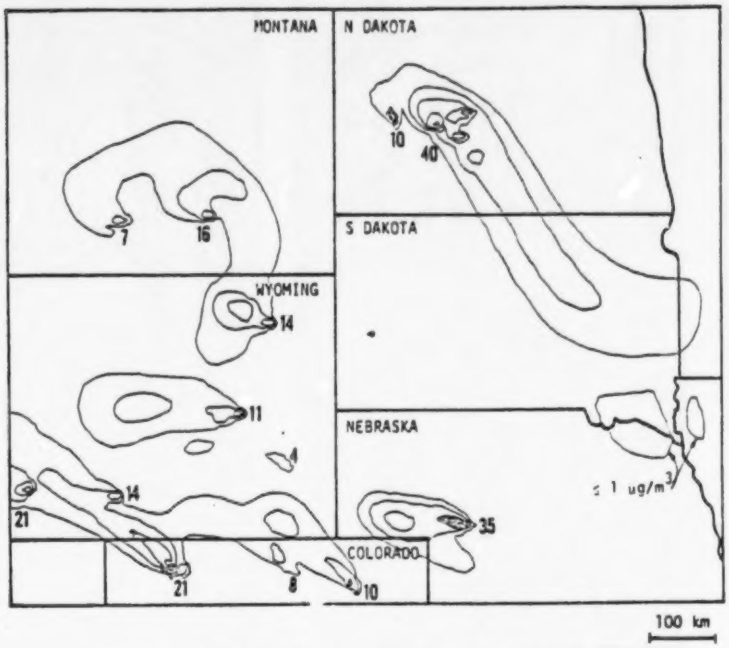

(a) SO_2; 1700-2000 MST 5 April 1976

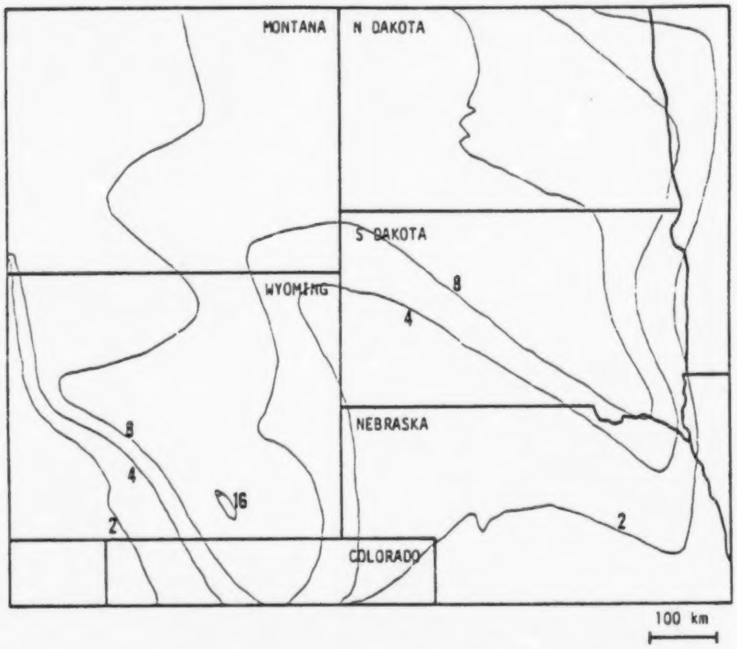

(b) Sulfate; 1700-2000 MST 6 April 1976

Figure 3. Concentrations predicted by the mesoscale air pollution model. Isopleths show concentrations at 2, 4, 8, and 16 $\mu g/m^3$.

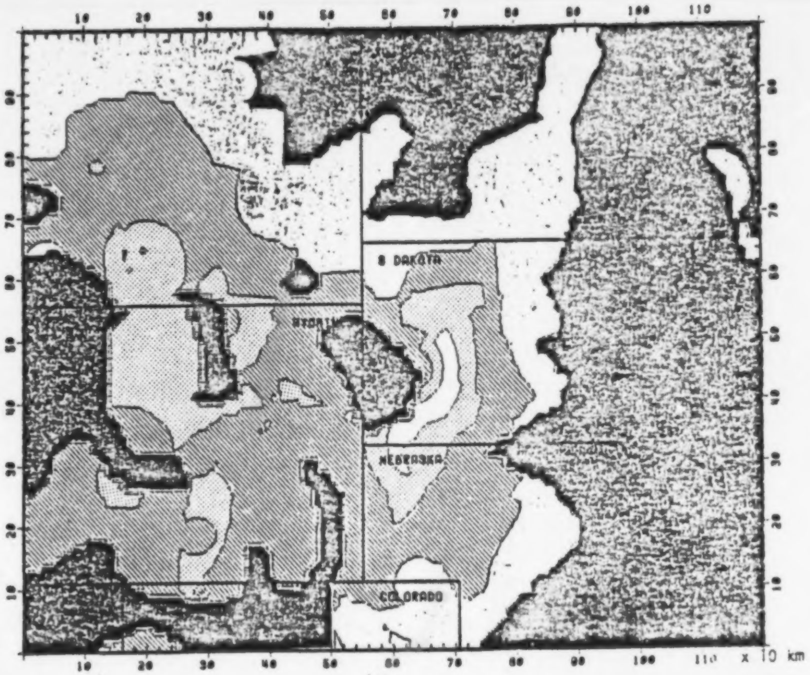

(a) 1400-1700 MST 4 April 1976

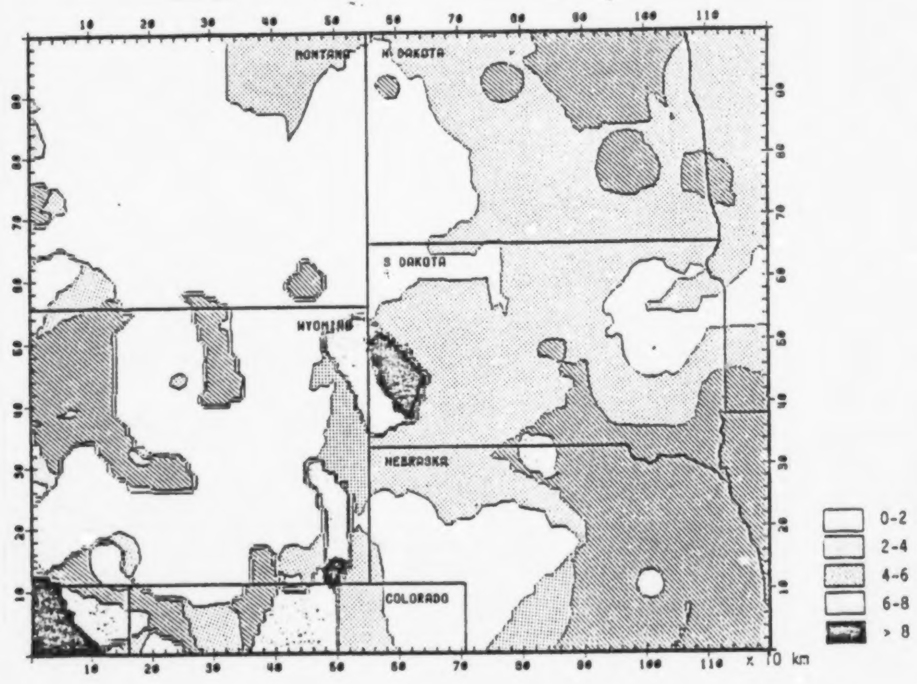

(b) 200-500 MST 5 April 1976

Figure 4. SO_2 deposition velocities (in mm/s) calculated by the mesoscale air pollution model.

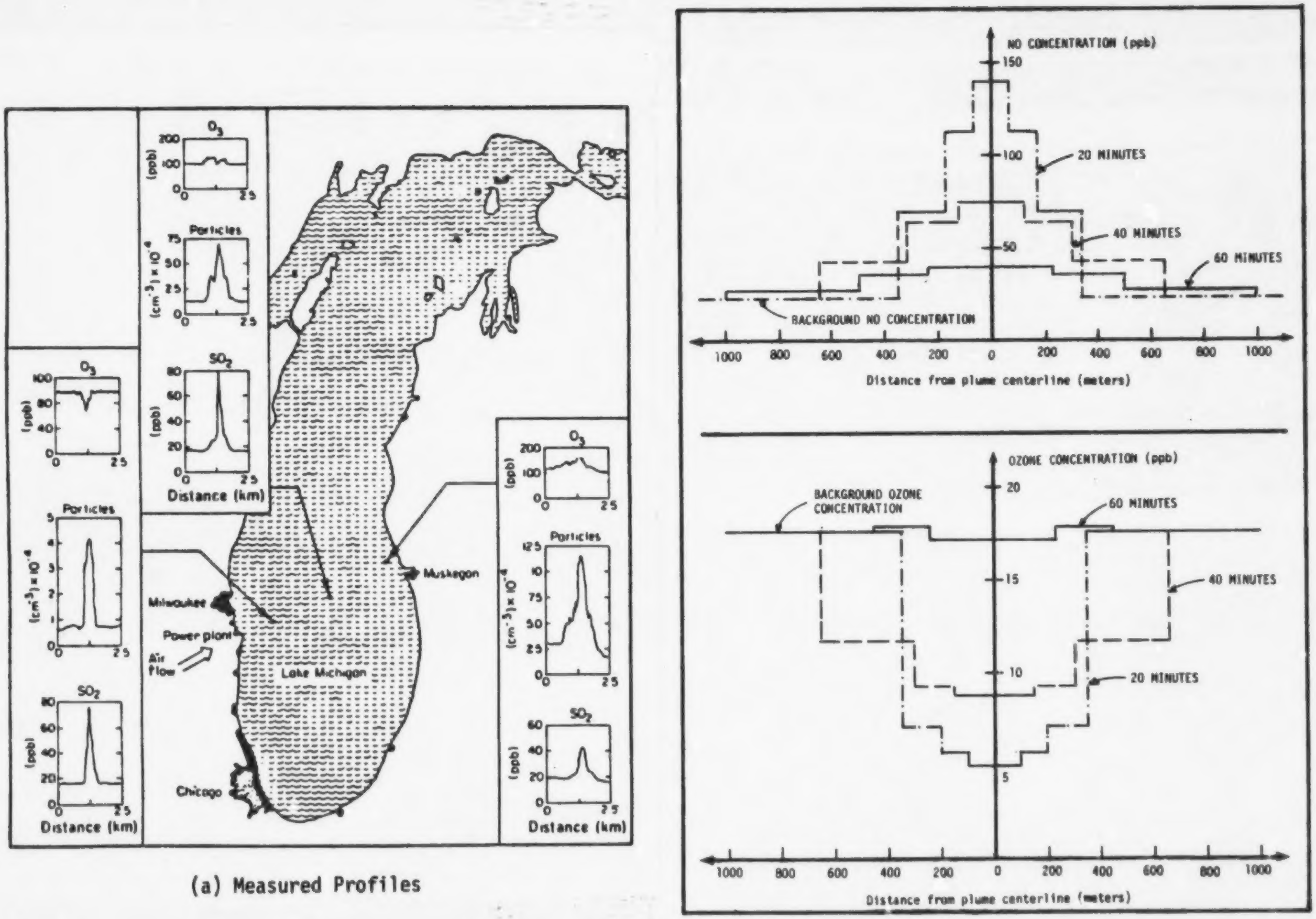

(a) Measured Profiles

(b) RPM-II Predicted Profiles

©1978 by the American Association for the Advancement of Science.
This figure originally appeared in an article by D. F. Miller in volume 202 of *Science*, pp. 1186-1188.

Source: Liu et al. (1978).

Figure 5. Comparison of measured and predicted profiles for a reactive plume.

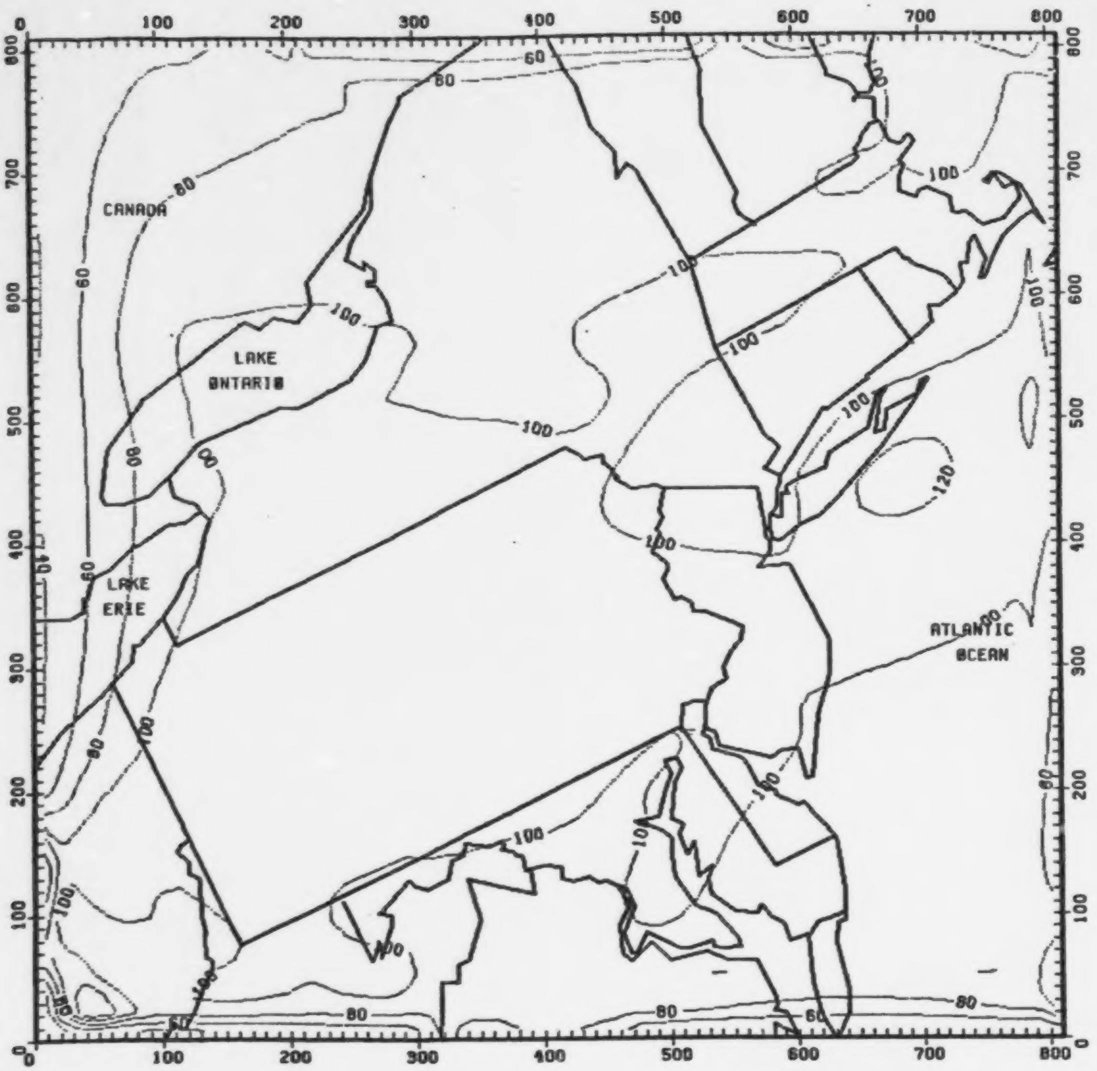

Figure 6. Preliminary results from the simulation of the 1975 northeast oxidant experiment (surface ozone concentrations in ppb).

EPRI'S AIR QUALITY STUDIES

Glenn R. Hilst

Electric Power Research Institute
Palo Alto, California

INTRODUCTION

Air quality studies and research, including the forthcoming PEPE project, which this Workshop addresses, have taken on new and larger degrees of importance as our society wrestles with the problems of restoring and preserving equitable environmental quality while keeping the costs of environmental protection in balance with the benefits to be gained. The complexities of atmospheric transport and dilution of airborne contaminants coupled with the chemical transformation and depositional losses of pollutants along the way from source to receptor have been the subject of scientific inquiry for decades. To be sure, these research studies have provided a great deal of insight, in particular, into the individual components of atmospheric processes that control pollution exposure patterns once the source strengths and configurations have been established.

Unfortunately, however, these bits and pieces of scientific wizardry are not adequate for present and future requirements for rational and cost-effective pollution control strategies for at least two reasons:

1. Either parts of the puzzle are very poorly understood or our present predictive capabilities are severely handicapped by erroneous and inadequate input information. Atmospheric transport on the regional scale and chemical transformation mechanisms and rates are prime examples. Another example is the depositional loss of gases and particles, also of fundamental importance in regional pollutant behavior.
2. The linkage of the transport-dilution/mixing chemistry-sources-sinks modules of air pollution models is still in a primitive state and represents a serious deficiency when we address such basic requirements as source attribution for pollutants originating from multiple sources. This problem is partly scientific

and partly technological, i.e., computer cost and size limitations. However, it is now very clear that we are dealing with a coupled, nonlinear system in which the consequences of feedback from one module to another can have drastic impacts on the accuracy of our predictions. Diffusive mixing limitations on fast chemical reactions in inhomogeneously mixed turbulent flow reactors, of which the atmosphere is one, are examples.

These limitations on our present ability to predict the transport and fate of airborne pollutants, and the very practical and urgent need for improved predictions, suggest two things to me:

1. We must accelerate research in this area significantly, but in a thoughtful and coordinated way, in order to produce results in a timely and efficient manner. Air pollution research, as we atmospheric scientists know it, is emerging into an era of "big science" with costs and management requirements to match. Large field measurements programs are essential, and our appetites for computer size and time are insatiable. If these expensive operations are to be efficient, we must learn from and synthesize all of the results of related programs that have gone on before and are going on around us now.
2. We must maintain a balance between the individual research studies that can improve our understanding of the inner workings of the atmospheric pollution system and the large, integrated measurements and model construction systems. This may seem self-evident, but it is my experience that accomplishing this objective is far from easy. It is all too convenient to focus on one or the other and lose sight of the fact that "small" science provides the tools that "big" science uses, and the societal problems that "big" science addresses are in fact the best rationale for a strong and vigorous "small" science program. As we think in terms of megabucks for our PEPE's, SURE's, STATE's, MAP3S's, and the like, we must also keep their life support system, the hundred kilobuck research projects, vigorous and healthy.

THE EPRI AIR QUALITY STUDIES

Faced, as it is, with the prospect of regulatory requirements for spending hundreds of billions of its rate payers' dollars on air pollution control equipment and operations during the decade ahead, to say nothing of highly restricted power plant siting options, the U.S. electric power industry has a very lively interest in establishing the factual base for the requirements and the strategies to be adopted for air pollution control. As a result, the research arm and center for the industry, EPRI, has developed a large (by industrial standards) research subprogram within the Physical Factors Program of its Environmental Assessment Department. This subprogram is called, aptly enough, the Air Quality Studies. At present the Air Quality Studies are strongly oriented toward pollutants associated with fossil fuel combustion, but the general thrust of the program is directed to three key questions: (1) where does the pollutant go, (2) in what concentration does it arrive, and (3) what is its chemical form when it arrives. We are equally concerned with primary and secondary pollutants, gases and particles, time scales from minutes to days, and travel distances from kilometers to continental dimensions. Naturally, our prime concern is with pollutants emanating from tall stacks, but the need to separate out utility contributions to ambient pollution levels from those attributable to other sources blurs this distinction quickly.

The EPRI Air Quality Studies have also been responsive to various regulatory forcing functions. Secondary formation of sulfates from SO_2, first as a potential health hazard and more recently as a factor in visibility impairment, gave rise to our Sulfate Regional Experiment (SURE). Visibility impairment and prevention of significant deterioration (PSD) as embodied in the 1977 Clean Air Act Amendments have been forcing functions as well. However, these immediate problems have not given rise to a "fire fighting" type of research. Rather, timely but thoughtful and thorough understanding and fact finding have been called for. Our typical research plan calls for a 3- to 5-year effort, or "time to pay off" if you will.

The organization of EPRI's Air Quality Studies can best be described under four major headings:

- Large-scale field measurements
- Integrated analyses and model development
- Supporting special studies
- Instrumentation development

As a measure of the level of effort called for in these categories, our 1979 budget allocates approximately $5,000,000 to the large-scale field measurements projects, $500,000 to integrated analyses and model development, $750,000 to supporting special studies, and $750,000 to instrumentation development. This allocation reflects our deep concern for the need to establish the facts concerning present baseline values of the magnitude and variability of air pollutants across the country, particularly on a regional basis. Prior monitoring and field experimentation have concentrated on pollution "hot spots" for obvious reasons; these areas have required immediate regulatory attention and they have provided the best targets for research studies. But do these measurements represent anything but the local situation? Through the SURE project, now nearing completion, and its sequel, the Regional Air Quality Studies (RAQS), we have set out to document the answer to that critical question. These activities will continue to dominate our program, from a budgetary point of view, for some time to come because they come closest to establishing the factual basis for regulatory actions and they provide the basic phenomenological record that scientific research must explain. However, we at EPRI see the "bottom line" of all of this as models that incorporate the scientific know-how and predict, within the irreducible uncertainty that nature herself provides, the environmental consequences of man's activities, including electric power generation.

The project content of EPRI's Air Quality Studies and the possible interactions with the EPA PEPE project can best be described under the major program categories listed above.

Large-Scale Field Measurements

As noted before, EPRI's first venture into large-scale field measurements projects is the Sulfate Regional Experiment (SURE), which has been underway since 1976 and will be completed in 1980. The details of this project and some of the early results will be discussed by Dr. George Hidy of Environmental Research and Technology, Inc., later in this Workshop. To say the least, the SURE is highly relevant to the PEPE study because we have measured pollution episodes over the eastern United States, as well as the much more frequent low-level pollution behavior characterizing the western United States. These data and analyses should provide a gold mine of information for fine tuning the PEPE's field measurements program, and I hope they will be used that way.

The SURE project, as the name implies, emphasized the $SO_2/SO_4^{=}$ problem, but it also gathered extensive information on the regional behavior of NO/NO_x, O_3, TSP, RSP, and various elements contained in airborne particulates. During the latter phases of the project we have also incorporated precipitation chemistry measurements. During 1979 we propose to initiate a two-station visibility study in this area. Although the basic data gathering for SURE has been completed, we are extending the lifetime of an augmented Class I station network into 1980. This network will consist of twelve surface aerometric stations and fourteen precipitation chemistry sites, as well as the two visibility field sites. This sequel to the SURE has been incorporated into our general RAQS as the eastern network (ERAQS). Depending upon the timing of PEPE and budgetary considerations, there is, of course, a large potential for coordinated data gathering between ERAQS and PEPE.

RAQS is also being extended to the western United States (WRAQS), but with somewhat different emphases. The regional air quality problems of the western United States clearly focus on the formation and transport of fine particles and their impact on visibility impairment. These are the problems we are addressing in WRAQS. During 1979 we propose to set up a visibility/fine particle network complementary to the EPA/NPS VIEW network. In 1980 and 1981 this network will be extended throughout the intermountain and high plains region. Again our intent is to gather the data necessary to define the regional behavior of air pollutants and develop regional models.

On another front and time and distance scale, during 1979 EPRI plans to initiate its Plume Model Validation project (PMV). This project has been described in a recent publication (EPRI EA-917-SY, "Plume Model Validation," October 1978). In brief, very extensive sets of measurements of plume behavior in various terrain and meteorological conditions are to be made in order to validate the modular performance of plume models as well as their general operational utility. These results are expected to pinpoint improvements in plume model performance and reliability; again, an analysis and model development component is also planned for this project.

The relevance of the PMV project to PEPE is not so obvious, but better understanding of the dilution and chemical behavior of plumes during their first few hours may shed some light on the regional episodic behavior of pollutants as well as their potential for long-distance transport.

Integrated Analyses and Model Development

Our primary effort in this area during 1979 will be the completion of the SURE analyses and modeling. However, as noted above, ERAQS, WRAQS, precipitation chemistry, and visibility are also headed toward extensive analyses and modeling efforts in our Air Quality Studies. For planning purposes, we anticipate that approximately one-third of our future efforts will be directed toward this area. However, we have also noted the need for closer liaison and coordination with similar efforts in other agencies and we welcome suggestions along these lines.

Supporting Special Studies

This category includes a veritable pot pourri of projects with limited but important objectives. For example, we have funded a number of plume studies designed to measure chemical conversion rates. We are funding two chamber studies, one for dark reactions of SO_2 as a function of temperature and humidity, including liquid water, and another to determine nitrogen chemistry in plumes under photochemical conditions.

In another area we are supporting a very fundamental study of turbulent transport as it affects dry deposition of gases and particles under various terrain and vegetation conditions. We have also pioneered in developing measurement techniques and assaying biogenic emissions of sulfur compounds in the eastern United States. Similarly, we have conducted a feasibility study for comparisons of various instrumental methods used to measure visibility in the southwest United States.

Instrumentation Development

Although our extensive field measurements projects have provided a natural forcing function for improved aerometric measurements techniques, EPRI has concentrated on the development of a new generation of remote sensing devices. At present we are funding the final design and construction of a differential absorption lidar system (DIAL) that shows great promise. This system is designed to measure concentrations of SO_2, NO_2, or O_3 out to distances of 3 to 4 km and with an axial resolution of 5 to 10 m. When field-proven, this instrument should revolutionize the study of close-in plume behavior.

On another front, we are supporting the final design and construction of an automated telephotometer that will systematize measurements of visual range. When completed, we propose to use this instrument extensively in our western visibility studies.

Finally, we are also supporting further development of remote sensing systems designed to resolve the three-dimensional wind and temperature fields through the depth of the planetary boundary layer. Such instrumentation is essential to plume behavior studies in complex terrain.

These descriptions of EPRI's Air Quality Studies are necessarily brief. Also, this program is evolving rapidly in its young life. However, I think it is evident that the electric power industry has made a substantial commitment to research and development in the area of air quality.

CONCLUSION

Beginning with the SURE project and its coordination with the DOE MAP3S and the EPA MISTT and STATE programs, as well as informal coordination with other work, the desirability of coordinated programs has been well demonstrated. It is our hope that this is only the beginning. To be sure, each of us will have our own peculiar goals, objectives, and timetables that must be met. Within this framework, however, there is ample room for making certain that the total results of our efforts are greater than the sum of the parts provided by each of us. We welcome the opportunity to coordinate our research with PEPE and other air quality studies.

ENSEMBLE TRAJECTORY ANALYSIS OF SUMMERTIME SULFATE CONCENTRATIONS IN THE EASTERN UNITED STATES

Perry J. Samson

New York State Department of Environmental
Conservation, Albany, New York

INTRODUCTION

Much of our present knowledge about the formation, movement, and eventual decay of regional scale episodes of high summertime sulfate concentrations has been obtained from spatial and temporal examination of individual episode periods. Trajectory analysis is a useful tool for tracing the movement of such systems either forward or backward in time. This technique has been employed by several authors including Hall et al. (1973), Husar et al. (1976), Samson and Ragland (1977), and Wolff et al. (1977) to demonstrate the advection of large areas of low visibility, high ozone concentrations, and/or high sulfate concentrations in the eastern United States.

There are, however, several potential problems inherent in constructing individual trajectories that add to the uncertainty of analysis of small data sets. Observational errors in the input winds can cause considerable error in trajectory location. If there exist significant large-scale vertical motions, then the sampled air may have its origin in a layer of the atmosphere different from the layer being traced. The net motion over a predetermined layer may not adequately describe the motion of the air column being studied if large vertical shears exist over the layer.

If we assume that these effects are random along the path of the trajectory then it would be useful to use ensembles of trajectories over a large number of days to smooth the random "noise". It is then possible to obtain general relationships between resultant sulfate concentrations and the history of the sampled air.

This paper describes the use of ensemble trajectory analysis for relating resultant sulfate concentrations to the upwind emissions burden, wind speed, and mixing height. The general technique is presented and preliminary results relating sulfate concentrations to upwind wind speed at several locations in the eastern United States are presented.

APPROACH

The trajectory model of Heffter et al. (1975) as modified by Heffter and Ferber (1977) has been used in this study. The model computes the trajectory of an air column within the mixed layer of the atmosphere. All motion is assumed horizontal and winds are integrated from the top of the surface inversion to the top of the mixed layer as determined from wind and temperature profiles. The endpoints of the trajectory segments of 3 hours' duration are stored in the computer.

This output can be used with a graphics plotting program labeled TRAJPLOTTER which, for each day of interest, draws a base map (designated by the user) and overlays the trajectories for that day. But the ensemble of trajectory endpoints can also be used with corresponding pollutant concentration to arrive at estimates of interrelationships.

For a well-mixed boundary layer, the conservation of mass equation can be solved for equilibrium conditions (see Lettau, 1970) to be of the form

$$C = \frac{\bar{Q}}{\bar{U}\ h} \cdot F(x;Ri) \qquad (1)$$

where C is the concentration (g/m^3), Q is the areal source strength per length of integration (g/m-sec), $\bar{U}$ is the wind speed average over the layer of interest (m/sec), and h is the mixing height. The function F describes the horizontal dispersion as a function of downwind distance from the source, x, and stability (Richardson Number, Ri).

For the purpose of this investigation, assume that the net effect of the dispersion function is small over a long time series (i.e., the horizontal gradient of sulfate concentrations is small). Then the resultant concentration of sulfate can be related to the upwind emissions burden, wind speed, and mixing height using the formula

$$C = C_o + \sum_{i}^{N} \frac{(a_i\bar{Q}_i)}{(\beta_i\bar{U}_i)(\gamma_i h_i)} \qquad (2)$$

where C_0 is the natural background concentration (assumed less than 1 μg/m^3 and ignored in the present study) and the subscripts refer to each of the N trajectory segments included in the analysis. The parameters α_i, β_i and γ_i represent the weight of that particular variable at that particular trajectory segment on the resultant concentration. These values can be determined from least squares analysis of the sulfate and trajectory data. Figure 1 shows a hypothetical trajectory calculation backward in time from a point A. The wind speed estimated for segment II upwind of point A would be the distance traversed between points B and C divided by the time increment for the segments. The emissions burden calculated for segment II is determined by an objective analysis scheme from the midpoint between points B and C. The area included in estimating the areal source strength increases with distance from the origin (because of the increased scatter of endpoints intuitively expected with increasing time from the origin). Further, the weighting of sources is elongated along the axis of the segment, the ratio of major to minor axes increasing with increasing wind speed.

The height of the mixed layer can be ascertained from analysis of vertical temperature and wind profiles. In their model, Heffter and Ferber (1977) use a technique whereby the observed vertical temperature profiles are examined for inversion levels and the wind profiles are examined for significant wind shear. This technique is to be tested against other, less stringent criteria such as those proposed by Meyers et al. (1976). Once a reasonable approach is determined, then the results will be included in the total analysis.

RESULTS

The relationships between resultant sulfate concentrations and upwind wind speed have been completed for several monitoring stations in the eastern United States. Figure 2 shows the location of the sites used thus far. Table 1 lists the sites along with the dates of operation and the investigators responsible.

In an earlier paper (Samson, 1978) it was shown, using the 1975 and 1976 sulfate data for the three sites in upstate New York, that no correlation existed between the measured sulfate concentration and the wind speed measured through the mixed layer at the same time. However, using estimated wind speeds from trajectory segments greater than 24 hr upstream produced a significant correlation. That is, the resultant concentration of sulfate measured at these rural locations could be explained, in part, statistically by stagnation occurring more than 24 hr upwind.

The analysis of an additional year of summertime sulfate values at those three stations and analysis of other sites in the eastern United States has verified this finding. Figure 3 shows the analysis between the inverse of wind speed and the resultant sulfate and nitrate concentrations as a function of hours upwind. The sulfate produces the same pattern as was reported previously for the upstate New York stations. For this short period the sulfate could be explained, in part, by stagnation occurring more than 48 hr upwind. The nitrates, on the other hand, have a high correlation nearer the point of measurement. Thus, more local stagnation appears to have affected nitrate concentrations rather than stagnation occurring well upwind.

Figure 4 shows these relationships for four other locations. In three of the four, the previously discussed relationship is true. Stagnation upwind of Keysville, VA, McKee, KY, and Allegheny Mountain, PA, was significantly correlated with resultant sulfate concentrations. The data from Brookhaven did not produce the pattern. There are a few possible explanations for this apparent discrepancy, the most likely being that due to Brookhaven's location near the sea many of its trajectories that tracked out over the ocean would have been ignored. As written, the trajectory model will terminate trajectory analysis if insufficient upper air data are available within a certain radius. Thus, the trajectories available for analysis for Brookhaven would be biased toward those of continental origin. Other possible explanations are the nearness of the New York metropolitan area, which could be masking upwind effects, and the importance of mesoscale wind features such as the sea breeze to pollutant concentrations.

Finally, the categorization of trajectories into those corresponding to low resultant sulfate concentrations ($<5\ \mu g/m^3$) and high resultant sulfate concentrations ($>15\ \mu g/m^3$) gives a graphic description of the general history of the sampled air. Figures 5, 6, 7, and 8 show the trajectories arriving in the middle of the sampling period for Holland, NY, Allegheny Mountain, PA, Keysville, VA, and McKee, KY, respectively. The duration of travel between arrowheads is 6 hr, each trajectory being computed backwards for 72 hr (or until insufficient wind data were available to continue).

The dichotomy between the high and low samples is striking at these stations. In Figure 5, Holland receives its lower concentrations from the west to north with relatively high winds in the boundary layer. The highest concentrations occur with winds from the south to west with several cases of upwind stagnation observable. The classification of Allegheny Mountain trajectories in Figure 6 shows a similar dichotomy.

The trajectories for Keysville, VA, show a markedly different pattern. The lowest concentrations occur with airflow out of the south or with fast moving air from the northwest. The higher concentrations occur with slower moving air from the north and west and stagnant conditions to the southwest.

One of the most striking dichotomies occurs in the classification of trajectories at McKee, KY, shown in Figure 8. Over the period of this study, the lowest concentrations were associated with airflow from the north to northwest moving at a moderately fast speed. The highest concentrations occur with a consistent pattern looping anticyclonically from the east. Since the trajectories to a point in Pennsylvania are similar to those shown in Figure 6a for low concentrations at Allegheny Mountain, PA, it would appear that production and/or accumulation south of that point must be responsible for the high concentrations.

DISCUSSION

This is a preliminary report on research intended to investigate the sensitivity of measured sulfate concentrations to upwind emission burden, wind speed, and mixing height. A consistent pattern has emerged between sulfate concentrations and upwind wind speed with a significant correlation with the inverse of wind speed occurring more than 24 hr upwind of the sampling point. This pattern could be due to:

1. The lag time between accumulation of sulfur dioxide and its transformation to high concentrations of sulfate, or

2. The relative location of these rural samplers to large source regions (i.e., stagnation near the sampler will not produce high concentrations in the absence of anthropogenic sources).

It is hoped that future work, including emissions burdens, will clarify the reason for this pattern and give an indication of how sensitive sulfate concentrations are to upwind emissions.

ACKNOWLEDGMENTS

The author would like to thank the investigators who offered their data for this analysis: Dr. Peter Coffey and Mr. Phil Galvin, New York State Department of Environmental Conservation; Dr. Paul Lioy, New York University; Dr. George Wolff, General Motors Research Lab; Dr. Roger Tanner, Brookhaven National Lab; and William Pierson, Ford Motor Company.

REFERENCES

Coffey, P. E., P. J. Galvin, J. Cline, and P. J. Samson. 1979. Results of the 1977 New York State Sulfate Sampling Network. New York State Department of Environmental Conservation Report (in preparation).

Galvin, P. J., P. J. Samson, P. E. Coffey, and D. Romano. 1978. Transport of Sulfates to New York State. Environ. Sci. Tech, 12:580-584.

Hall, F. P., C. E. Duchon, L. G. Lee, and R. R. Hagan. 1973. Long-Range Transport of Air Pollution: A Case Study, August 1970. Mon. Wea. Rev., 101:404-411.

Heffter, J. L., A. D. Tayler, and G. J. Ferber. 1975. A Regional-Continental Scale Transport, Diffusion and Deposition Model. NOAA Tech. Mem. ERL-ARL-50, Air Resources Lab., Silver Springs, MD.

Heffter, J. L. and G. J. Ferber. 1977. Development and Verification of the ARL Regional-Continental Transport and Dispersion Model. Proc. Joint Conf. on Appl. of Air Poll. Meteor. 29 November-2 December 1977, Amer. Meteor. Soc., Boston, Mass., pp. 400-403.

Husar, R. B., N. V. Gillani, J. D. Husar, C. C. Paley, and P. N. Turcu. 1976. Long-Range Transport of Pollutants Observed Through Visibility Contour Maps, Weather Maps and Trajectory Analysis. Proc. 3rd Symp. Atmospheric Turbulence, Diffusion, and Air Quality. 19-22 October 1976.

Lettau, H. H. 1970. Physical and Meteorological Basis for Mathematical Models of Urban Diffusion Processes. In Proc. of Symp. on Multiple-Source Urban Diffusion Models (edited by A. C. Stern). U.S. Environmental Protection Agency, AP-86, Research Triangle Park, NC, pp 2-1 to 2-26.

Lioy, P. J., G. T. Wolff, J. S. Czachor, P. E. Coffey, W. N. Stasiuk, and D. Romano. 1977. Evidence of High Atmospheric Concentrations of Sulfates Detected at Rural Sites in the Northeast. J. Environ. Sci. Hlth., A12: 1-14.

Lioy, P. J., G. T. Wolff, K. A. Rahn, D. M. Bernstein, and M. Kleinman. 1979. Characterization of Aerosols Upwind of New York City, II: Aerosol Composition. Annals of the New York Academy of Sciences (in press).

Meyers, R. E., R. T. Cederwall, W. D. Ohmstede, and W. aufm Kampe. 1976. Transport and Diffusion Using a Diagnostic Mesoscale Model Employing Mass and Total Energy Conservation Constraints. Proc. 3rd Symp. Atmospheric Turbulence, Diffusion, and Air Quality. 19-22 October 1976.

Pierson, W. R., W. W. Brachaczek, T. J. Truex, J. W. Butler, and T. J. Korniski. 1978. Ambient Sulfate Measurements on Allegheny Mountain and the Question of Atmospheric Sulfate in the Northeastern United States. Research Report, Scientific Laboratory, Ford Motor Company, Dearborn, MI.

Samson, P. J. 1978. Ensemble Trajectory Analysis of Summertime Sulfate Concentrations in New York State. Atmospheric Environment, 12:1889-1893.

Samson, P. J., and K. W. Ragland. 1977. Ozone and Visibility Reduction in the Midwest: Evidence for Large-Scale Transport. J. Appl. Meteor., 16:1101-1106.

Tanner, R. 1979 Sulfate, Nitrate and Related Ionic Species in Airborne Particles. New York Acad. of Science Conf. on Aerosol; Anthropogenic and Natural Sources and Transport, 9-12 January 1979.

Wolff, G. T., P. J. Lioy, G. D. Wight, R. E. Meyers, and R. T. Cederwall. 1977. An Investigation of Long-Range Transport of Ozone Across the Midwestern and Northeastern United States. Atmospheric Environment, 11:797-805.

Wolff, G. T., P. R. Monson, and M. A. Ferman. 1978. On the Nature of the Diurnal Variation of Sulfates at Rural Sites in the Eastern United States. Presented at American Chemical Society Meeting, 11-14 September 1978, Miami, Florida, (also General Motors Research Rpt. GMR-2772, ENV #46, General Motors Research Laboratries, Warren, MI, July 1978).

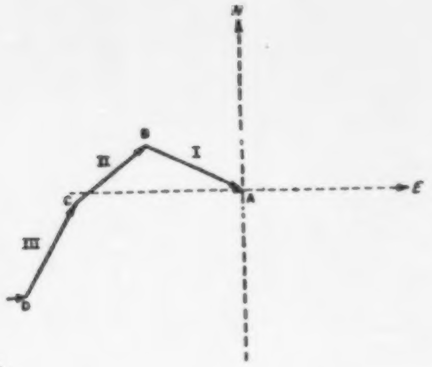

Figure 1. Hypothetical trajectory calculation.

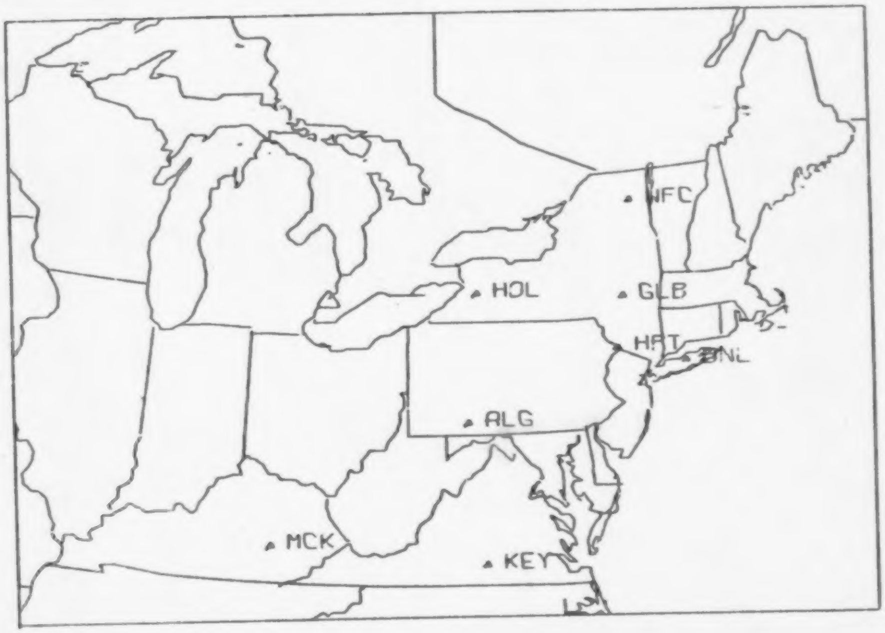

Figure 2. Location of stations used in this report. A listing of the station names along with dates of operation and investigators responsible appears in Table 1.

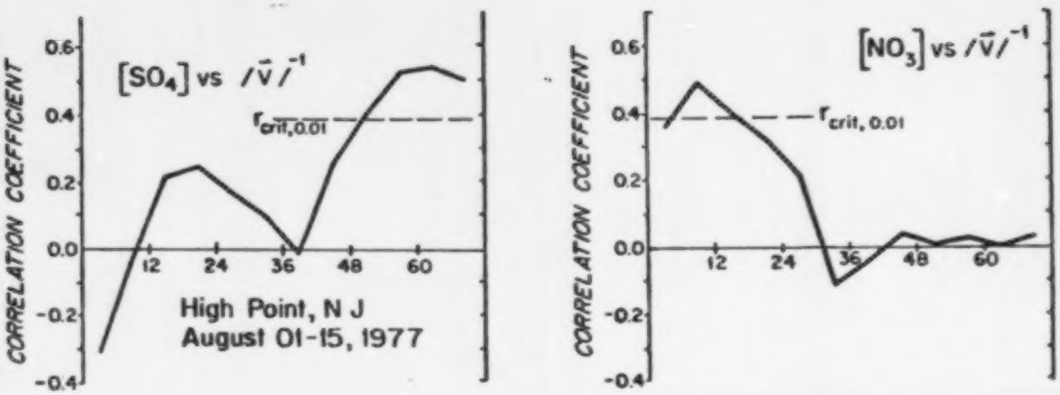

Figure 3. Correlation between the inverse of wind speed and resultant sulfate and nitrate concentrations as a function of hours upwind.

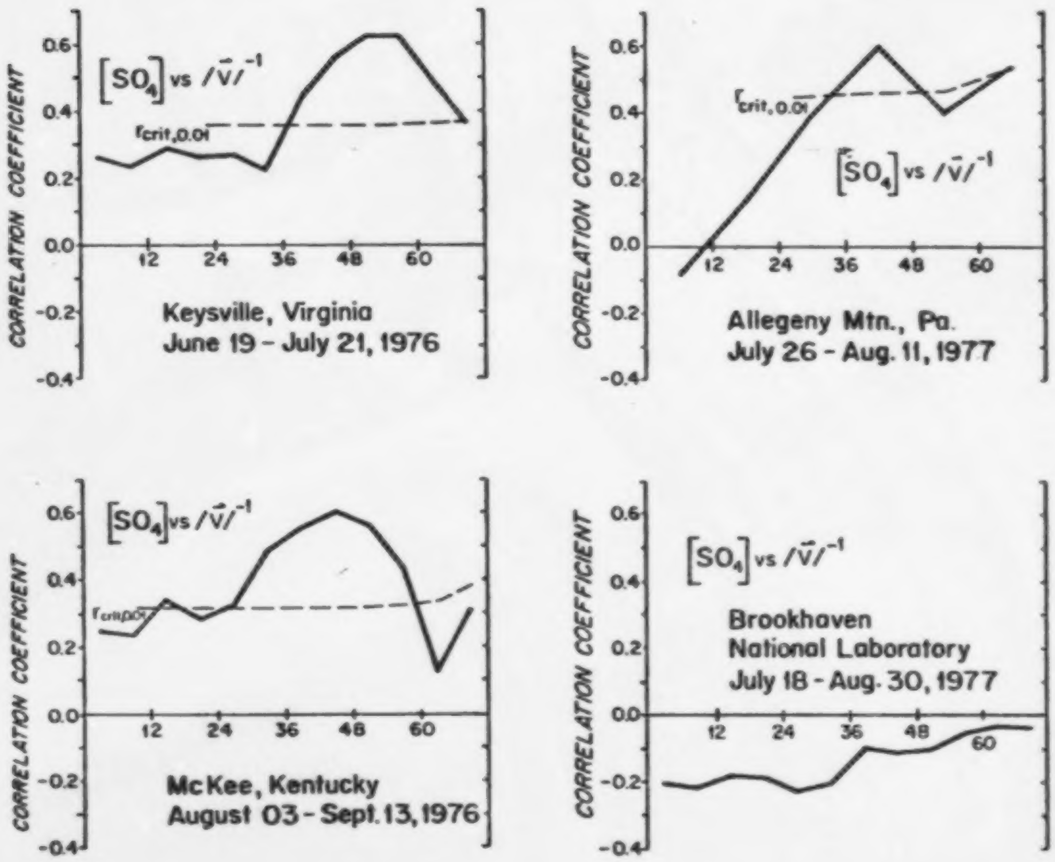

Figure 4. The correlation between the inverse of wind speed and resultant sulfate concentrations as a function of hours upwind.

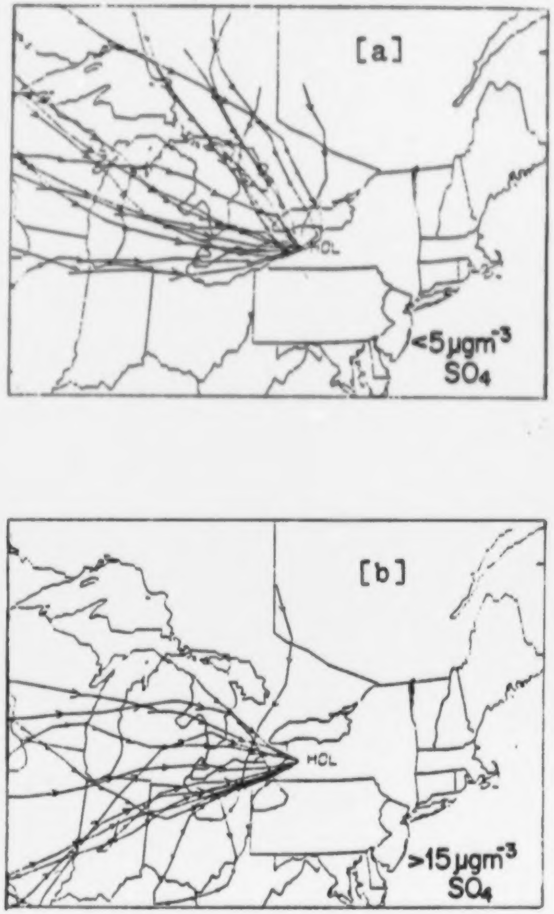

Figure 5. Trajectories arriving at Holland, NY, at 1400 EDT on days of low and high sulfate concentrations.

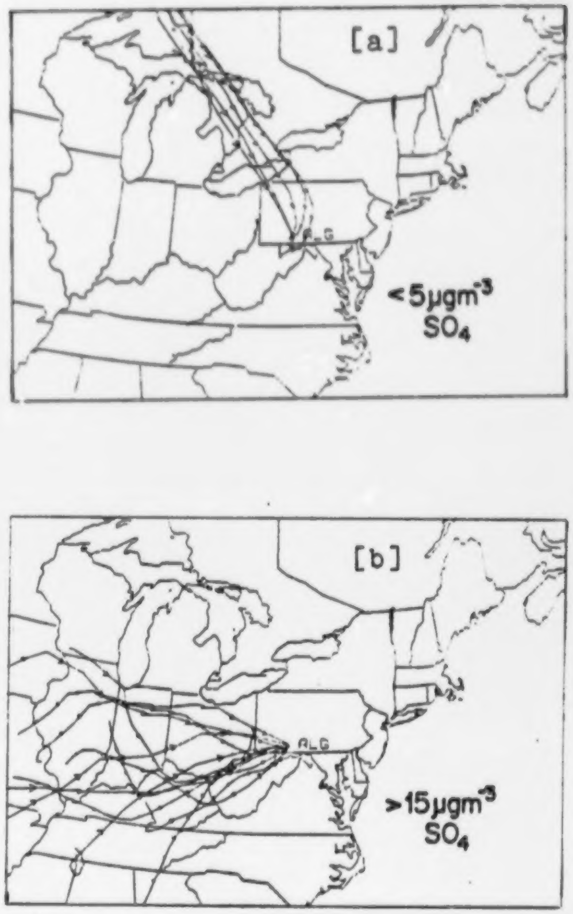

Figure 6. Trajectories arriving at Allegheny Mountain, PA, at midpoint of sampling period (12 hr) for low and high sulfate concentrations.

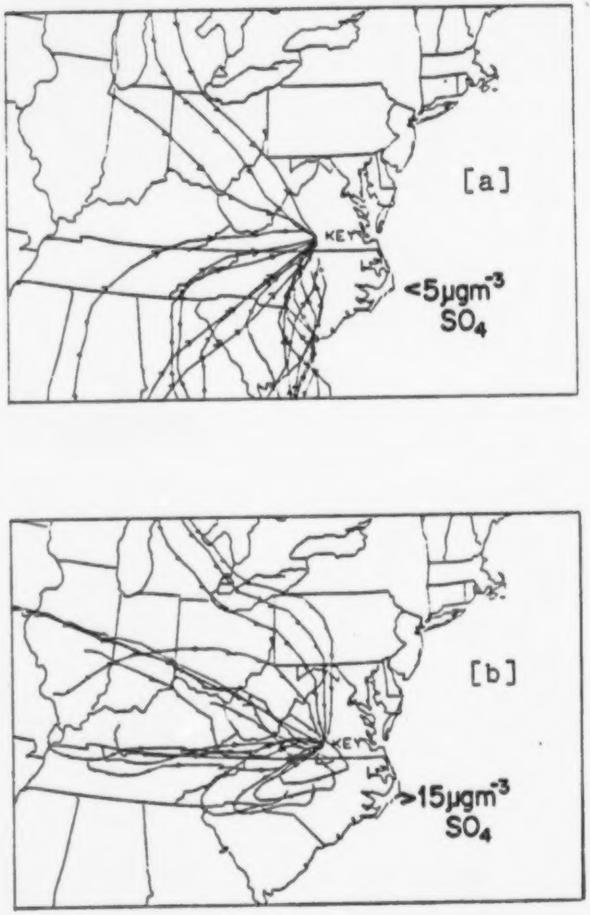

Figure 7. Trajectories arriving at Keysville, VA, at midpoint of sampling period (4 hr) for low and high sulfate concentrations.

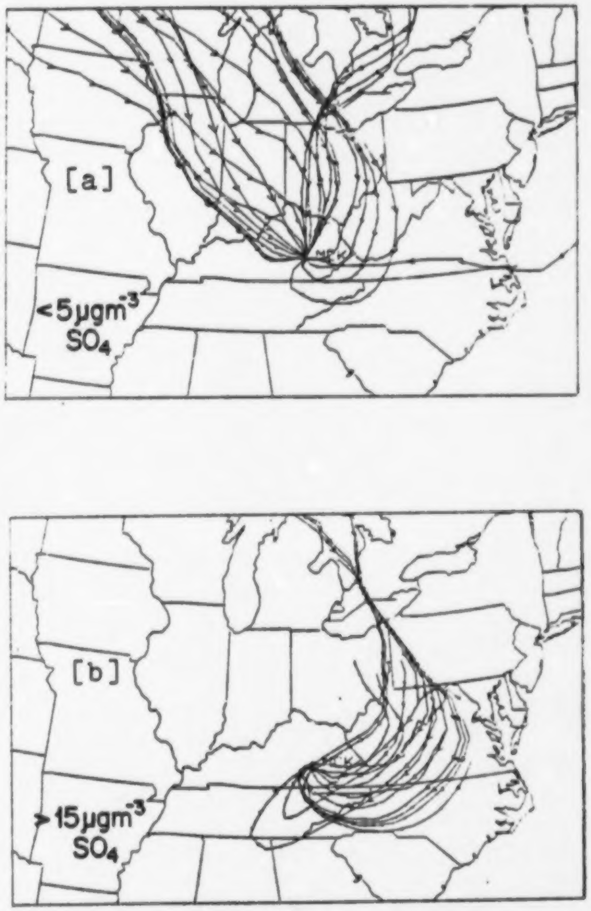

Figure 8. Trajectories arriving at McKee, KY, at midpoint of sampling period (4 hr) for low and high sulfate concentrations.

TABLE 1. SOURCES OF SULFATE DATA AND PERIODS OF STUDY

Site	Location	Investigators	Period
WFC	Whiteface Mountain, NY	Lioy et al. (1977)	1-31 July 1975
GLB	Gilboa, NY (Schoharie, NY)	Galvin et al. (1978)	6-31 July 1976
HOL	Holland, NY	Coffey et al. (1979)	15 June - 15 Aug. 1977
HPT	High Point, NJ	Lioy et al. (1979)	1-15 Aug. 1977 (6 hr)
BNL	Brookhaven National Laboratories, NY	Tanner (1979)	18 July - 30 Aug. 1977 (6 hr)
KEY	Keysville, VA	Wolff et al. (1978)	19 June - 21 July 1976 (4 hr)
MCK	McKee, KY	Wolff et al. (1978)	3 Aug. - 13 Sept. 1976 (4 hr)
ALG	Allegheny Mountain, PA	Pierson et al. (1978)	26 July - 11 Aug. 1977 (12 hr)

SOME RESULTS OF THE SULFATE REGIONAL EXPERIMENT (SURE) AND THE PEPE EXPERIMENT DESIGN

G. M. Hidy,* P. K. Mueller, and T. F. Lavery
Environmental Research and Technology, Inc.
Westlake Village, California

INTRODUCTION

Because of the emerging results of studies of long-range pollutant transport in Europe (e.g., OECD 1977), researchers have begun to suspect that the occurrence of regional scale phenomena is also important in North America. Early evidence suggested that regional pollution over scales exceeding 1,000 km occurred in the northeastern United States. The occurrence of transport of pollution over such distances, as compared with multiple source interactions over distances of hundreds of kilometers, could not be distinguished. Investigation of such processes in the Northeast led to the design and implementation of the Sulfate Regional Experiment (SURE) (Hidy et al., 1976), as well as other studies including the Multistate Atmospheric Power Production Pollution Study (MAP3S), and the Ohio River Basin Study (ORBS). The planned investigation of Prolonged Elevated Pollution Episodes (PEPE's) represents a second generation of regional projects in the Northeast. Operationally, we define a PEPE as an occurrence of pollution for more than one day over a geographical extent of several hundred kilometers. A PEPE is signalled by the occurrence of high concentrations of particulate sulfate and ozone at ground level and aloft. These events are believed to be associated with mesoscale and synoptic-scale meteorology, and the interactions of sulfur or nitrogen oxide emissions from tall stacks and from urban plumes.

To assist in the design of the PEPE experiment, consideration should be given to the experience of programs nearing completion. This paper is intended to provide a perspective on the occurrence of PEPEs as identified in the SURE results.

THE SURE AND ITS RESULTS

The SURE is a major study that involved the operation of a ground network of 54 monitoring stations in the region shown in Figure 1. The stations are located by number as indicated. The first nine stations (Class I stations) were heavily instrumented for sampling pollutant gases (SO_2, NO, NO_2, and O_3) and airborne particulate matter and were run continuously from August 1977 through October 1978. The additional 45 stations monitored only SO_2 and suspended particulates in six center-season months: August 1977, October 1977, January-February 1978, April 1978, July 1978, and October 1978. The SURE ground measurements were supplemented by sampling aloft using two aircraft during a 12-day period in each of the center-season months. The aircraft were instrumented in a manner equivalent to the Class I stations; in addition, they included an integrating nephelometer, a condensation nuclei counter, and turbulence instrumentation. The experiment also involved extensive collection and use of emission data for SO_2, NO_x, particulate, and hydrocarbons, as well as National Weather Service meteorological observations. The experimental concept of the SURE and its relationship to MAP3S and other programs is discussed in detail by Mueller et al. (1978).

---

*Speaker.

The SURE field program has been completed, and the data are currently being analyzed. The results to date have revealed certain important features of regional scale pollution patterns in the northeastern United States. Some of the results relevant to the PEPE studies are summarized below.

The occurrence of elevated sulfate concentrations is characterized from data taken at the nine continuously operating stations (Class I) over the 1-year period between August 1977 and July 1978. The cumulative frequency of occurrence of different sulfate levels is shown in Figure 2. The differences among these rural stations are relatively small throughout the region. The annual median level of sulfate is about 6 $\mu g/m^3$ for all nine stations. Concentrations greater than 20 $\mu g/m^3$ occurred less than 6 percent of the time, and concentrations of 10 $\mu g/m^3$ less than 25 percent of the time. Using the 20-$\mu g/m^3$ level as a criterion for a PEPE, Figure 2 shows that PEPE's occur only a small fraction of the time.

Looking at the regional events in a different way, we estimated the sulfate concentration in each of the 690 80 km × 80 km grid squares in the SURE region by extrapolating the 54 station measurements (Mueller et al., 1979). The extent of coverage of the region by different sulfate levels of ≥ 10 $\mu g/m^3$, ≥ 15 μ g/m^3 , and ≥ 20 $\mu g/m^3$ is shown in Figure 3. These estimates cover the summer months of August 1977 and July 1978. For the purpose of discussion, we have defined a regional event in terms of grid squares and land area covered: 40-50 percent in the $\geq$10-μg/m^3 isopleth, accompanied by 25 percent in the $\geq$15-μg/m^3 isopleth, and 10 percent in the $\geq$20-μg/m^3 isopleth. We see that two events of a regional nature took place in each of the summer months and each lasted for at least 3 days. From these two samples, a PEPE is likely to occur not more than twice during the duration of a planned summer experiment of 6 weeks.

The geographical extent of elevated pollutant levels may be characterized by the number of days of $\geq$10 μg/m^3 sulfate or by $\geq$20 μg/m^3 calculated from extrapolation of the network data. (See the isopleth maps for August 1977 in Figure 4.) The estimated heaviest regional concentration of sulfate in summer is focused on the middle to upper Ohio Valley and Pennsylvania. On this basis, and taking into account the heavy concentration of moderate to large-sized cities and the intense industrialization in this region, the PEPE experiments should be conducted here.

It is interesting to compare the distributions of monthly geometric mean sulfate and nitrate for August 1977, as given in Figure 5. Here, the sulfate concentrations are estimated to be regionally widespread, but nitrate is more localized around urban or isolated source complexes. Furthermore, the nitrate levels in August 1977 at the ground are nearly an order of magnitude lower than sulfate concentrations, despite a much smaller difference in regional SO_2 and NO_x precursor emissions. Such observations underscore the differences in the behavior of the two anion species, and emphasize the need for future work on nitrogen oxide behavior on an urban and regional scale.

The SURE aircraft sampling provided a useful indicator that, indeed, the occurrence of sulfate involves significant activity aloft. Observations were taken over the ground station at Duncan Falls, OH, during all four seasons. Duncan Falls is roughly in the center of the zone of high regional pollution. In Table 1 the average values of sulfate and nitrate are listed for the six flights in each month for Duncan Falls. Data reported for the ground, for 500 to 5,000 ft, and for 5,000 to 10,000 ft suggest that sulfate concentration is higher in the 500- to 5,000-ft layer than at the ground for all sampling months except January-February 1978. Furthermore, the July 1978 observations and others given in the table suggest that (total) nitrate is considerably higher in concentration aloft than at the ground (see also Hidy et al., 1979). Thus, it will be crucial to the PEPE program to provide as much sampling aloft as practicable within budgetary limitations.

From the early analysis of the SURE data, a distinction was made in the character of PEPE's between the buildup of pollution associated with regional scale air mass stagnation and that associated with the long-range transport situation. Lavery et al. (1979) have identified long-range transport with the regional scale "ducting or channeling" of air flow between the west side of the Appalachian Mountains and east-west oriented summer cold fronts. The differences in these events are summarized in Table 2. Here, the transport winds are identified as those at 300 m. Zones of influence are defined qualitatively in terms of the extent to which elevated sulfate concentrations are identifiable with a fixed source complex (an 80 × 80 km square in the SURE grid).

The structure of the ducting situation is illustrated for August 3 and 5, 1977, in Figure 6. The hatched squares denote the zones of high SO_2 emission density. The two graphs show the isopleths of sulfate estimated from 24-hr data of the ground network. In this case, the isopleths are elongated with the 300-m winds. Also shown are the isobars in millibars. Moist, warm air flows at moderate speed northeastward with the anticyclonic flow, accumulating pollution behind the large high-pressure area over the high emission density zones of the midwest, and passing along the western part of the Appalachians. Unlike the stagnation situations, the zone of maximum sulfate concentration "detaches" from the areas of high-emission density and moves "downwind" into areas to the east with lower emission density. The apparent movement of the zone of high pollution passed eastward with the winds over a 3-day period before precipitation and other processes associated with the southward drifting of the front dissipated that event. To date, such situations have been identified only three or four times in the SURE set, and only in summer when the cold fronts are more east-west oriented than in winter. Thus, it is expected that such conditions for a regional event would be accessible on at least a 24-hr forecast basis over the proposed PEPE study area. Examination of the SURE results and results from the National Aerometric Data

Bank, with meteorological data, should provide a basis for such forecasts, perhaps extending well beyond 24 hr.

RECOMMENDATIONS

The SURE served a very useful purpose by providing a comprehensive set of basic measurements of air quality at rural locations in the eastern States. As a second generation study, EPA's proposed PEPE program offers an opportunity to investigate several aspects of regional pollution events in detail using more sophisticated techniques. Some of the areas that need additional investigation are suggested in the following list.

- Rural hydrocarbon vapors, including oxygenates, in the PEPE region need quantification both at the ground and aloft for improvement of regional scale photochemical models.
- Some of the chemical links require characterization, including the rate of production of OH radicals, H_2O_2, PAN, and HNO_3. The vertical and horizontal distribution of these constituents is of interest in the PEPE.
- Knowledge of the chemical processes taking place in clouds is needed to clarify certain aspects of the SO_2 and NO_x oxidation processes.
- The linkage to cloud chemistry requires elucidation between chemical reactions and wet and dry removal processes in regional pollution events.

These four factors combined with other meteorological activity (e.g., transport and mixing), undoubtedly can explain the "sudden" genesis and death of PEPE's. The details of the dynamics of these events are unclear after initial analysis and interpretation of the SURE data. We recommend that the PEPE studies attempt to focus on these four areas in extending knowledge of regional scale pollution processes.

ACKNOWLEDGMENT

This work was sponsored in part by the Electric Power Research Institute under Project 862-2.

REFERENCES

Hidy, G. M. et al. 1976. The Design for the Sulfate Regional Experiment. Report EC-125, Electric Power Research Institute, Palo Alto, CA.

Hidy, G. M., et al. 1979. Air Chemistry in the Rural Northeastern United States. To be submitted to Environ. Sci. & Technol.

Lavery, T. F., et al. 1979. Occurrence of Long Range Transport of Sulfur Oxides in the Northeastern United States. In Proc. 4th Symposium on Turbulence, Diffusion and Air Pollution, American Meteorological Society, Boston, p. 330.

Mueller, P. K., et al. 1978. Implementation and Coordination of the Sulfate Regional Experiment (SURE) and Related Research Programs. Electric Power Research Institute Report, Palo Alto, CA, in press.

Organization for Economic Cooperation & Development (OECD) 1977. The OECD Programme on The Long Range Transport of Air Pollutants Measurements and Findings. OECD, Paris, France.

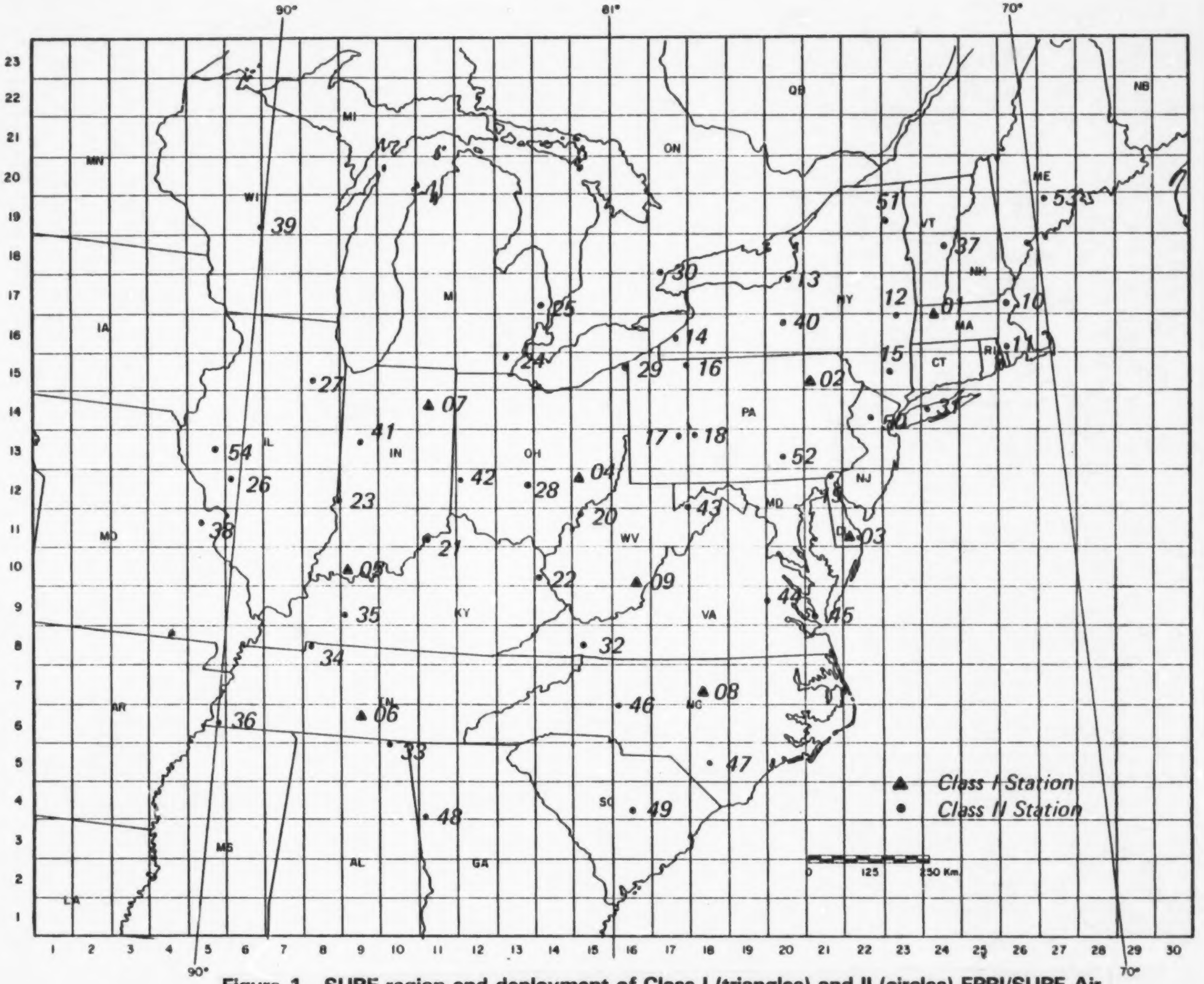

Figure 1. SURE region and deployment of Class I (triangles) and II (circles) EPRI/SURE Air Quality Monitoring Stations.

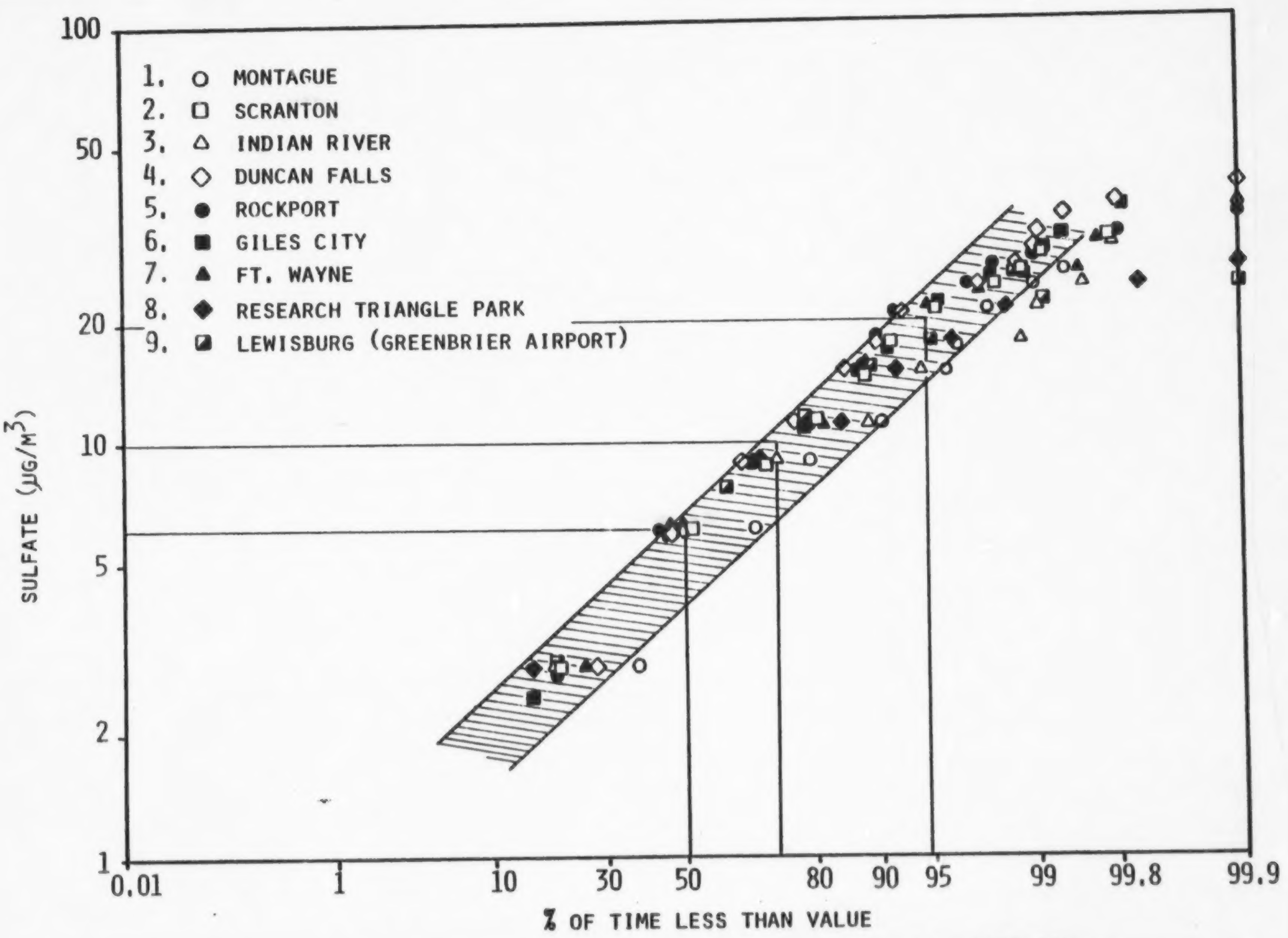

Figure 2. Frequency of occurrence of 24-h average sulfate concentrations in the SURE region based on August 1977 to July 1978 results.

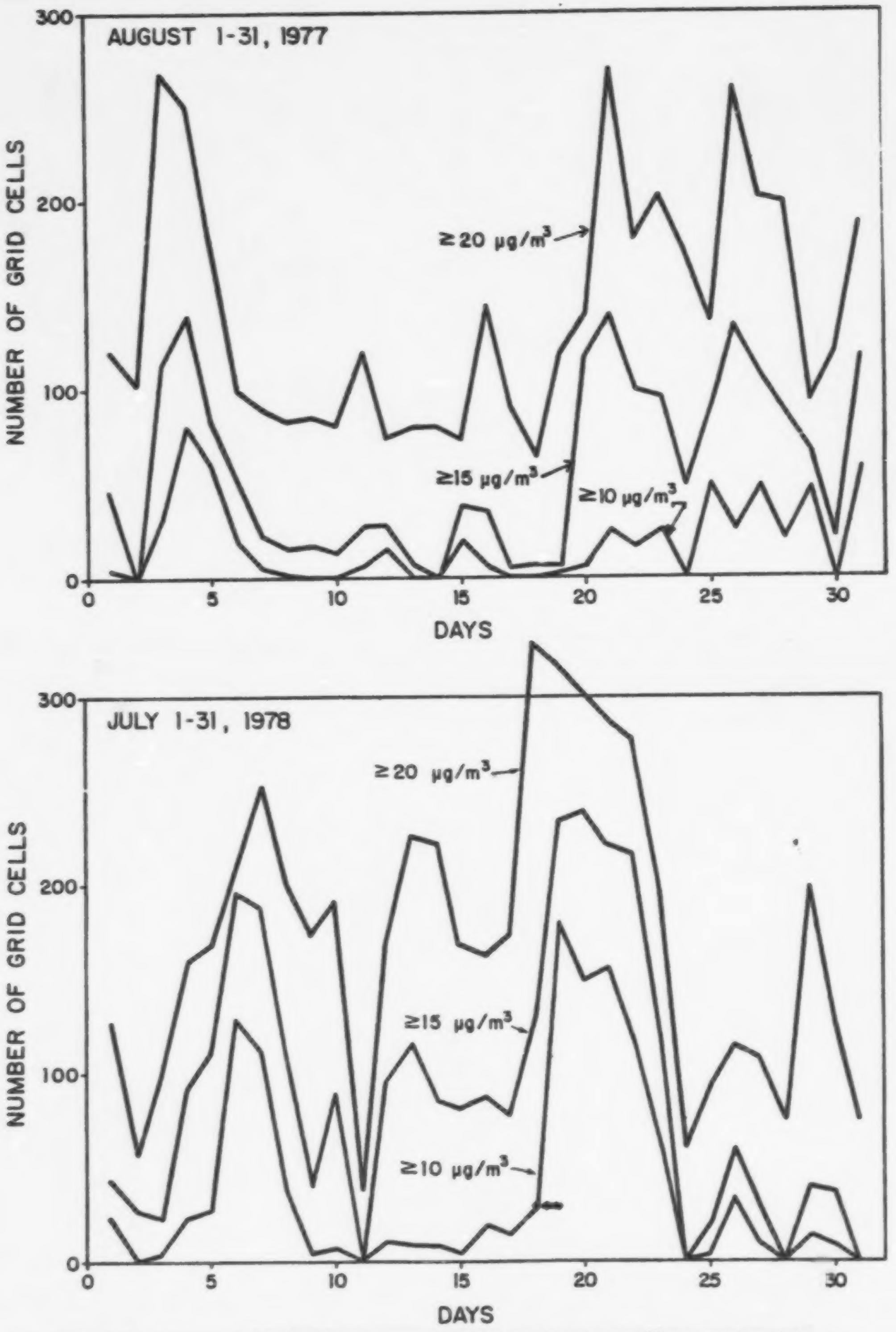

Figure 3. Extrapolated grid coverage of 24-h average sulfate concentrations ≥ 10 μg/m³, ≥ 15 μg/m³, and ≥ 20 μg/m³. Extrapolation was based on inverse distance squared from the SURE ground stations over the SURE grid.

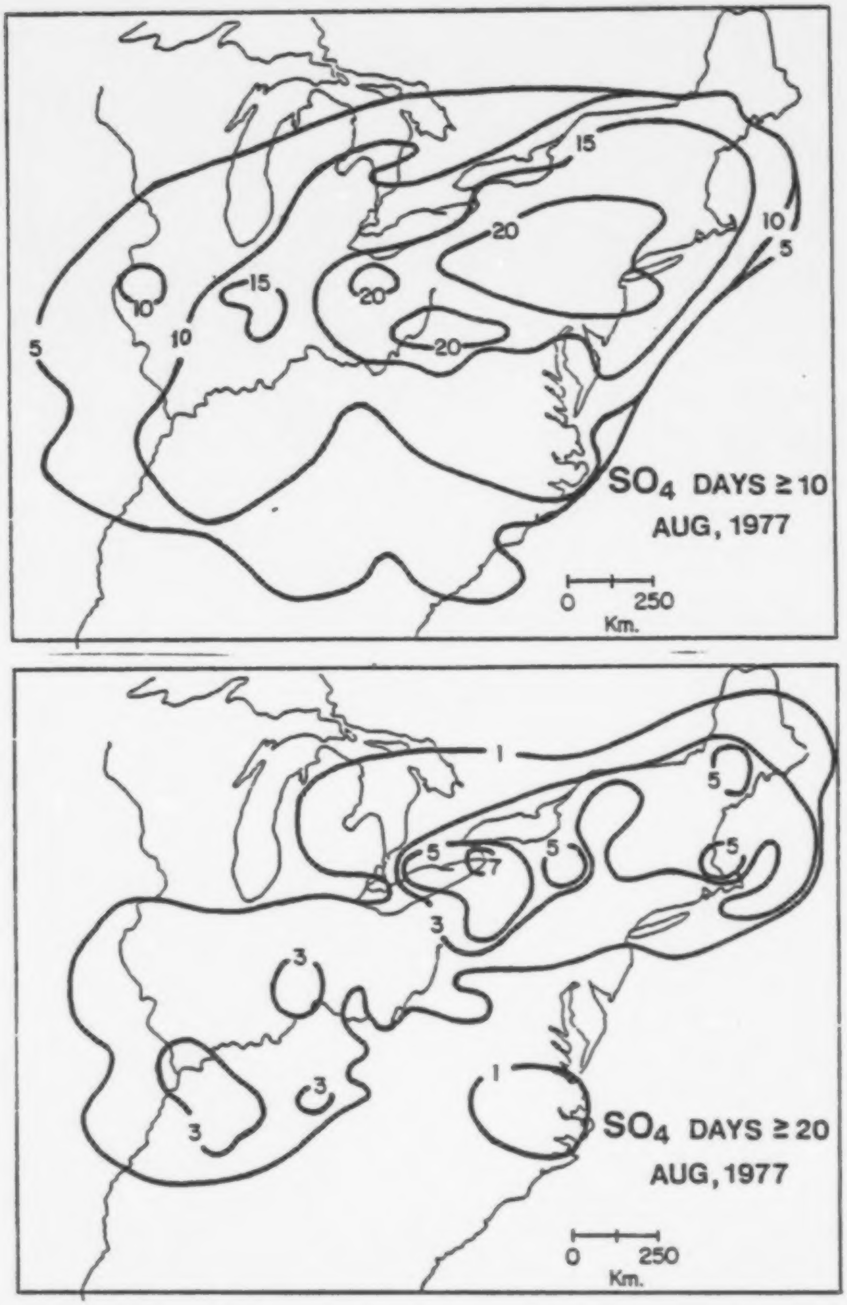

Figure 4. Calculated dosages of sulfate based on extrapolation of the SURE network data for August 1977. Isopleths are number of days ≥ 10 $\mu g/m^3$ (top) and ≥ 20 $\mu g/m^3$ (bottom).

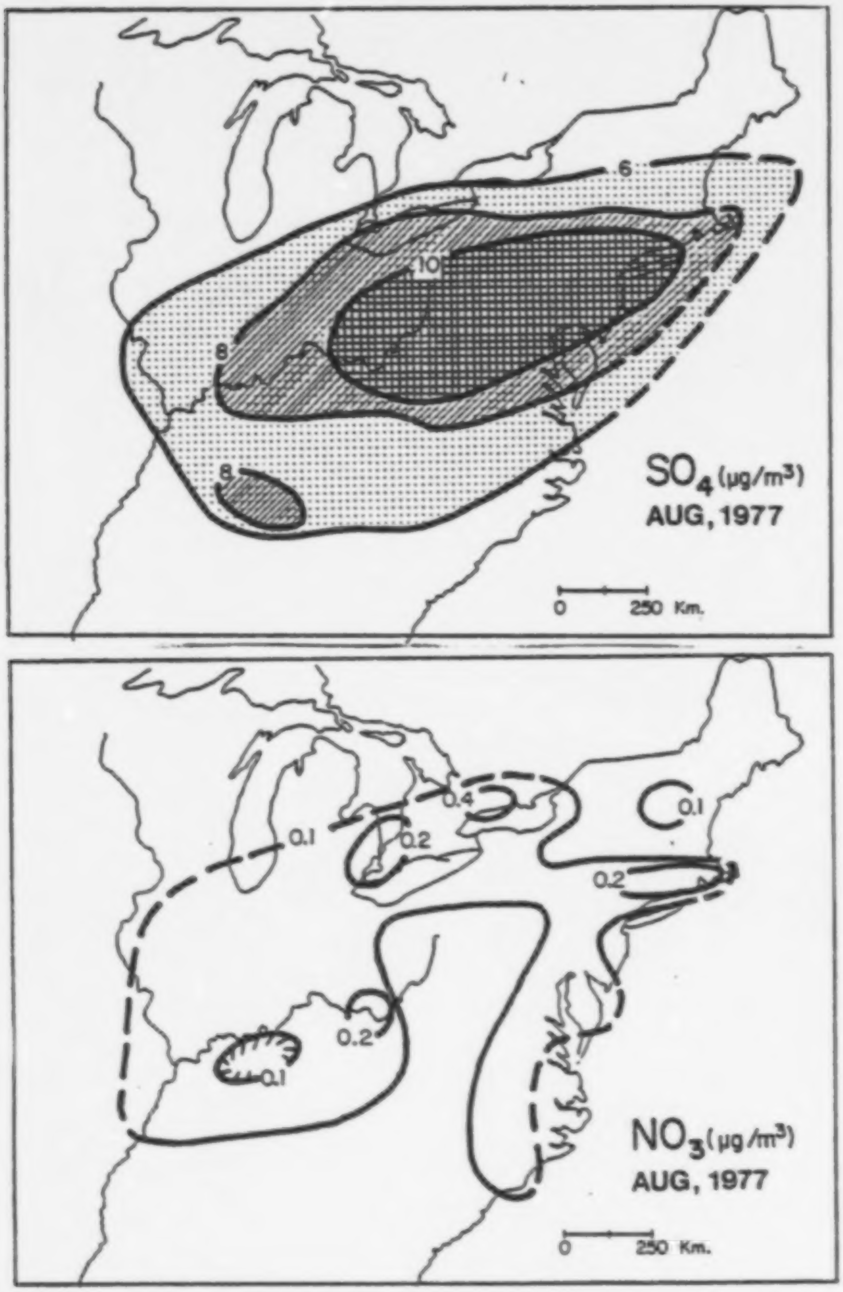

Figure 5. Distributions of monthly geometric mean values of 24-h average sulfate and nitrate concentrations extrapolated from the SURE network data.

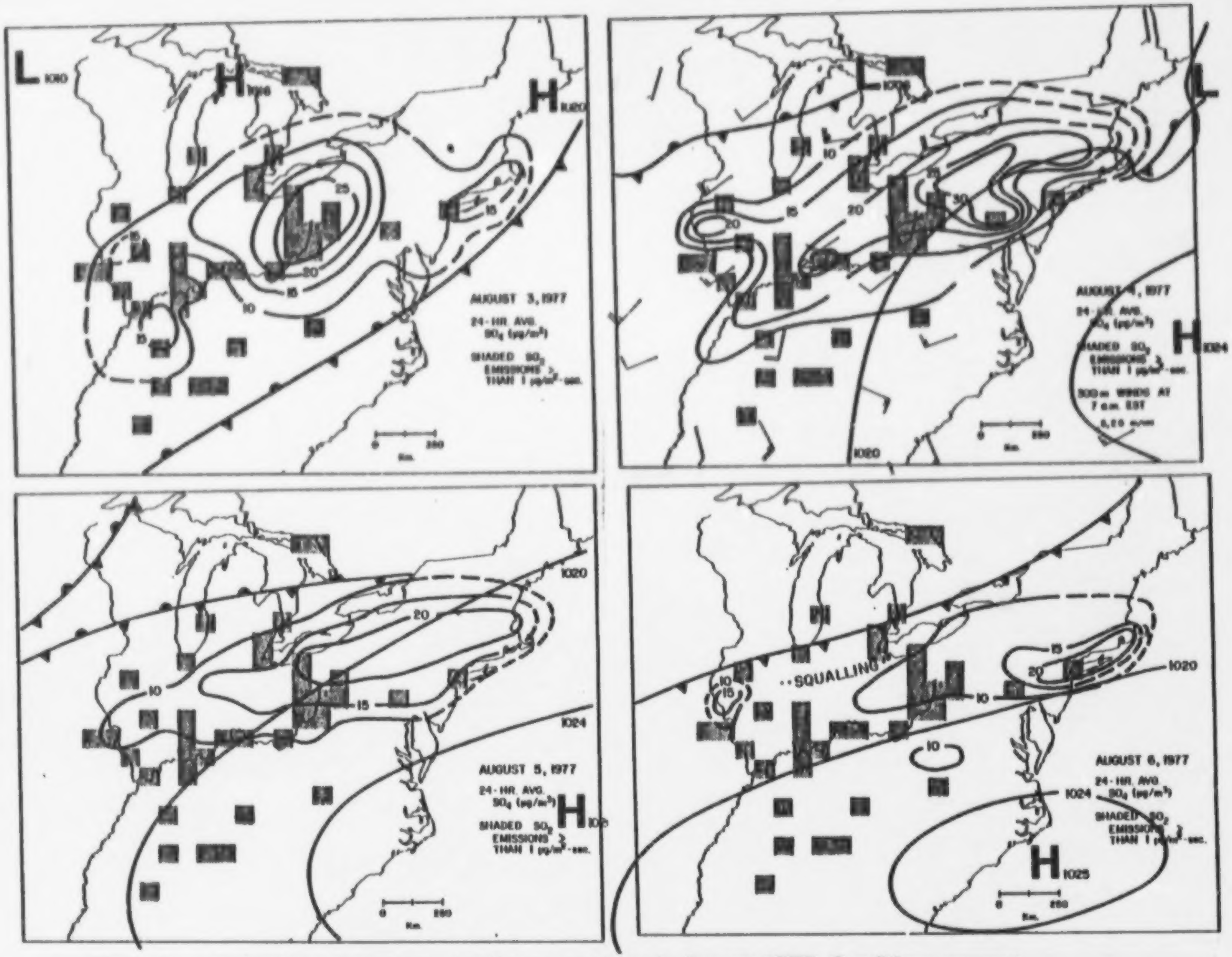

Figure 6. Evaluation of an elevated sulfate event in early August 1977. Conditions suggest long-range transport across the Northeast associated with a channeling or ducting of moist air flow. Pressures associated with highs and lows are in millibars; isobars are drawn in with the sulfate isopleths. The sulfate levels are in two digits compared with the isobars in four digits.

TABLE 1. AVERAGE AIRCRAFT OBSERVATIONS* FOR SULFATE AND NITRATE FOR DUNCAN FALLS, OH

Period	Maximum height (10^{-3} ft)	$SO_4^=$ (μg/m³)	NO_3^- (μg/m³)
August 1977	Surface	9.1	---
	5	12.5	2.6
	10	7.5	2.4
Jan-Feb 1978	Surface	10.1	---
	5	5.6	1.1
	10	2.0	0.09
April 1978	Surface	3.9	---
	5	4.8	0.7
	10	1.9	0.1
July 1978	Surface	10.6	0.18
	5	18.0	1.0
	10	3.1	0.6
October 1978	Surface	---	---
	5	6.3	0.9
	10	2.7	0.1
Mean (Duncan Falls)	5	9.4	1.3
	10	3.4	0.7

*Excludes horizontal traverses; average of all flights per sampling period.

TABLE 2. METEOROLOGICAL REGIMES CONDUCIVE TO REGIONAL SULFATE ACCUMULATION AND TRANSPORT

Type	Synoptic pattern	Seasonal preference	Transport winds	Afternoon mixing heights	Zone of influence	Thermo-dynamics
Stagnation	Dominant high-pressure cell (surface and aloft)	Any season	Light (~5 m/s)	Low <1,000 m	100-300 km	Any temperature; generally moist
Channeling or ducting	Stationary front along Great Lakes and/or westward extension of Bermuda high	Summer	Moderate SW winds (7-12 m/s)	Moderate (1,000-1,500 m)	Long-range transport (>500 km)	Warm; moist

PERFLUOROCARBON TRACER SYSTEM FOR ATMOSPHERIC TRANSPORT AND DISPERSION STUDIES

Gilbert J. Ferber

National Oceanic and Atmospheric Administration
Silver Spring, Maryland

INTRODUCTION

A variety of atmospheric transport and dispersion models are being developed under the auspices of EPA, DOE, and others to simulate the behavior of air pollutants and estimate regional air concentrations under various scenarios. With increasing concern over regional and international aspects of air pollution, reliable model calculations are required at distances out to 1,000 km from pollution sources.

Attempts to verify model calculations, using air quality data, are complicated by the presence of multiple sources and imprecise knowledge of emission amounts. There is a need for nonreactive, nondepositing tracers that could be released at precisely controlled rates and measured accurately at very low concentrations. This will allow us to conduct tracer experiments that isolate atmospheric transport and dispersion from the other complexities and provide data for verification of this basic aspect of all model calculations. Regional scale model verification experiments require tracers that can be unambiguously identified and measured out to hundreds of kilometers or several days' travel time. Sulfur hexafluoride, SF_6, has been used out to about 100 km, but its relatively high and variable background concentration militates against its use to much greater distances.

PERFLUOROCARBON TRACER SYSTEM

Investigations by J. E. Lovelock in England indicated that a perfluorocarbon tracer system could be developed that would be ideal for long-range dispersion studies. The perfluorocarbons are extremely stable, nontoxic compounds, measurable at very low concentrations by electron capture gas chromatography. Atmospheric background concentrations are well below that of SF_6. Under DOE funding, the NOAA Air Resources Laboratories (ARL) contracted with Lovelock to develop three different prototype samplers as the first step in the development of a perfluorocarbon tracer system.

The first instrument, a sequential sampler, consists of a pump and a cassette of 24 tubes containing molecular sieve material to trap the tracer. Air is pumped through each sampling tube in a preset automated sequence. The cassette is returned to the laboratory and inserted into an analyzer unit, which automatically heats each tube in turn, to desorb the sample into a catalytic reactor that destroys unwanted components. The sample then flows through a chromatograph column that separates the perfluorocarbon tracer from other surviving compounds and then tracer concentrations are determined with an electron capture detector.

Another prototype instrument combines the sampling and analysis functions into a single unit. The unit contains two sampling tubes so that one is sampling while the other is being analyzed. This instrument provides readout of concentrations every 5 minutes at the sampling site.

A third instrument was designed to be flown in a small aircraft. Ambient air is drawn through a catalytic reactor that reduces the O_2 and other electron-absorbers, leaving the perfluorocarbon and nitrogen. This is passed directly to an electron capture detector providing continuous concentration readout with a 3-second delay.

Prototype instruments were delivered by Lovelock in June 1976. Since then ARL has been working closely with the DOE Environmental Measurements Laboratory (EML) and Brookhaven National Laboratory (BNL) in a cooperative effort to develop a practical perfluorocarbon tracer system.

Comparative data on SF_6 and perfluorocarbons (PDCH, PMCH and PDCB) are shown in Table 1. The atmospheric background concentration of PDCH is about 0.02 ppt by volume (2×10^{-14}), about 1/25 of the SF_6 background. Background of the other ~~two~~ perfluorocarbons (PMCH and PDCB) is an order of magnitude lower. The amount of tracer released in any experiment must be sufficient to distinguish the plume from background at the maximum sampling distance. The required release rate for PDCH is about 10 percent of that for SF_6; for PMCH and PDCB it is about 1 percent of the SF_6 rate. Taking the higher price of the perfluorocarbons into account, the PDCH required for an experiment would cost about 70 percent as much as SF_6; the cost of PMCH and PDCB would be about 5 percent of the SF_6 cost.

Perfluorocarbon release, sampling, and analysis techniques were tested in a field experiment in Idaho in April 1977. Three perfluorocarbons were released simultaneously with SF_6 and samples were collected along arcs out to 90 km from the release point. The experiment demonstrated that release techniques worked well with all tracers released uniformly over a 3-hr period as planned. Five sequential samplers performed well on the 50-km arc. About 60 half-hour samples were taken and all data were consistent. As the plume passed the arc, PDCH concentrations were measured from the background of about 0.02 ppt to a peak near 10 ppt and down to background again as shown in Figure 1. Perfluorocarbon measurements from these samplers agreed well with SF_6 measurements from whole-air samples taken at the same locations.

The real-time continuous sampler did not operate properly in this test. Subsequently, the BNL version of this instrument was successfully flown in the MAP3S-AMBIENS experiment in October 1977.

IMPROVED SEQUENTIAL SAMPLER

The Idaho experiment established that the sequential samplers worked well and that PDCH can be measured reliably down to its background level of about 0.02 ppt. However, the molecular sieve traps used in these instruments do not collect PDCB or PMCH, both of which have background concentrations about 1/10 that of PDCH. In exploring perfluorocarbon trapping and analysis techniques at BNL, it was found that charcoal efficiently traps all three tracers but also collects many unwanted components that interfere with perfluorocarbon analysis. A laboratory analysis scheme has been devised that effectively eliminates interferences and achieves a sensitivity better than 0.001 ppt (1×10^{-15}). This achievement has led to a new concept for a sequential sampler, using charcoal traps, that is smaller, lighter (under 20 lb with self-contained batteries), simpler to operate, and less costly than the Lovelock samplers. The sampler will automatically start at a preselected time and take a preset number of samples (up to 24) of preselected duration (up to 24 hr per sample). Two prototype units are scheduled for delivery in April 1979. Tests should be completed by June and we plan to contract for production units to be delivered early in 1980.

DEMONSTRATION EXPERIMENT

We plan to conduct an atmospheric tracer experiment in the spring of 1980 to demonstrate the capabilities of the perfluorocarbon tracer system. Two perfluorocarbons will be released simultaneously with at least one other tracer and the new sequential samplers will be operated on several arcs out to about 500 km from the release point. Measurements of the different tracers will be compared to establish the reliability and precision of release, sampling, and analysis techniques. The BNL real-time continuous monitor will be used to measure the vertical distribution of tracer and cross-wind concentration profiles. Data will be used to estimate diffusion parameters and to test model calculations of plume dispersion.

The perfluorocarbon tracer system will provide a capability, for the first time, to perform long-range atmospheric transport and diffusion experiments, at reasonable cost, for verification and improvement of air quality models. Other applications of interest to EPA include:

1. Tracer studies of atmospheric transport and dispersion from proposed plant sites;
2. Simultaneous release of several perfluorocarbons at different sites to determine their relative contributions to the gross pollutant burden at locations of interest; and
3. Study of long-range pollutant transformation and deposition rates by injection of tracer into the stack and measurement of pollutant/tracer ratios as a function of plume travel time.

APPLICATION TO PEPE STUDIES

The feasibility of using perfluorocarbons in studies of prolonged elevated pollution episodes (PEPE) can be examined with a computer-simulated tracer release. The ARL Regional Scale Transport and Diffusion Model[1 2] was used to calculate tracer concentrations for 5 days following a release of PMCH. The simulation assumes a release rate of 100 lb/hr for 3 hr (1,030-1,330 GMT) at Nashville, TN, on August 18, 1976. A stagnating high-pressure system dominated the weather over the eastern half of the United States during this period. The calculated trajectory, shown in Figure 2, travels clockwise around the high, arriving over Michigan on the fifth day. Calculated tracer concentrations are shown for 12-hr air samples collected on the third and fifth day after release. Contours are drawn for concentrations at the limit of detection (0.002 ppt) and ten times the detection limit (0.02 ppt). The simulation indicates that the tracer should be measurable over a large area up to 5 days after a total release of 300 lb of PMCH.

REFERENCES

1. Heffter, J. L., A. D. Taylor, and G. J. Ferber. 1975. A Regional-Continental Scale Transport, Diffusion, and Deposition Model. NOAA Tech. Memo. ERL ARL-50, Air Resources Laboratories, Silver Spring, MD 20910, 29 pp.

2. Telegadas, K., G. J. Ferber, J. L. Heffter, and R. R. Draxler. 1978. Calculated and Observed Seasonal and Annual Krypton-85 Concentrations at 30-150 km from a point source. Atmospheric Environment, 12:1769-1775.

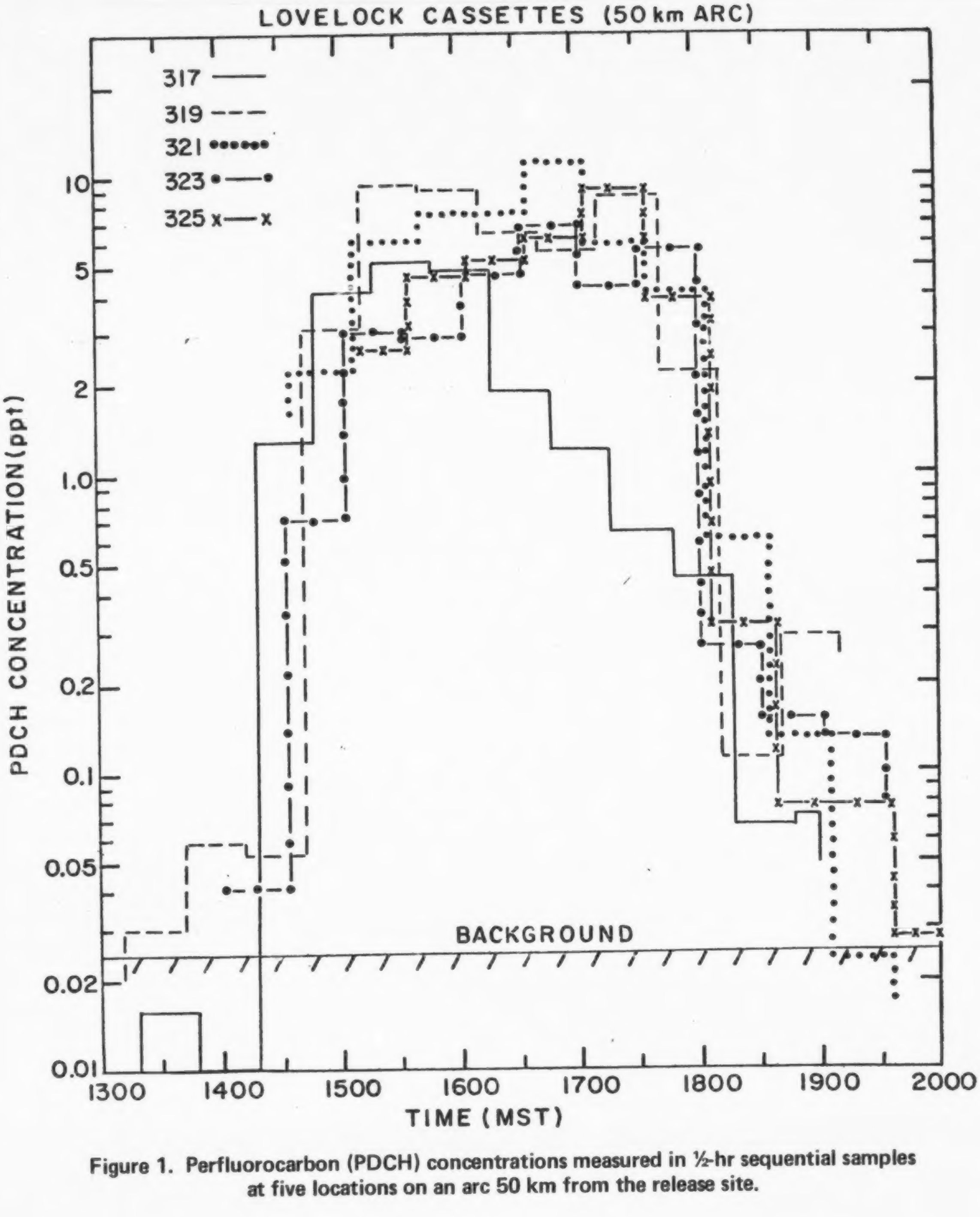

Figure 1. Perfluorocarbon (PDCH) concentrations measured in ½-hr sequential samples at five locations on an arc 50 km from the release site.

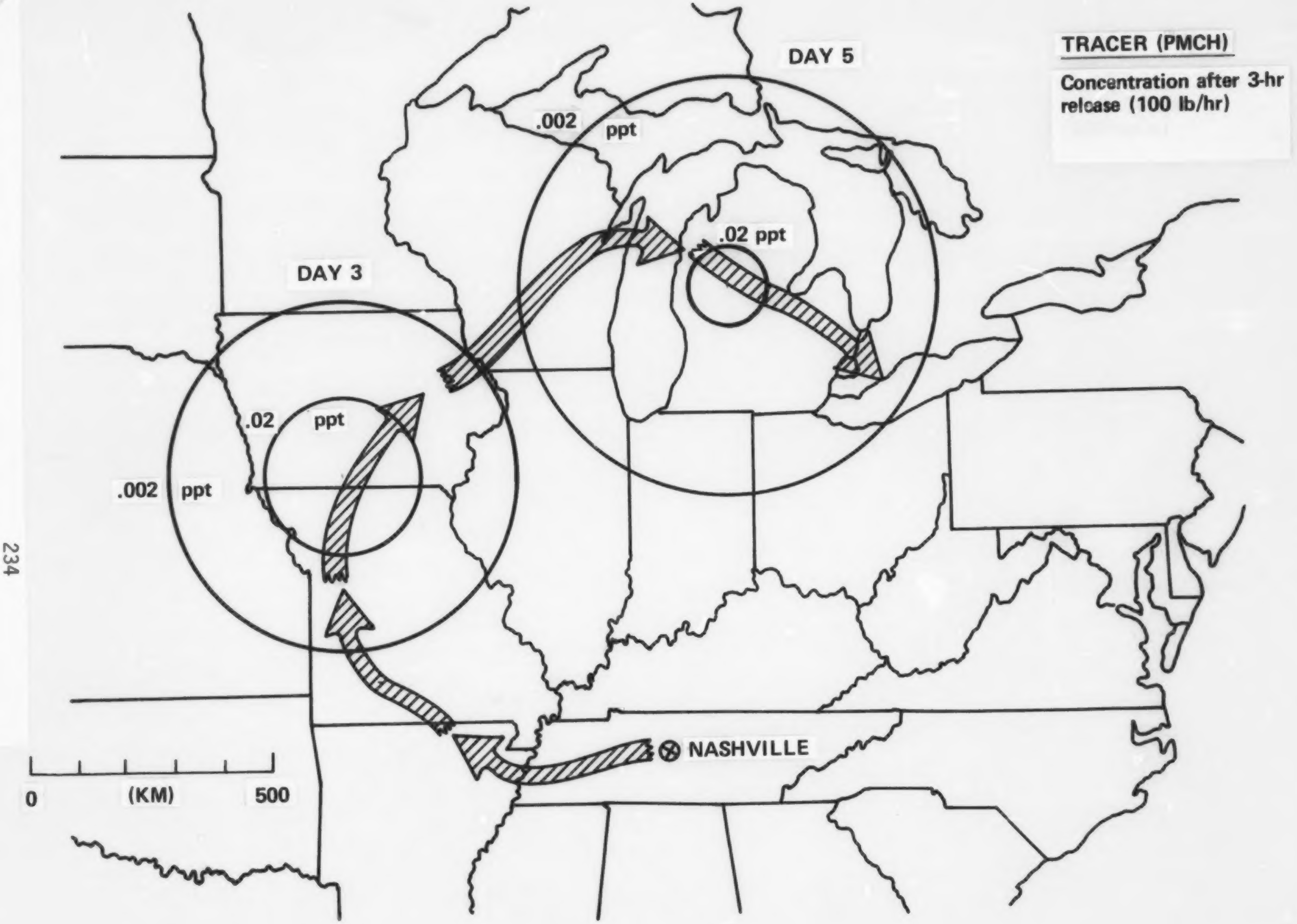

Figure 2. Calculated tracer concentrations (ppt) in 12-hr samples taken 3 and 5 days after release at Nashville, TN.

TABLE 1. COMPARATIVE DATA ON SF_6 AND PERFLUOROCARBONS

Tracer	Sulfur-hexa-fluoride	Perfluoro-dimethyl-cyclohexane (PDCH)	Perfluoro-methyl-cyclohexane (PMCH)	Perfluoro-dimethyl-cyclobutane (PDCB)
Formula	SF_6	C_8F_{16}	C_7F_{14}	C_6F_{12}
Mol. wt.	146	400	350	300
Background (pptv)	0.5	0.02	0.002	0.002
Cost/kg	$7	$45	$45	$45
Relative release rate	100	11	0.9	0.8
Relative cost/ release	100	70	6	5

MAP3S PROGRAMS APPLICABLE TO PEPE'S

Michael C. MacCracken

University of California, Livermore, California

SUMMARY

The MAP3S goal is to improve the capability to simulate the behavior of energy-related pollutants in the atmosphere. This requires improving the understanding of atmospheric behavior and of the processes affecting pollutant evolution in the atmosphere. MAP3S has conducted a wide variety of field experiments and characterization studies to improve understanding of wet and dry deposition, pollutant transformation, planetary boundary layer evolution, aerosol speciation, long-range pollutant transport, precipitation chemistry, and pollutant budgets. While MAP3S will be continuing in FY 1980 to focus on its own program objectives, the objectives of PEPE (Persistent Elevated Pollution Episode) are sufficiently related to those of MAP3S to permit consideration that some MAP3S resources could be diverted to PEPE studies during limited intensive periods in the summer of 1980. Resources and capabilities that may be available can be divided into the following three areas, with subareas also listed.

A. Network Support

1. Precipitation chemistry network data from the eight MAP3S and nine Electric Power Research Institute event-basis sites can be used to measure the final removal stages of PEPE's.
2. Aerosol acidity of fine particles, in terms of the molar ratio of hydrogen ion to sulfate ion, with a 4-hr time resolution at five sites.
3. Turbidity data may be available if the network that operated from the summer of 1977 to fall of 1978 is reestablished so as to interface with the National Oceanic and Atmospheric Administration (NOAA) network.

B. Field Capabilities

1. Pacific Northwest Laboratories and Brookhaven National Laboratory (BNL) instrumented aircraft may be available for episode studies by diverting them from ongoing MAP3S studies.
2. MAP3S funded tracer capabilities, developed by a team from BNL, Environmental Measurements Laboratory, and NOAA, are expected to be ready for major field implementation in 1980. (Refer to paper by G. Ferber in this volume.)
3. Special sampling instruments, including the diffusion processor, BNL filter packs, and the BNL-developed real-time sulfate/sulfuric acid monitor.

C. Modeling and Analysis Capabilities

1. Data from the August 1977 and July 1978 studies of elevated $SO_4^=$ concentrations can serve as the basis for PEPE preplanning.
2. Source emission data are available that may indicate likely PEPE source regions.
3. MAP3S trajectory models are expected to be able to operate using National Weather Service forecast trajectories as a means of estimating the evolution and movement of the polluted air mass.

Because of uncertainty in the planning of MAP3S activities for 1980 and beyond, resources in addition to those now available to MAP3S participants may be required.

ACKNOWLEDGMENTS

This work was supported by the U.S. Environmental Protection Agency through interagency agreement with the Department of Energy. The work was performed by the Lawrence Livermore Laboratory under contract no. W-7405-Eng-48.

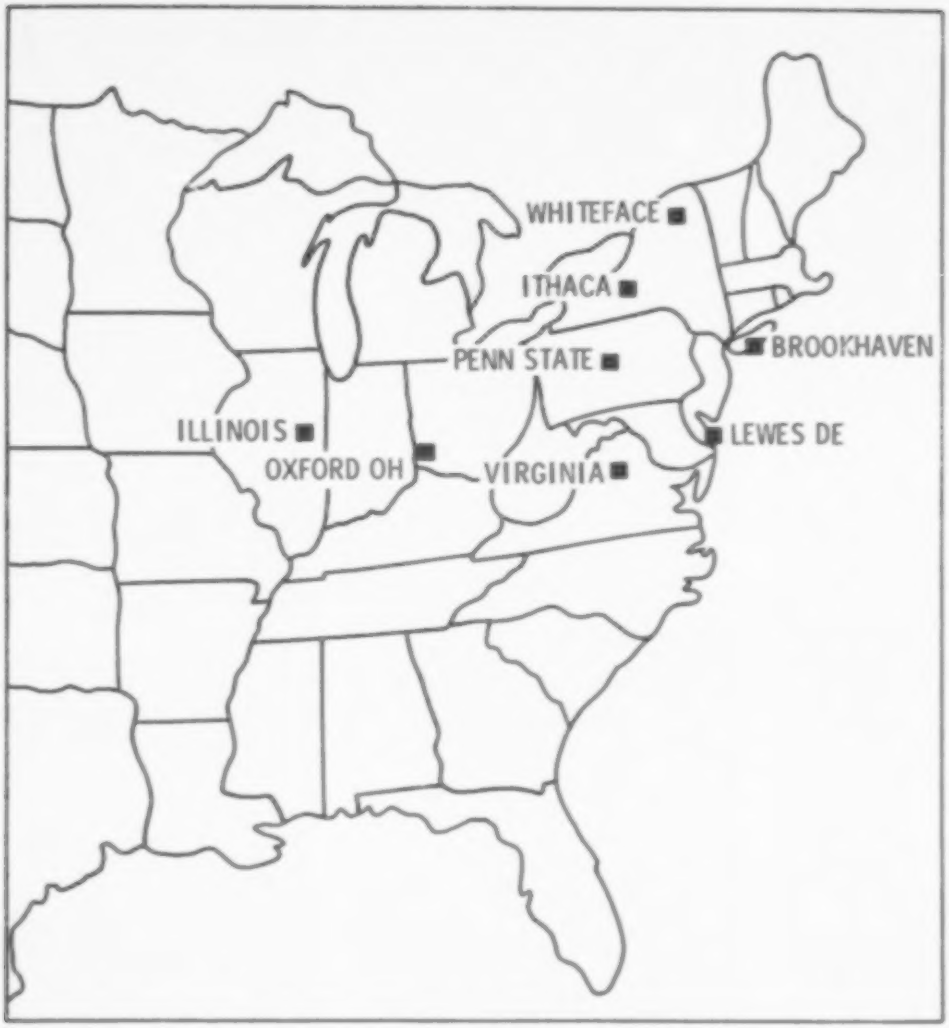

Figure 1. Locations of MAP3S precipitation chemistry sites.

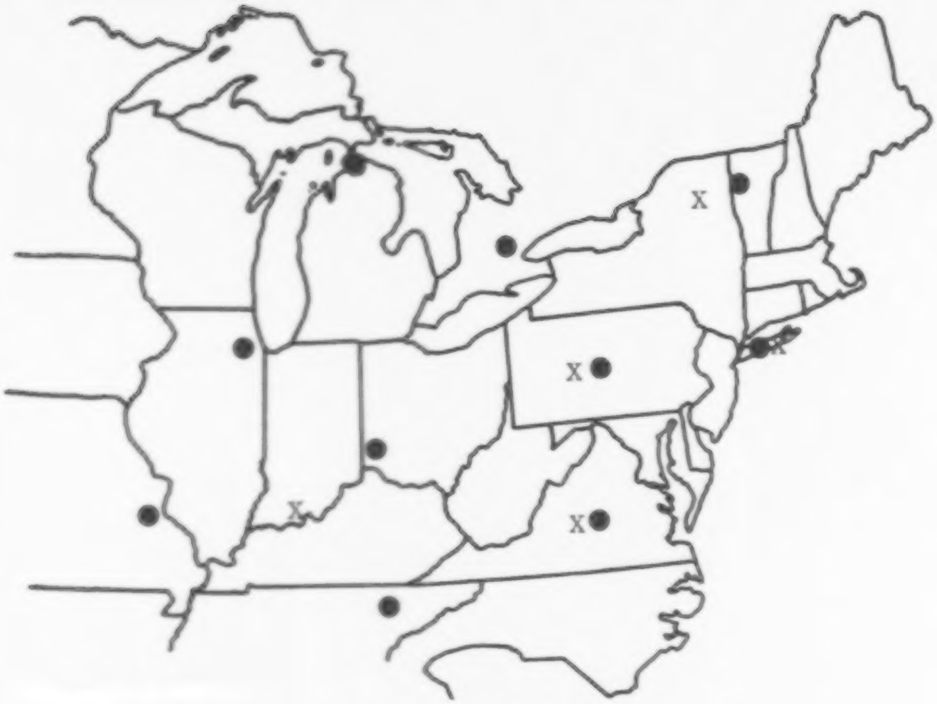

Figure 2. Location of MAP3S aerosol acidity (X) and (former) turbidity network (●) sites.

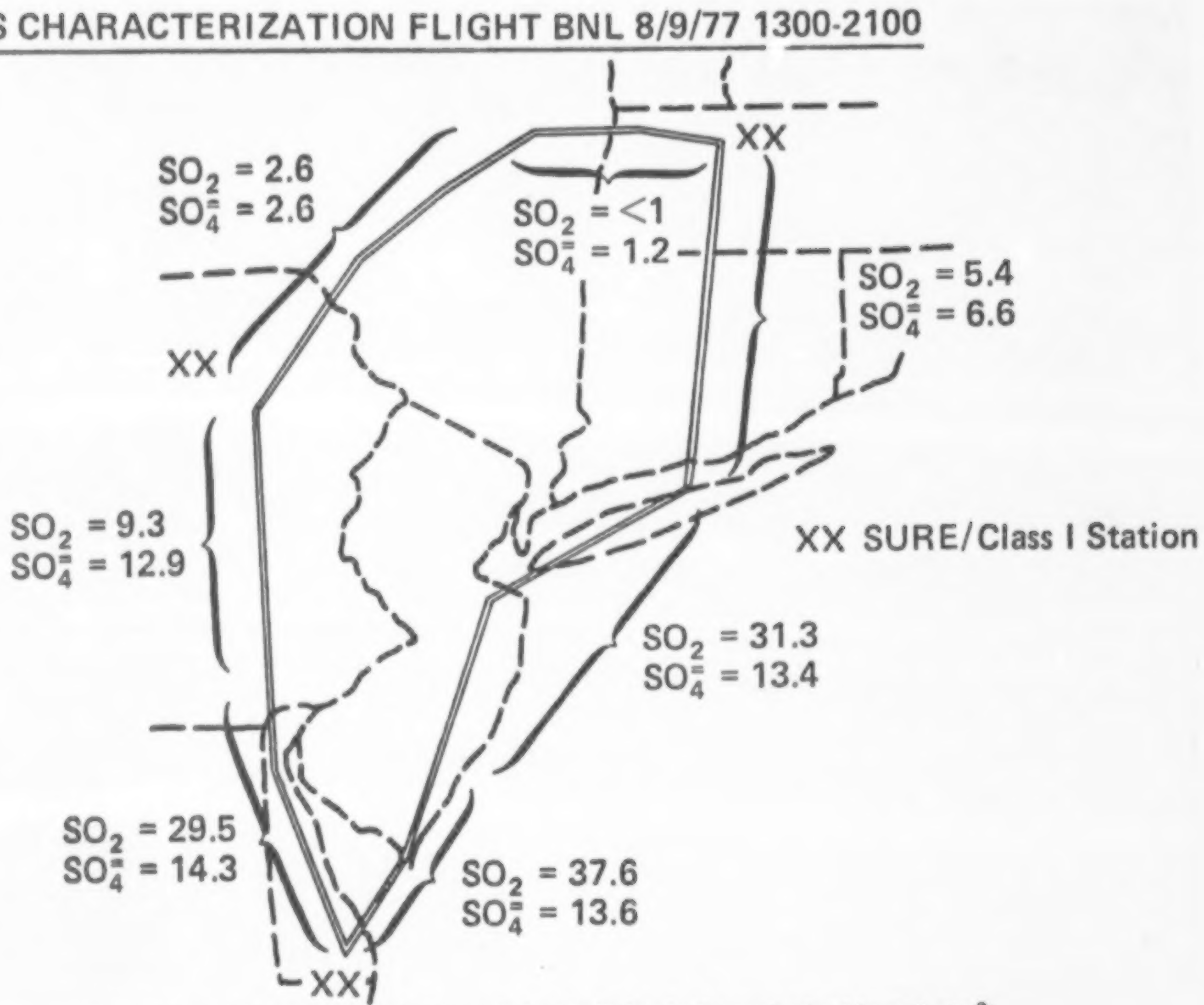
MAP3S CHARACTERIZATION FLIGHT BNL 8/9/77 1300-2100

Figure 3. Typical result from horizontal aircraft flights in the well-mixed layer ($\mu g/m^3$).

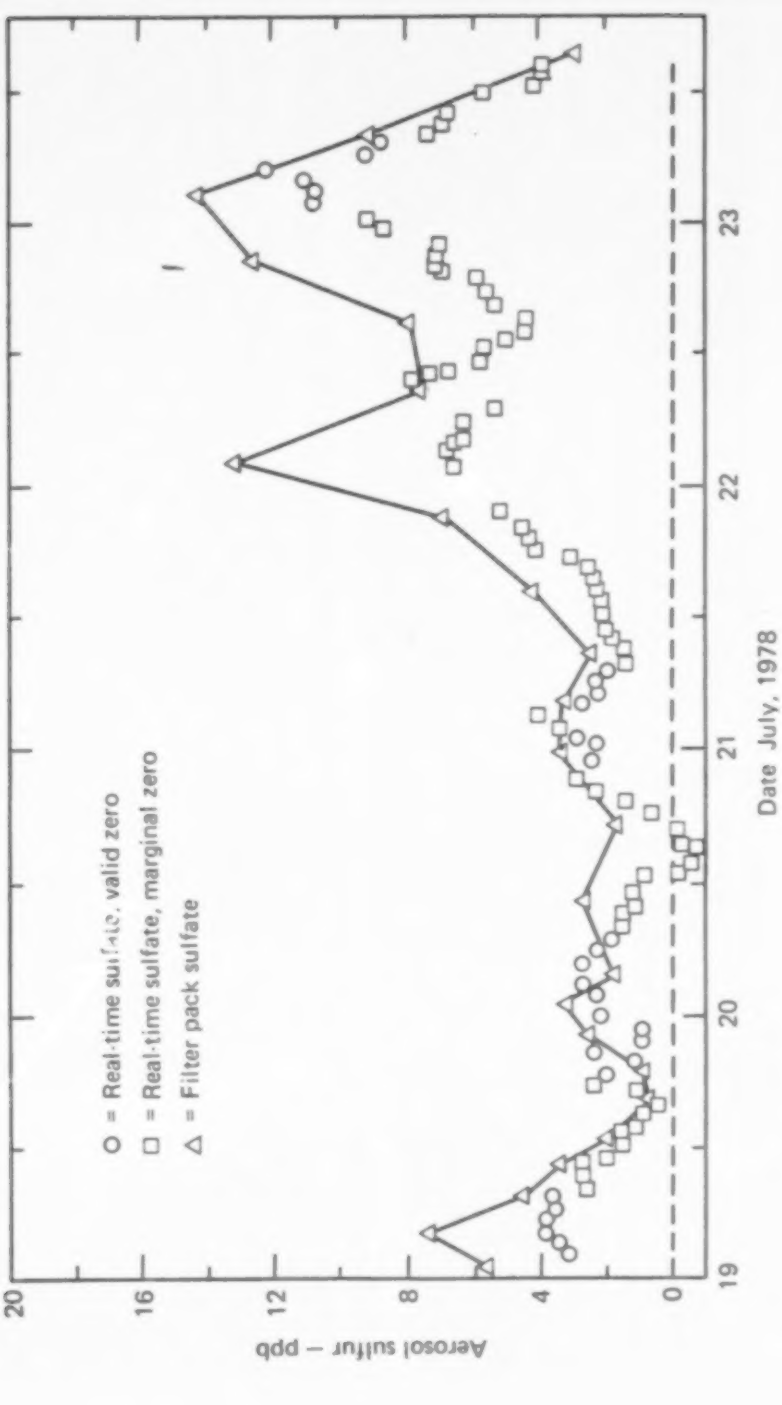

Figure 4. Comparison of BNL real-time and filter pack measurements of sulfate.

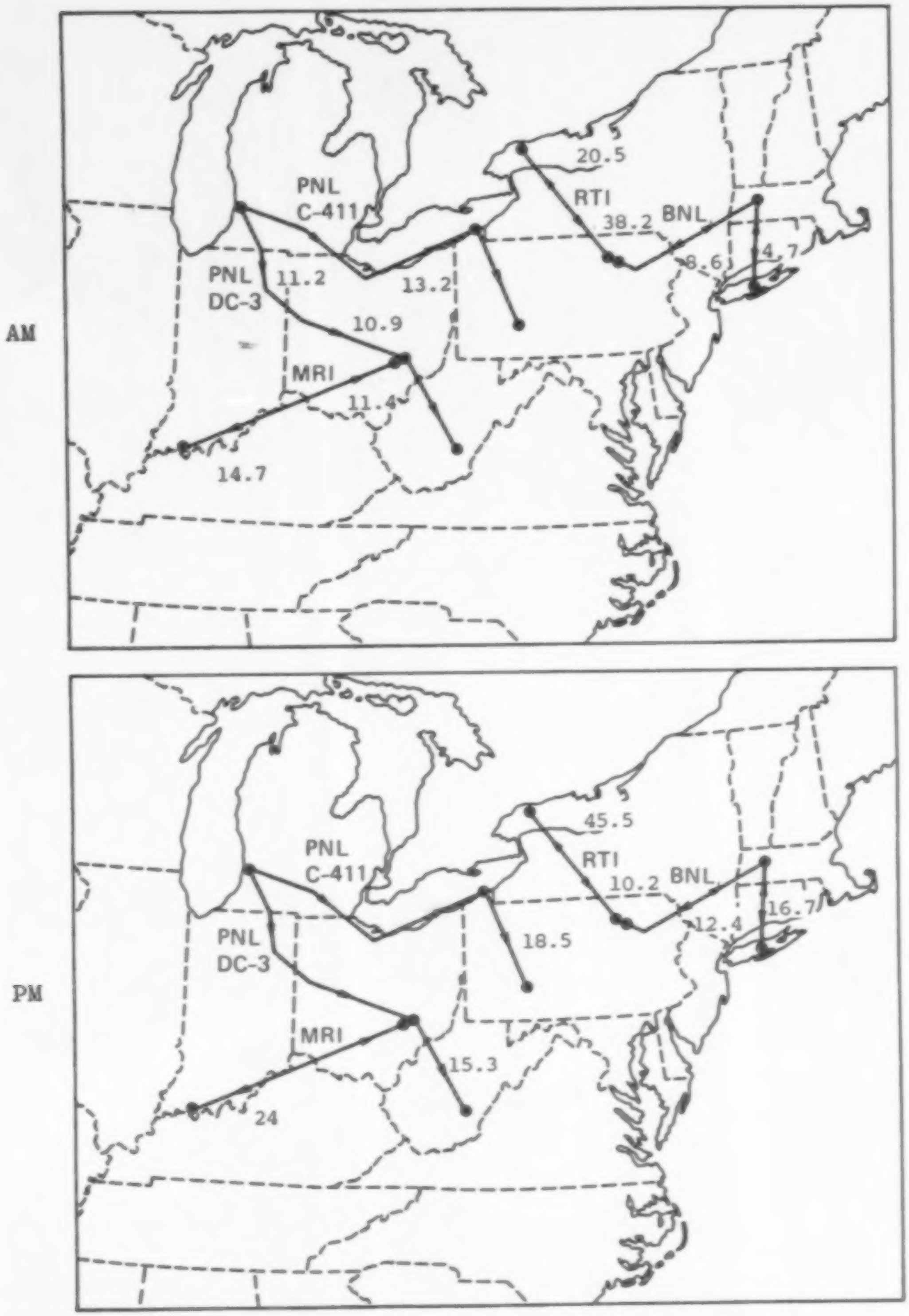

Figure 5. Aircraft sulfate measurements during SURE/MAP3S intensive study on July 19, 1978 ($\mu g/m^3$).

REGIONAL SCALE AIRCRAFT MAPPING OF HAZY AIR MASSES DURING PROJECT MISTT, 1975 and 1976

D. E. Patterson, J. M. Holloway, and R. B. Husar*
Washington University, St. Louis, Missouri

1.0 INTRODUCTION

The measurements reported in this document were made as part of the 1975 and 1976 field programs of the Midwest Interstate Sulfur Transformation and Transport (MISTT) study. Project MISTT is an integrated interdisciplinary research program of field, laboratory, and theoretical studies sponsored by the U.S. Environmental Protection Agency. The principal objective is to obtain a physical understanding and quantitative estimation of the nature and fate of atmospheric sulfur in large power plant and urban-industrial plumes.

Although MISTT focused on plume studies, there were a few flight days in which measurements were made on a regional scale. Four such missions have been chosen for analysis in the context of this PEPE seminar. Each mission characterizes the air mass of interest on a scale of hundreds of kilometers over a period of at least 8 hr, and each represents a different sampling approach. It is hoped that these missions can serve as examples (good or bad) for use in designing future regional scale sampling programs.

The analysis of each day consists of four levels of information:

1. The meteorological setting is described through isopleth maps of noon surface temperature, dewpoint, sea level pressure, relative humidity, and wind field over the eastern United States. The observed noon visibilities (corrected to 60 percent RH) are displayed as light extinction coefficient, b_{ext}. The extinction coefficient, or haziness, has been shown to be a qualitative surrogate for sulfate concentrations.

---

*Speaker.

2. The flight path, time of day, and altitude of sampling are described in detail. Locations of traverses and vertical soundings are shown on an appropriate regional map.
3. Pollutant parameters are displayed by superimposing the measured values on the flight path for ease of interpretation. The continuous measurements usually include SO_2 and ozone in addition to three aerosol parameters: condensation nuclei count (CNC), aerosol charge, and the light scattering coefficient (b_{scat}). Particulate sulfur (as sulfate) was obtained from filter samples by the flame photometric detection (FPD) method.
4. Vertical profiles of gaseous and aerosol parameters add the third dimension to the picture of the atmosphere. Profiles of temperature, turbulence, and dewpoint are also provided where available. Sulfate concentrations are averages over each spiral and are listed in the corner of each plot.

The information is primarily in graphical form, so that much of the report is to be found in the figure captions.

2.0 JULY 29-30, 1975

2.1 Flight Description

A large high-pressure area dominated the eastern portion of the country from the Missouri Valley to the east coast. The center of the ridge, both aloft and on the surface, was situated over the eastern Great Lakes. To the west, a rather well-defined trough, extending from the surface to 9,145 m MSL, was located over the western plains. Since the Mississippi Valley was between these two features, a strong pressure gradient pattern favoring south to southeasterly winds affected Missouri, Iowa, and Illinois throughout the air sampling period. Since the flow pattern tended to be more southerly closer to the trough, winds favored a southeasterly direction east of the Mississippi River and a southerly direction west of it.

Skies were clear throughout the period but considerable haze caused daytime visibilities to be 7 to 8 km and nighttime readings to average near 5 km. Lower visibility readings were particularly evident east of the Mississippi and south of Iowa and Wisconsin.

Temperature soundings displayed nearly adiabatic lapse rates from the surface to 1,830 m MSL. Above that level, neutral conditions capped a shallow +1° C inversion. The diurnal surface inversion started to establish itself by midnight on the 29th, extending up to about 460 m MSL by sunrise on the 30th.

Wind direction variation with height was more than 10° to 15° throughout the period of sampling. Along the east of the Mississippi River, directions were from 120° to 150° while directions from 170° to 190° became apparent west of the river, especially during the early hours of the 30th. Wind speeds at all the sampling locations were between 10 and 20 m/s at all levels.

The flight consisted of traverses at several discrete altitudes oriented crosswind to the air mass trajectory. In addition, spirals were made at each downwind distance. The mission began at 1300 CDT July 29 and ended at 1130 CDT on July 30.

2.2 Summary

The July 29-30, 1975, mission sampled a very hazy air mass as it passed over St. Louis, covering over 20 hr from beginning to end. Sulfate concentrations in excess of 60 $\mu g/m^3$ and light scattering coefficient near 10 × $10^{-4}m^{-1}$ were encountered northeast of Quincy, IL.

The sampling pattern consisted of multiple traverses at discrete downwind distances complemented by spirals over a fixed location. This technique provides excellent resolution of the three-dimensional structure of the air mass, but requires too much time for truly regional scale sampling.

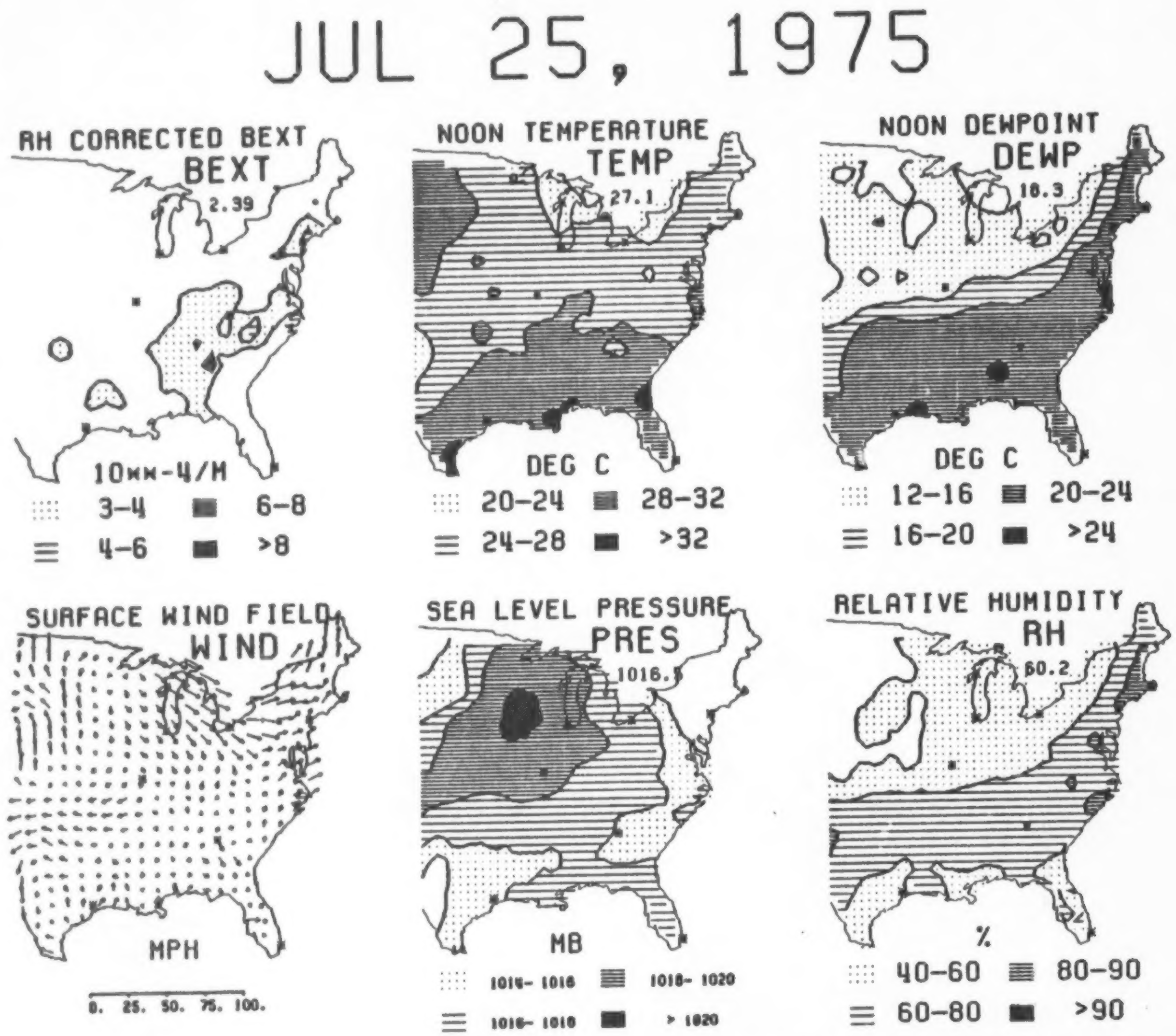

Figure 2-1. Stagnating winds from the Ohio River Valley south to Florida are associated with the beginning of this episode. Noon surface readings indicate temperature near 28° C, dewpoint 20-24° C, RH of about 60-80 percent with extinction coefficient of ~$3 \cdot 10^{-4}m^{-1}$ (visibilities of ~8 mi).

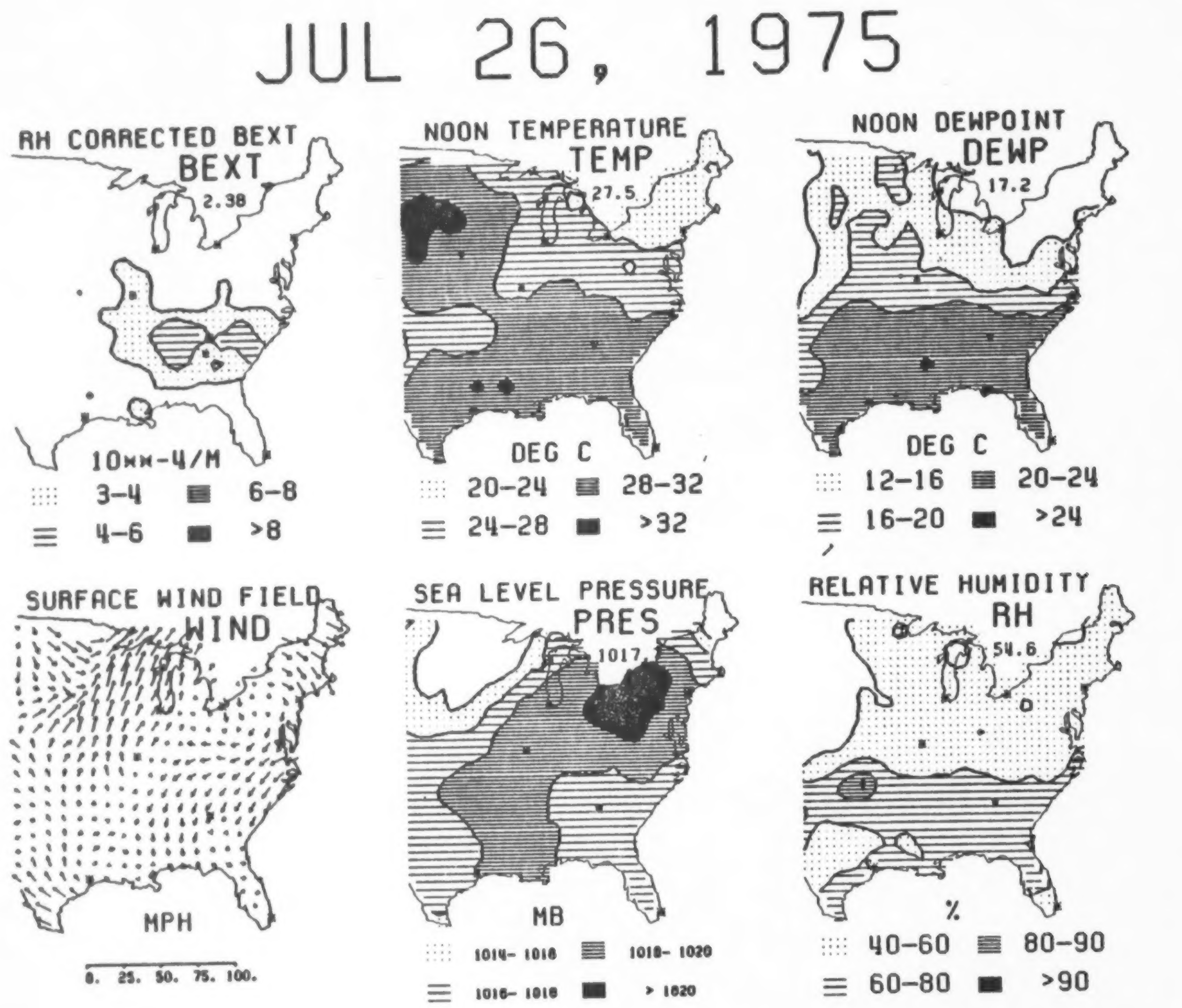

Figure 2-2. The region with $b_{ext} > 3 \cdot 10^{-4} m^{-1}$ has expanded into the MO-IL-IO area. Note the stagnant region in the upper IN-OH region associated with the high-pressure cell.

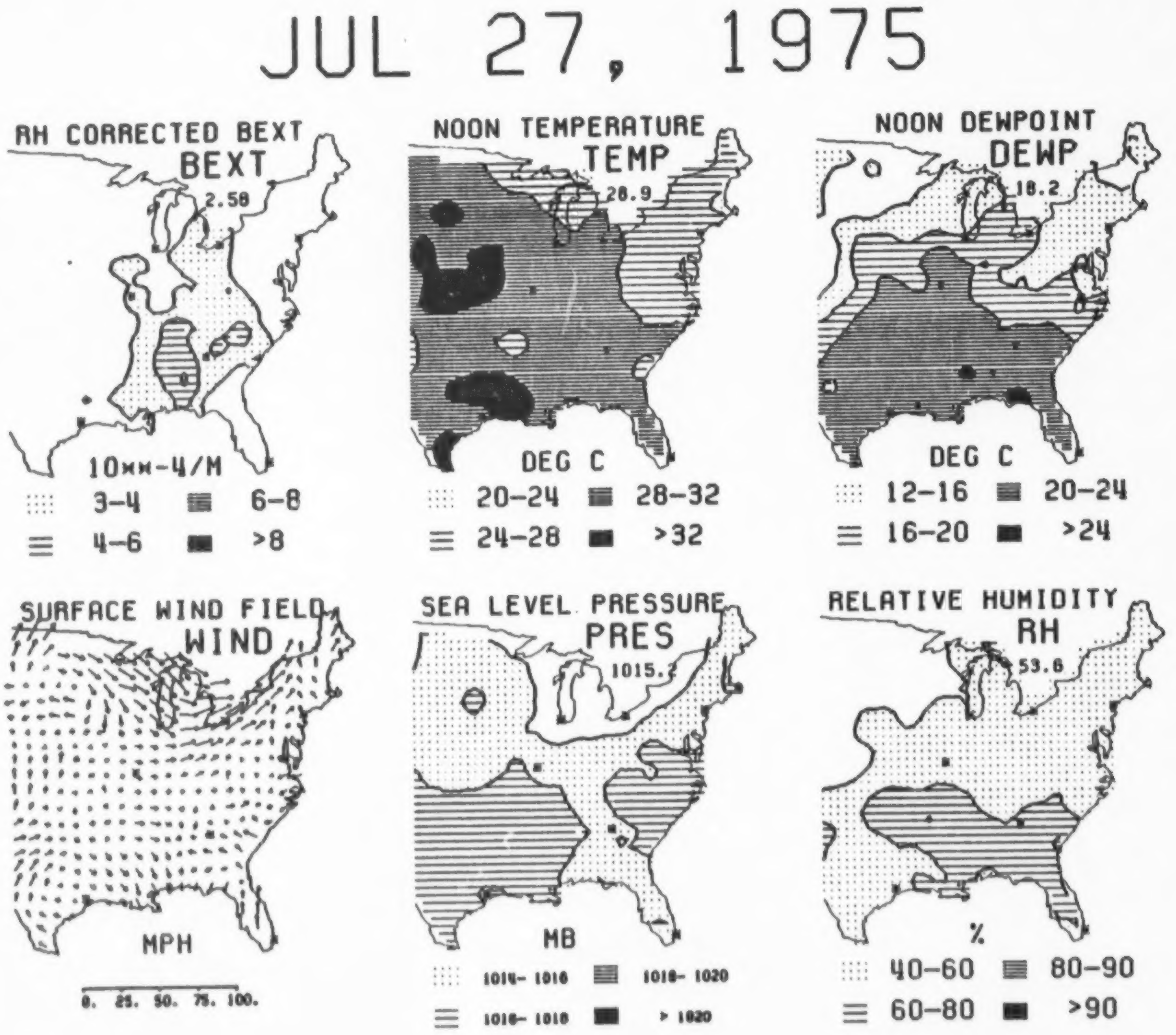

Figure 2-3. The region of haze covers a large part of the east-central United States by July 27.

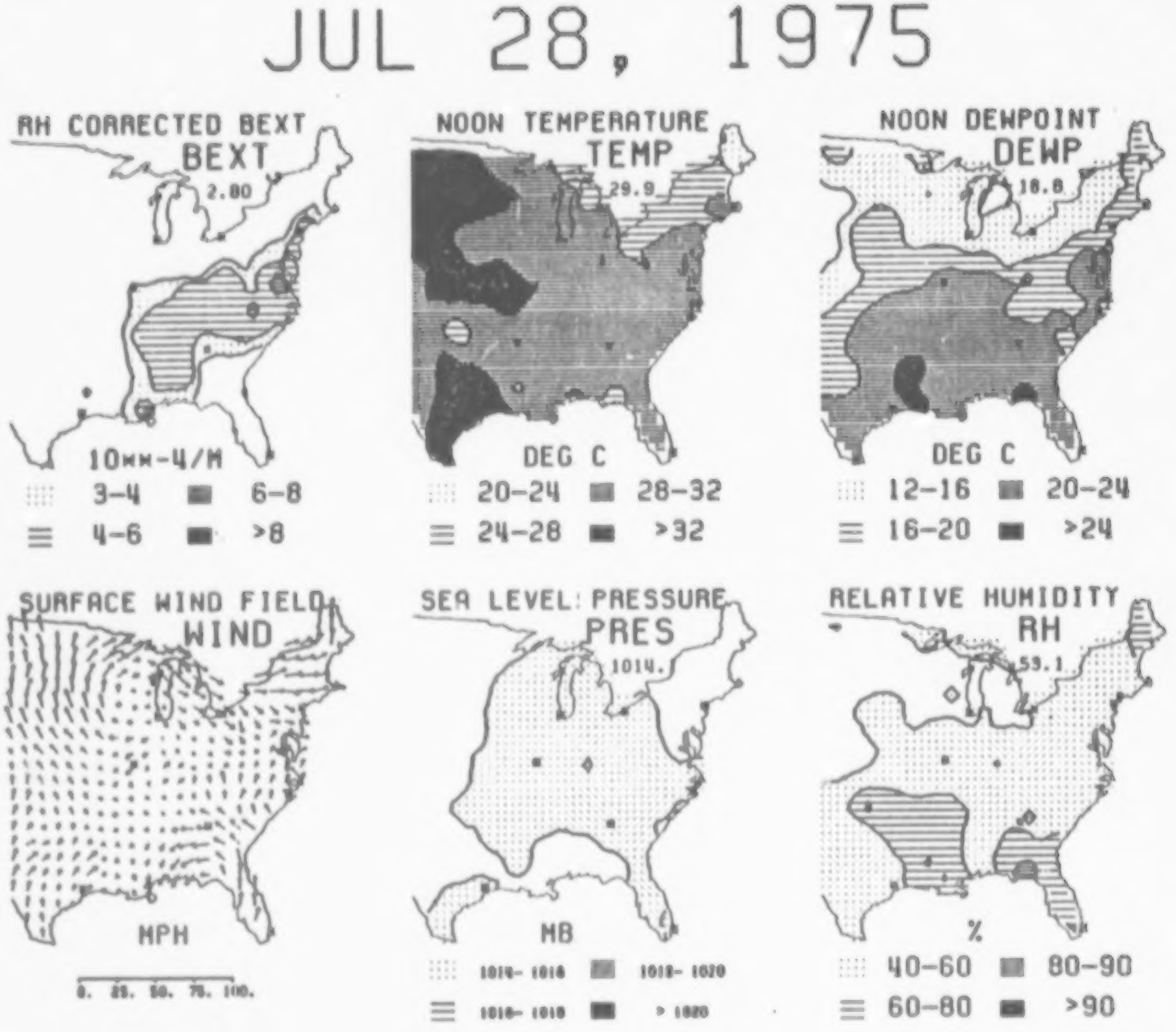

Figure 2-4. Continued stagnation in the Ohio River Valley is associated with extinction coefficient $>4 \cdot 10^{-4} m^{-1}$. Noon surface temperatures are 28°-32° C with relative humidity typically 40-60 percent. The area around St. Louis, MO, is stagnant.

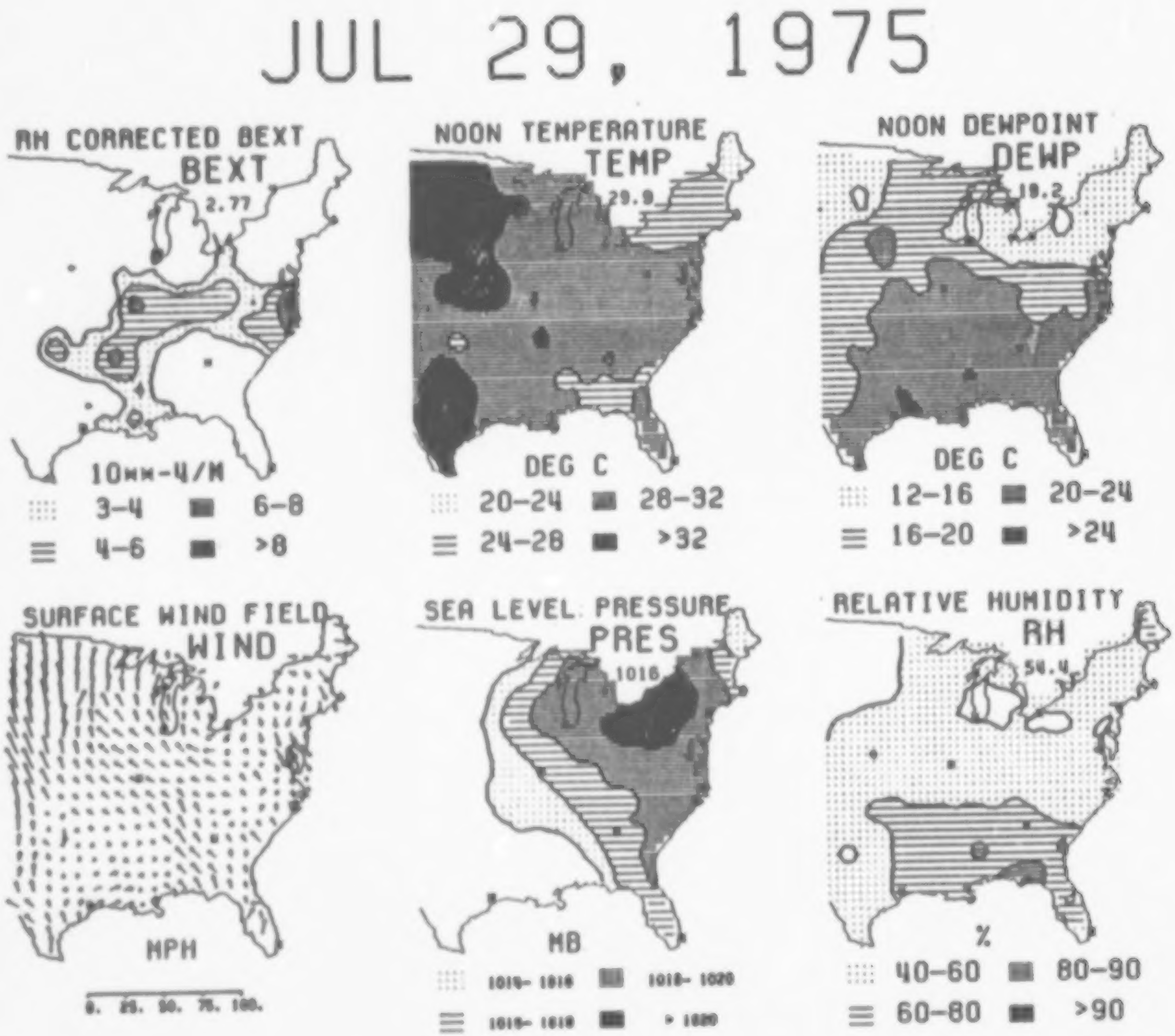

Figure 2-5. This is the first day of the sampling mission. The wind and pressure fields have changed dramatically over the past 24 hr; the St. Louis area is in the region of lowest visibility.

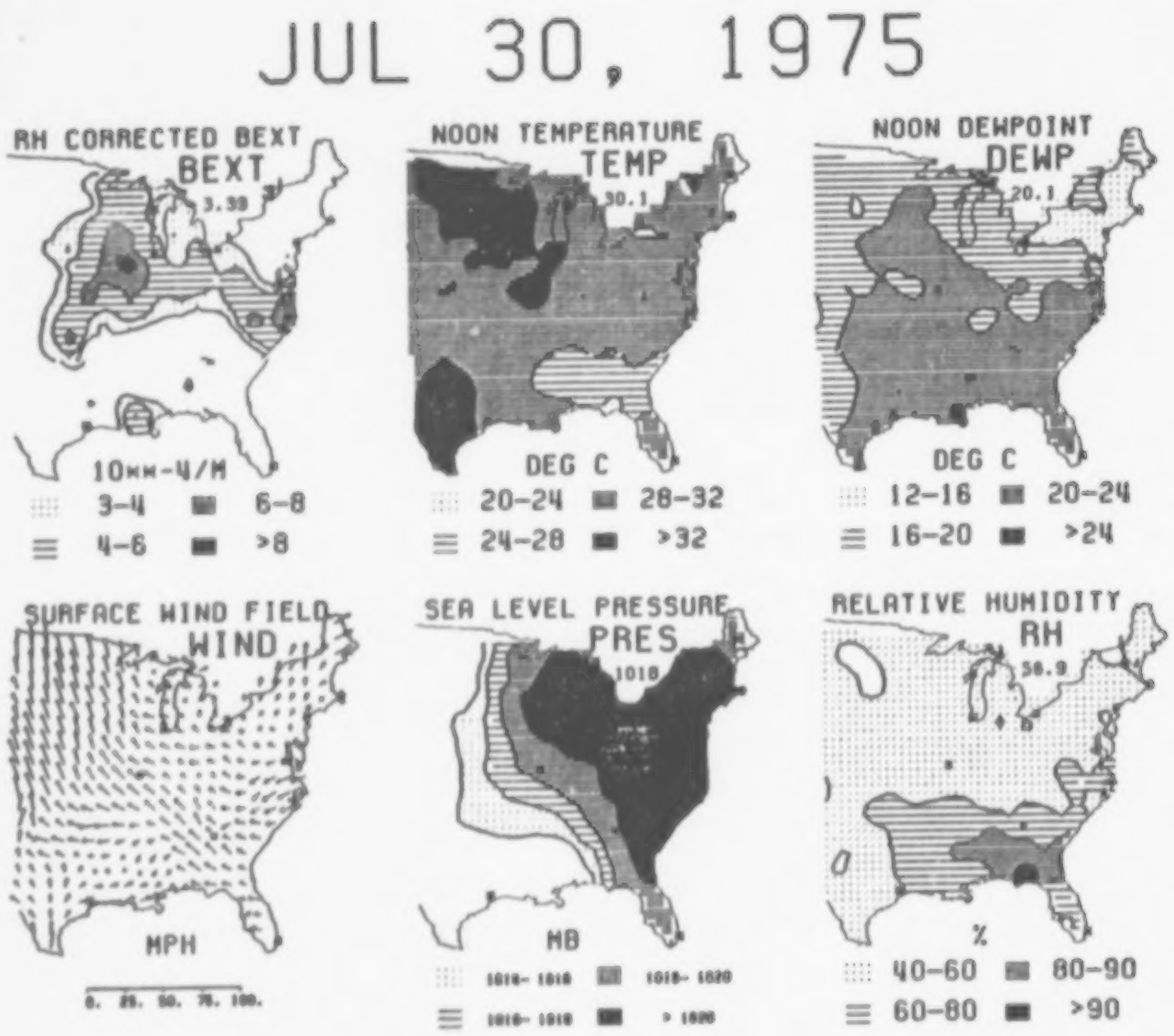

Figure 2-6. The MO-IL-IA region is the area of lowest visibility; the aircraft have moved to the north along with the hazy air mass. Temperatures have increased since the 29th along with dewpoint. The black area on the b_{ext} plot represents noon visibility less than 3 mi.

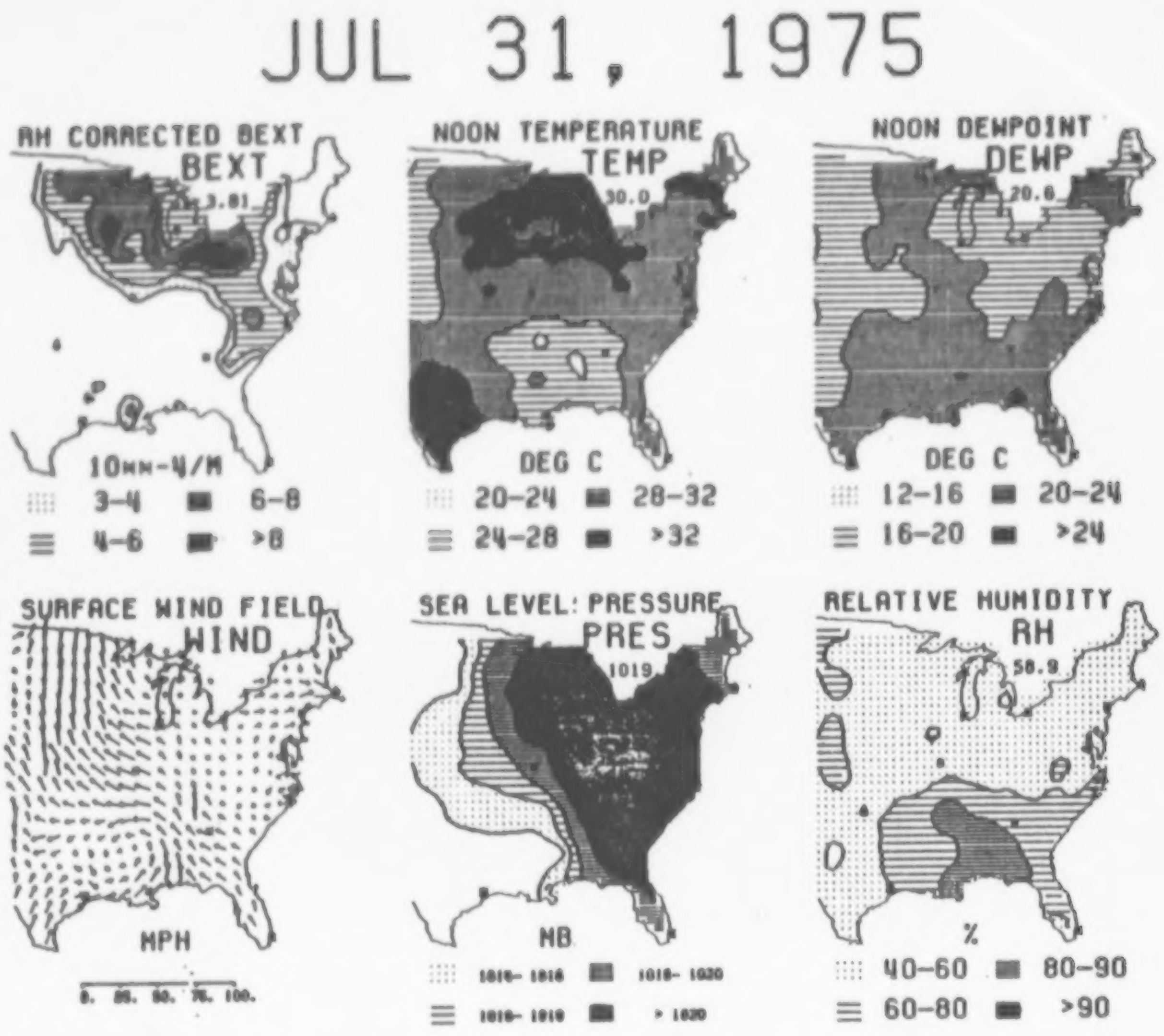

Figure 2-7. The hazy air is now moving out of the St. Louis area toward the Canadian border.

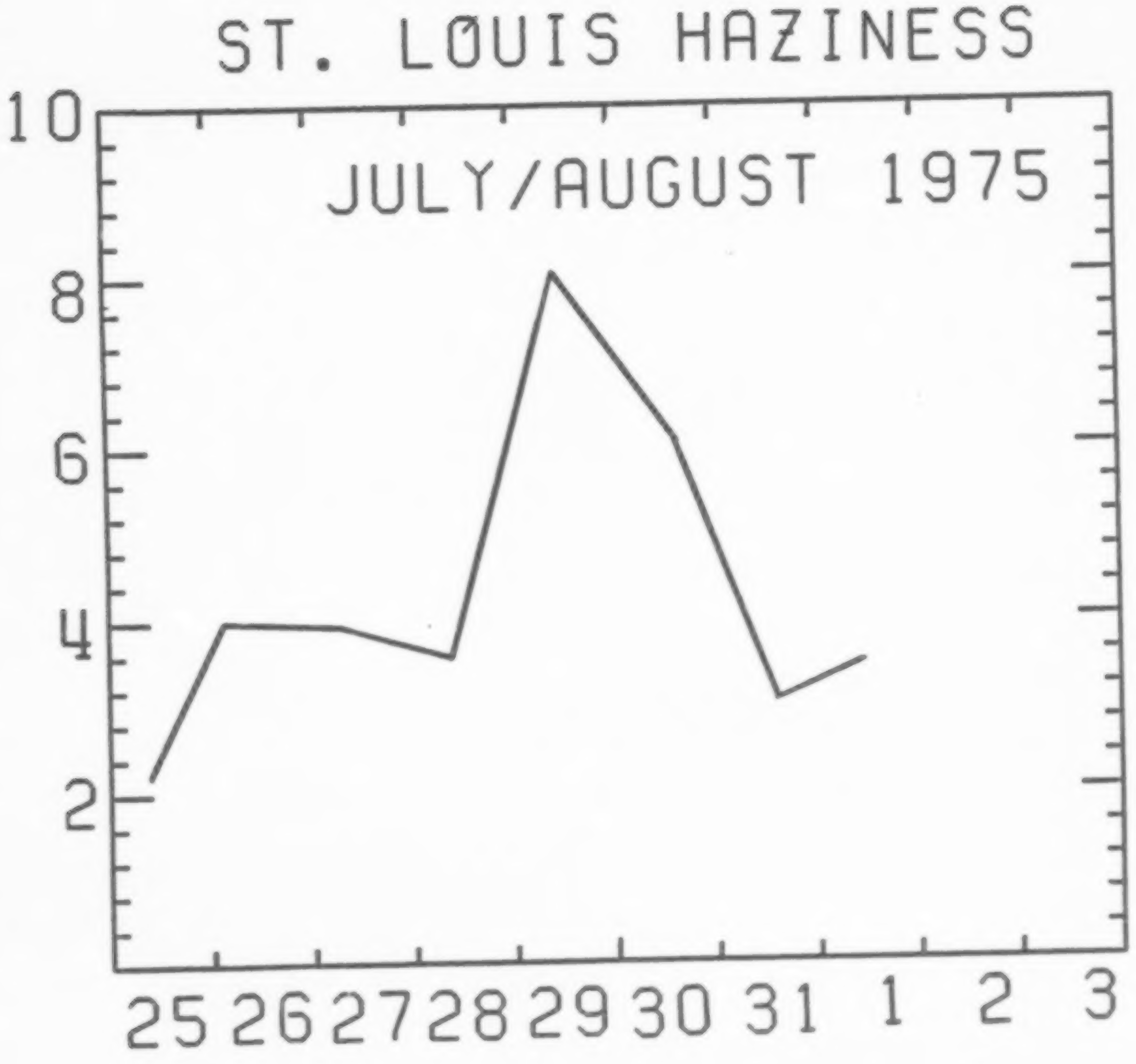

Figure 2-8. Noon extinction coefficient in St. Louis, MO, calculated from surface visibility. The haze episode peaked on July 29, dropping off sharply by the 31st.

TABLE 2-1. FLIGHT OUTLINE, JULY 29-30, 1975

Altitude (m MSL)	Route	Time (CDT)
451	Point A to Brighton (tuned to St. Louis VOR)	1335-1342
610	Brighton to Point A	1345-1351
762	Point A to Brighton	1354-1400
915	Brighton to Point A	1403-1409
1460-410	10 km NE of Point A (spiral)	1418-1427
	INOPERATIVE	
762	Point C to Point D	1502-1511
915	Point B to Point C	1525-1540
1460-290	Point E (spiral)	1546-1556
451	Hettick to Point F	1620-1628
457	Pearl to Point G (tuned to Maples VOR)	1643-1657
	INOPERATIVE	
	Refuel	
180-2590	Jacksonville (spiral)	1854-1920
1061	Pearl to Point G (tuned to Maples VOR)	1949-2009
1475-390	Point H (spiral)	2024-2043
915	Point I to Point J	2045-2053
915	Point K to Point L	2056-2119
756	Point L to Point K	2124-2146
610	Point K to Point L	2148-2210
1650-450	Point M (spiral)	2222-2231
	Refuel	
1900-400	Point N (spiral)	0014-0028
604	Monroe City to Havana (tuned to Maples VOR)	0042-0135
909	Havana to Monroe City (partial)	0140-0233
	INOPERATIVE	
	Refuel	
762	Peoria VOR to Macomb (tuned to Peoria VOR)	0519-0543

TABLE 2-1 (continued)

Altitude (m MSL)	Route	Time (CDT)
756	Macomb to Point O	0544-0612
756	Point O to Point P (partial) (tuned to Macon VOR)	0613-0640
1067	Point P to Point R	0648-0719
451	Navoo to Point S	0739-0832
1061	Point S to Kirksville	0837-0852
	Refuel	
1990-290	Cannon Memorial Apt. (spiral)	0901-0912
756	Kirksville VOR to Chillicothe	1034-1052
604	Chillicothe to Point T	1054-1125

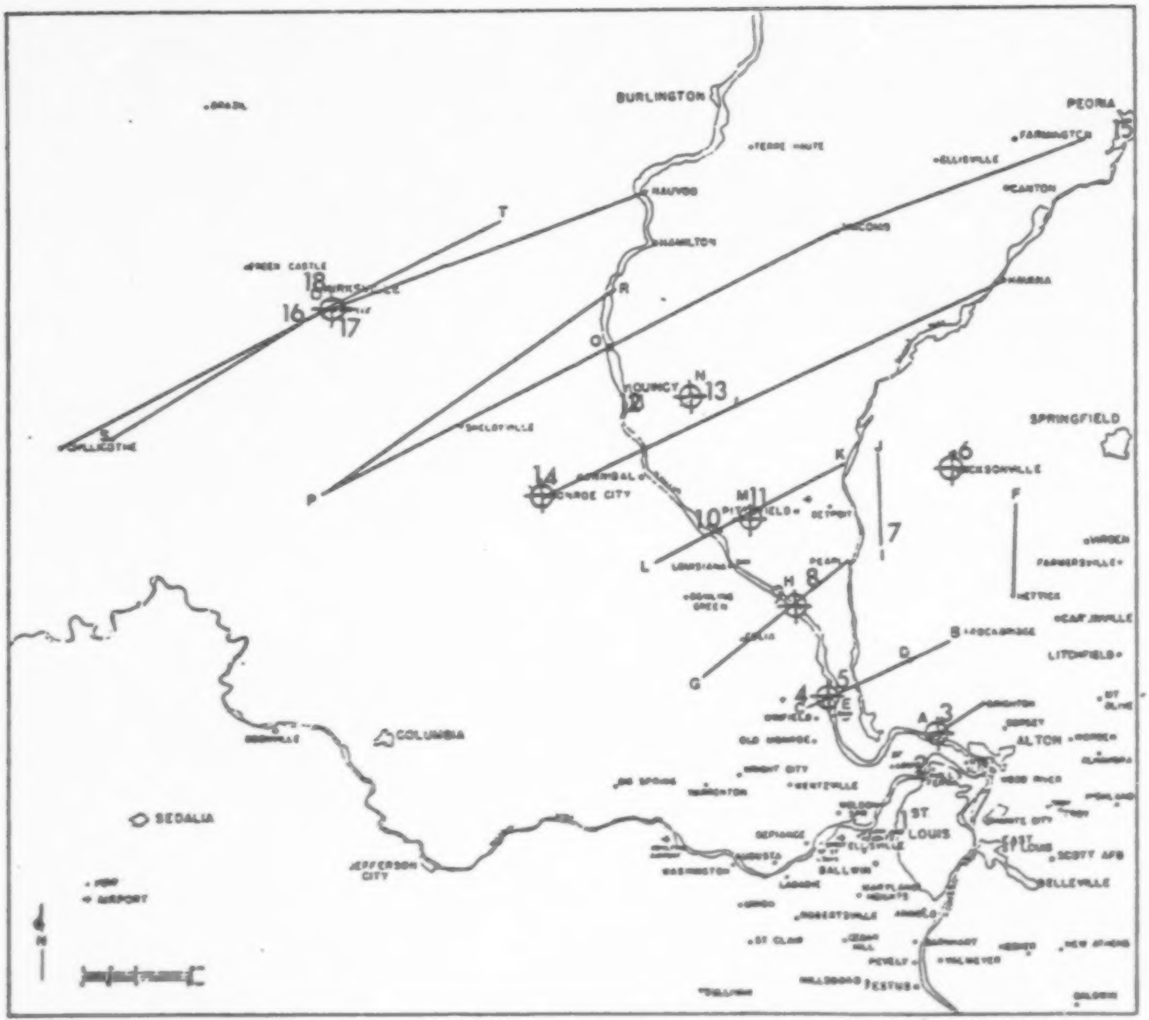

July 29-30, 1975
1330 - 1130 CDT

⊕ - Spiral

Figure 2-9. Map showing location of traverses and spirals for July 29-30, 1975. The numbers 1 through 18 indicate the positions of the spirals displayed in Figures 13-18.

OZONE

JULY 29-30, 1975

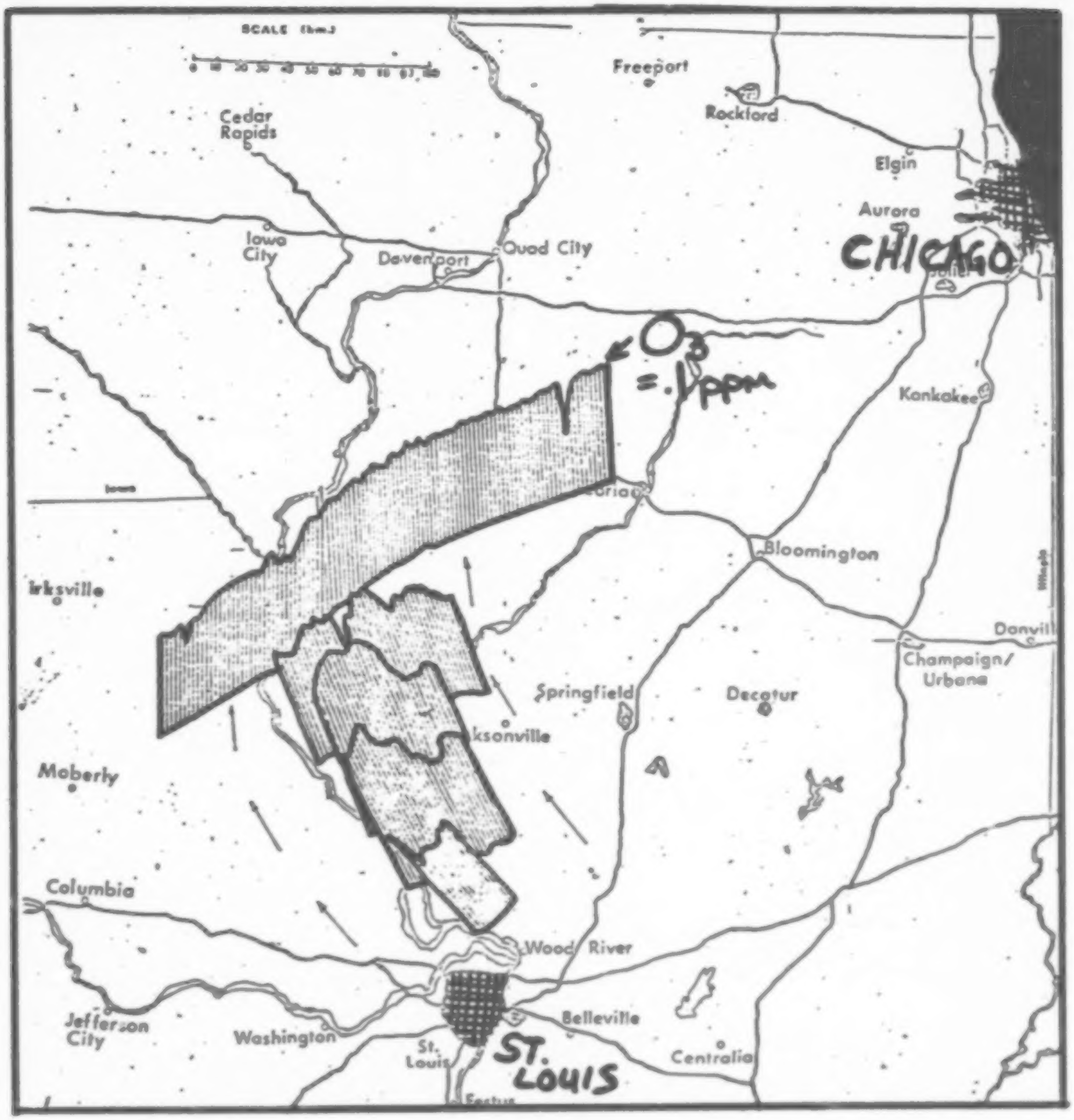

Figure 2-10. Crosswind profiles of ozone at 760 m MSL. Peak ozone concentration is approximately 140 ppb, with levels generally near 100 ppb ozone.

SO_2

JULY 29-30, 1975

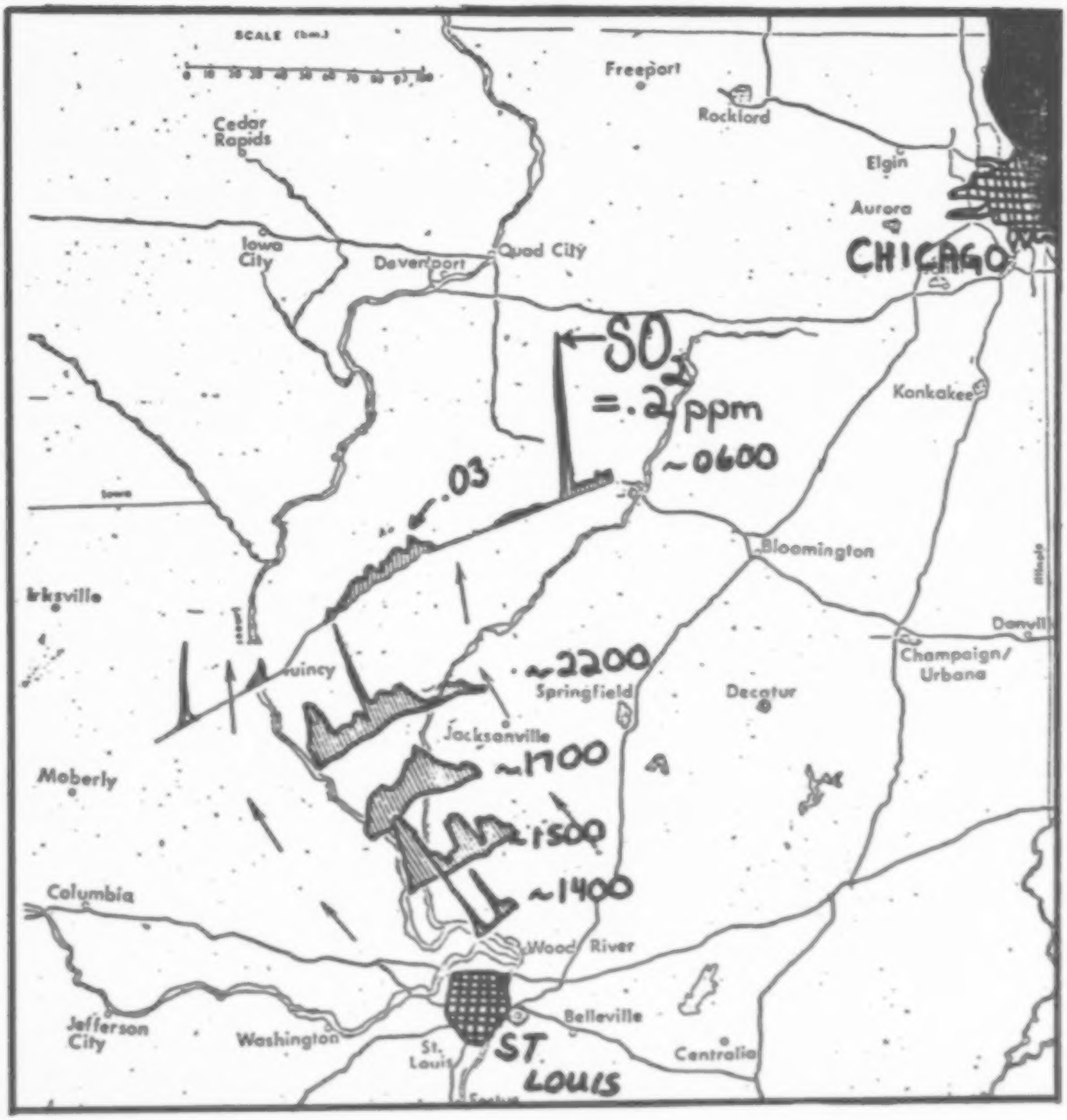

Figure 2-11. Crosswind profiles of SO_2 at 760 m MSL on July 29-30, 1975. At 1400 CDT (the closest traverse) the easternmost peak corresponds to the Wood River, IL, power plant/refinery complex; the western SO_2 peak is due to the Portage des Sioux power plant. Both sources may be detected at the next two downwind distances as well.

B_{SCAT}

JULY 29-30, 1975

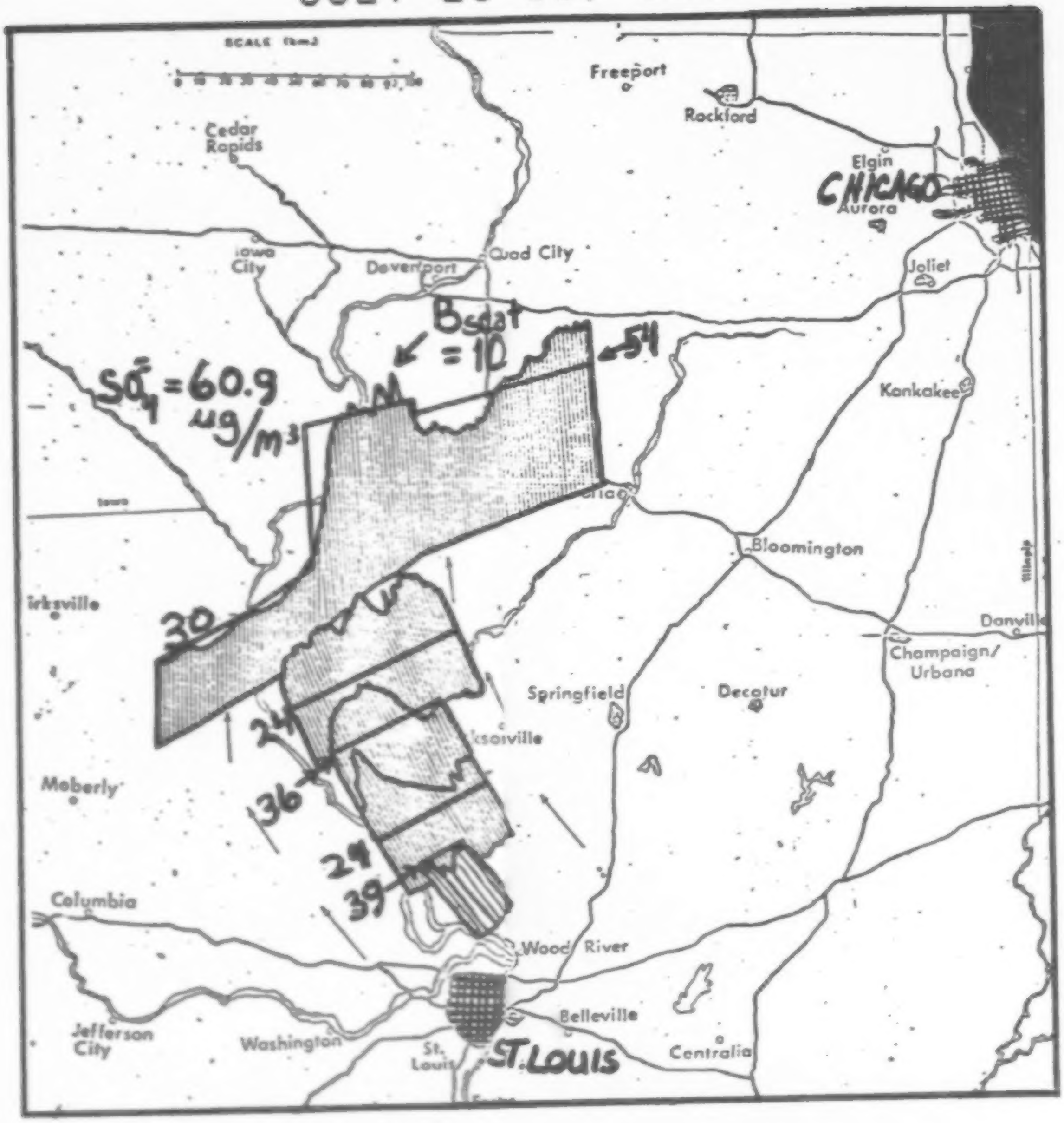

Figure 2-12. Average sulfate concentration at 760 m MSL ranged from 24 to 61 µg/m³. The highest SO_4 was associated with extreme haze of b_{scat} $10 \cdot 10^{-4} m^{-1}$. Light scatteing coefficient ranged from 5 to $10 \cdot 10^{-4} m^{-1}$, showing evidence of the contribution of many area and point sources.

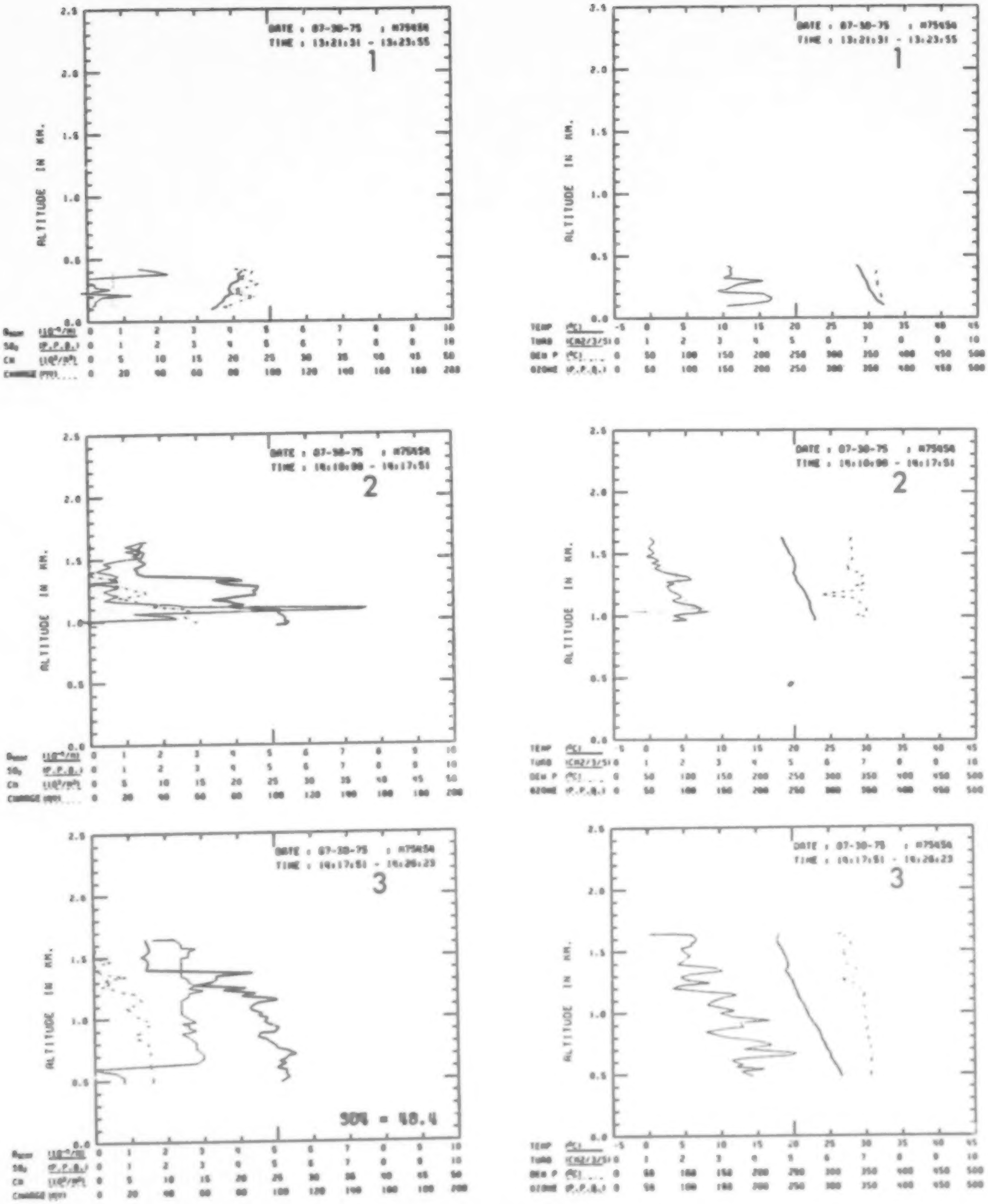

Figure 2-13. The left column contains b_{scat} (heavy line) and SO_2 (thin line) measured simultaneously are in the righthand plots. Spiral #3 is reasonably complete; below 1,400 m, b_{scat} ranges between $4-5 \cdot 10^{-4} m^{-1}$. Average sulfate is 48 $\mu g/m^3$ with 3 ppb SO_2. Spiral #2 shows the influence of a fresh power plant plume at 1,050 m.

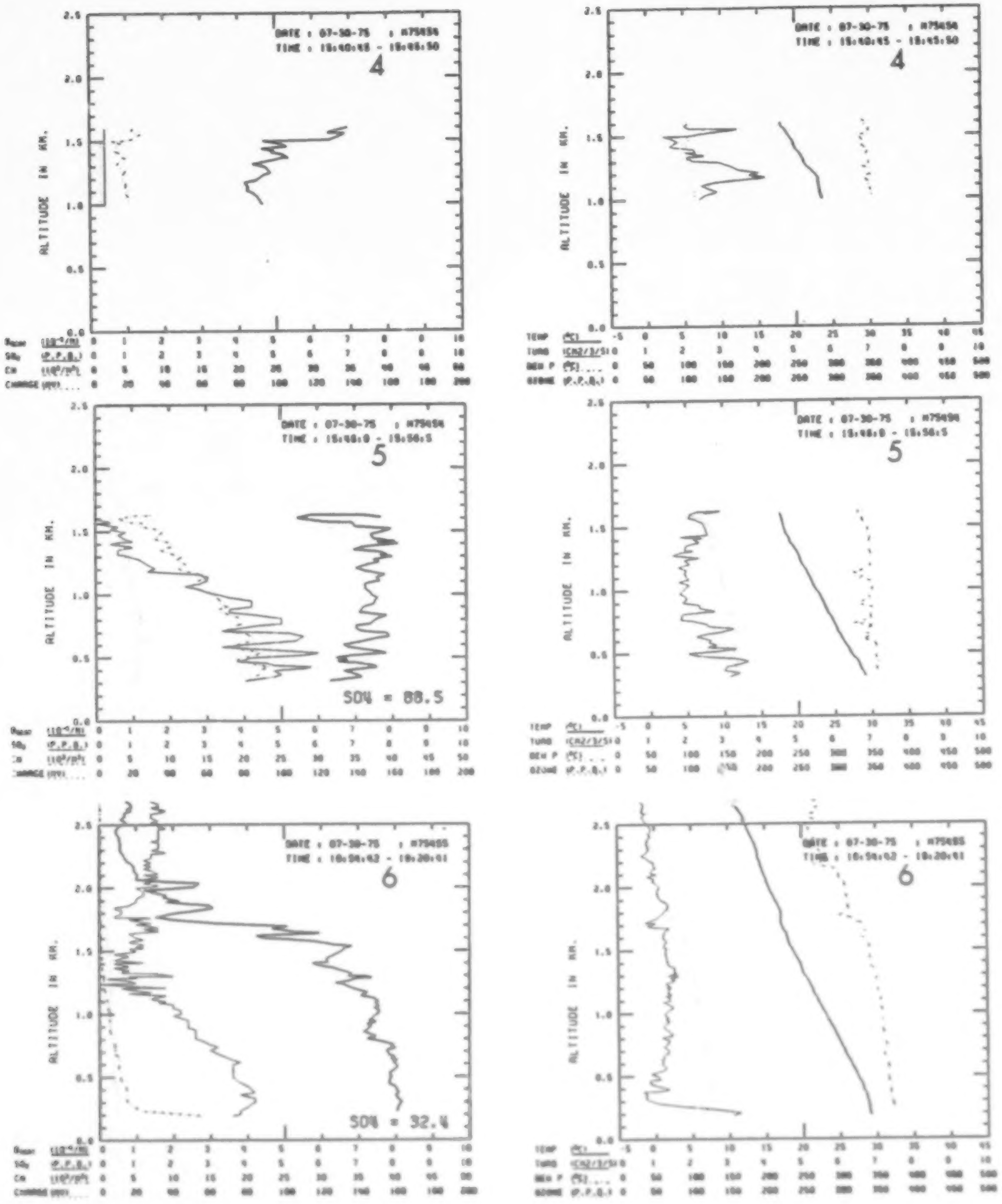

Figure 2-14. Spirals #4 and #5 show elevated haze layers at about 1,600 m in the early afternoon of July 29. Spiral #5 shows b_{scat} 6.5-7.5 with ozone at 150 ppb; spiral #4 is 5 km west with sharply lower b_{scat} of 4.5-5 and ozone 120 ppb. At Jacksonville, IL (spiral #6), at about 1900 CDT, b_{scat} was $8 \cdot 10^{-4} m^{-1}$ near the surface with evidence of several layers of haze above 800 m.

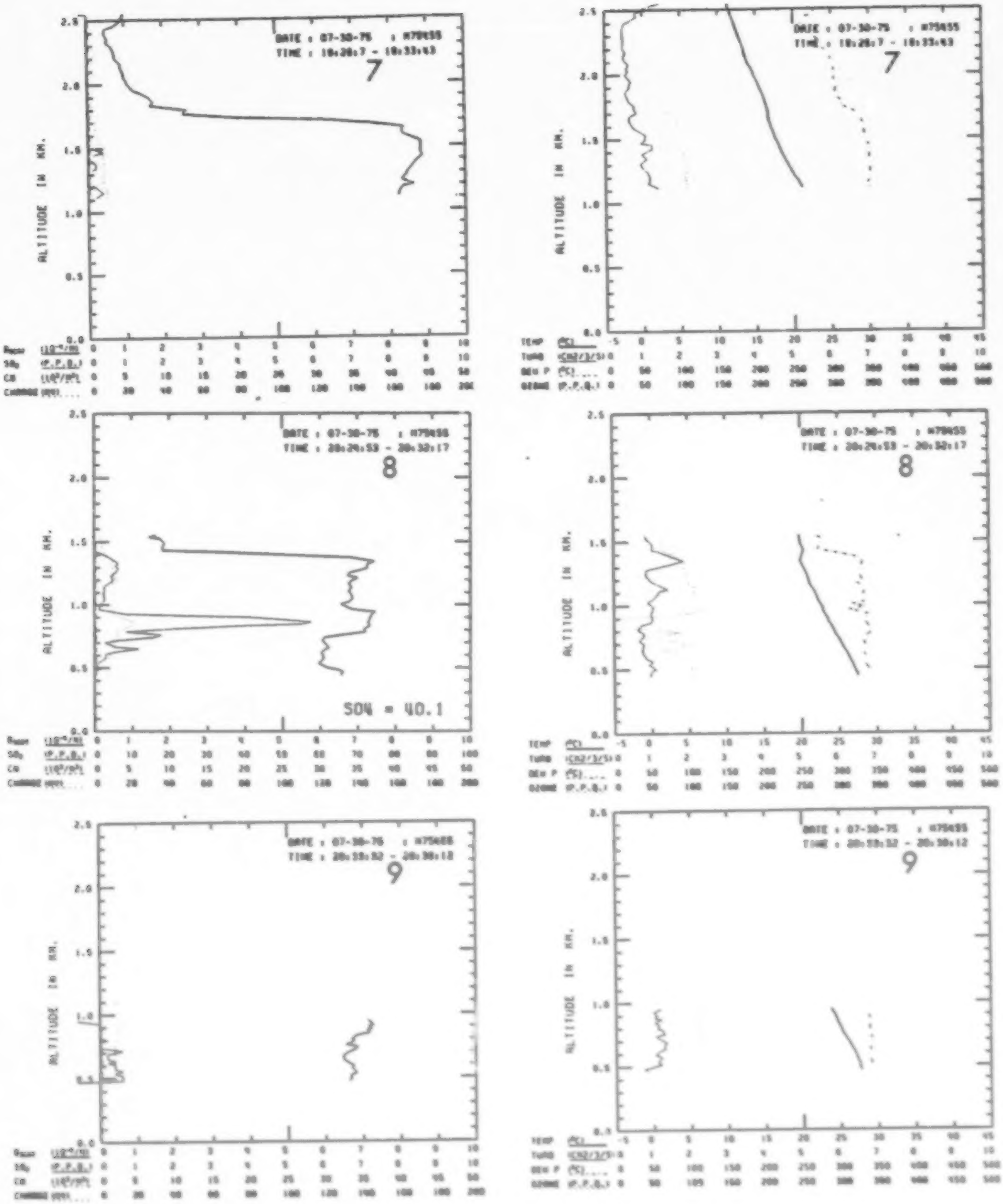

Figure 2-15. Spiral #7 indicates a "lid" at 1,700 m, capping the mixed layer with b_{scat} of 8.5. Here SO_2 is less than 1 ppb, with ozone 100 ppb. One hour later, at 2030 CDT, a fresh power plant plume was encountered at 850 m with peak SO_2 of 60 ppb; b_{scat} shows a marked vertical inhomogeneity.

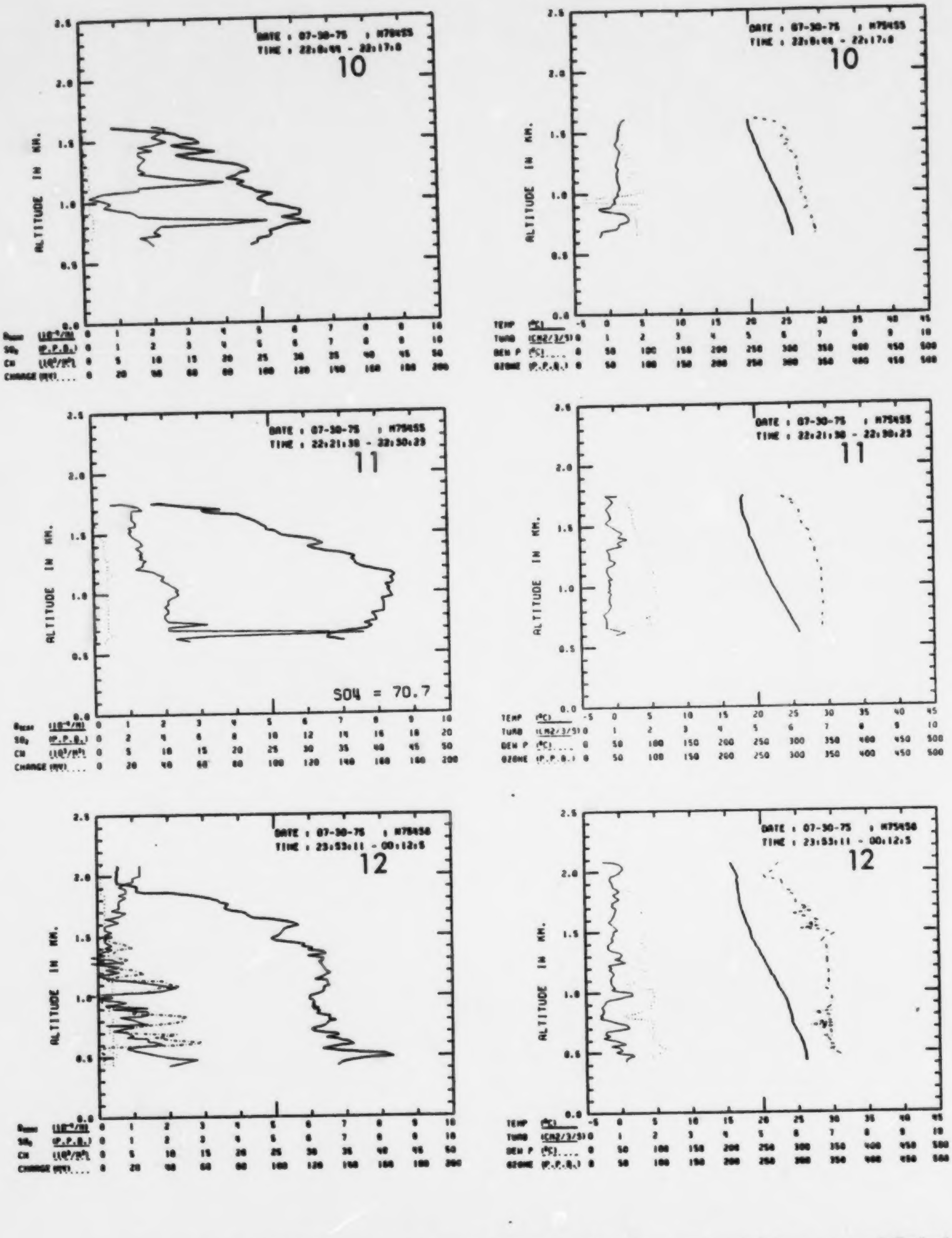

Figure 2-16. Spiral #11 was obtained immediately after and ~10 km east of Spiral #10. Both the vertical structure and the levels of b_{scat} are substantially different. At Quincy, IL (spiral #12), b_{scat} is 6.

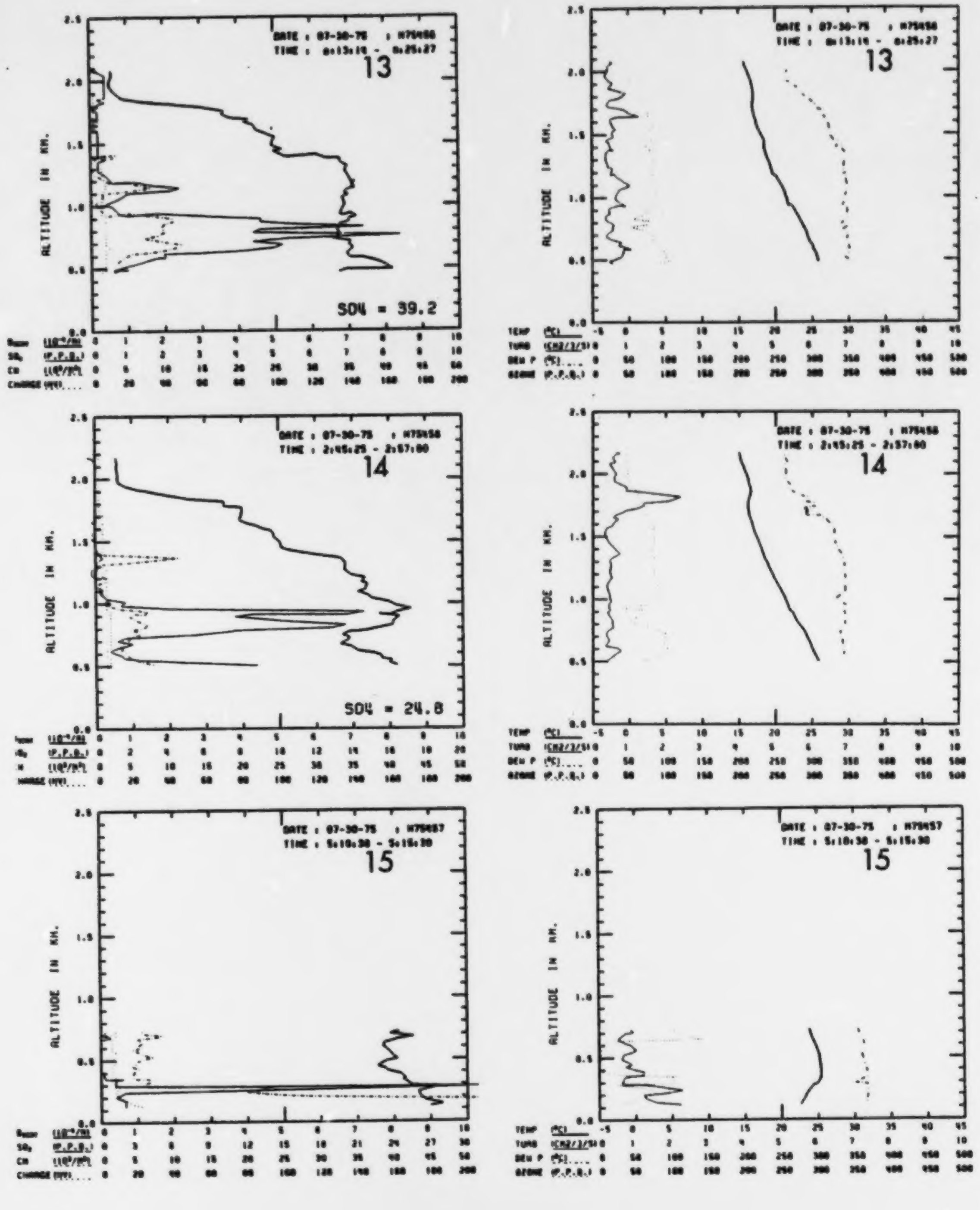

Figure 2-17. Spiral #13 indicates that the layer from the surface to 1,400 m is a well-mixed layer with b_{scat} of 7. At 3 a.m. on July 24 (spiral #14), b_{scat} is not well mixed, ranging between 7 and 8.5 in the lowest 1,400 m. B_{scat} at Peoria, IL, at 5 a.m. was 8.5-9 below the nocturnal inversion.

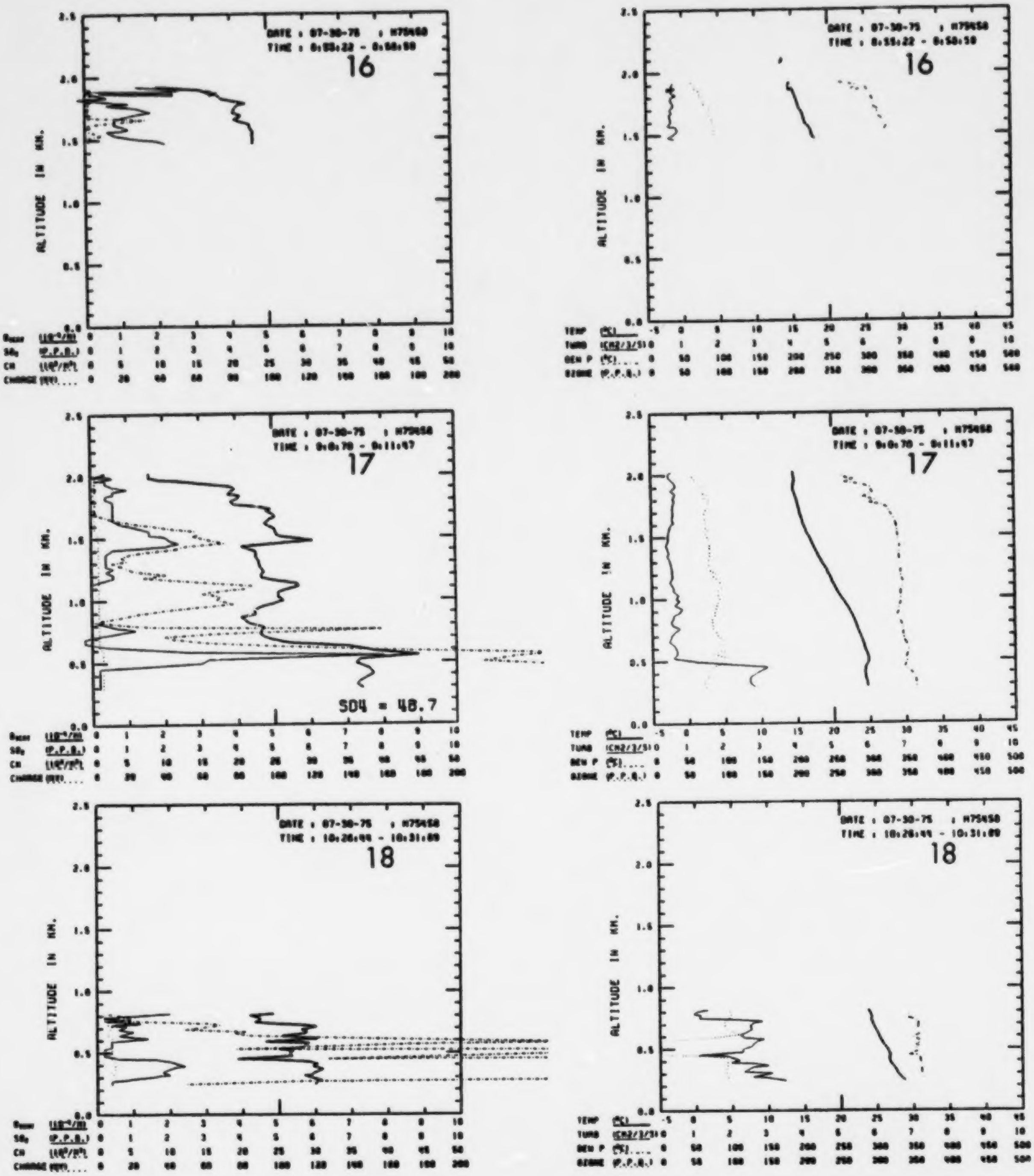

Figure 2-18. Spiral #17 indicates b_{scat} of 7-7.5 within the 500-m mixed layer at 9 a.m. on July 30, with elevated haze layer of $4-5 \cdot 10^{-4} m^{-1}$. Average sulfate concentration from surface to 2,000 m was 48 $\mu g/m^3$. By 10:30 a.m., b_{scat} is more nearly mixed in the lowest 800 m.

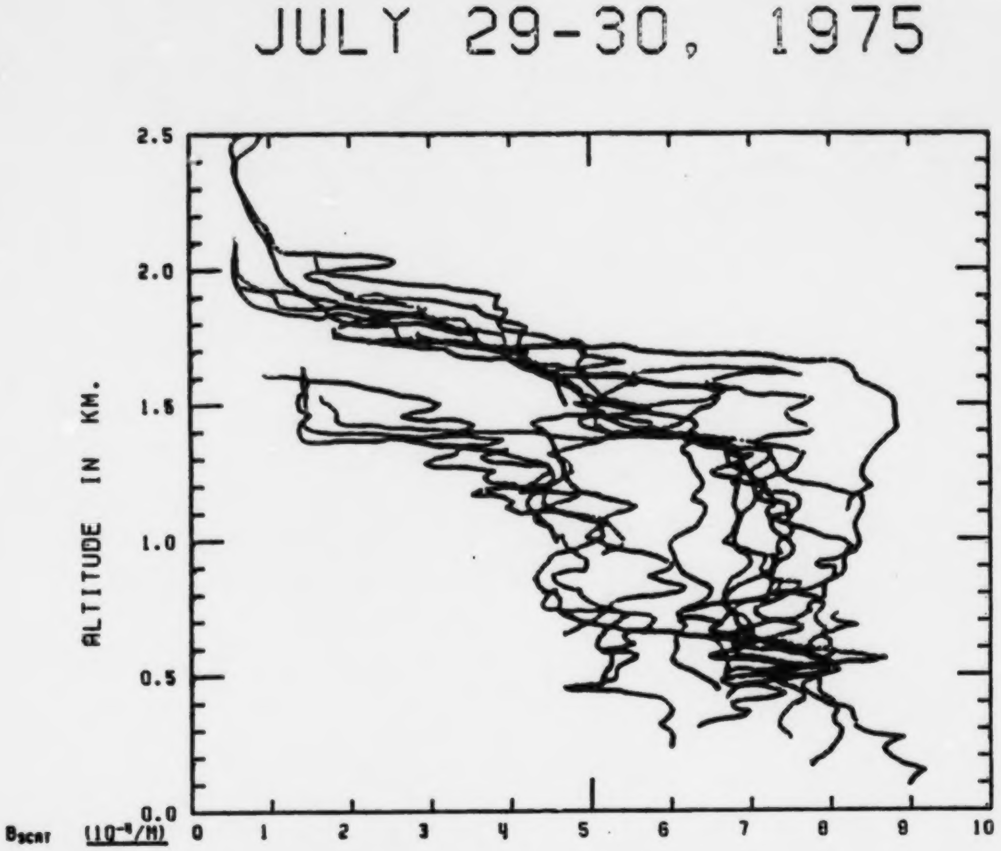

Figure 2-19. Overlaid soundings from July 29-30, 1975. This period was very hazy, with b_{scat} ranging from about 4 to 8 in the lowest 1,300 m over a 24-hr period. Sulfate concentrations varied from 25 to above 80 $\mu g/m^3$.

3.0 AUGUST 10, 1975

3.1 Flight Description

A large flat-surface high-pressure area dominated the entire eastern portion of the country from the Mississippi Valley to the coast. A strong zonal flow pattern did exist aloft over southern Canada but it only extended as far south as the northern plains. The southern two-thirds of the country was influenced by a very featureless upper and midlevel pattern. Stagnant air conditions were common from St. Louis to New York. A well-defined surface low moved across southern Canada, just south of James Bay bringing a cold front behind it. However, the front never moved farther south than central Nebraska and Iowa before it became stationary. The more northerly portion of the front did follow the Canadian border eastward enough to clear Minnesota and Wisconsin. A large outbreak of air-mass thunderstorms occurred in Ohio and eastern Indiana while a line of showers and weak thunderstorms moved out of Iowa and southeastern Minnesota into Wisconsin and northern Illinois.

Sky conditions were generally clear from Kansas to Indiana through most of the day. Visibility was only 3 to 7 km over eastern Missouri, Illinois, and western Indiana during the morning with improving visibility in the afternoon. The area of lowest visibility moved into Ohio, southern Michigan, and northeastern Indiana by 1300 CDT. Visibility improved significantly about 150 mi east of the cold front throughout the day.

Wind flow patterns were south-southeasterly during the early morning, becoming southerly--then south-southwesterly by late morning, through the afternoon. This pattern had a tendency to move the area of lowest visibility toward the northeast.

The main leg of the flight consisted of a pass at 750-m altitude from Chillicothe in Northeast Missouri to Indianapolis, with few spirals taken. The main path began at 1000 CDT and ended about 1400 CDT; the overall mission covered 0500-1800 CDT on this date.

3.2 Summary

The main traverse of August 10, 1975, was at a constant 750-m altitude. The aircraft found a wide haze plume in central Illinois and a sharp gradient of b_{scat} near the Illinois-Indiana border. Both aerosol charge and condensation nuclei count also increased sharply from eastern Illinois into Indiana. The flight plan provided a good "snapshot" of the atmosphere across the central midwest, but provided relatively little vertical information. It appears that on this day there were several hazy layers aloft, even at midday, and thus the evolution of a hazy air mass may well involve variations in day-to-day mixing height.

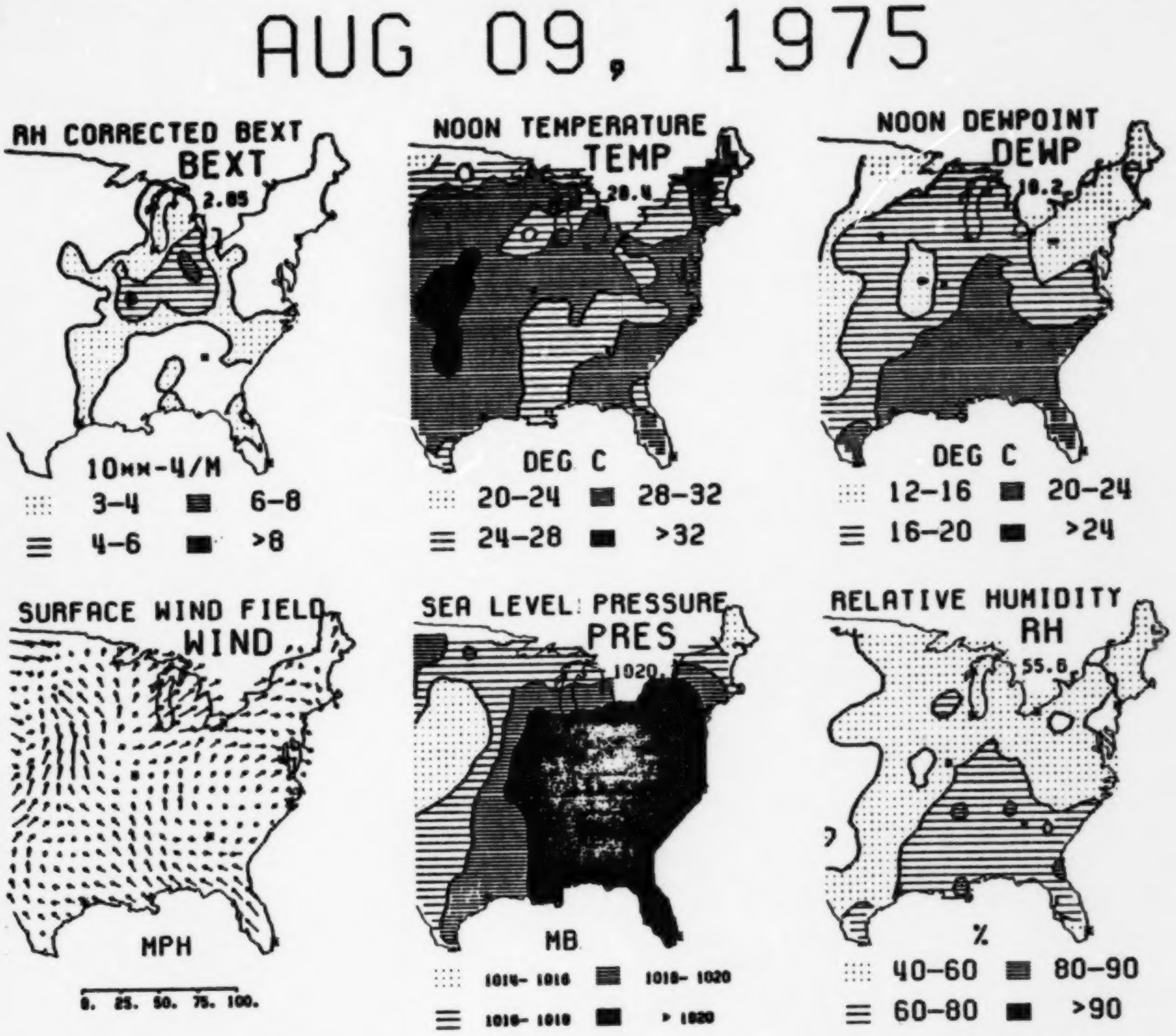

Figure 3-1. A high-pressure system was present over the entire eastern United States. Noon surface temperatures were in the range of 28°-32° C. The center of the hazy air mass was in south-central Illinois.

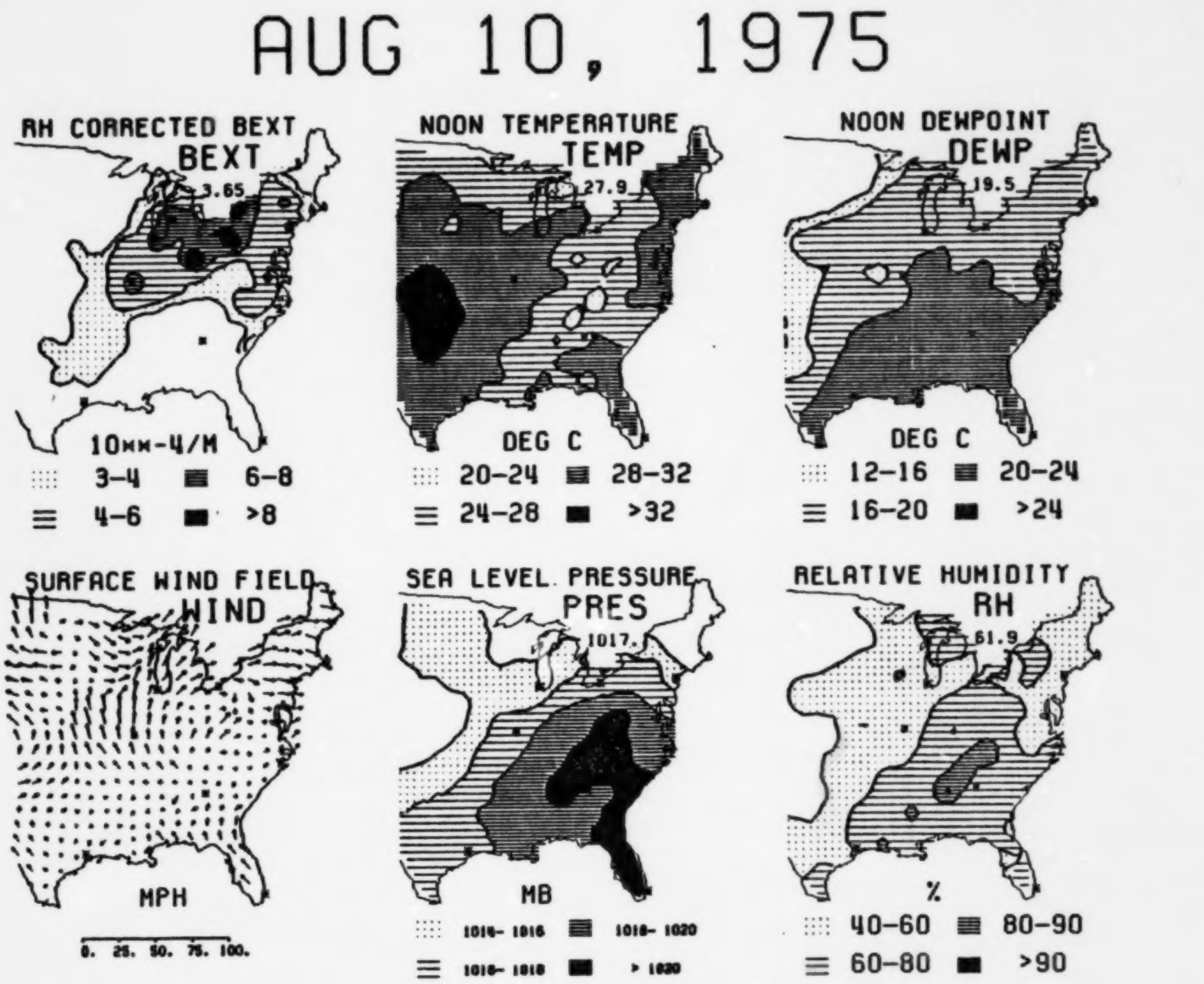

Figure 3-2. The haziest portion has moved into the Indiana-Ohio region, with expansion of the region of reduced visibility into all of Missouri. Winds from St. Louis to Indianapolis are out of the South. The high-pressure system still prevails over the eastern United States.

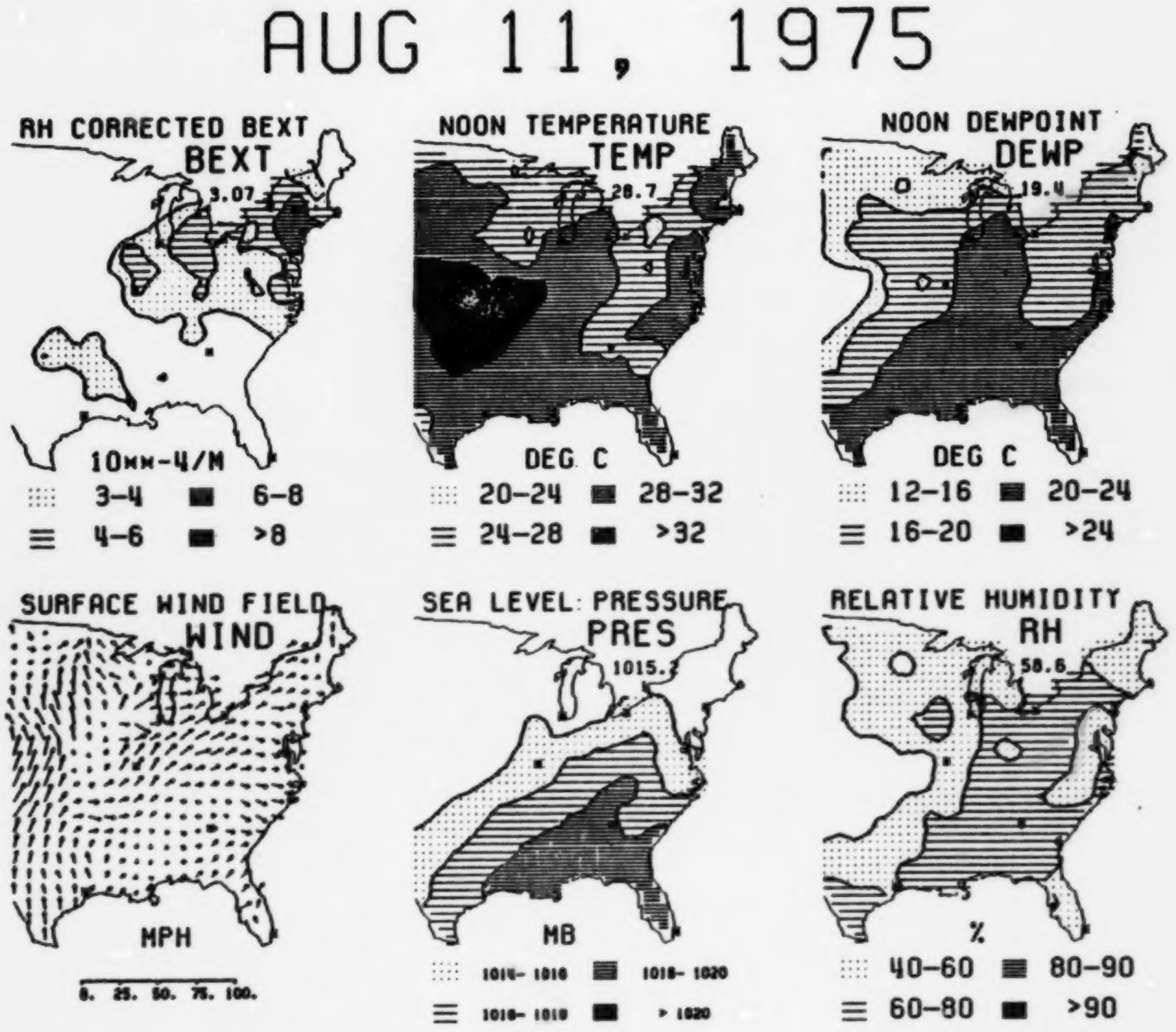

Figure 3-3. The pressure and wind fields have become disorganized; St. Louis is still in a hazy region.

TABLE 3-1. FLIGHT OUTLINE, AUGUST 10, 1975

Altitude (m MSL)	Route	Time (CDT)
590-2570	Wentzville (Spiral)	0512-0534
762	Wentzville to Boonville (Tuned to Maryland Heights VOR)	0542-0637
770-2570	Boonville (Spiral)	0639-0653
762	Boonville to Blue Springs (Tuned to Blue Springs VOR)	0659-0745
756	Cameron to Chillicothe	0812-0832
	Refuel	
310-1960	Chillicothe (Spiral)	1012-1030
762	Chillicothe to Hannibal (Tuned to Quincy VOR)	
730-1960	Hannibal (Spiral)	1125-1138
756	Hull (Hannibal) to Tuscola (Tuned to Capital VOR, changed to Decatur VOR at 1247:00)	1142-1259
820-2110	Tuscola (Spiral)	1259-1310
762	Camargo (Tuscola) to Indianapolis	1317-1353
	Refuel	
756	Green Castle to Brazil (Tuned to Lafayette VOR)	1530-1541
756	Terre Haute to Casey (Tuned to Terre Haute VOR at 1601:36)	1550-1609
756	Springfield to Hillsboro (Tuned to Capitol VOR)	1707-1729
756	Litchfield (Hillsboro) to Brighton (Tuned to St. Louis VOR)	1733-1750

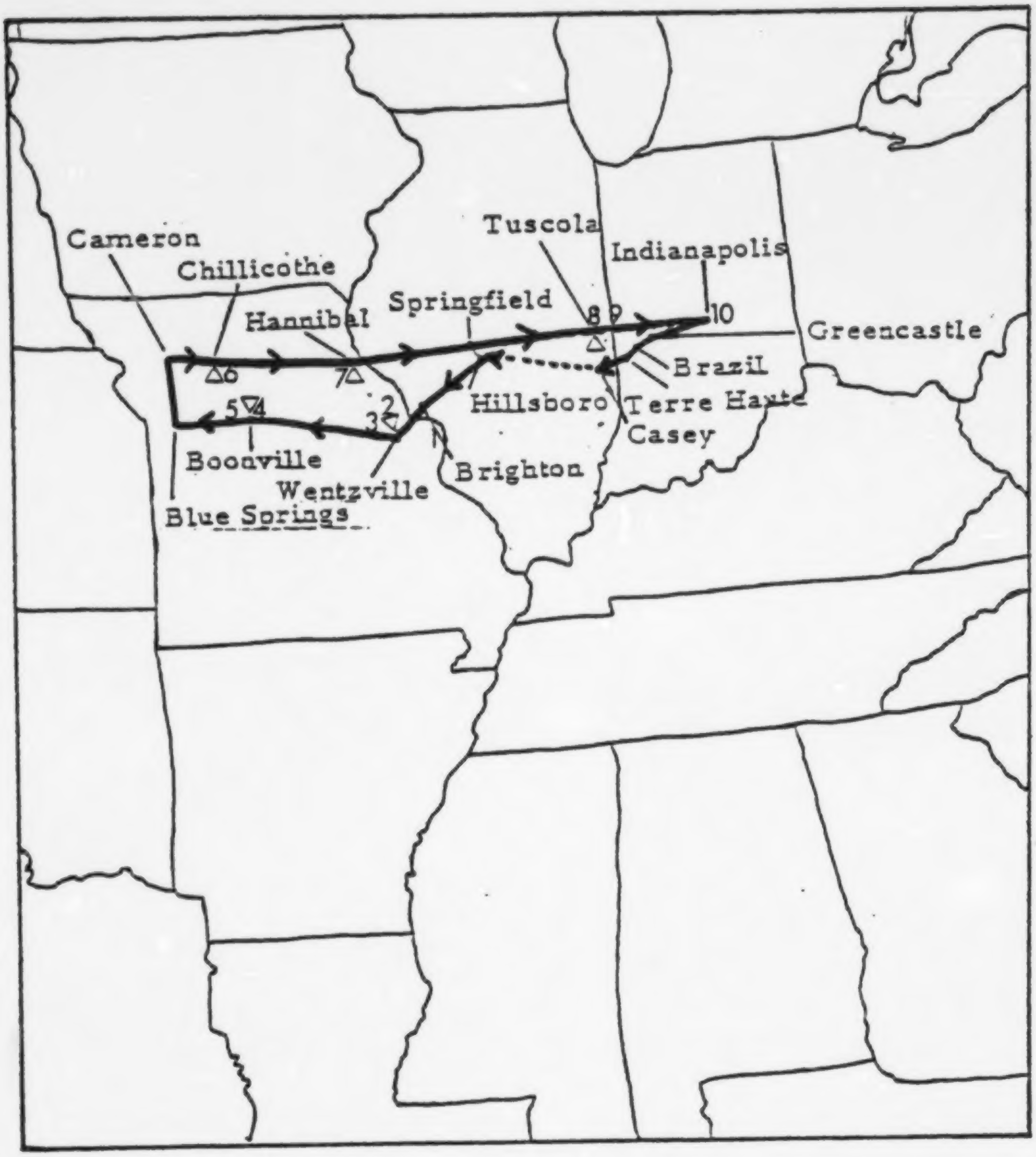

August 10, 1975

0500-1800 CDT

Δ - Spiral

Figure 3-4. Map showing the flight path and location of spirals for August 10, 1975. The numbers 1 through 10 indicate the positions of the spirals displayed in Figures 3-10 and 3-11.

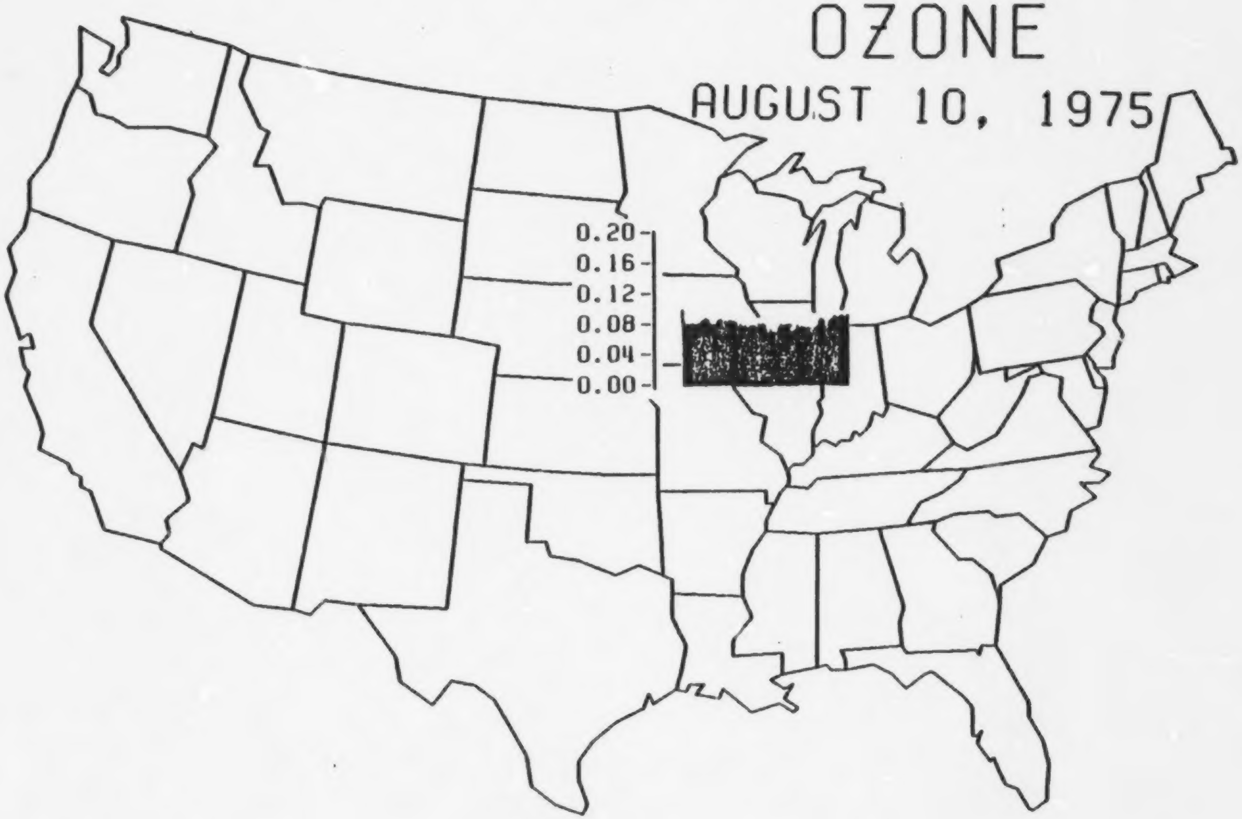

Figure 3-5. Ozone was slightly higher in western Missouri than in the Mississippi Valley, with a small gradient from Illinois into Indiana.

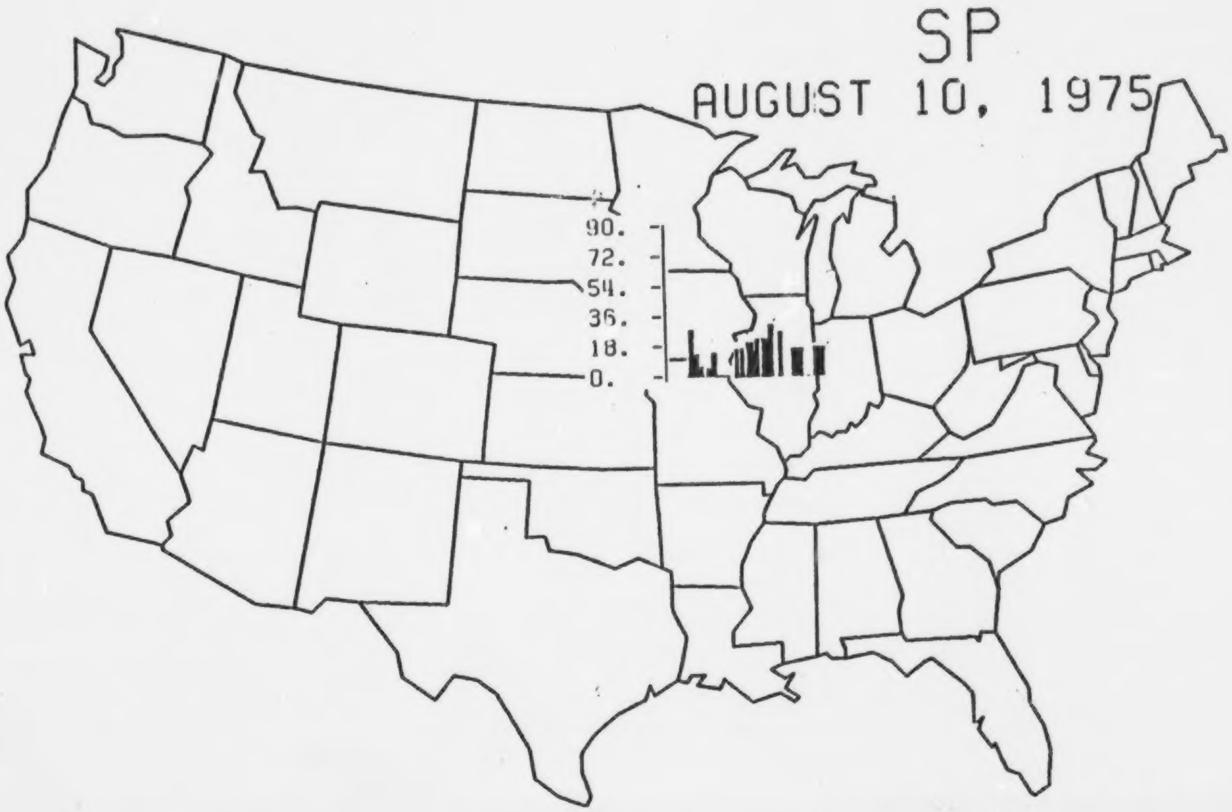

Figure 3-6. Particulate sulfur was highest in western Missouri and western Illinois.

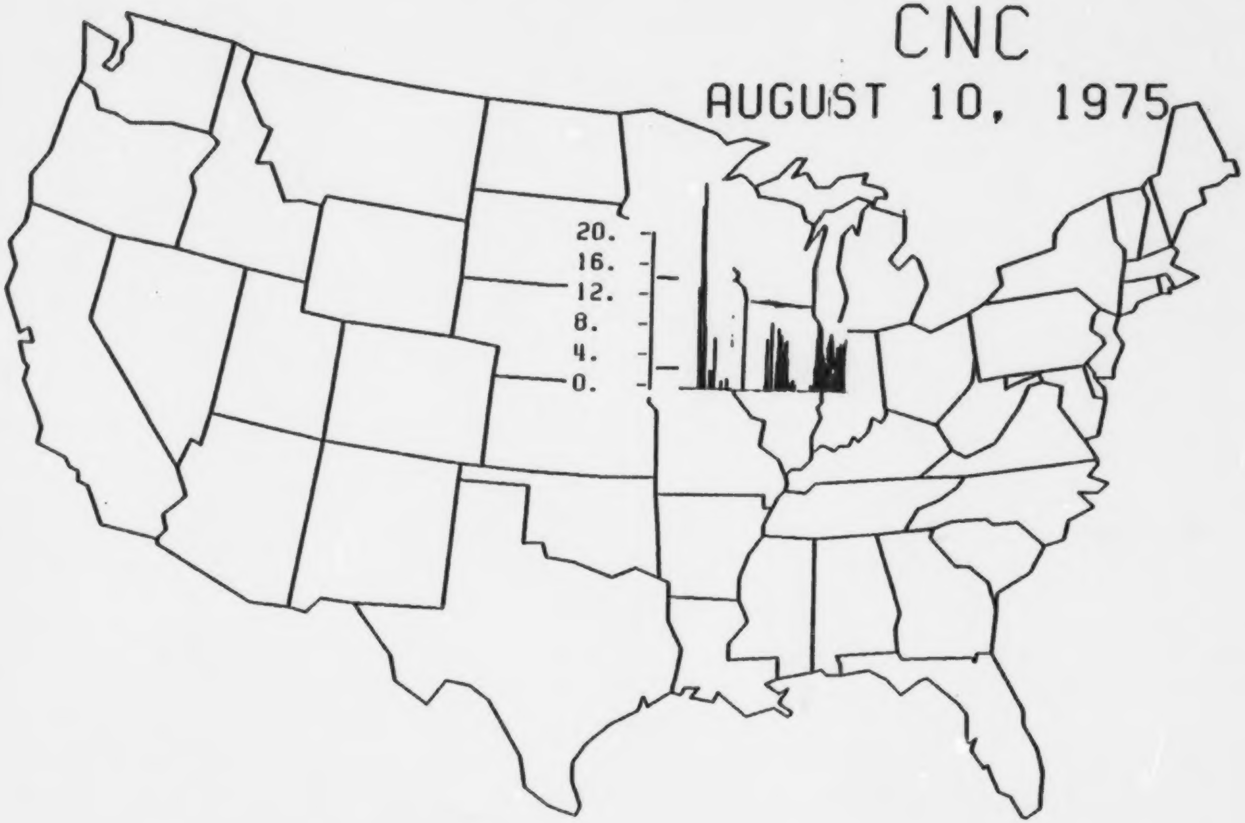

Figure 3-7. Condensation nuclei were present in high concentration in western Missouri and central Illinois, wth a strong consistent peak east of the Illinois-Indiana border.

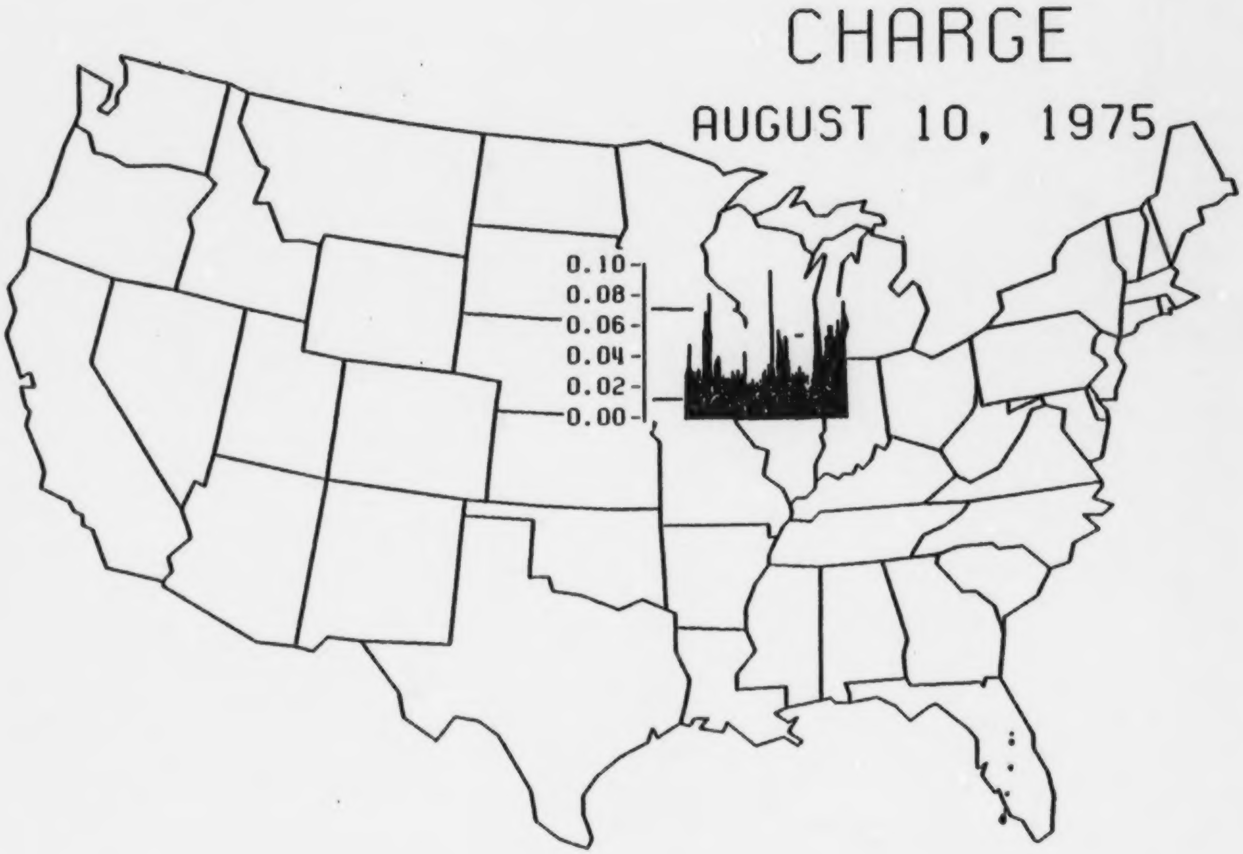

Figure 3-8. Aerosol charge shows the influence of several point and area sources in Missouri and Illinois, with a strong and consistent increasing gradient from the Illinois-Indiana border heading toward Ohio.

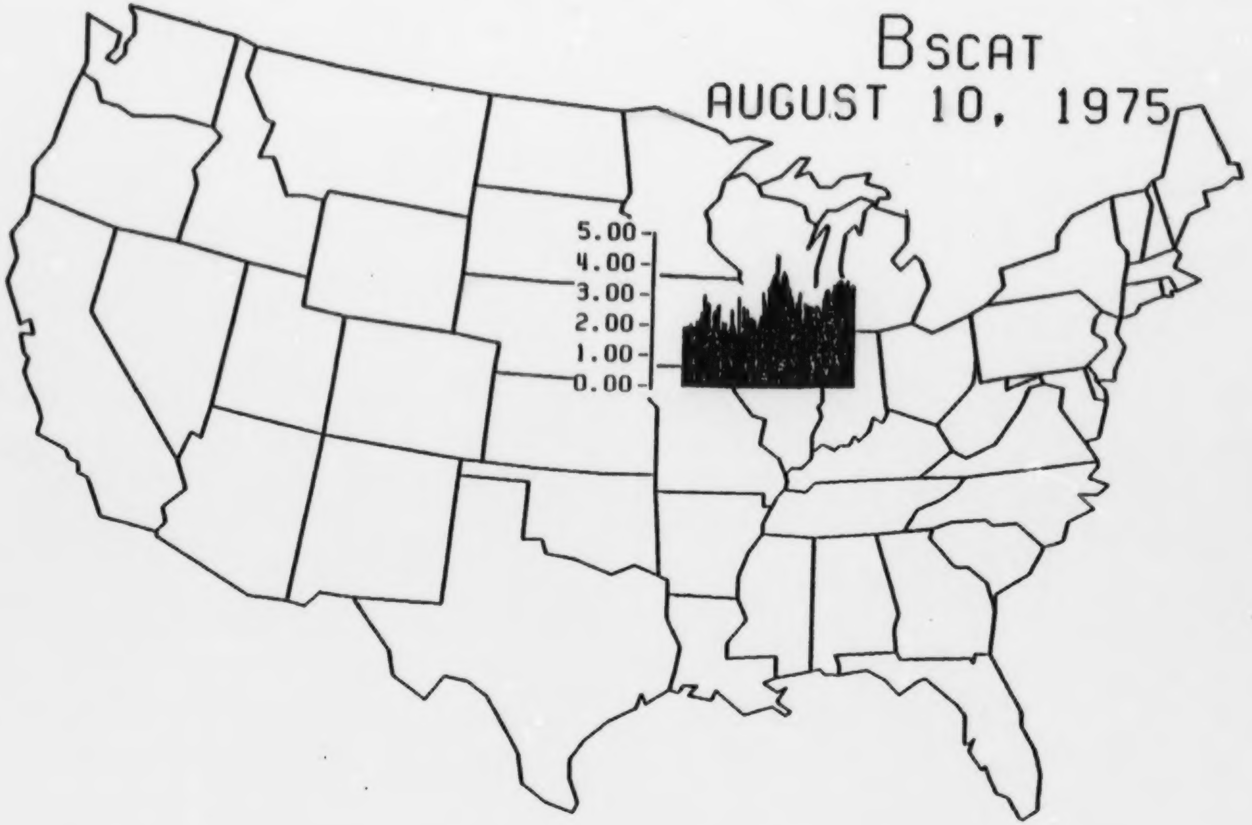

Figure 3-9. Light scattering (haziness) behaved much like CNC and charge, peaking in central Illinois with a strong gradient east of the Illinois-Indiana border.

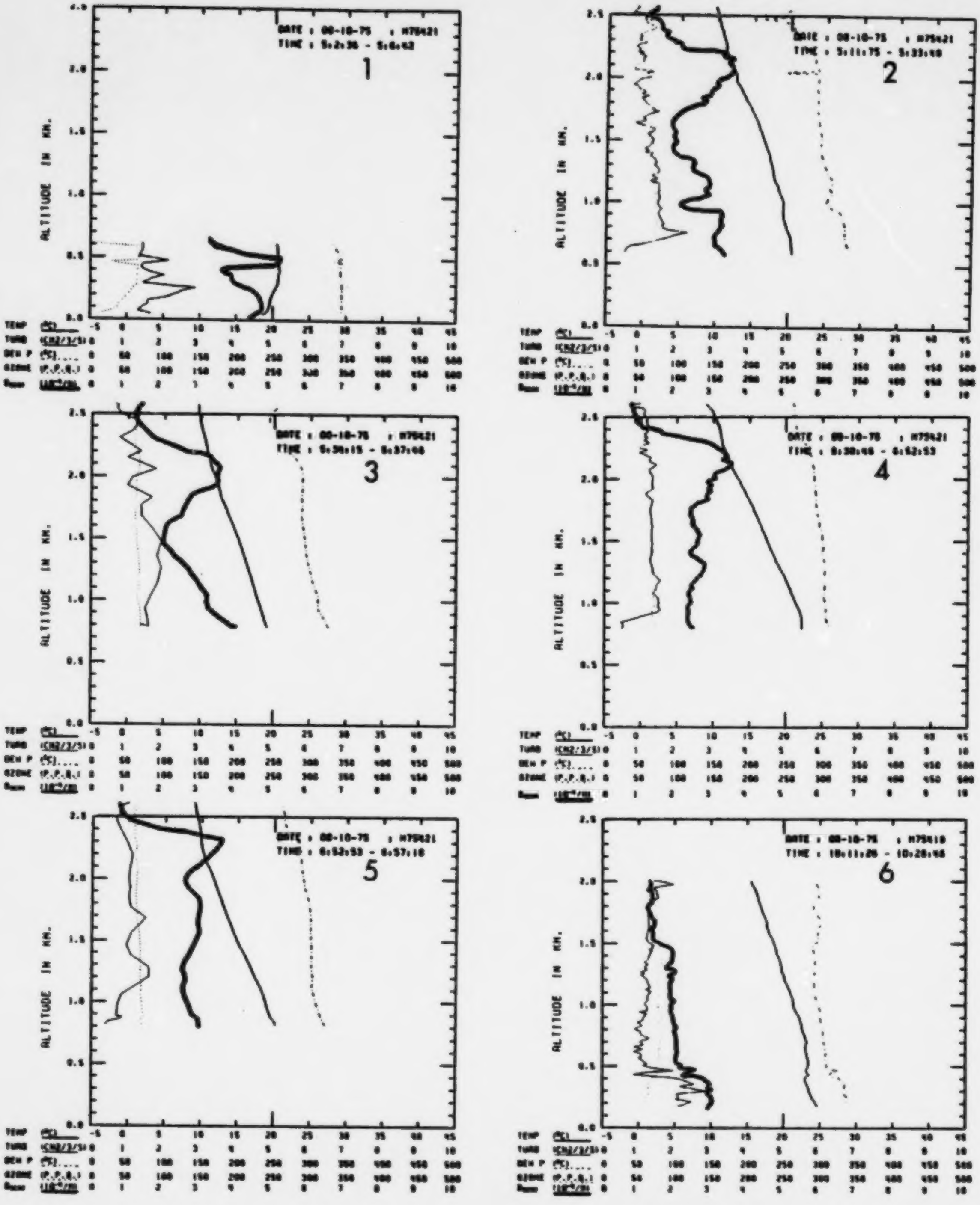

Figure 3-10. The bold solid line is b_{scat}. At 5 a.m. there are several haze layers, with b_{scat} 4-5. Spiral #2 indicates peak b_{scat} from 1,700-2,200 m. Spirals #4 and #5 found b_{scat} of 2-2.5 from 600-1,700 m with hazier layer above. At 10 a.m. (#6) there are distinct well-mixed regimes with b_{scat} of 3 (to 400 m), 2 (500-1,400 m), and 1.2 (1,500-2,000 m).

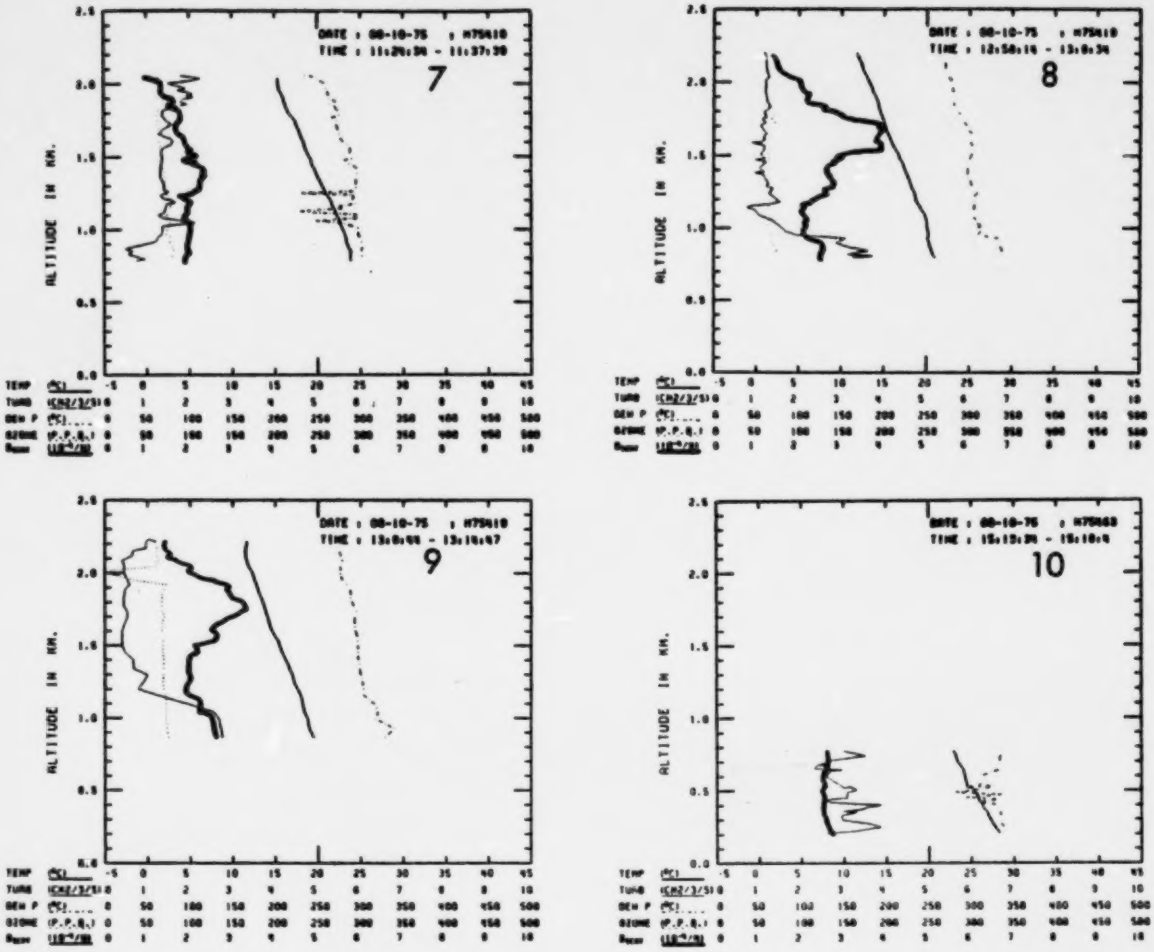

Figure 3-11. Hannibal, Missouri, at 11:30 (spiral #7) exhibits b_{scat} ~ 2 from 700-1,500 m. By 1300 (spirals #8 and #9, at Tuscola), there is an elevated layer with b_{scat} of 3.5 superimposed on the characteristic readings of b_{scat} ~ 2. At Indianapolis the 1300 sounding shows a uniform light scattering coefficient of about 2.5 in the lowest 700 m.

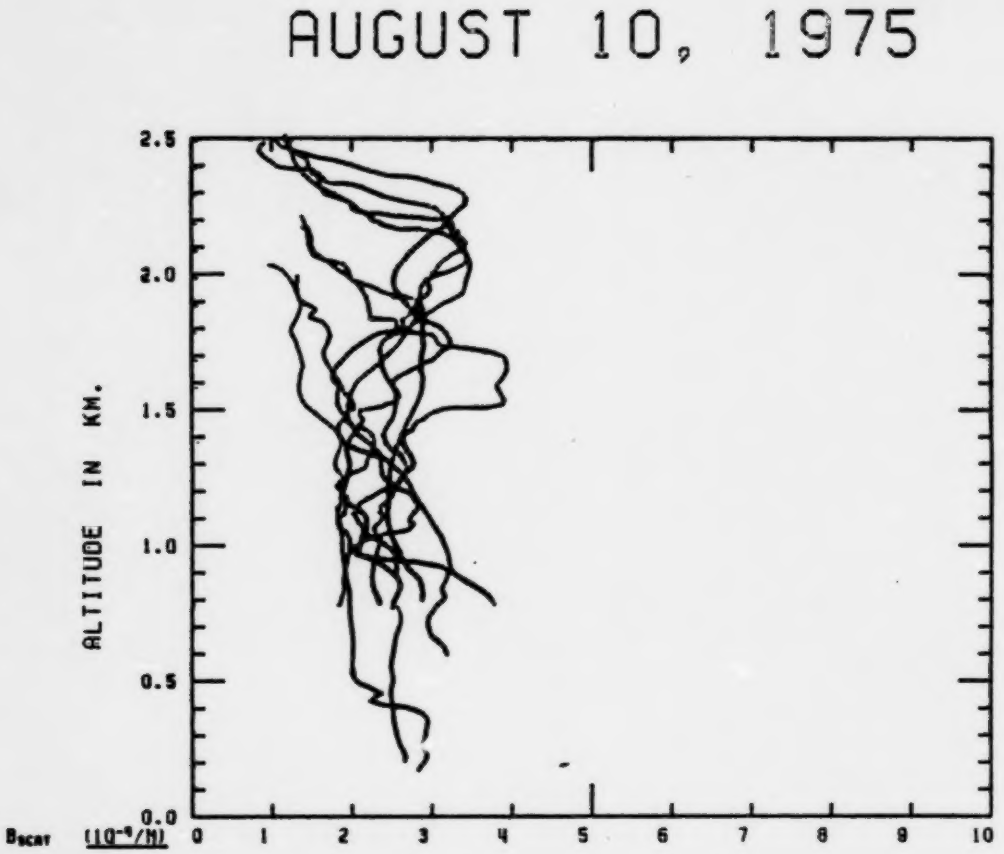

Figure 3-12. Overlaid soundings from August 10, 1975. Even at midday, the soundings in the Illinois-Indiana region show marked layers of haze with peak b_{scat} aloft.

4.0 JULY 30, 1976

4.1 Flight Description

A large high-pressure cell with related stagnant air was predicted to occur in the region to the east and north of south-central Illinois. Also, during the night preceding the sampling missions, winds from the Chicago region were expected to deliver an accumulation of pollution into the region along the Illinois-Indiana border. Consequently, a "long-range" flight aimed at characterization of a large stagnant air mass along the Illinois-Indiana border was planned.

The flight plan called for an approach to the target area from the south. Thus, the first leg of the mission consisted of a flight from St. Louis south along the Mississippi River to Paducah, Kentucky, then east to Bowling Green, Kentucky. In the second leg, which was expected to be the principal component of the sampling mission, the flight consisted of zigzagging northward, up along the Illinois-Indiana border (also Wabash River Valley). The flight was broken up into an alternating ferry-dolphin-ferry... sequence in order to obtain horizontal gradients going into the stagnant air mass and to resolve the structure of the atmosphere. The northernmost point reached was north of Danville, Illinois. A strong gradient of visual range was observed along the Illinois-Indiana border. A sharp increase in haziness also existed across central Illinois. The predicted meteorology did prevail, with nearly stagnant flow conditions in the Wabash River Valley. Several power plant plumes were encountered along the flight path.

Figure 4-1 shows a schematic of the ferry-dolphin flight pattern used on the July 30 and August 2, 1976, missions. The ferry is a conventional traverse at constant altitude and provides purely horizontal information. The dolphin pattern of ascent-descent-ascent is designed to measure the vertical structure within and above the mixed layer. It combines the horizontal progress of the ferry with the altitude variation of an aircraft spiral.

In an operational sense, an attempt is made to schedule the dolphin segments of the flight at locations where there is reason to expect several layers of pollutants. As seen in the illustration, a ferry at a poorly chosen altitude could provide a misleading measurement. Dolphin measurements, on the other hand, can be difficult to interpret because there is no natural axis (horizontal or vertical) to the pattern. This approach, ideally, can provide vertical resolution over a large horizontal extent.

4.2 Summary

For the July 30, 1976, flight the ferry-dolphin sampling technique provided a large number of vertical soundings over a range of about 50 km.

A strong gradient of b_{scat}, sulfate, and ozone was seen along the Illinois-Indiana border with higher concentrations in the northern loop of the flight. The atmosphere became layered by the evening hours, with strong plume effects in central Illinois.

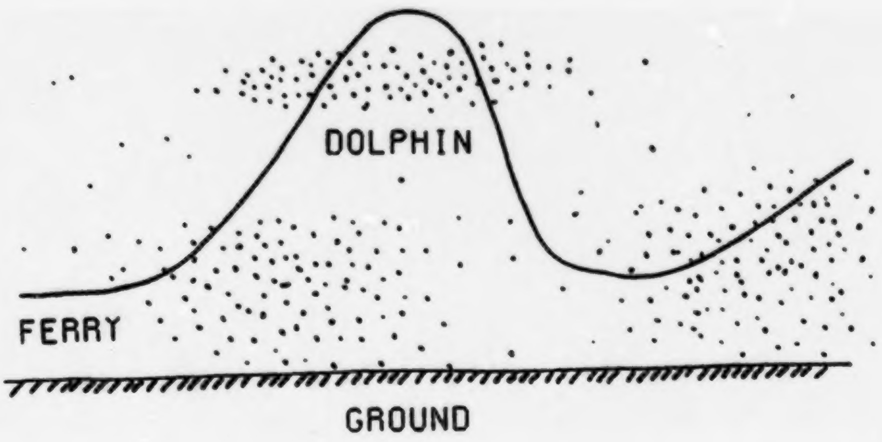

Figure 4-1. Ferry-dolphin flight pattern schematic for July 30 and August 2, 1976.

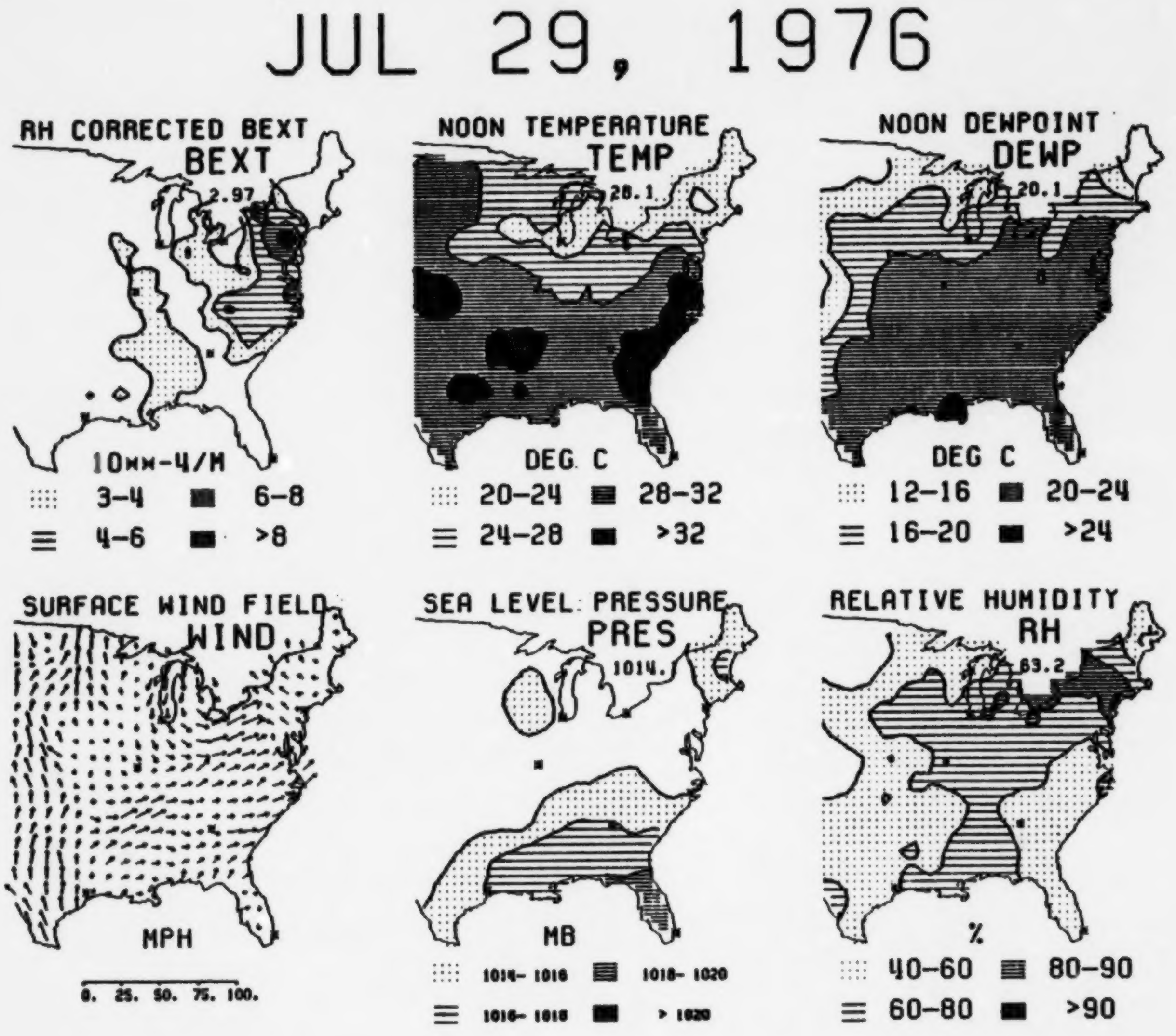

Figure 4-2. July 29, 1976—winds were stagnant over Missouri and Illinois the day before the flight.

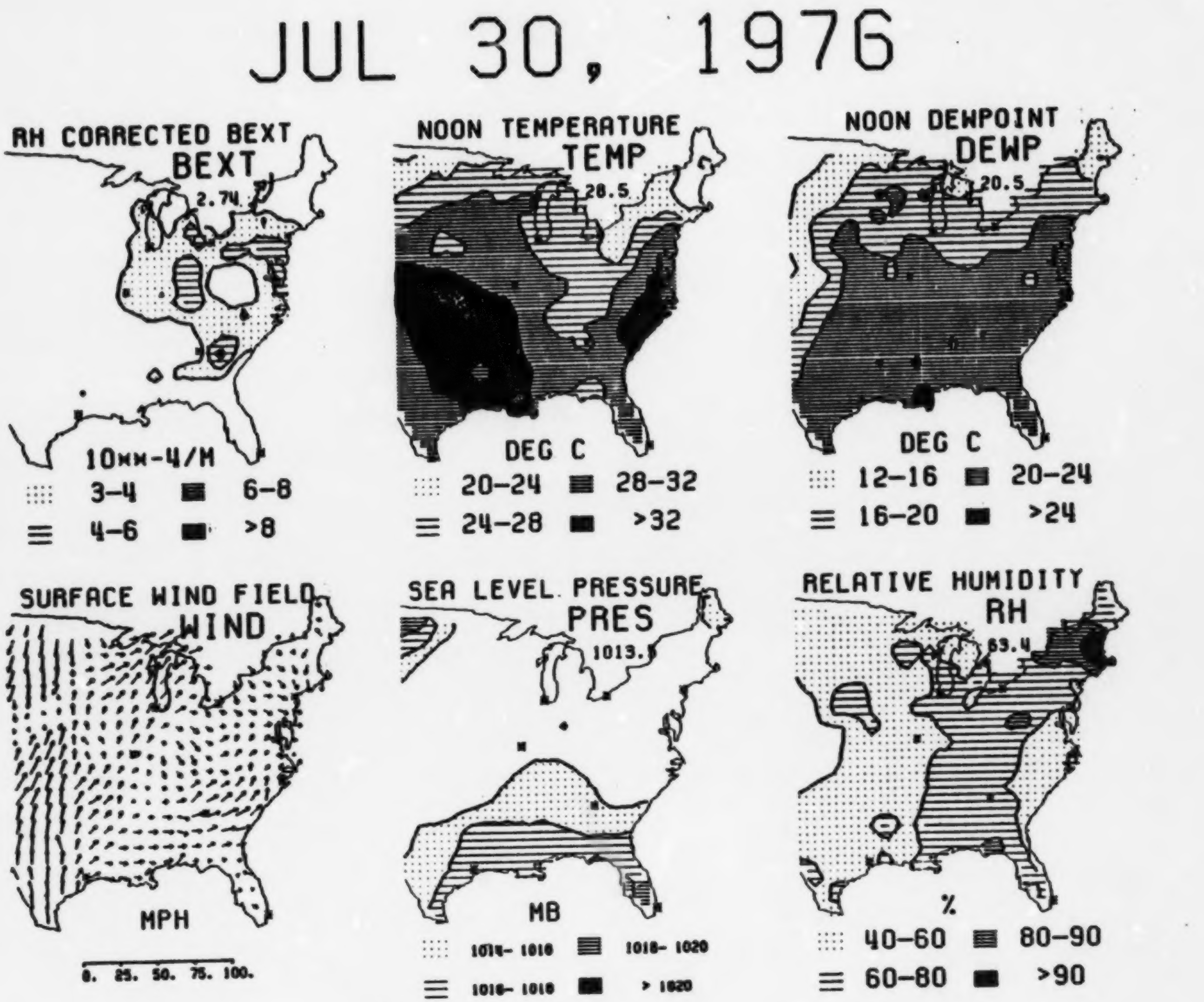

Figure 4-3. July 30, 1976—continued stagnation over the central midwest, with the region of lowest visibility in Indiana. Noon surface temperatures along the path were near 28° C, with dewpoint 20°-24° C. A high-pressure system is moving in from the Northern Great Plains.

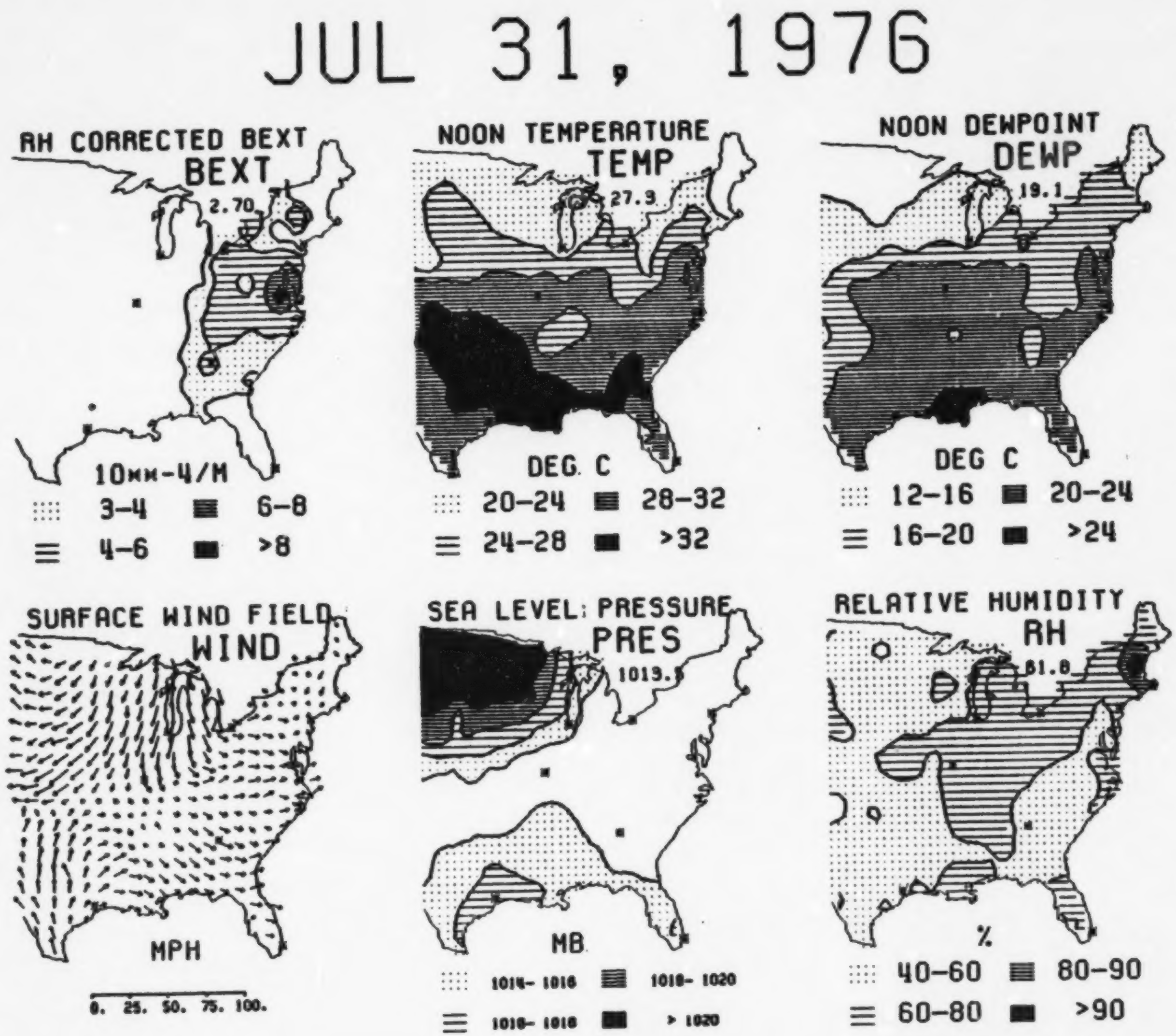

Figure 4-4. July 31, 1976--the high-pressure system induced a major change in the wind field, pushing the hazy air mass toward the east coast.

TABLE 4-1. FLIGHT OUTLINE, JULY 30, 1976
(Cartridge No. 021)

Event No.- Type	ALT (m MSL)	Route	Time (CDT)
1. Dolphin	450-1650	B - C - D	1250 - 1308:30
2. Ferry	600	D - E - F	1310 - 1330
3. Dolphin	450-1800	F - G - H - I	1330 - 1350
4. Ferry	600	I - J	1351 - 1401
5. Dolphin	600-1650	J - K - L - M	1402 - 1416
6. Ferry	1050	M - N - O	1416 - 1430
7. Dolphin	450-1500	P - Q - R	1431 - 1443
8. Ferry	1050	R - S - T	1443 - 1456
Landing/T.O.		Evansville, Ind.	1457 - 1632
9. Ferry	1050	U - V - W	1637 - 1649
10. Dolphin	540-1500	W - X - Y	1651 - 1659
11. Ferry	900	Y - Z - A'	1701 - 1711
12. Dolphin	480-1500	A'-B'-C'-D'	1712 - 1721
13. Ferry	600	E' - F' - G'	1722 - 1732
14. Dolphin	600-1650	G' - H' - I'	1733 - 1745
15. Ferry	600	I' - J' - K'	1746 - 1758
16. Dolphin	640-1600	K' - L' - M'	1759 - 1812
17. Ferry	600	M' - N' - O'	1813 - 1820
Landing/T.O.	-	Terre Haute	1828 / 1915
18. Ferry	600	P' - Q' - R'	1923 - 1930
19. Dolphin	480-1800	R' - S' - T'	1931 - 1946
20. Ferry	600	T' - U'	1947 - 1957
21. Dolphin	600-1500	U' - V' - W'	1958 - 2012
22. Ferry	600	W' - X' - Y'	2013 - 2022
23. Dolphin	600-2300	Y' - Z' - A'	2024 - 2042
Landing	-	Spirit	2052

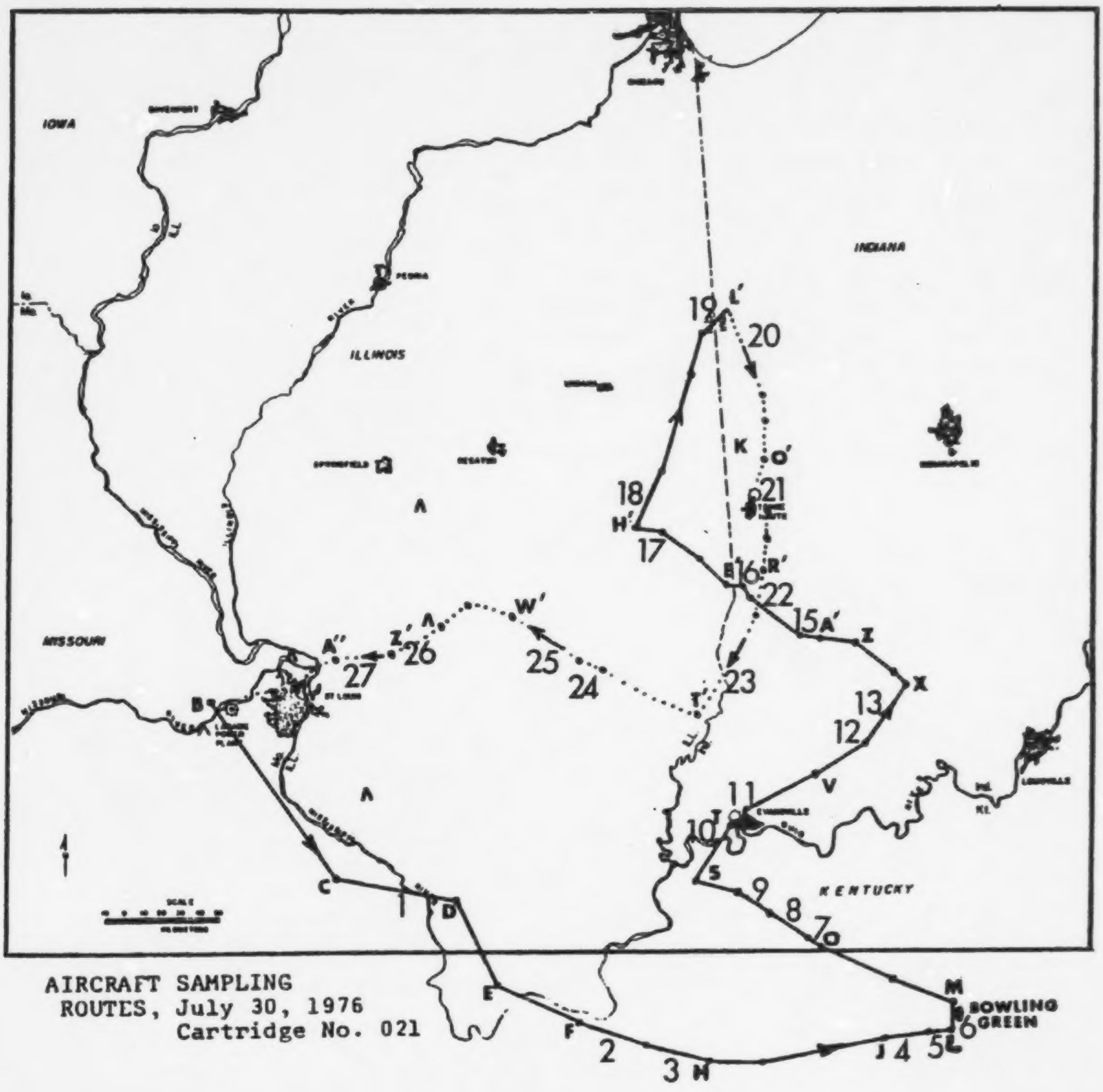

Figure 4-5. Map showing flight path and location of spirals for July 30, 1976. The numbers 1 through 27 indicate the positions of the spirals displayed in Figures 4-18 through 4-22.

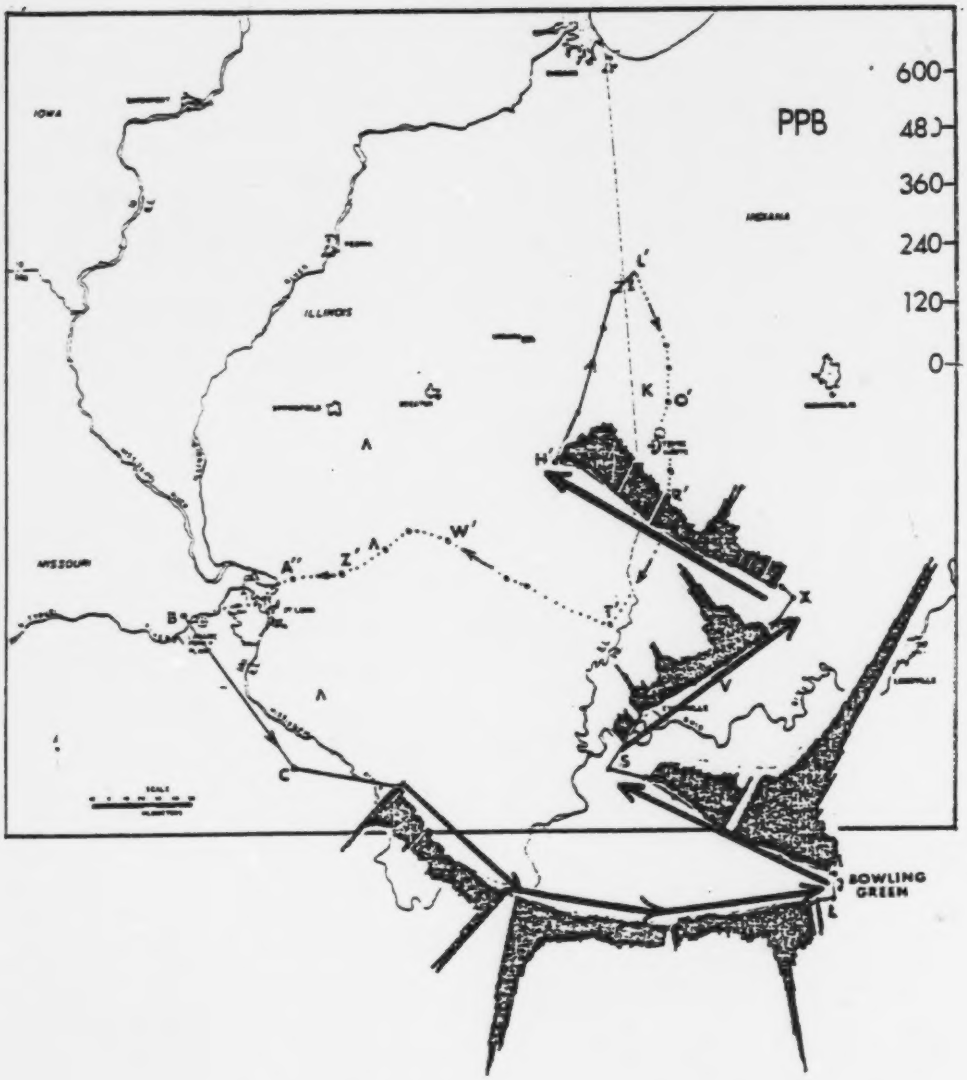

JULY 30, 1976

SO_2

Figure 4-6. During the flight several SO_2 plumes were encountered, especially along the southern leg. Winds are light, predominantly from the southwest. Note that concentration is displayed perpendicular to the aircraft path and does not represent prevailing wind directions. Note: The systematic decrease-increase in concentration is due to the dolphin pattern of flight.

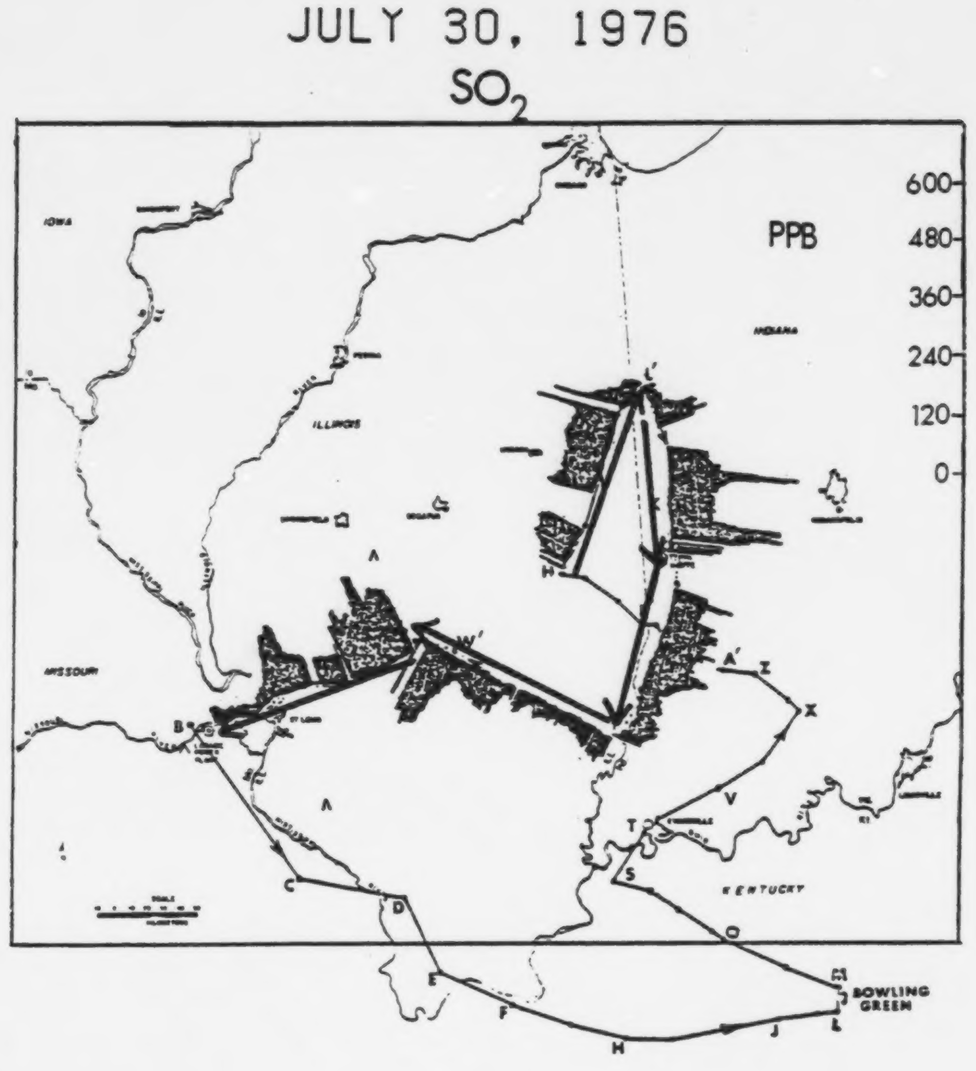

Figure 4-7. Continuation of SO_2 concentrations. Note: The systematic decrease-increase in concentration is due to the dolphin pattern of flight.

JULY 30, 1976
OZONE

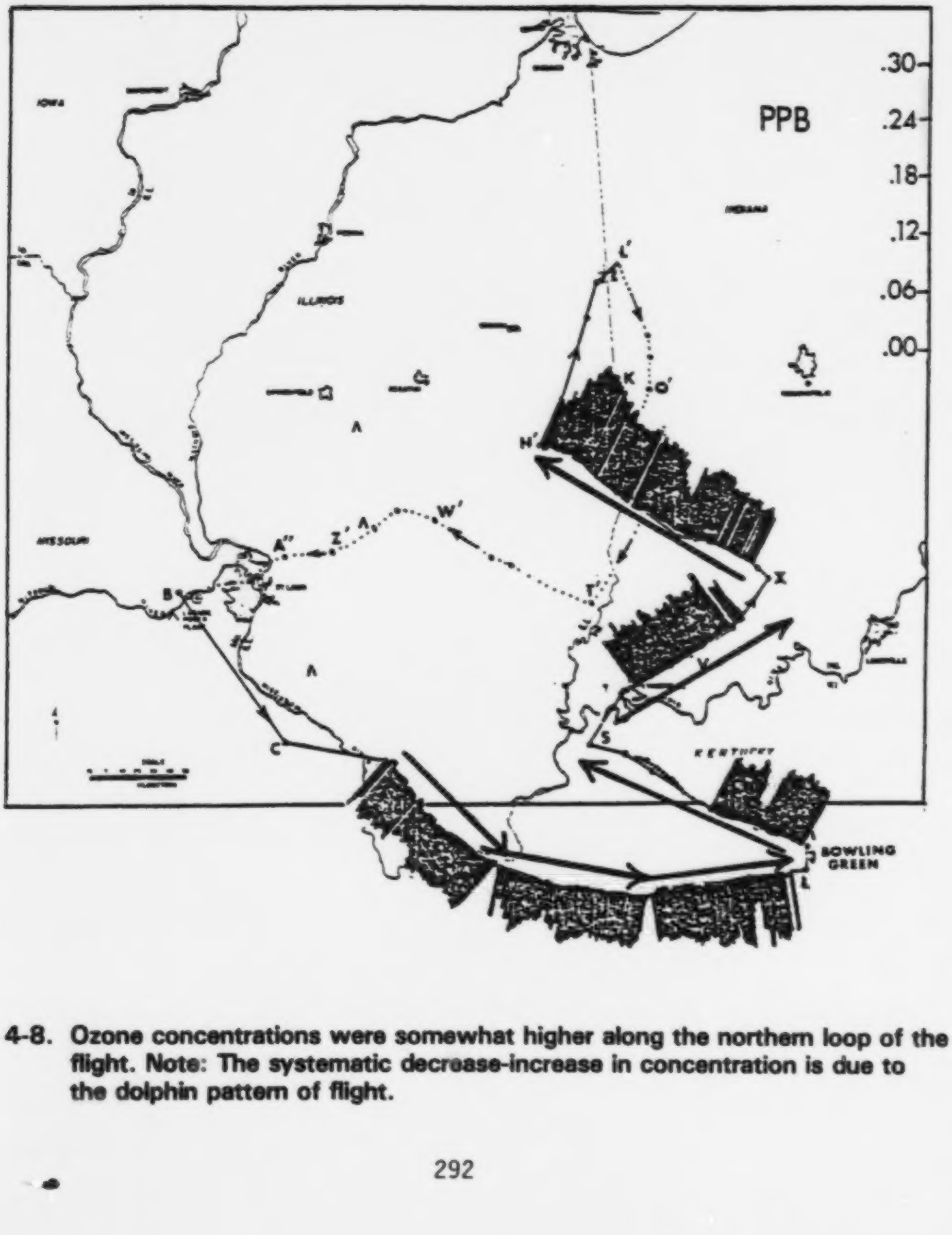

Figure 4-8. Ozone concentrations were somewhat higher along the northern loop of the flight. Note: The systematic decrease-increase in concentration is due to the dolphin pattern of flight.

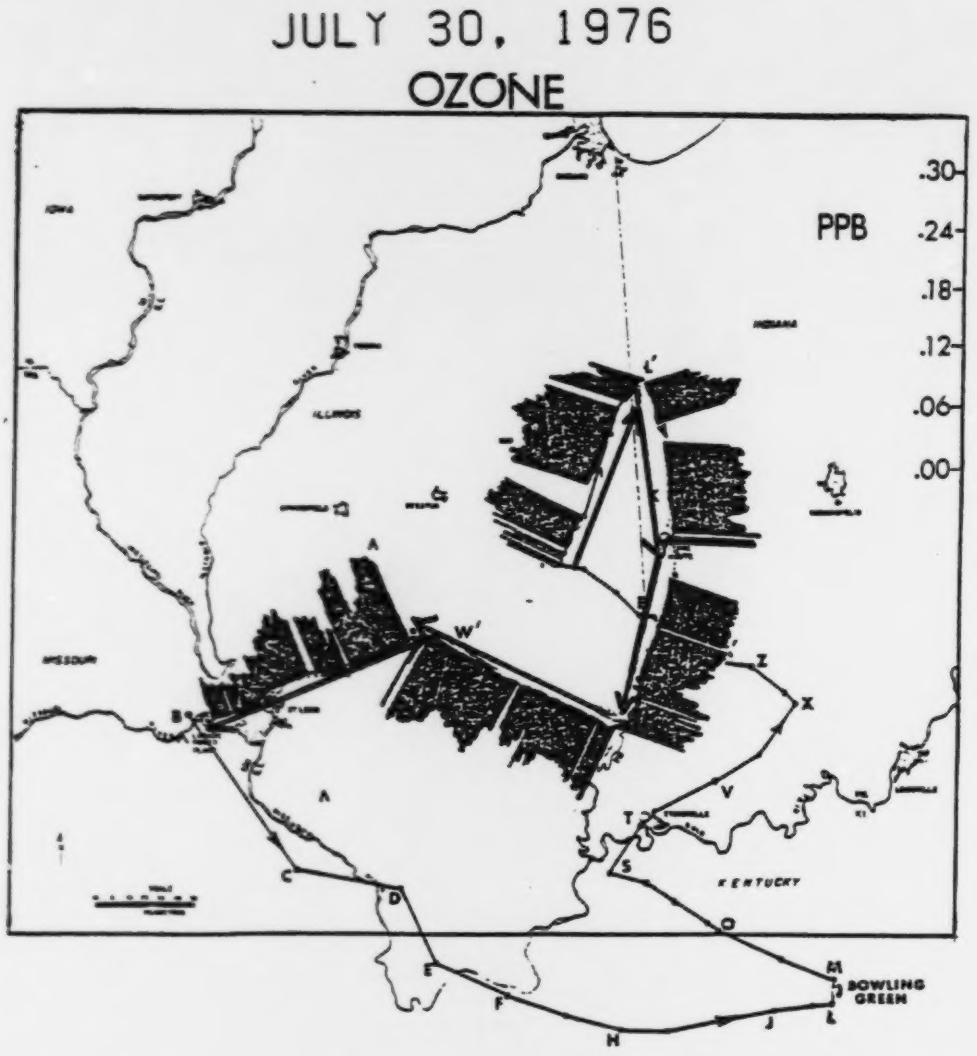

Figure 4-9. Continuation of ozone concentration. Note: The systematic decrease-increase in concentration is due to the dolphin pattern of flight.

JULY 30, 1976

SO_4

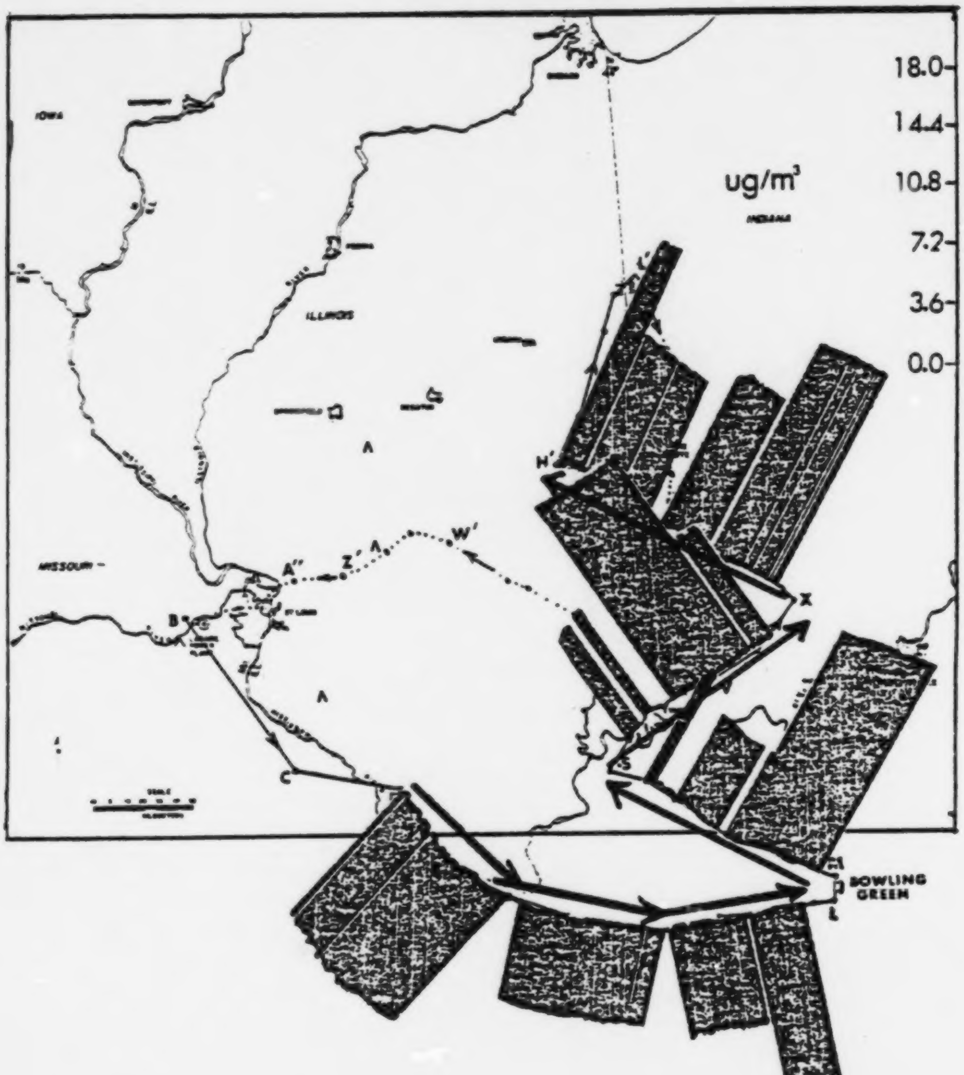

Figure 4-10. Sulfate concentration was much higher along the northern loop of the flight. Note: The systematic decrease-increase in concentration is due to the dolphin pattern of flight.

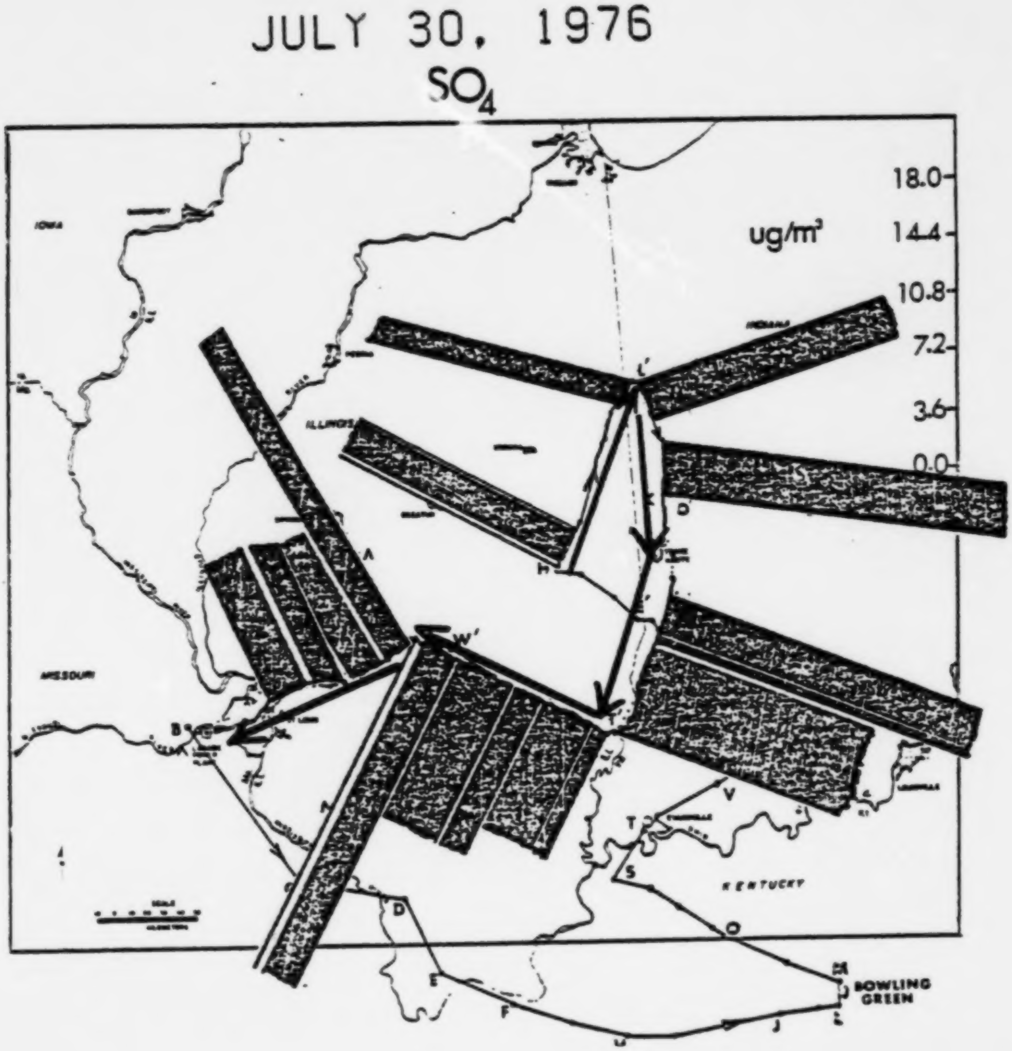

Figure 4-11. Continuation of sulfate concentrations. Note: The systematic decrease-increase in concentration is due to the dolphin pattern of flight.

JULY 30, 1976

CNC

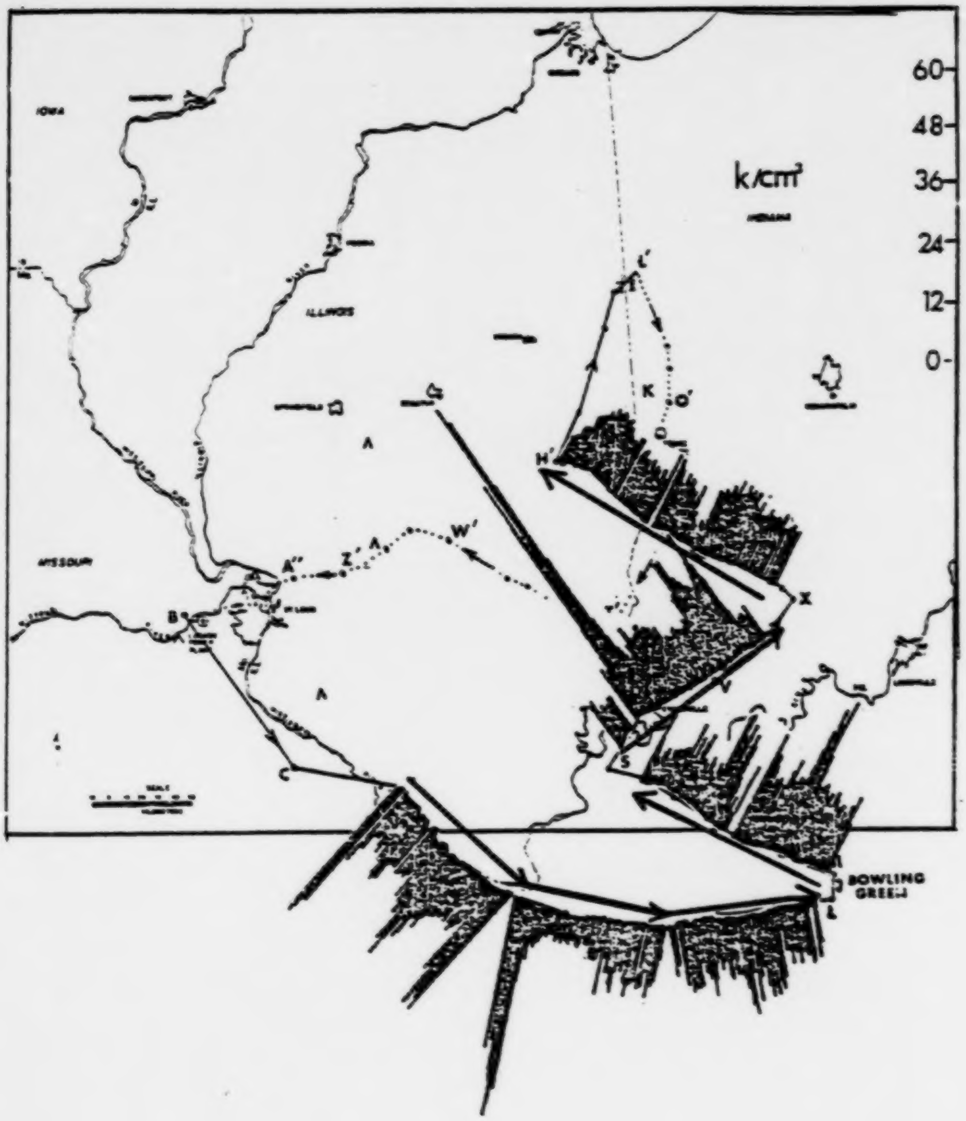

Figure 4-12. Condensation nuclei count. Note: The systematic decrease-increase in concentration is due to the dolphin pattern of flight.

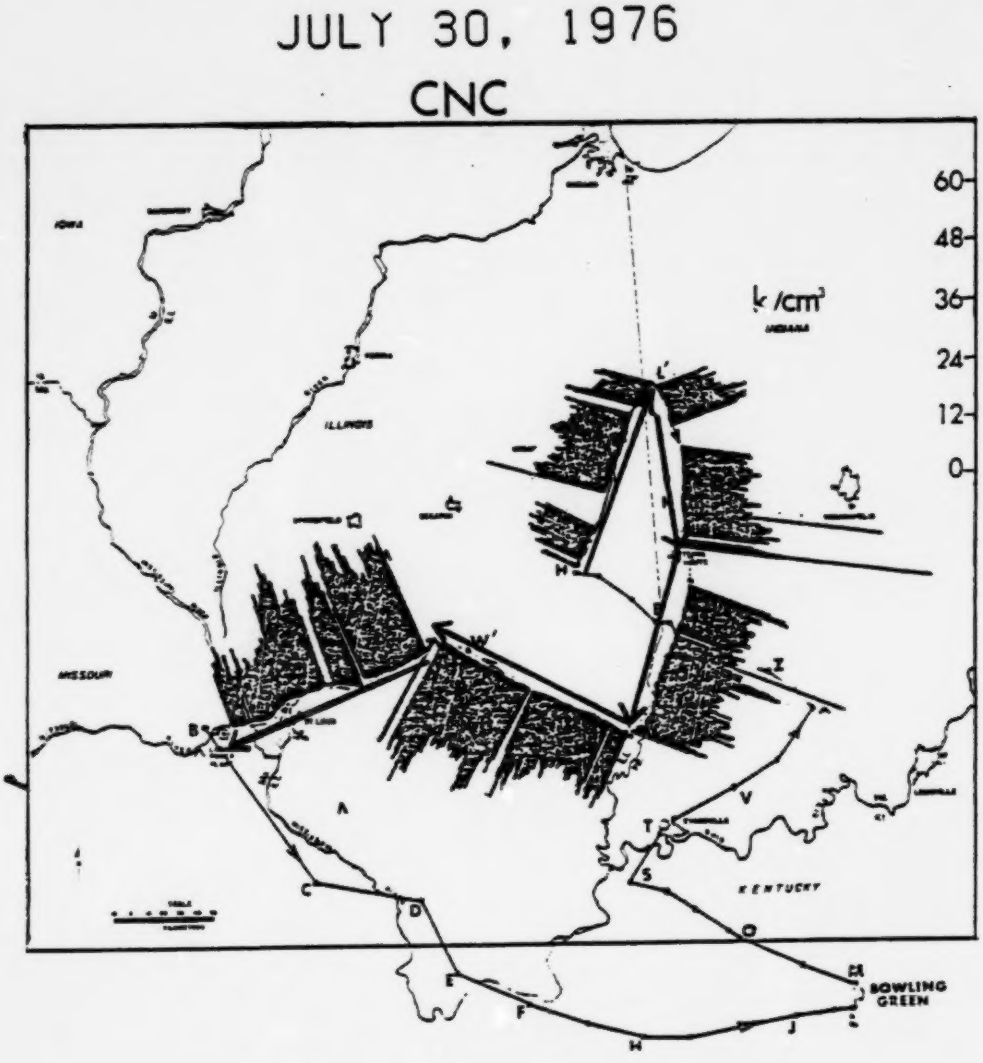

Figure 4-13. Continuation of condensation nuclei count. Note: The systematic decrease-increase in concentration is due to the dolphin pattern of flight.

JULY 30, 1976
CHARGE

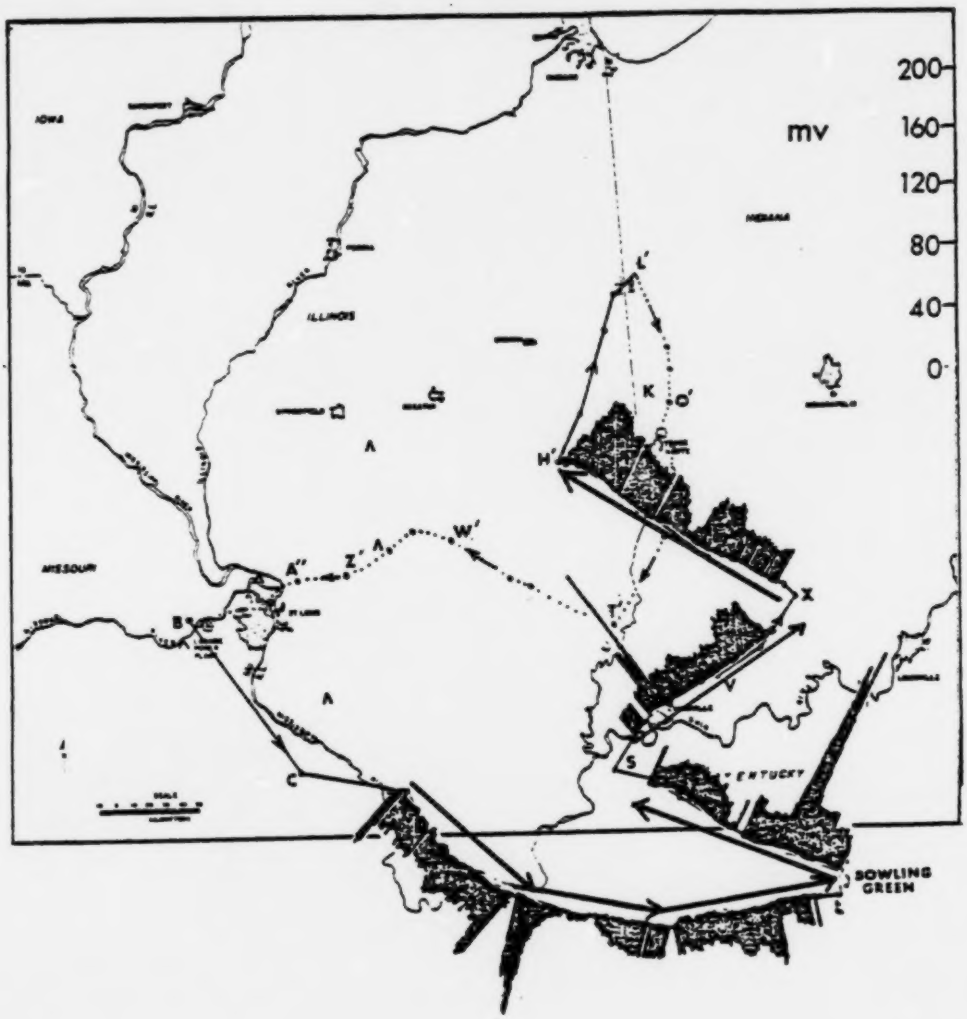

Figure 4-14. Aerosol charge reveals the contribution of major urban areas as well as power plant plumes. Wide charge plumes are seen along the northern loop and in central Illinois. Note: The systematic decrease-increase in concentration is due to the dolphin pattern of flight.

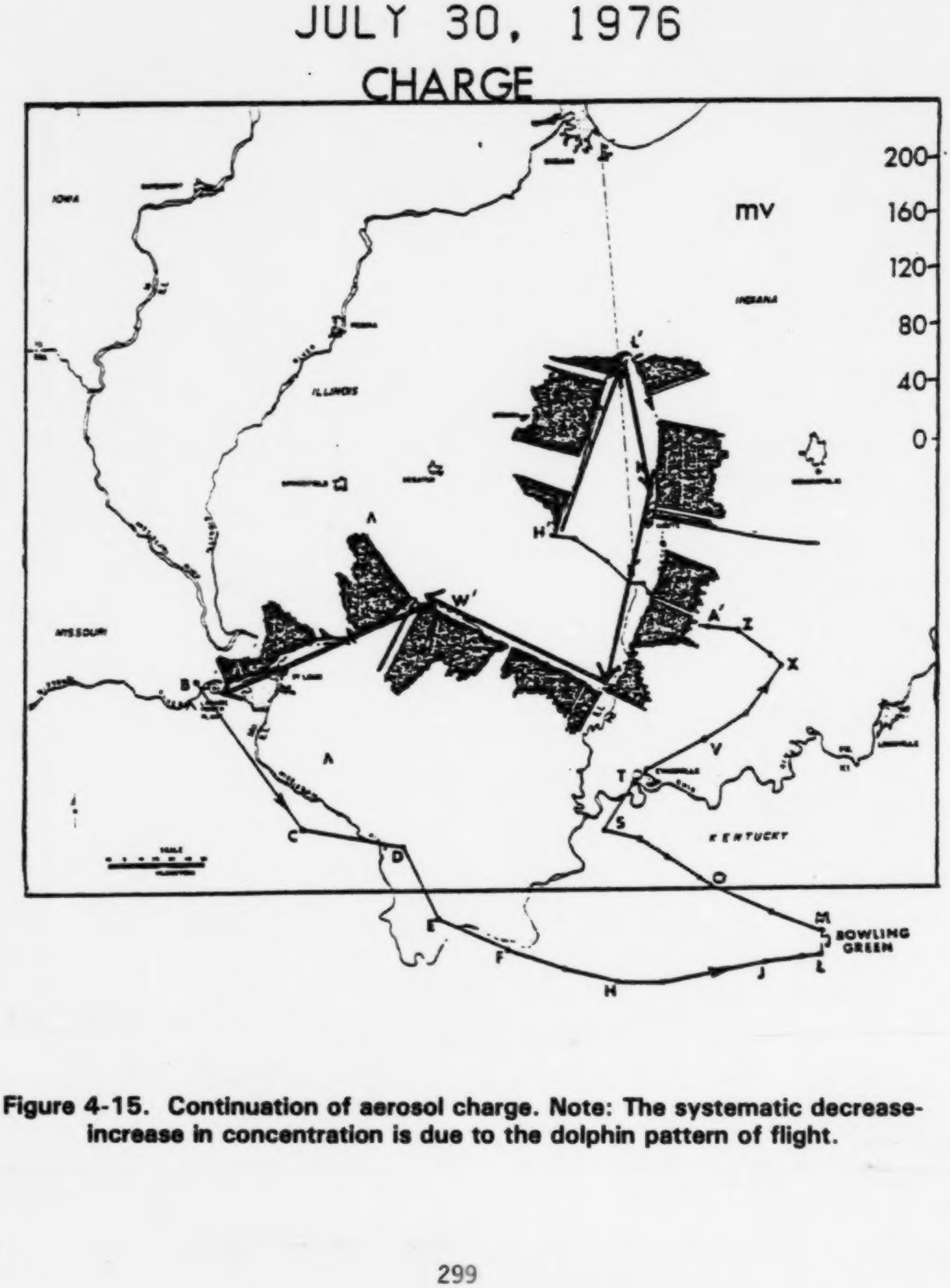

Figure 4-15. Continuation of aerosol charge. Note: The systematic decrease-increase in concentration is due to the dolphin pattern of flight.

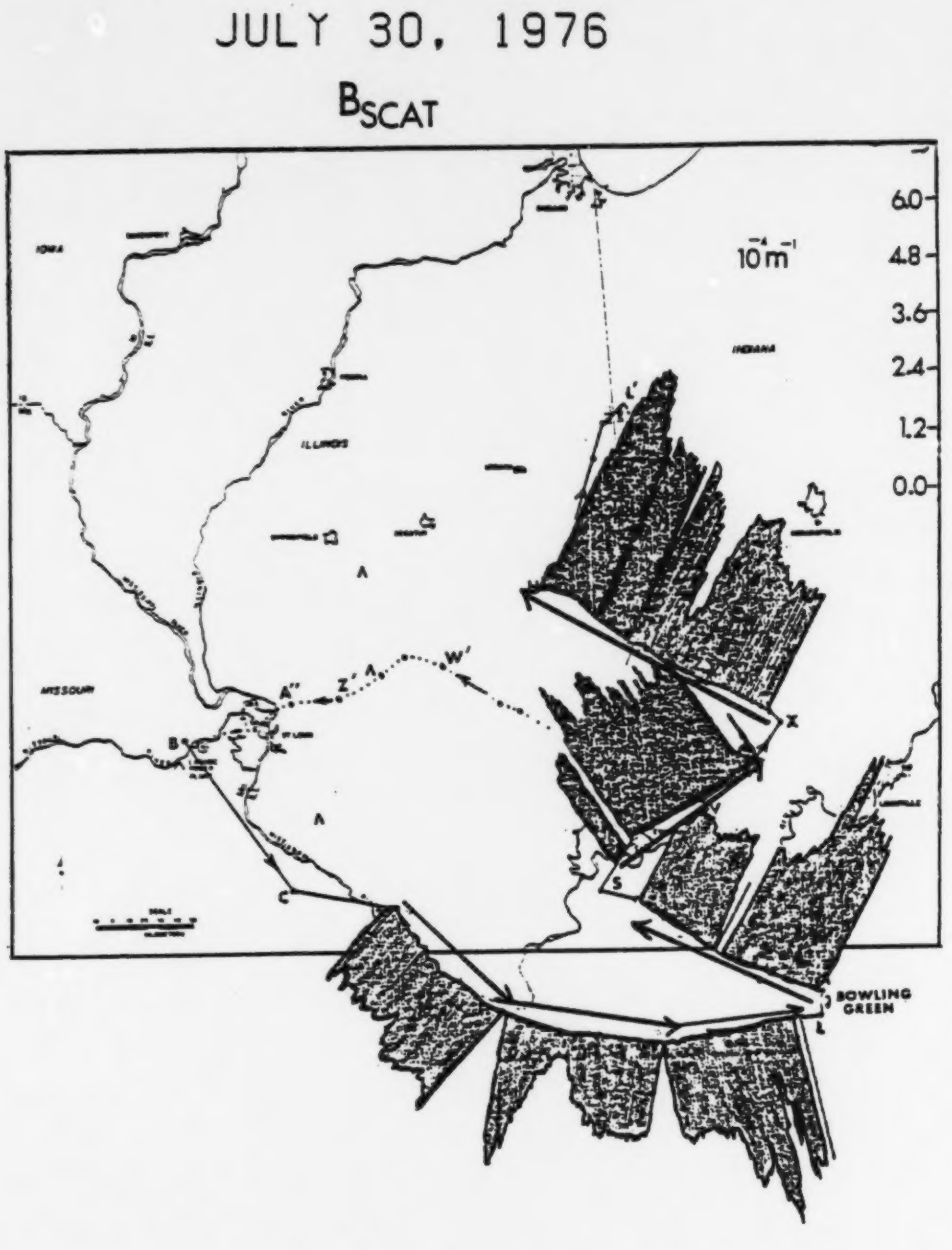

Figure 4-16. Haziness, as measured by b_{scat}, was also much higher on the northern Illinois-Indiana border region than farther south, with an additional peak in central Illinois shown on the following page. Note: The systematic decrease-increase in concentration is due to the dolphin pattern of flight.

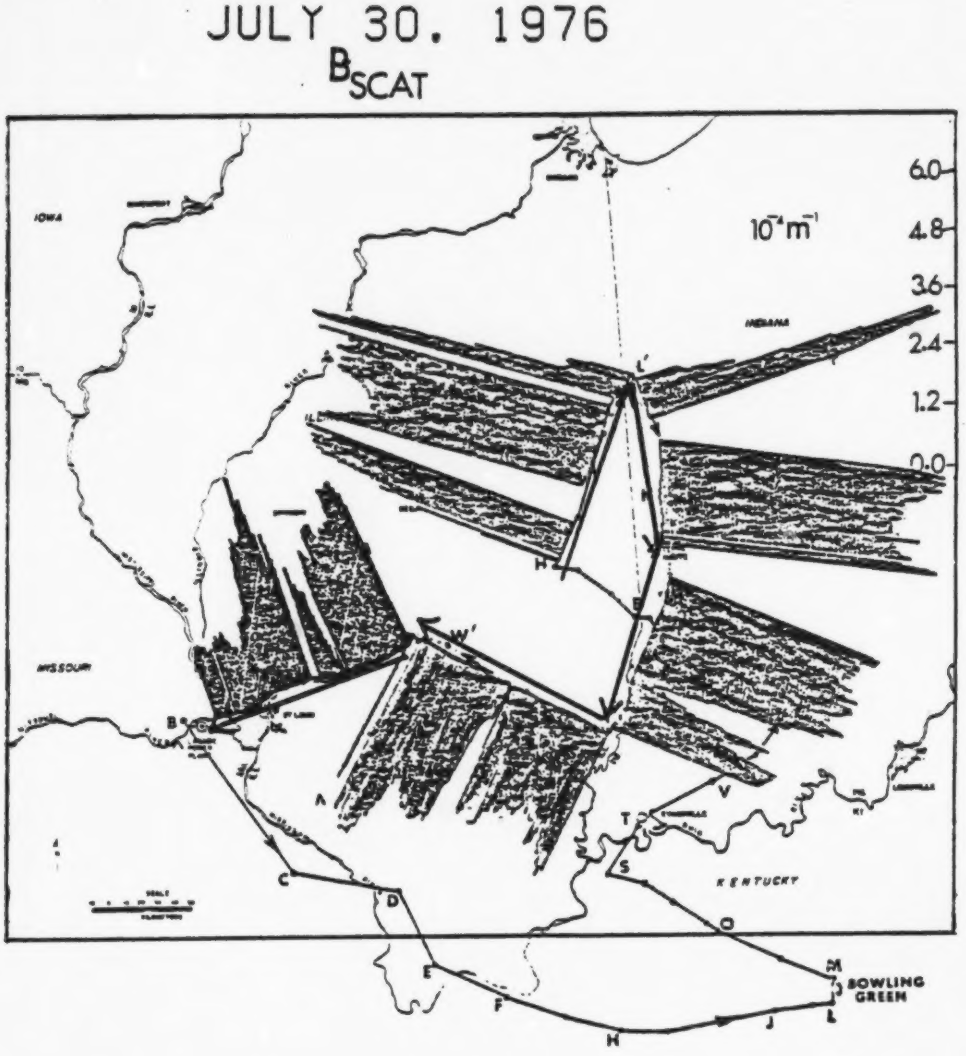

Figure 4-17. Continuation of b_{scat} concentrations. Note: The systematic decrease-increase in concentration is due to the dolphin pattern of flight.

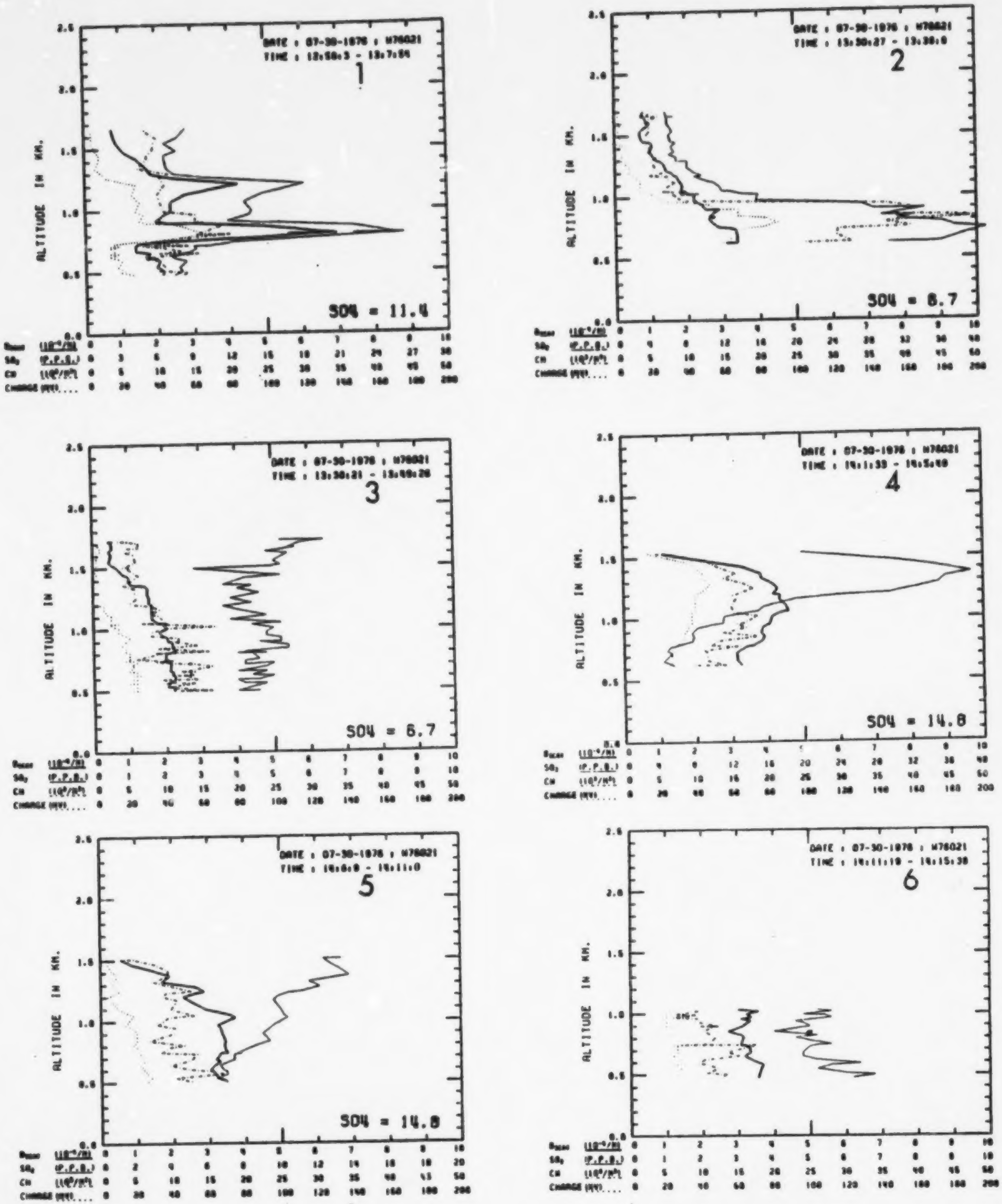

Figure 4-18. The first two dolphins encountered two elevated plumes. The third, along the southernmost leg of the flight, indicates a rather well-mixed layer up to 1 km with b_{scat} of 2. Dolphins 4, 5, and 6 were taken in the vicinity of Bowling Green, with b_{scat} 3-3.5.

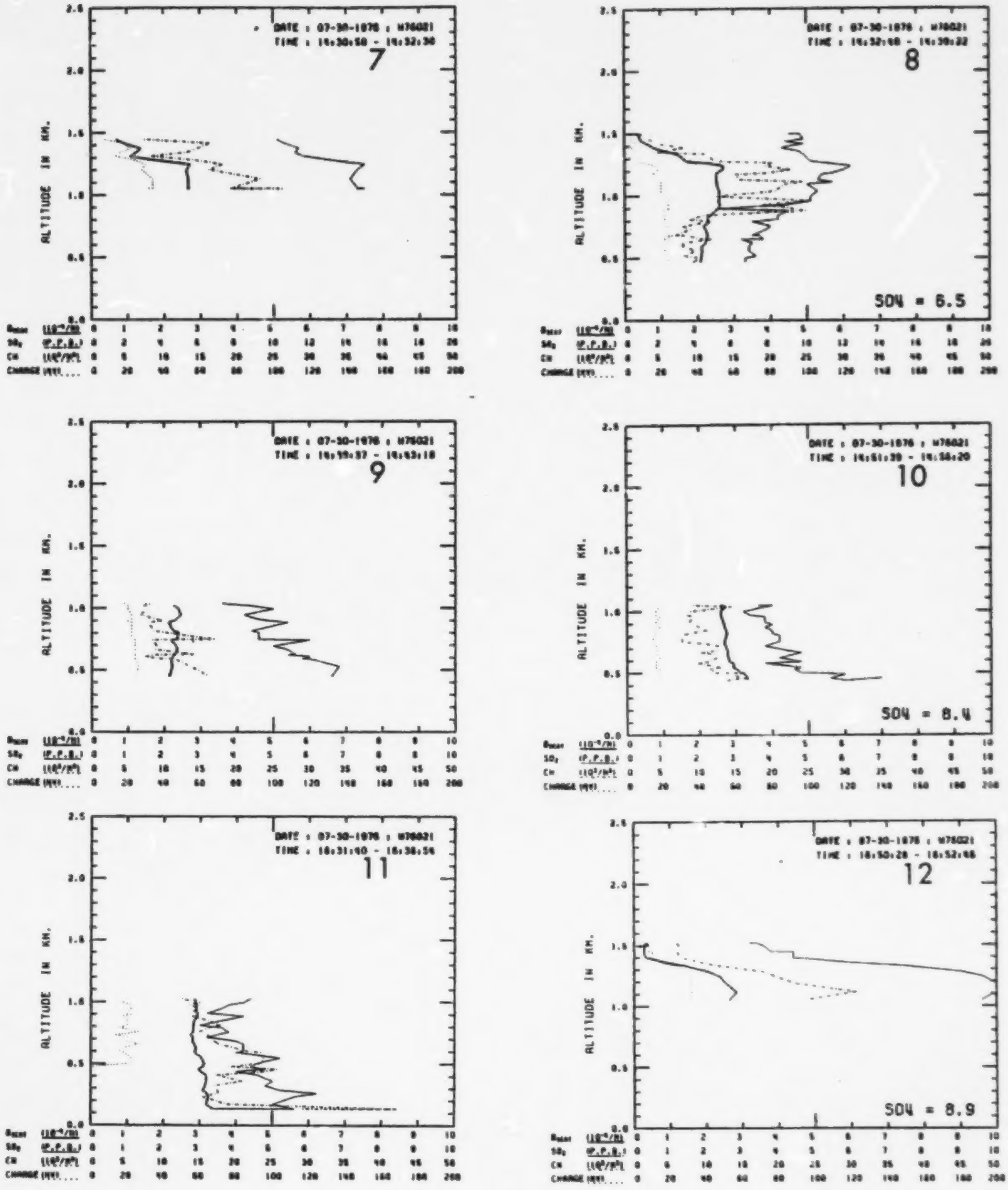

Figure 4-19. Dolphins 7-9 occurred along a line heading northwest from Bowling Green, with 10 and 11 (separated by 2 hr) at Evansville, Indiana. Within the 1,250-m mixed layer the characteristic levels of b_{scat} increased from 2.5 to 3.0 along this path.

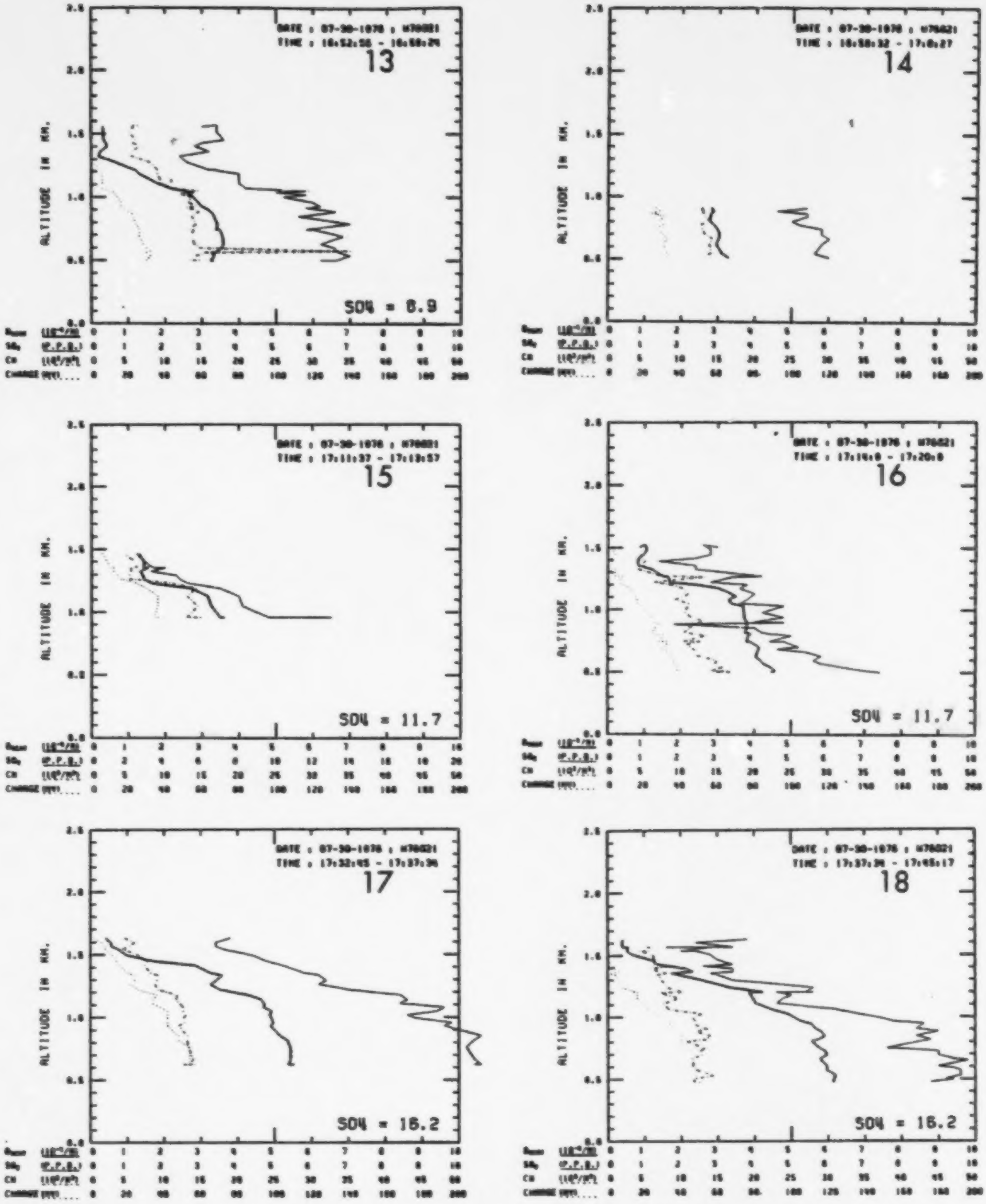

Figure 4-20. Near point X on the map (spirals 13 and 14), light scattering coefficient is near $3 \cdot 10^{-4} m^{-1}$. Heading northwest toward point H', b_{scat} is approximately 4 at spiral 16, increasing to 5 at spiral 17. The northeast path of spiral 18 indicates b_{scat} of 6 near the surface at 1730 CDT.

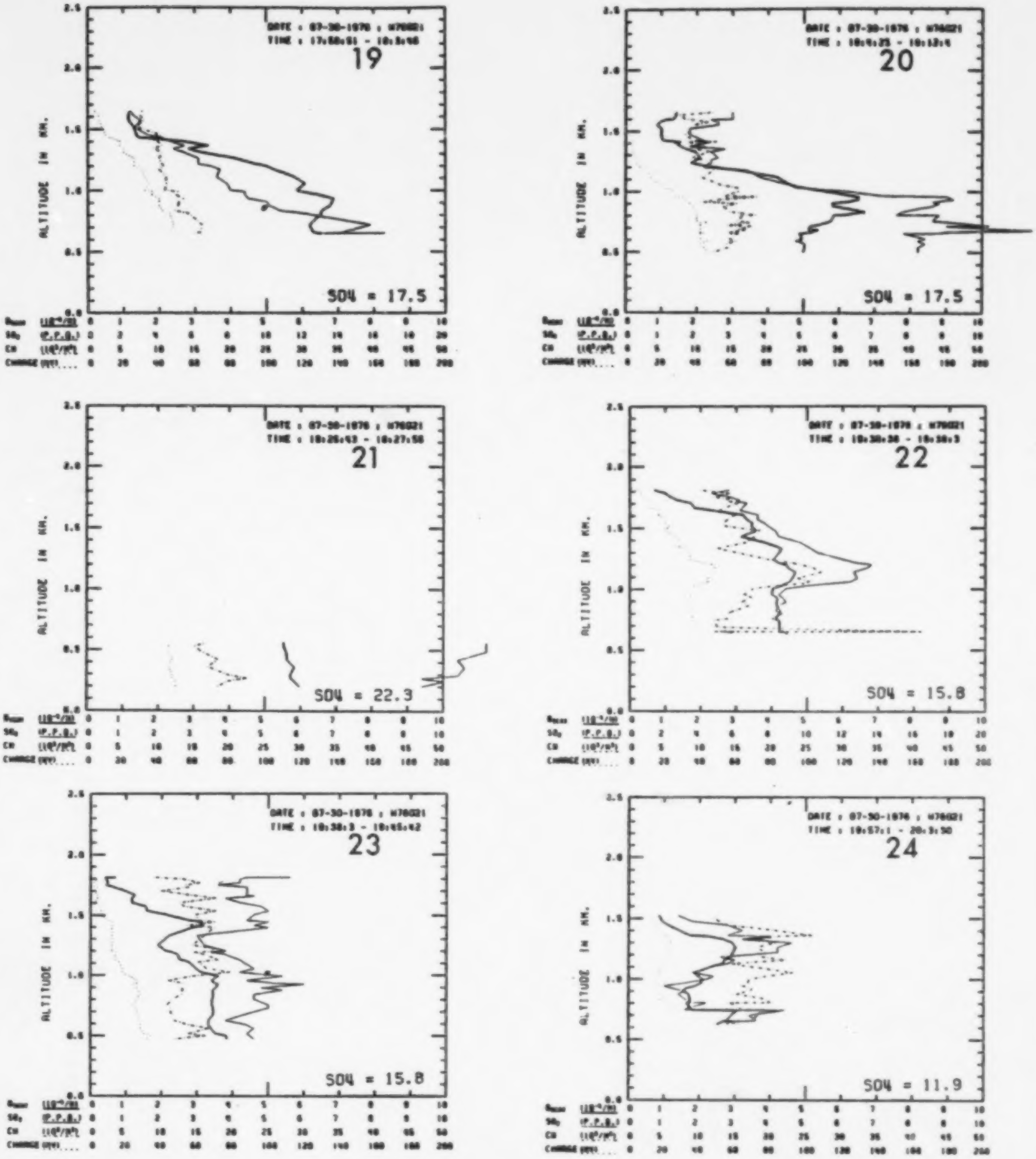

Figure 4-21. Spirals 19 and 20 are at the northernmost part of the flight, near the Illinois-Indiana border, where the most severe haze was encountered. South of Terre Haute b_{scat} has dropped to 4-4.5. Near point T' the characteristic level is again lower (23). Spiral 24, in east south-central Illinois, reveals strong haze layering effects with peak b_{scat} of 3.

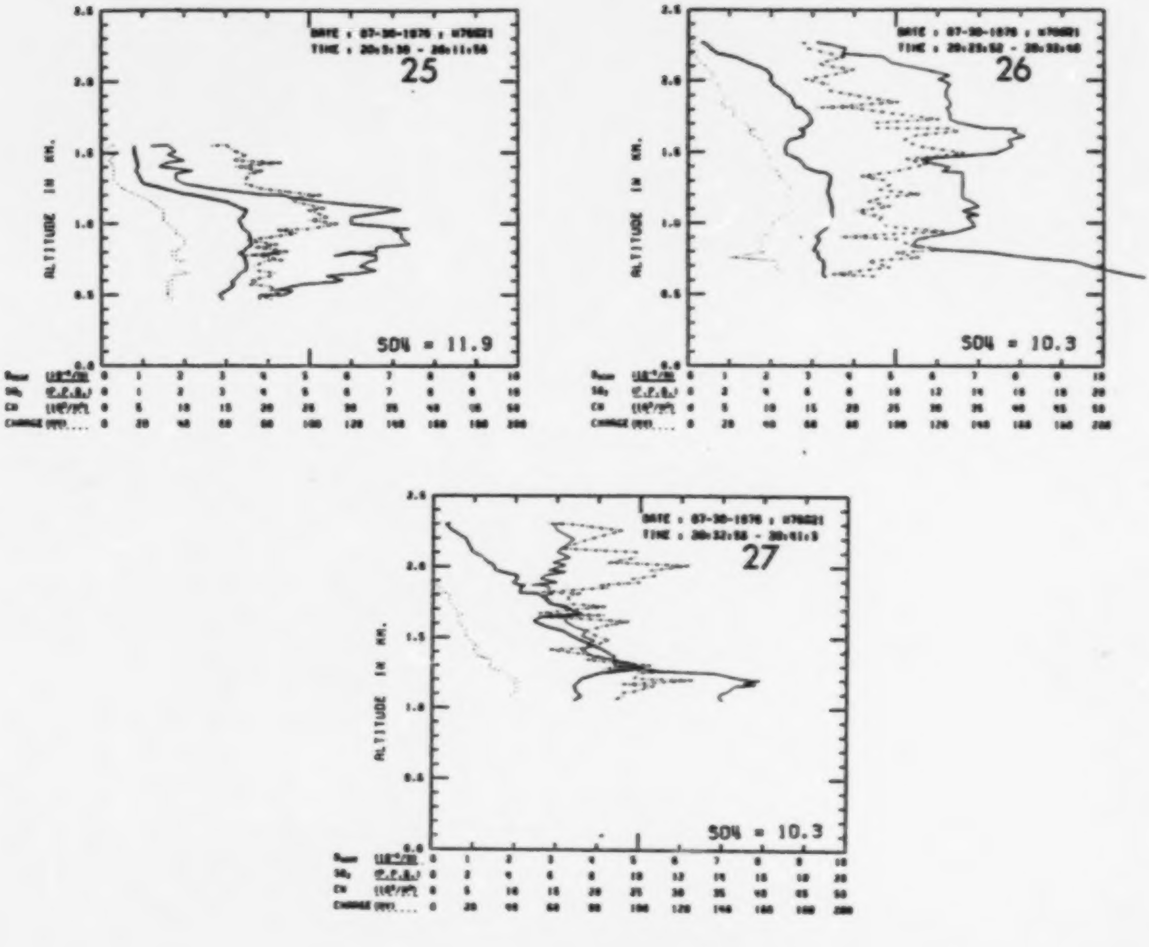

Figure 4-22. In south-central Illinois (25-26) at 2000 CDT b_{scat} is approximately 3.5 in the lowest 1,200 m.

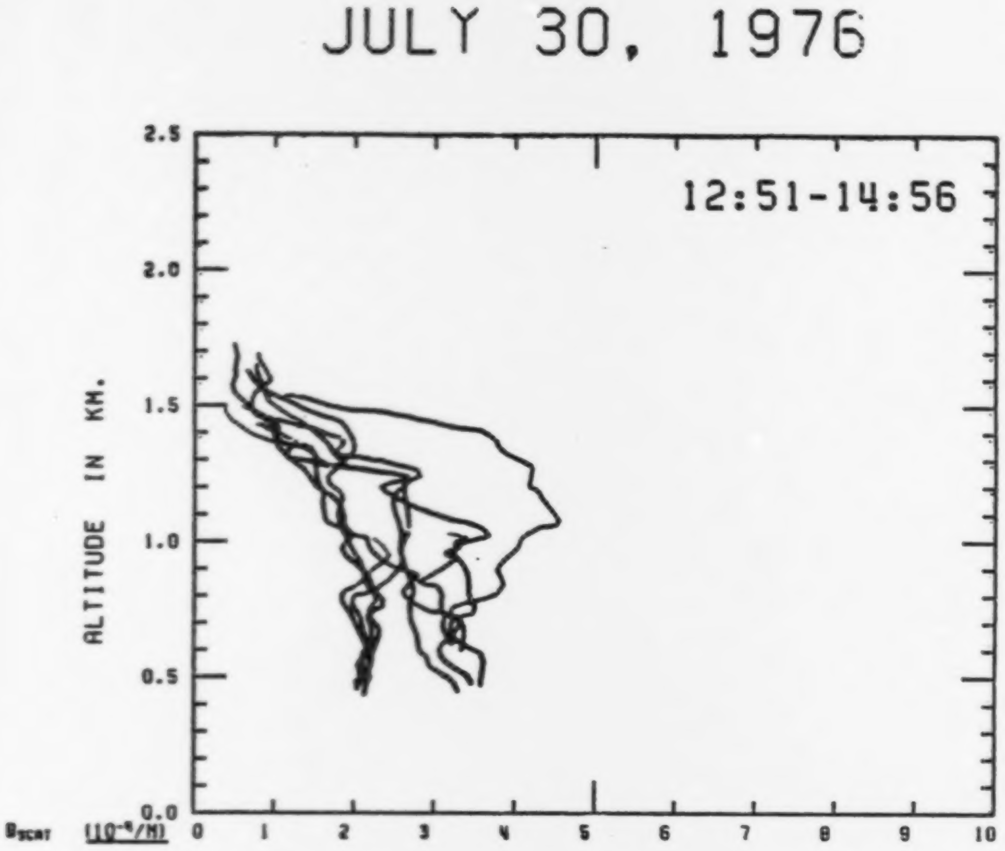

Figure 4-23. Overlay of soundings 1-10. This leg of the flight ran southeast from St. Louis to Paducah, east to Bowling Green, and northwest to Evansville. Highest sulfate and haze were near Bowling Green. B_{scat} is typically 2-3 in the southern portion of the flight.

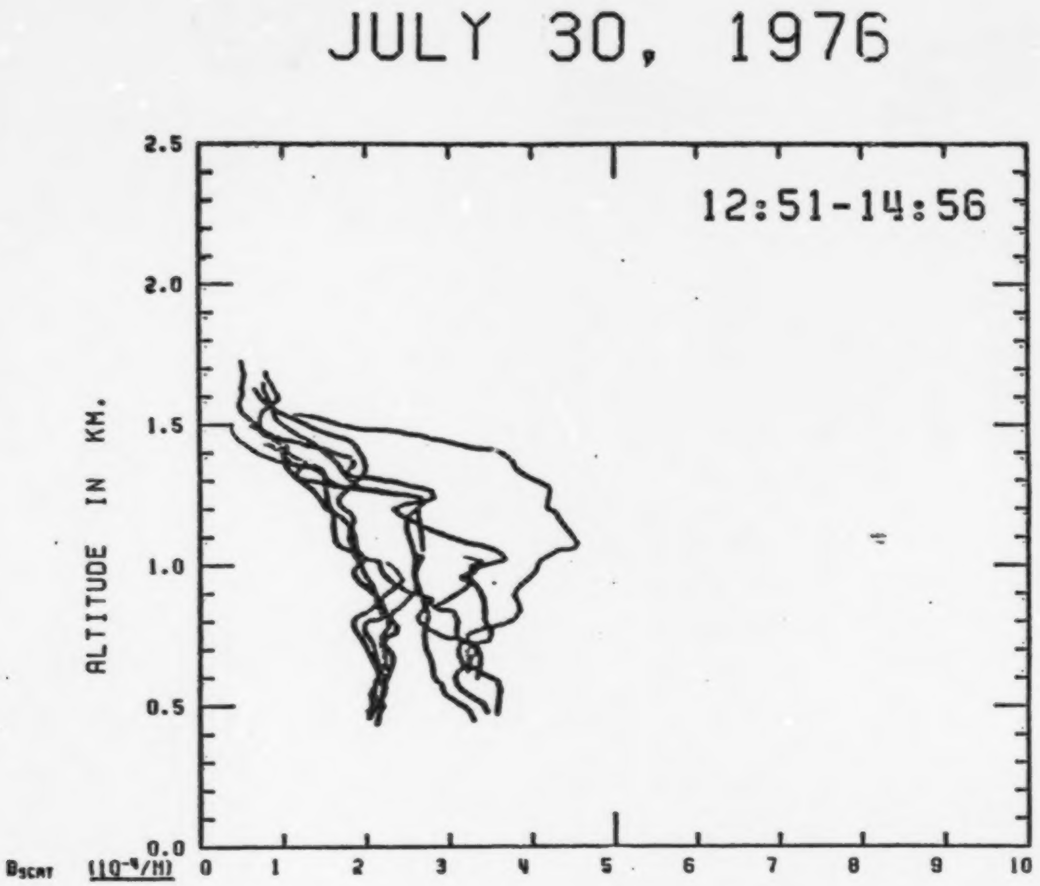

Figure 4-24. Overlay of soundings 1-10. This leg of the flight ran southeast from St. Louis to Paducah, east to Bowling Green, and northwest to Evansville. Highest sulfate and haze were near Bowling Green. B_{scat} is typically 2-3 in the southern portion of the flight.

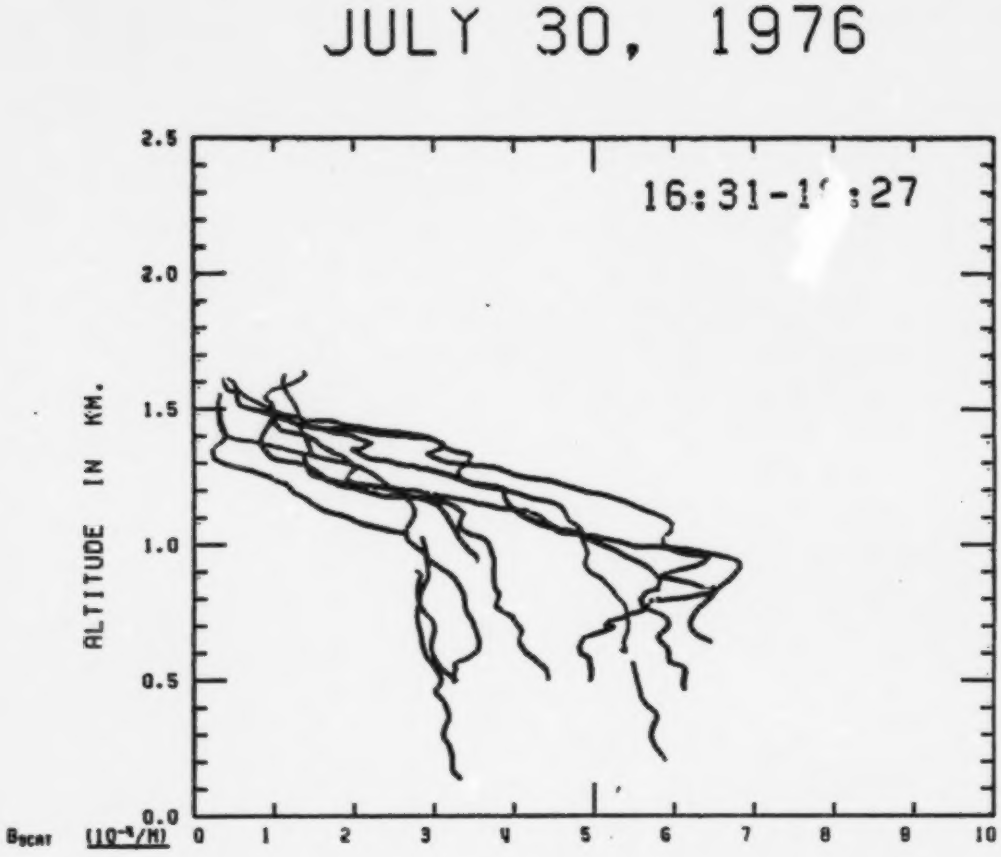

Figure 4-25. Overlay of soundings 11-21. In late afternoon the IL-IN border region has highest b_{scat} of 5-6 along the northern loop, with sulfate concentration 15-20 $\mu g/m^3$.

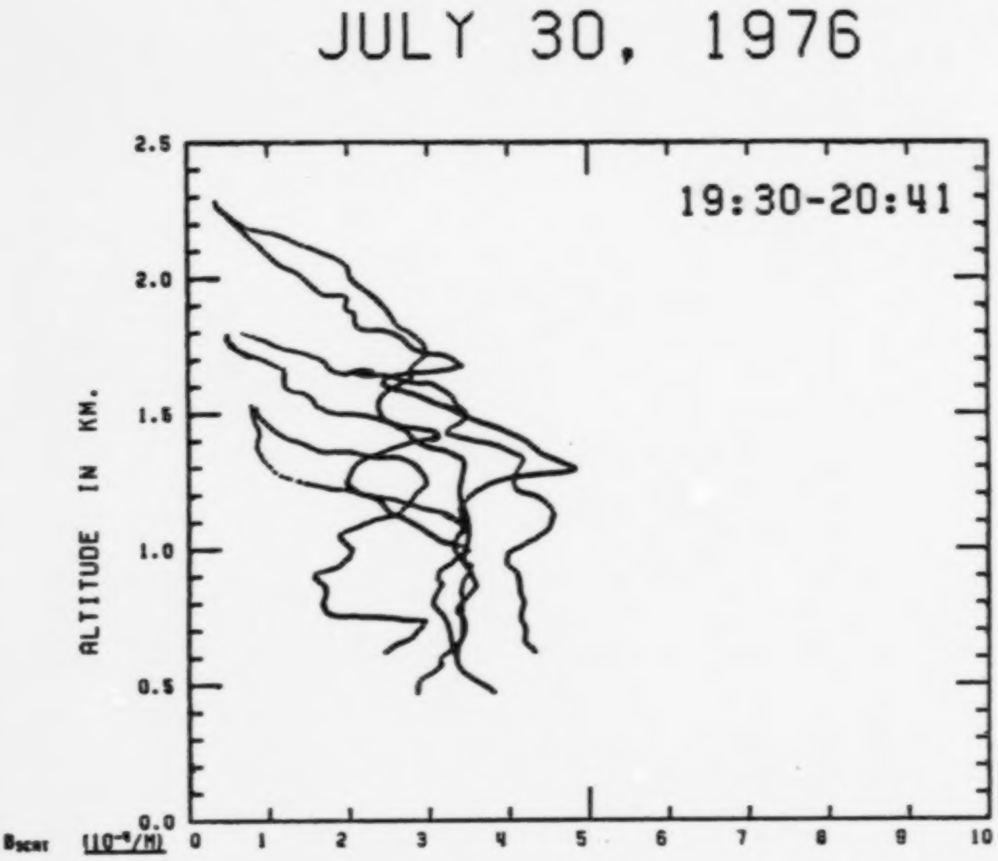

Figure 4-26. Overlay of soundings 22-27. Across central Illinois, about 2000 CDT, several plumes of haze are encountered, with b_{scat} 3-4 near the surface.

5.0 AUGUST 2, 1976

5.1 Flight Description

Once again, the objective was to collect data over a long-range flight. Under predicted northerly wind conditions, the decision was to make a box flight enclosing the Ohio River Valley approximately between Louisville and Paducah, Kentucky.

In the first leg of the mission (1100-1300), an eastward flight from St. Louis ended in Louisville, Kentucky; the route included the northern border of the "box." The second flight traveled down the eastern edge of the box, then proceeded east almost to the Virginia border. Three traverses were then made along the south edge of the box, being close to and parallel to the Kentucky-Tennessee border. The return to St. Louis completed the western edge of the box. Several power plant plumes from the Ohio River Valley and from central Kentucky were picked up in the east-west traverses along the southern leg.

The entire flight lasted about 10 hr, and was carried out by the Washington University aircraft alone. The entire mission was carried out in an alternating ferry-dolphin-ferry...sequence.

5.2 Summary

The August 2, 1976, sampling mission consisted of a box flight enclosing the lower Ohio River Valley. The region was reasonably clean, with peak b_{scat} of approximately $2 \times 10^{-4} m^{-1}$ and maximum sulfate concentration of approximately 8 $\mu g/m^3$.

The horizontal traverses indicated a north-south gradient with increased haze along the Kentucky-Tennessee border area. From St. Louis, Missouri, to Louisville, Kentucky, the levels of b_{scat} were near 1, with little variation either horizontally or vertically. The southern leg encountered higher levels of all aerosol parameters, with a more pronounced vertical structure, indicating the effect of several urban and point sources. Thus, this mission yields information about the isolated contribution of emissions within the box.

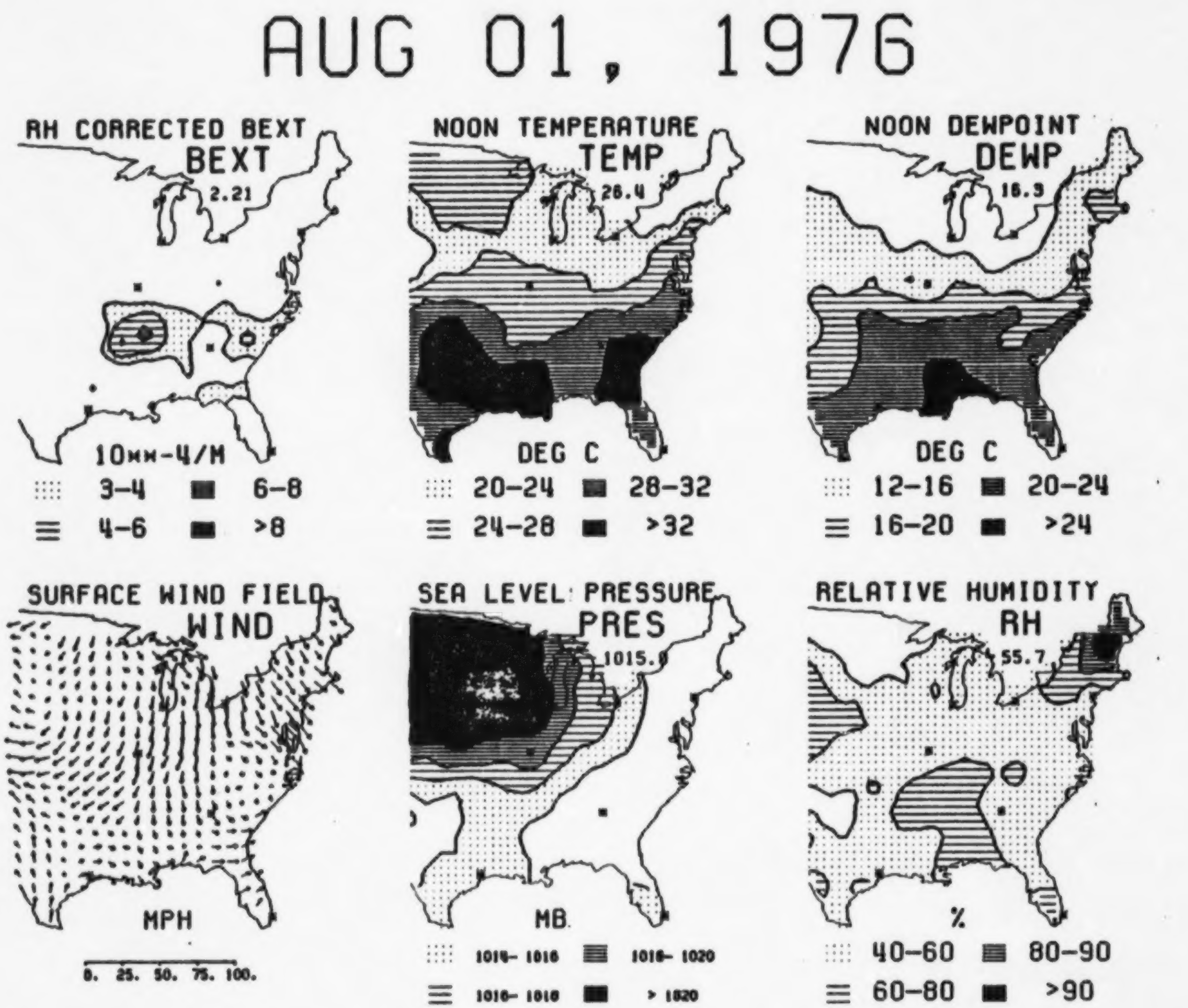

Figure 5-1. August 1, 1976—a large hazy air mass was centered south and east of St. Louis, Missouri. Temperature and dewpoint were relatively low, with northerly winds.

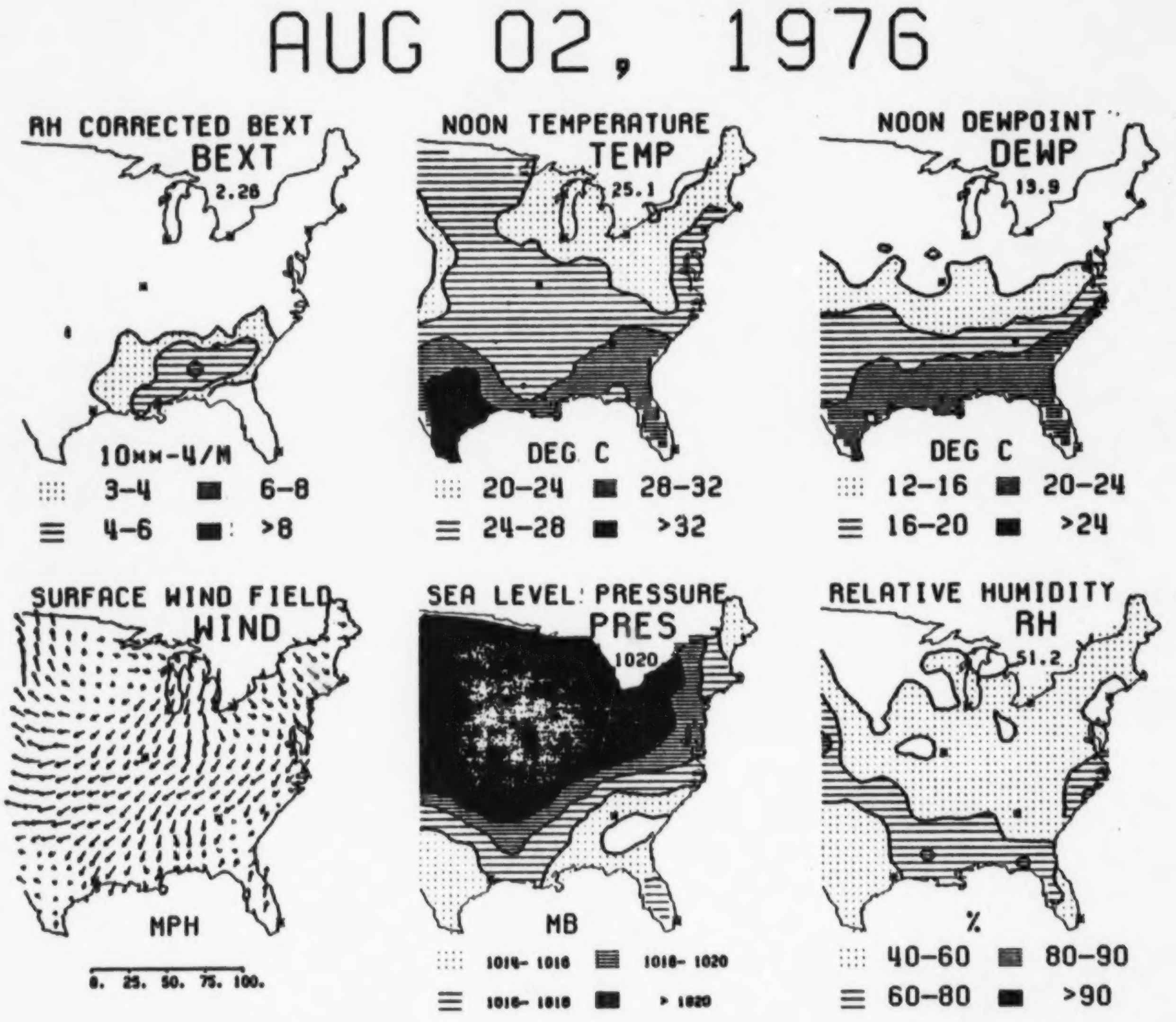

Figure 5-2. August 2, 1976—the region of haze moved south of the flight pattern by August 2nd. The Ohio River Valley region had good visibility with low RH. Winds are out of the north to the northeast.

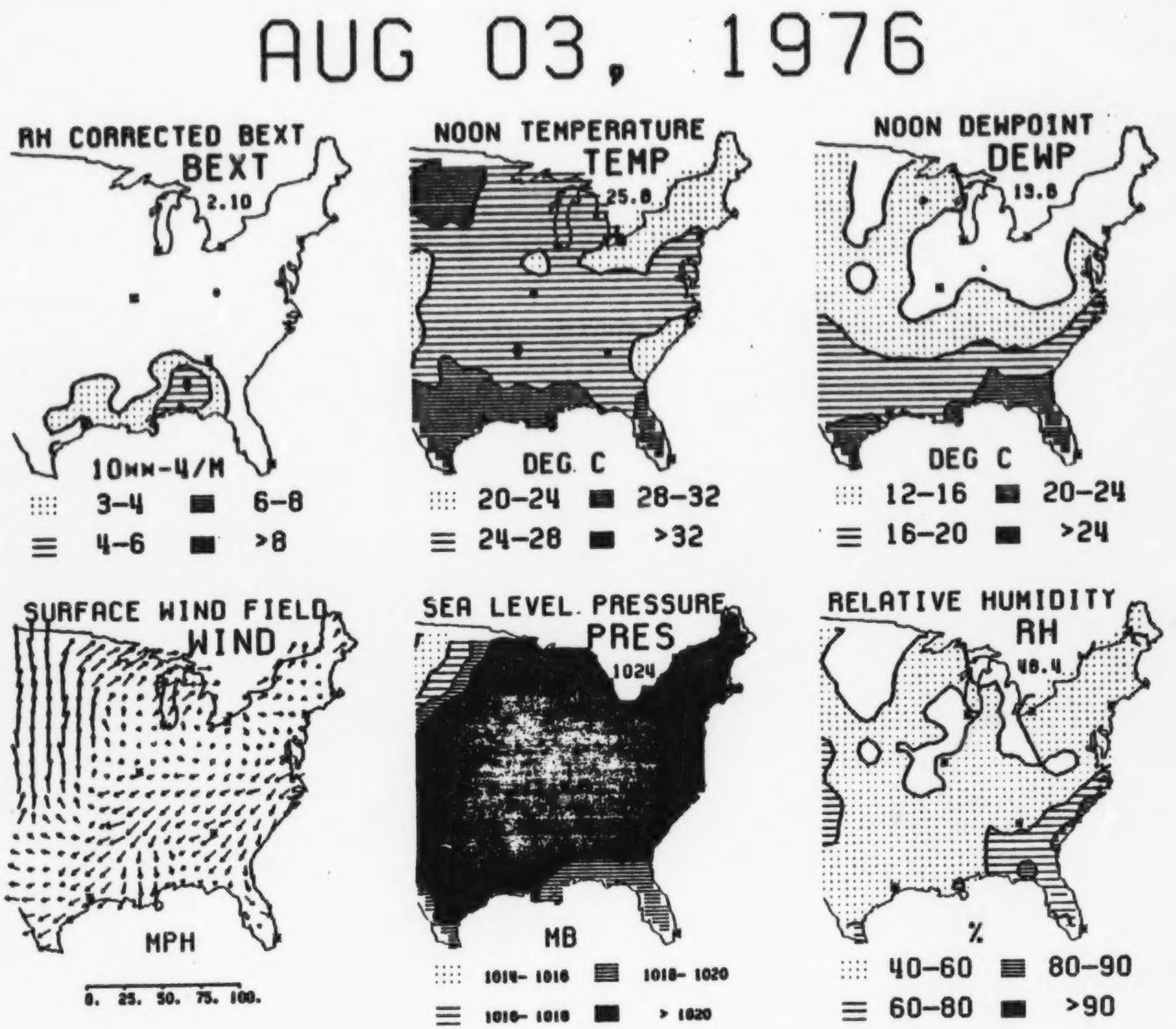

Figure 5-3. August 3, 1976—a large clean cool dry high-pressure system covers the entire eastern United States on the day after this flight.

TABLE 5-1. FLIGHT OUTLINE, AUGUST 2, 1976
(Cartridge No. 022)

Event No.-	Type	ALT (m MSL)	Route	Time (CDT)
1.	Ferry	690	A - B	1111 - 1128
2.	Dolphin	420-1200	B - C	1128 - 1139
3.	Ferry	540	D - E	1141 - 1151
4.	Dolphin	420-1350	E - F	1151 - 1207
5.	Ferry	570	F - G	1209 - 1221
6.	Dolphin	450-1410	G - H	1222 - 1241
7.	Ferry	810	H - I - J - K	1242 - 1303
Landing/T.O.		-	Louisville, Ky.	1310 / 1420
8.	Ferry	600	M - N	1443 - 1501
9.	Dolphin	640-1890	N - O	1502 - 1518
10.	Ferry	600	O - P - Q	1518 - 1531
11.	Dolphin	600-1800	Q - R - S - T	1532 - 1549
12.	Ferry	540	T - U - V - W	1551 - 1606
13.	Dolphin	600-1650	W - X	1606 - 1620
14.	Ferry	600	X - Y	1622 - 1629
15.	Dolphin	450-2220	Y - Z - A'-B'	1631 - 1651
16.	Ferry	600	B' - C'	1653 - 1707
17.	Dolphin	450-1950	C' - D'	1708 - 1727
18.	Ferry	750	D' - E'	1727 - 1747
Landing/T.O.		-	Bowling Green	1751 / 1838
19.	Dolphin	390-2400	F'-G'-H'-I'	1841 - 1909
20.	Ferry	690	I' - C'	1910 - 1937
21.	Dolphin	450-2160	C'-J'-K'-L'	1938 - 2004
22.	Ferry	600	L'-M'-N'-O'	2005 - 2028
23.	Ferry	810	P' - Q'	2031 - 2047
Landing		-	Spirit	2056

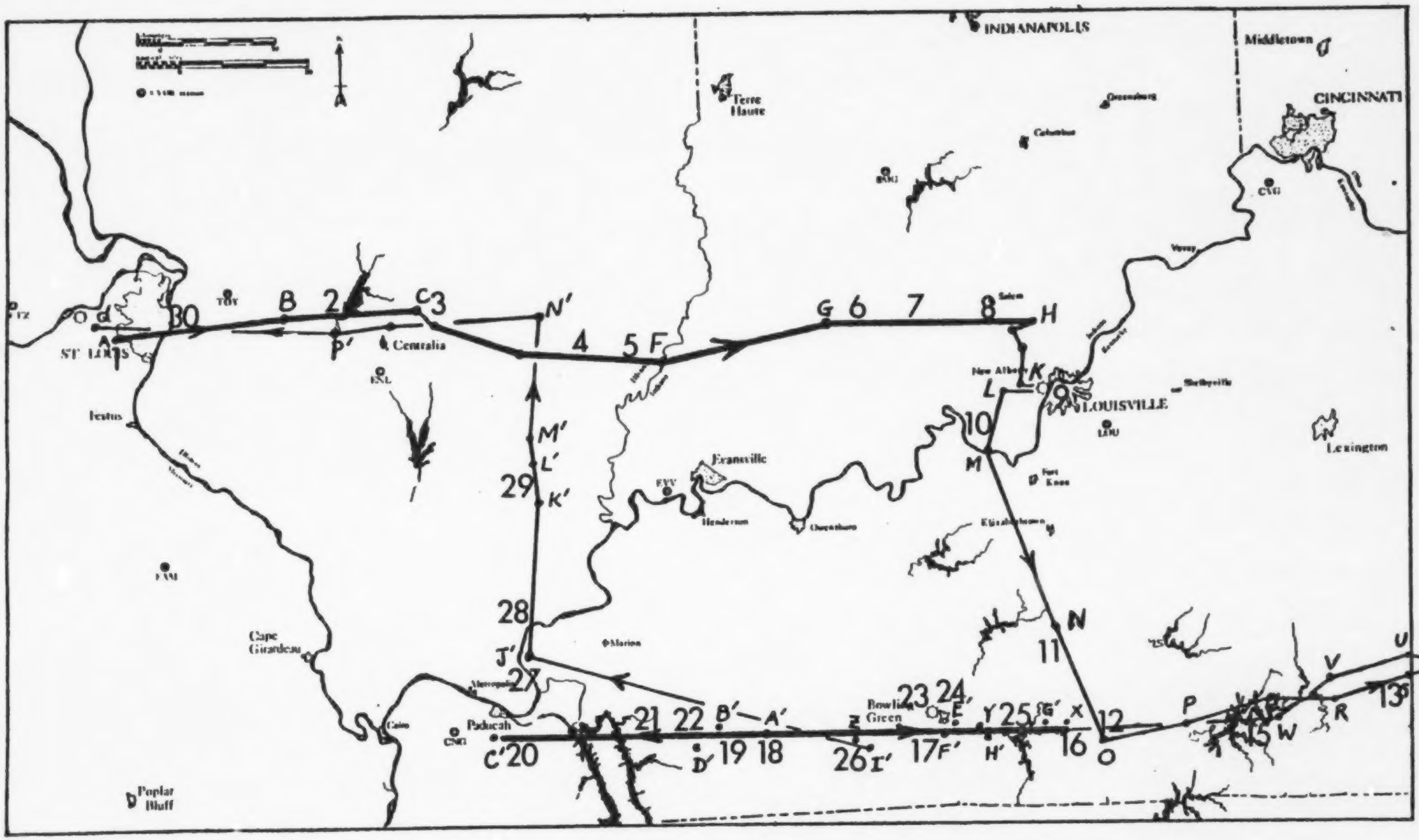

LOCATION OF AIRCRAFT SAMPLING ROUTES, August 2, 1976
Cartridge No.: 022

Figure 5-4. Map showing flight path and location of spirals for August 2, 1976. The numbers 1 through 30 indicate the positions of the spirals displayed in Figures 5-20 through 5-24.

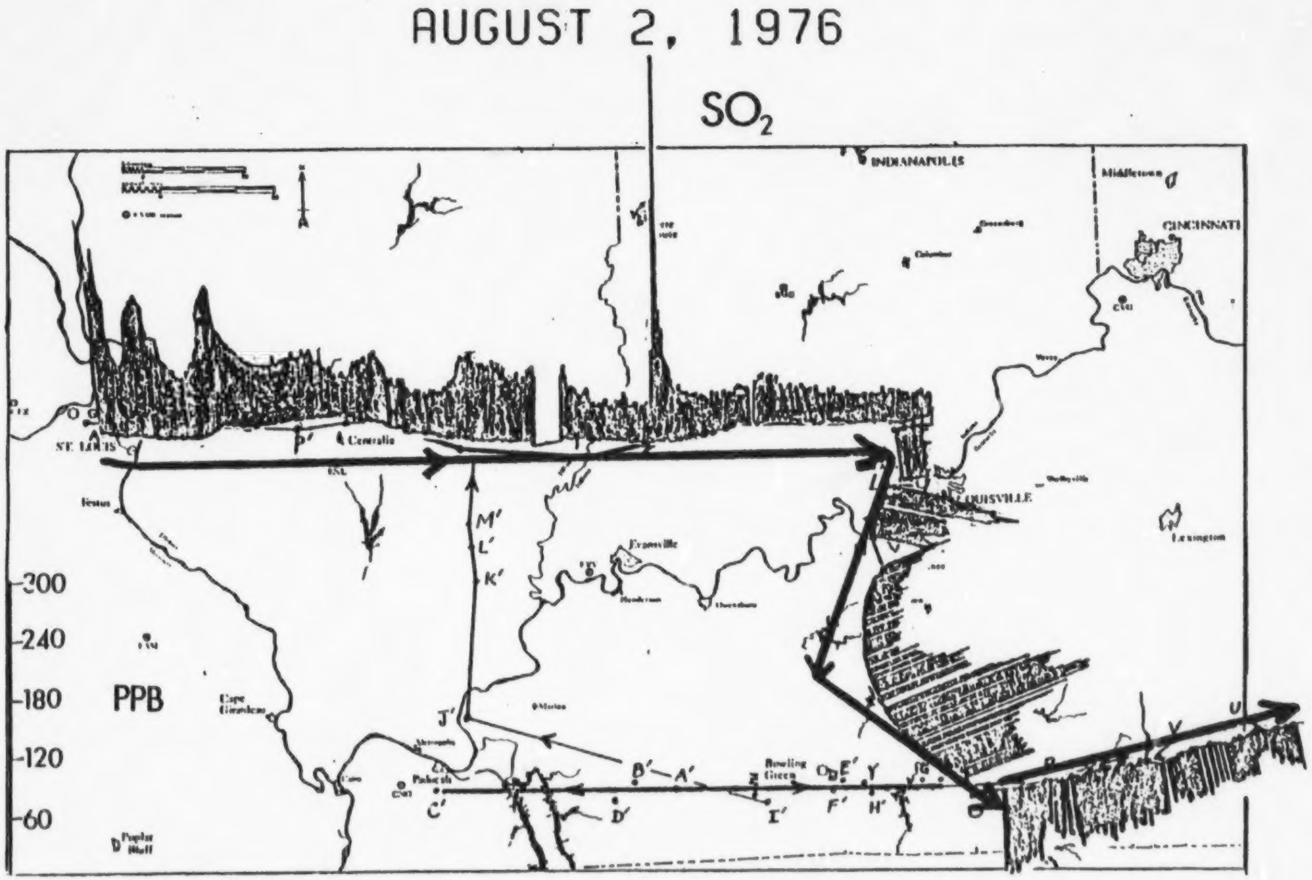

Figure 5-5. SO$_2$ concentration is generally higher along the southern edge of the box, with numerous individual plumes encountered near St. Louis and by the Illinois-Indiana border. Note: The systematic decrease-increase in concentration is due to the dolphin pattern of flight.

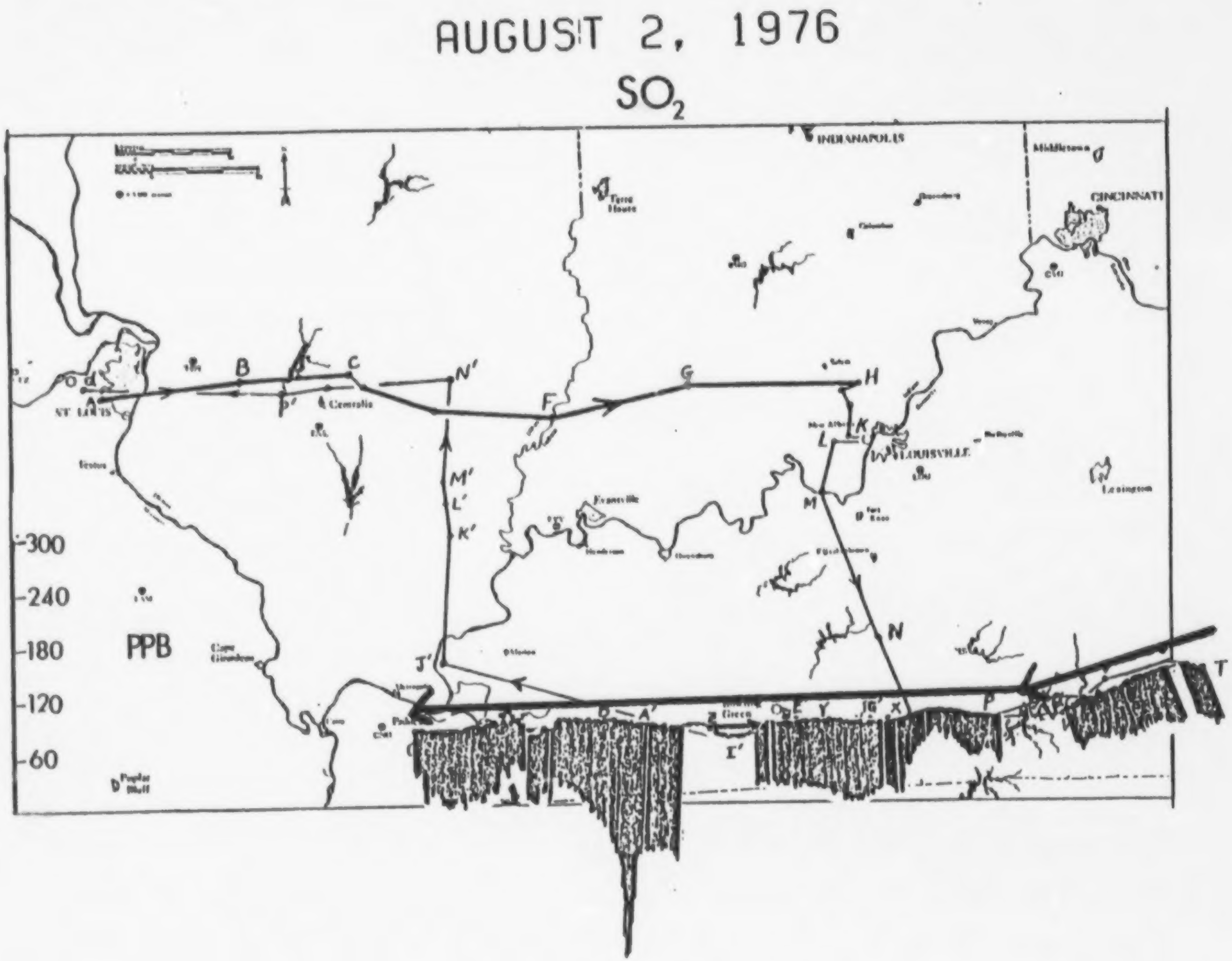

Figure 5-6. Continuation of SO_2 concentrations. Note: The systematic decrease-increase in concentration is due to the dolphin pattern of flight.

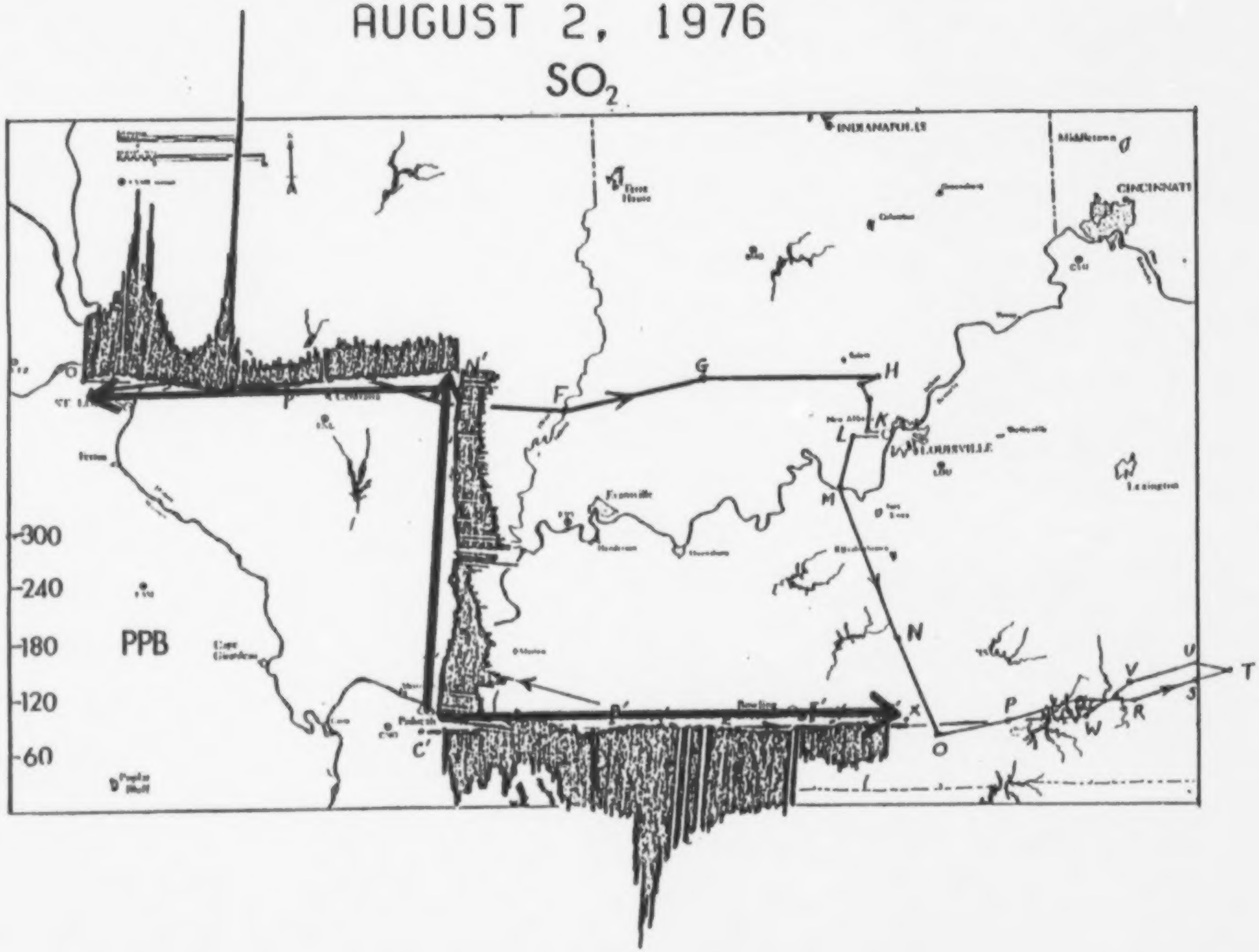

Figure 5-7. Continuation of SO_2 concentrations. Note: The systematic decrease-increase in concentration is due to the dolphin pattern of flight.

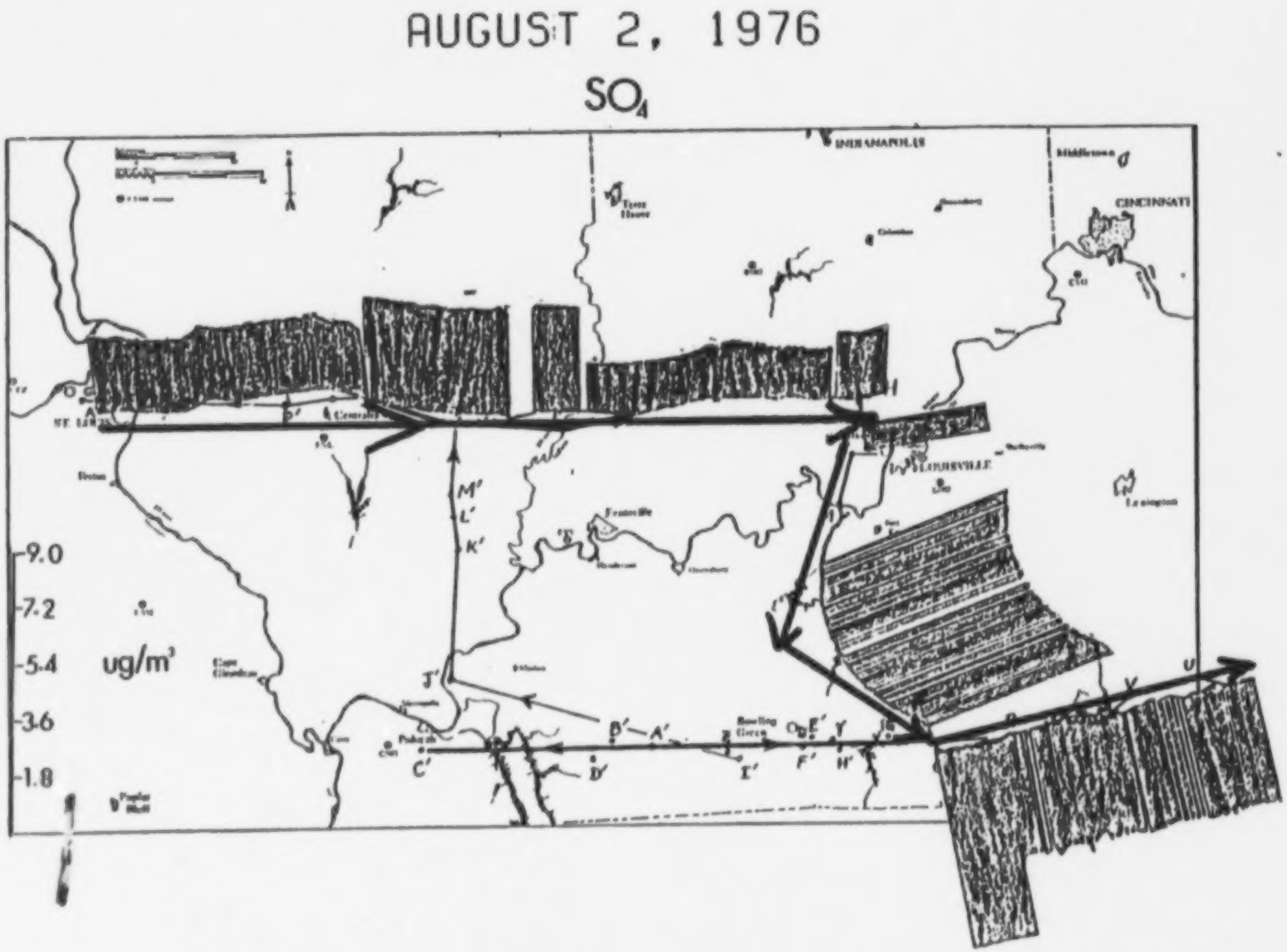

Figure 5-8. Sulfate concentrations are low over the entire area, with peak of about 8 $\mu g/m^3$ in the vicinity of Bowling Green. Note: The systematic decrease-increase in concentration is due to the dolphin pattern of flight.

AUGUST 2, 1976

SO_4

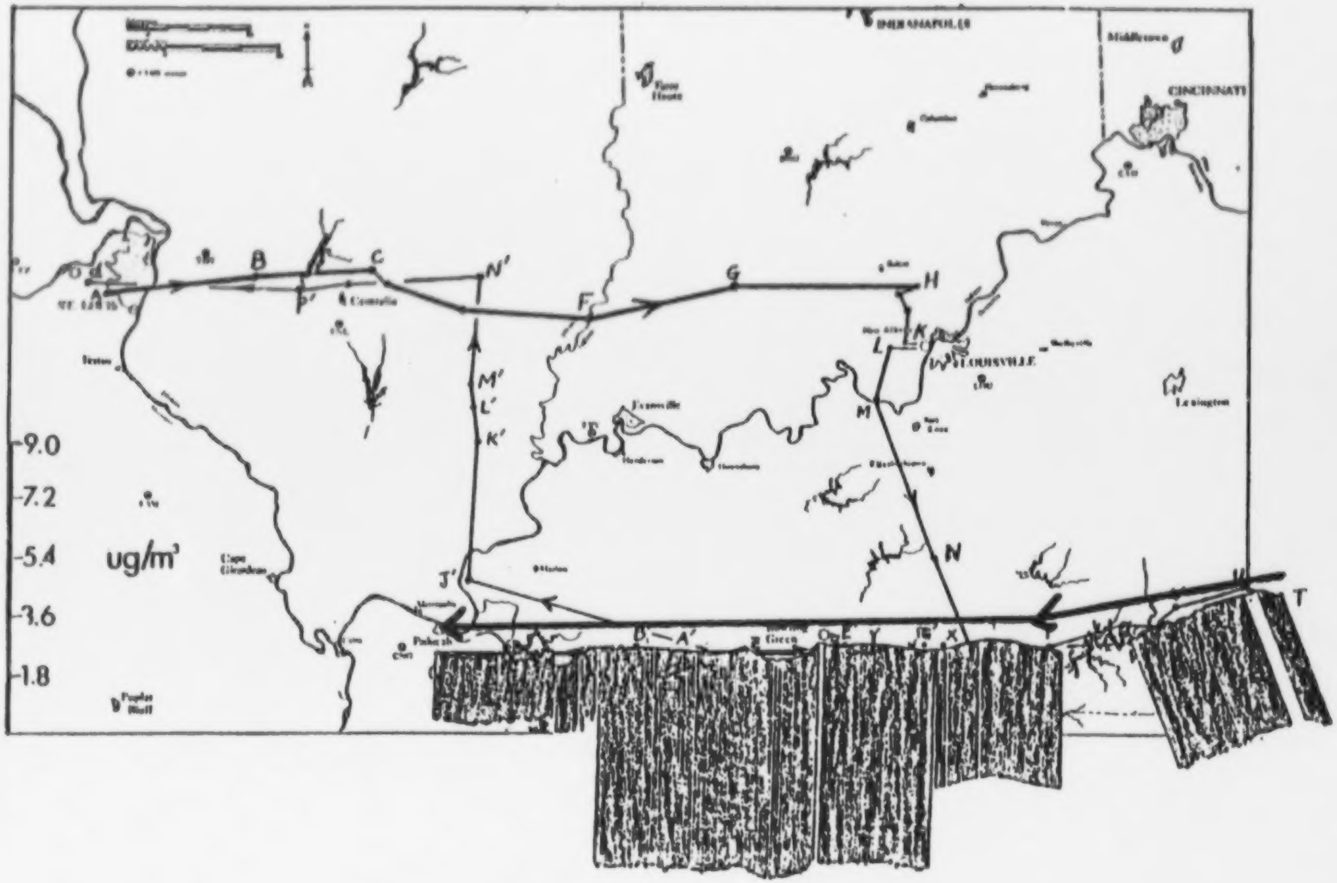

Figure 5-9. Continuation of sulfate concentrations. Note: The systematic decrease-increase in concentration is due to the dolphin pattern of flight.

AUGUST 2, 1976

SO_4

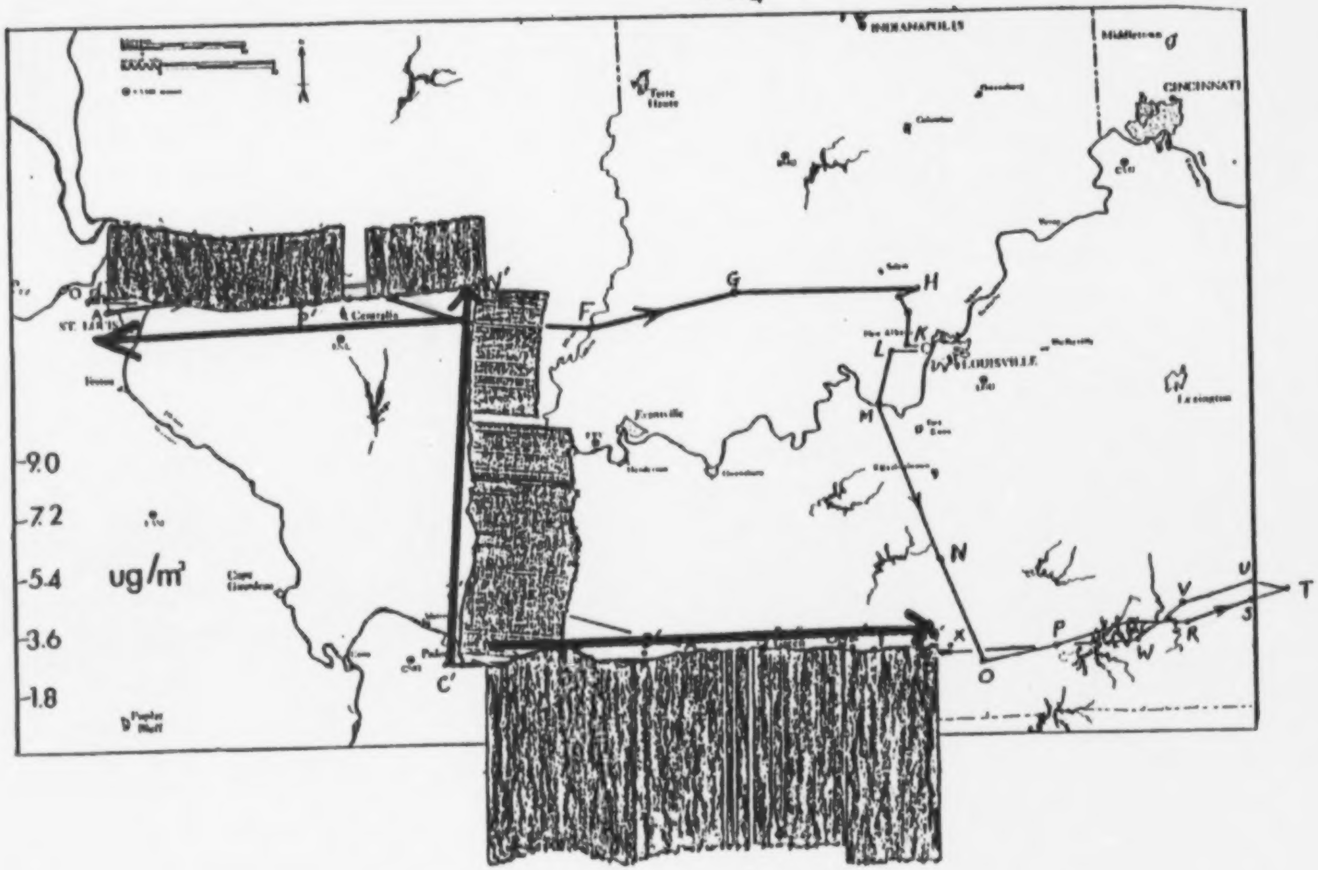

Figure 5-10. Continuation of sulfate concentrations. Note: The systematic decrease-increase in concentration is due to the dolphin pattern of flight.

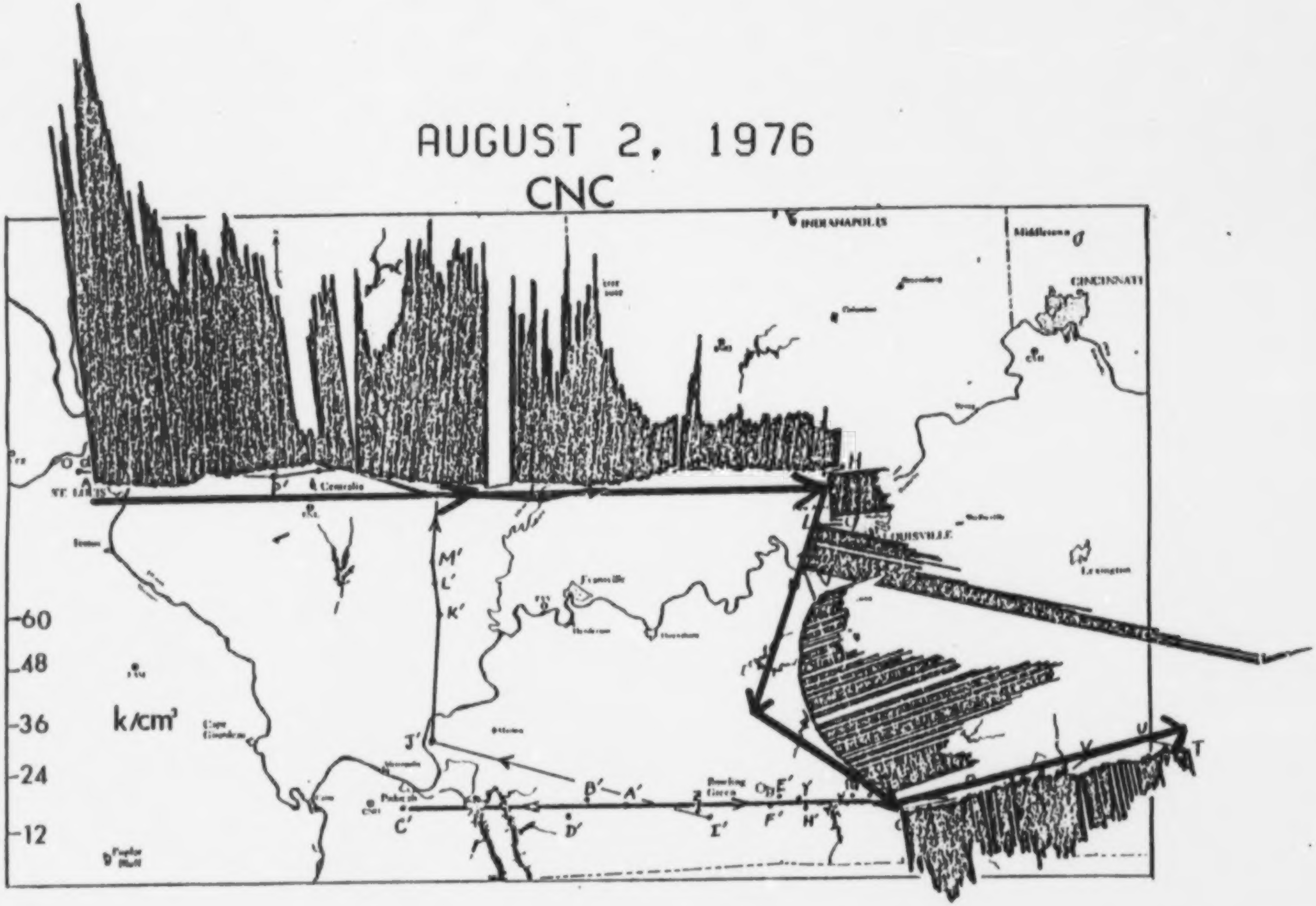

Figure 5-11. Condensation nuclei concentration is highest in central Illinois; apparently the southern region contains relatively more aged aerosol. Note: The systematic decrease-increase in concentration is due to the dolphin pattern of flight.

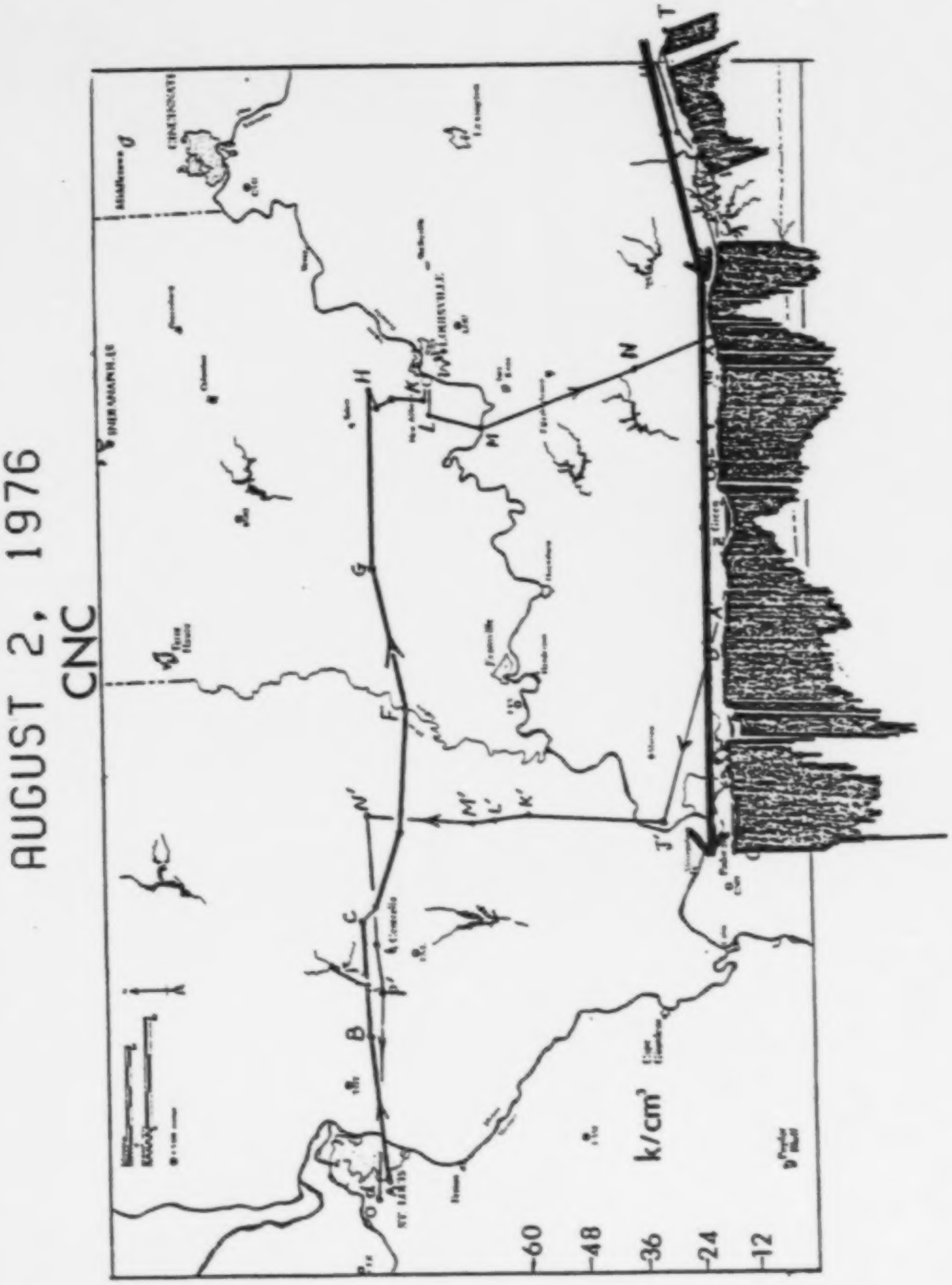

Figure 5-12. Continuation of condensation nuclei. Note: The systematic decrease-increase in concentration is due to the dolphin pattern of flight.

AUGUST 2, 1976

CNC

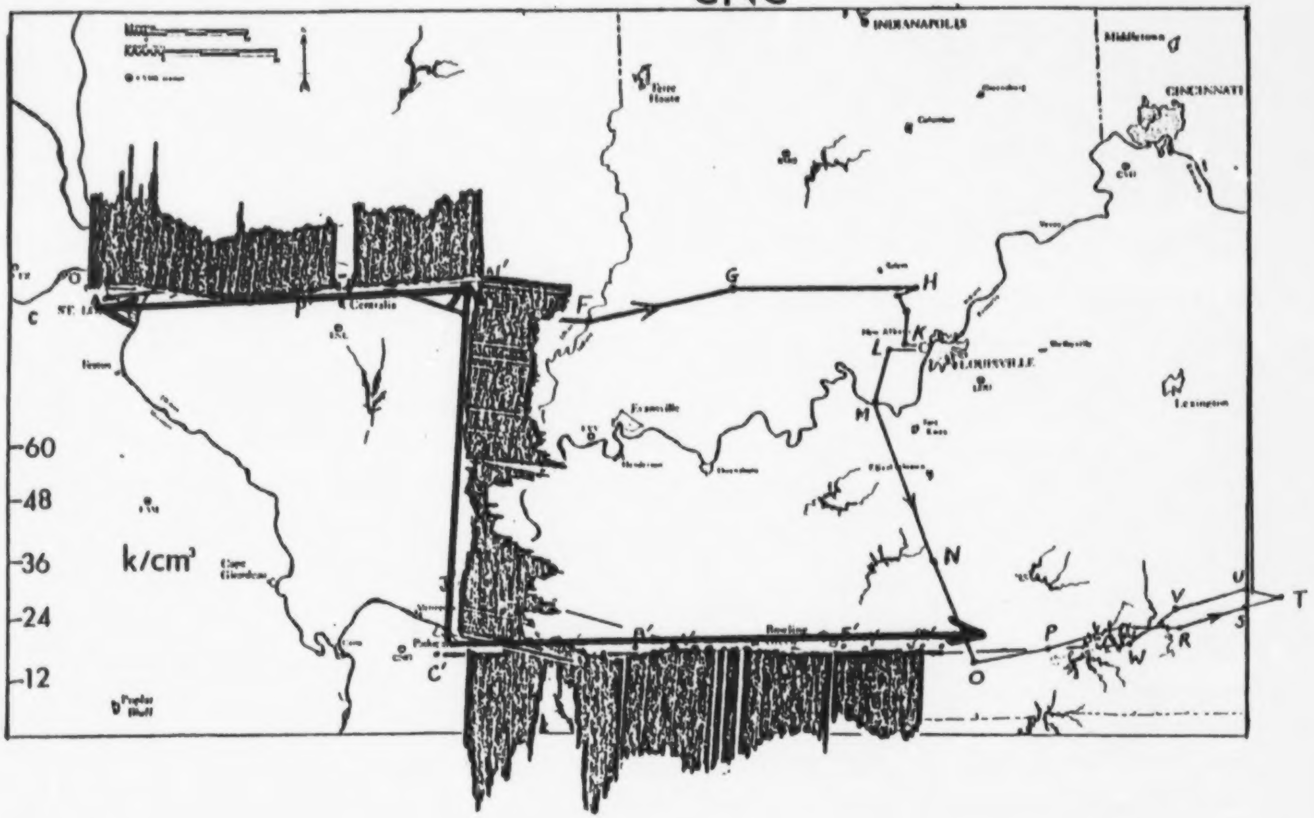

Figure 5-13. Continuation of condensation nuclei. Note: The systematic decrease-increase in concentration is due to the dolphin pattern of flight.

AUGUST 2, 1976

CHARGE

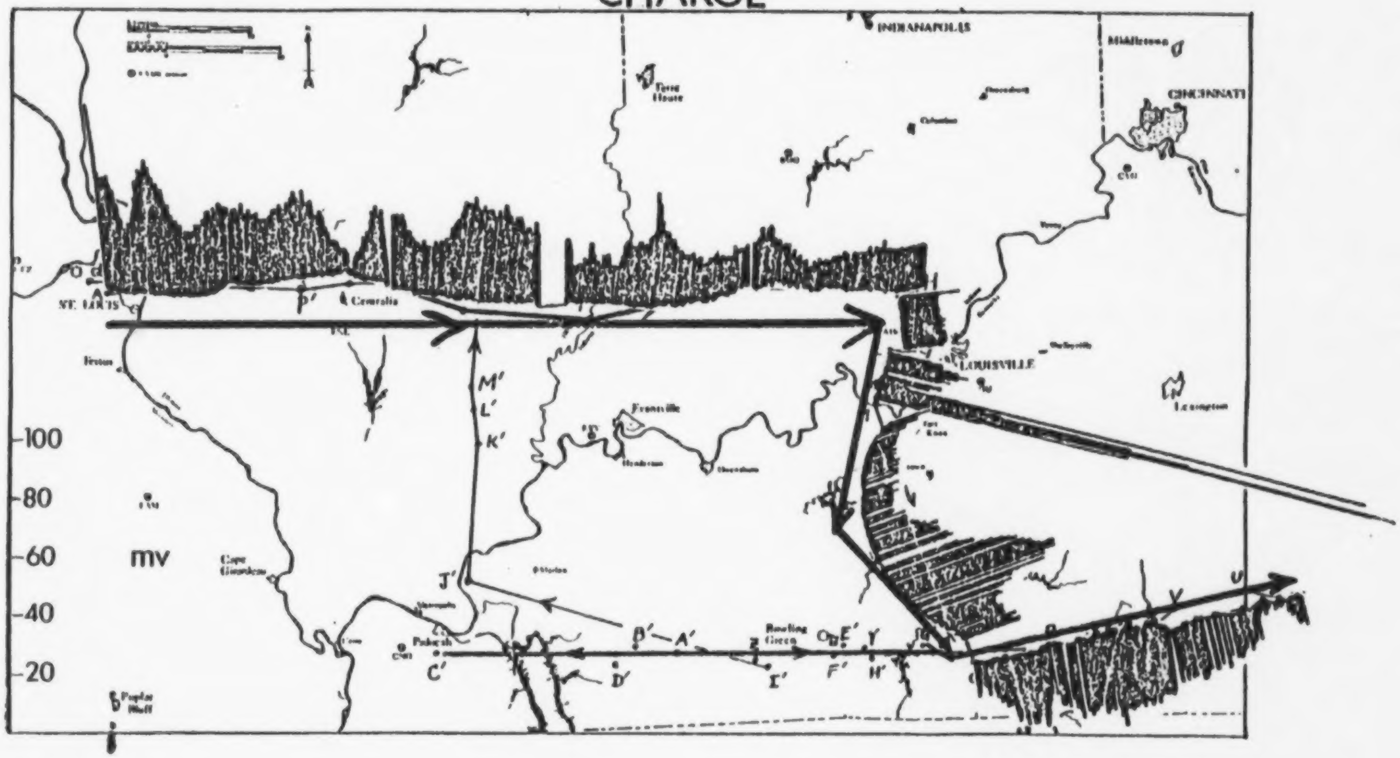

Figure 5-14. Aerosol charge also peaks along the stretch between Paducah and Bowling Green. Note: The systematic decrease-increase in concentration is due to the dolphin pattern of flight.

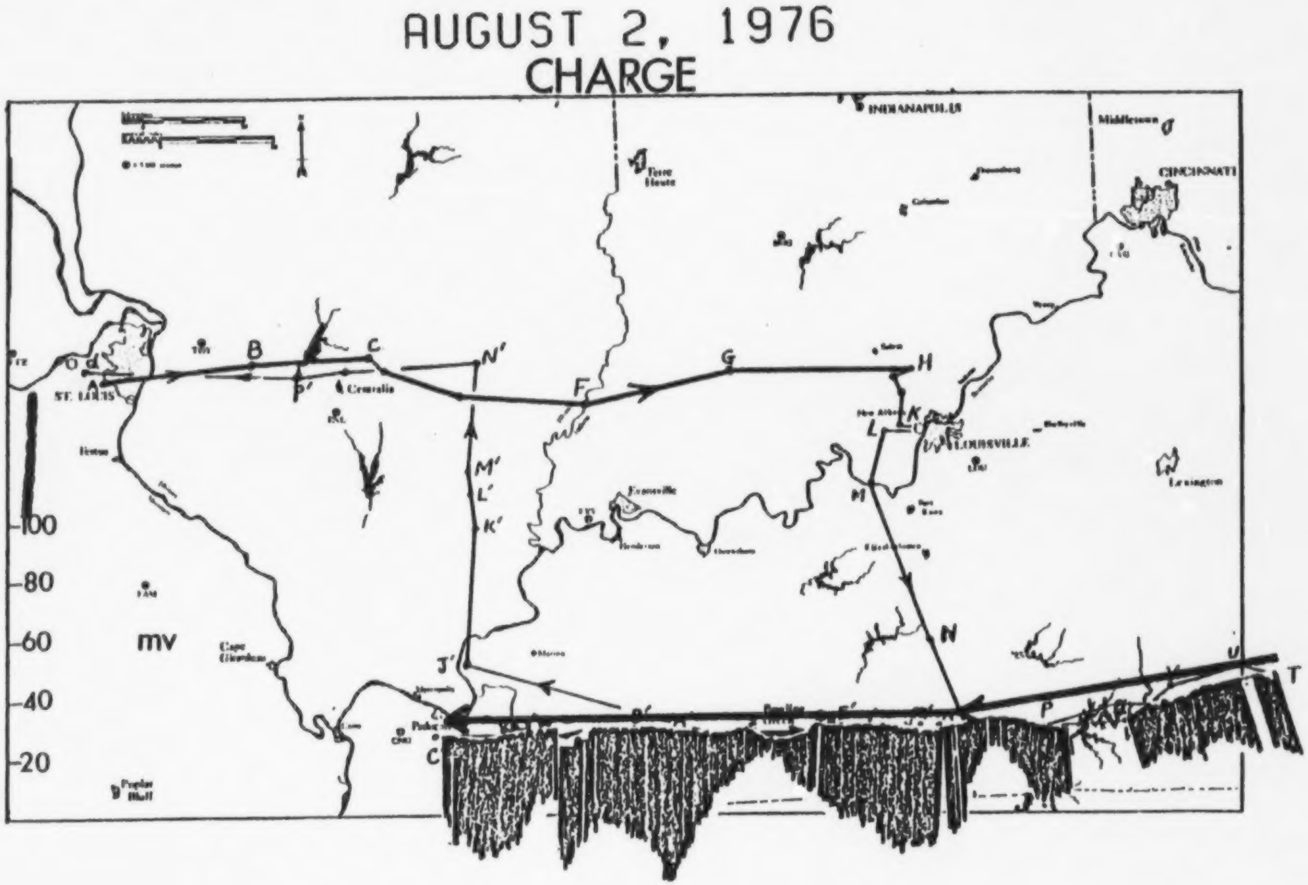

Figure 5-15. Continuation of aerosol charge. Note: The systematic decrease-increase in concentration is due to the dolphin pattern of flight.

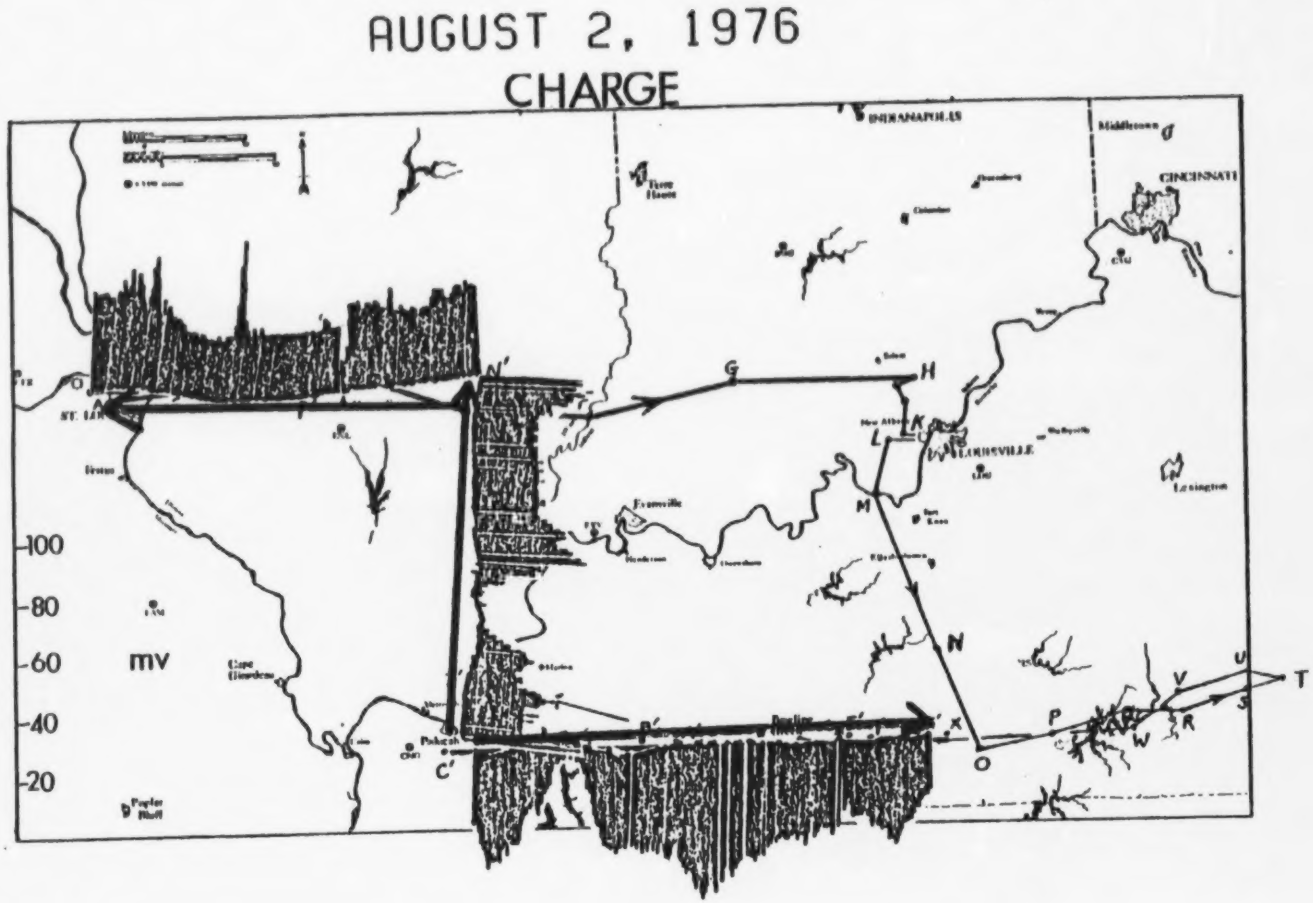

Figure 5-16. Continuation of aerosol charge. Note: The systematic decrease-increase in concentration is due to the dolphin pattern of flight.

AUGUST 2, 1976

B_{SCAT}

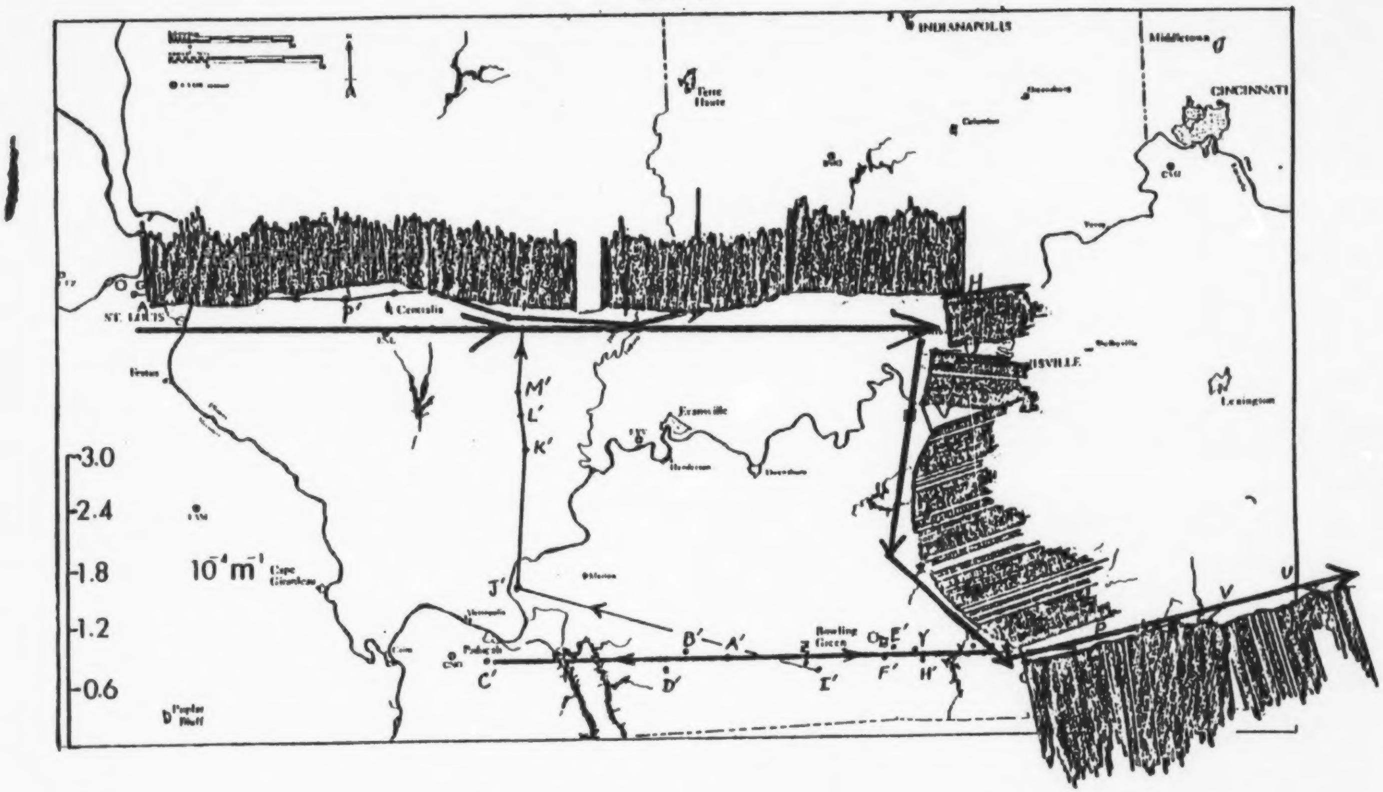

Figure 5-17. B_{scat} is much higher along the southern leg of the flight. This was a relatively clean day, especially in central Illinois, with b_{scat} typically less than $1 \cdot 10^{-4}m^{-1}$. Note: The systematic decrease-increase in concentration is due to the dolphin pattern of flight.

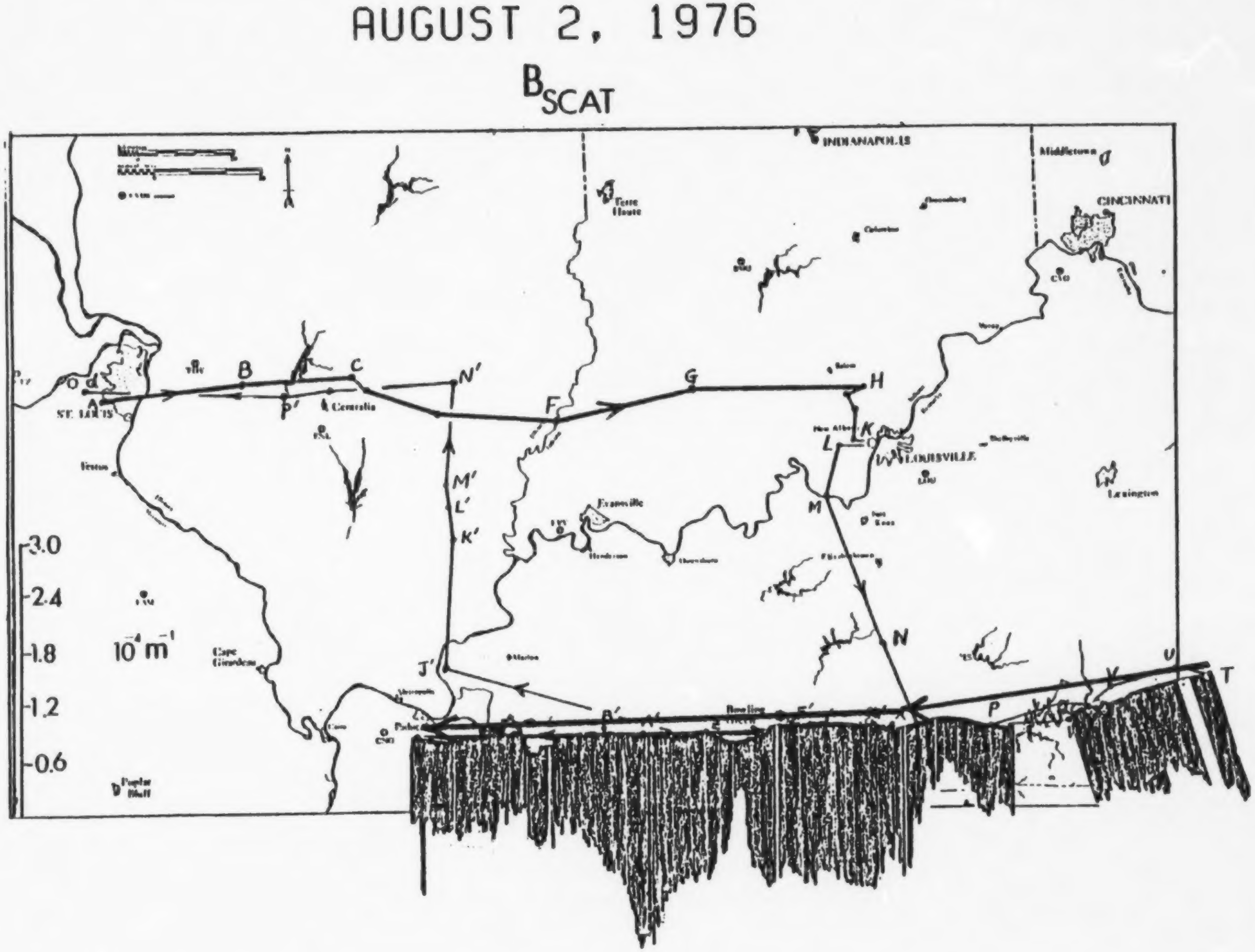

Figure 5-18. Continuation of b_{scat} concentrations. Note: The systematic decrease-increase in concentration is due to the dolphin pattern of flight.

AUGUST 2, 1976

B_{SCAT}

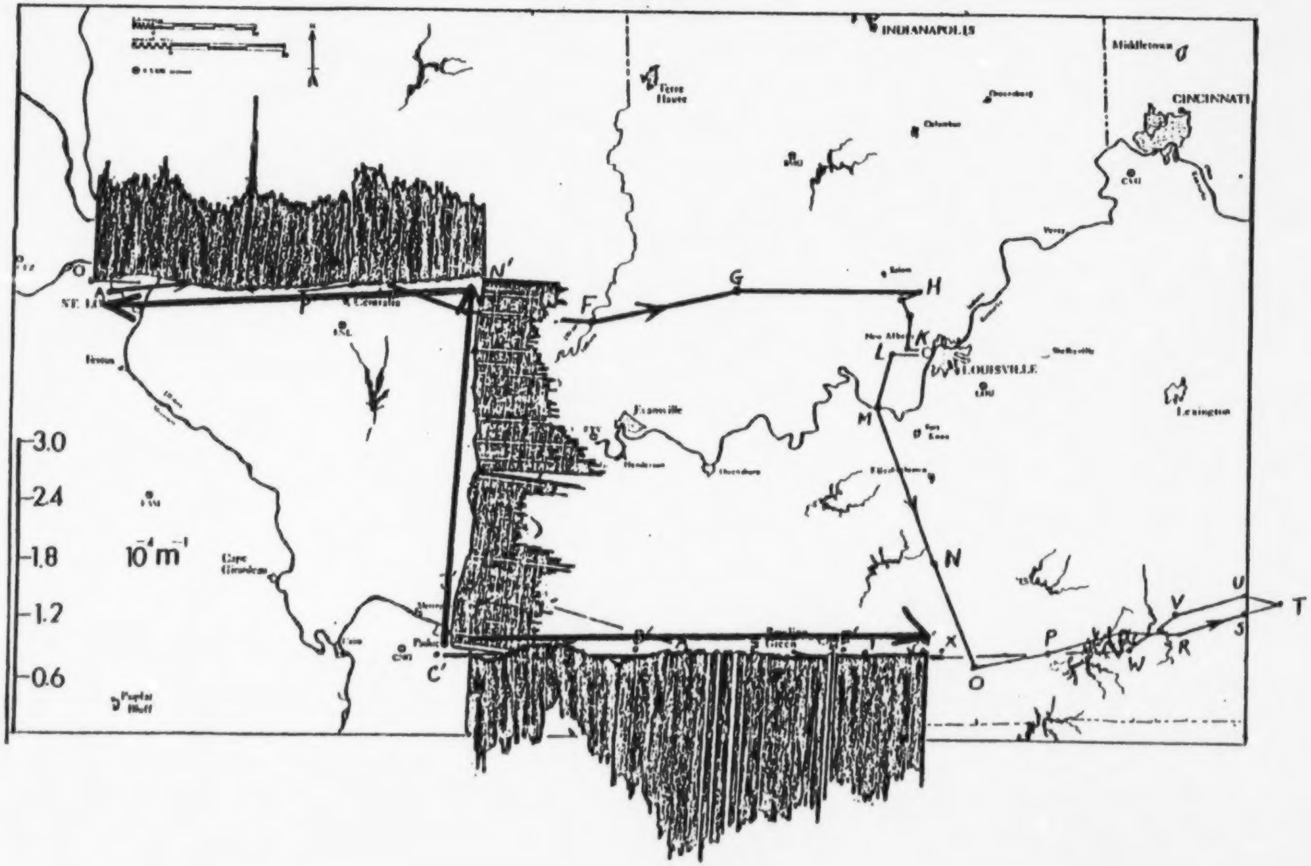

Figure 5-19. Continuation of b_{scat} concentrations. Note: The systematic decrease-increase in concentration is due to the dolphin pattern of flight.

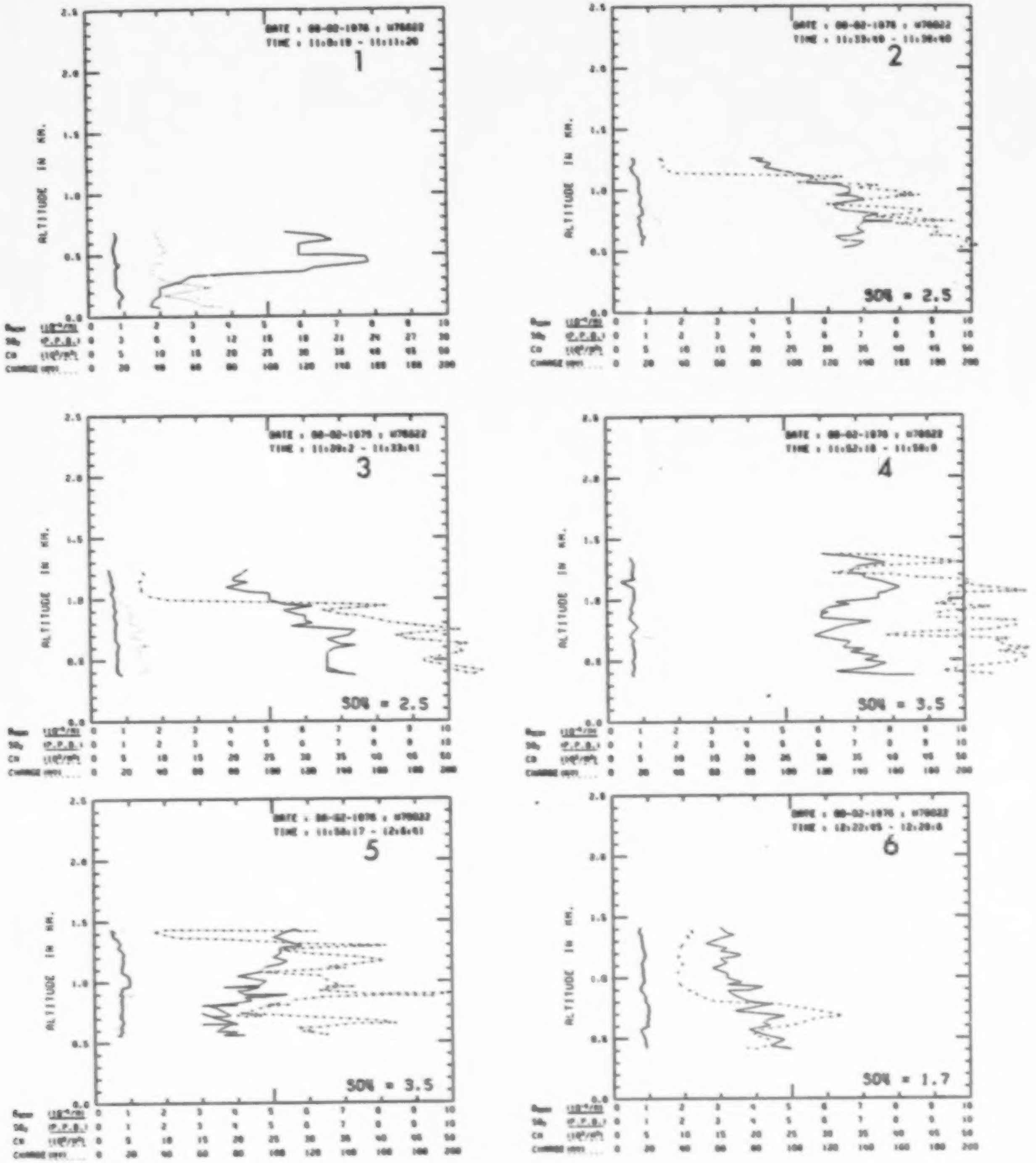

Figure 5-20. Along the line from St. Louis to Louisville, near noon, b_{scat} is relatively uniform with respect to height and is below $1 \cdot 10^{-4} m^{-1}$.

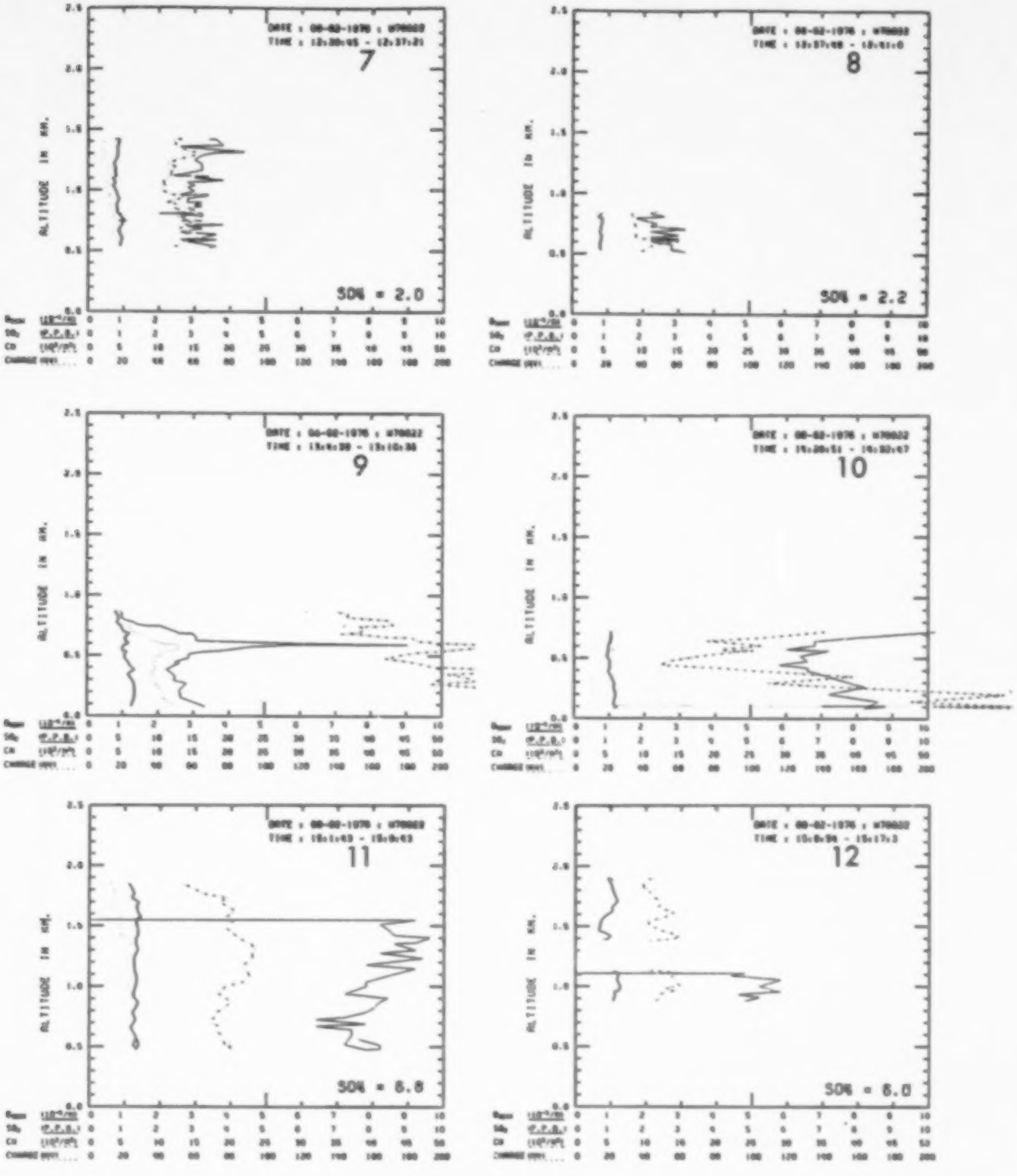

Figure 5-21. Spirals 7 and 8 display the same vertical profiles of b_{scat} along the northern leg of the mission. Near Louisville, b_{scat} is slightly above 1 in the early afternoon. Spiral 11 indicates a very uniform profile of light scattering aerosol.

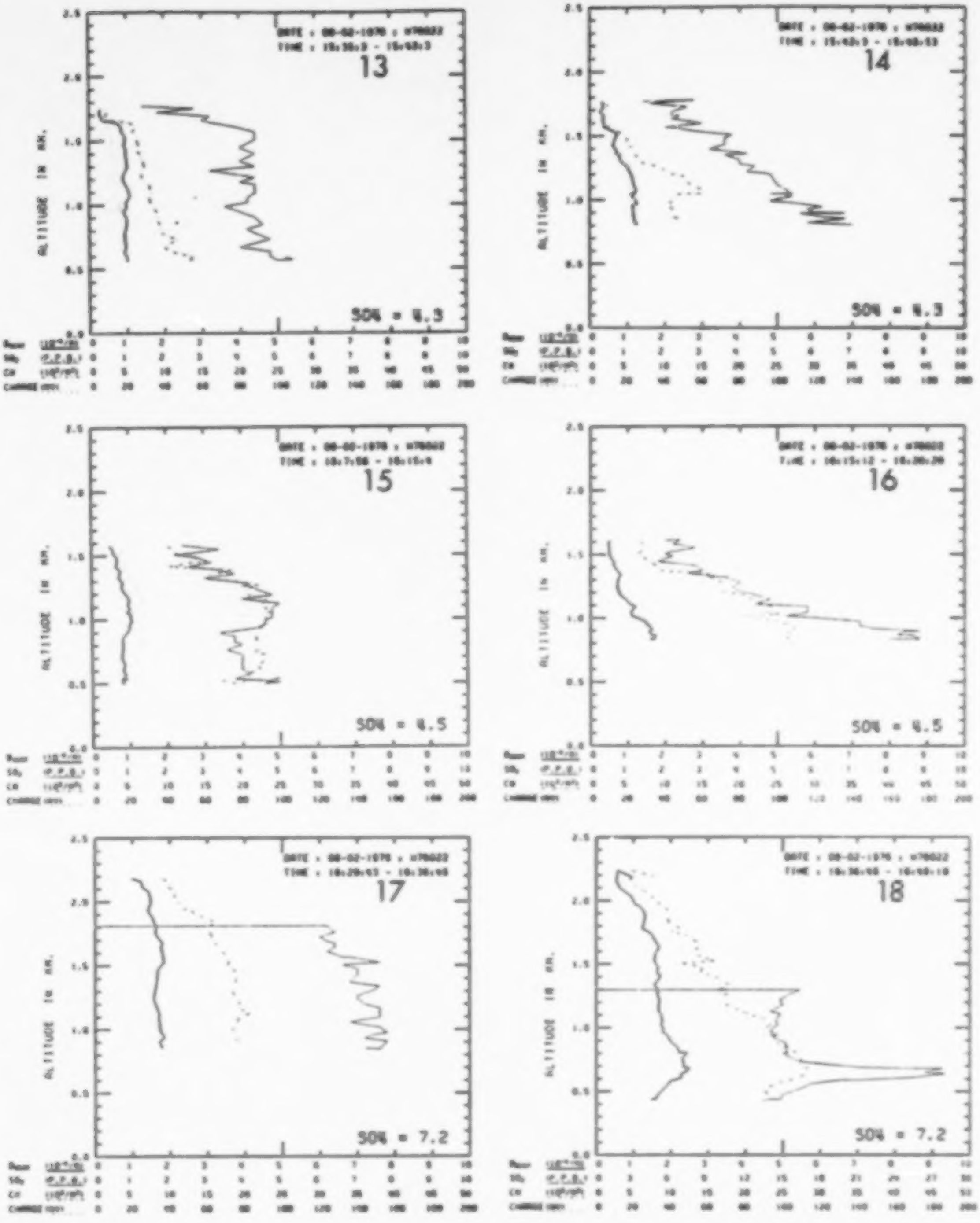

Figure 5-22. On the eastern corner of the sampling path there is a well-mixed 1,600-m layer with b_{scat} = 1. Spiral 17, near Bowling Green, exhibits b_{scat} of 1.5. Spiral 18 indicates an SO_2 plume with associated b_{scat} peak of 2.5.

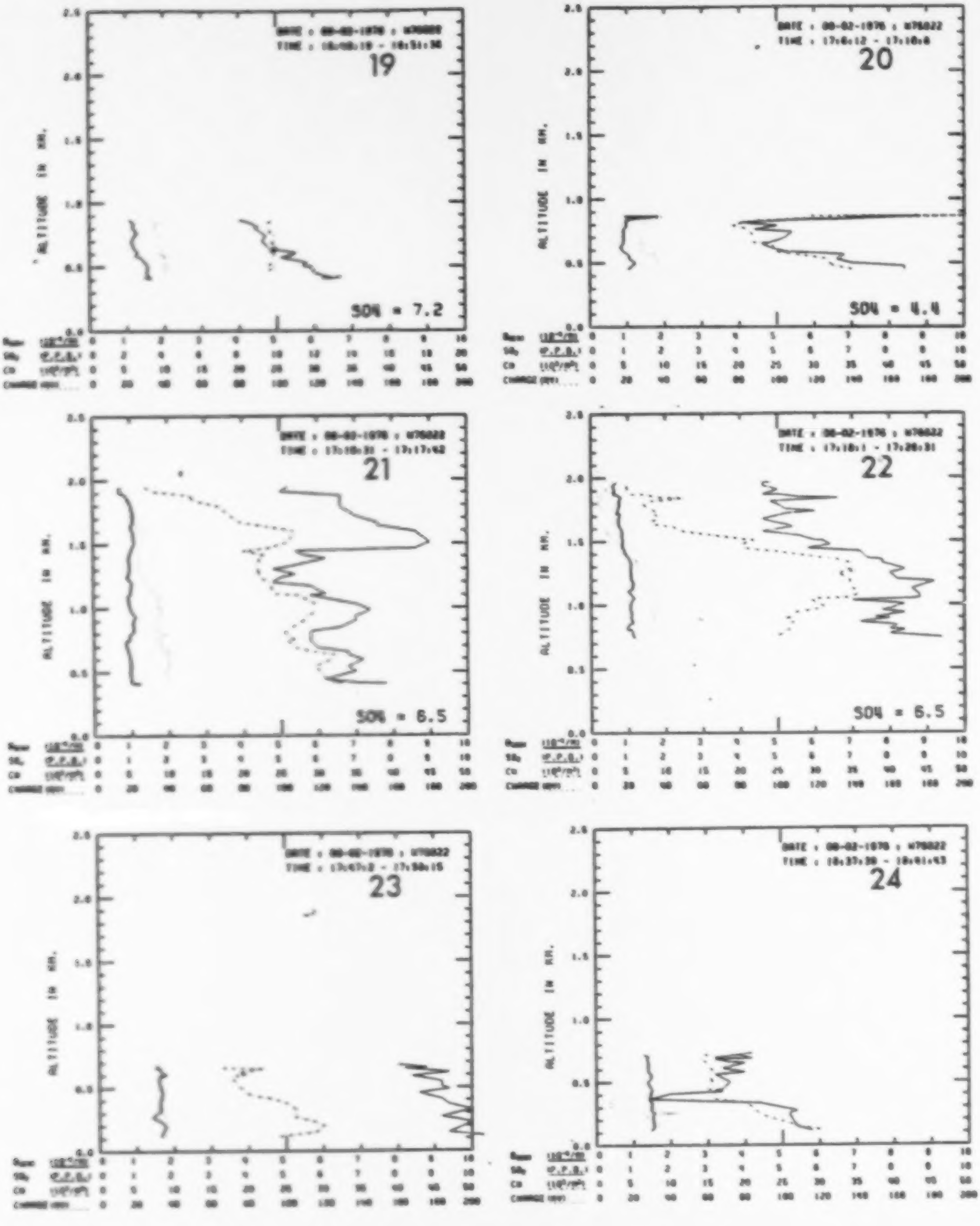

Figure 5-23. South and east of Paducah (spirals 20-22) the light scattering coefficient has again dropped to $1 \cdot 10^{-4} m^{-1}$ with little vertical structure. Near Bowling Green (23 and 24), b_{scat} is measured at 1.5-2.

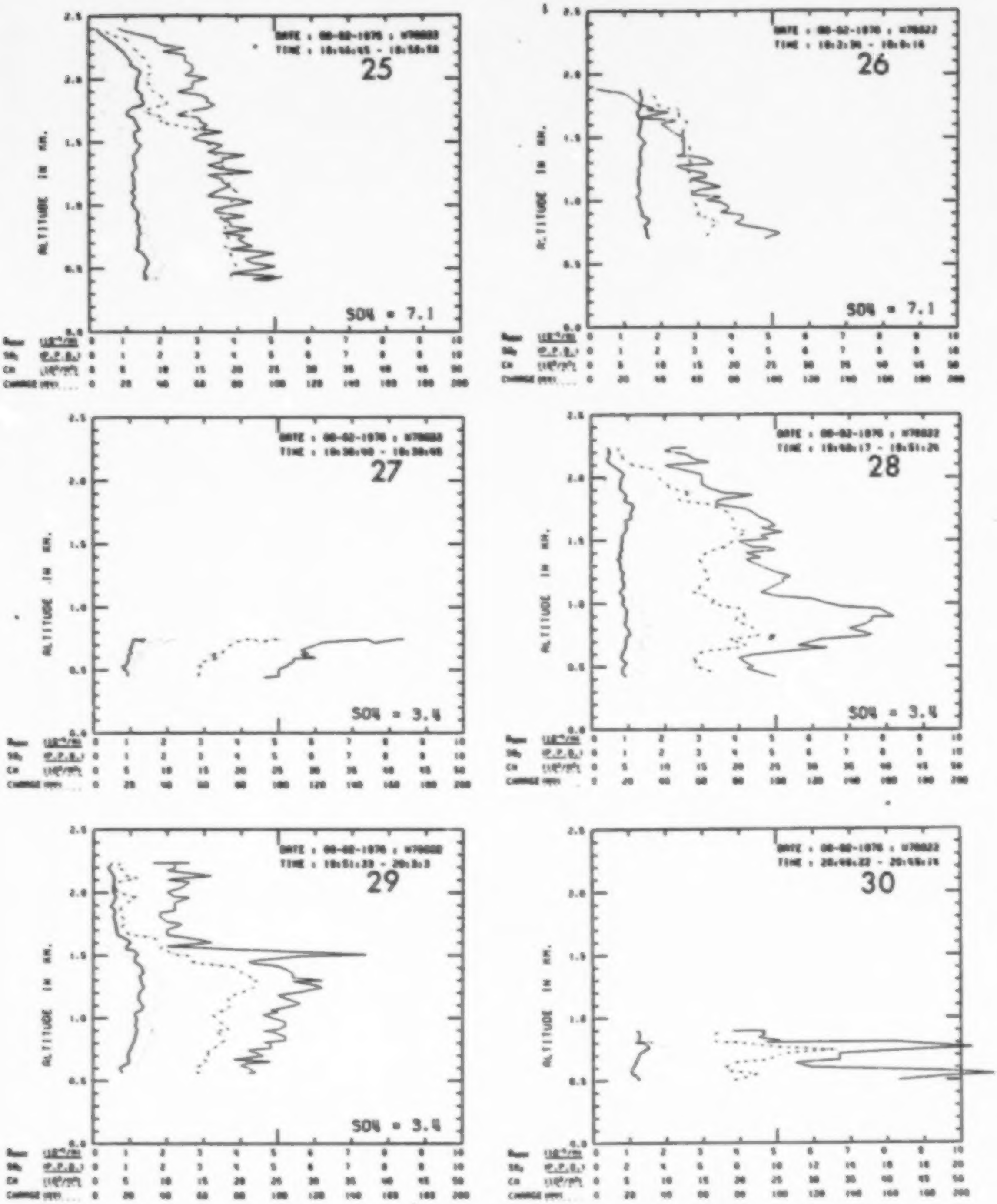

Figure 5-24. About 1900 CDT, south of Bowling Green, b_{scat} is 1-1.5, again with no obvious layering. From points J' to K' (spiral 28), b_{scat} is below 1 and well mixed.

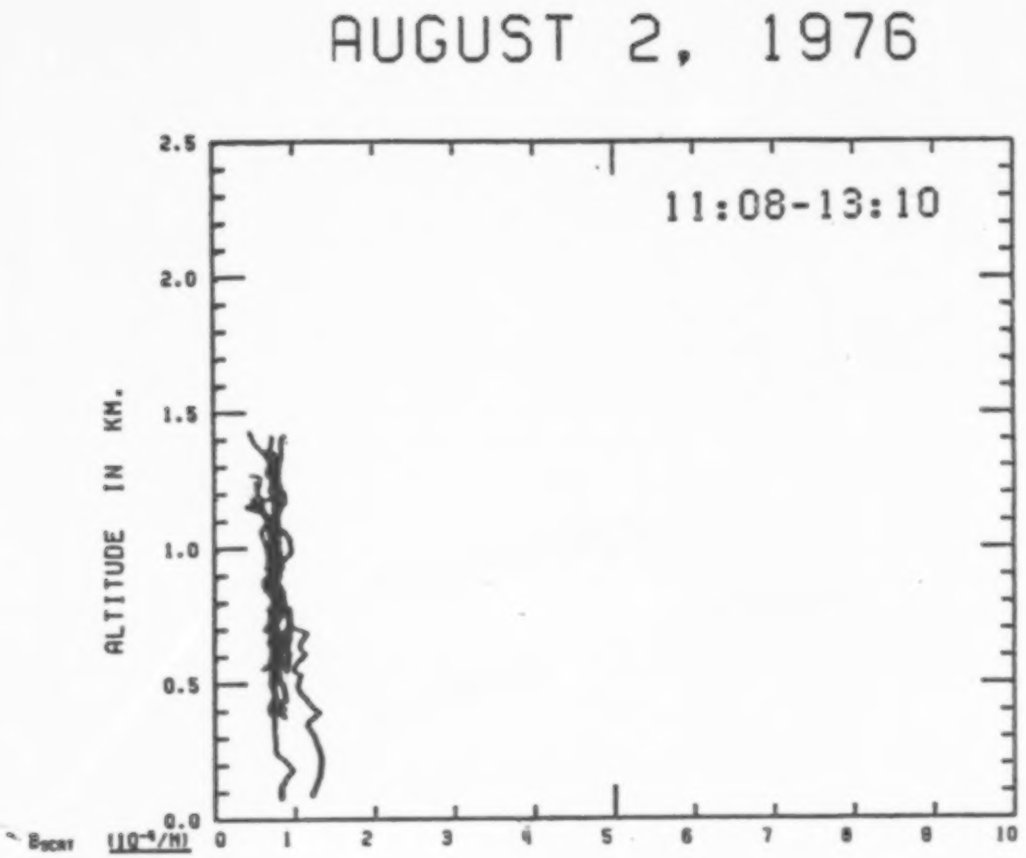

Figure 5-25. Overlay of soundings 1-9. Along the northern leg from St. Louis to Louisville there is little vertical structure around noon; b_{scat} is near 1 within the lowest 1,400 m, with sulfate 2-3 $\mu g/m^3$.

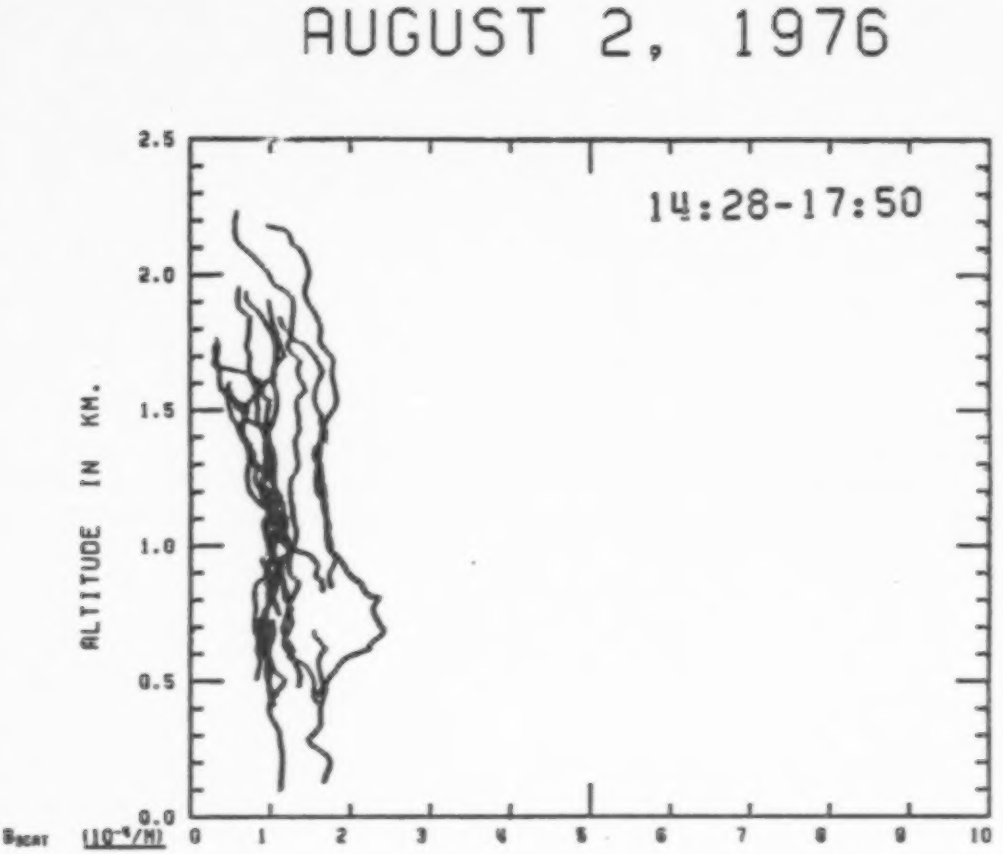

Figure 5-26. Overlay of soundings 10-23. Along the southern leg, 1500-1800 CDT, b_{scat} is slightly higher at 1-2, with evidence of several layers of haze and sulfate 4-7 μg/m^3.

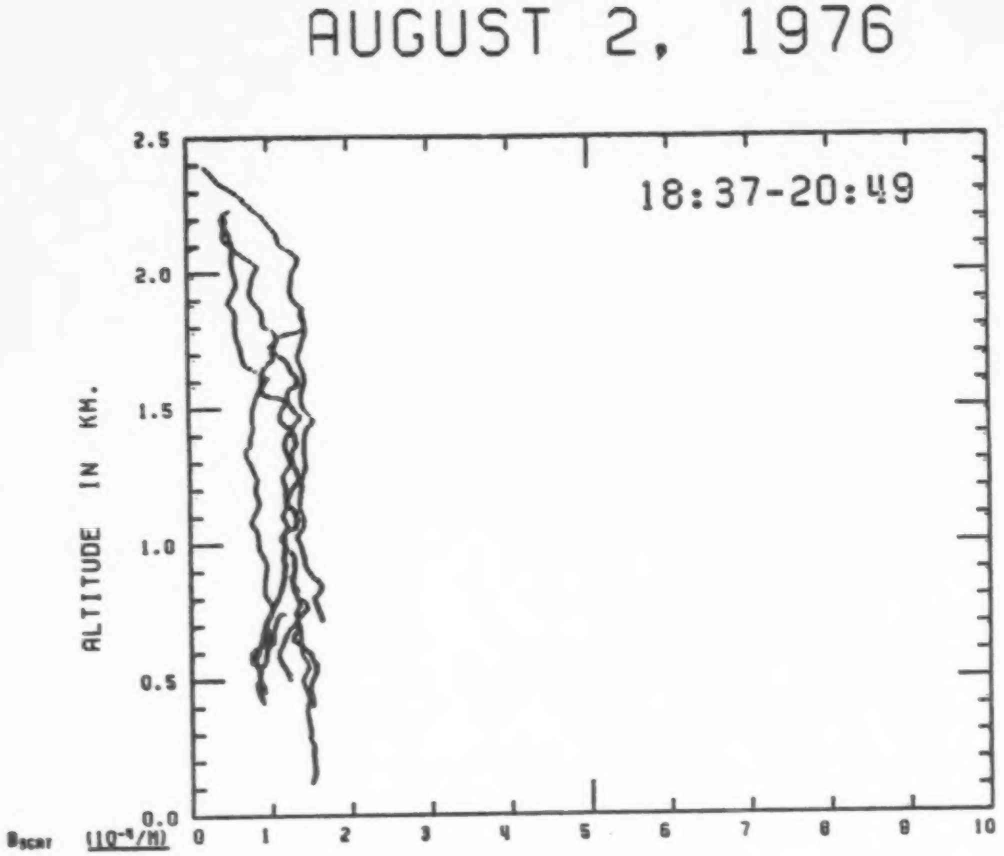

Figure 5-27. Overlay of soundings 24-30. Returning north in the early evening b_{scat} drops from 1.5 to below 1, with sulfate again near 2 $\mu g/m^3$.

6.0 CONCLUSIONS

Four days' sampling missions from Project MISTT have been presented in graphical form as an aid in designing future regional scale aircraft experiments. The July 29-30, 1975, mission caught a major sulfate and haze episode and was designed to provide detailed cross sections of the air mass at a few discrete distances. The August 10, 1975, flight obtained measurements across three Midwestern States at a single altitude. A new approach of the alternate ferry-dolphin sequences was adopted for the July 30, 1976, mission, which concentrated on characterizing the pollutant gradients along an east-west and north-south radial. The ferry-dolphin technique was used again for the August 2, 1976, experiment to "box in" a section of the Ohio River Valley.

These attempts to characterize large air masses encountered two major problems: (1) balancing the need for large horizontal coverage versus the vertical resolution, and (2) designing methods to conveniently examine the data generated on a large spatial-temporal scale.

ACKNOWLEDGMENT

This report draws upon the extensive data base of project MISTT. We wish to acknowledge the participants of the project for preparation of the data volumes, with special appreciation to Meteorology Research, Inc., for preparation of the daily weather summaries, flight outlines, and flight maps for the July 29-30, 1975, and August 10, 1975, flights.

GROUND MEASUREMENTS OF REGIONAL HAZE

Kenneth T. Whitby* and Peter H. McMurray

University of Minnesota, Minneapolis, Minnesota

Abstract

This report describes some of the first results from physical and chemical measurements on the haze measured during the STATE study in Tennessee during the summer of 1978. These results show that most of the haze aerosol mass can be accounted for by sulfate in equilibrium with water. There is good agreement between the size distributions measured by a low pressure impactor (LPI) and those measured by the electrical aerosol analyzer (EAA). Also, aerosol volumes computed by assuming that the aerosol is H_2SO_4 in equilibrium with water agree within 20 percent of the volumes measured by the EAA, and LPI sulfur values agree within 30 percent of those measured by X-ray fluorescence. These data also suggest that the aerosol is partly neutralized H_2SO_4 and that the aerosol is internally mixed.

Findings from a recent analysis of the aerosol formation and growth in the St. Louis urban plume (Whitby, 1979) are reviewed. Analysis of aerosol measurements in the St. Louis urban plume on July 18, 1975, showed nuclei formation rates of up to several hundred $cm^{-3}hr^{-1}$. Nuclei formation rates and ozone formation rates correlated well with the ground-level ultraviolet intensity. Aerosol volume formation rates of up to 6.7 $\mu m^3 cm^{-3} hr^{-1}$ during the middle of the day were observed. These also appeared to correlate well with the ultraviolet radiation. Using a simple aerosol growth model based on the experimental results, the total weight of secondary aerosol formed in the plume during one irradiation cycle was found to be 1,000 metric tons day^{-1}.

CHARACTERIZATION OF AEROSOL SULFUR IN PEPE'S

During August 1978, researchers on the University of Minnesota Mobile Laboratory (UMML)† used several independent but complementary measuring techniques to study chemical and physical properties of haze aerosols in Tennessee. These measurements included X-ray fluorescence (XRF) of filter samples collected with a dichotomous sampler, measurements of aerosol sulfur distributions collected with a low pressure impactor (LPI), measurements of the hygroscopic properties of aerosols with the tandem differential mobility analyzer (TDMA), and measurements of aerosol physical properties with the electrical aerosol analyzer (EAA) and optical particle counters (OPC).

---

*Speaker.

†Background material on the University of Minnesota Mobile laboratories is presented as an appendix to this report.

The low-pressure cascade impactor used in this study (design and calibration described by Hering et al., 1979) had five stages; the top stage had a lower cut at 0.5 μm, while the lower cut point for the bottom stage was 0.05 μm. This insured that virtually all of the accumulation mode aerosol mass was collected. Samples were collected on small stainless steel strips and analyzed by the flash volatilization technique described by Roberts and Friedlander (1976). The validity of the impactor results was checked by comparing the total sulfur mass detected on all five impactor stages with the total sulfur measured by XRF for samples collected during similar time periods. Results of this comparison are shown in Figure 1. Note that the two independent techniques agree to within about 30 percent.

If the aerosol is assumed to be sulfuric acid in equilibrium with ambient humidities, the aerosol volume associated with measured sulfur values can be calculated. Although the sulfate in the aerosol was probably partially neutralized by NH_3, this should still give a reasonable estimate for the volume. While H_2SO_4-$(NH_4)_2SO_4$ mixtures do exhibit hysteresis properties upon humidification and dehumidification, humidities must be reduced to extremely low values (~5-15 percent) to observe this effect. For summer haze in Tennessee, where humidities typically vary from 90 percent to 50 percent during the diurnal cycle, the particles are probably always supersaturated and hygroscopic properties of H_2SO_4 and H_2SO_4-$(NH_4)_2SO_4$ mixtures will be similar. This hypothesis is supported by Figures 2 and 3, taken from a report by McMurray and Liu (1978). Note from Figure 3 that hygroscopic properties of H_2SO_4-$(NH_4)_2SO_4$ solutions do not appear to vary a great deal with composition as humidities are decreased from 95 percent. With this assumption, total aerosol volumes measured with the EAA and OPC can be compared with those calculated from impactor sulfur data. Results of this comparison are shown in Figure 4. Note that impactor values are, on the average, about 20 percent higher than those measured with the EAA and OPC. This is remarkably good agreement, and supports the hypothesis that most of the aerosol volume in the haze is associated with sulfur. If this were not the case, one would expect EAA and OPC volumes to exceed the volume associated with the aerosol sulfur. Independent measurements to determine the volume associated with other constituents (e.g., nitrates and organics) are required for a better understanding of the aerosol.

If the aerosol sulfur distributions are converted to volume distributions by making the assumption discussed above, volume distributions measured with the LPI can be compared with those measured with the EAA and OPC. Results of a typical comparison are shown in Figure 5. Note that the agreement below 0.3 μm is quite good, but that the impactor detects more volume in the 0.3- to 1-μm size range. A possible explanation for this discrepancy is that the lower cut point for the top stage of the impactor was 0.5 μm. Therefore, any coarse particles that penetrated through the sampling system would also be collected on that stage. For future experiments, stages with larger cut points will be added to the impactor to test this hypothesis. If this is true, however, it follows that there is a considerable amount of sulfur associated with the coarse particle mode as well as the accumulation mode, which is generally assumed to contain most of the secondary aerosol volume.

It has been shown above that most of the aerosol volume in this continental haze can be accounted for by sulfur. Measurements of the hygroscopic properties of these aerosols with the TDMA gave some insight into the composition of these particles. [The TDMA was described in detail by Liu et al. (1978). Essentially, the instrument generates a monodisperse aerosol from a polydisperse aerosol (e.g., from ambient aerosol), manipulates the monodisperse aerosol (e.g., by humidification), and determines the new particle size after this manipulation.] Data collected during the night of August 5 and 6, 1978, are shown in Figure 6. In this figure, growth of the ambient aerosols with humidity is shown to agree favorably with laboratory data for growth of internally mixed solutions of H_2SO_4 and $(NH_4)_2SO_4$ in the molar ratio 1:3. Laboratory data for pure H_2SO_4 or for solutions that contained relatively more $(NH_4)_2SO_4$ did not agree as well. It was concluded that during these measurements, about 25 percent of the H_2SO_4 was neutralized by NH_3. The degree of neutralization did vary from day to day, but aerosols were generally found to contain more H_2SO_4 than $(NH_4)_2SO_4$.

The TDMA data can also be used to show that haze aerosols are internally mixed. If the haze aerosol consisted of several distinct types of particles, then it is likely that the hygroscopic properties of these particles would vary. Thus, if a monodisperse, dry aerosol were humidified (as is done in the TDMA), particles of several sizes would be expected. This was never observed. Humidification of a monodisperse aerosol always resulted in another (usually larger) monodisperse aerosol. This result was true for all particle sizes investigated (initial sizes at 10 percent humidity of 0.05, 0.07, 0.1, and 0.2 μm). These results are demonstrated by the data presented in Figure 7.

In conclusion, it appears that most of the haze aerosol volume can be accounted for by the volume associated with measured aerosol sulfur levels, if it is assumed that the sulfur is in the form of H_2SO_4 in equilibrium with ambient humidities. Comparisons of volume distributions measured by the EAA and OPC with sulfur distributions collected with the LPI suggests that there may be a significant amount of sulfur associated with coarse particles (larger than 1 μm). Studies of the hygroscopic properties of these haze aerosols suggest that the aerosol consists of partially neutralized H_2SO_4 and that the particles are internally mixed.

AEROSOL FORMATION IN URBAN PLUMES

Recently, Whitby (1979) did an analysis of the July 18, 1975, St. Louis urban plume measurements with the goal of determining the rate of aerosol formation during a daily irradiation cycle. Some of the more important results from that analysis and the implications for regional haze studies are presented here.

The principal conclusions from that analysis are as follows:

1. Nucleation rates exceeding 200 $cm^{-3}sec^{-1}$ were found in the St. Louis urban plume on July 18, 1975. The nucleation rate was found to correlate with the ultraviolet intensity.
2. Using a simple model in which it was assumed that the accumulation mode aerosol volume formation rate was proportional to the ultraviolet intensity, aerosol concentrations similar to those observed were predicted.

3. Using the above model, it was estimated that St. Louis produces about 1,000 metric tons per day of secondary aerosol in one irradiation day.
4. Our results agree with those of White et al. (1976) and Isaksen et al. (1978) that the entire secondary aerosol can be accounted for by assuming it is a sulfate such as H_2SO_4.

It will be noted that nothing has been said about conversion rates. The reason is that, except in the near-source region of plumes, the SO_2 concentrations and the concentrations of other gaseous precursors are so low that conversion rate calculations based on gaseous precursors are rather inaccurate. Rather, the approach that must be taken in urban plumes and in hazy areas is to determine the rates of formation of aerosol or other chemical species. Also, it is likely that as the concentration of SO_2 or other gases reaches low levels, the rates of aerosol formation are related in a more and more complex way to the concentrations of the gaseous precursors. Last summer we made an attempt to determine the rate of aerosol formation in the hazes of Tennessee. Although only a small part of the data has been analyzed, one episode in the Great Smoky Mountains of Tennessee was of such a nature that the growth rate could be calculated.

McMurray et al. (1978) found that the aerosol volume in the Smokies grew from 4 to 20 $\mu m^3 cm^{-3}$ over a 2-day period. At the same time, the b_{scat} grew from 0.3 to about 1.3 m^{-1}, or about 0.5 b_{scat} per day. Husar et al. (1976) states that the average growth of b_{scat} in the most hazy parts of the smog blobs he has been studying in the eastern United States is about 1 b_{scat} per day. Since the calculated growth rate for the St. Louis urban plume from this study is 36 $\mu m^3 cm^{-3} day^{-1}$ and 2.2 b_{scat} day^{-1}, it appears that the urban plume growth rates are about four times that observed by McMurray in the Smokies, and about twice those in the hazier parts of the smog blob.

Table 1 compares the various measures of aerosol growth for the St. Louis plume, the eastern haze, and the Smokies. The rate of aerosol sulfur formation has also been calculated for 70 percent relative humidity. Although comparing the aerosol growth rates in the urban plume with those in the general haze is something like comparing apples and oranges because the urban plume concentrations will be diluted by overnight travel, the data do suggest the range that probably exists from plume to haze.

Future haze studies should make an effort to determine the rates of formation on successive days of irradiation, travel, etc. The results cited above suggest that aerosol formation rates are much higher in the urban plume than on succeeding days after the plume has mixed, aged, and traveled. However, the data are much too scarce to be sure of what effect we have measured.

ACKNOWLEDGMENT

Most of the work reported here, including the preparation of this paper, was supported by EPA Research Grant No. R 803851-03. We would also like to acknowledge the help of Mr. Norman Valentine in the data reduction and of Mr. Joseph Wolf in the design and construction of the UMML.

REFERENCES

Hering, S. V., S. K. Friedlander, J. J. Collins, and L. W. Richards. 1979. Design and Evaluation of a New Low Pressure Impactor - II. Atmos. Environ., in press.

Husar, R. B., N. V. Gillani, J. D. Husar, C. C. Paley, and P. N. Turcu. 1976. Long-Range Transport of Pollutants Observed through Visibility Contour Maps, Weather Maps, and Trajectory Analysis. Presented at the 3rd Symposium on Atmospheric Turbulence, Diffusion and Air Quality, Raleigh, NC.

Isaksen, I. S. A., E. Hesstvedt, and O. Hov. 1978. A Chemical Model for Urban Plumes: Test for Ozone and Particulate Sulfur Formation in St. Louis Urban Plume. Atmos. Environ., 12:599-604.

Liu, B. Y. H., D. Y. H. Pui, K. T. Whitby, D. B. Kittelson, Y. Kousaka, and R. L. McKenzie. 1978. The Aerosol Mobility Chromatograph: A New Detector for Sulfuric Acid Aerosols. Atmos. Environ., 12:99-104.

McMurray, P. H., and B. Y. H. Liu. 1978. The Tandem Differential Mobility Analyzer Applied to Studies on Particle Growth and Gas Phase Titration. Final Report to DOE on Contract No. EY-76-S-02-1248.

McMurray, P. H., B. Y. H. Liu, and K. T. Whitby. 1978. Recent Progress in Fine Particle Research at the University of Minnesota. Presented at the GAF Conference, Vienna, Austria.

Roberts, P. T., and S. K. Friedlander. 1976. Analysis of Sulfur in Deposited Aerosol Particles by Vaporization and Flame Photometric Detection. Atmos. Environ., 10:403-408.

Whitby, K. T. 1979. Aerosol Formation in Urban Plumes. Presented at New York Academy of Sciences Conference on Aerosols: Anthropogenic and Natural-Sources and Transport, New York, NY.

Whitby, K. T. 1979a. University of Minnesota Particle Technology Laboratory Mobile Laboratories. Technical Report, U.S. EPA Grant No. R803851.

White, W. H., J. A. Anderson, D. L. Blumenthal, R. B. Husar, J. D. Husar, and W. E. Wilson. 1976. Formation and Transport of Secondary Air Pollutants: Ozone and Aerosols in the St. Louis Urban Plume. Science 194:187-189.

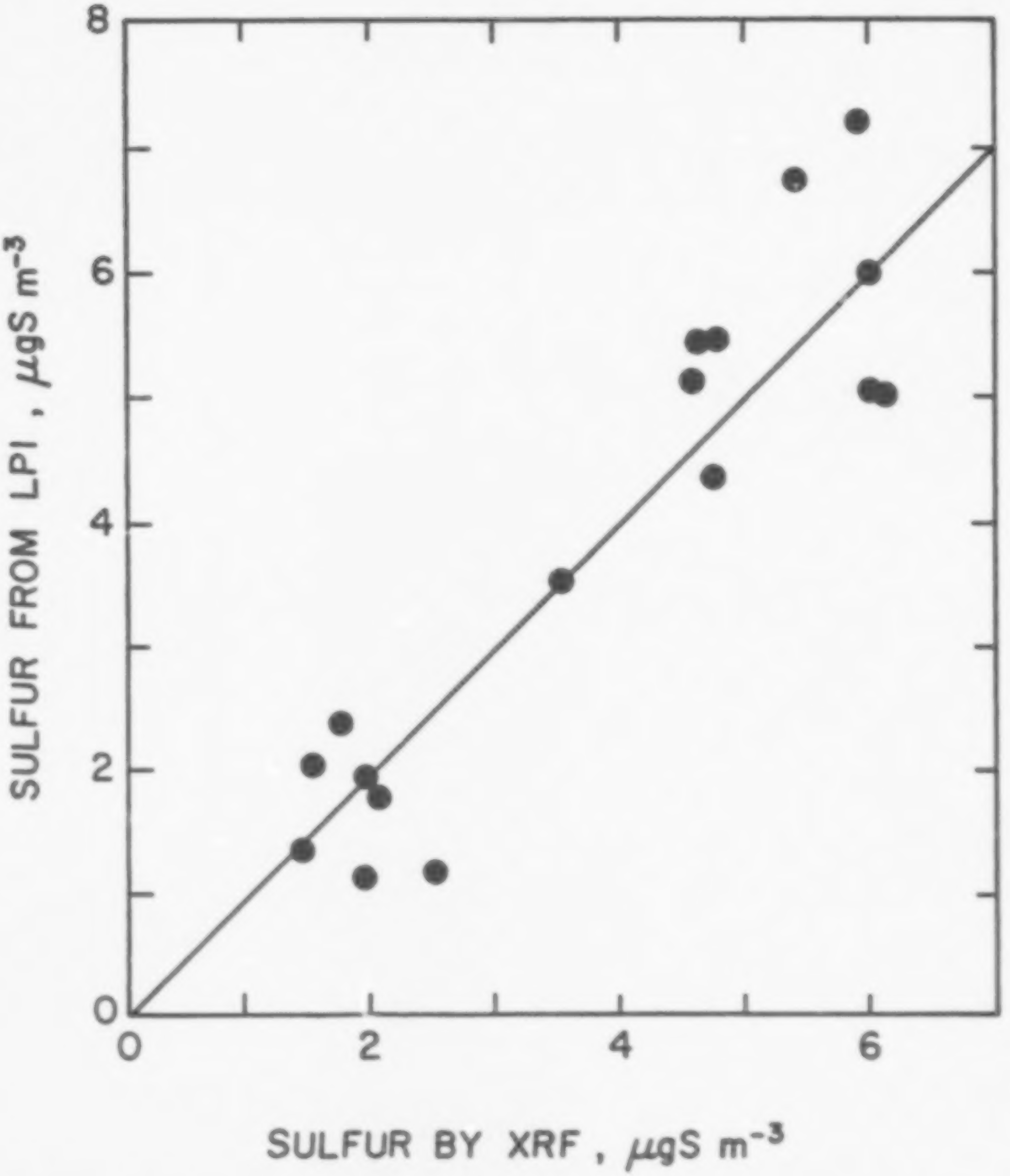

Figure 1. Comparison of total sulfur measured with XRF and with the LPI during the STATE program in August, 1978.

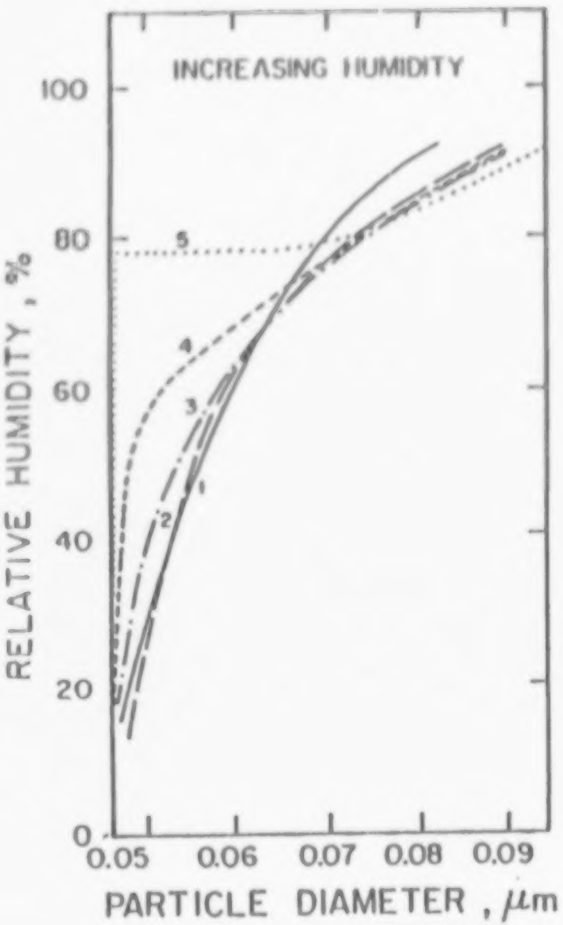

Source: McMurray and Liu, 1978.

Figure 2. Particle diameters achieved when aerosols consisting of mixtures of H_2SO_4 and $(NH_4)_2SO_4$, internally mixed in various proportions, are exposed to relative humidities shown on the ordinate. The initial humidity in all cases was about 8 percent.

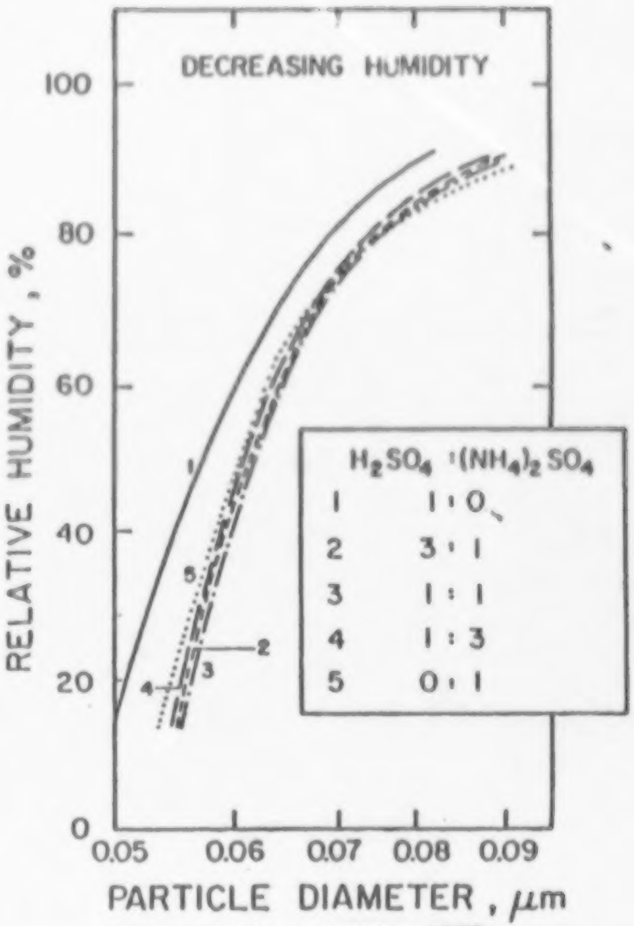

Source: McMurray and Liu, 1978.

Figure 3. Particle diameters achieved when aerosols consisting of mixtures of H_2SO_4 and $(NH_4)_2SO_4$, internally mixed in various proportions, are exposed to relative humidities shown on the ordinate. The initial humidity in all cases was about 95 percent.

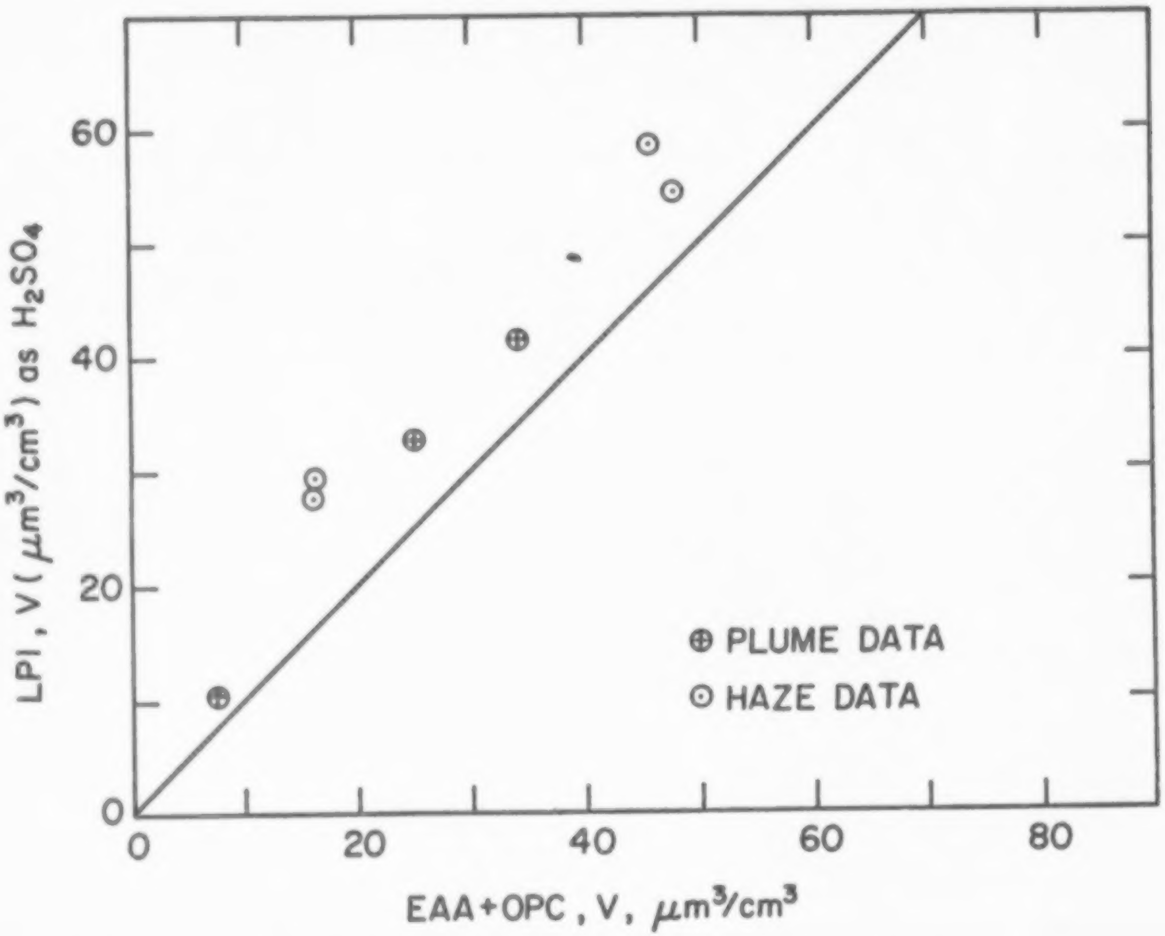

Figure 4. Comparison of total volume measured by the EAA and OPC with volumes calculated from LPI data. For LPI volumes, the aerosol was assumed to be pure H_2SO_4 in equilibrium at ambient humidities.

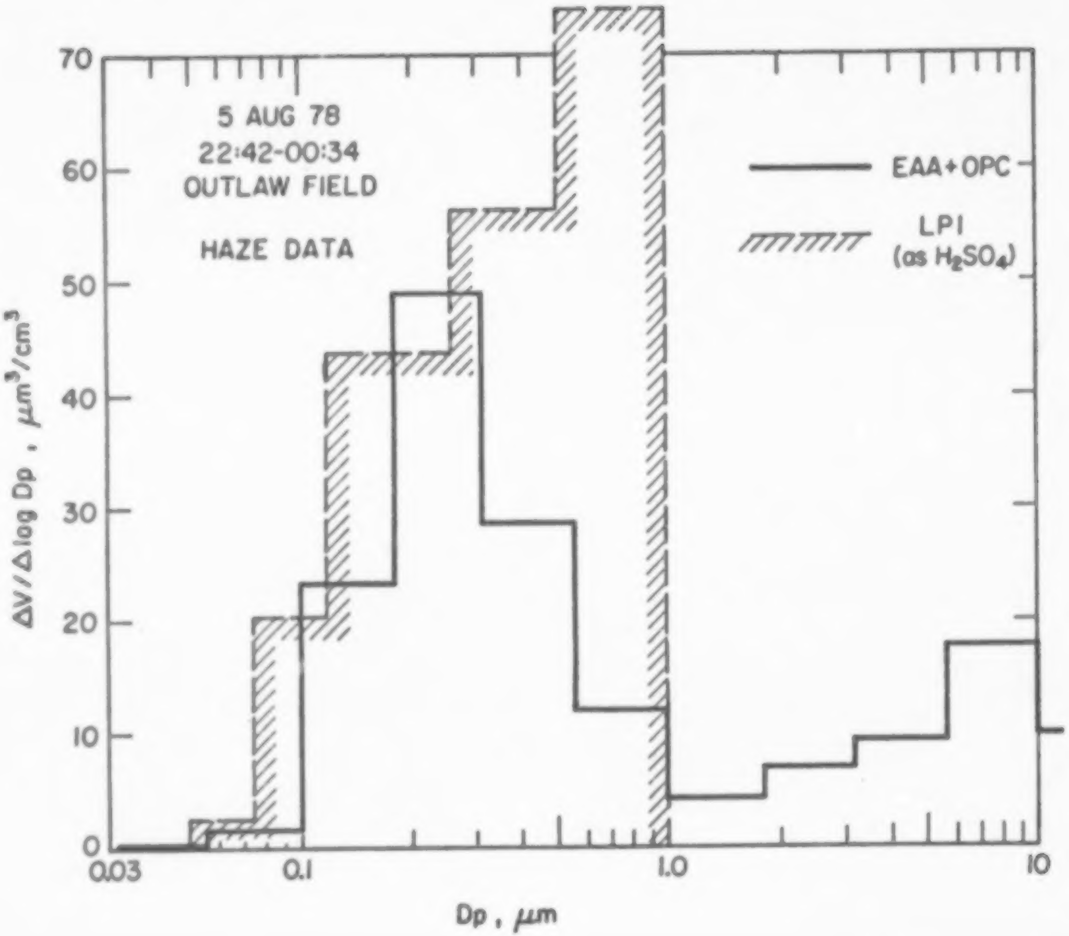

Figure 5. Comparison of an aerosol volume distribution measured by the EAA and OPC with one calculated from LPI sulfur distributions.

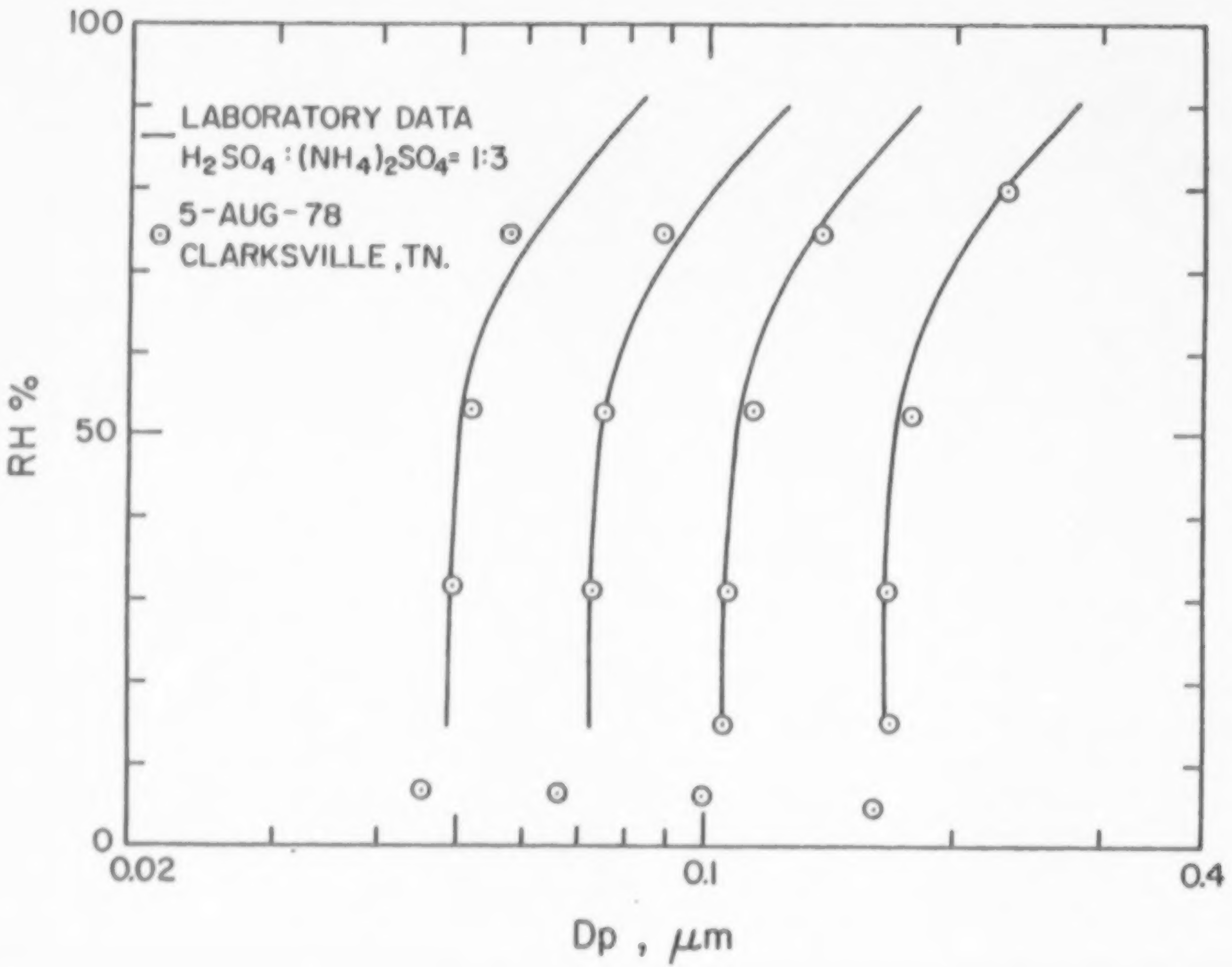

Figure 6. Comparison of laboratory and field data for the growth of particles with increasing humidity. These data were measured with a TDMA.

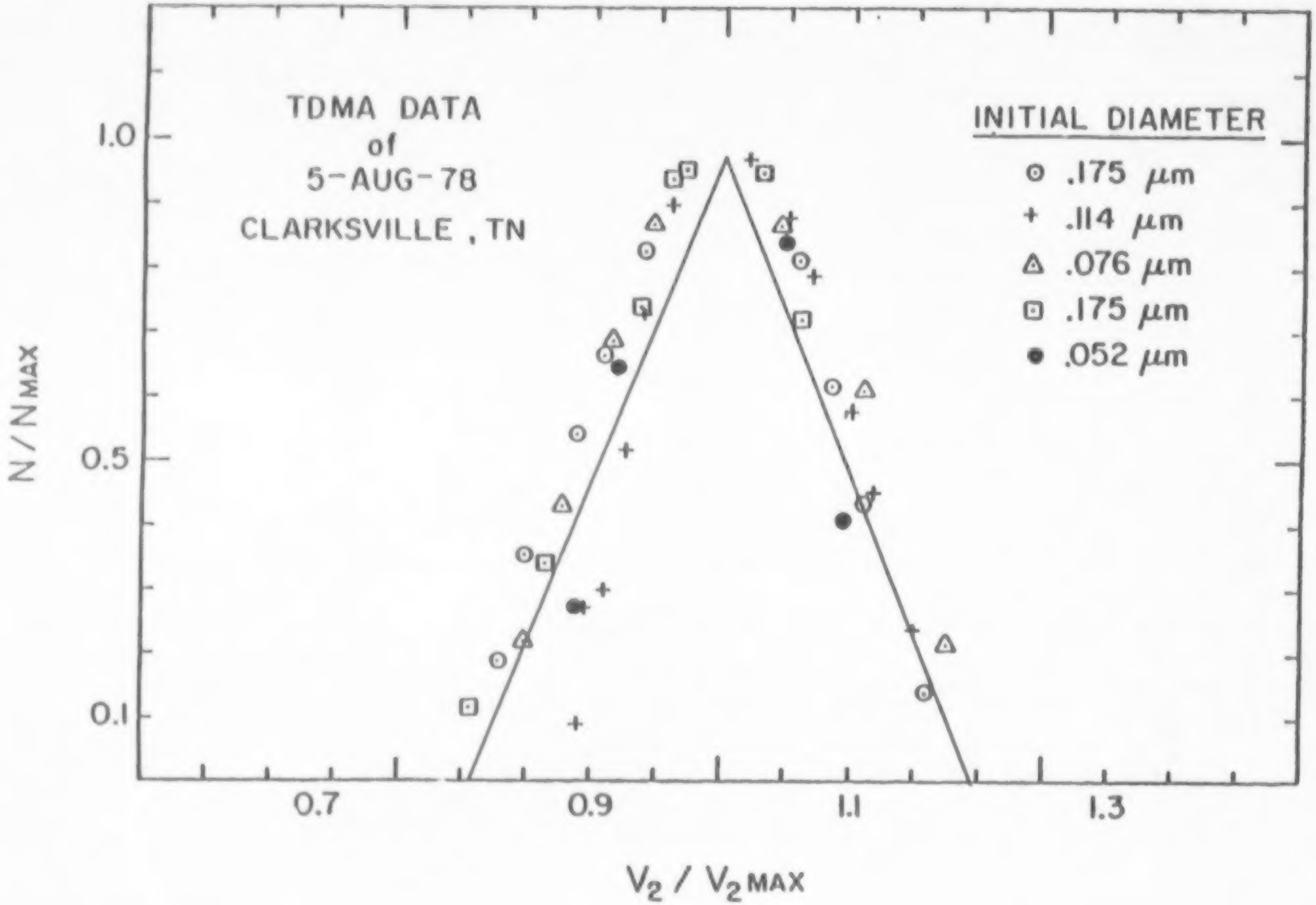

Figure 7. Number of particles (N) penetrating the second differential mobility analyzer (DMA2) normalized with respect to the maximum number observed during a voltage scan (N_{max}) versus the voltage on the DMA2 collector rod (normalized with respect to the voltage at N_{max}). The solid lines represent the theoretical curve for a monodisperse aerosol entering DMA2. This agreement between data and theory suggests the aerosol was internally mixed.

TABLE 1. COMPARISON OF THE b_{scat}, VOLUME FORMATION RATE (dV/dt), AND AEROSOL SULFUR FORMATION RATE FOR THREE LOCATIONS

Location	bscat/ day	dV/dt, μm^3 $cm^{-3} day^{-1}$	(dV/dt)/ b_{scat}	ΔS/dt,* μg S/day
St. Louis urban plume	2.2	36	16.4	5.2
Husar PEPE's estimate	1	(16.4)†		2.4
Great Smoky Mountains	0.5	8	16	1.2

*$\Delta S/dt = \frac{\rho_{P_{H_2SO_4}}}{3} \times dV/dt = \frac{0.44}{3} \times dV/dt$ (0.44 for 70 percent RH).

†Calculated using $(dV/dt)/b_{scat} = 16$.

APPENDIX A
UNIVERSITY OF MINNESOTA PARTICLE TECHNOLOGY LABORATORY MOBILE LABORATORIES*

PURPOSE

The University of Minnesota Mobile Laboratory (UMML) and the University of Minnesota Mobile Home (UMMH) were developed to make possible physical and chemical aerosol and gas measurements of an advanced nature anywhere there are roads passable to medium-sized trucks and motor homes. These vehicles are not intended for long-term monitoring, but rather for intensive measurement.

The vehicles have been designed so that all the electrical power and necessary support hardware are built in. All instruments are in racks that can be easily removed because we have found that practically no two studies are alike and that the complement of instruments is always somewhat different for each study.

The emphasis has been on continuous real-time measuring instruments, although a reasonable assortment of filter, virtual impactor, and cascade impactor samplers may be used.

The data logger used is capable of sampling all electrical signals every 0.6 seconds. Nine-track magnetic tapes recorded by this data acquisition system (DAS) can be reduced in the field on a PDP 11/10 minicomputer that is carried along. This off-line mode of operation has been found to be more satisfactory than on-line data acquisition directly into the computer.

UNIVERSITY OF MINNESOTA MOBILE LABORATORY

Description

The UMML is a 1975 General Motors 15½-ft Step-Van constructed of aluminum. The body is 16 ft from the driver's seat to the rear, 8 ft wide, and 80 in. high. Into this shell have been built two Onan generators, one on each side.

---

*Not presented at the symposium.

Two electrical systems have been installed, one delivering power to instruments and the other delivering power to two 13,000 Btu air conditioners in the forward part of the vehicle. An additional 13,000 Btu air conditioner is installed towards the rear, powered by the vehicle engine. Provisions have also been made for external power of up to 50 A at 220 V to be plugged in from the side. The heavy-duty towing package has been installed so that trailers or, as has often been done, an additional generator can be towed. When extra power is required, a 15 kW generator may be towed.

A double roof has been installed to provide a sturdy surface on which to walk and also a suitable mounting surface for instruments.

Figure A-1 shows the left side interior of the UMML. Two laboratory benches with drawers for supplies are mounted above the generators and wheel wells, one on each side. Instruments are mounted by bolting to the bench, bolting to laboratory strips mounted vertically, or by strapping to logistic strips mounted horizontally on the walls at several heights.

Electrical System

Two 6.5 kW Onan generators are built in, one on each side. The left-hand generator supplies power for the instruments and the right-hand supplies power for the air conditioners, pumps, and lights. An external connection on the right side also can be plugged into line power or a towed generator. Operating on internal generators, a total of 13 kW is available, and while operating with an external generator, a total of 21.5 kW of power is available.

Two 3.5-kW Sorenson line regulators have been provided to regulate power to the instruments and data acquisition system. Enough transfer switches and plugs have been provided so that almost any combination of power transfer can be accommodated.

Pump Systems

Two identical pump compartments, one on each side at the rear of the vehicle, have been provided. Each contains a 1-hp Gast vacuum pump and a 1-hp Rotron blower. These pumps and blowers provide enough suction to operate most of the filters and transfer systems under normal conditions. There is room in the pump compartments for additional pumps as necessary. For example, a high-vacuum pump has been installed to operate a low-pressure impactor for some studies.

Sampling Systems

Two multiple-inlet sampling feed-throughs have been provided, one on each side. The one on the left side is underneath the bag sampling system shown in Figure A-2 and is used primarily for aerosol sampling. The sampling feed-through on the right side is used both for gas sampling and for aerosol sampling to a virtual impactor located below it on the laboratory bench. In addition, some gas sampling inlets may be fed through the upper center part of the front of the vehicle for more direct access to the instruments.

Sampling probes extend forward of the vehicle on both sides and are arranged so that they can sample at either the roof level or from a level of about 1 m above the ground. The roof-level sampling is used for most sampling, and the lower-level sampling is used when it is desired to simulate what a driver of a vehicle on a roadway would inhale through the intake of an automobile.

Bag Sampling System

Figure A-2 shows the present bag sampling system. A bag sampler is necessary when making aerosol measurements under nonsteady conditions on roadways because the electrical aerosol analyzer requires that the aerosol concentration be stable through its operating cycle of about 2 min.

The bag sampler has an electronic control that automatically empties it, fills it, and holds an aerosol in it for the required 2-min measurement cycle. This automatic system can be either set to operate automatically with sampling times from 2 min to 1 hr, or the bag sampling cycle can be initiated by pushing a button.

Figure A-3 shows the measured transport efficiency of the system shown in Figure A-2.

Instrument Complement

The instrument complement varies from study to study. Table A-1 lists the instruments that will be used for two field studies during the summer of 1979. Figure A-1 shows the instruments on the left side as used during the 1976 Los Angeles Roadway Study. Since that figure was made, a Royco 245 sensor optimized for the 5- to 40-μm size range has been mounted on a platform at roof level in front of the windshield.

Data Acquisition

The present data acquisition system is a modified Metrodata 640 data logger recording on nine-track magnetic tape. The unit has been modified to accept 0.1-, 1-, and 10-V signals. Normally, the data logger is operated at its fastest scan rate of abut 0.6 s per scan in order to catch the flags from the aerosol analyzing system. However, the scan rate can be slowed down during periods in which monitoring over long periods must be done.

Eight or more channels of strip chart recording are also provided. There are enough strip charts and visual indicators on all instruments, as well as several digital volt meters aboard, so that if the data system logger is inoperative, all instruments can be operated and data recorded, albeit at a lower frequency.

Data Reduction

Because the only way to determine whether data recording is satisfactory is to reduce the data on a computer, a Digital Equipment Corp. PDP 11/10 with 32 K of memory and two floppy discs is ordinarily brought along, unless we are operating close to our home base.

Meteorology Equipment

Wind speed, direction, and outside temperature are measured with a Meteorology Research, Inc., meteorological package. The meteorology mast is arranged so that it can be erected in about 1 min. Thus, wind direction and velocity can be obtained if the vehicle is stationary for as little as 10 min.

Vehicle Position

Vehicle position is determined by a combination of distance measurement by an onboard instrument, which records distance on the data logger, and laboratory digitization of vehicle position from maps marked in the field with location and time.

Crew and Operation

Normally, three or four people are required to operate the UMML in motion. Two people can operate it satisfactorily when stationary and during long runs overnight; it has been found that one person can operate all the instruments, although at a reduced frequency.

When the two vehicles are operating together in the field, normal crew is five or six, with three or four in the UMML and two in the UMMH.

Detailed checklists for starting up and shutting down the labs have been developed and found to work quite well.

UNIVERSITY OF MINNESOTA MOBILE HOME (UMMH)

Description

The UMMH is a Winnebago 28-ft motor inn with one 6.5-kW generator installed. Two air conditioners, one forward and one aft, have been installed. The electrical system has been rebuilt so that it can operate on either 220-V internal generator or 110- or 220-V external power. Both air conditioners can only be operated on external power. The UMMH has a refrigerator, stove, toilet, shower, and considerable storage built in. In addition, a standard four-drawer file cabinet has been installed for project records and supplies. Other than the file cabinet, no other furniture has been built in. Experience has shown that it is best to strap in the facilities needed for each study. Instruments and facilities are secured by means of logistic strips placed at several levels on each side.

Communications

Both the UMML and UMMH have a CB radio installed. In addition, the UMML has a 720-channel aircraft radio. During some field studies, such as the STATE study in Alabama and Tennessee, an additional ground communication radio was installed in each vehicle. Thus, in the STATE program, it was possible to communicate between vehicles and with aircraft with the base station. For some studies, a standard radio telephone has also been installed.

MEASUREMENT PROJECTS PERFORMED WITH UMML/UMMH

Following is a brief summary of the measurement programs that have been completed, and the two that are planned in 1979, with the UMML and UMMH. Also given are a few comments about the major objectives and results of each study.

St. Louis, August 1976

In St. Louis in August 1976, the UMML made its first measurements of the Labadie power plant plume as part of the MISTT program. Because this was the first trip, only a modest amount of useful data was produced. Because the operating speed of the PDP/11-10 computer as a data acquisition system was too slow, the use of the on-board computer was discontinued, and the Metrodata 640 data logger was used for data acquisition in all subsequent studies.

Los Angeles Roadway Study, October 1976

Under EPA sponsorship, the UMML was equipped with a variety of instruments aimed at determining the amount of sulfuric acid from a catalyst-equipped car that might be seen on major freeways. Although useful data on roadway aerosol were obtained, the study showed that there were no significant concentrations of H_2SO_4.

State of Minnesota Regional Copper-Nickel Project, Summer 1977

In the summer of 1977, under the sponsorship of the State of Minnesota Regional Copper-Nickel Project and EPA, measurements were made of the mine and road dust concentrations found around several iron mines in northern Minnesota. The most important conclusion was that dirt roads contributed significant amounts of dust, perhaps even more dust than the mines. This study showed the feasibility of measuring dust size particles in real time with the UMML.

Diesel Exhaust Studies, June 1978

Under General Motors sponsorship, the UMML was used to measure diesel exhaust aerosols behind diesel cars. Size distributions and concentrations were measured and found to agree reasonably well with laboratory measurements.

Sherco Project, June 1978

In June of 1978, the Sherburne County NSP Sherco power plant was studied in collaboration with the University of Washington, EPA, EPRI, NSP, and Midwest Research Institute. The purpose of this project was to characterize a clean power plant equipped with scrubbers operating on low sulfur coal.

Pine Bend Refinery, July 1978

In July of 1978, a 1-day study of the Pine Bend refinery in Minnesota was made. High concentrations of pollutants are observed in the shallow valley where this refinery is located. Some very high sulfuric acid aerosol concentrations were found.

STATE Program, Summer 1978

The major study of 1978 was participation in the EPA-sponsored STATE program in Tennessee and Alabama. Measurements on the Cumberland and Widow's Creek power plants were made. Also, a large amount of data was collected on the hazes of the east central United States, both in western Tennessee and the Great Smoky Mountains.

Diesel Exhaust Studies, December 1978

In December 1978, additional diesel exhaust plume studies were done under Coordinating Research Council sponsorship. The UMML was mounted on a flatbed trailer that was towed behind a Cummins diesel-powered tractor. Aerosol samples were obtained at various positions in the exhaust plume.

VISTTA Program, Summer 1979

In the summer of 1979, it is planned to participate in the EPA VISTTA visibility program in the Four Corners area (Utah, Colorado, New Mexico, Arizona) of the southwestern United States. The major objective will be detailed physical and chemical characterization of the haze aerosols in that area.

Bureau of Mines, Summer 1979

Following the VISTTA study, it is planned to make a dust study for the U.S. Bureau of Mines at a coal mine near Craig, Colorado. The objective will be to characterize the size distribution and concentration of dust generated around this mine.

Other Projects, Summer 1979

Before and after the VISTTA and Bureau of Mines studies, additional studies of diesel aerosols over roadways will be made.

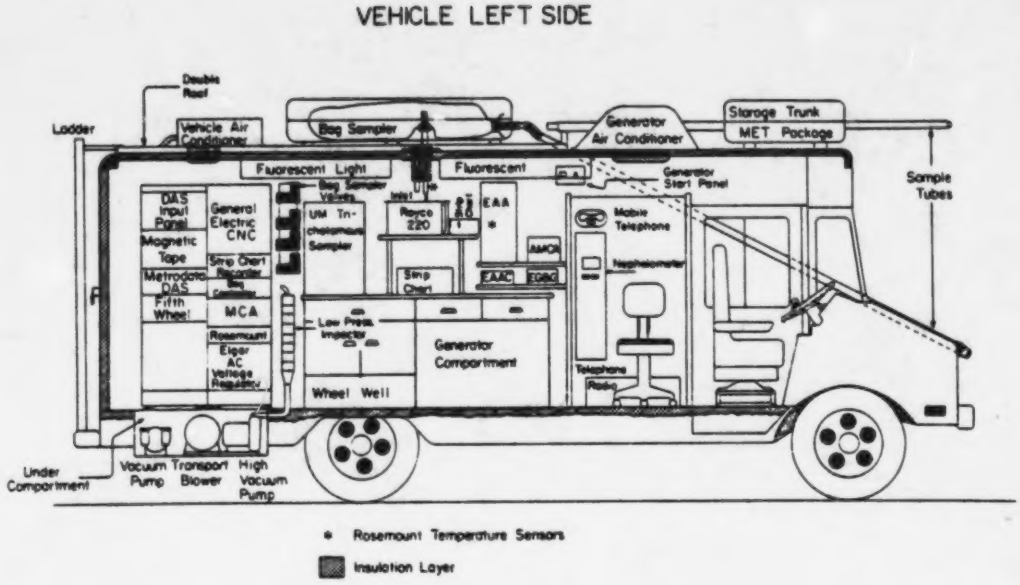
VEHICLE LEFT SIDE

Figure A-1. Interior schematic of the left side of the UMML showing the instrumentation as used during the 1976 Los Angeles Roadway Study.

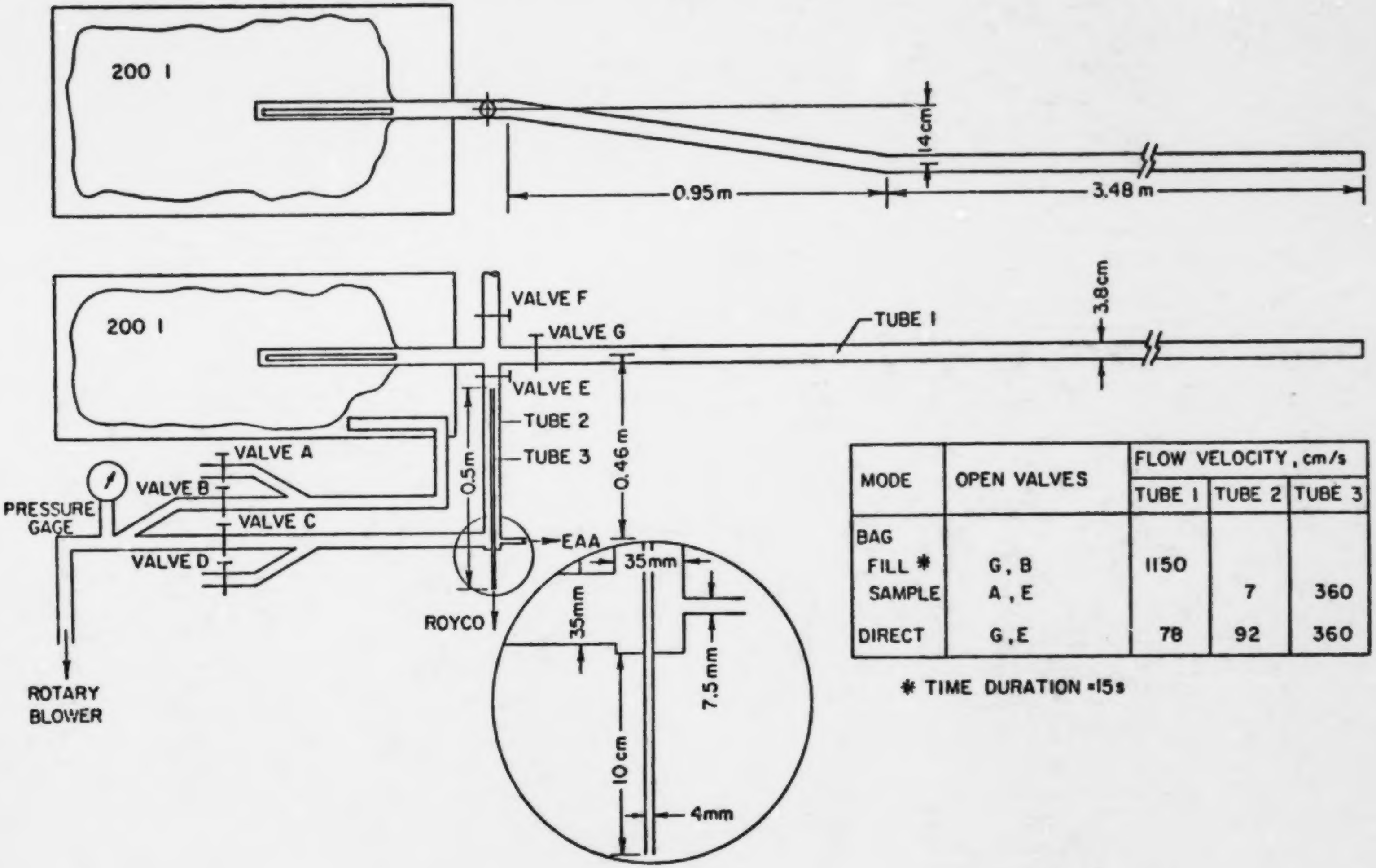

MODE	OPEN VALVES	FLOW VELOCITY, cm/s		
		TUBE 1	TUBE 2	TUBE 3
BAG				
FILL *	G, B	1150		
SAMPLE	A, E		7	360
DIRECT	G, E	78	92	360

* TIME DURATION ≈15s

Figure A-2. Schematic of the new bag sampler constructed in the spring of 1978. In addition to somewhat reduced losses, this system permits direct sampling from straight above the UMML.

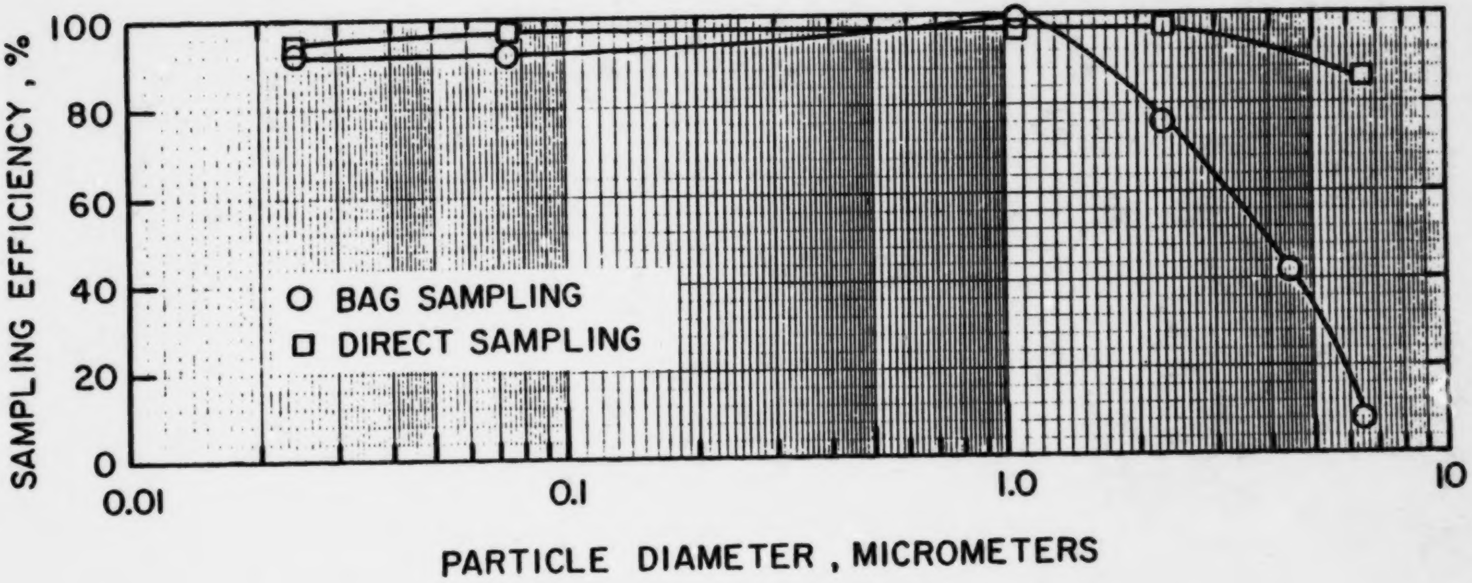

Figure A-3. Sampling efficiencies of the UMML sampling system used in 1978. Efficiencies were measured experimentally using monodisperse aerosol. "Direct Sampling" refers to drawing the sample through the horizontal tube and directly down to the instruments at a flow of 531 lpm. "Bag Sampling" refers to drawing a sample into the bag through the horizontal tube at about 780 lpm, and then drawing the sample from the bag at 6.8 lpm. The inside of the bag was coated with a thin soap film to reduce particle losses due to electric fields.

TABLE A-1. UMML/UMMH INSTRUMENTATION
(available summer 1979)

Variable or Function	Instrument
Position - maps - speed and location - distance traveled	SPACEKOM, Inc., Auto Company
Meteorology	
Inside temperature	Rosemount Engineering Temperature Sensors
Dew point	EG & G, Model 820 Hygrometer
Wind speed & direction (stationary) and outside temperature	MRI, Model 840-1 T sensor Model 1074 WSPD & WDIR Model 840 Aspirated Temperature Sensor
Visibility, b_{scat}	Modified MRI, Inc., Model 1561 Integrating Nephelometer
Gas Chemistry	
SO_2 (gaseous S)	Meloy SA 285
NO, NO_2, NO_x	TECO Series 14
O_3	Dasibi, Model 1003 - AH
CO	Energetics Science, Inc., 2000 Series
Aerosol Size Distribution	
Aitken Nuclei	General Electric GE-1 Condensation Nuclei Counter Environment/One Rich 100 or TSI Model 3020
0.0056 - 1 μm	TSI Model 3030 EAA
0.056 - 6μm	Royco 220, MCA and Ratemeter
5.6 - 40 μm	Royco 245, MCA and Ratemeter
30 +	Filter & Microscope
Aerosol Chemistry	
X-ray fluorescence	50 l/min dichotomous virtual impactor--collection on filters--cut at 2.5 μm
Sulfur	Low pressure impactor
X-ray fluorescence	Micro-orifice impactor--cuts at 0.1, 0.3, 1, and 2.5 μm--collection on 37-mm filter
Carbon analysis	47-mm filters for carbon analysis
Aerosol sulfur	Pulsed Meloy SA 285--continuous
Aerosol growth with humidity	TDMA--TSI Model 3020 CNC
Single particle XFL	Filter analysis at Penn State

(continued)

TABLE A-1 (continued)

Data	
Data acquisition	Metro Data Model 640 DL
Data recording	Digi Data Corp. Model 1309-8-B2 9-track magnetic tape
Data reduction	DEC PDP 11/10 Minicomputer - off-line
Strip charts	Two Chessel 3-channel, one Linear 3-channel, one Linear 2-channel
Communication	
Ground	40-channel CB in UMML & UMMH
Air	Genave Model 720 p 720 channel aircraft radio in UMML
Miscellaneous	
Telephotometer	(Provided by EPA)
Sun photometer	5-band Voltz sun photometer--modified
Photography	35-mm camera
Time lapse	Super 8 movie camera
Calibration	
O_3, SO_2, NO_x	Monitor Labs. Model 8500 gas calibrator
Flow	TSI Model 1352 and 1050 mass flow meters
OPC's	Aerosolized PSL & Polystyrene
Solar radiation	
Broad-band and ultraviolet radiation	Eppley pyrheliometer

COMPARISON OF AIR QUALITY WITHIN THE MIXED LAYER WITH THAT AT THE SURFACE

James J. B. Worth

Research Triangle Institute, Research Triangle Park, North Carolina

Abstract

Data collected during the Sulfate Regional Experiment were investigated to determine how well data collected at surface stations compared to data collected on board an instrumented aircraft flown within the mixed layer. Data were compared for all flights and for flights grouped by time of day by calculating correlation coefficients (r-values). The gaseous species, O_3 and SO_2, and measurements of particulate sulfate and total suspended particulate were considered in this analysis. The SO_2 and sulfate data within the two measurement regimes were found to have correlations significantly different than zero for all time periods and the ozone data appeared to be correlated in the afternoon.

Other analyses were made using averages of all the aircraft data, and data from selected individual flights. These additional analyses were performed to provide information useful in understanding the results of the correlations. The additional analyses included:

1. Averaging the aircraft data over all flights within the mixed layer, above the mixing height, and in 60-m (200-ft) increments.
2. Examination of aircraft data collected on individual flights through the near-surface layer to an altitude of 15 m (50 ft) above the ground.
3. Comparison of data collected on three vertical spirals separated by no more than 80 km (50 mi).

INTRODUCTION

A primary objective of this study was to identify those conditions under which surface air quality can be expected to represent the air quality in the mixed layer. This was done by comparing air quality data collected at the surface with that collected by aircraft during the Sulfate Regional Experiment (SURE). The results provide guidance for the development of study designs that will make optimum use of valuable aircraft flight time in future studies. The SURE program provided an excellent data base for this work because air quality measurements made aboard aircraft on spiral flights above surface stations were available at several locations, during the four seasons, and at three times of the day.

Flight plans for the SURE aircraft called for two flights per day consisting of three vertical spirals per flight. These flights were conducted at sunrise and at midday during the first four measurement periods and at midnight and midday during the remaining two measurement periods. A total of approximately 400 spirals were flown by SURE aircraft. Spirals between the surface and 3 km were flown upwind of, over, and downwind of a specified SURE Class 1 station. The spacing between the spirals during the first four intensives was 25 km (15 mi) and during the last two intensives was 80 km (50 mi). A typical flight pattern is shown in Figure 1.

Measured parameters included meteorology, position, and air quality data. Continuous air quality data included SO_2, O_3, NO/NO_x, b_{scat}, and condensation nuclei concentration (CNC) data. Sulfur dioxide was also determined by analysis following 30 min of sampling through filter packs. Particulate samples were collected for 15-min and 30-min periods. The 30-min samples were collected such that they provide resolution from the surface to 1.5 km and from 1.5 to 3.0 km. Particulate samples were subsequently analyzed for $SO_4^=$, NO_3^-, and NO_4^+ in addition to particulate mass.

Data from selected flights were examined first to determine the agreement between the air quality measured on the three spirals flown within 50 km of one another. Second, the data collected on low-altitude extensions of the typical spirals, which tied the aircraft data to the surface data, were examined. This analysis provided insight into the causes of poor agreement between surface and aircraft data.

Statistical procedures were applied to the entire aircraft ground data set. These analyses included averaging air quality data over all spirals and calculating correlations between corresponding measurements at the surface and aboard the aircraft. The results of these procedures provided information on the agreement between surface and aircraft data in general. The analysis was not extended to investigate the relationship between surface and aircraft air quality data between seasons at the same location or during the same season at different locations. The available data were not sufficient to provide meaningful results for individual locations or seasons.

RESULTS AND DISCUSSION

Comparison of Data from Three Spirals at the Same Locations

The standard three-spiral flight plan followed during the SURE made an important analysis possible. The measurements made during individual spirals of the separate flights were compared by testing the mean concentrations of gaseous parameters above and below the mixing height to determine if there was any significant difference between the mean concentrations on the three spirals.

Figures 2 and 3 present the data of three spirals overlaid on one another for the morning and afternoon flights of 15 April 1978, respectively. These flights took place at Research Triangle Park, NC, and were separated by approximately 24 km (15 mi). These figures clearly show the agreement that can be expected between spirals with this separation, not only with respect to O_3 and SO_2, but for the other parameters measured as well.

Throughout the first four periods of intensive measurements (intensives) the agreement among the data from the three spirals at 24-km (15-mi) separations was consistent. As a result of this, it was decided to extend the distance between spirals to approximately 80 km (50 mi) during the remaining two intensives. Table 1 lists the spiral means and results of tests of significance for O_3, SO_2, and NO_x among the spirals separated by 80 km (50 mi) during the July and October 1978 intensives. During these intensives at Scranton, PA, and Zanesville, OH, there was no significant difference in the mean concentrations of O_3, SO_2, or NO_x below 1.5 km (nominal mixing height) at the 80-km (50-mi) separation. There was a significant difference for NO_x above the mixing height during both intensives and for O_3 above the mixing height during the October intensive at Zanesville, OH. These results suggest that, depending on the needs of a particular measurement program, individual spirals flown more frequently during the day may be a more efficient use of valuable aircraft flight time than the flight plans followed in this study. Figures 4 and 5 represent the data of the three spirals overlaid on one another from the noon and midnight flights of 12 July 1978 at Scranton, PA, respectively. Once again, in both of these figures the data for all parameters agree quite well. Note in Figure 5 that while the mixing height varied considerably over the three spirals in the midnight flight, the concentrations of O_3 above and below the mixing height on the three spirals were in good agreement.

Low-Approach Flight Data

Vertical spirals were extended from the typical spiral base altitude (0.45 km [1,500 ft] MSL) down to approximately 15 m (50 ft) above the ground near a surface station to examine the vertical distribution of the measured pollutants near the surface. Figures 6 through 9 show selected examples of these data along with the corresponding surface station measurements. These data have been helpful in understanding the reasons for the poor correlations between the surface and aircraft measurements.

Figure 6 represents the low-approach and surface station measurements made during the morning flight on 12 April 1978 at Research Triangle Park, NC. For this flight, the extension of the aircraft spiral was completed at RDU airport approximately 4.8 km (8 mi) from the surface station. On the morning flight of 12 April 1978, there were steep gradients of NO, NO_x, and O_3 near the surface. These gradients were a direct result of the presence of a nocturnal radiation inversion. The nocturnal inversion served to trap NO_x emissions through the night in a shallow layer near the surface. The rapid reaction between NO and O_3 caused a decrease in the O_3 concentration and an increase in the NO_2 concentration (represented by the difference between NO_x and NO). Figure 7 represents data from a similar low-approach comparison flight at Research Triangle Park, NC, during the afternoon of 24 April 1978. By the time of the afternoon flight, the surface inversion had dissipated and good mixing had been established. The lowest part of the vertical profile agreed quite well with the surface station measurements during this flight. On this flight the ozone concentration up to 0.59 km (2,000 ft) MSL agreed well with the surface measurements. These results suggest that there is an apparent relationship between surface ozone and the mean ozone concentration within the mixed layer during the afternoon.

Local sources sometimes have a serious impact on the comparison between surface and aircraft data. The effect of a local source is illustrated by the low-approach and surface station data from the afternoon flight of 13 October 1978 at Zanesville, OH, shown in Figure 8. There is a local source of SO_2 in the area and, as seen in the figure, the SO_2 at the surface was much greater than the concentration measured aboard the aircraft. These data also illustrate the effect of sampling aboard an aircraft on the edge of a large urban-type plume. The spiral path may have caused the aircraft to periodically enter and leave an area of high NO and NO_x concentration characteristic of an urban plume.

Figure 9 represents the low-approach and surface station data collected on the night flight of 23 October 1978. The influence of a shallow surface inversion is evident in the steep gradient of ozone very near the surface. The inversion layer is formed shortly after sunset and continues to deepen and become progressively more stable through the night. The destruction of reactive species such as ozone is influenced not only by chemical reaction with other pollutants but also by uptake and reaction at the surface. The data in Figure 9 show that while the NO_x concentration has not increased significantly at the surface, the ozone concentration has already decreased considerably below the mean ozone concentration above the inversion.

Mean Concentrations

The means and ranges of O_3 and SO_2 concentrations at the surface, below the mixing height, and above the mixing height for all flights considered in this analysis are presented in Tables 2 and 3. The means and ranges for all flights grouped by the separate time periods are also listed in Tables 2 and 3. The mean ozone concentrations increased with increasing altitude over all flights. These observations were consistent even when the data were averaged over the flights within the separate time periods, although during the midday flights the mean ozone concentrations at the surface, below, and above the mixing height were nearly equal.

The behavior of SO_2 was quite different from that of ozone. Both the mean and maximum SO_2 concentrations generally decreased with altitude over all flights as well as over the flights within the separate time periods.

Mean ozone concentrations above the mixing height were consistently greater than the mean concentration either below the mixing height or at the surface, although the difference was small during the noon flights. The mean ozone concentration above the mixing height was nearly the same in each of the time periods. There was a significant difference, however, between the ozone concentration at the surface during the midnight and early morning flights compared to the mean surface ozone concentration during the noon flights. The mean ozone concentration within the mixed layer, although lower than that above the mixing height, was also quite consistent across the separate time periods. These trends suggest that the effects of transport, synthesis, and destruction of ozone are more in balance above the surface on the diurnal time scale than they are at the surface. The impact that the ozone above the mixing height has on surface air quality is as yet not fully understood. However, as atmospheric conditions change, some of the ozone above the mixing height may be mixed to the near-surface layer and affect surface air quality.

The mean concentrations of SO_2 at the surface, below, and above the mixing height were similar acoss the separate time periods, although the maximum concentrations differed considerably. The consistency of the means over the time periods may suggest that the primary SO_2 sources are continuous throughout the day. Large stationary sources of SO_2, such as coal-fired power plants, may therefore be the dominant influence on the mean surface concentrations, with the large ranges observed resulting from the presence or absence of the direct influence of relatively local sources.

Table 4 lists the means and ranges of the sulfate concentration measured at the surface, below 1.5 km (5,000 ft), and above 1.5 km (5,000 ft) over all flights and for the morning and afternoon flights. The data from midnight flights were too few to establish any meaningful conclusions and were not considered. The data in Table 4 indicate that, on the average, the sulfate concentrations at the surface and below 1.5 km (5,000 ft) agreed quite well. The agreement between the 3-hr average sulfate concentration at the surface and the mean sulfate concentration below 1.5 km (5,000 ft), averaged over all three spirals, was within 10 percent on both the morning and midday flights. The sulfate concentrations measured above 1.5 km (5,000 ft) were consistently lower than those measured both below 1.5 km (5,000 ft) and at the surface. The sharp decrease in sulfate concentration above 1.5 km (5,000 ft) confirms that atmospheric sulfate arises primarily from surface-related sources.

Mean Vertical Spirals

All of the available spiral data were averaged in 60-m (200-ft) increments, and the results for each individual parameter were plotted as mean vertical spirals. There is one plot for data below 1.5 km (5,000 ft) and one for data above 1.5 km (5,000 ft) for each parameter. These plots appear in Figures 10 through 17 for SO_2, NO_x, and O_3, respectively. The solid dots represent plus and minus one standard deviation from the mean in each of the 60-m (200-ft) increments. To provide good visual resolution, the concentration data for individual species were scaled differently in the two altitude regions.

Figures 10 and 11 show the plots of mean SO_2 concentrations below and above 1.5 km (5,000 ft) MSL, respectively. The maximum mean SO_2 concentration was approximately 0.015 ppm and occurred at 0.4 km (1,400 ft), approximately 180-240 m (600-800 ft) above the average surface elevation. At the lowest elevation, the mean concentration was approximately 0.009 ppm, and the mean surface concentration was 0.014 ppm. In the low-altitude portion of the mean spiral, the standard deviation for SO_2 was large, nearly 100 percent of the mean concentration, indicating that there was a large variability in SO_2 concentration measured near the surface. These plots represent data averaged over spirals flown at several different locations, and much of the variability is suspected of resulting from local sources and variations in surface terrain. At altitudes above 0.4 km (1,400 ft), both the mean SO_2 concentration and the standard deviation decreased continually. The occurrence of the maximum at 0.4 km (1,400 ft) suggests that stationary ground sources with tall stacks have a significant impact on the initial vertical distribution of SO_2. The rapidly decreasing mean SO_2 concentrations all the way to 3 km (10,000 ft) result from dilution and chemical reaction as the SO_2 is mixed away from the source area.

The mean vertical spiral for NO_x shown in Figures 12 and 13 is similar to that for SO_2. The maximum value of approximately 0.013 ppm occurred at 0.35 km (1,200 ft). There was a secondary maximum of approximately 0.012 ppm in the very lowest altitude layer and the mean NO_x concentration at the surface was 0.010 ppm. The maximum mean concentration at 0.35 km (1,200 ft) is probably a result of the same type of emissions as were suggested for SO_2. The secondary maximum in the lowest altitude increment shows the importance of surface sources, primarily automobiles, on the vertical distribution of NO_x. The standard deviation for NO_x, like that for SO_2, was large very near the surface and decreased with altitude, especially below 1.5 km (5,000 ft). The variability of local source strengths and surface terrain are, again, suspected of contributing to the large variability in NO_x concentrations observed near the surface. The decreasing concentrations with altitude are also a result of dilution and chemical reaction.

Unlike SO_2 and NO_x, the mean vertical concentrations of ozone, which are shown in Figures 14 and 15 increased with altitude up to 1.5 km (5,000 ft). The standard deviation remained nearly constant over the entire altitude range. The lack of significant amounts of NO_x and SO_2 at altitudes above 1.5 km (5,000 ft) indicates that these surface-related primary emissions are diluted and chemically altered as they are mixed in the atmosphere. The mean profile of ozone, however, further suggests that there is a more stable balance among synthesis, destruction, and transport at altitudes above 1.5 km (5,000 ft) than at the surface. The standard deviations of the means for ozone were consistent over the entire altitude range, further substantiating the stability of high ozone concentrations above 1.5 km (5,000 ft).

The mean values of b_{scat} decreased, in general, from the lowest portions of the aircraft spirals to 1.5 km (5,000 ft) as shown in Figure 16. The standard deviation from the mean was similar over that altitude range. This is to be expected because the surface itself can serve as a source of particles that are included in the measurement of b_{scat}. Above 1.5 km (5,000 ft), however, the mean b_{scat} values, shown in Figure 17, decreased more slowly, and above 2.1 km (7,000 ft) they remained nearly constant. The standard deviation started to vary consistently above 2.1 km (7,000 ft). There is often a concentration of b_{scat} just below an inversion layer and the large and variable standard deviations shown in Figure 17 above 2.1 km (7,000 ft) were a result of variation in the mixing depth over the spirals.

Correlations Between Surface and Aircraft Data

Correlations were calculated between aircraft data and surface station data for comparison. Table 5 lists the correlations obtained for the data of all flights. A statistical test was performed to determine if the correlations were significantly different from zero; those correlations in Table 5 that were significant are marked by an asterisk. Selected scatter diagrams of the data used in calculating these correlations are shown in Figures 18 through 23. Although some of the correlations were determined to be significant, inspection of the scatter diagrams reveals, in some cases, that the correlations were apparently fortuitous and not actually meaningful.

The SO_2, sulfate, and ozone concentrations within the mixed layer and SO_2 above the mixing height were found to be correlated with the corresponding surface data. Figure 18 is the scatter diagram for SO_2 within the mixing layer versus SO_2 at the surface for all flights. Although a large fraction of the data are clustered around the origin, there does appear to be the potential for significant correlation between the two sets of data. There are two outliers for which the surface SO_2 was approximately 0.07 ppm and the average SO_2 within the mixed layer was below 0.015 ppm. Undoubtedly the correlation would be improved considerably if these two outliers were removed. Even with them included, the correlation of 0.56 was significant. The scatter diagram of sulfate below 1.5 km (5,000 ft) versus sulfate at the surface, shown in Figure 19, with a correlation of 0.61 also shows a potential for a significant correlation. In addition, a linear regression equation fit to these data would have a slope very close to unity. There were no outliers in this data set, indicating that, in general, the surface sulfate concentration is similar to the sulfate concentration in the mixed layer. This result further substantiates the agreement between surface sulfate and sulfate concentrations below 1.5 km (5,000 ft) inferred from the table of mean concentrations.

The correlations between surface and aircraft data for flights within the separate time periods are listed in Table 6. Once again the asterisk marks those correlations that are significantly different from zero.

The scatter diagrams for SO_2 and sulfate within the mixed layer versus SO_2 and sulfate at the surface for morning flights, both of which have a correlation of 0.54, are shown in Figures 20 and 21. In both cases the data appear to justify the significance of the correlation. The correlation of 0.69 for SO_2 above the mixing height versus SO_2 at the surface for morning flights was determined to be significant. The scatter diagram of these data, however, shown in Figure 22, indicates that a single outlier influenced the correlation significantly, and the remainder of the data did not support the significance of the correlation.

The scatter diagram for SO_2 within the mixed layer versus SO_2 at the surface for afternoon flights, shown in Figure 23, strongly supports the significance of the 0.80 correlation. For these data the regression equation would have a slope near unity as was the case for sulfate below 1.5 km (5,000 ft) over all flights. At the present time, it appears that a potential for significant correlation exists between SO_2 and sulfate at the surface and within the mixed layer at all times. The O_3 concentration within the mixed layer is also likely to be correlated with surface ozone concentrations in the afternoon.

CONCLUSIONS

The mean concentrations of O_3 increased with altitude over all flights from the surface to above the mixing height. The mean concentrations of SO_2 decreased with height over all flights from the surface to above the mixing height, and the mean sulfate concentrations were approximately equal at the surface and below 1.5 km (5,000 ft) and decreased by approximately 50 percent above 1.5 km (5,000 ft).

Due to the mean vertical distribution of ozone, large amounts of ozone can be isolated from rapid destructive influences near the surface, and may be transported large distances downwind. The vertical distribution of ozone was found to be dependent on time of day. The mean concentrations of ozone at the surface, within the mixed layer, and above the mixing height during the afternoon flights, were within 10 percent of one another.

The mean concentrations of SO_2 and sulfate at the surface below the mixing height and above the mixing height, in general, were not dependent on the time of day.

The mean concentration of O_3 in 60-m (200-ft) increments increased with height and the standard deviation remained approximately the same with altitude. The mean concentrations of SO_2 and NO_x had maxima at 0.40 km (1,400 ft) and 0.35 km (1,200 ft), respectively, and the standard deviations decreased continually with height.

Correlations of SO_2 and sulfate at the surface and within the mixed layer were found to be significantly different from zero. Ozone concentrations at the surface and within the mixed layer showed an apparent correlation for the afternoon flights but not during the morning flights.

Data collection aboard the aircraft down to altitudes within 15 m (50 ft) above the ground provides information useful in understanding the reasons for poor correlations between the surface air quality and the mean air quality within the mixed layer.

Evidence suggests that there may be no significant difference between the mean concentration of ozone or SO_2 below the mixing height on spirals separated by 24 km (15 mi) or 80 km (50 mi).

More efficient use of valuable aircraft flight time may be possible if single spirals are flown more frequently during the day.

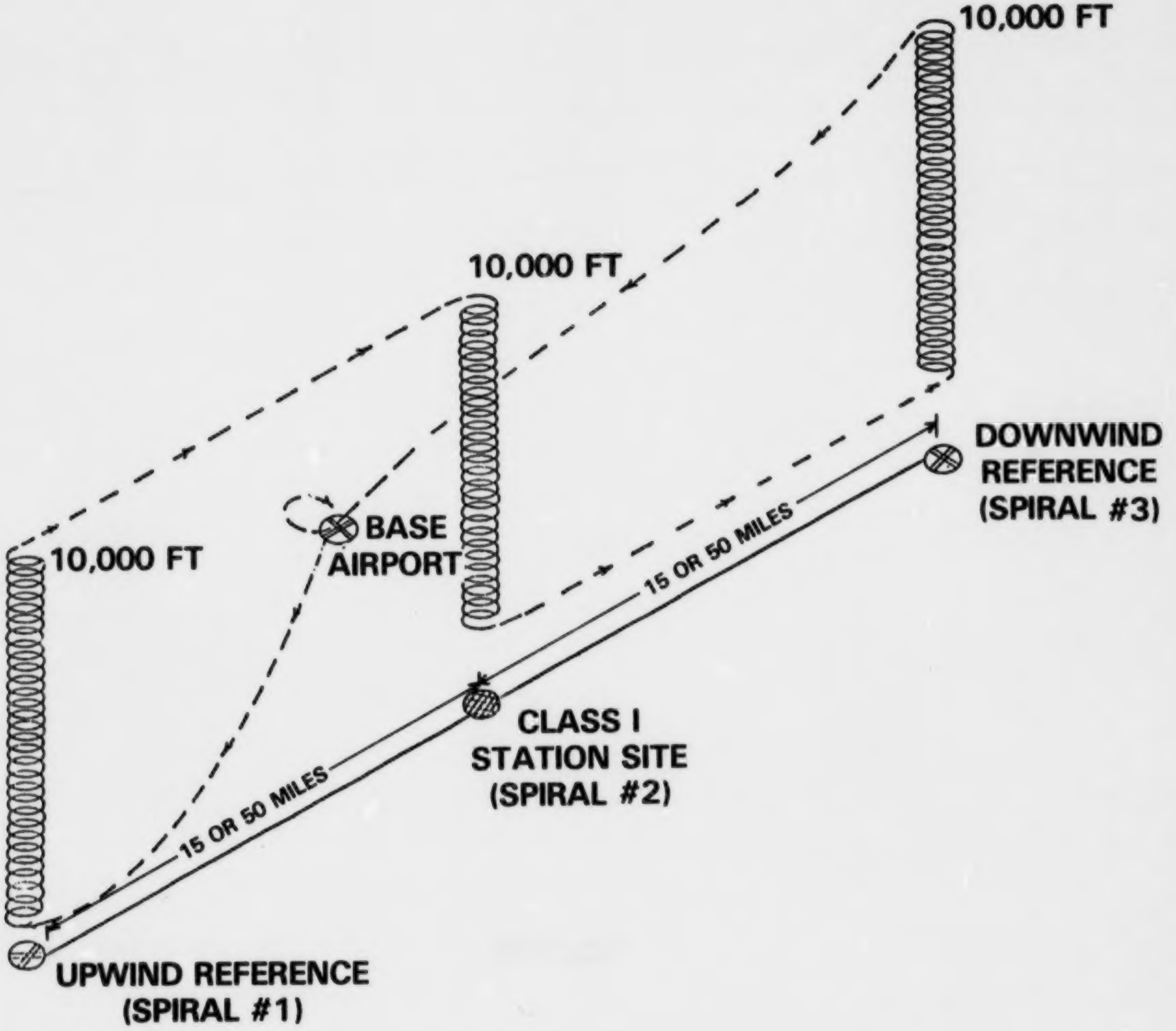
10,000 FT
10,000 FT
10,000 FT
BASE AIRPORT
15 OR 50 MILES
15 OR 50 MILES
DOWNWIND REFERENCE (SPIRAL #3)
CLASS I STATION SITE (SPIRAL #2)
UPWIND REFERENCE (SPIRAL #1)

Figure 1. Typical three-spiral SURE aircraft flight plan.

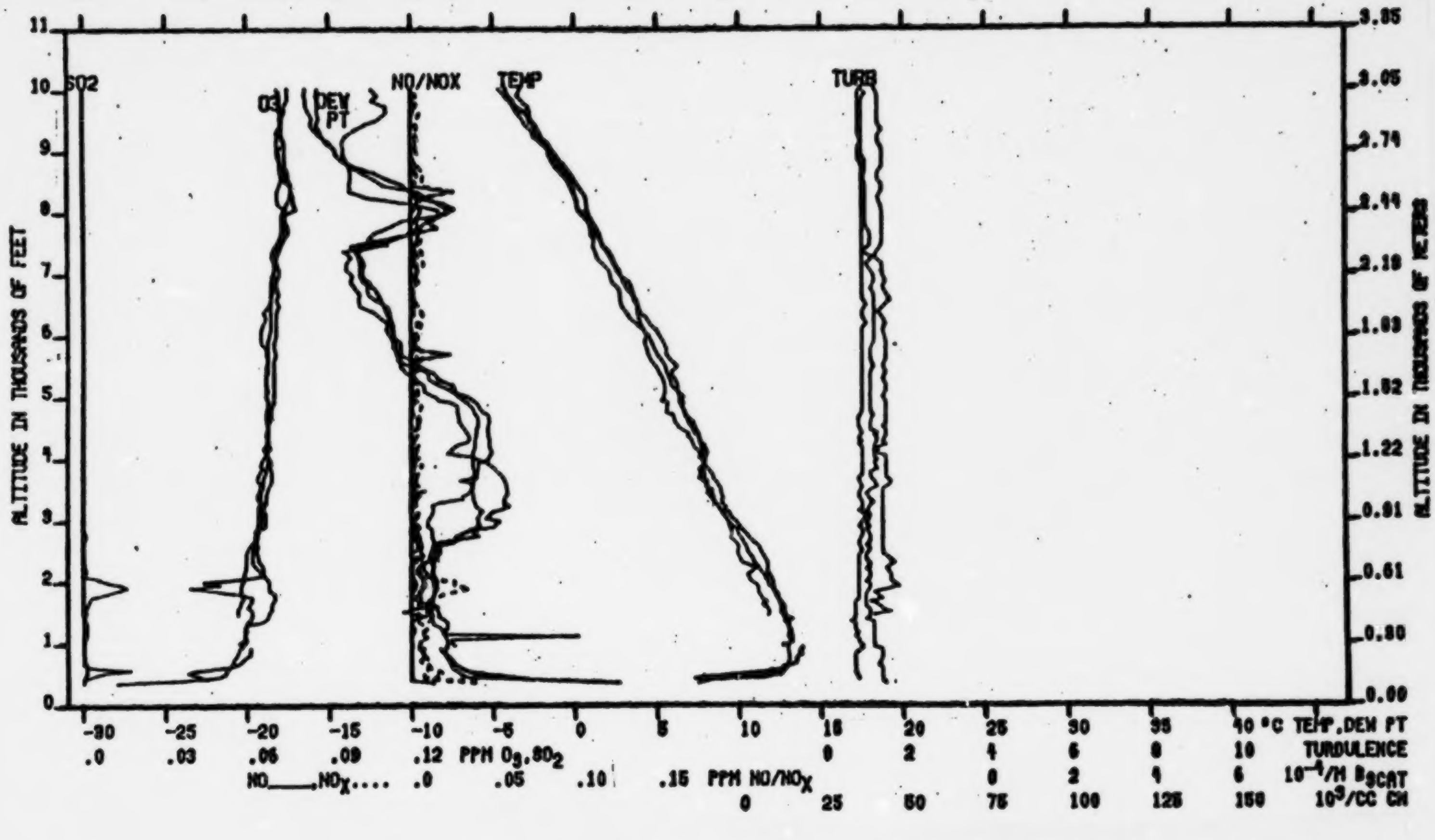

Figure 2. Concentration profiles of all three spirals of the morning flight of 15 April 1978 overlaid on one another.

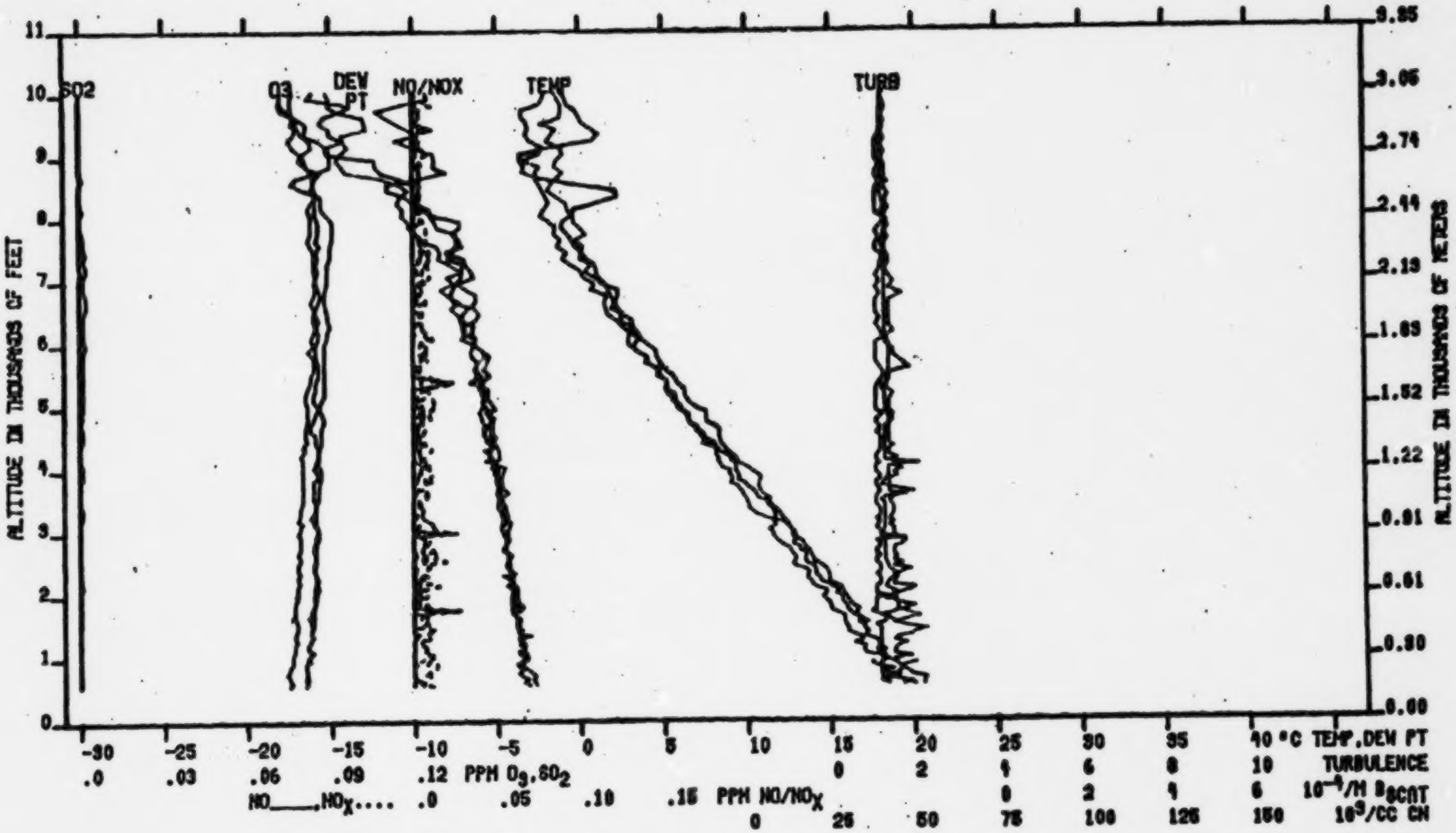

Figure 3. Concentration profiles of all three spirals of the afternoon flight of 15 April 1978 overlaid on one another.

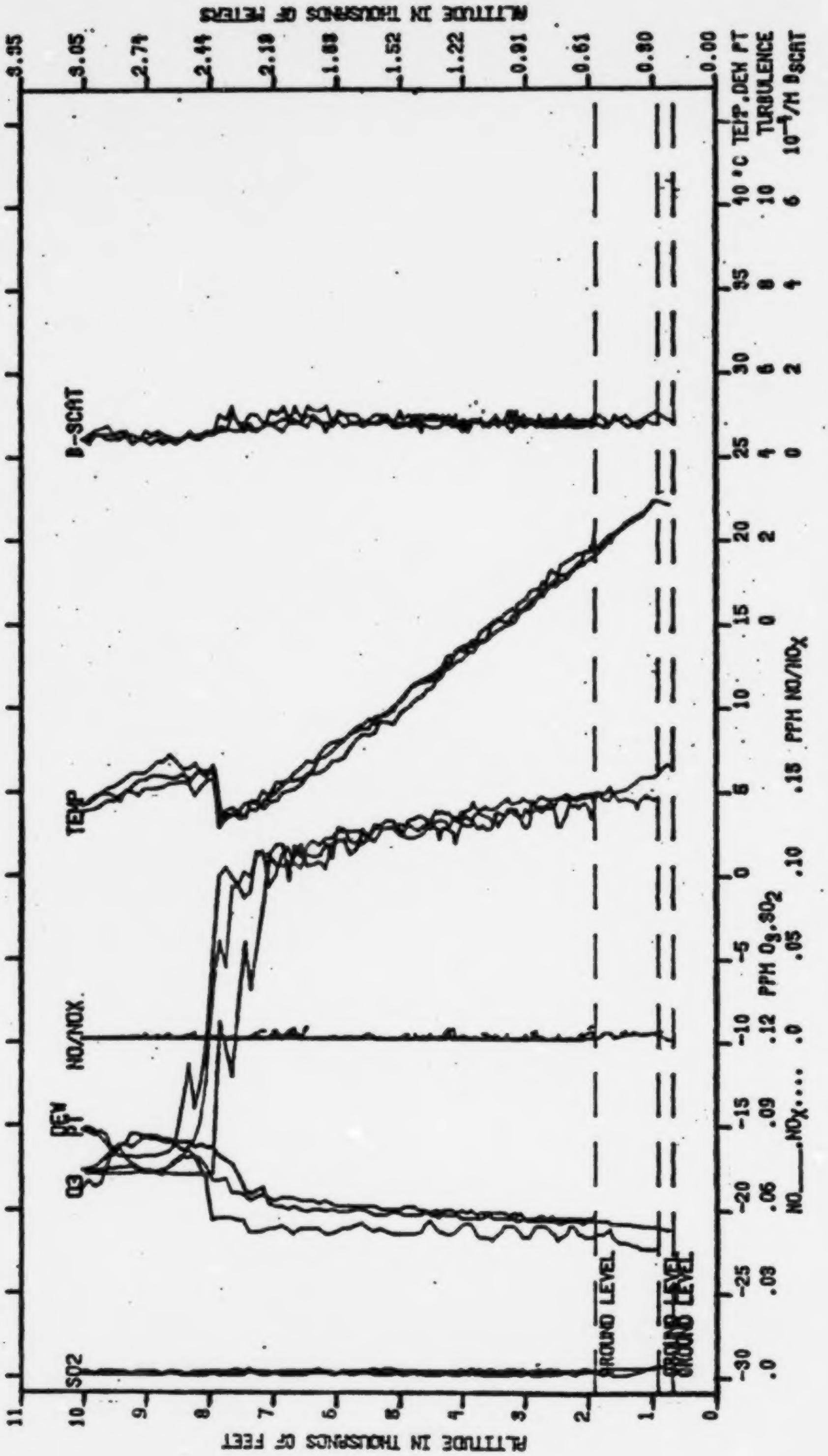

Figure 4. Concentration profiles of all three spirals of the afternoon flight of 12 July 1978 overlaid on one another.

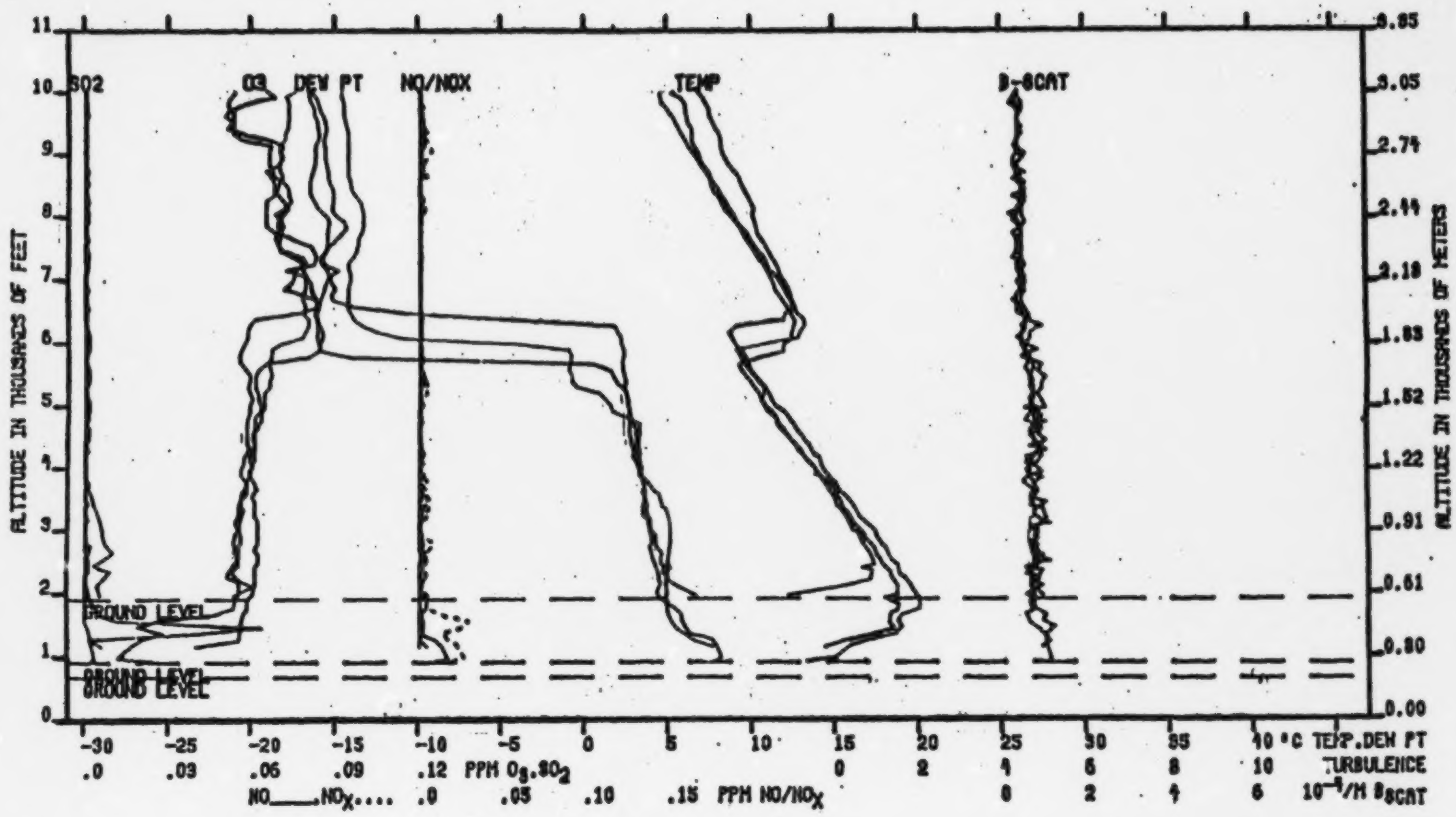

Figure 5. Concentration profiles of all three spirals of the midnight flight of 12 July 1978 overlaid on one another.

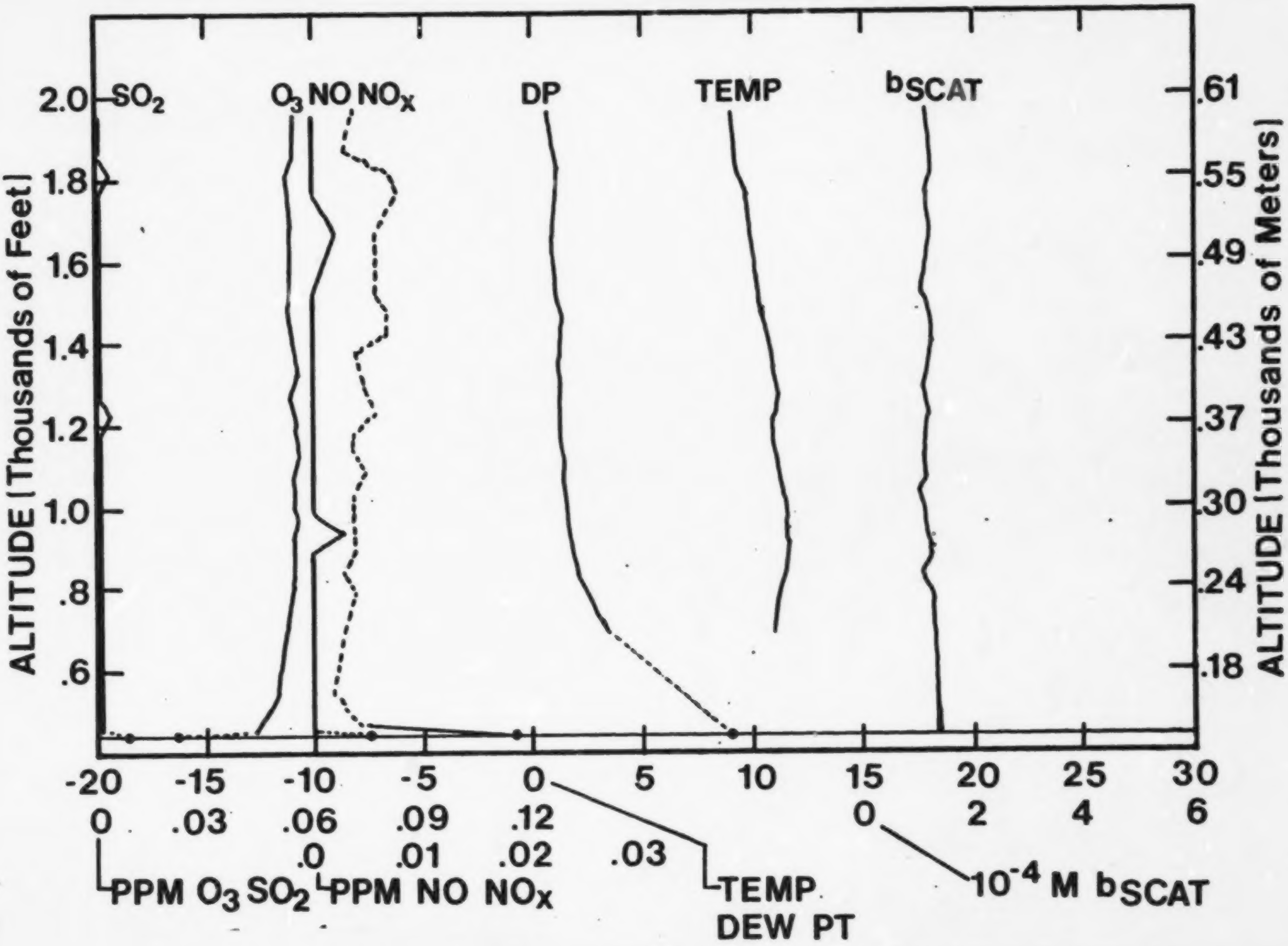

Figure 6. Low approach and surface station data collected during the morning flight on 12 April 1978 at Research Triangle Park, NC.

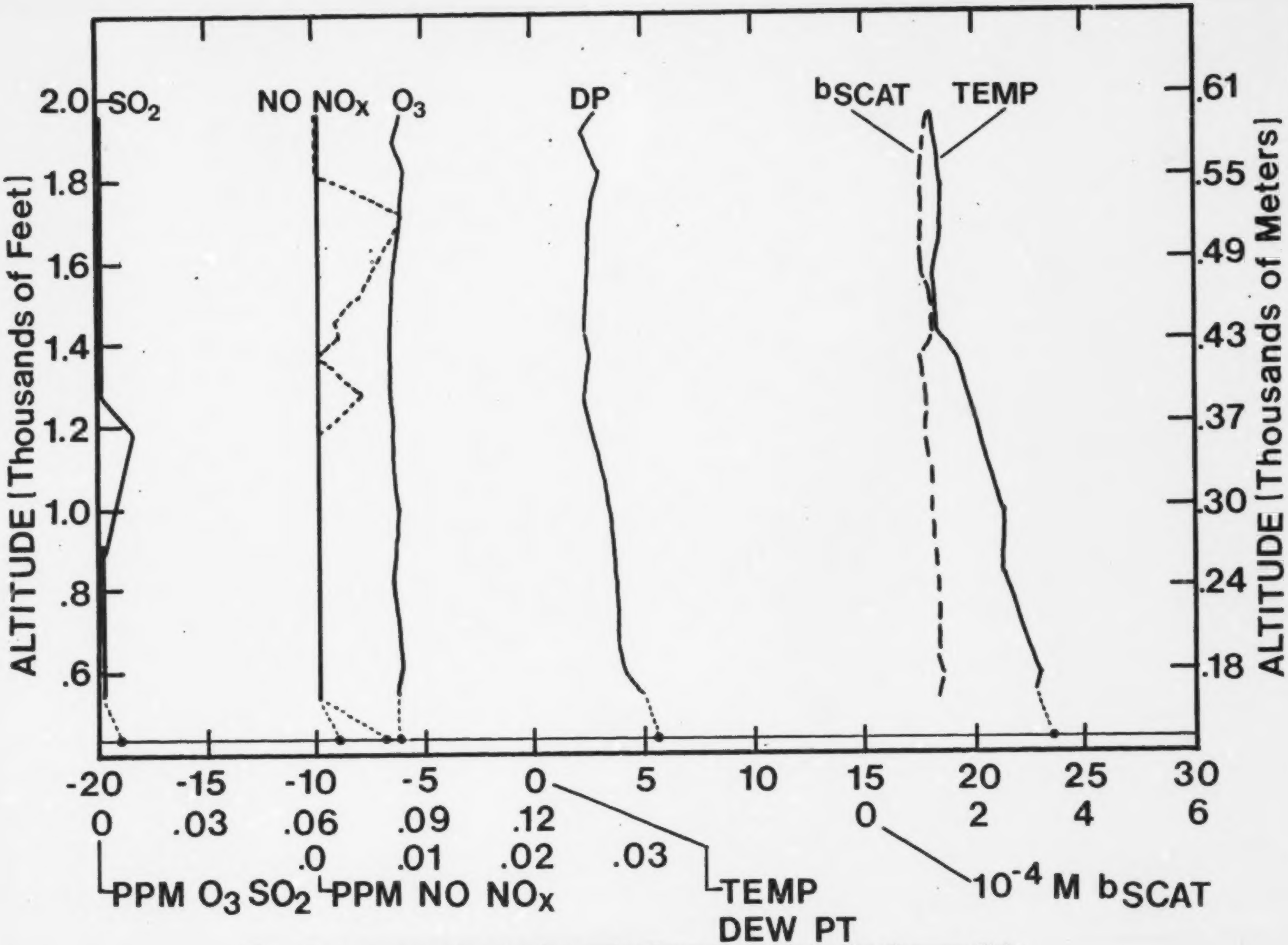

Figure 7. Low approach and surface station data collected during the afternoon flight on 4 April 1978 at Research Triangle Park, NC.

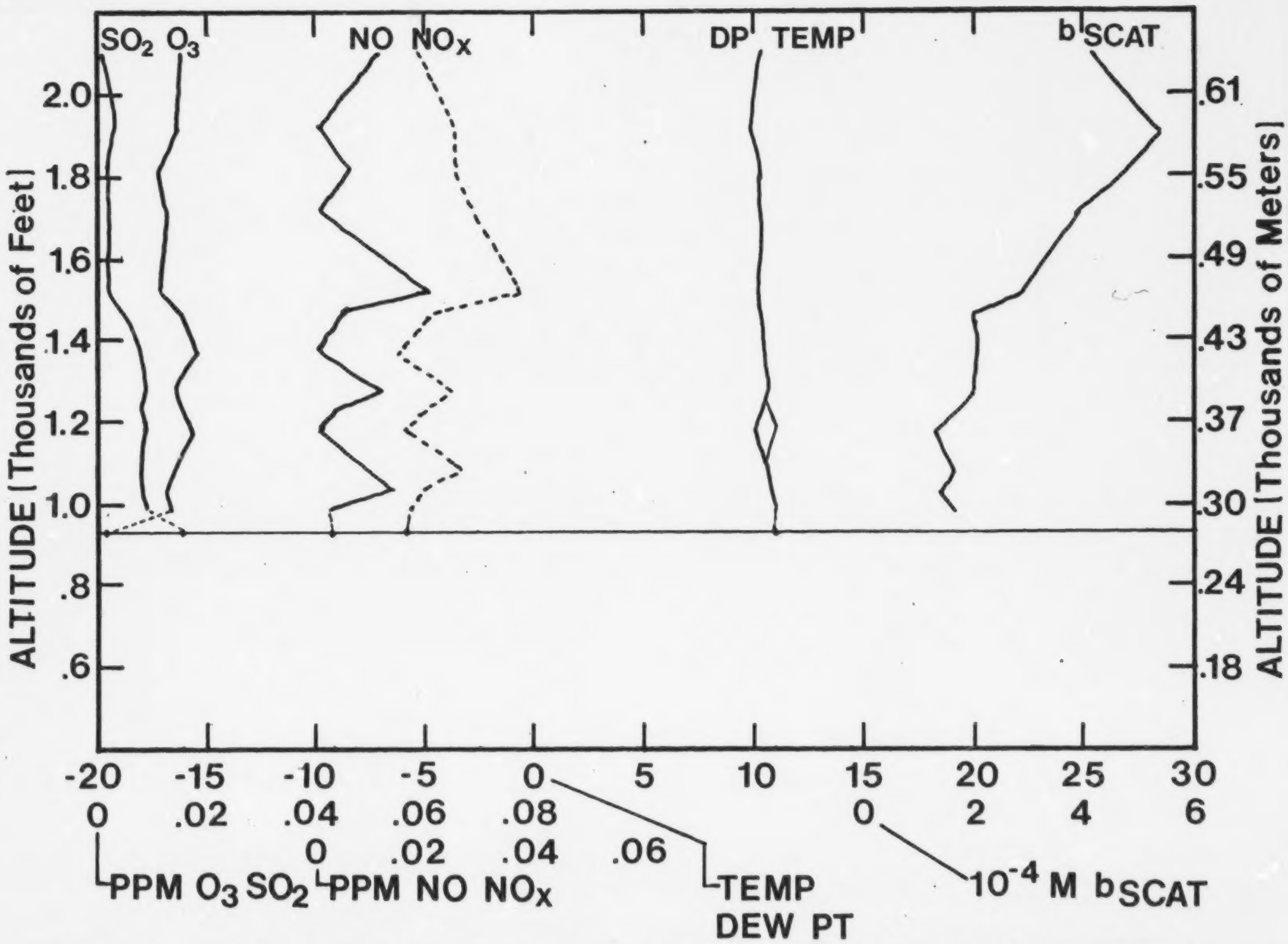

Figure 8. Low approach and surface station data collected during the afternoon flight on 13 October 1978 at Zanesville, OH.

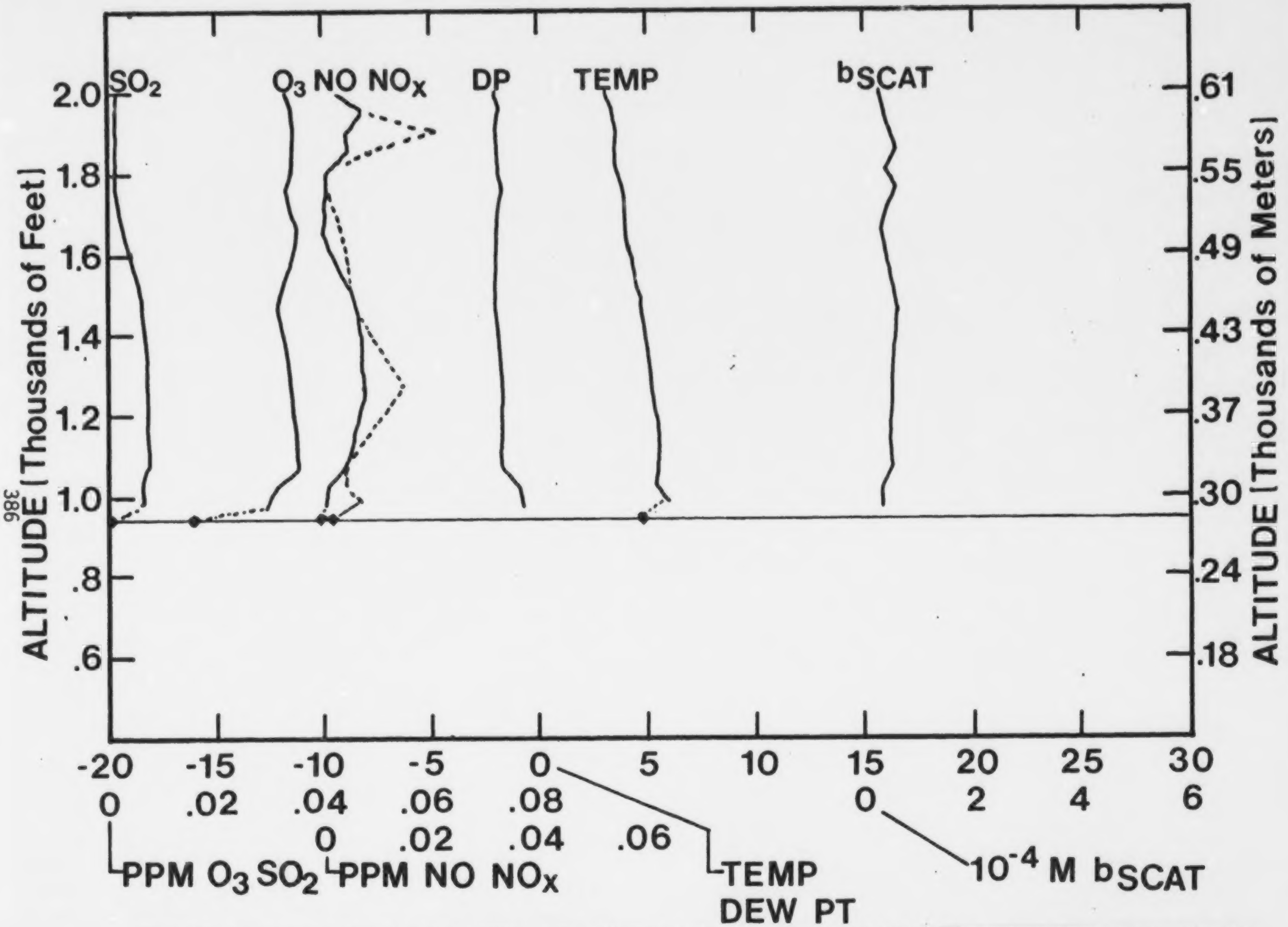

Figure 9. Low approach and surface station data collected during the midnight flight on 23 October 1978 at Zanesville, OH.

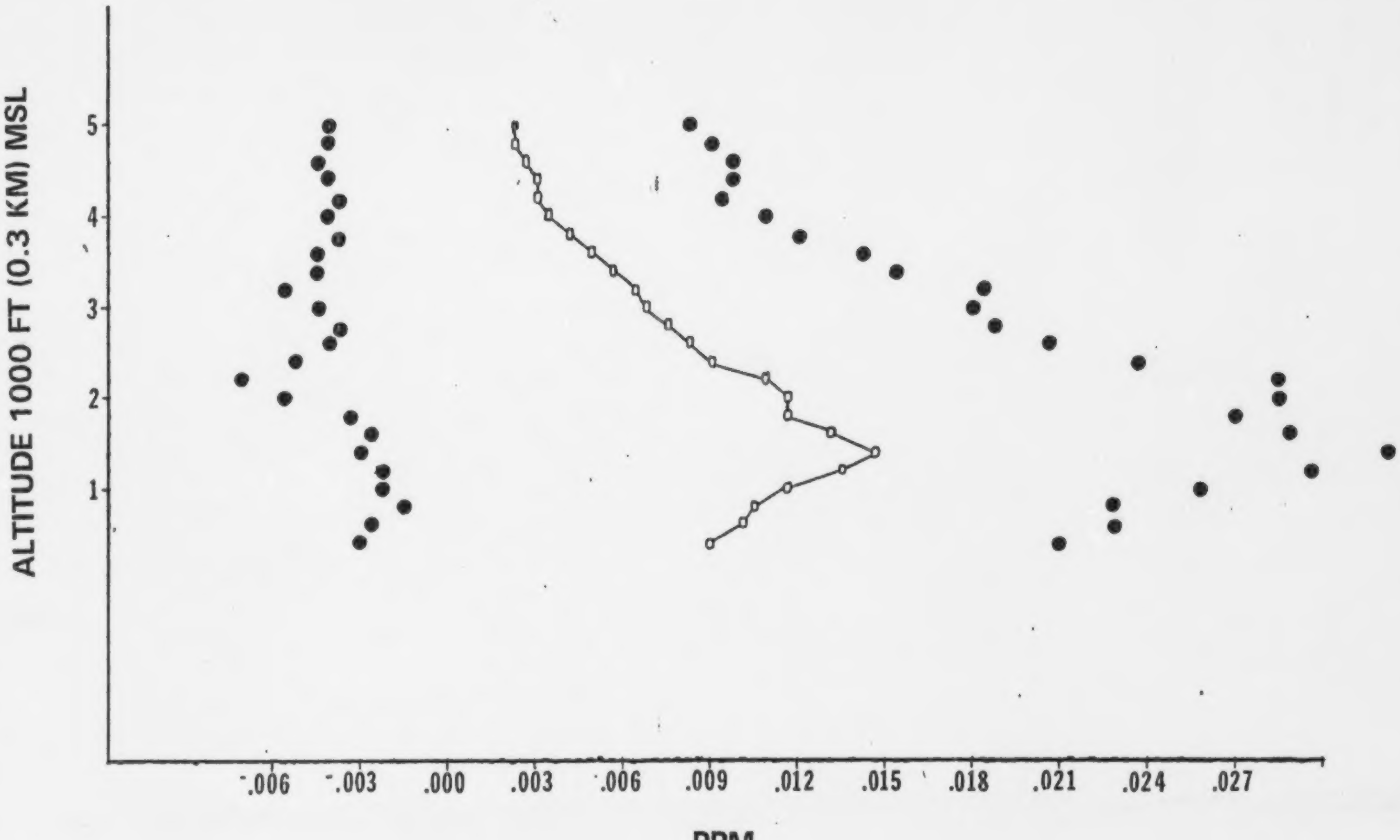

Figure 10. Mean SO_2 concentrations in 200-ft increments below 1.5 km (5,000 ft) over all SURE aircraft spirals.

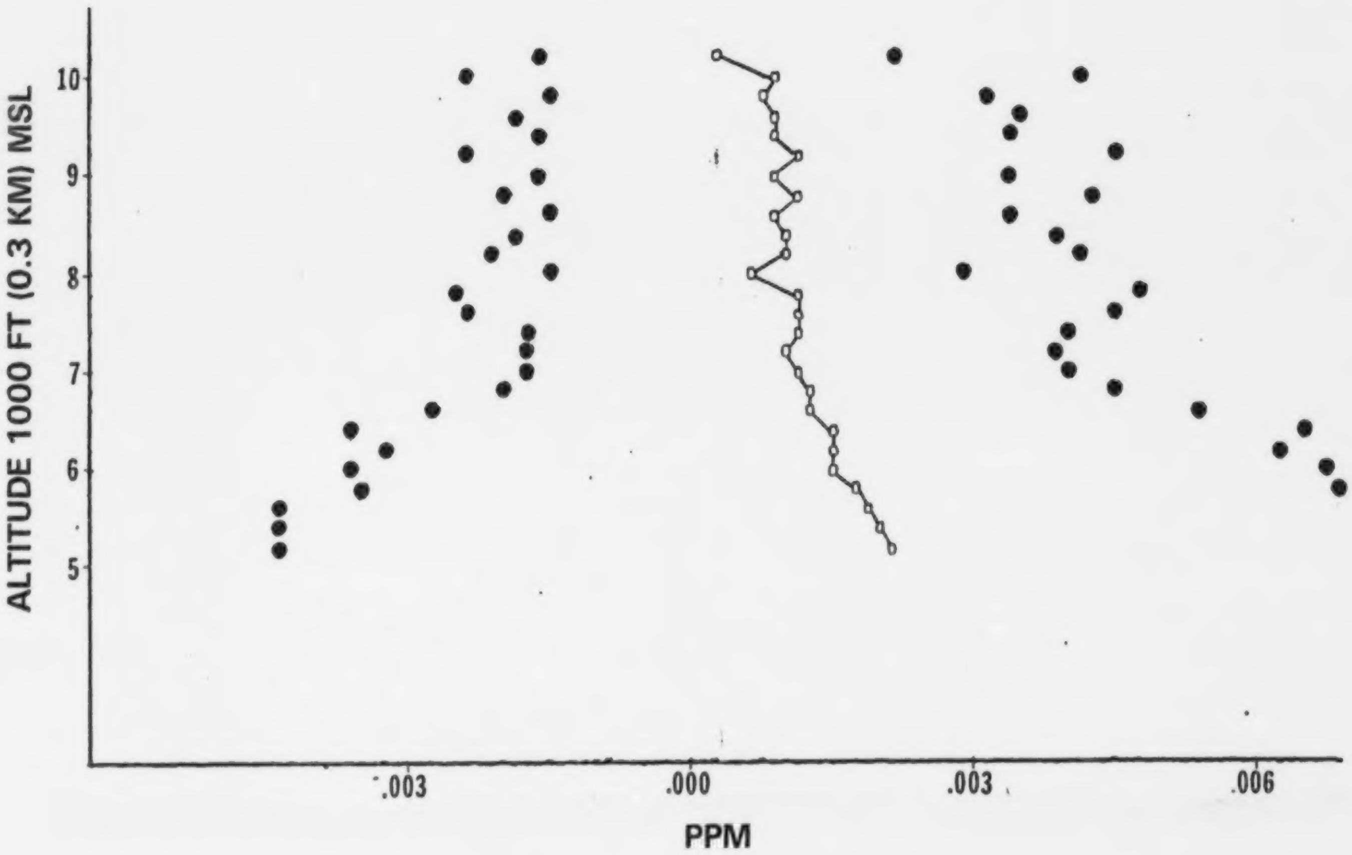

Figure 11. Mean SO_2 concentrations in 200-ft increments above 1.5 km (5,000 ft) over all SURE aircraft spirals.

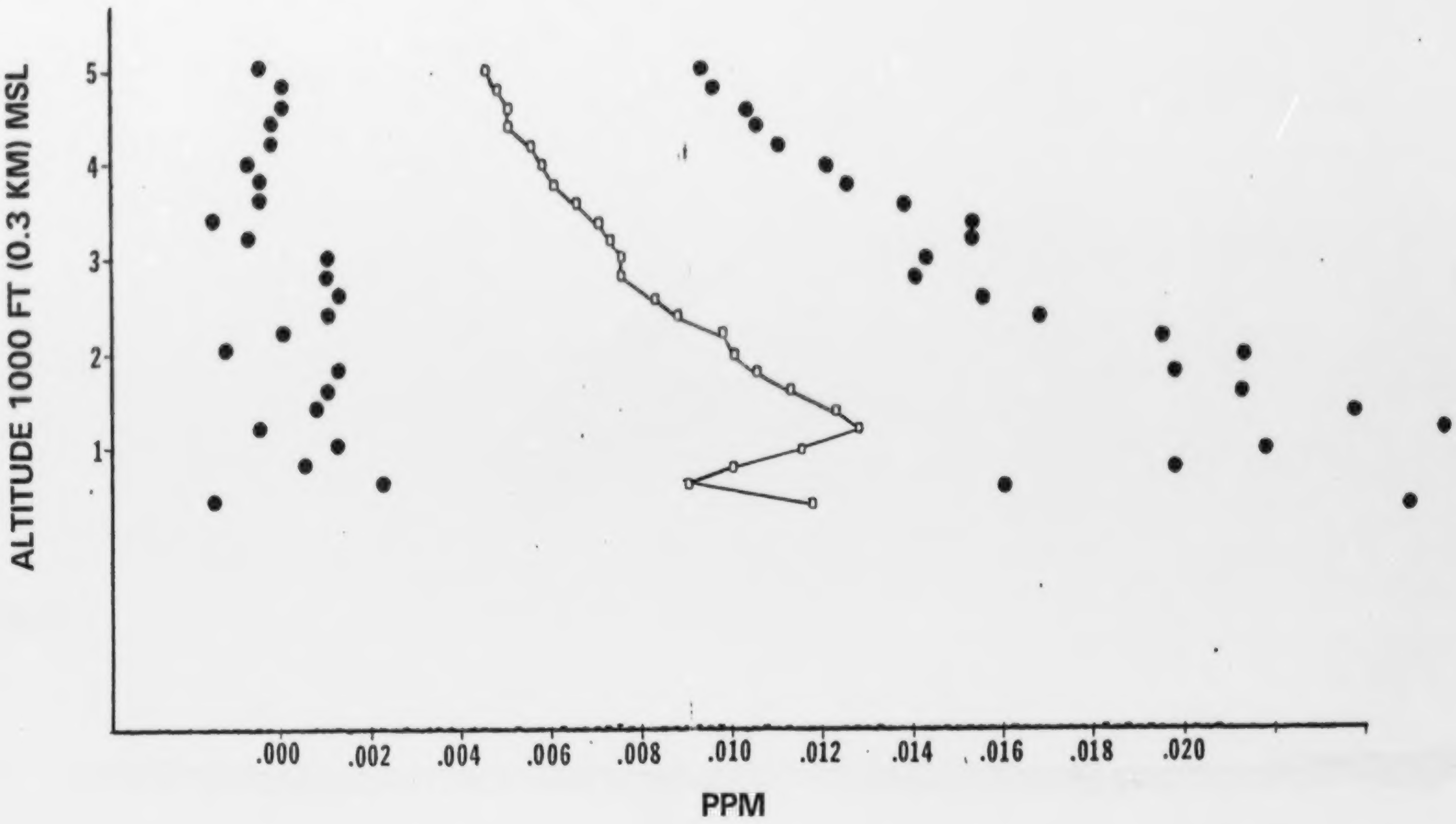

Figure 12. Mean NO_x concentrations in 200-ft increments below 1.5 km (5,000 ft) over all SURE aircraft spirals.

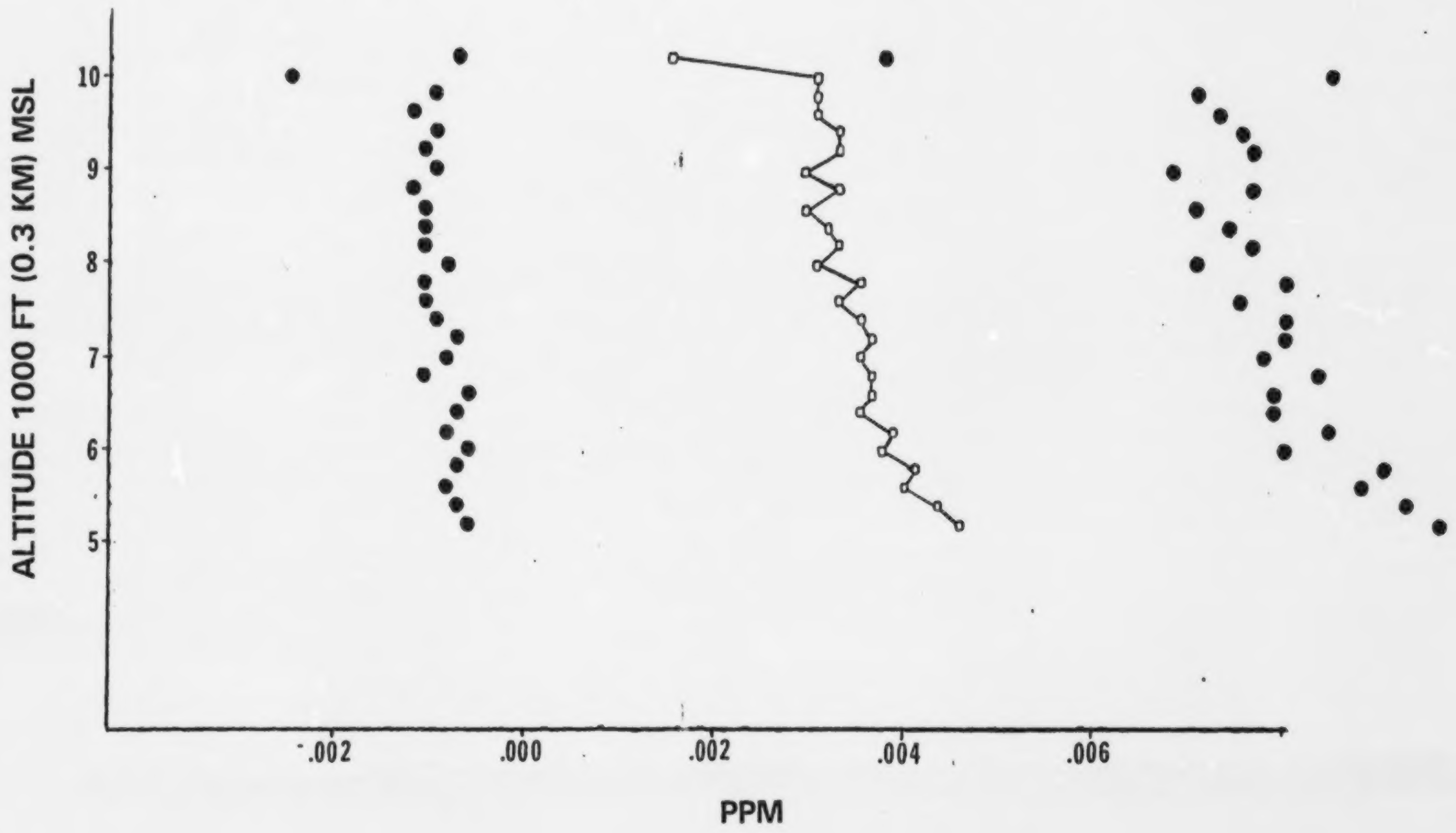

Figure 13. Mean NO_x concentrations in 200-ft increments above 1.5 km (5,000 ft) over all SURE aircraft spirals.

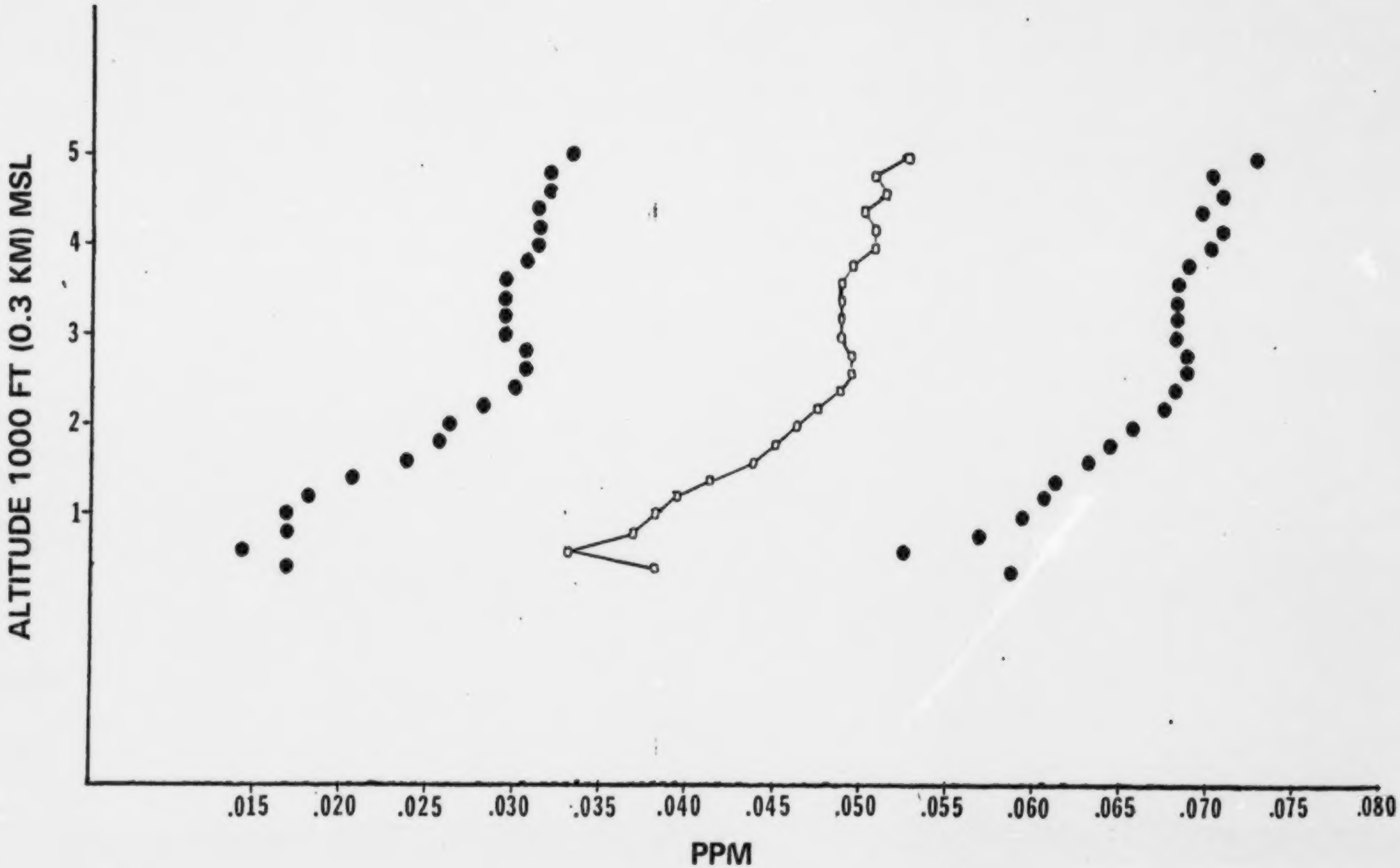

Figure 14. Mean O_3 concentrations in 200-ft increments below 1.5 km (5,000 ft) over all SURE aircraft spirals.

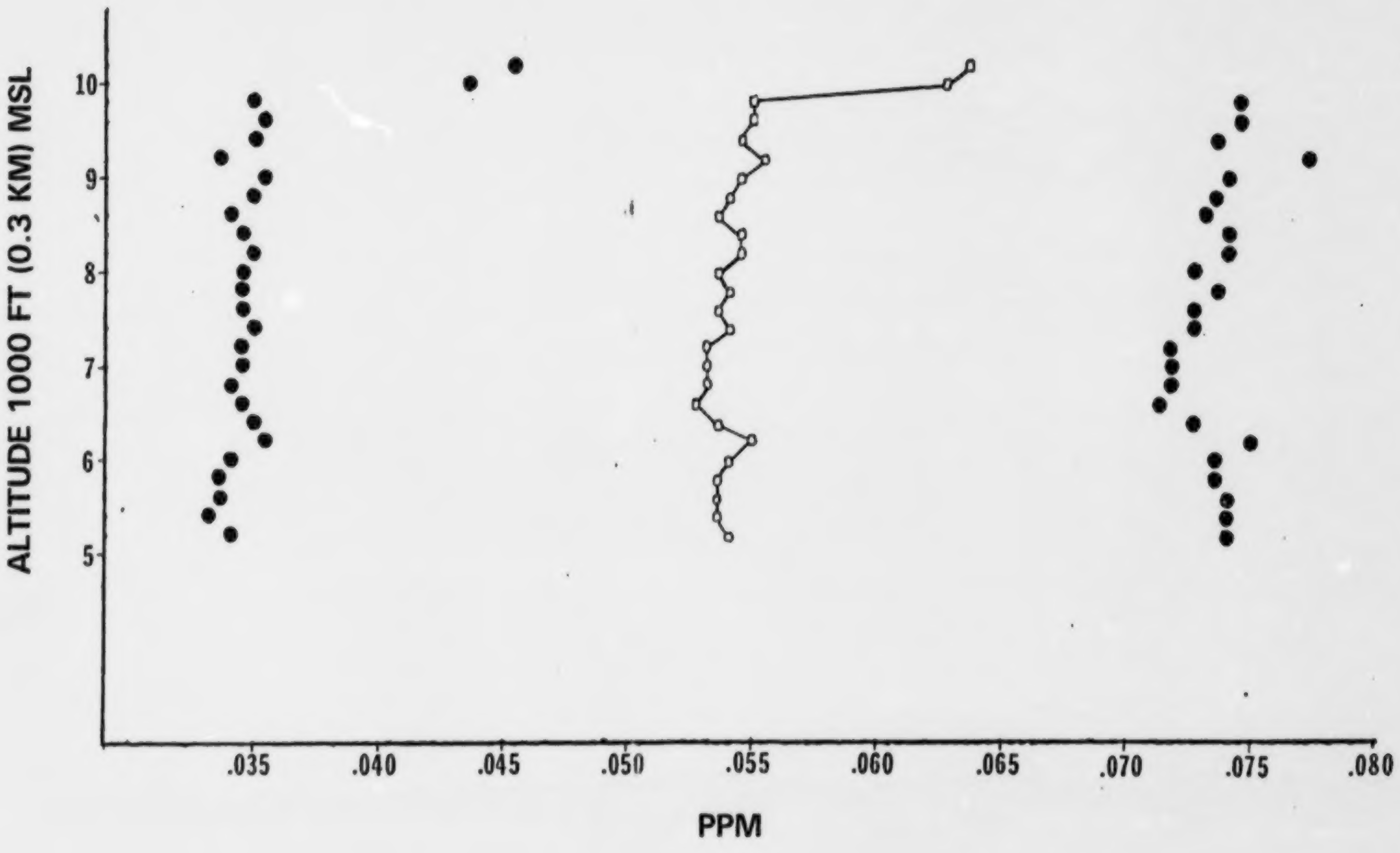

Figure 15. Mean O_3 concentrations in 200-ft increments above 1.5 km (5,000 ft) over all SURE aircraft spirals.

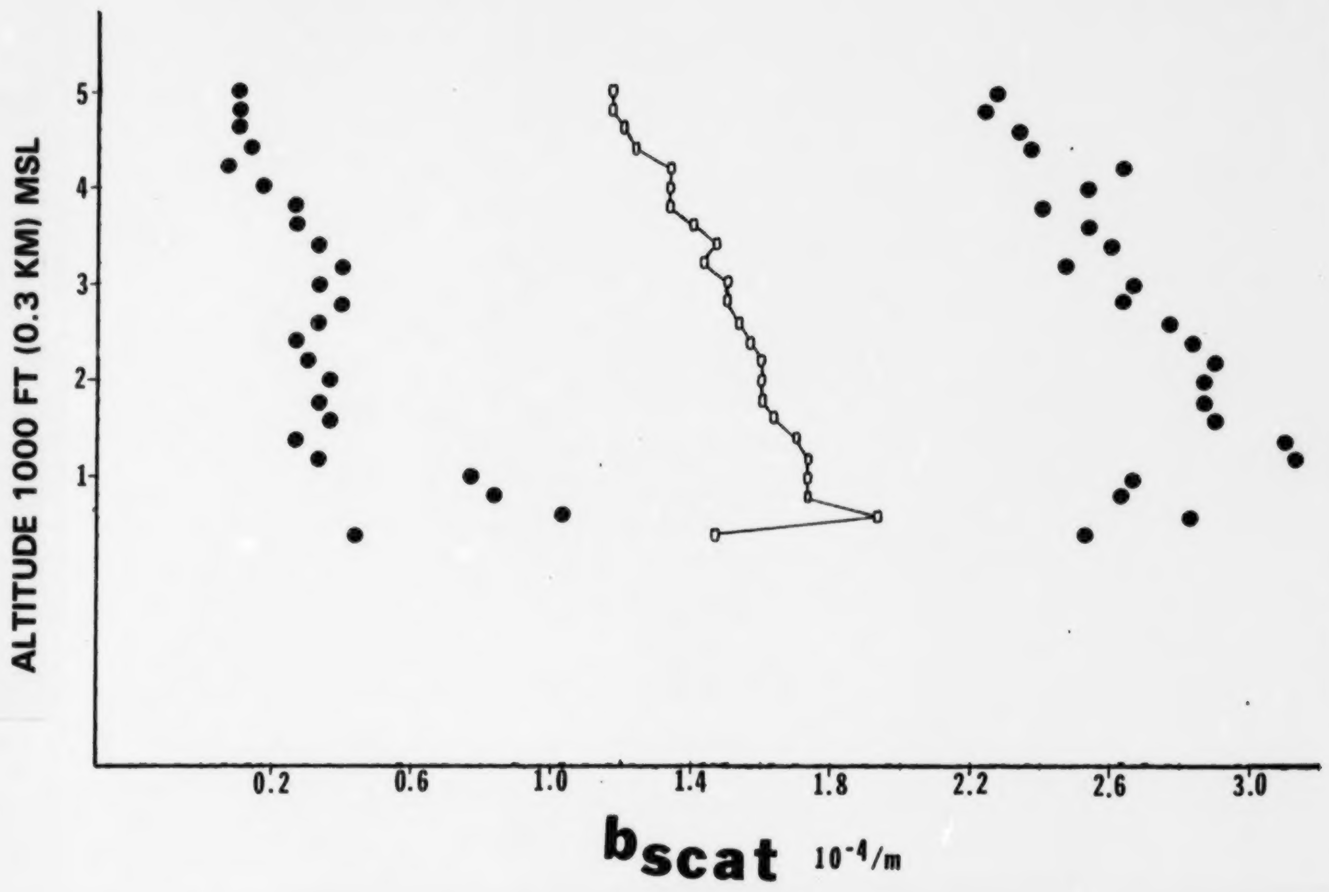

Figure 16. Mean b_{scat} values in 200-ft increments below 1.5 km (5,000 ft) over all SURE aircraft spirals.

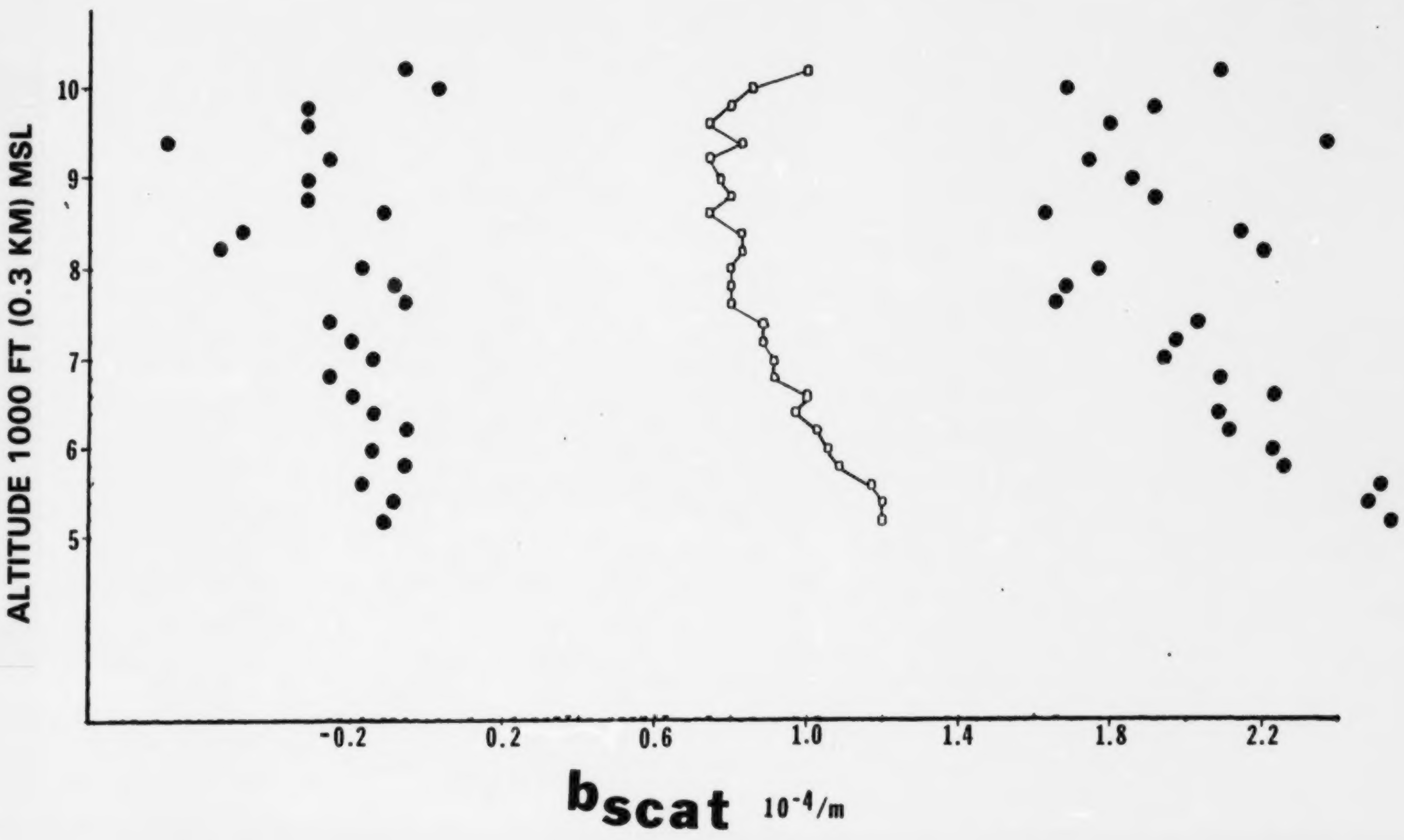

Figure 17. Mean b_{scat} values in 200-ft increments below 1.5 km (5,000 ft) over all SURE aircraft spirals.

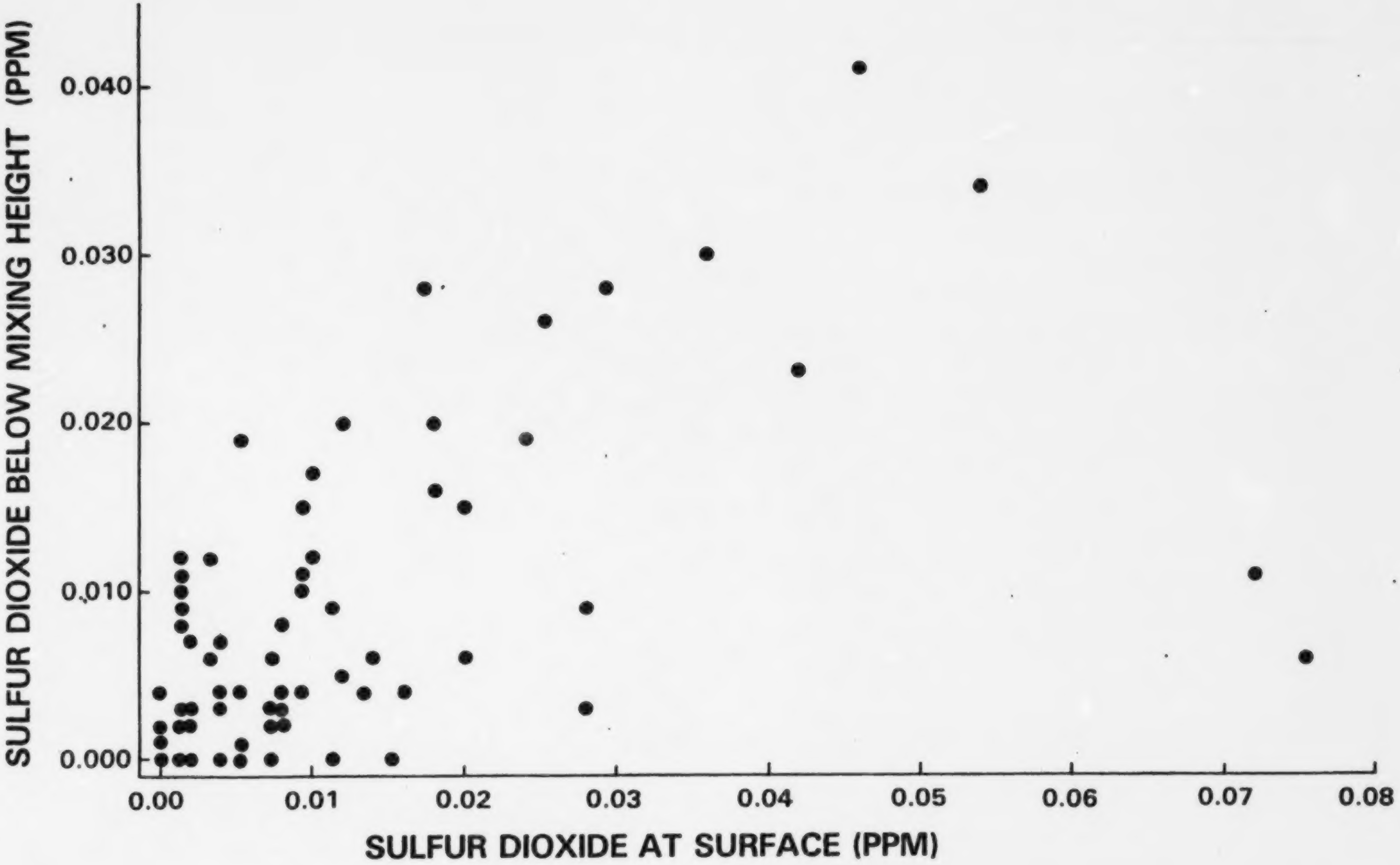

Figure 18. Scatter diagram of sulfur dioxide concentrations at the surface versus below the mixing height for all flights.

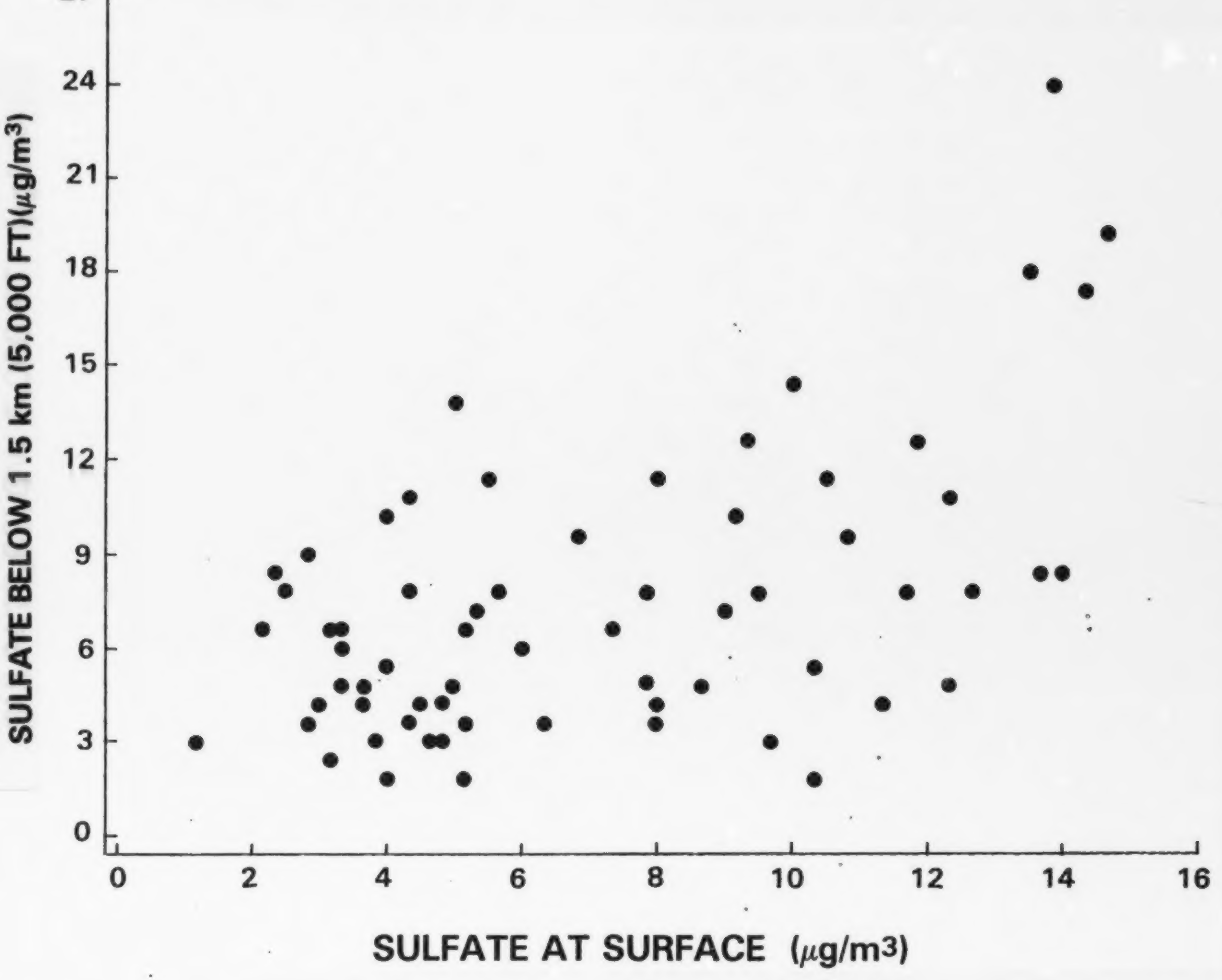

Figure 19. Scatter diagram of sulfate concentrations at the surface versus below 1.5 km (5,000 ft) MSL for all flights.

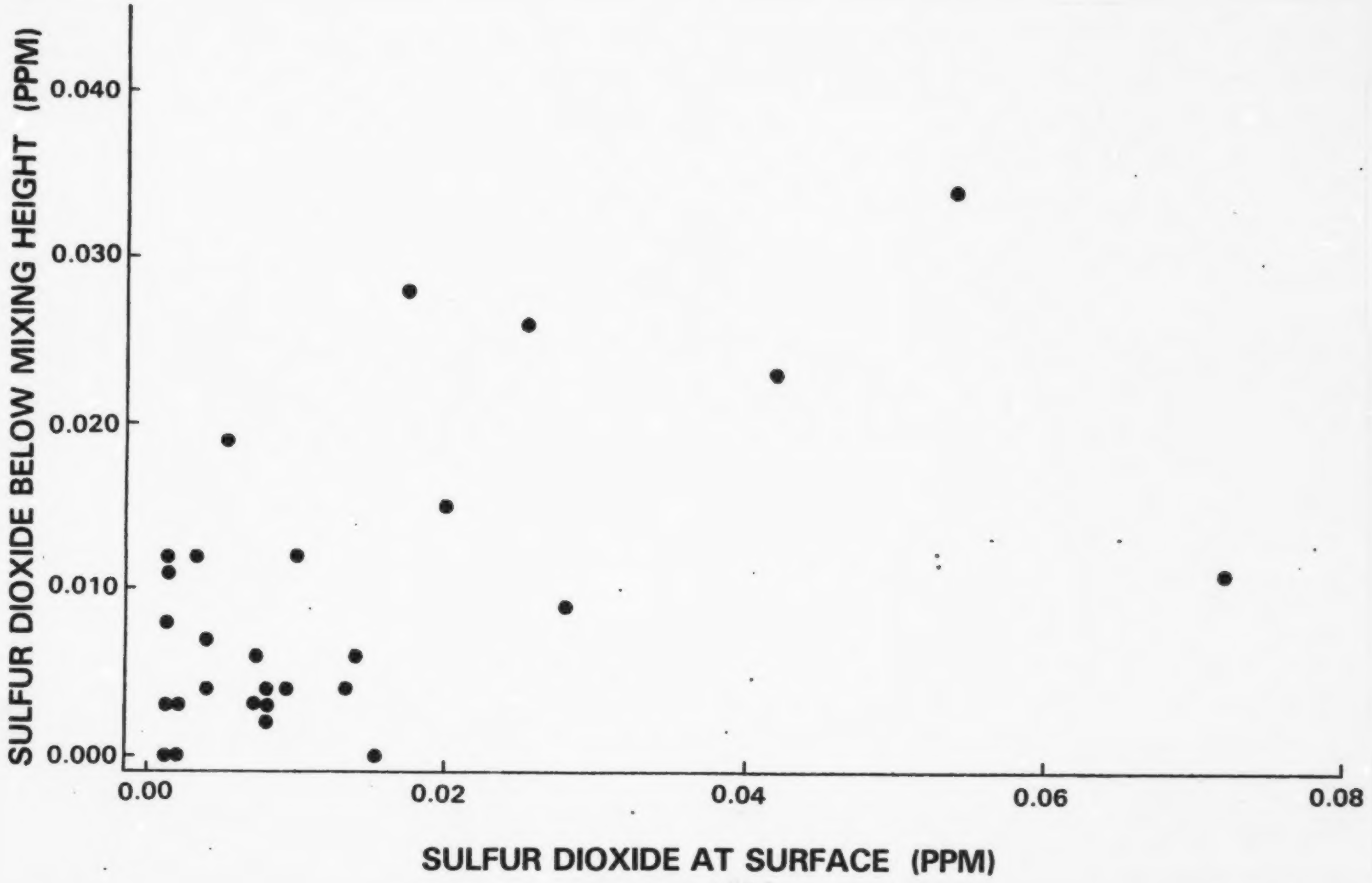

Figure 20. Scatter diagram of sulfur dioxide concentrations at the surface versus below the mixing height for all morning flights.

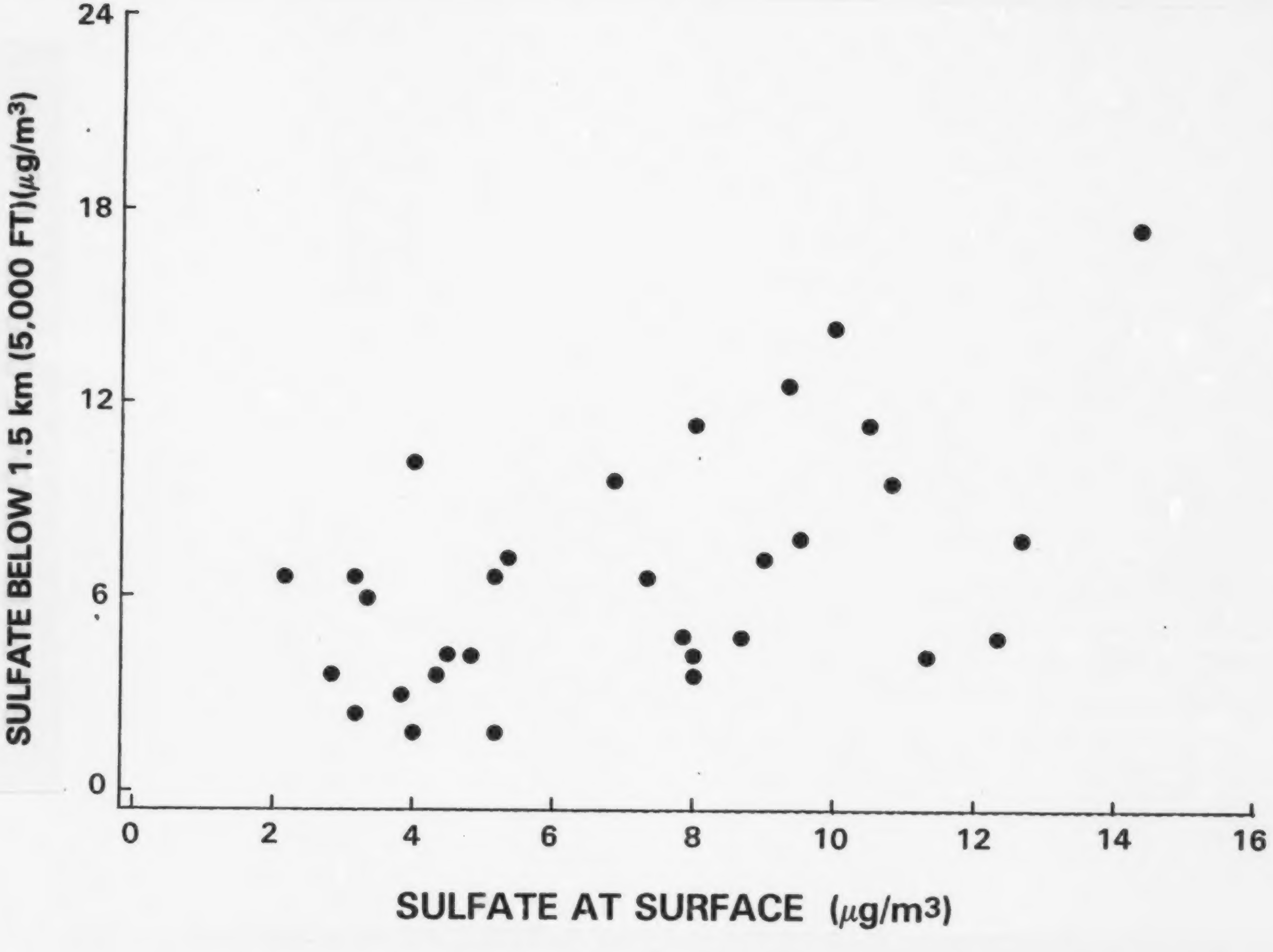

Figure 21. Scatter diagram of sulfate concentrations at the surface versus below 1.5 km (5,000 ft) for all morning flights.

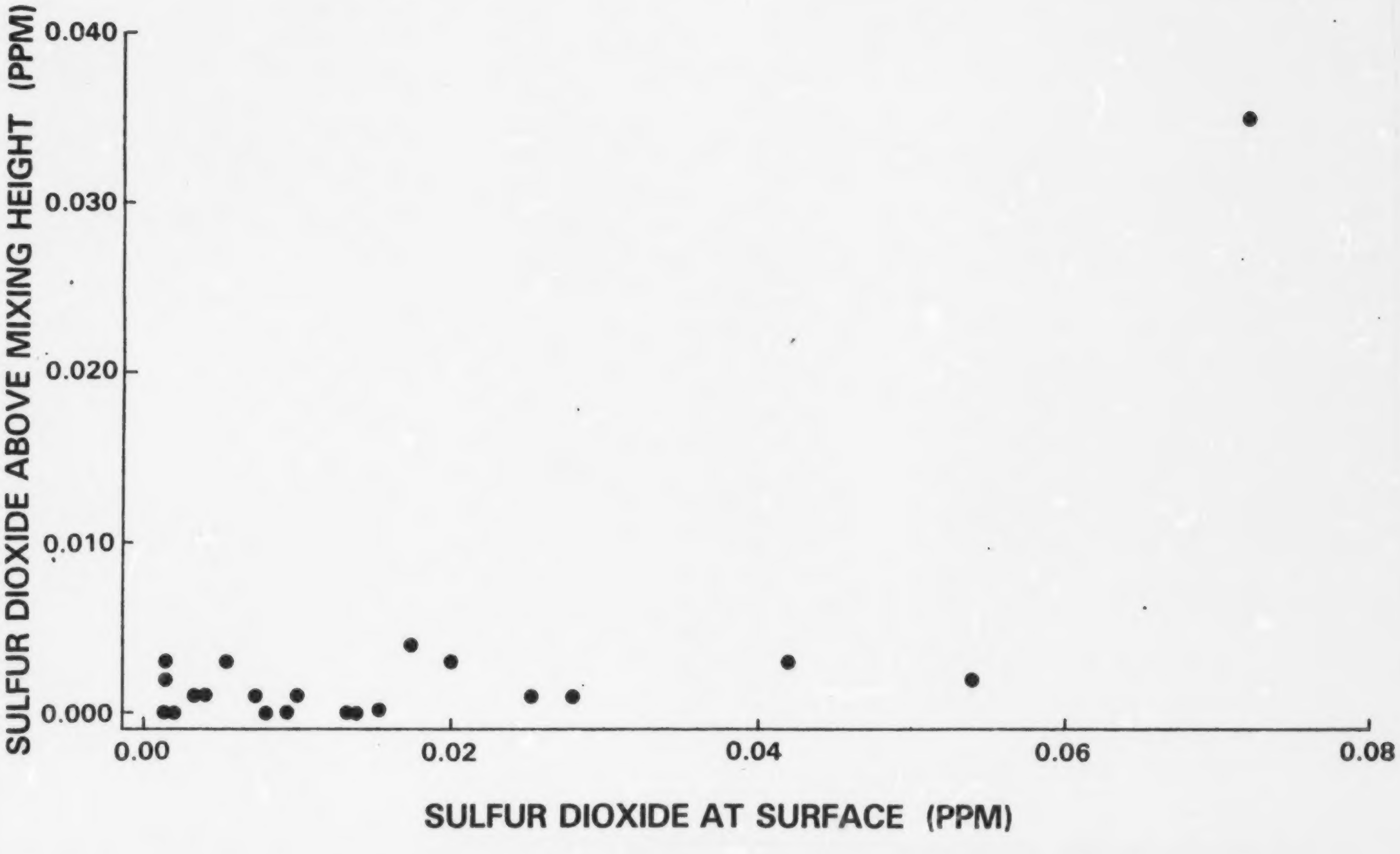

Figure 22. Scatter diagram of sulfur dioxide concentrations at the surface versus above the mixing height for all flights.

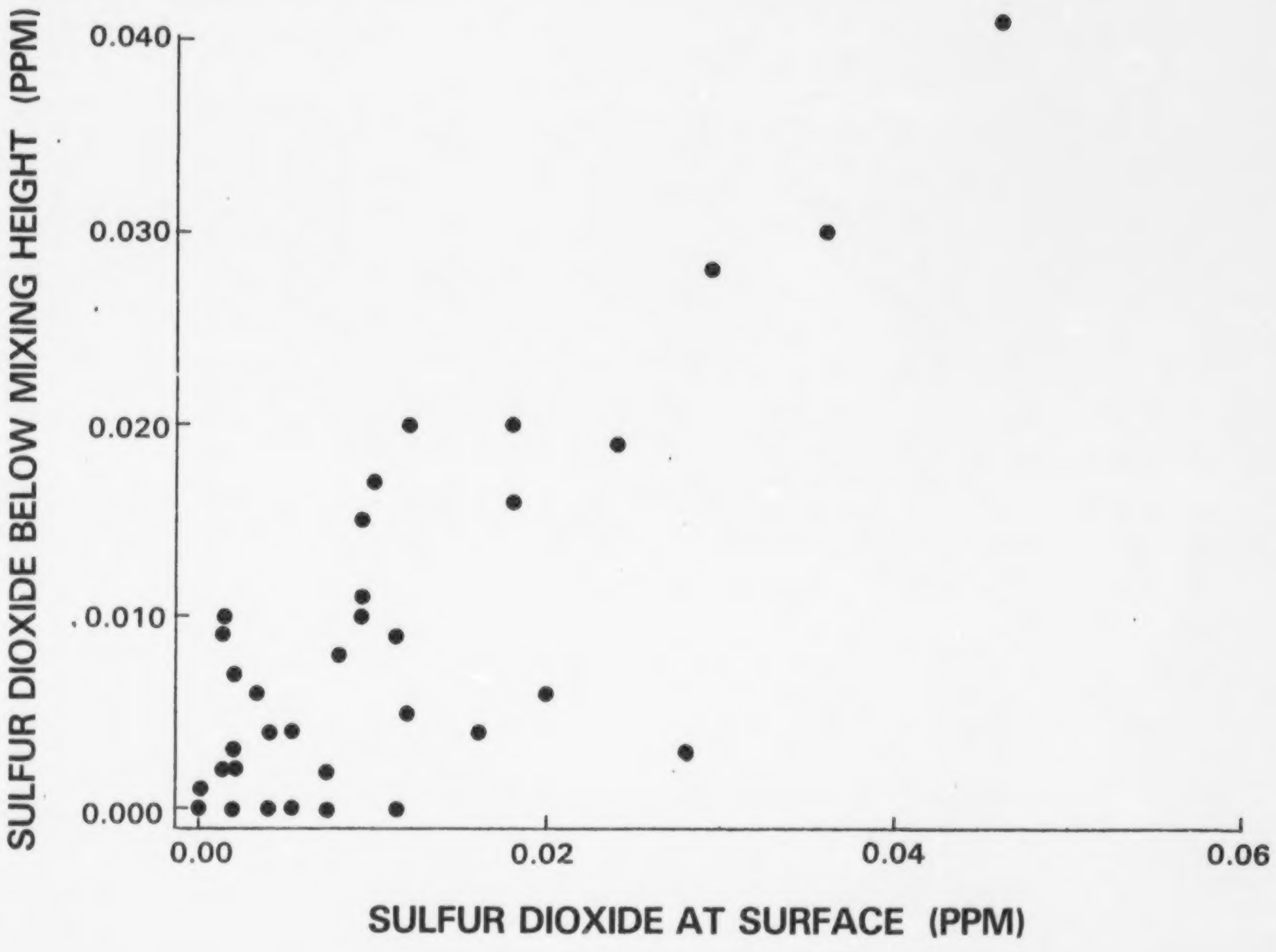

Figure 23. Scatter diagram of sulfur dioxide concentrations at the surface versus below the mixing height for afternoon flights.

TABLE 1. MEAN SO_2, NO_x, AND O_3 CONCENTRATIONS ON THREE SPIRALS DURING JULY AND OCTOBER 1978 INTENSIVES

	Spiral	Below mixing height		Above mixing height	
		Sample mean (ppm)	Level of significance	Sample mean (ppm)	Level of significance
July 1978 Scranton, PA					
SO_2	1	.0011	NS	.0002	NS
	2	.0012		.0006	
	3	.0019		.0002	
NO_x	1	.004	NS	.002	0.05
	2	.002		.001	
	3	.003		.001	
O_3	1	.068	NS	.079	NS
	2	.077		.077	
	3	.082		.085	
October 1978 Duncan Falls, OH					
SO_2	1	.0032	NS	.0008	NS
	2	.0030		.0006	
	3	.0044		.0006	
NO_x	1	.013	NS	.005	0.05
	2	.010		.003	
	3	.010		.004	
O_3	1	.043	NS	.054	0.05
	2	.044		.052	
	3	.040		.049	

NS = Not significant.

TABLE 2. VERTICAL DISTRIBUTION OF OZONE DURING SURE INTENSIVE MEASUREMENT PERIODS

	Mean $[O_3]$, ppm	Range, ppm
All flights		
Surface	0.034	0.000 - 0.084
Below mixing height	0.047	0.004 - 0.113
Above mixing height	0.054	0.018 - 0.101
Sunrise flights		
Surface	0.020	0.000 - 0.044
Below mixing height	0.042	0.010 - 0.077
Above mixing height	0.052	0.026 - 0.101
Noon flights		
Surface	0.047	0.001 - 0.084
Below mixing height	0.052	0.004 - 0.113
Above mixing height	0.054	0.018 - 0.092
Midnight flights		
Surface	0.022	0.005 - 0.039
Below mixing height	0.049	0.023 - 0.079
Above mixing height	0.060	0.025 - 0.089

TABLE 3. VERTICAL DISTRIBUTION OF SO_2 DURING SURE INTENSIVE MEASUREMENT PERIODS

	Mean $[SO_2]$, ppm	Range, ppm
All flights		
Surface	0.014	0.000 - 0.186
Below mixing height	0.007	0.000 - 0.041
Above mixing height	0.002	0.000 - 0.035
Sunrise flights		
Surface	0.013	0.001 - 0.072
Below mixing height	0.008	0.000 - 0.034
Above mixing height	0.002	0.000 - 0.035
Noon flights		
Surface	0.015	0.000 - 0.186
Below mixing height	0.008	0.000 - 0.041
Above mixing height	0.001	0.000 - 0.010
Midnight flights		
Surface	0.013	0.000 - 0.075
Below mixing height	0.003	0.000 - 0.006
Above mixing height	0.001	0.000 - 0.004

TABLE 4. VERTICAL DISTRIBUTION OF SULFATE DURING SURE INTENSIVE MEASUREMENT PERIODS

	$[SO_4^{=}]$, μg/m³	Range, μg/m³
All flights		
Surface	7.456	1.200 - 32.100
Below 1.5 km (5,000 ft) MSL	7.301	0.170 - 27.760
Above 1.5 km (5,000 ft) MSL	3.615	0.000 - 10.860
Sunrise flights		
Surface	6.934	2.100 - 14.300
Below 1.5 km (5,000 ft) MSL	6.206	0.170 - 17.180
Above 1.5 km (5,000 ft) MSL	3.100	0.000 - 8.420
Noon flights		
Surface	7.913	1.200 - 32.100
Below 1.5 km (5,000 ft) MSL	8.305	2.060 - 27.760
Above 1.5 km (5,000 ft) MSL	4.096	0.000 - 10.860

TABLE 5. CORRELATIONS BETWEEN SURFACE STATION MEASUREMENTS AND MEAN AIRCRAFT MEASUREMENTS ABOVE AND BELOW THE MIXING HEIGHT OVER ALL FLIGHTS

	Ground				
Air	SO_2	O_3	SO_4	TSP	Sample size
Below mixing height					
SO_2	.56*				75
O_3		.41*			78
SO_4			.61*		69
TSP				-.14	20
Above mixing height					
SO_2	.45*				75
O_3		.10			78
SO_4			.19		67
TSP				-.60	6

*Correlations significantly different from zero.

TABLE 6. CORRELATIONS BETWEEN SURFACE STATION MEASUREMENTS AND MEAN AIRCRAFT MEASUREMENTS ABOVE AND BELOW THE MIXING HEIGHT FOR FLIGHTS GROUPED BY TIME OF DAY

		Ground				
	Air	SO_2	O_3	SO_4	TSP	Sample size
Below mixing height						
a.m.	SO_2	.54*				30
	O_3		-.07			32
	SO_4			.54*		32
	TSP				-.73	7
p.m.	SO_2	.80*				38
	O_3		.49*			39
	SO_4			.65*		31
	TSP				.40	13
Midnight	SO_2	.71				7
	O_3		.93*			7
Above mixing height						
a.m.	SO_2	.69*				30
	O_3		-.20			32
	SO_4			.11		37
p.m.	SO_2	.06				38
	O_3		.26			39
	SO_4			.24		36
Midnight	SO_2	-.25				7
	O_3		.64			7

*Correlations significantly different from zero.

PASSIVE REMOTE SENSING OF SO_2

Millán M. Millán
Atmospheric Environment Service, Toronto, Canada

INTRODUCTION

Over the last decade or so it has become increasingly evident that atmospheric pollutants can be transported much farther and remain airborne for longer periods than had previously been expected. In turn, the need to study and characterize the behavior of the polluted air parcels has resulted in a requirement for the development of increasingly sophisticated measurement techniques. Among these are remote sensors that can analyze airborne pollution from ground, airborne, and satellite-based platforms.

The spectroscopic techniques used for this purpose can be broadly divided into the active, which use a controlled radiation source, and the passive, which use naturally available radiation. So far, two main instrumental families have emerged to the level of extended and routine operation: lidars and correlation spectrometers. The former are inherently active instruments, and the latter have been utilized mainly in a passive mode of operation. Here we will examine the application of passive correlation spectroscopic techniques. In particular, we will concentrate on the application of the commercially available COSPEC (Barringer Research Ltd.) with emphasis on the work carried out in the Canadian Department of the Environment.

For a more extensive review of both lidar and correlation spectrometers as they apply to the detection of SO_2 in the atmosphere, the reader is referred to the review paper by Hamilton et al. (1978).

INSTRUMENTAL SYSTEM AND OPERATIONAL CHARACTERISTICS

The correlation spectrometer (COSPEC) is an instrument designed to measure the quantity of a specific target gas (SO_2 or NO_2 in the commercial version) along its line of sight to a suitable source of radiation. For passive remote sensing, the radiation source is the scattered solar light from the sky. The instrument consists of a telescope to collect the radiation, a grating spectrometer that disperses and displays the spectrum of the incoming radiation onto a disc in its exit plane (Figure 1), and a photodetector with associated signal processing electronics. Engraved on the disc are four masks or arrays of exit slits, which have been designed to coincide alternatively with the absorption maxima and minima of the target gas (Millán and Hoff, 1977a; 1978). By rotating the disc, the photodetector (a photomultiplier tube) receives a modulated signal that is processed to yield an output proportional to the line-integral of the concentration of the target gas along the line of sight.

Two calibration cells containing known amounts of SO_2 (or NO_2) can be inserted in the optical path to provide a suitable calibration of the output.

From the point of view of data reduction and interpretation, the simplest mode of operation is to use the sensor looking vertically upward to the zenith sky (Millán, 1979). The sensor is usually mounted on a vehicle that travels underneath the target gas cloud. Figure 2 shows the conceptual relationship between the output and the plume parameters for the case of a Gaussian plume when a sensor is used to traverse under a plume.

The operational characteristics of any passive remote sensing instrument are, to a large extent, dominated by the peculiarities of the background. In the case of the COSPEC measuring SO_2, Figure 3 shows the kind of variation in the spectral radiance of the zenith sky as a function of the solar elevation. The intensity of the radiation and penetration of the shorter wavelengths increases with solar elevation, and, accordingly, follows a well-marked diurnal cycle. The results of this diurnal variation are nominally: (a) a zero, no-gas signal, or baseline diurnal drift; and (b) a diurnal sensitivity change (Millán and Hoff, 1978).

The present COSPEC design allows for the cancellation or minimization of the baseline drift (see below). The diurnal sensitivity variation remains, however, and must be overcome by frequent instrumental calibrations. Figure 4 shows the diurnal baseline behaviour in a well-compensated sensor.

RESEARCH IN THE ATMOSPHERIC ENVIRONMENT SERVICE OF CANADA (AES)

The use of this type of remote sensing technique in the Canadian Department of the Environment was considered under the aegis of the following broad objectives: (1) to conduct fundamental and applied research on the application of remote sensing techniques to determine air pollution concentrations and atmospheric processes related to pollution dispersal and transport in the atmosphere, and (2) to optimize data handling methodologies for the application of field observations to the development of diffusion models from point and area sources.

The data collection and processing methodologies have been reported by the author and his colleagues (Millán, 1978; Hoff et al., 1978; Millán et al., 1978) and will not be discussed in any detail here. For the purpose of this presentation, it should be indicated that individual plume profiles obtained during a preselected time period (½ or 1 hr) are projected onto a plane perpendicular to the average plume direction during the same period. These profiles are averaged directly, as they occur, to yield an Eulerian average. They can also be recentered with respect to their individual centers of gravity (COG) and averaged to yield a fixed-distance Lagrangian average. This latter process nominally removes from the average the meandering of the plume centerline during the time period considered. The two averaging processes are illustrated in Figure 5.

Present areas of research that may be of direct applicability to a PEPE type program are those concerned with the measurement of plume diffusion from tall stacks in the regional scale (up to ~500 km), and with the measurement of transboundary fluxes of SO_2; i.e., the profiling of large and low concentration SO_2 clouds. These applications require sensors that are very stable and very sensitive and that have an extended operational time. To this effect, some of the objectives of our present work are:

1. To extend the time of operation of the COSPEC to very low, or zero, solar elevation angles.
2. To minimize the diurnal baseline drift.
3. To investigate methods of establishing an absolute zero for SO_2 and NO_2 burden measurements.

The first two objectives have now been successfully completed (Millán and Hoff, 1976; 1977b) and Figure 4 shows the result of the baseline stabilization method developed. Our first experience with the regional transport of the plume from a tall stack took place during the development of this methodology. As Figures 6 and 7 illustrate, the departure of the baseline (Figure 6) toward SO_2 readings at ~1600 hr (LST) can be attributed to the plume from the INCO superstack (381 m) in Sudbury, Ontario. This was established by calculating the back trajectories for the air parcel over Toronto at the time of the observation (Millán and Chung, 1977). These are shown in Figure 7. After this serendipitous observation, a program was initiated to use the baseline-stabilized COSPEC's together with appropriate trajectory forecasting to study the dispersion of the plume from this source on the regional scale and under similar meteorological conditions. Figure 8 shows six plume profiles obtained on May 10, 1977, at approximately 300 km from Sudbury on Highway 9 in southwestern Ontario between Orangeville and Palmerston. Two COSPEC vehicles were used (nearly) simultaneously for the first four profiles, and one for the last two. The plume remains quite cohesive and meandering until approximately 1400 hr (EDT). After this time it starts spreading laterally very quickly. This is caused, presumably, by the convection activity reaching the plume level. This program of measurements is continuing at present.

PLUME DIFFUSION AT THE LOCAL SCALE (up to ~50 km)

Characterization of plume behaviour in this scale is intended to support the development and verification of plume diffusion models. For this work, the COSPEC vehicle(s) is also outfitted with an SO_2 point monitor to delineate the plume impingement area, or ground plume, and several units are normally used simultaneously at various distances from the source. Figure 9, for example, shows two half-hour Eulerian averages of seven plume profiles each. These profiles were obtained in a lakeshore environment at approximatley 14 km from the plant under conditions of strong and well-defined wind. Both graphs include the averages of the vertically integrated as well as the ground SO_2 plumes.

Our experimental evidence indicates that under conditions of strong and well-defined winds (i.e., near neutral conditions): (1) the averages are well-behaved, i.e., reasonably smooth; (2) the ground plume is usually displaced to the left of the verticallly integrated plume; and (3) this is always associated with the usual turning (veering) of the wind with height.

The situation can be quite different for the plume of the same plant under a well-developed fumigation due to its interaction with the thermally induced boundary layer (TIBL). In Figure 10a, the wind backed with height throughout the thickness of the boundary layer. For this case, the center of gravity of the ground plume is to the right of the overall plume. As seen in Figure 10b, 2 hr later when the wind had reverted to a veering profile, the COG of the ground plume is again to the left of the overall plume. Some thousand profiles with these characteristics strongly indicate that wind directional shear effects play a very important role in plume diffusion, both in the enhancement of plume spread and in the location of the ground plume vs. the plume aloft.

Another example of a sheared plume propagating downwind is provided by the profiles shown in Figures 11 and 12. These are compositions of fixed-distance Lagrangian averages (½ hr) of plume profiles obtained with three COSPEC's operating simultaneously at increasing distances from the stack. The time lag between the averages shown was selected to represent the time required for a representative air parcel to travel from one distance to the next.

AIRBORNE APPLICATIONS

Initially, one can envisage two modes of operation for an airborne COSPEC or similar instrument: upward looking and downward looking. In the first mode, the operational characteristics and data reduction procedures are not very different from those for a ground-based sensor. The coverage is much faster, and traverses are no longer dependent on the availability of a suitable road network. Information on the gas burden from the ground to aircraft altitude, however, is lost. This method of operation has been used successfully to quantify the transboundary flux of SO_2 between Germany and the Netherlands (Van Egmond et al., 1978).

It is important to realize that in any type of remote sensing of atmospheric components, one is confronted with a radiation transfer problem. This indicates that, in general, the data must be processed (i.e., "inverted") in order to retrieve the desired information. Under certain conditions, however, the radiation transfer problem is sufficiently simple that an instrumental calibration is all that is required to retrieve the signal. This is mostly the case for the upward-looking geometry of observation of a sensor like the COSPEC, operating in the near ultraviolet (SO_2) or in the blue-visible (NO_2).

Up to this point it has been considered that the COSPEC output is proportional to the line-integral of the target gas concentration along the line-of-sight (to the zenith sky). This assumes that the SO_2 lies in a clear particle-free atmosphere and is illuminated entirely from behind. In practice, the gas will be accompanied by particles that scatter radiation into the line of sight from other angles. If the sulfur dioxide is distributed uniformly, this can only increase the effective pathlength and increase the measurement of the vertical burden. It can be shown, however, that under most atmospheric conditions the increase is not more than 4 to 10 percent of the true burden (Millán, 1979). The same applies to the aircraft-based upward-looking application.

For the downward mode of operation, the data reduction is not as simple. A fraction of the available radiation is reflected from the surface after traversing at various angles through the atmospheric layer below the aircraft, and the rest of the radiation is scattered upward from the particles in the field-of-view of the sensor. Retrieval of the desired information now requires the development of a suitable radiation transfer model and a data inversion procedure, which, up to the present, has not been seriously pursued.

FUTURE DEVELOPMENTS

The development of an improved or a new generation of sensors with a diurnal baseline drift of less than 10-15 ppm-m, and/or an absolute zeroing technique, can be expected within 1 or 2 years. These would be particularly useful for the measurement of transboundary fluxes with more accuracy than is easily achievable at present. Software techniques, such as the radiation transfer model and data inversion procedures for downward-looking airborne application, can be developed at present for use by the current generation of sensors. The development of this work, however, appears to be utimately related to program requirements and may not be initiated until all the possibilities of the ground-based and aircraft-based upward-looking modes of operation are exhausted.

REFERENCES

Hamilton, P. M., R. H. Varey, and M. M. Millán. 1978. Remote sensing of sulphur dioxide. Atmos. Environ. 12:127-133.

Hoff, R. M., A. J. Gallant, and M. M. Millán. 1978. Data processing procedures for the Barringer Correlation Spectrometer (COSPEC). 1978. Technical Memoranda, TEC 860. Atmospheric Environment Service, Downsview, Ontario, Canada.

Millán, M. M., and R. M. Hoff. 1976. The COSPEC remote sensor, II Electronic set-up procedures. Report ARQT-6-76, Atmospheric Environment Service, Downsview, Ontario, Canada.

Millán, M. M., and R. M. Hoff. 1977a. Dispersive correlation spectroscopy: A study of mask optimization procedures. Appl. Opt. 16:1609-1618.

Millán, M. M., and R. M. Hoff. 1977b. How to minimize the baseline drift in a COSPEC remote sensor. Atmos. Environ. 11:857-860.

Millán, M. M., and Y-S, Chung. 1977. Detection of a plume 400 km from the source. Atmos. Environ. 11:939-944.

Millán, M. M. 1978. Remote sensing of SO_2, a data processing methodology. Proceedings, 4th Joint Conference on Sensing of Environmental Pollutants, American Chemists Society.

Millán, M. M. and R. M. Hoff. 1978. Remote sensing of air pollutants by correlation spectroscopy--instrumental response characteristics. Atmos. Environ. 12:853-864.

Millán, M. M., A. J. Gallant, and J. Markes. 1978. Nanticoke Environmental Study: COSPEC/SIGN-X project. Report ARQT-6-78, Atmospheric Environment Service, Downsview, Ontario, Canada.

Millán, M. M. 1979. Remote sensing of air pollutants: A study of some atmospheric scattering effects. Atmos. Environ. (in press).

Van Egmond, N. D., O. Tissing, D. Onderdelinden, and C. Bartels. 1978. Quantitative evaluation of mesoscale air pollution transport. Atmos. Environ. 12:2279-2287.

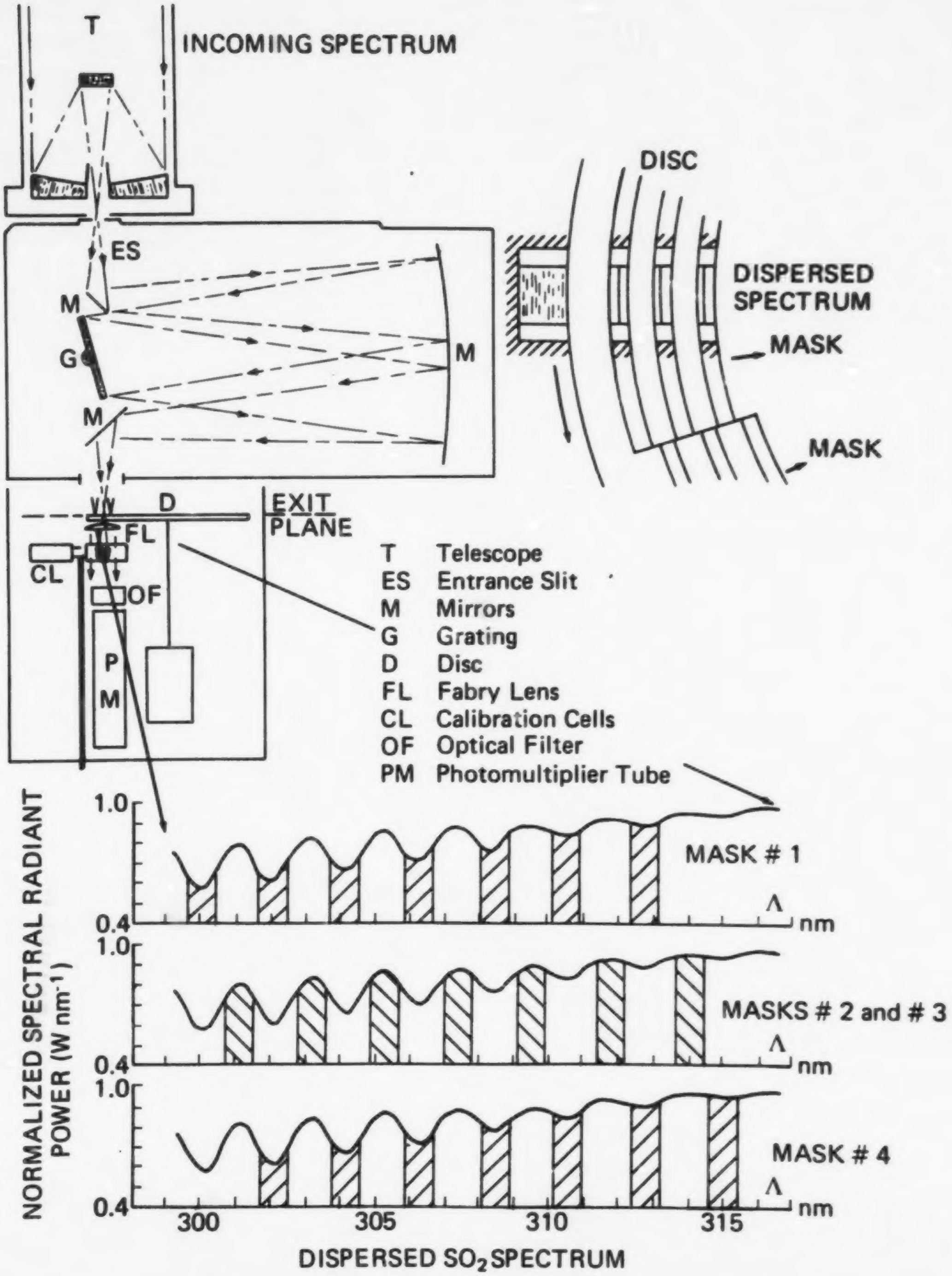

300 ppm-m ABSORPTION ON A SPECTRALLY FLAT BACKGROUND
SPECTRAL ENTRANCE SLIT 0.8nm WIDE

Figure 1. Schematic of the COSPEC optical layout. The masks are shown in their designed positions with respect to the dispersed spectrum (Millán and Hoff, 1978).

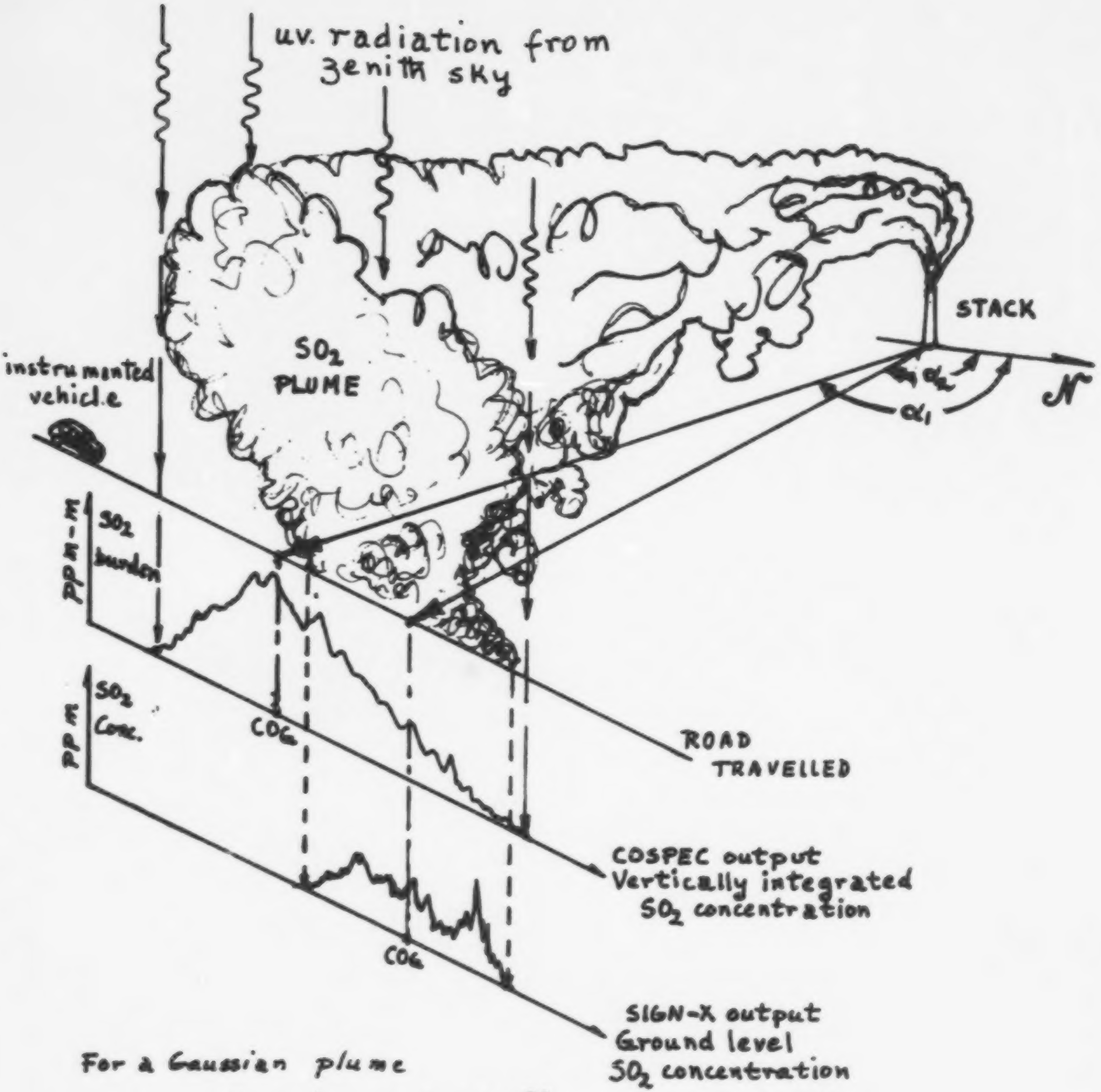
u.v. radiation from zenith sky
SO₂ PLUME
instrumented vehicle
STACK
α₂
α₁
N
SO₂ burden
ppm-m
SO₂ Conc.
ppm
COG
ROAD TRAVELLED
COSPEC output Vertically integrated SO₂ concentration
COG
SIGN-X output Ground level SO₂ concentration

For a Gaussian plume

$$\chi(x,y,z) = \frac{Q}{\bar{u}} \frac{1}{\sqrt{2\pi}\,\sigma_y} \exp\left\{-\frac{1}{2}\left(\frac{y}{\sigma_y}\right)^2\right\} \times \frac{1}{\sqrt{2\pi}\,\sigma_z} \exp\left\{-\frac{1}{2}\left(\frac{z}{\sigma_z}\right)^2\right\}$$

$$\text{COSPEC output} = \int_0^\infty \chi(x,y,z)\,dz = \frac{Q}{\bar{u}} \frac{1}{\sqrt{2\pi}\,\sigma_y} \exp\left\{-\frac{1}{2}\left(\frac{y}{\sigma_y}\right)^2\right\}$$

i.e. the lateral diffusive term

Figure 2. Plume profiling concept using a COSPEC remote sensor to measure the overall or vertically integrated SO_2 plume and an SO_2 point monitor to define the ground plume. The conceptual relationship between the COSPEC line-integrated measurement (burden) and the plume parameters is shown for an idealized Gaussian plume.

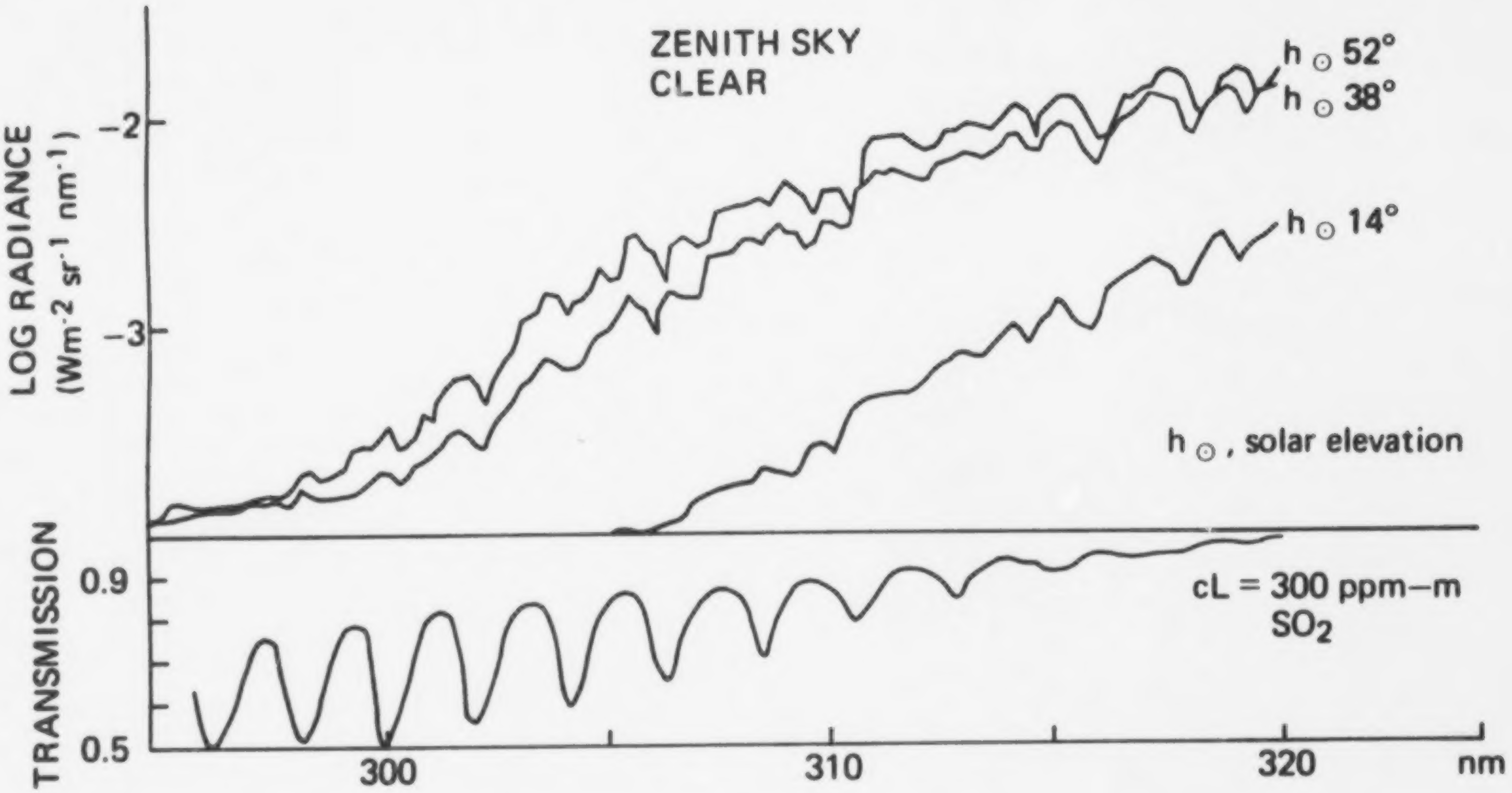

Figure 3. SO_2 transmission spectrum in the spectral region used for passive SO_2 measurements, and three typical zenith sky backgrounds in the same region (Millán and Hoff, 1978).

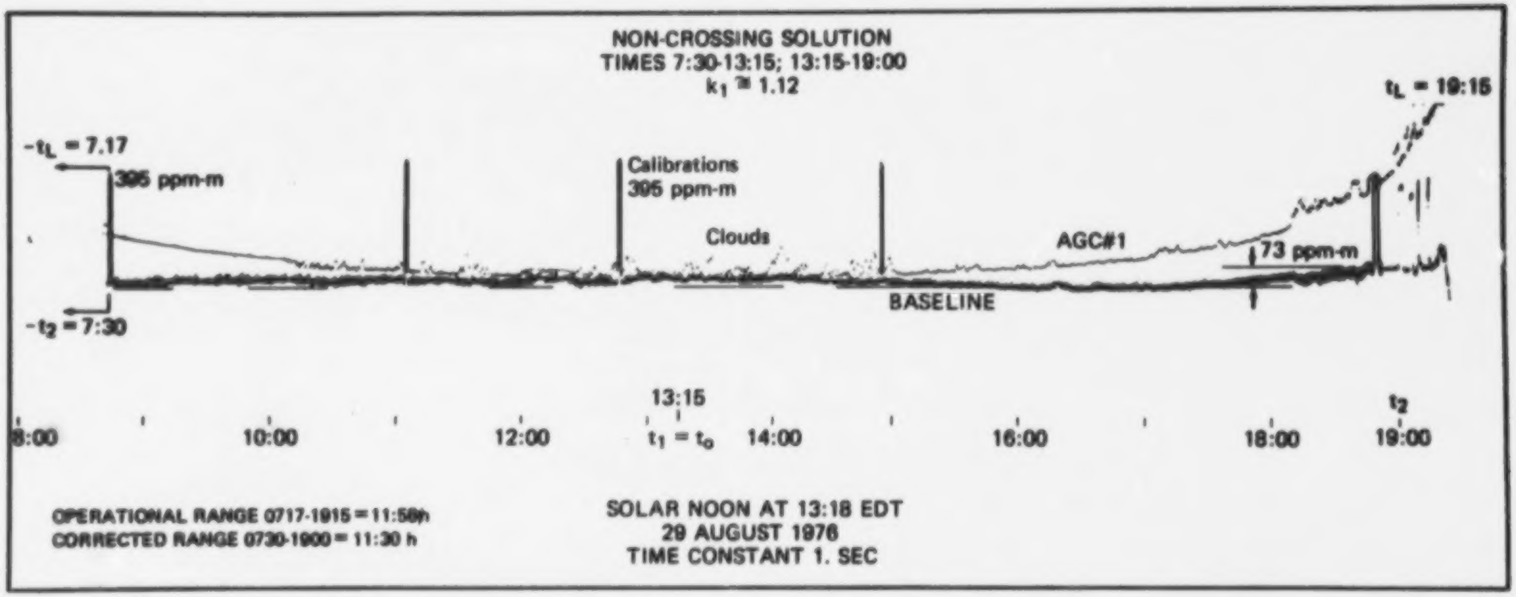

Figure 4. Example of a COSPEC diurnal baseline drift in a compensated instrument. Times $\pm t_L$ indicate the ends of the operational day; $\pm t_2$ are the ends of the compensated time period for minimization of baseline drift. The AGC curve is inversely proportional to the amount of radiation available (Millán and Hoff, 1977b).

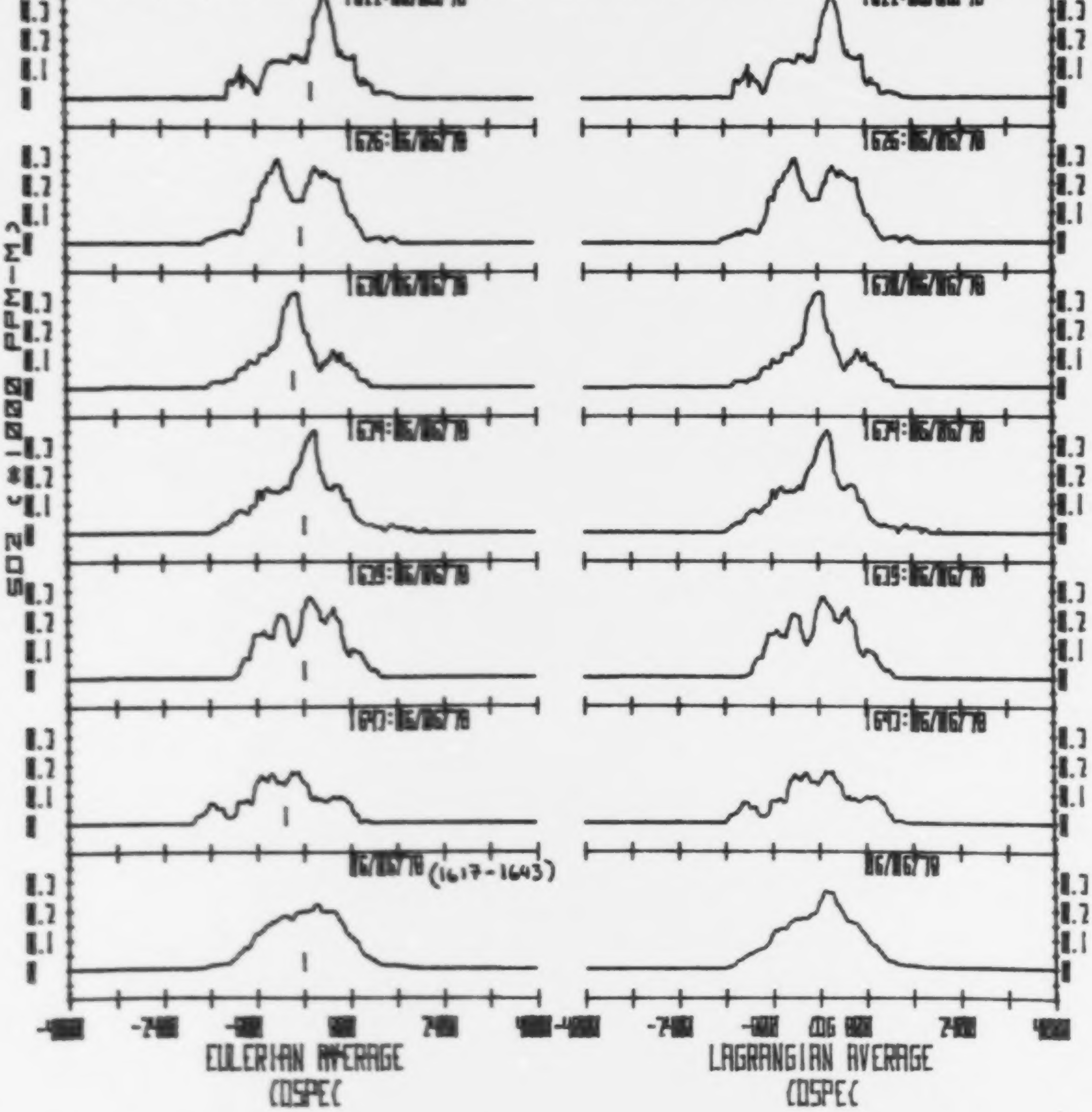

Figure 5. Example of the Eulerian and Lagrangian averages of seven COSPEC plume profiles. These are always presented as seen from the stack looking downwind. The Eulerian average is the same used in Figure 9a.

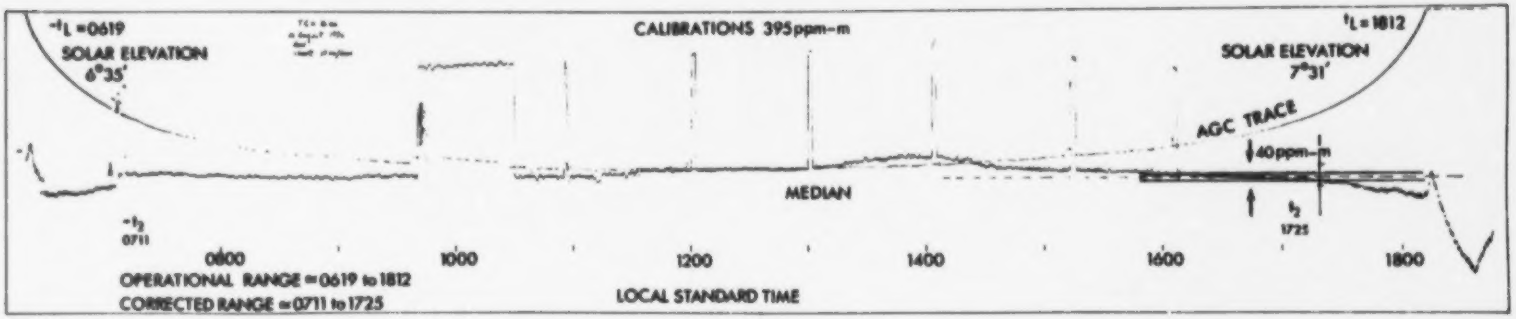

Figure 6. COSPEC diurnal baseline run of August 30, 1976, at the AES building in the northern edge of Toronto, Canada. The departure toward SO_2 readings centered at approximately 1400 hr (LST) indicates the passage of an SO_2 cloud overhead (Millán and Chung, 1977).

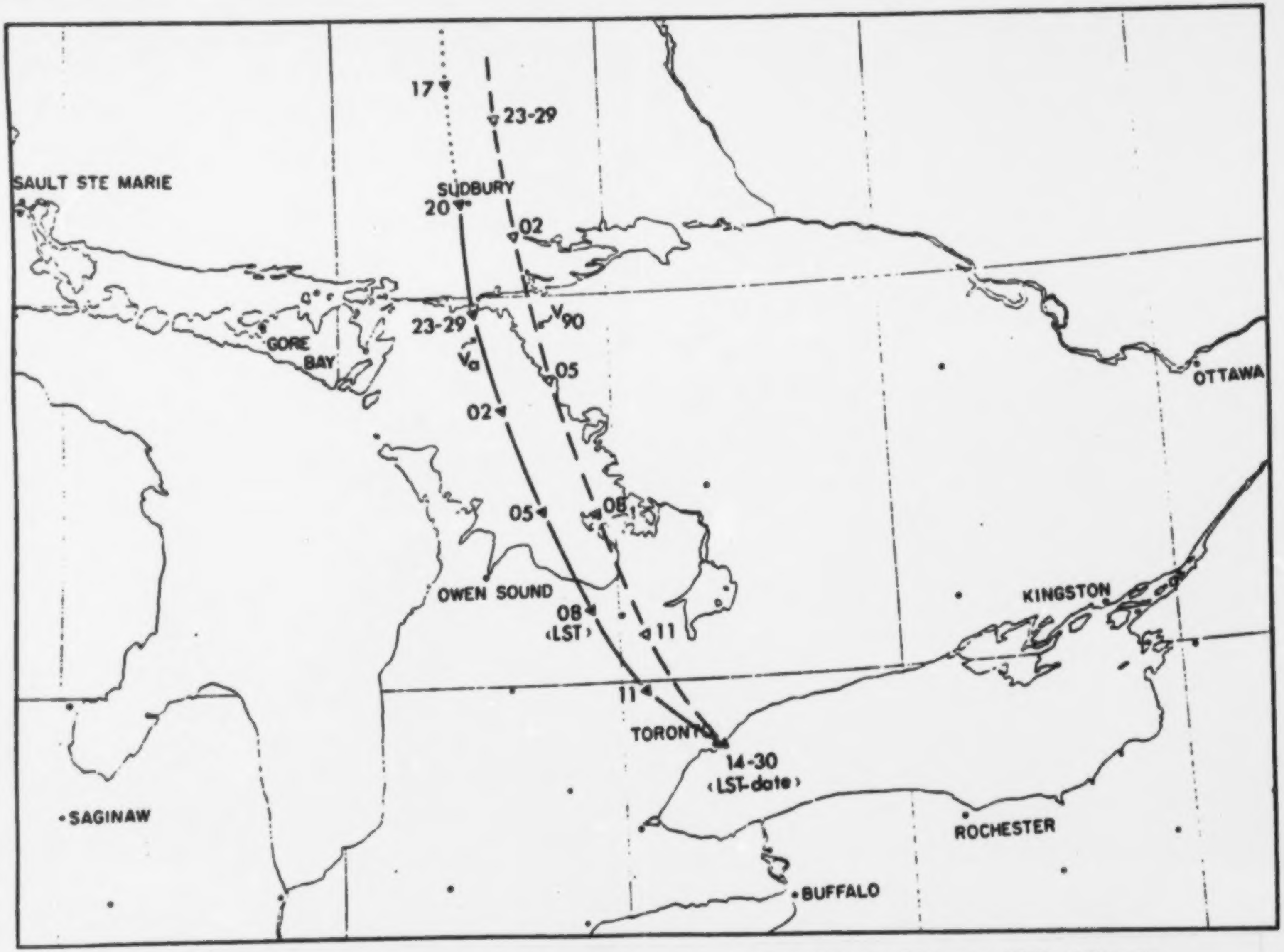

Figure 7. Air parcel back trajectories in the boundary layer terminating 1400 LST, 30 August 1976, at Toronto. V_a and V_{90} represent trajectories at the levels of ~300 and 600 m, respectively, above ground (Millán and Chung, 1977).

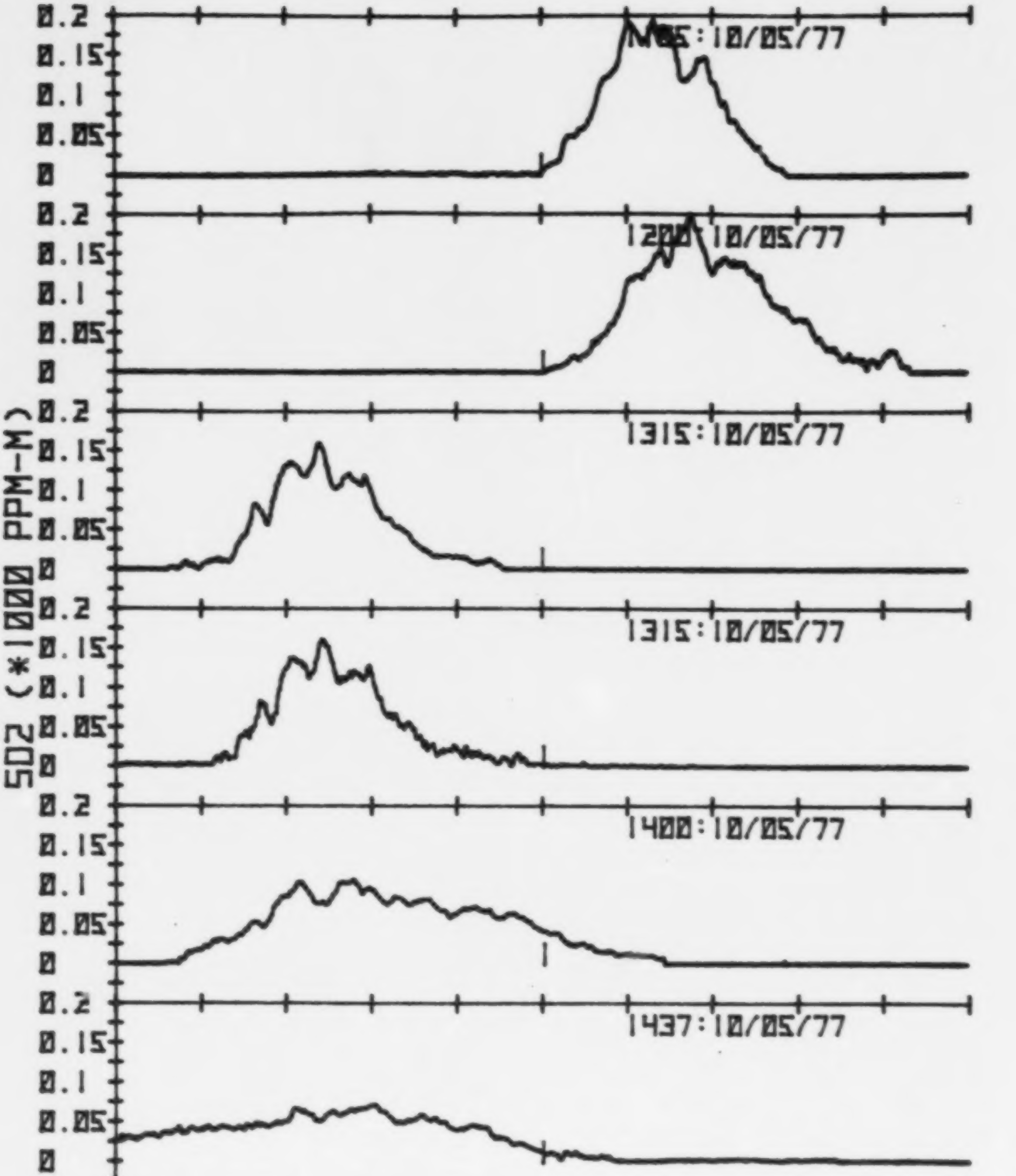

Figure 8. Six plume profiles over Highway 9, in southern Ontario on May 10, 1977. Forecast of the approximate plume position for most efficient deployment of the COSPEC's was provided by Y-S Chung.

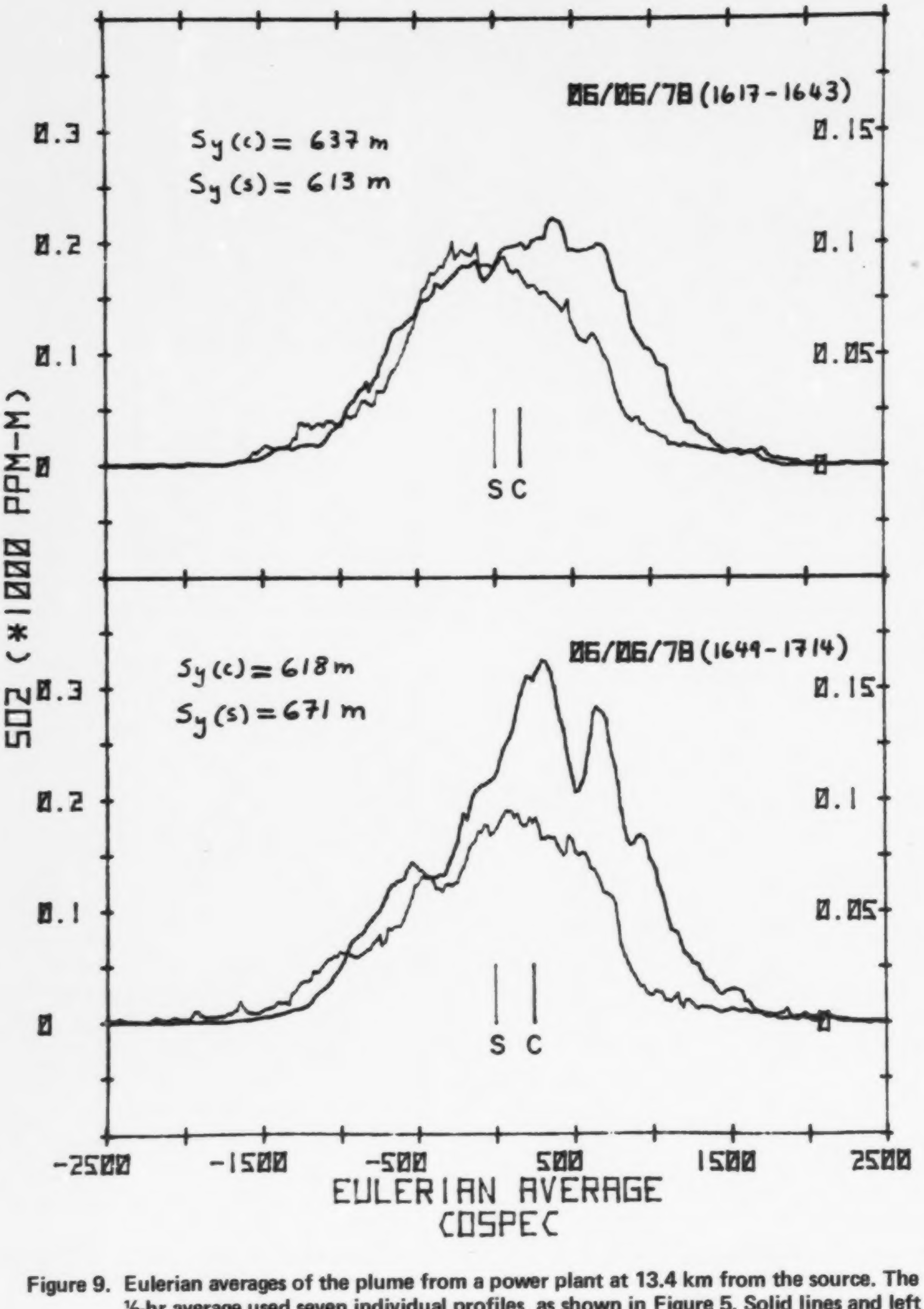

Figure 9. Eulerian averages of the plume from a power plant at 13.4 km from the source. The ½-hr average used seven individual profiles, as shown in Figure 5. Solid lines and left scales are for the vertically integrated SO_2 average plumes, weaker lines and right scales are for the SIGN-X ground level SO_2 average plume. Vertical bars indicate the position of the centers of gravity of each average, c for COSPEC, s for SIGN-X. Sy(c), Sy(s) are the standard deviations of the distributions represented by the vertically integrated and ground plumes, respectively. Time shown in brackets are the beginnings of the first and last profiles used in the average.

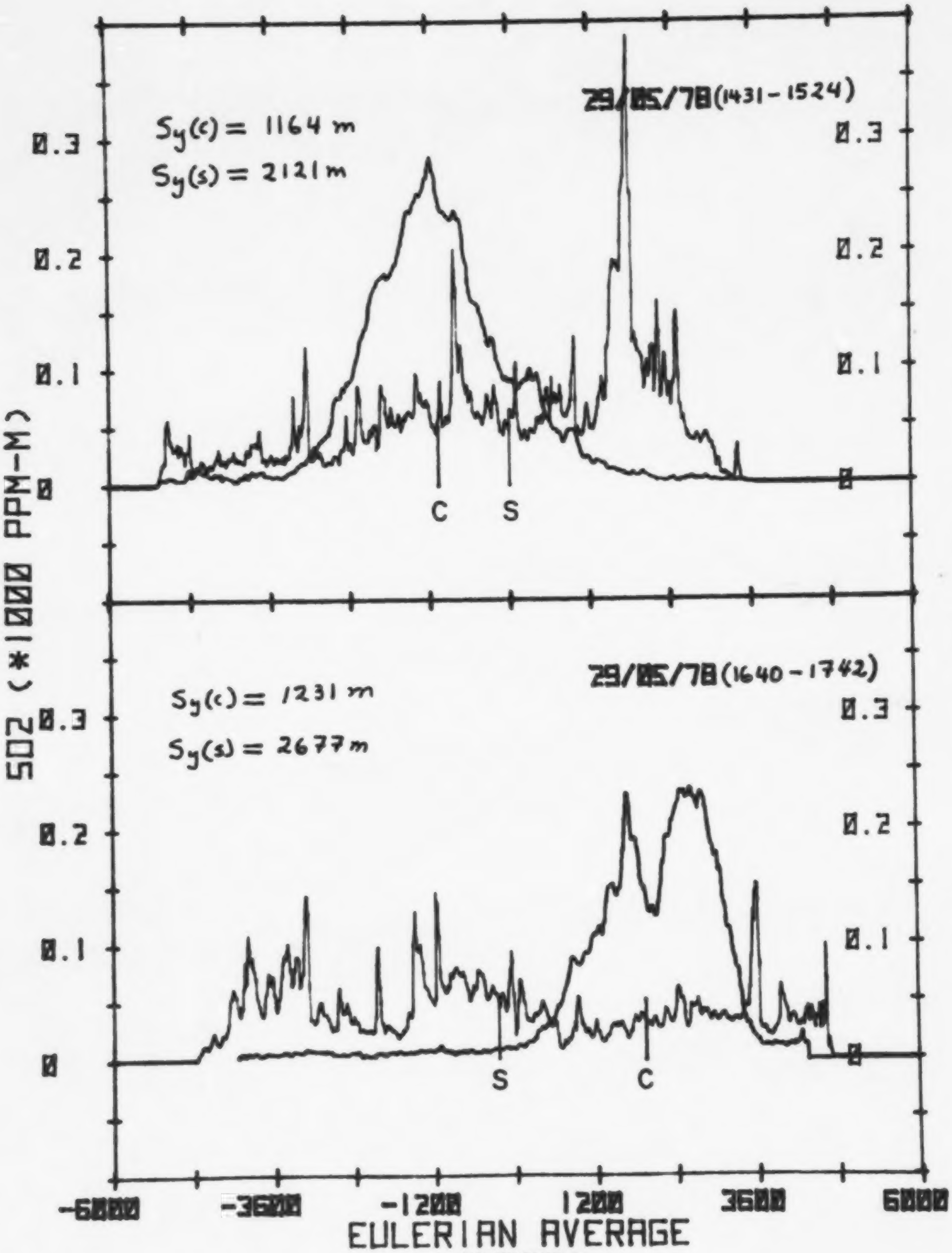

Figure 10. The same as for Figure 9 at 10.5 km from the source under fumigation conditions. These are hourly averages of seven plume profiles. Note the irregularity of the ground level SO_2 average under the unstable (fumigation) conditions.

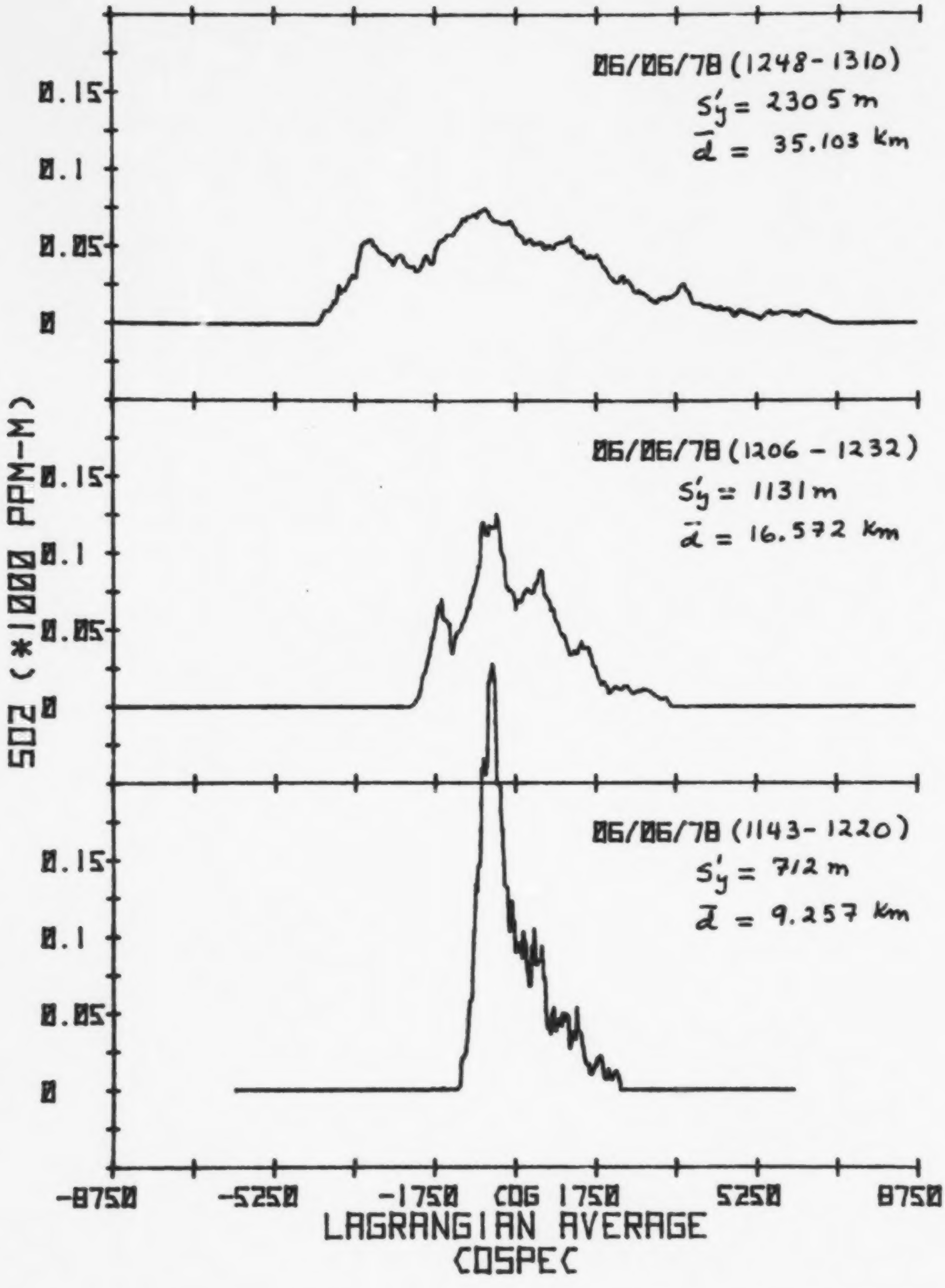

Figure 11. Composite of three half-hour Lagrangian averages of a plume at three distances downwind from the source. The time lag between successive averages was selected to represent the time required to transport a representative air parcel from one location to the next.

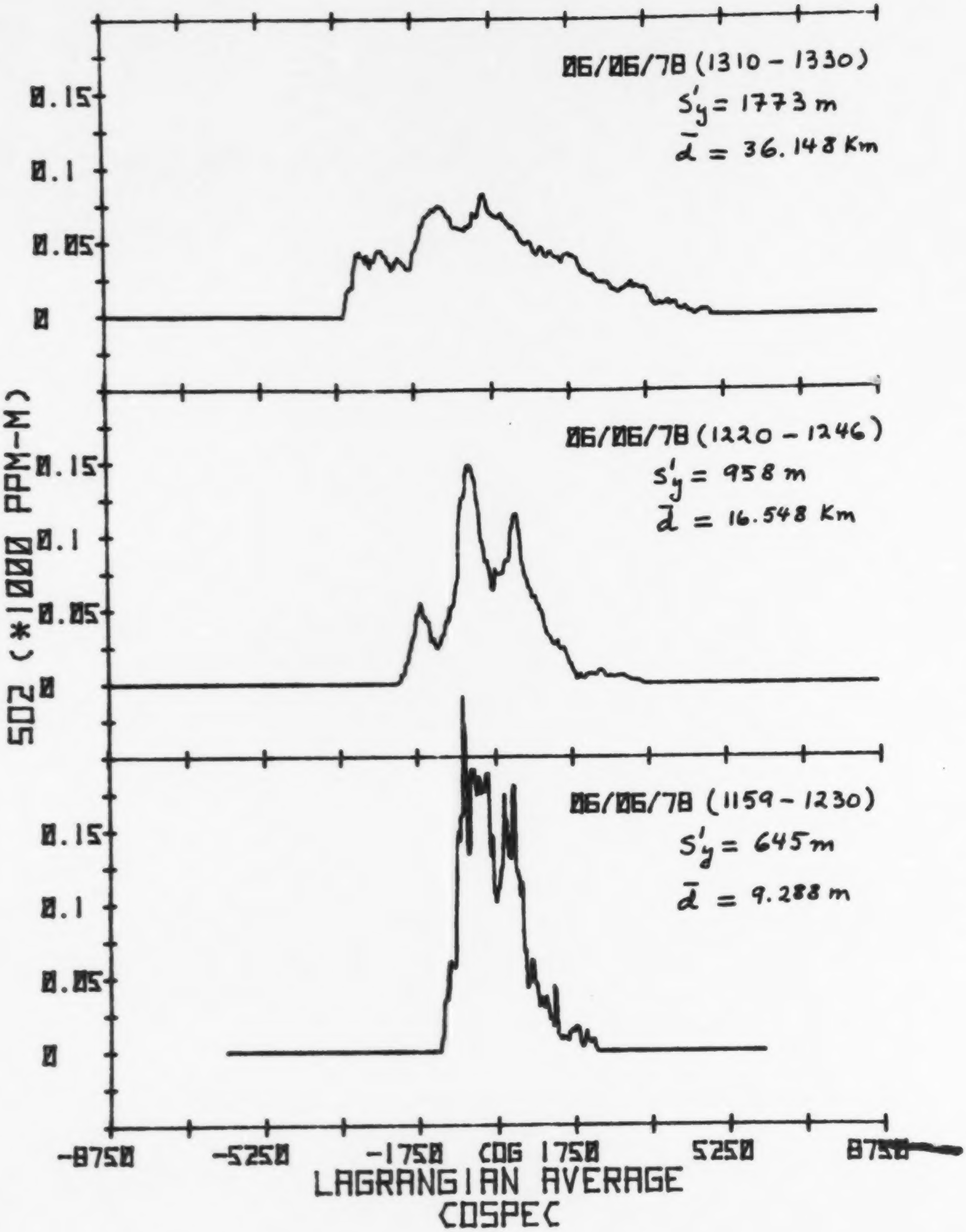

Figure 12. The same as for Figure 11. In both these figures, the skewness of the average profile is transported downwind.

SUMMARY OF THE NASA REMOTE SENSING PROGRAM

S. H. Melfi

Office of Space and Terrestrial Applications
National Aeronautics and Space Administration, Washington, D.C.

INTRODUCTION

Over the past few years, concern with the quality of the atmosphere has matured to one of the many important but often competing national goals. The role of anthropogenic activities in affecting the quality of the atmosphere remains a complex process because complete understanding of the physics and chemistry of the natural atmosphere requires understanding the photochemistry, dynamics, and radiation budget of the atmosphere and their interactive processes. Improved understanding of atmospheric processes requires a combination of atmospheric computer modeling; global, regional, and localized measurements; and laboratory studies. Remote sensors capable of obtaining wide spatial coverage and measuring temporal variability of gaseous and aerosol species are valuable tools for performing measurements in the global and regional troposphere. The National Aeronautics and Space Administration (NASA), in response to the national concern for understanding the physics and chemistry of the atmosphere, has developed unique satellite, aircraft, balloon, and ground-based remote sensing instrumentation for measuring atmospheric gaseous and aerosol species, meteorological parameters, and earth resource parameters.

NASA has been engaged in a technology development and measurement program to develop remote sensors for studying the global and regional troposphere. Airborne remote sensing technology has matured to the point that it has the potential to complement traditional measurements in Environmental Protection Agency (EPA) regional field studies. Unique capabilities of airborne remote sensors include wide spatial coverage, measurements of temporal variability, multiple species detection (i.e., O_3, SO_2, aerosols, CO,. . .), and vertical ranging. Remote sensors will supplement in situ sensors both in characterizing pollution sources and in providing the synoptic coverage needed to address local and particularly regional problems. Ultimately remote sensors from space may provide measurements of the photochemistry and transport of the global troposphere and provide valuable scientific understanding of the impact of anthropogenic activity on the natural troposphere.

In this paper, a summary of the remote sensing technology in the NASA Environmental Quality Program is presented in three categories including:

1. Earth observation satellite systems that have potential application to improved prediction of Persistent Elevated Pollution Episodes (PEPE's).
2. Passive remote sensing technology that can be used for detection of trace species in the troposphere on a regional scale that will provide complementary measurements in EPA regional studies.
3. Active remote sensing technology that can be used for measuring range-resolved and total burden of gaseous and aerosol species in the troposphere on a regional scale that could be used to perform complementary measurements in the 1980 EPA regional studies.

It must be realized that in studies related to the global and regional troposphere, measurements of meteorological parameters to understand the photochemistry and dynamics of the troposphere are important to obtain a complete understanding of the underlying physics and chemistry of the global and regional troposphere. This summary will not include the instrumentation and technology developed by NASA for obtaining meteorological parameters such as pressure, temperature, winds, and cloud cover, although identification of these "state" variables with remote sensing technology has been developed by NASA for application from satellite, aircraft, balloon, and ground-based platforms.

EARTH OBSERVATION SATELLITE SYSTEMS

The occurrence of high atmospheric sulfate aerosols in the United States has become a problem of national concern and is being given national attention in aerometric measurement programs such as those conducted by the EPA, the Department of Energy (DOE), and the Electric Power Research Institute (EPRI). Strong evidence has emerged in the last several years to support the need for regional, if not subcontinental, consideration of the effects of sulfur pollution. Of particular interest are the regional characteristics of atmospheric sulfate occurrences that are now thought to be of more direct epidemiological consequences than gaseous SO_2. While a network of ground-based pollution sensors is needed to provide accurate measurements of pollutant concentrations, the localized measurements are limited to tracking and evaluating episodes of regional dimensions. Airborne remote sensing techniques have the potential for extending the regional coverage requirements but are difficult to implement in a program to identify regional pollution episodes in the formative stages. Earth observation satellites can potentially complement the ground-based network and airborne remote sensors by providing complete areal coverage of regional pollutant concentrations, identifying regional pollution episodes in the formative stages, and tracking the episodes as they move across various regions and locales. Therefore, the combination of satellite observations, aircraft flights, and a network of in situ sensors should provide the necessary information for the verification of models that will be used for the design of environmental air quality control strategies.

NASA has developed a number of earth observation satellite systems for various meteorological and earth/water resource applications. Table 1 is a summary of Earth Observation Satellite Systems that have been developed for specific applications such as the generation of high-resolution earth images for meteorology, the measurement of sea surface and cloud top temperatures, land use and water resource studies, and agricultural surveys. These instruments are classified generically as visible/infrared spectroradiometers and operate in spectral bands ranging from the visible (0.45 μm) through the infrared (12.5 μm) range of the electromagnetic spectrum, in selected spectral bands. Spatial resolution of the instruments ranges from 30 m to 13.6 km. In Table 1, the satellite system used as the instrument platform, the orbits, and the launch schedule are indicated for each sensor as well as the application and objective originally intended for the instrumentation. Additional information on the specifications for the satellite observation instruments summarized in Table 1 are found in references 1, 2, and 3.

A review of the current status of satellite imagery for the detection of regional haze, with potential application to the PEPE program has been presented in proceedings of this conference.[4] [5] Under sponsorship of the

NASA Environmental Quality Program, two research efforts are currently in progress to study the quantitative interpretation of selected satellite imagery to measure and detect aerosol loadings in regional haze over land,[6] and to measure tropospheric aerosol loadings over inland bodies of water.[7]

The objective of the first study[6] is to perform visual and digital analyses of satellite visible and infrared data for selected high-sulfate episodes over the northeastern United States, and to compare results of satellite data to ground truth information from a unique and comprehensive aerometric data base available in Environmental Research and Technology's data archive. Data from the NOAA/VHRR, DMSP, GOES and Landsat satellite systems are being evaluated.

Analysis of satellite data for three selected high-sulfate episodes over the northeastern United States has been completed. The dates of these high-sulfate episodes are: (1) 8-10 July 1974, (2) 26 June-3 July 1975, and (3) 3-5 August 1977. In addition to analysis of satellite data for the above three cases, selected NOAA/VHRR and GOES imagery has been acquired and analyzed for a suspected high-sulfate episode during the period between 19 and 24 July 1978. Figures 1 and 2 show typical examples of satellite imagery obtained with the SMS satellite system on 9 and 10 July 1974 at 2100 GMT and identify an area of elevated pollution (haze blob) associated with a high-sulfate episode over the northeastern United States. Comparison of the two images demonstrates extension of a high-sulfate episode east of the northeastern coast over a 24-hr period. Detailed analysis of the satellite data has shown that in three of four cases analyzed, areas of higher reflectance are observed to correlate well with the location of highest sulfate measurements. The synoptic weather pattern over the northeast during the period from 19-24 July 1978 is similar to other verified high-sulfate episodes. Analysis of the preliminary 24-hr average sulfate values for eight of the nine Class I SURE stations indicates that a regional sulfate episode did occur over the northeast during this time period. Also, this very limited data sample displays a transport of high-sulfate levels from the Ohio Valley region eastward to off the mid-Atlantic coast, with maximum levels in the 30- to 40-$\mu g/m^3$ range. The location of the maximum sulfate levels shows a distinct correlation with the location of the patterns of increased brightness levels observed in the satellite imagery and the regions of reduced surface visibility.

The objective of the second study[7] is to provide the capability of quantitatively monitoring tropospheric aerosols over land masses by evaluating the relationship of upwelling near-infrared radiance over inland bodies of water to the atmospheric aerosol optical thickness. The technique is similar to one previously developed in the Landsat program for observations over oceans,[8] and will utilize raw data tapes from Landsat 2 MSS7 for five inland sites for which ground truth data were obtained in the previous Landsat study. From initial results of brightness contrasts as seen from space, regional pollution episodes in the form of haze blobs have the potential to be detected even at the early formative stage. These results are promising for future planning for satellite monitoring of pollution episodes. However, these results must be tempered with the realization that other meteorological conditions (most frequently clouds) and surface conditions (different ground albedos) will obscure and limit the quantitative evaluation of pollution episodes from satellite imagery.

PASSIVE REMOTE SENSORS

This section summarizes the current status of passive remote sensing instrumentation for measurement of trace gaseous pollutants in the troposphere. The feasibility of utilizing passive remote sensors from aircraft and space platforms for measuring trace gaseous pollutants was established in a study performed in 1969.[9] Since that time, instruments and associated software systems have undergone laboratory testing and aircraft flight tests leading to the NASA approval for a passive CO sensing instrument to fly on the second Shuttle Orbital Flight Test (OFT-2).

Passive remote sensors represent that class of remote sensors that utilizes radiation existing naturally in the system whose properties are being measured. For tropospheric measurements, two sources of radiation are available: reflected solar radiation and the thermal radiation emitted by the earth-atmosphere system. In general, at wavelengths shorter than 2.5 or 3 μm, the primary radiation is reflected solar energy, while at wavelengths longer than 3.5 or 4.5 μm, the primary radiation is emitted by the earth-atmosphere system. Within the region from 2.5 to 4.5 μm, both sources contribute significantly and must be considered. For ground-based systems measuring tropospheric gaseous species, a third source of radiation is direct solar radiation through the measurement of absorption of solar radiation by the intervening atmospheric absorption lines of pollutants of interest. Although this technique is limited in spatial coverage, measurements of this type can be extremely important for uniformly mixed gases in which study of transport is not a major scientific objective, or for gases whose concentrations are extremely low and whose vibration-rotation lines are weak. Techniques of this type, from ground-based mobile platforms, could play an important role in establishing variability of gases whose sources or sinks depend upon the nature of the terrain (i.e., NH_3). This may be important as a sentinel measurement to detect changes in the atmospheric absorption spectra that can later be analyzed retrospectively for trace constituent trends.

In establishing the feasibility of a remote sensor to detect tropospheric pollutant gases, several basic parameters must be established prior to instrument design. These general parameters include: (1) instrument spectral bandpass, trading off interference effects of gases with overlapping bands with total signal; (2) required noise level to achieve adequate signal-to-noise ratios for the expected gas concentrations and atmospheric conditions; and (3) for some instruments, high-resolution filter characteristics to set the signal level and height in the atmosphere at which the gas concentration is being measured. In general, the major atmospheric pollutant gases have line widths at atmospheric pressure on the order of 0.1 cm^{-1}, and because of the overlap of the pollutant gas spectra with spectra of naturally occurring constituents, it is necessary that passive sensors have an effective resolution that is less than 0.1 cm^{-1}. Further, high spectral resolution also provides the sensor with the ability to provide sharper vertical distribution of gaseous pollutants in the troposphere. However, higher spectral resolution must be evaluated against the loss of incoming signal and the fundamental limitation of the upwelling thermal radiation from the atmosphere to provide vertical resolution. In general, spectral bandpasses less than 0.01 cm^{-1} do not provide any significant improvement in providing the ability to vertically discriminate tropospheric gases.

The energy received at a wavelength and altitude is a composite of the energy emitted and absorbed by the atmosphere at all altitudes between the source and the sensor. Because of the pressure broadening of the absorption lines, the energy received in the wings of the line should represent the effect of the pollutant gas located at greater pressures (i.e., lower altitude), while the energy received near the line center should be more representative of the effects of the pollutant gas that is located at lower pressure (i.e., high altitudes). This gives rise to the possibility that by selectively measuring the radiation at various distances from the line center, one could, in principle, generate vertical profiles of the gas concentration. This is analogous to the inference of temperature profiles by remote sensing methods using thermal infrared wavelengths where measurements in various parts of the absorption band are used to effect the altitude discrimination. For measurement of tropospheric pollutant gases, the bands are generally very weak and current instrumentation is not sufficiently sensitive to allow significant height discrimination from aircraft altitudes. This situation is alleviated when the sensor is utilized from a space platform, and vertical discrimination is possible although it is still difficult to isolate the air mass less than a few kilometers above the ground (i.e., biosphere).

A summary of the current passive remote sensors developed under the NASA remote sensing program is given in Table 2. The instruments have been categorized generically into four classes of instruments: (1) Gas Filter Correlation (GFC) techniques; (2) Interferometry; (3) Infrared Heterodyne Radiometry, and (4) UV/VIS/IR Spectroradiometers. Characteristics of the instruments including detectable species, spectral coverage, field of view, and vertical resolution are shown on the table. Three viewing modes are delineated including the thermal IR (≥4.5 µm), solar reflected (2.0-4.5 µm), and direct solar (3-15 µm). In general, instruments in the thermal IR and solar reflected viewing modes have immediate application in aircraft and space platforms while instruments in the direct solar viewing mode have immediate application to ground-based platforms. Technology developments in cryogenic cooling of sensor systems (i.e., viewing optics) and in high quantum efficiency wideband photomixers will allow application of these sensors to aircraft and satellite platforms in the nadir viewing mode.

For immediate application to the EPA 1980 regional field studies, however, the aircraft MAPS (measuring air pollution from satellites) Gas Filter Correlation instrument can be utilized to measure the dispersion of urban plumes from an aircraft platform. Aircraft MAPS has undergone extensive testing and evaluation, and is the prototype instrument for OFT MAPS, which is scheduled to fly on the OFT-2 Shuttle flight to measure interhemispheric mixing of CO. Figure 3 represents some recent results obtained with the aircraft MAPS instruments to identify dispersion of the urban plume from the Chicago area, and demonstrates the ability of passive remote sensing technology to measure total burden of CO in the atmosphere and to use atmospheric CO as a tracer of the urban plume.

ACTIVE REMOTE SENSORS

NASA has been engaged in a variety of technological programs in active remote sensing to develop, evaluate, and apply lidar techniques to perform remote measurements of gaseous and aerosol species in the lower troposphere from airborne platforms in order to study the spatial and temporal variability of these species in the regional and global troposphere. Programs at NASA have evolved from initial studies with fixed-wavelength ruby lidar systems[10] to the use of tunable and narrow bandwidth lidar systems for remote measurements of atmospheric gases and aerosol characteristics.[11] Large telescope lidar systems have been applied to the measurement of stratospheric aerosols and an airborne version of the instrument is currently being used to provide correlative measurements for the Stratospheric Aerosol Measurement (SAM) and the Stratospheric Aerosol and Gas Experiment (SAGE II) satellite experiments. Investigations have been conducted using Raman scattering techniques for remote measurements of water vapor and SO_2 but this technique is limited to nighttime operation, high gas concentration, and short measuring distances. The differential absorption lidar (DIAL) technique can overcome these limitations and has emerged as the primary lidar technique for providing range-resolved and total column measurements of trace gases. The NASA-developed or -sponsored DIAL systems are in various stages of development and cover the spectral region from the ultraviolet through the infrared. In the evolutionary lidar program at NASA, ground-based mobile lidar systems have been applied to measurements of plume rise and dispersion studies, model validation studies, and optical extinction analysis through measurement of atmospheric aerosols and sulfur dioxide. As an example, experiments were conducted by the NASA Langley Research Center and Old Dominion University at the Virginia Electric and Power Company (VEPCO) plant at Yorktown, Virginia, in July 1976 and at the Morgantown Generating Plant of the Potomac Electric Power Company, Morgantown, Maryland, in September and October of 1976 and June 1978. Detailed discussion of the instrumentation and experimental results through 1977 are given in reference 11. Recent results from the 1978 studies are shown in Figure 4, in which the SO_2 column content (ppm-meters) measured at different times was obtained as a function of the horizontal coordinate across the plume. The plume investigated was a high stack vertical plume with the horizontal lidar scans 275 m above the stack exit, and through comparison with correlative measurements including the JPL, Multispectral Observation of Pollutant Species (MOPS) sensor, feasibility of DIAL SO_2 measurements and system sensitivity was established. Long-path measurements in the IR portion of the spectrum (9-12 μm) using cooperative reflectors have also been used by the Jet Propulsion Laboratory to measure O_3 and NO in heavily congested travel areas in Southern California, and have provided the technology for the design and implementation of the Laser Absorption Spectrometer remote IR lidar system for measurement of total column O_3.

Measurements from mobile ground-based platforms with prototype engineering models have provided NASA with the data base to develop airborne remote sensors for cooperative efforts with EPA in regional field studies to complement EPA remote sensors and in situ sensors. Three airborne active remote sensors available for cooperative efforts in the 1980 regional program are:

1. Airborne UV-VIS-IR Differential Absorption Lidar (DIAL)
2. High Spectral Resolution Lidar (HSRL)
3. Laser Absorption Spectrometer (LAS)

A fourth system, Airborne IR Lidar System, is currently being assembled into an airborne system and has the potential for participation in the 1980 field studies with accelerated development.

A summary chart of the current active remote sensors under the NASA program is given in Table 3. Instrument parameters including detectable species, spectral coverage, type of transmitting laser, receiver telescope diameter, viewing mode, and platform are specified for each sensor. The last two columns summarize current status and field application programs for each instrument. A summary of the four airborne active remote sensors that are potential candidates for participation in 1980 EPA field studies follows.

Airborne UV-VIS-IR DIAL System

The airborne DIAL system was developed by NASA to simultaneously measure the vertical and horizontal distribution of O_3 and aerosols or SO_2 and aerosols with the potential, with future modifications, to measure the three species simultaneously. The present system contains two Nd:YAG pump lasers and two high-conversion-efficiency dye lasers for conducting measurements of SO_2, or O_3 in the ultraviolet, and aerosols in the visible spectral range. The airborne DIAL system also has the capability to measure NO_2 in the 0.40-μm range and H_2O in the 0.70-μm range. Simultaneous measurements of the concentration and distribution of SO_2, O_3, and aerosols and their temporal variations are important to improve current understanding of the atmospheric chemistry and transport of these species. Complete understanding of regional chemistry and transport requires the rapid acquisition of concentration and distribution of pollutants on a regional scale, requirements that are satisfied by the Airborne DIAL System. In addition, regional measurements of NO_2 can provide information on transformation, transport, and budgets in the atmosphere with respect to photochemical oxidant problem, and with complementary measurements of total hydrocarbons (Airborne IR Lidar System) can provide the fundamental data for improved understanding of the atmospheric reactions involved in the photochemical oxidant production.

High Spectral Resolution Lidar (HSRL)

Measurements of the atmospheric spatial distribution of aerosol optical extinction coefficients are needed to characterize the transport and development of regional scale hazy air masses. Such information can be used alone or in connection with satellite and conventional information to assess the impact of pollutant sources on visibility and air quality. An accurate measurement of the optical extinction coefficient is required to protect visibility in Class I Federal Areas from manmade impairment related to air pollution.

The HSRL has been developed to measure the vertical and horizontal distribution of the atmospheric optical extinction coefficient, the aerosol-to-molecular scattering ratio, and the aerosol backscattering phase function from aircraft platforms. The HSRL is eye safe, can be operated under daylight conditions over centers of population, and has the potential for providing correlative measurements for the interpretation and analysis of elevated pollution episodes monitored by satellite imagery. The HSRL could complement the interpretation of the EPA two-wavelength lidar for the characterization of atmospheric contaminant mass loading, size distribution, and composition.

An engineering model of the HSRL has been developed by the University of Wisconsin under NASA sponsorship for aircraft flight testing aboard the NASA CV-990 in the October 1979 time frame. Details of the instrument and experiment concept are given in reference 11. Recent results obtained with the HSRL are shown in Figures 5 and 6, in which the aerosol-to-molecular scattering ratio and the aerosol optical extinction coefficient as a function of vertical range (km) obtained from HSRL data are shown. These data were generated from typical daytime HSRL signals obtained from a "clear" atmosphere at Madison, Wisconsin, on June 10, 1978, at 0900 CDT. Airborne data of this kind can be used to map the temporal and spatial distribution of the aerosol optical extinction coefficient in regional scale hazy air masses, and can be used to characterize the regional transport of aerosols and regional variation of mixed layer depth.

Laser Absorption Spectrometer (LAS)

The LAS is a remote sensing instrument developed by the Jet Propulsion Laboratory under NASA sponsorship and designed to interface with a twin-engine Beechcraft aircraft. The LAS was flown in the NASA CV-990 as part of the space simulation mission in 1977. The LAS utilizes the differential molecular absorption technique with reflection from ground targets to obtain the total column content of O_3 from the aircraft altitude to the ground. Two 1-W waveguide CO_2 lasers operating at two closely spaced wavelengths are used for laser transmitters; one wavelength overlaps an absorption line of the molecule of interest, and the second operates at a nearby "clear" wavelength to discriminate interfering effects from speckle ground reflection and atmospheric interferants (i.e., H_2O, CO_2). Heterodyne detection is used to monitor the back-scattered laser radiation with two high quantum efficiency mercury-cadmium-telluride photomixers. The present LAS instrument has monitored ozone column abundances and will be used in future programs to measure atmospheric ammonia. The LAS is a prototype instrument for a potential Space Shuttle System to monitor global distributions of ozone, ammonia, water vapor, ethylene, methyl chloride, and other species with absorption spectra in the 9- to 12-µm spectral region.

In July 1978, JPL participated in the Southeastern Virginia Urban Plume Study to investigate the formation of O_3 in parcels of air that originated from urban areas during morning hours (Figure 7). Figure 8 shows four measurements taken on four different aircraft passes over the same path at different hours of the day. The wind direction was initially from the southwest, so that the Norfolk area plume was swept up toward Wallops, Virginia. On these plots, the diamonds are measurements performed with a Dasibi Ozone Monitor on board the Beechcraft and the circles are the LAS measurements. A plume of polluted air can clearly be identified at the region near position F' for the passes at 11:40, 3:30, and 5:45. For regional field studies, the LAS instrument can be utilized to perform similar measurements of total O_3 or NH_3 with the capability to obtain vertical profiles by changing aircraft altitudes over different areas.

Airborne IR Lidar System

Measurements of hydrocarbon (HC) concentrations and spatial distributions are needed on a regional scale to determine the impact of anthropogenic and natural sources on the production of photochemical oxidants. Such information can be used in evaluating the relationship between HC emissions and levels of ozone in the atmosphere. A measurement of HC transport and ozone production would permit the assessment of current control strategies and provide data for planning future strategies. The combustion of coal and oil provides a significant anthropogenic source of nitrous oxide (N_2O). This gas is the primary sink for ozone in the stratosphere and is third only to CO_2 and H_2O in its impact on the Earth's temperature due to the greenhouse effect. Since there are no known sinks for N_2O in the troposphere, measurements need to be made initially on a regional scale and ultimately on a global scale to determine the fluxes of N_2O being emitted into the atmosphere from anthropogenic and natural sources (e.g., lightning).

Several key components of the IR DIAL system, including the IR laser constructed by Westinghouse and the IR detection system, have been developed under the previous Energy-Related Remote and In Situ Instrument Development Program (EPA Project 80 BLEU). The IR laser has the capability to be tuned from 1.4 to 3.9 μm. This permits measurements to be made of HC near 3.4 μm and N_2O near 3.85 μm. The IR laser is eye safe, and it can be operated in the daytime. In conjunction with the measurement of ozone in the troposphere by the Airborne DIAL System, the relationship between the distribution and transport of HC and ozone production could be studied in support of EPA's regional modeling effort. In addition, the IR DIAL will have a high sensitivity for the measurement of HCl, which has been detected in coal field power plants and in vinyl chloride flares.

SUMMARY

NASA has been engaged in the development of remote sensing instrumentation for performing scientific measurements of the quality of the earth's air, land, and water resources. This technology has matured to the point that satellite measurements with application to earth and ocean resources are being performed routinely. Additional measurements are taken to determine meteorological parameters in the stratosphere and troposphere, and to study the photochemistry, transport, and radiation budget of the stratosphere. An important gaseous species in determining the quality of the natural and polluted troposphere, carbon monoxide will be measured in an early Space Shuttle flight to determine its interhemispheric mixing ratio, important in understanding the impact of anthropogenic activity on the sources and sinks of global CO.

This paper has summarized the current NASA Remote Sensor Technology for studying the global and regional troposphere from space, aircraft, balloon, and ground-based platforms in the NASA Environmental Quality Program.

As part of its program to develop remote sensors for utilization from space, NASA has developed a series of passive and active remote sensors that have undergone extensive testing from aircraft platforms. Four of these sensors, including aircraft MAPS, UV/VIS DIAL, HSRL, and LAS, can be implemented to supplement in situ and remote sensors (developed by EPA) in the 1980 regional field test program. A fifth lidar system, the Airborne IR

Lidar System, is currently being assembled into an aircraft system and with accelerated development has the potential for participation in the field test program.

Similarly, earth observation satellite systems have demonstrated the ability to detect regions of elevated pollution and have the potential to supplement current in situ and aircraft systems in identifying elevated pollution episodes in the formative stages.

REFERENCES

1. Goddard Space Flight Center. LANDSAT Data Users Handbook. Document no. 76SDS 4258 September 2, 1976.
2. Hussey, John W. The TIROS-N Polar Orbiting Environmental Satellite System. National Oceanic and Atmospheric Administration, U.S. Department of Commerce, Washington, D.C., October 1977.
3. Remote Sensing Handbook. Marshall Space Flight Center, June 30, 1977.
4. Husar, Rudolf B. Identification of PEPE's by Visibility Isopleths. Proceedings of the Seminar/Workshop on Persistent Elevated Pollution Episodes, March 19-23, 1979, Environmental Sciences Research Laboratory, Research Triangle Park, N.C.
5. Lyons, Walter A. Satellite Measurements of PEPE's. Proceedings of the Seminar/Workshop on Persistent Elevated Pollution Episodes, March 19-23, 1979, Environmental Sciences Research Laboratory, Research Triangle Park, N.C.
6. Barnes, James C., and W. Ayers. Study to Evaluate the Capabilities of Satellite Imagery for Monitoring Air Pollution Episodes. Environmental Research and Technology, Inc., and NASA, Langley Research Center, Hampton, Virginia.
7. Griggs, M., and W. Ayers. Satellite Measurements for Tropospheric Aerosols. Science Applications, Inc., and NASA, Langley Research Center, Hampton, Virginia.
8. Measurement of Atmospheric Aerosol Optical Thickness Using ERTS-1 Data. J. Air Poll. Contr. Assoc., 25:622, 1975. Comment on Relative Atmospheric Aerosol Content From ERTS Observations. J. Geophys. Res., 82:4972, 1977.
9. Ludwig, C. B., et al. Study of Air Pollutant Detection By Remote Sensors. NASA CR-1380, July 1969.
10. Lawrence, J. D., et al. Optical Radar Studies of the Atmosphere. Proceedings of the Fifth Symposium on Remote Sensing of the Environment, Ann Arbor, Michigan, April 16-19, 1968.

11. Browell, E. V. Lidar Remote Sensing of Tropospheric Pollutants and Trace Gases-Programs of NASA Langley Research Center. *Proceedings of the 4th Joint Conference on Sensing of Environmental Pollutants*, American Chemical Society, 1978.

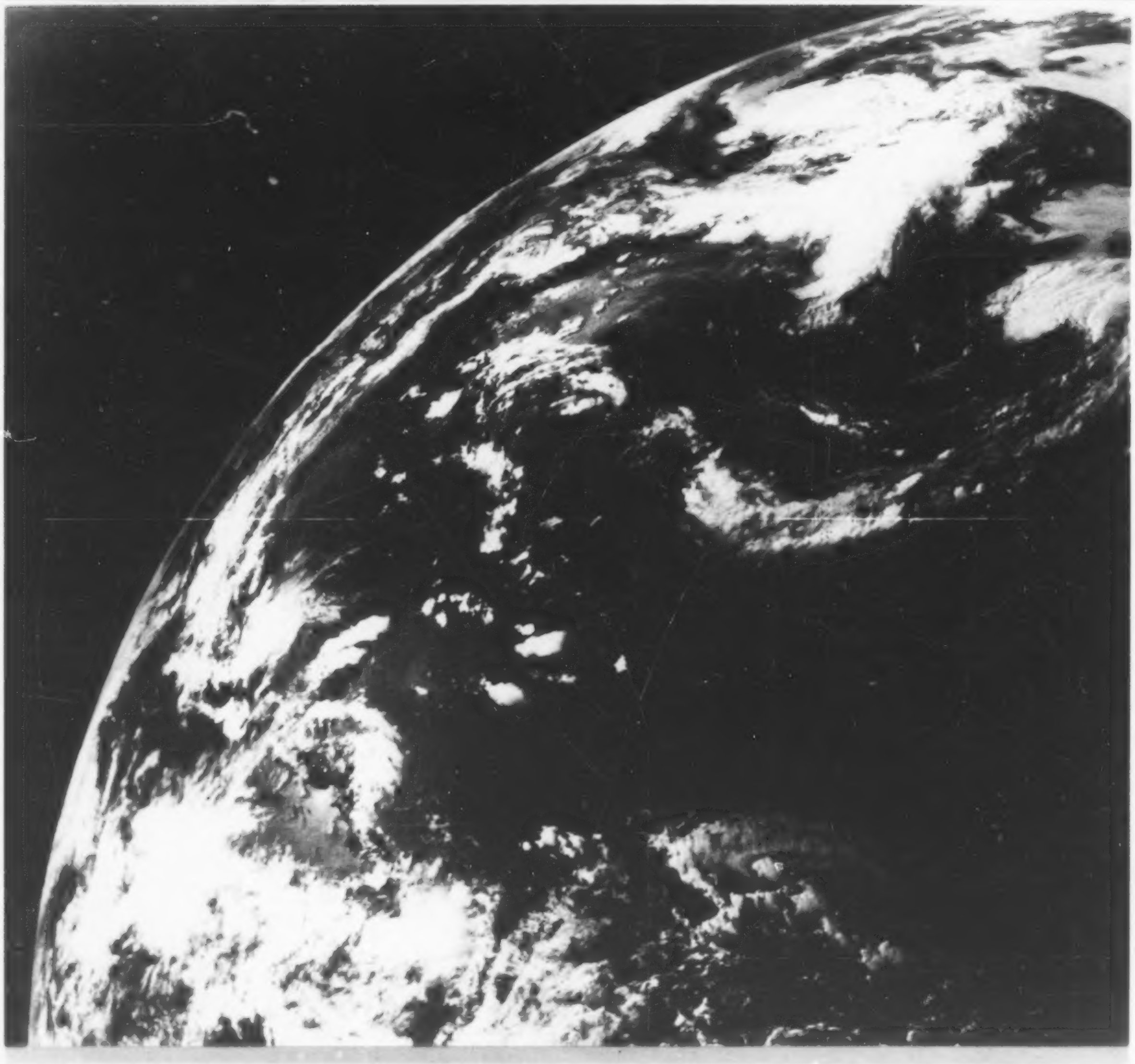

Figure 1. Satellite imagery with SMS satellite system, July 9, 1974, @ 2100 GMT.

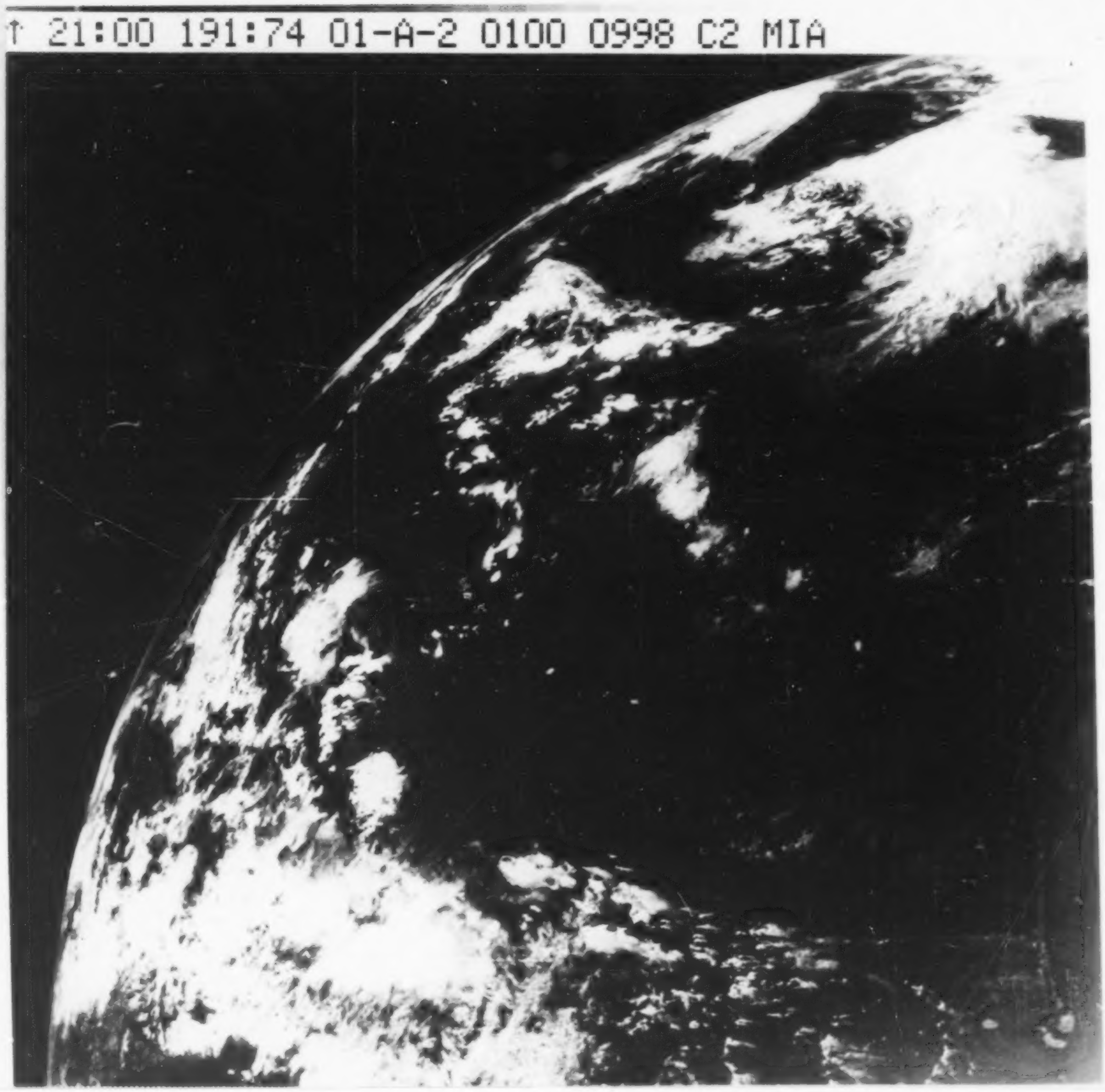

Figure 2. Satellite imagery with SMS satellite system, July 10, 1974, @ 2100 GMT.

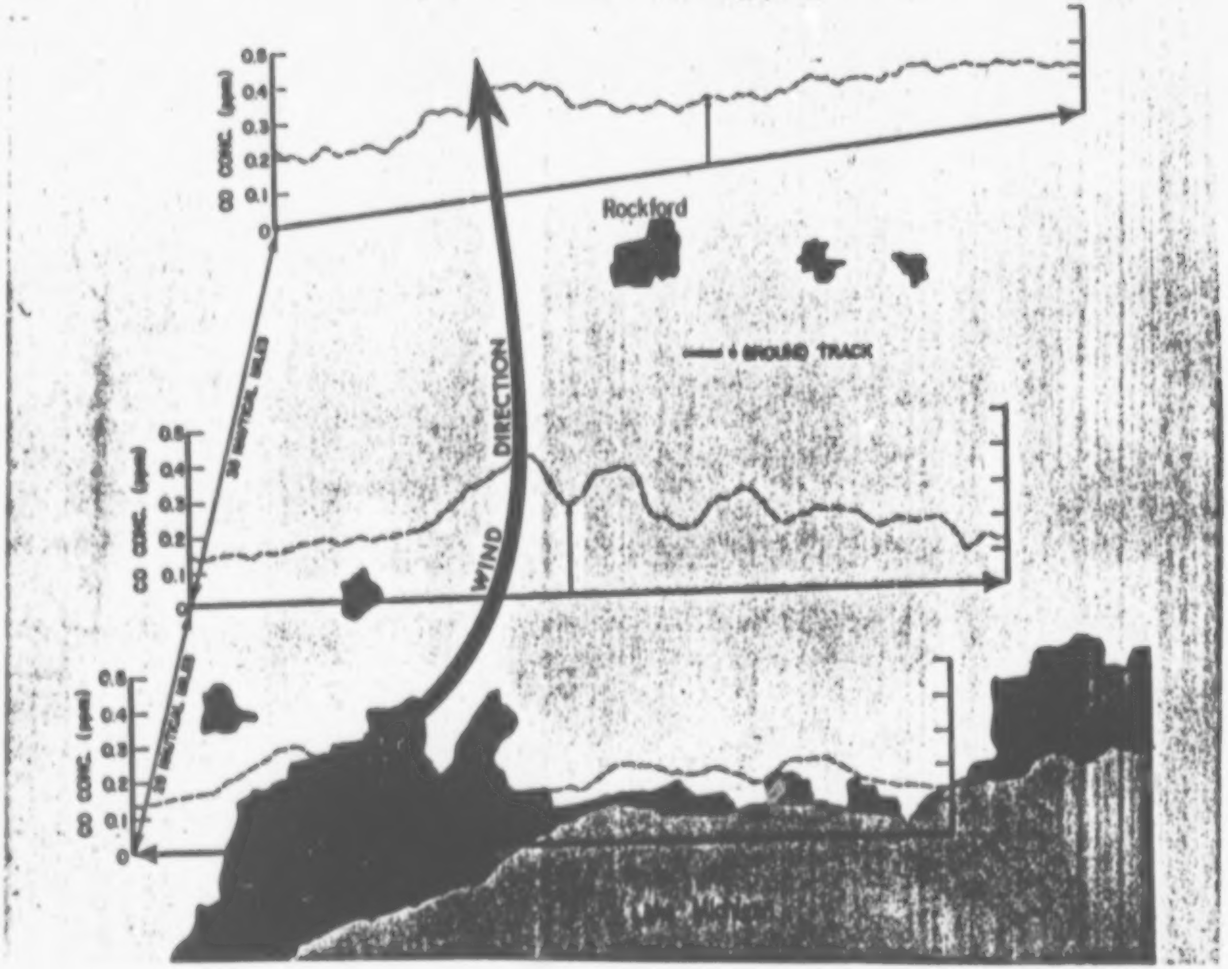

Figure 3. Dispersion of urban plume from Chicago area using the A/C MAPS instrument.

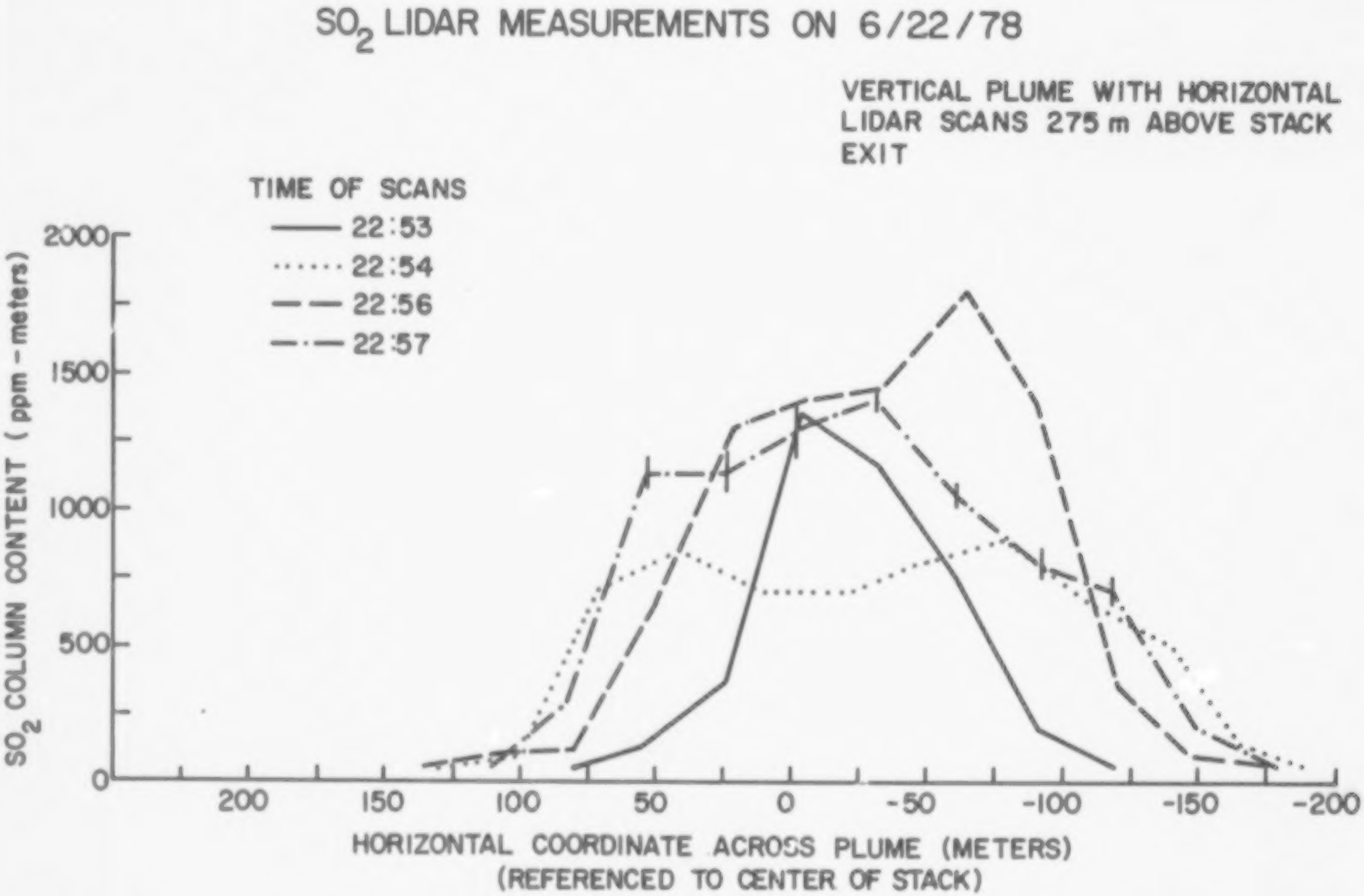

Figure 4. Sulfur dioxide column content measured at different times as a function of horizontal coordinate across plume.

HSRL AEROSOL DATA

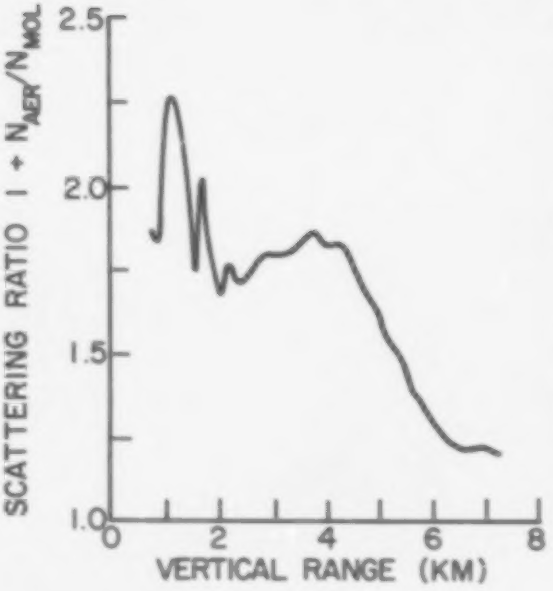

Figure 5. Aerosol-to-molecular scattering ratio as a function of vertical range (km) (HSRL).

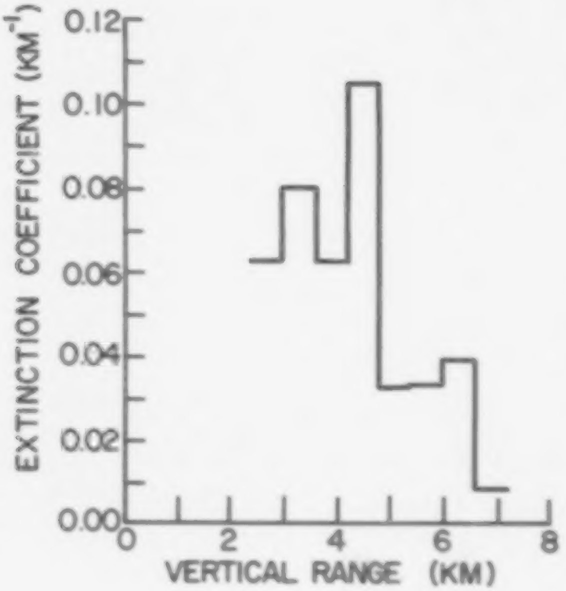

Figure 6. Aerosol optical extinction coefficient as a function of vertical range (km) (HSRL).

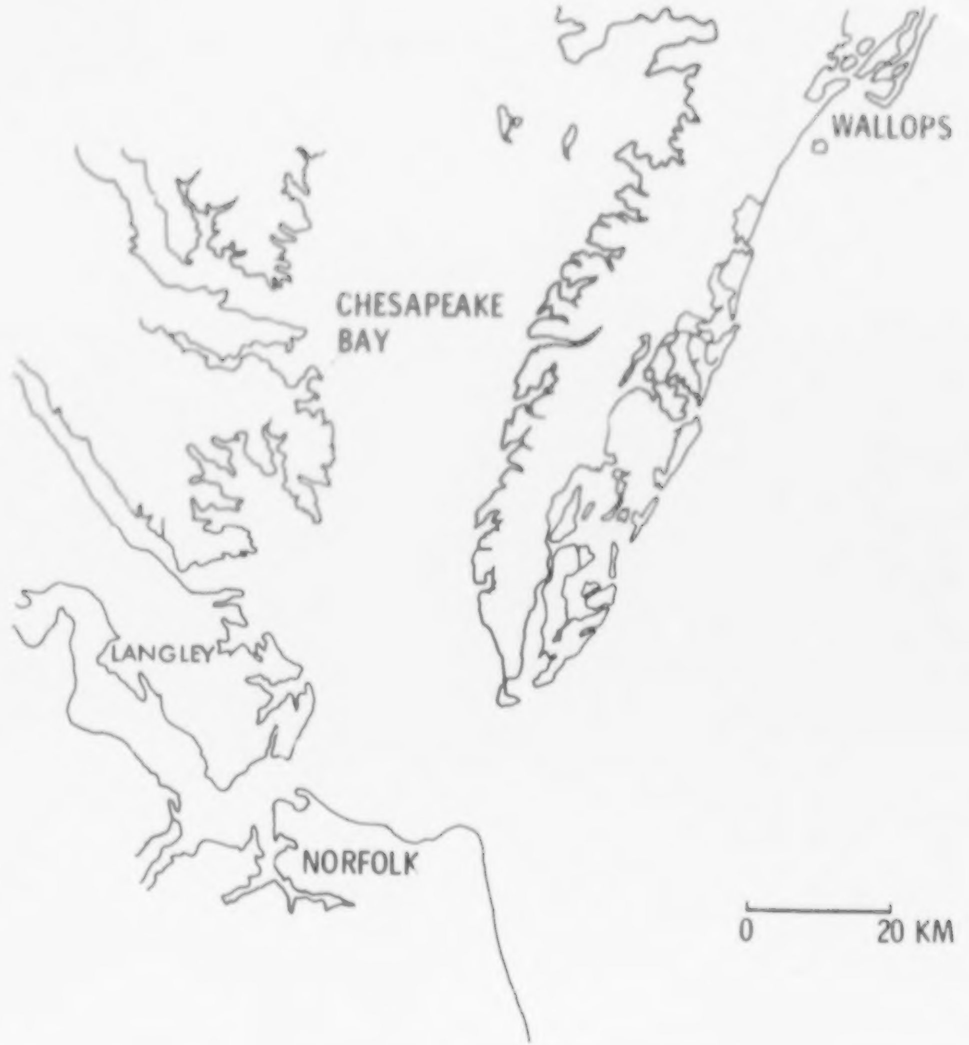

Figure 7. Virginia urban plume study geography.

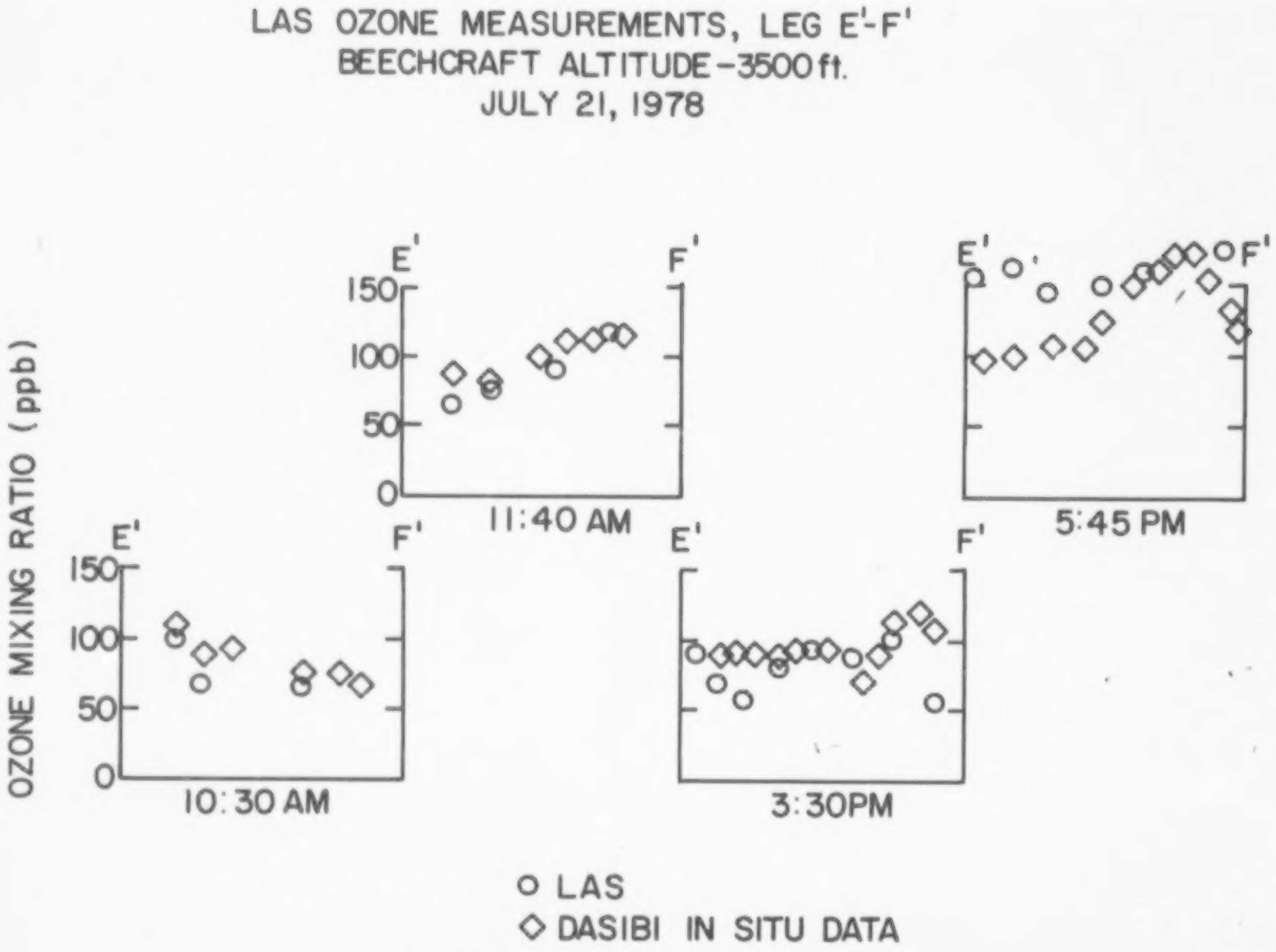

Figure 8. LAS measurements of total burden ozone in the southeastern Virginia plume study.

TABLE 1. EARTH OBSERVATIONS SATELLITE SYSTEMS

EARTH OBSERVATIONS SATELLITE SYSTEMS

CATEGORY AND INSTRUMENTS	SPECTRAL COVERAGE (MICRONS)	SPATIAL RESOLUTION (KM)	SATELLITE SYSTEM	ORBIT	LAUNCH SCHEDULE	APPLICATIONS/OBJECTIVE
• VISSR VISIBLE SPIN SCAN RADIOMETER	IR IMAGES (10.5 - 12.6) VIS IMAGES (.55 - .75) VIS IMAGES (.55 - .75) VIS IMAGES (.55 - .75) VIS IMAGES (.55 - .75)	8 4 2 1 and 2 1 and 2	SMS/GOES 1-3	GEOSYNCHRONOUS	SMS-1 5/74 SMS-2 2/75 SMS-3 10/75 GOES-2 6/77 GOES-3 6/78	• CLOUD IMAGES • SEA SURFACE TEMPERATURE • HIGH RESOLUTION IMAGES
• VAS (VISSR ATMOSPHERIC SOUNDER)	IR & VIS IMAGING IDENTICAL TO VISSR WITH ADDITIONAL SOUNDING CHANNELS AT IR (3.73 - 8.0) IR (8.0 - 14.7)	16 KM	GOES D/E/F (NOAA REIMBURSABLE)	GEOSYNCHRONOUS	D E F 7/80 2/81 7/83	• ATMOSPHERIC SOUNDING • SEA SURFACE TEMPERATURE • CLOUD TOP TEMPERATURES • METEOROLOGICAL HIGH RESOLUTION EARTH IMAGES
• AVHRR (ADVANCED VERY HIGH RESOLUTION RADIOMETER)	VIS IMAGES (0.55 - 0.70) NEAR IR IMAGES (0.725 - 0.90) IR IMAGES (3.55 - 3.93) IR IMAGES (10.5 - 11.5)	1.1 1.1 1.1 1.1	TIROS N A THRU G	SUN SYNCHRONOUS	TIROS N 10/78 NOAA A B* C* 4/79 79 80 D* E* F* G* 81 82 83 84 *AS NEEDED	• CLOUD IMAGES • SEA SURFACE TEMPERATURE • HIGH RESOLUTION IMAGES
• MSS (MULTI-SPECTRAL SCANNER) • RBV (RETURN BEAM VIDICON CAMERA)	VIS (0.5 - 0.6) IR (0.6 - 0.7) IR (0.7 - 0.8) IR (0.8 - 1.1) BLUE-GREEN (.475 - .575) ORANGE-RED (.580 - .680) NEAR IR (.690 - .830)	.08	LANDSAT 1 & 2	SUN SYNCHRONOUS 910 KM	1 2 7/72-1/78 1/75	SOLAR REFLECTED • LAND USE • WATER RESOURCES • AGRICULTURAL SURVEY
• MSS (5-BAND MULTI-SPECTRAL SCANNER) • RBV (RETURN BEAM VIDICON CAMERA)	SAME AS LANDSAT 1 & 2 WITH ADDITIONAL MSS CHANNEL IR (10.4 - 12.6)	.08 .237	LANDSAT 3	SUN SYNCHRONOUS 917 KM	3/78	SOLAR REFLECTED • LAND USE • WATER RESOURCES • AGRICULTURAL SURVEY
• THEMATIC MAPPER	VIS (.45 - .52) VIS (.52 - .60) VIS (.63 - .69) IR (.79 - .90) IR (1.55 - 1.75) IR (10.4 - 12.5)	.03 .03 .03 .03 .03 .120	LANDSAT-D	SUN SYNCHRONOUS	3RD QUARTERS 81	SOLAR REFLECTED RADIATION • LAND USE • WATER RESOURCES • AGRICULTURAL SURVEY

TABLE 2. PASSIVE REMOTE SENSORS

PASSIVE REMOTE SENSORS

CATEGORY AND INSTRUMENTS	SPECIES	SPECTRAL COVERAGE MICRONS	FIELD OF VIEW (DEGREES)	VERTICAL RESOLUTION (KM)	VIEWING MODE	PLATFORM	CURRENT STATUS
GAS FILTER CORRELATION (GFC)							
• A/C MAPS	CO, CH_4 Extendable to Other Gases	4.52 - 4.8	7.5°	<5	THERMAL IR	A/C	A/C OPERATIONAL
• OFT MAPS (SHUTTLE)	CO Extendable to Other Gases	4.52 - 4.8	4.9°	<5	THERMAL IR	SHUTTLE	CY 80 FLIGHT TEST
• PMR	CH_4, CO, N_2O, NH_3 SO_2	4.52 - 4.8 8.00 - 11.0	4.5°	<5	THERMAL IR	A/C	PROPOSED ENGINEERING MODEL DEVELOPMENT
• DCR	CH_4, NH_3, CO, H_2O, HCl, NO_2, SO_2, (NMHC)	4.0 - 9.0	2-7°	TOTAL BURDEN	SOLAR REFLECTED	A/C	PROPOSED A/C DEVELOPMENT
INTERFEROMETRY							
• COPE	CO, CH_4	2.30	7°	TOTAL BURDEN	SOLAR REFLECTED	A/C	A/C OPERATIONAL
• CIMATS	NH_3, H_2O, N_2O, CO, CH_4 CO, SO_2	2.0 - 2.4 4.0 - 9.0	2-7°	<5 km	SOLAR REFLECTED THERMAL IR	A/C	ENGINEERING MODEL DEVELOPED
• HSI	SPECTRALLY SCANNING	1.0 - 6.0 µm	2°	TOTAL BURDEN	DIRECT SOLAR	BALLOON Gnd-BASED	BALLOON/Gnd-BASED OPERATIONAL
INFRARED HETERODYNE RADIOMETRY							
• IHR	O_3, NH_3	9 - 12 µm (DISCRETE STEPS WITH CO_2 LASER)	0.25 mr	<5	DIRECT SOLAR THERMAL IR	A/C A/C	A/C Gnd-BASED OPERATIONAL REQUIRES TECHNOLOGY DEVELOPMENT IN PHOTOMIXER QUANTUM EFFICIENCY
• LHS	SPECTRAL COVERAGE (CONTINUOUS)	7.5 - 13.0 µm	0.25 mr	<5	DIRECT SOLAR	Gnd-BASED	LABORATORY ENGINEERING MODEL
SPECTRORADIOMETERS							
• SBUV - TOMS	O_3 12 SELECTED CHANNELS	(0.25 - .34)	3°	TOTAL BURDEN	SCANNER, SOLAR REFLECTED (UV)	NIMBUS-3 NIMBUS-4 NIMBUS-7	SATELLITE OPERATIONAL
• MULTISPECTRAL OBSERVATION OF POLLUTANTS (MOPS)	SO_2, O_3, NO_2	(0.30 - .60)	MULTI-SPECTRAL IMAGING	TOTAL BURDEN (1 PPM-M)	DIRECT SOLAR NADIR	A/C	A/C OPERATIONAL

TABLE 3. ACTIVE REMOTE SENSORS

ACTIVE REMOTE SENSORS

CATEGORY AND INSTRUMENT	SPECIES	SPECTRAL RANGE (MICRONS)	TRANSMITTING LASER	RECEIVER TELESCOPE DIAM. (CM)	VIEWING MODE	PLATFORM	CURRENT STATUS	FIELD APPLICATIONS
FIXED WAVELENGTH								
• LARGE TELESCOPE LIDAR SYSTEM	STRATOSPHERIC AEROSOL'S	.693	RUBY	122	ATMOS. BACKSCATTER	MOBILE GND	OPERATIONAL	• GND TRUTH FOR SATELLITES (SAM II, SAGE) • VOLCANIC ERUPTIONS
• A/C STRATOSPHERIC AEROSOL LIDAR SYSTEM	STRATOSPHERIC AEROSOL'S	.693	RUBY	36	ATMOS. BACKSCATTER	A/C	OPERATIONAL	• GND TRUTH FOR SATELLITES (SAM II, SAGE)
• GND-BASED RUBY LIDAR SYSTEM	TROPOSPHERIC AEROSOL'S	.693	RUBY	31	ATMOS. BACKSCATTER	MOBILE GND	OPERATIONAL	• POWER PLANT PLUME STUDIES
• LASER ABSORPTION SPECTROMETER (LAS)	O_3, NH_3	9-12 (DISCRETELY TUNABLE)	CO_2 WAVEGUIDE LASER	15	REFLECTED GND (MOLECULAR ABSORPTION)	A/C	OPERATIONAL	• TOTAL BURDEN
• HIGH SPECTRAL RESOLUTION LIDAR (HSRL)	AEROSOL EXTINCTION	.4-.46	N_2 - PUMPED DYE	36	ATMOS. BACKSCATTER	A/C	SYSTEM ASSEMBLY FOR 8/79 FLGT. (CV-990)	• REGIONAL AEROSOL EXTINCTION PROFILES
TUNABLE WAVELENGTH								
• UV DIAL	SO_2, O_3, NO_2, AEROSOL'S	.28-.31	Nd:YAG PUMPED DYE	31	DIFFERENTIAL ABSORPTION FROM ATMOS. BACKSCATTER	MOBILE GND.	OPERATIONAL	• REGIONAL/URBAN PLUME STUDIES
• NEAR IR DIAL	H_2O, PRESSURE, TEMPERATURE PROFILES	.70-.75	RUBY PUMPED DYE	51	DIFFERENTIAL ABSORPTION FROM ATMOS. BACKSCATTER	GND/VERTICAL PROFILES	OPERATIONAL	• TROPOSPHERIC METEOROLOGICAL PARAMETERS
• MID IR DIAL	CO, HCl, CH_4, CO_2, H_2O, N_2O, NH_3, H_2S (NMHC)	1.4-3.7	OPTICAL PARAMETRIC OSCILLATOR	36	DIAL, GND REFLECTION	A/C	SYSTEM ASSEMBLY FOR 8/79 FLGT.	• REGIONAL (HC) & TROP. SPECIES SURVEY
• A/C DIAL SYSTEM	SO_2, O_3, NO_2, H_2O, AEROSOL'S, TEMPERATURE, PRESSURE	.28-.9	Nd:YAG PUMPED DYE	36	DIFFERENTIAL ABSORPTION FROM ATMOS. BACKSCATTER	A/C	SYSTEM ASSEMBLY FOR 8/79 FLGT.	• REGIONAL STUDY OF O_3, SO_2, AEROSOL'S, TROP. H_2O PROFILES
• DIFFERENTIAL ABSORPTION POLLUTION SENSOR	H_2O, CO, NH_3	.45-.60 7.5-13.0	TUNABLE DIODE LASERS	6	LASER ABSORPTION IN 20 METER PATH	A/C	OPERATIONAL	• REGIONAL STUDY OF TROPOSPHERIC BUDGETS & DYNAMICS
• SHUTTLE LIDAR	MULTIPLE SPECIES, CLOUDS, AEROSOL'S, MET PARAMETERS	.30-13.0	EVOLUTIONARY LIDAR SYSTEM	125	ATMOS. BACKSCATTER FLUORESCENCE DIAL	SPACELAB	PHASE-B STUDY COMPLETE	• GLOBAL TROPOSPHERE STRATOSPHERE MESOSPHERE THERMOSPHERE

VALIDITY OF BALLOONS FOR AIR PARCEL TRACKING

Frank B. Tatom*
Engineering Analysis, Inc., Huntsville, Alabama

George H. Fichtl
NASA/George C. Marshall Space Flight Center,
Marshall Space Flight Center, Alabama

Abstract

Constant-volume balloons (CVB's), tetroons, and similar types of balloons are commonly used for measuring atmospheric winds.[1] These balloons are assumed to follow the mean wind and thus represent a logical choice for tracing air parcel trajectories during "persistent elevated pollution episodes" (PEPE's). Various aerodynamic and thermodynamic forces, however, may interact with the balloon and cause it to deviate from the mean wind path. The discussion that follows is divided into three separate areas:

- Examples of tetroon behavior.
- Analytical studies of CVB motion.
- Displacement of CVB's due to the vertical component of wind.

This material is designed to provide a better insight into the question of the validity of balloons for air parcel tracking.

EXAMPLES OF TETROON BEHAVIOR

A large amount of tetroon tracking data has been collected covering a wide range of altitudes and conditions.[2] Two examples of such data are provided in Figures 1 and 2. These radar tracks of tetroons were collected by NASA in August 1967 at Cape Kennedy.

The first tetroon track (Figure 1) corresponds to a morning launch commencing at 0800 EST. As shown in the altitude history plot, the tetroon ascended to an altitude of roughly 425 m and generally remained at that altitude for a major portion of the track. Vertical oscillations appear to have a period of about 20 min with an amplitude of 25 m. The direction and speed of the balloon remained relatively constant with respect to time.

---

*Speaker.

The second tetroon track (Figure 2) corresponds to a late morning launch (1100 EST). The altitude history is characterized by sizeable vertical oscillations with amplitudes as great as 200 m and time periods on the order of 16 min. The corresponding direction history is more erratic than for the first case, but the mean direction of drift is roughly the same. The speed history for the second case is also more erratic, with a magnitude that is approximately twice that observed in the earlier launch.

These two examples illustrate the general observation that atmospheric conditions are generally more stable in the early morning than later in the day. The amplitude and period of the observed oscillations are also of interest as subsequently discussed.

ANALYTICAL STUDIES OF CVB MOTION

As part of an earlier study^2 of CVB's, the computer program BALLOON was written to provide a means of predicting the response of a CVB to a three-dimensional transient flow field.

Basic Governing Equations

The motion of a CVB is governed by the conservation of momentum equation, which in dimensionless form can be written as

$$\frac{d\tilde{v}_i}{d\tilde{t}} = 36\left(\frac{\tilde{\rho}}{2+\tilde{\rho}}\right)\tilde{\nu}\,(\tilde{u}_i - \tilde{v}_i) + \frac{3}{2}\left(\frac{\tilde{\rho}}{2+\tilde{\rho}}\right)C_{D\ell}\,(\tilde{u}_i - \tilde{v}_i)\,|\vec{\tilde{u}} - \vec{\tilde{v}}|$$

$$+ 3\left(\frac{\tilde{\rho}}{2+\tilde{\rho}}\right)\frac{D\tilde{u}_i}{D\tilde{t}} + \left(\frac{\tilde{\rho}}{2+\tilde{\rho}}\right)(\tilde{v}_j - \tilde{u}_j)\frac{\partial\tilde{u}_i}{\partial\tilde{x}_j} - \frac{2(1-\tilde{\rho})}{2+\tilde{\rho}}\,\tilde{g}\,\delta_{i3}$$

$$- 18\left(\frac{\tilde{\rho}}{2+\tilde{\rho}}\right)\sqrt{\frac{\tilde{\nu}}{\pi}}\int_0^{\tilde{t}} \frac{\frac{d(\tilde{v}_i - \tilde{u}_i)}{d\tilde{t}'}\,d\tilde{t}'}{\sqrt{\tilde{t} - \tilde{t}'}} \qquad (i = 1,2,3)$$

This equation is numerically integrated by means of a fourth-order Runge-Kutta technique to obtain the response of the CVB to the flow field. A periodic flow field model was used to represent the atmosphere. The model, which is nonhomogeneous, transient, and three-dimensional with mean translational motion, has the form

$$\tilde{u}_i = \bar{\tilde{u}}_1 \, \delta_{i1} + \sin \left[\tilde{k} \, (\tilde{x}_1 + \tilde{x}_2 + \tilde{x}_3) - \tilde{\omega}\tilde{t} + \theta_i \right] \quad (i = 1,2,3) \qquad (2)$$

By selecting the 3 values of θ_i spaced 120° apart, the model satisfies the continuity equation.

Natural Period of Oscillation

Based on first-order theory,[3] the natural period of oscillation of an air parcel is

$$\tau_{B.V.} = 2\pi \sqrt{\frac{T_o}{g(\Gamma_s - \Gamma)}} \qquad (3)$$

The reciprocal of this expression is generally referred to as the Brunt-Väisälä frequency. The corresponding period of oscillation for a CVB,[4] is

$$\tau_{CVB} = 2\pi \sqrt{\frac{T_o}{g(\Gamma_\rho - \Gamma)}} \qquad (4)$$

The adiabatic lapse rate, Γ_s, has a value of 9.76° K/km while the constant density lapse rate, Γ_ρ, has a value of 34.2° K/km. Examination of equations (3) and (4) indicates that the natural period of oscillation of the CVB will always be less than that of the air parcel. For example, with an equilibrium temperature, T_o, of 300° K and a lapse rate, Γ, of 6° K/km,

$$\tau_{B.V.} = 566.76 \text{ sec or } 9.45 \text{ min}$$

while

$$\tau_{CVB} = 206.95 \text{ sec or } 3.45 \text{ min}$$

The periods of oscillation of the tetroons discussed previously appear more representative of the natural frequency of an air parcel than of a balloon.

Taylor's Hypothesis

In the course of the earlier investigation, the relative magnitude of three velocities was observed to be of special significance. These three velocities were the mean wind, $\tilde{\bar{u}}_1$, the mean balloon velocity, $\tilde{\bar{v}}_1$, and the phase velocity, $\tilde{c}$, where

$$\tilde{c} = \tilde{\omega}/\tilde{k} \tag{5}$$

With respect to these three velocities, two versions of Taylor's Hypothesis were identified. The first, which is Taylor's hypothesis for the fluid (THF), is satisfied when the mean wind velocity equals the phase velocity or

$$\tilde{\bar{u}}_1 = \tilde{c}$$

The second version, which is Taylor's hypothesis for the balloon (THB), is satisfied where the mean balloon velocity equals the phase velocity or

$$\tilde{\bar{v}}_1 = \tilde{c}$$

Numerical Prediction

A series of balloon trajectories was generated with the program BALLOON. Table 1 presents typical input values. The outputs included the position and velocity of the balloon as a function of time and also the velocity of the wind at the same position and time.

The results were examined in terms of both the periodic motion and the mean motion of the balloon. With regard to the mean motion it was observed that the balloon displayed mean transverse motion in the horizontal plane when THB was not satisfied. This feature is illustrated in Figures 3, 4, and 5. In addition to transverse motion, the mean x_1-velocity component of the balloon did always match the mean wind velocity u_1. When the x_1-component of the mean wind velocity greatly exceeded the phase velocity ($\bar{u}_1 >> c$), the balloon mean x_1-velocity component generally was slightly less than the wind velocity component ($\bar{v}_1 < \bar{u}_1$), as shown in Figure 6. However, as c increased relative to $\bar{u}_1$, $\bar{v}_1$ also increased until, as THF was approached, $\bar{v}_1$ first equaled and then exceeded $\bar{u}_1$. Subsequently, when THF was satisfied, $\bar{v}_1$ exceeded both $\bar{u}_1$ and c. For a value of c slightly greater (~5 percent) than $\bar{u}_1$, THB was satisfied, with c becoming equal to $\bar{v}_1$. Further increases in c resulted in a reduction in $\bar{v}_1$ until, for cases where c was very large compared with $\bar{u}_1$, $\bar{v}_1$ became essentially equal to $\bar{u}_1$.

VERTICAL DISPLACEMENT OF CVB's DUE TO THE VERTICAL COMPONENT OF WIND

In the presence of a steady vertical velocity, the CVB will be displaced from its normal equilibrium altitude. The new equilibrium altitude is reached when two forces, drag and buoyancy, are balanced. In dimensionless form the relationship between the vertical velocity and the displacement is

$$W = [(1-\gamma Z)^{\frac{\gamma-1}{\gamma}} - 1]^{1/2} \quad (Z \geq 0) \tag{6}$$

$$W = -[1 - (1-\gamma Z)^{\frac{\gamma-1}{\gamma}}]^{1/2} \quad (Z < 0) \tag{7}$$

where

$$W = \sqrt{\frac{A_c C_{D\ell}}{2gV}}\, u_3$$

$$Z = \frac{g(x_3 - x_{3o})}{R\ T_o}$$

$$\gamma = \frac{\Gamma R}{g}$$

For values of γ ranging from 0 to 0.287, the variation of W with Z is presented in Figure 7. The dimensionless form of this plot, while useful because of its general nature, does not permit immediate appreciation of the magnitude of typical dimensional parameters. For the case of a lapse rate of 6° K/km and a balloon with a 1-m radius and a drag coefficient of 0.75, the corresponding dimensional plot is shown in Figure 8. This figure clearly indicates that a steady vertical velocity component of 2 m/s could cause a displacement of ~1,200 m. If the conditions associated with the second tetroon track (Figure 2) were similar to those in Figure 8, the vertical velocity component involved would be on the order of 1 m/s.

SUMMARY

The preceding discussion provides a description of certain effects produced by aerodynamic and thermodynamic forces that might cause a tetroon or CVB to deviate from the motion of the mean wind. Based on such material there is reason to believe that under certain conditions the balloon velocity may deviate from the mean velocity in both magnitude and direction. In addition, the balloon may be displaced a significant distance from its equilibrium altitude due to vertical currents. None of the material presented, however, is based on a flow field with the random characteristics of atmospheric turbulence. Thus, these conclusions must be applied with caution. To fully resolve the issues would involve coupling the BALLOON program with a three-dimensional simulation of atmospheric turbulence.

LIST OF SYMBOLS

English Symbols

Symbol	Definition
A	amplitude of periodic flow field model
A_c	area of balloon cross section
c	phase velocity, ω/k
$\tilde{c}$	dimensionless phase velocity, $\tilde{\omega}/\tilde{k}$
$C_{D\ell}$	balloon drag coefficient ($10^3<Re<10^5$)
D	diameter of balloon
g	gravitational acceleration
$\tilde{g}$	dimensionless gravitational acceleration, gD/A^2

Symbol	Definition
k	wave number
$\tilde{k}$	dimensionless wave number, kD
R	specific gas constant
t	time
$\tilde{t}$	dimensionless time, At/D
T_o	fluid temperature at equilibrium altitude
u_i	fluid velocity
$\tilde{u}$	dimensionless fluid velocity, u_i/A
v_i	balloon velocity
$\tilde{v}_i$	dimensionless balloon velocity, v_i/A
V	volume of balloon
W	dimensionless vertical velocity, $\sqrt{\frac{A_c C_{D\ell}}{2gV}}\, u_3$
x_{30}	equilibrium altitude
x_j	Cartesian coordinate
$\tilde{x}_j$	dimensionless Cartesian coordinate, x_j/D
Z	dimensionless vertical displacement, $g(x_3 - x_{30})/(RT_o)$

Greek Symbols

Symbol	Definition
γ	dimensionless lapse rate, $\Gamma R/g$
Γ	atmospheric lapse rate
Γ_s	adiabatic lapse rate
Γ_ρ	constant-density lapse rate
δ_{ij}	Kronecker delta function
θ_i	phase angle of flow field model
ν	kinematic viscosity
$\tilde{\nu}$	dimensionless kinematic viscosity, $\nu/(AD)$
ρ	fluid density
$\tilde{\rho}$	dimensionless fluid density, ρ/σ
σ	balloon density
τ	period of oscillation
ω	frequency of flow field model
$\tilde{\omega}$	dimensionless frequency of flow field model, $\omega D/A$

REFERENCES

1. Tatom, F. B., and G. H. Fichtl. The Response of a Constant-Volume Balloon to Periodic Three-Dimensional Flow. Seventh Conference on Aerospace and Aeronautical Meteorology and Symposium on Remote Sensing from Satellites. November 16-19, Melbourne, Florida.

2. Tatom, F. B., and R. L. King. Determination of Constant-Volume Balloon Capabilities for Aeronautical Research. NASA CR 2805. George C. Marshall Space Flight Center Space Sciences Laboratory, Marshall Space Flight Center, Alabama, May 1976.

3. Hess, S. L. Introduction to Theoretical Meteorology. Holt, Rinehart and Winston, New York, 1959.

4. Angell, J. K., and D. H. Pack. Analysis of Low-Level Constant Volume Balloon (Tetroon) Flights from Wallops Island. Journal of The Atmospheric Sciences, 19:87-98, 1962.

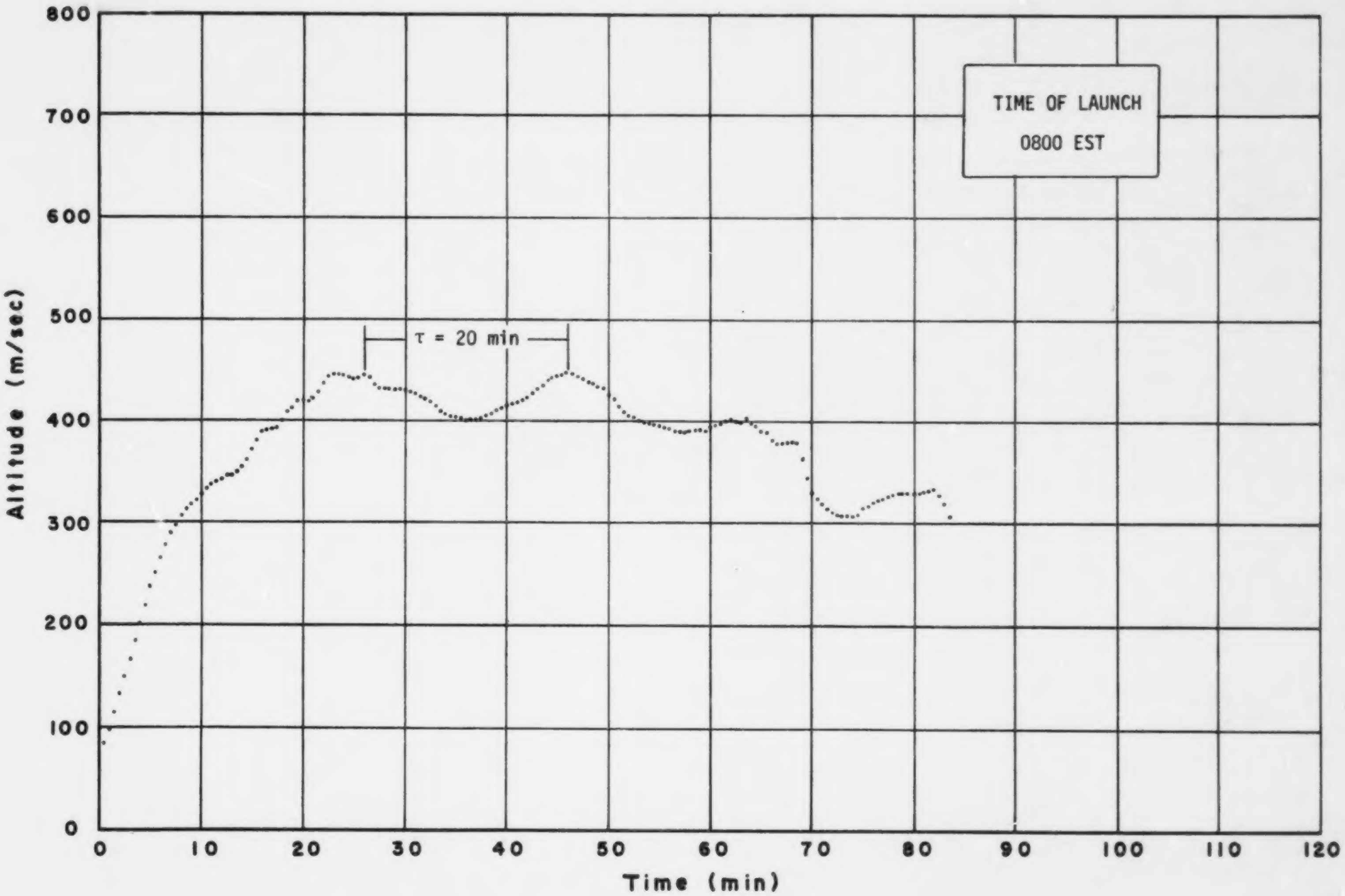

Figure 1a. Tetroon altitude history (morning launch).

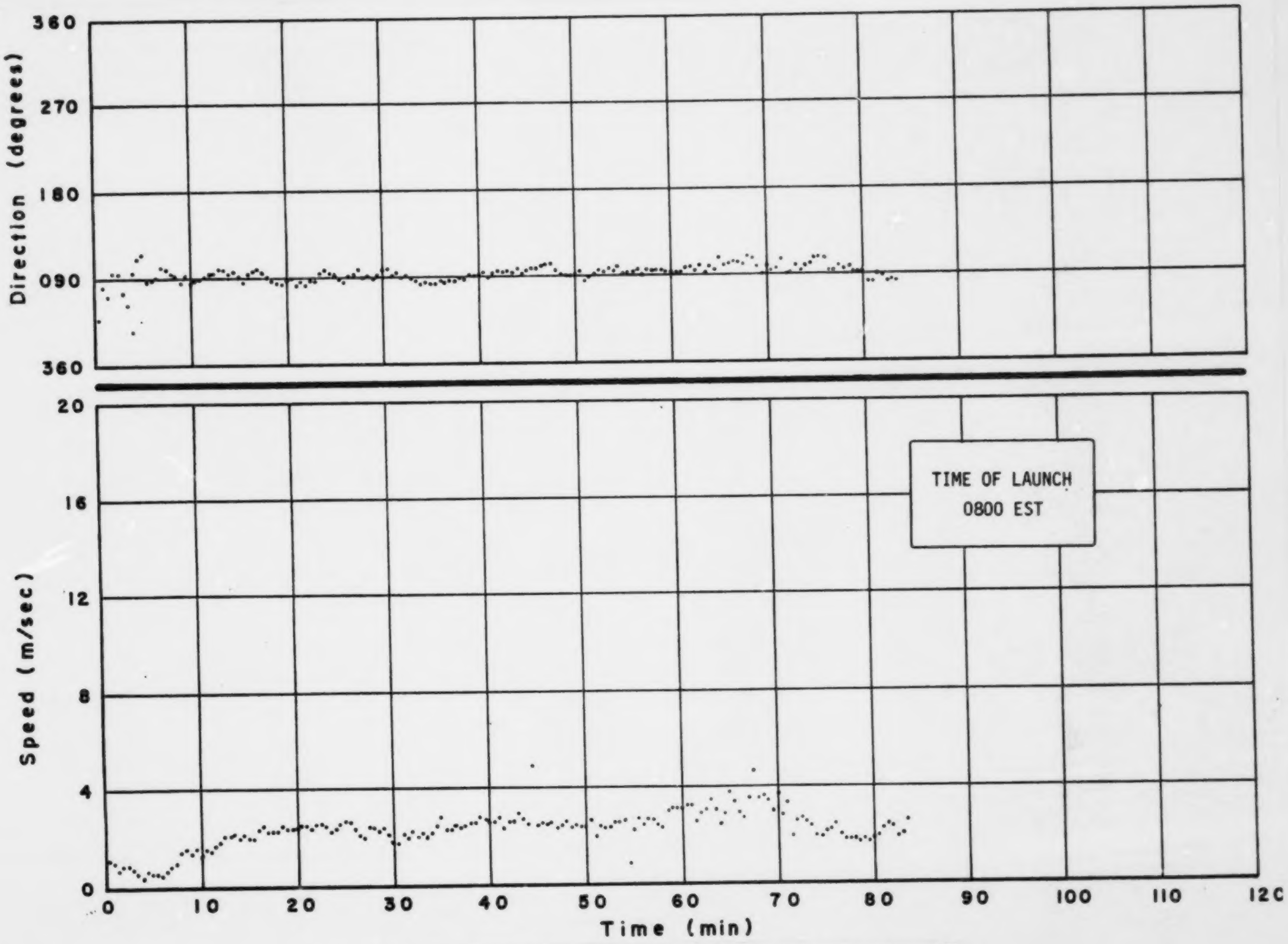

Figure 1b. Tetroon direction and speed history (morning launch).

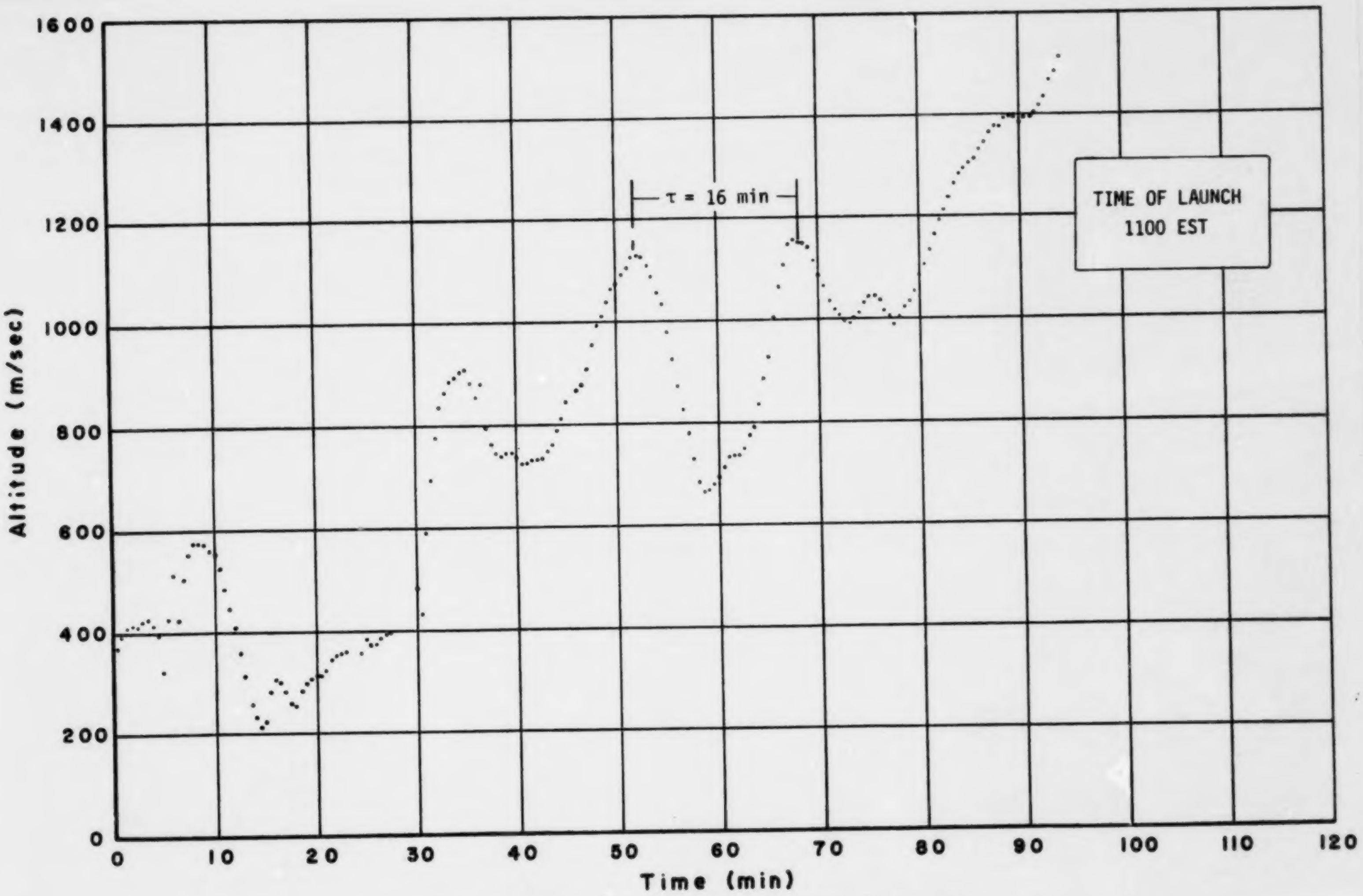

Figure 2a. Tetroon altitude history (late morning launch).

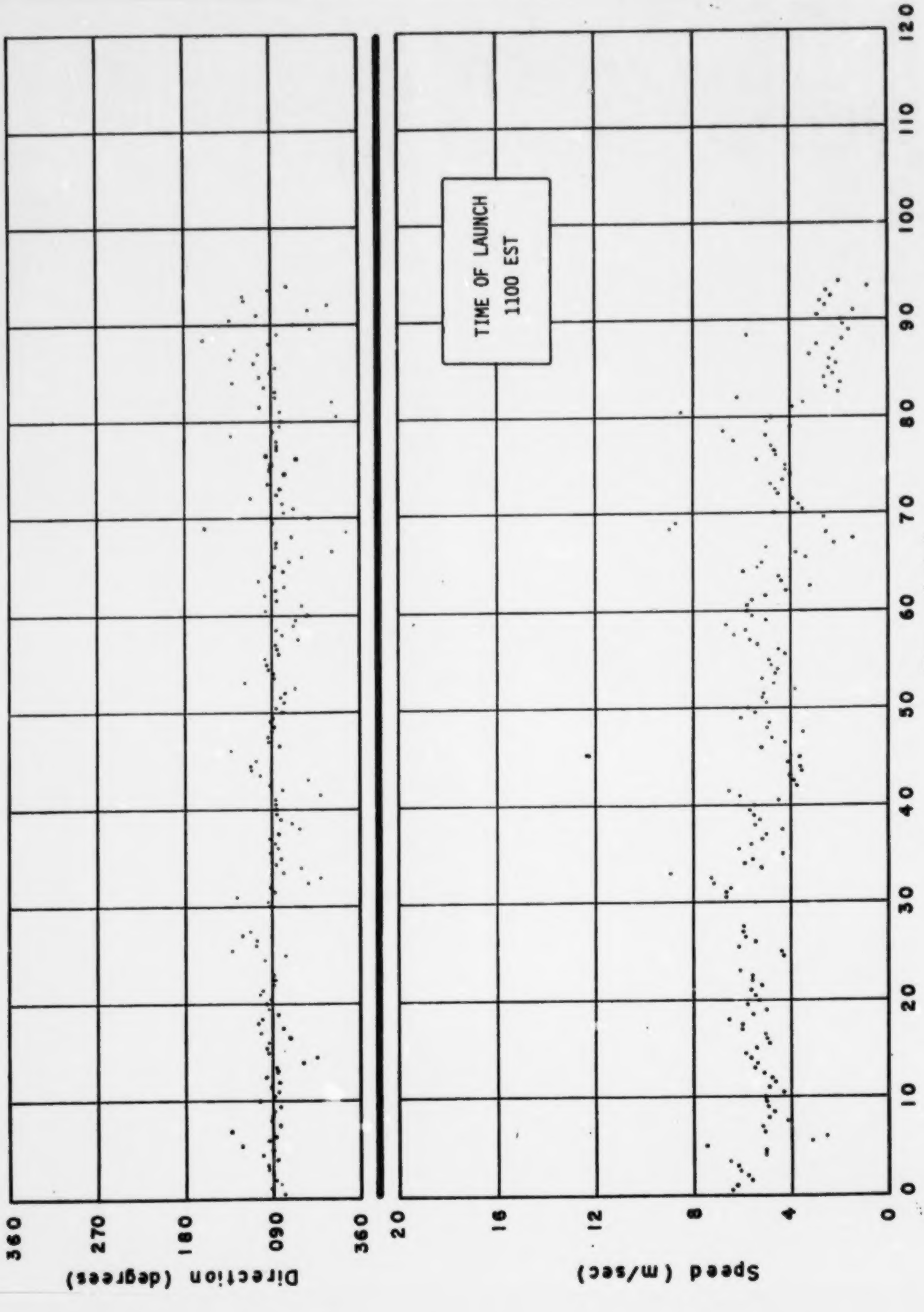

Figure 2b. Tetroon direction and speed history (late morning launch).

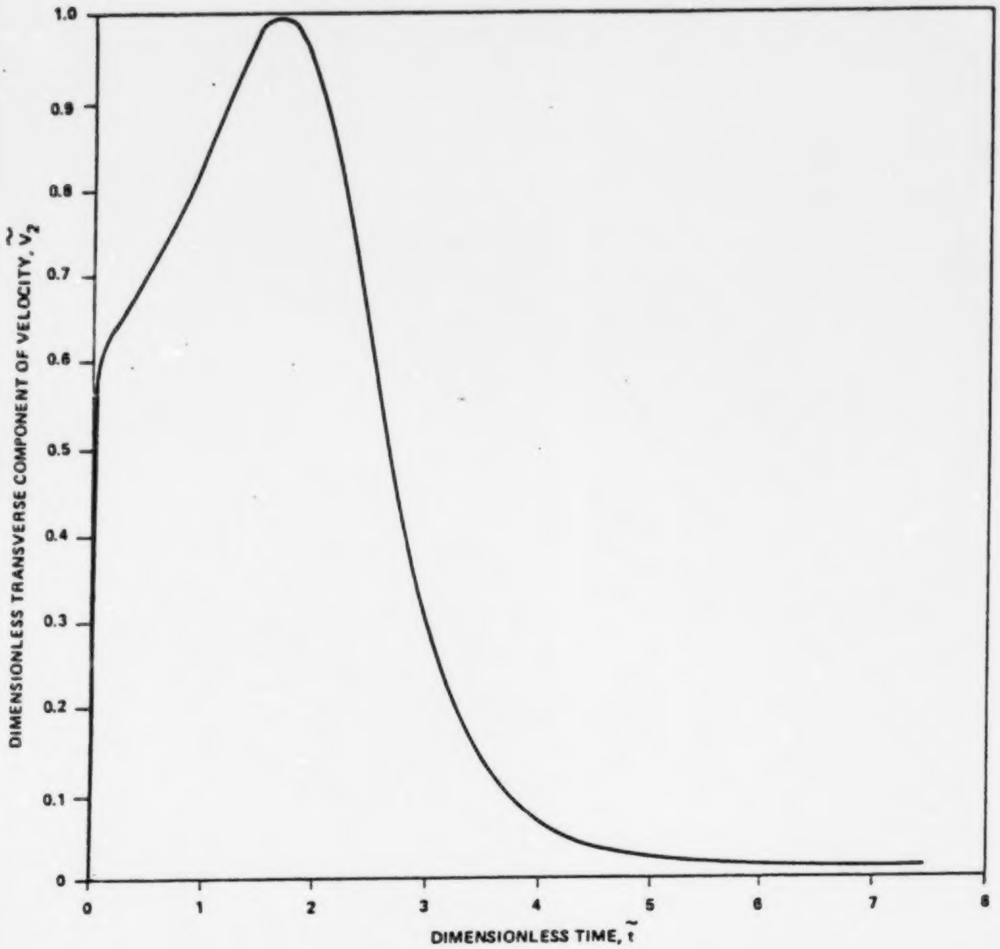

Figure 3. Transverse balloon velocity for case T_1 ($\bar{v} < c$).

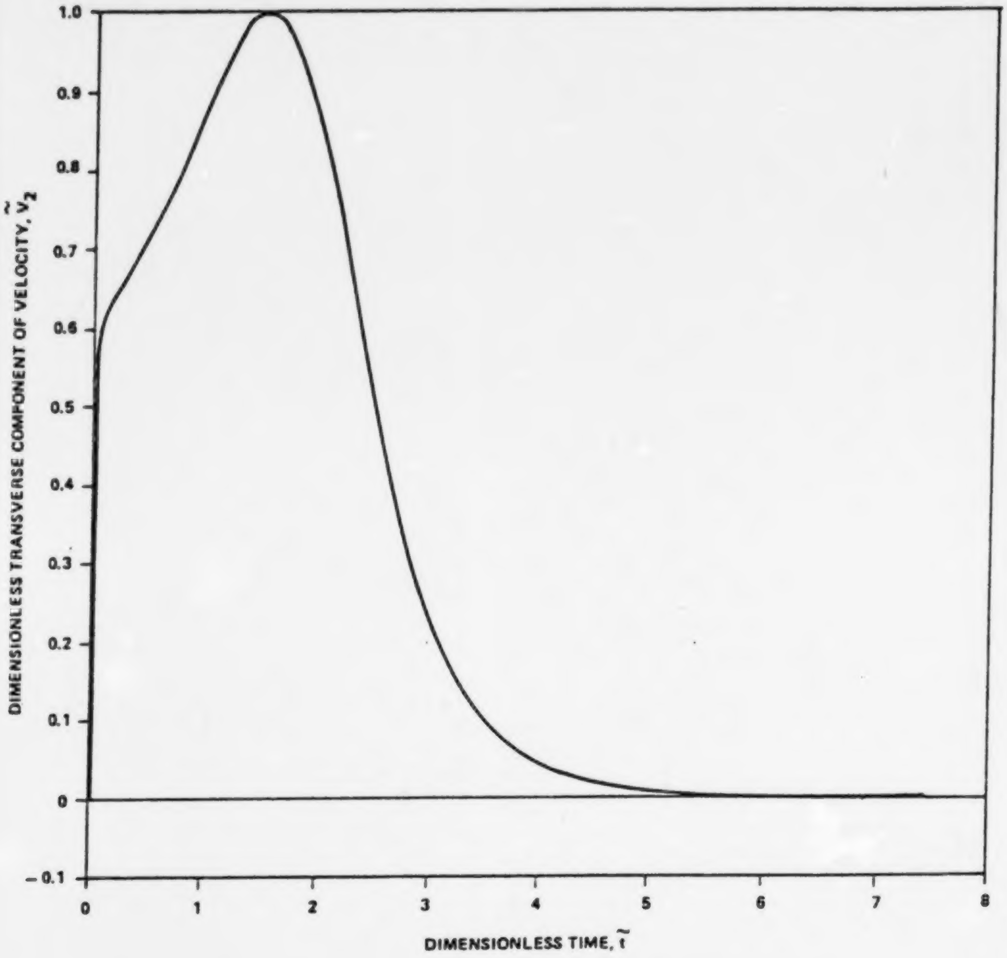

Figure 4. Transverse balloon velocity for case T_2 ($\bar{v} = c$).

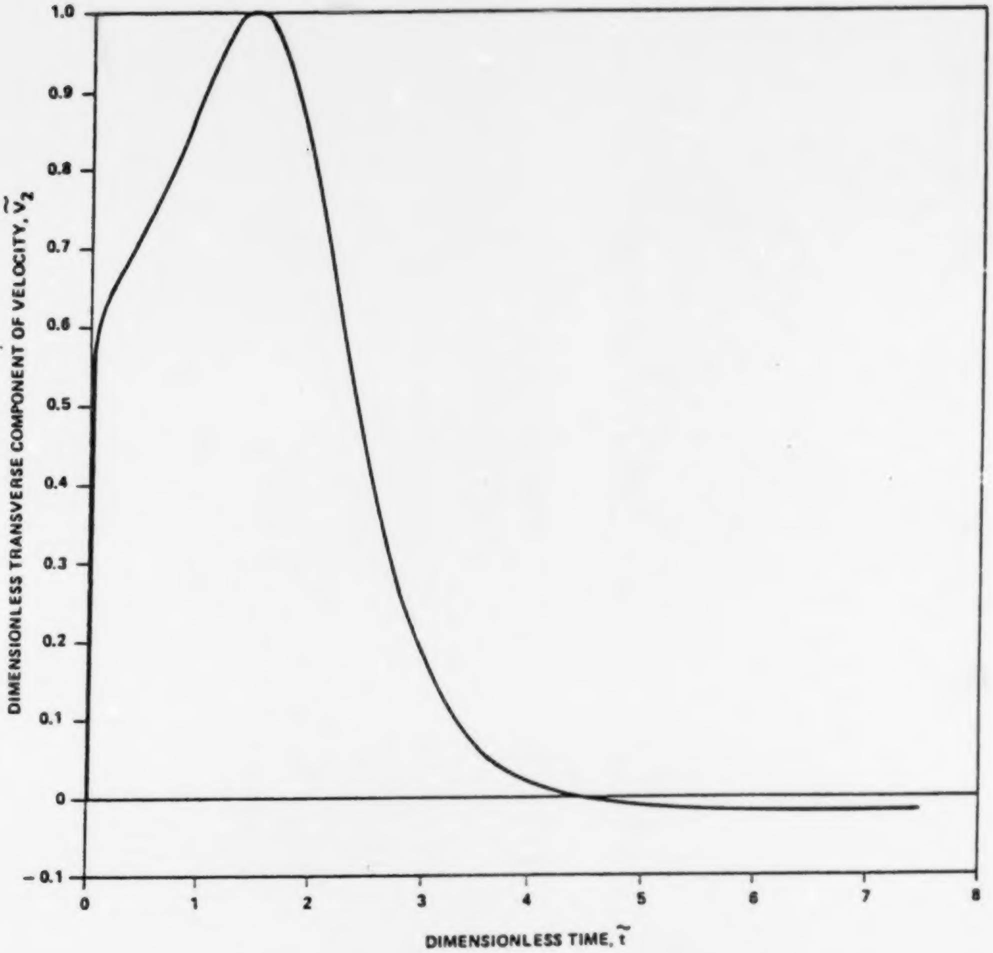

Figure 5. Transverse balloon velocity for case T_3 ($\bar{v} > c$).

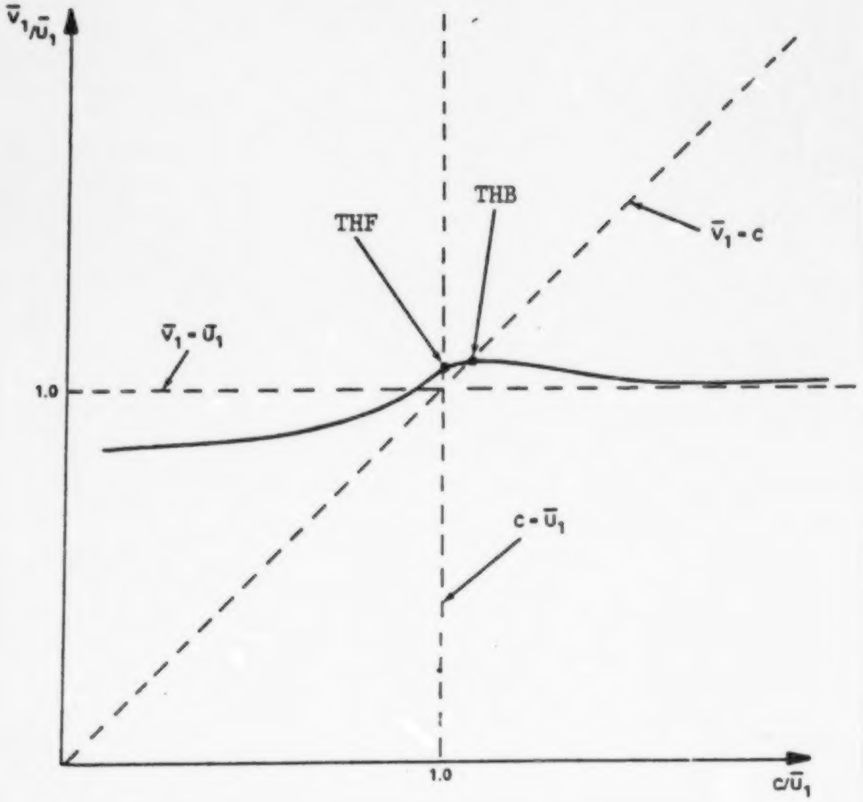

Figure 6. General variation of mean balloon velocity with phase velocity based on numerical results.

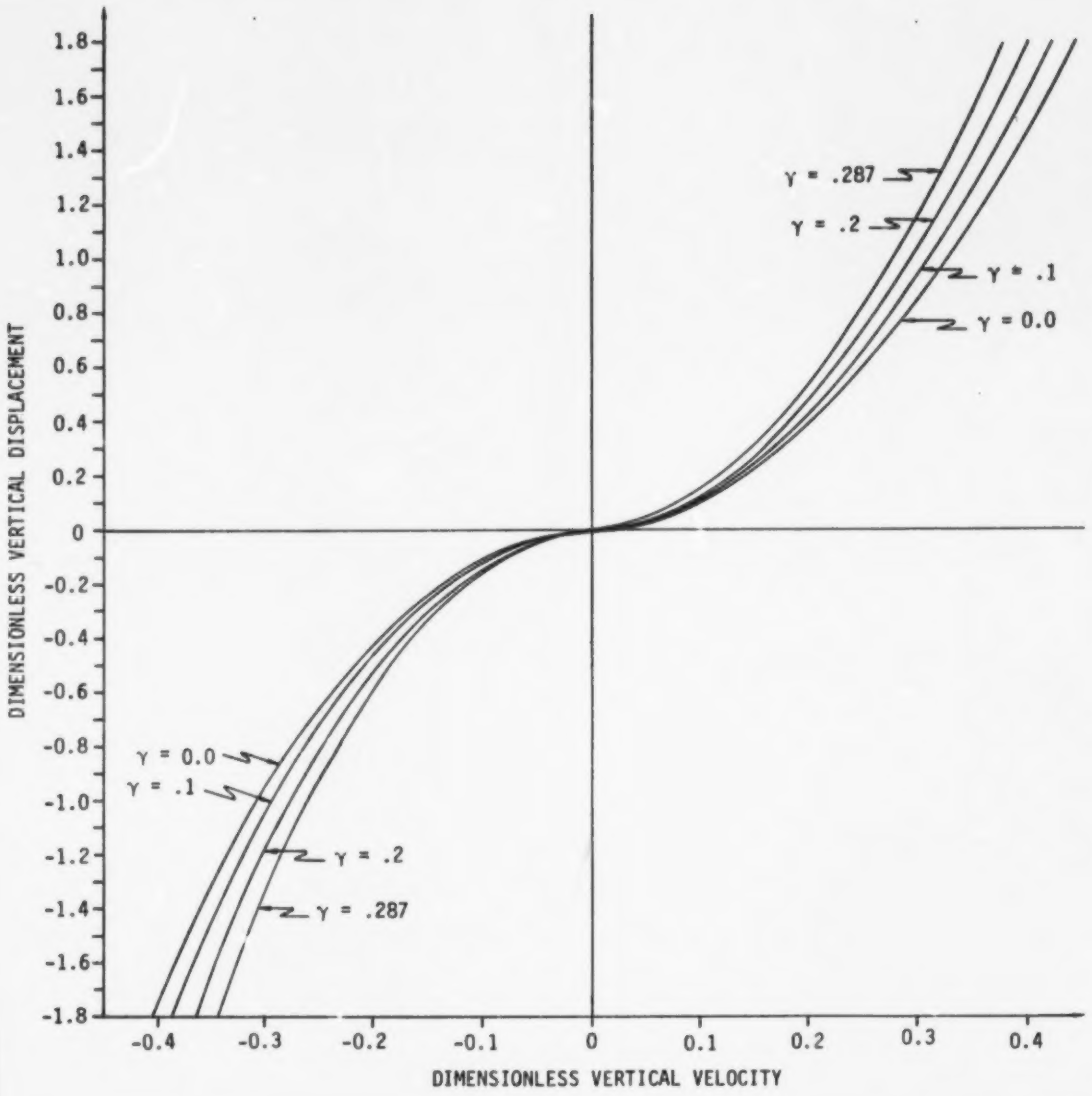

Figure 7. Dimensionless variation of vertical displacement with vertical velocity.

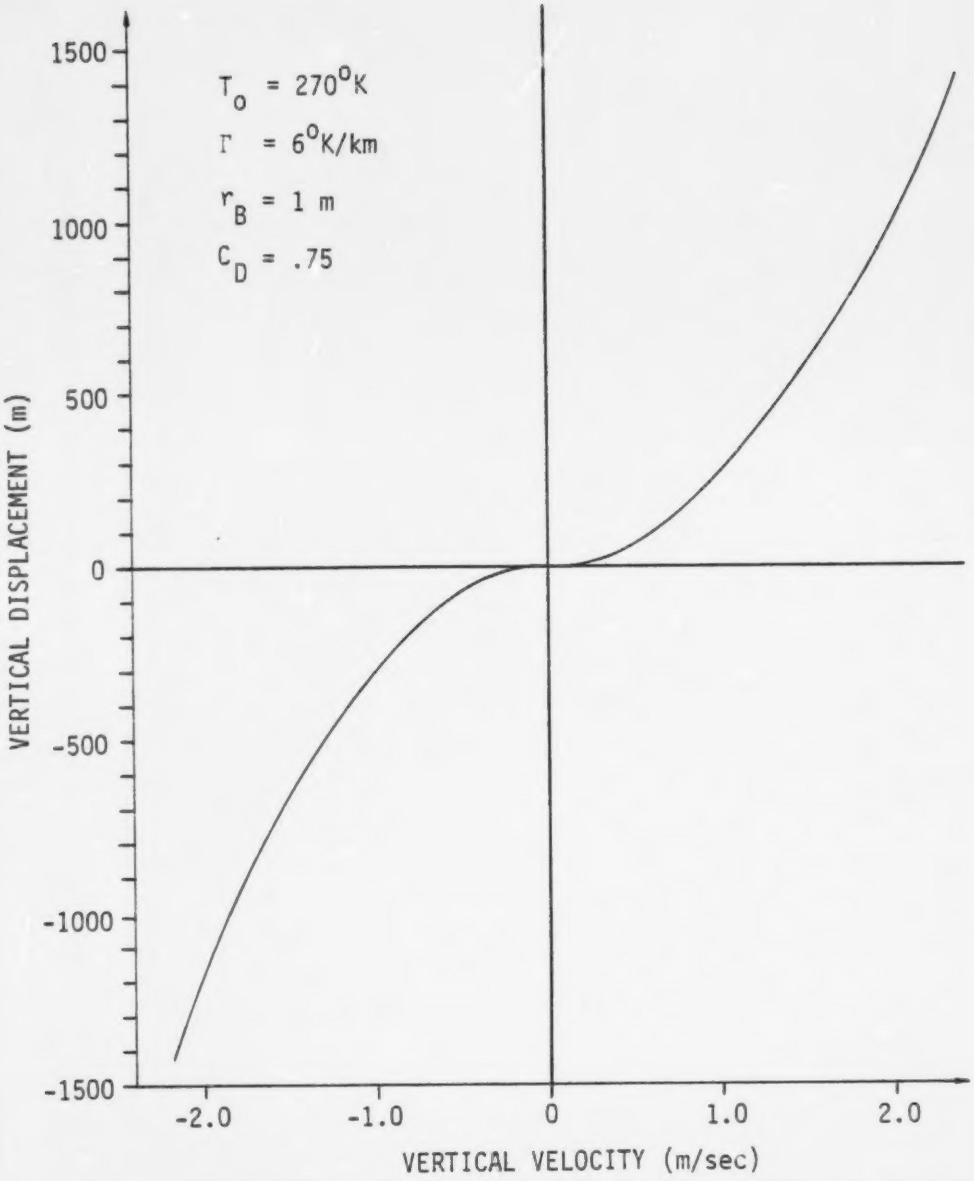

Figure 8. Dimensional example of variation of vertical displacement with vertical velocity.

TABLE 1. TYPICAL DIMENSIONAL VALUES

Physical parameter	Value
T_o	218° K
R	2.870224×10^6 cm^2/s^2 °K
Γ	0.0° K/cm
g	980.6 cm/s
μ_o	1.40646×10^{-4} g/cm s
A	100.0 cm/s
D	130.0 cm
$\bar{u}_1$	1000.0 cm/s
σ	3.61494×10^{-4} g/cm^3
ρ_o	3.61494×10^{-4} g/cm^3
k	6.28×10^{-6} to 6.28×10^{-3} cm^{-1}*
ω	6.28×10^{-3} to 6.28×10^{-1} sec^{-1}*

*Such ranges of k and ω correspond to spatial wavelengths from 10 m to 10 km and time periods of 1 s to 1,000 s.

NAVIGATIONAL AIDS FOR AIR PARCEL TRACKING

James G. Haidt

Research Triangle Institute, Research Triangle Park, North Carolina

Abstract

The purpose of this paper is to discuss the application of radio navigation systems to the tracking of tetroons used as air parcel markers. It is concluded that an acceptable tracking system could be designed that used either Omega or Loran-C but that several problems, both technical and logistical, remain to be faced.

RETRANSMISSION CONCEPT

The various means by which one might follow the progress of a tetroon, as it is carried along in a parcel of air, divide themselves naturally into two categories according to whether or not the tetroon payload includes electronic gear devoted specifically to the tracking function. For tetroons that include no such electronic gear, tracking techniques rely on sighting the tetroon either visually or with a primary radar; techniques of this sort are not discussed further here. Tracking systems in the complementary "electronic" category, those which are of interest here, are conveniently distinguished according to the type of electronic payload carried by the tetroon. Figure 1 illustrates three generic classes of electronic instrumentation: beacon, transponder, and receiver/retransmitter (or simply retransmitter).

In the beacon class of tracking systems, the tetroon carries a transmitter that periodically broadcasts a modulated signal. A receiver monitoring these broadcasts can then determine the position of the transmitter along with its identity. The beacon may also be equipped to transmit data in its broadcasts. The primary example of a beacon tracking system is that which employs satellites (e.g., Tiros-N) as the monitoring receivers. Other monitoring platforms can be used in principle, subject to the constraints that they achieve line-of-sight communication with the transmitter and that they know time and their position and velocity accurately.

The transponder class of systems carries a receiver/transmitter pair that responds to electronic interrogation from a radar. In this case, the position of the transponder is determined in the standard radar way (antenna-pointing direction and time delay in the transponder reply to interrogation). Position determination of the transponder obviously requires that the position of the radar be known. As in a beacon system, the transponder may relay data (e.g., identification code) in its reply.

In the retransmitter class of systems a distinctly different approach is taken to positioning the tetroon. Here the electronic payload includes a navigation receiver, by means of which the tetroon effectively determines its own position, and a transmitter, which relays this information to a monitor receiver. It follows, therefore, that the monitor need not know its own position and may, in fact, be moving, an important consideration in assessing the ease with which tetroons may be tracked. Along with position data, the navigation retransmitter may pass along other data in a natural way.

The retransmitter principle of tracking is depicted in greater detail in Figure 2a. The standard radio navigation receiver, as shown, consists of three main elements that have been labelled demodulator, processor, and tracker for convenience. The demodulator element is meant to include all of the radio frequency (RF) gear of the receiver, i.e., antenna, RF amplifier, etc. It is responsible for accepting the signals appropriate to the navigation system in use (e.g., Omega) and extracting from these signals the raw data (e.g., phase differences) from which position can be determined. The actual conversion of raw data into position data is performed by the second element of the receiver, the processor. The periodic position updates so produced are fed into a tracker where they are assembled into a smooth trajectory.

Adaptation of the standard navigation receiver to the retransmitter concept involves breaking it as shown in Figure 2b and inserting a transmitter/receiver pair in the gap. In the new configuration, the demodulator and transmitter comprise the tetroon payload while the receiver, processor, and tracker become part of the monitor receiver. Clearly the original navigation receiver could be divided at some other point besides that shown in Figure 2b to achieve the same end, but minimization of the electronics carried by the tetroon dictate the arrangement shown.

CANDIDATE RADIO NAVIGATION SYSTEMS

Tracking Requirements

It is not the intent of this paper to lay out an experimental design from which a list of requirements concerning a tetroon tracking system would be forthcoming. To provide a basis for discussion, however, it is useful to have at least a list of desirable attributes that the ideal tracking system might possess. Such a listing is advanced in Figure 3.

The parameters displayed in Figure 3 must be viewed, to reiterate, more as being desirable than necessary. Indeed, it is highly unlikely that any of the tracking systems mentioned earlier can realize all of them in practice. For example, an hourly position update rate will not be possible with the satellite set currently in orbit or projected to be operational in the near future. Likewise, neither a radar nor a retransmitter system is capable of a faithful hourly update rate over extended periods of time without sizeable expenditures of either manpower or money.

These and similar caveats should be borne in mind in the following discussion, the point being that some compromises will need to be made.

Navigational Systems

Table 1 lists three candidate radio navigational systems that could be used in a retransmitter tracking system. It should be noted at the outset that both Omega and Loran-C are currently operational; the last, GPS, is in the process of being implemented and tested but will probably not be available for routine operation until near the middle of the next decade. It is included in the lineup for completeness and to set forth a future candidate that may prove desirable. (Indeed, GPS is the only system of the three that will give three-dimensional position.)

Table 1 rates the various systems according to the criteria of accuracy, coverage, weight/volume, and cost. The ratings pertain to the baseline parameters set forth in Figure 3.

With respect to tracking accuracy, Omega is the poorest performing system but is, nevertheless, marginally capable of meeting a specification of 1-mile position uncertainty. Although the system can perform to this accuracy during daytime, at night 2-mile errors are more realistic when RF propagation at very low frequencies (10-14 kHz) tends to become less predictable.* The other systems, Loran-C and GPS, should always provide position estimate accuracy to 1 mile.

Omega presently provides full coverage of the United States through use of the stations in Hawaii, North Dakota, and Norway. However, in the region west of the Rocky Mountains it is usually more desirable to substitute the station in Japan for that in Norway. The station in Liberia is also a possibility, but the inferiority of east-to-west propagation makes its use marginal. GPS, likewise, will provide full coverage of the United States. Loran-C, originally designed to service marine traffic in the coastal confluence region, leaves the region between the Rocky Mountains and the Mississippi River largely uncovered (see Figure 4). Plans are being formulated to rectify this situation, but no timetable for implementation has been forthcoming.

With regard to weight/volume, both Omega and Loran-C appear capable of meeting a 750-g payload limit. Evidence of this assertion is provided by equipment currently manufactured (e.g., by Beukers Laboratories, Inc.). Thus, it is reasonable to assume that in either case a receiver/retransmitter combination weighing less than 200 g (perhaps half this value) could be assembled. If power were provided by high energy-density lithium cells, an additional 100 g of payload would suffice to power the electronics for 3 to 6 days depending on the transmitter duty cycle employed. Although these numbers are admittedly estimates, they do indicate that a 750-g payload limit does not present a fundamental difficulty to either Omega or Loran-C. The weight of a GPS receiver/retransmitter is projected to be roughly twice that of Omega, implying that it, too, will be capable of meeting the weight allowance.

The cost of either an Omega or Loran-C receiver/retransmitter is thought to be in the neighborhood of $100; that of GPS, perhaps two to three times greater.

---

*It should be noted that differential Omega, a distinct possibility in tetroon tracking, reduces position uncertainty to one-half mile, day or night.

Again, there appears to be no difficulty in meeting a $1,000 ceiling, even with the cost of tetroons.

IMPLEMENTATION

The preceding discussion indicates that any of the radio navigation systems considered would be feasible for use in what might be called the "air segment" of a tetroon tracking system; i.e., that portion of the overall system carried aloft by the tetroons. That is to say, one should experience no fundamental problem in: (1) designing a receiver that is capable of giving position data continuously if need be and to the desired accuracy; and (2) designing a companion retransmitter, the total package weighing 200 to 300 g and costing $100 to $200.

Problems do arise, however, when one attempts to envision how one might monitor the movements of multiple tetroons simultaneously over extended periods of time and make tracking data available to, say, a central facility on a near real-time basis. In this regard, two questions must be answered:

- How does one handle several transmitters operating simultaneously?
- How does one position oneself to listen to these transmitters when the tetroons carrying them may see their paths stretching over hundreds of miles and diverging by like distances?

The first question has a straightforward answer: encode the transmissions so as to create a code-division multiplex scheme. Such an approach is used routinely in military systems and would require little additional hardware to be added to the tetroon payload.

The second question is not so susceptible to solution. Indeed, the only answer would appear to be one or more aircraft monitors in the air virtually continuously, receiving the tetroon broadcasts and relaying them to a central control point. Such an approach is obviously quite demanding on men and equipment.

Were one to relax either the position update rate or the data turnaround time requirement, however, several interesting possibilities arise that exploit the unique characteristics of a retransmitter tracking system; to wit, that tetroon position is an air-derived measurement (distinct from a radar tracking system in which tetroon position is a ground-derived measurement). From this property of retransmitter systems, two important observations emerge:

- One can easily relocate the tetroons after extended periods of no surveillance. Indeed, on the basis of very crude position predictions, one need only send an aircraft up to 10,000 ft, for example, in the general vicinity of the tetroons to be able to receive all their broadcasts emanating from within a range of several hundred miles.

- Position data generated by the tetroon can be recorded for later broadcast on command to the observation aircraft considered in the preceding paragraph. In this way, one could recreate the complete trajectory a tetroon has followed by monitoring it twice a day, for example.

It is recognized, of course, that the last concept requires still more airborne equipment, but with solid-state memories it should be feasible.

In summary, the concept of using the retransmission technique for multiday tracking of air parcels appears feasible within a set of requirements somewhat less demanding than those of Figure 3 concerning positions update rate and data turnaround rate. Furthermore, a starting point for the design of the required equipment is commercially available.

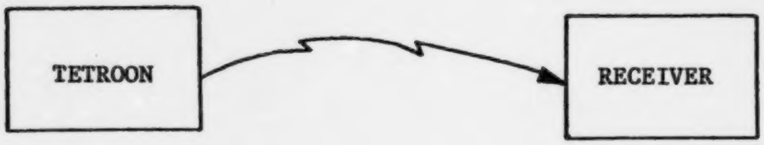

BEACON SYSTEM

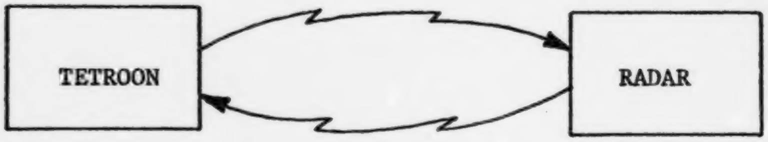

TRANSPONDER
SYSTEM

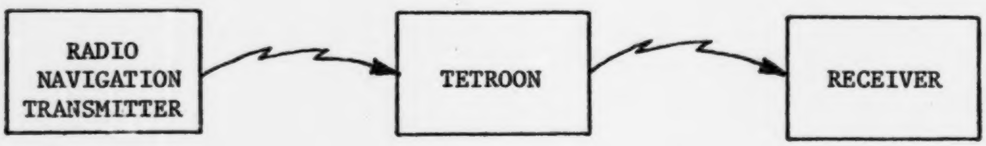

RETRANSMITTER
SYSTEM

Figure 1. Classes of tracking systems.

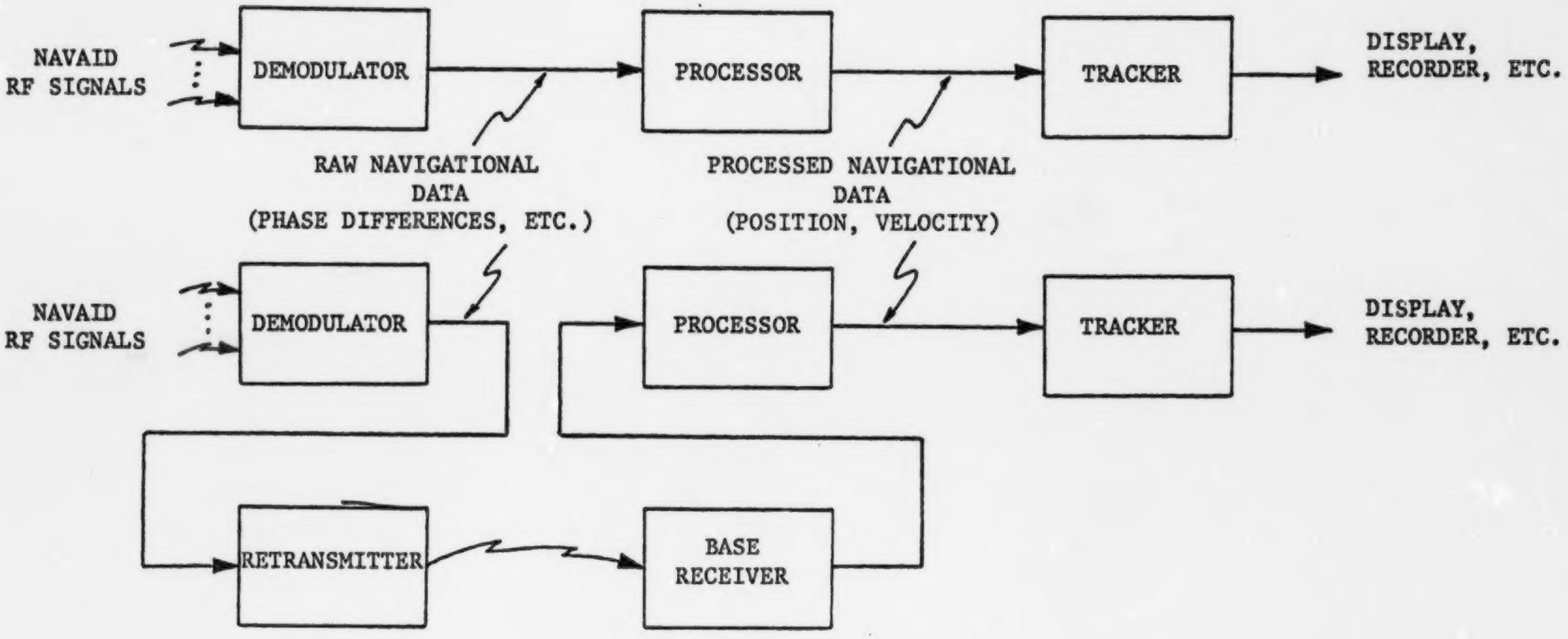

Figure 2. Retransmission System Principle. Figure 2a (top) shows standard navigation receiver. Figure 2b (bottom) shows conversion to retransmission system.

- EXPENDABLE SENSORS (MAXIMUM COST: $1,000)
- MINIMAL AVIATION HAZARD (MAXIMUM WEIGHT: 750 g)
- MULTIDAY DURATION (MINIMUM BATTERY LIFE: 72 HR)
- LOW ALTITUDE (3,000-4,000 FT)
- MULTIPLE SENSORS (MINIMUM 3-5)
- POSITION DATA ONLY
- MODERATE TRACK UPDATE RATE (HOURLY IF POSSIBLE)
- MODERATE POSITION ACCURACY (1 MILE IF POSSIBLE)
- RAPID DATA TURNAROUND (REAL-TIME IF POSSIBLE)

Figure 3. Idealized mission requirements.

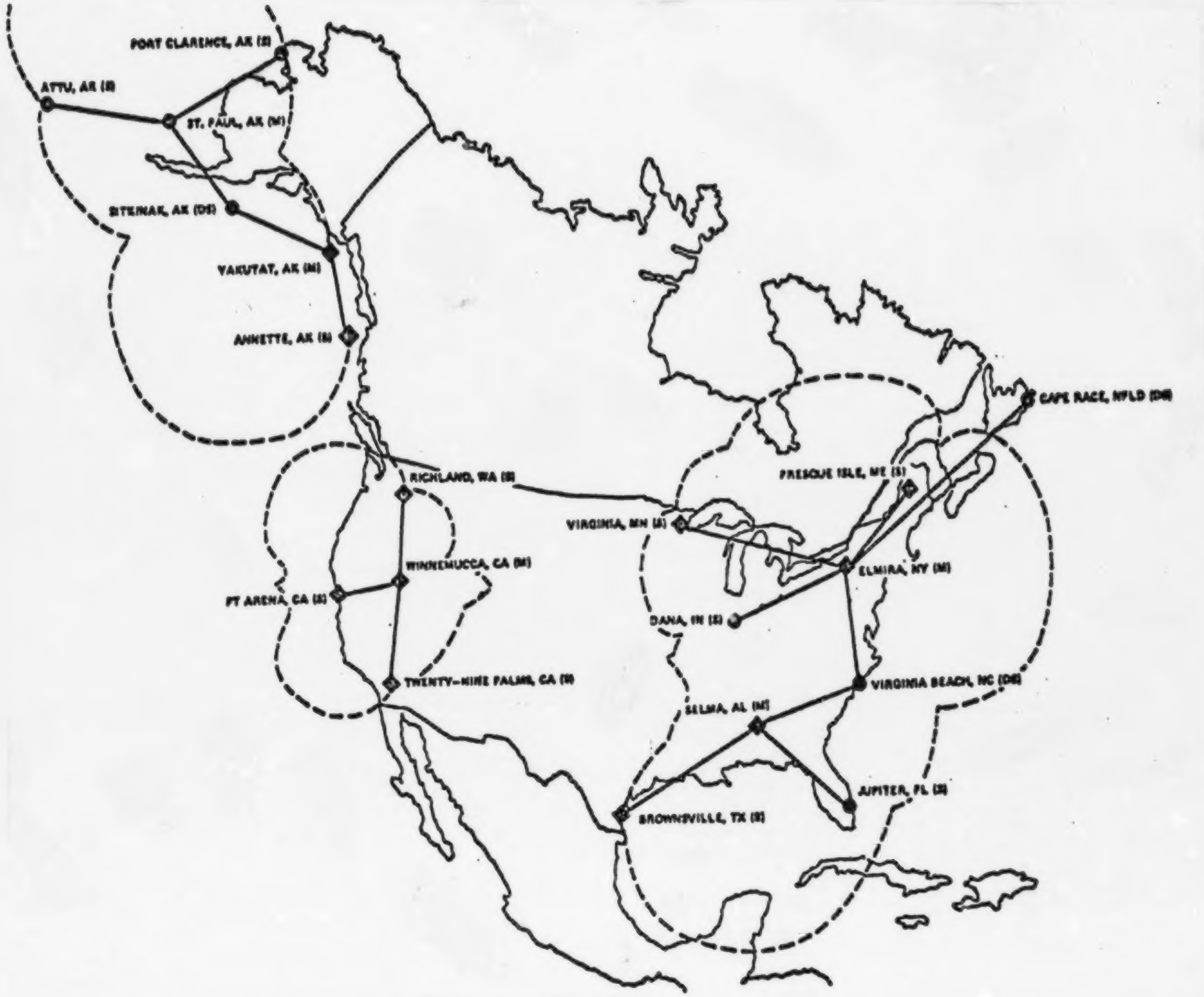

Figure 4. Loran-C coverage of the United States.

TABLE 1. CANDIDATE RADIO NAVIGATION SYSTEMS

	Accuracy	Weight/ volume	Coverage	Cost
Omega	Moderate	Low	High	Low
Loran-C	Moderate to high	Low	Moderate	Low to moderate
Navstar-GPS	High	Moderate (projected)	Very high	Moderate (projected)

SATELLITE POSITIONING OF TRACERS

James J. B. Worth

Research Triangle Institute
Research Triangle Park, North Carolina

The availability of the Random Access Measurement System (RAMS) on the later satellites of the NIMBUS series, and the successful use of this system for tracking balloons in air currents and buoys in the ocean, suggested that the RAMS might be used for tagging air parcels in which pollutant transformations were taking place. The RAMS consists of the radio transmitter for which the position is to be determined and the receiver-storage-transmitter in the satellite. Position data are retrieved by transmission from the satellite to a ground station with each orbit (minimum 12 hr, with possibility of every 6 hr).

The transmitter being tracked transmits a coded radio signal periodically (1 s of each minute). This signal is received by the satellite if the satellite's position in its orbit gives it a line-of-sight view of the transmitter. From the coded signal, the transmitter can be identified, and from repeated signals from the transmitter (at 1-min intervals) during one pass of the satellite, the position can be determined by the Doppler shift of the signal frequency. The period and the inclination of the satellite's orbit determine the number of position determinations that can be made in a 24-hr period. With the usual orbit of NIMBUS-type satellites, a minimum of two positions per day is obtained. Up to 100 transmitters can be handled by a single satellite.

The transmitter, or beacon, shown in Figure 1 is a prototype designed and built to test the circuitry (Figures 2 through 7) rather than to demonstrate a model feasible for use on low-altitude balloons or tetroons in crowded air space. With development we anticipate that this prototype that now weighs 822 g (with batteries) and measures 22 × 8 × 8 cm can be reduced in weight to less than 280 g and in size to approximately 20 × 4 × 3 cm. With these reductions the marker beacon could easily be carried by a single 1-m^3 tetroon and would be acceptable to the FAA as a flight package. The batteries would give this package a transmitting life of approximately 72 hr--a reasonable fraction of the lifetime of a PEPE.

For use in investigating the transformation of pollutants in PEPE's, we envision a cluster of four to six tetroon-supported beacons being released at a point within the developing system. The release location would be selected with the anticipation that the trajectories followed by the tetroons would be within the PEPE for a period of several days. Since superpressure balloons do not always hold their planned altitude, wind shear can be expected to disperse the tetroons of the cluster during the several-day period. With successive positions of the tetroons at 12-hr intervals, reasonable estimation of the path of a parcel of air within the PEPE can be made and approximations of the dispersion within the PEPE can be obtained from the separation of the tetroons.

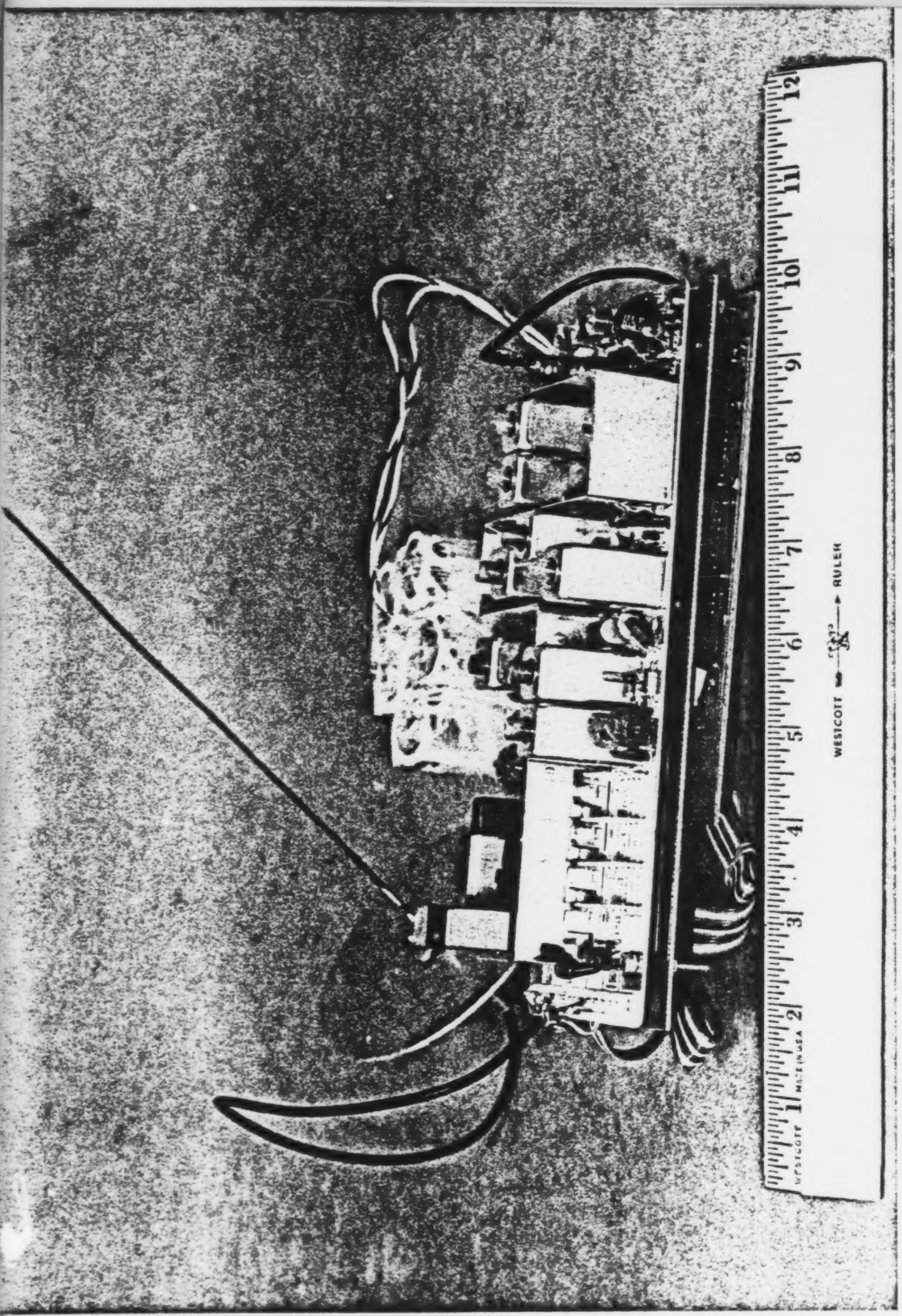

Figure 1. Random access measurement system beacon.

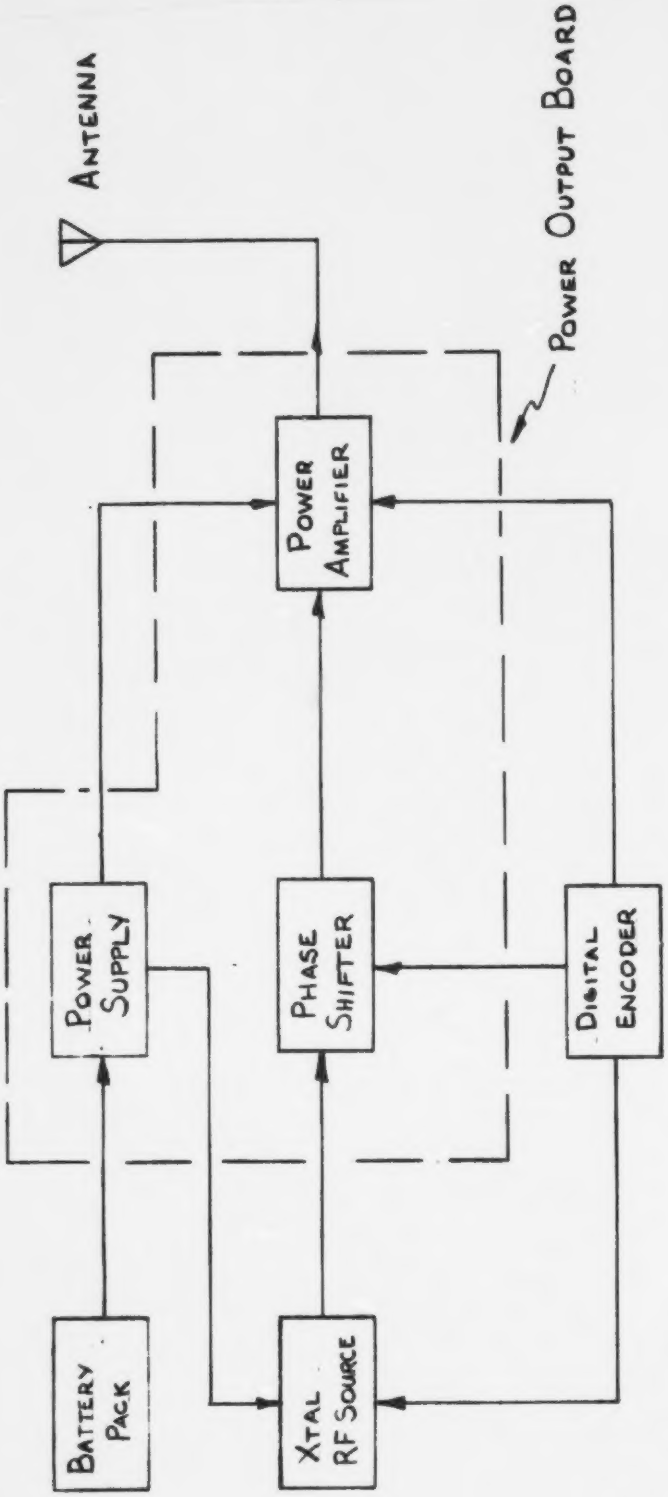

Figure 2. System block diagram.

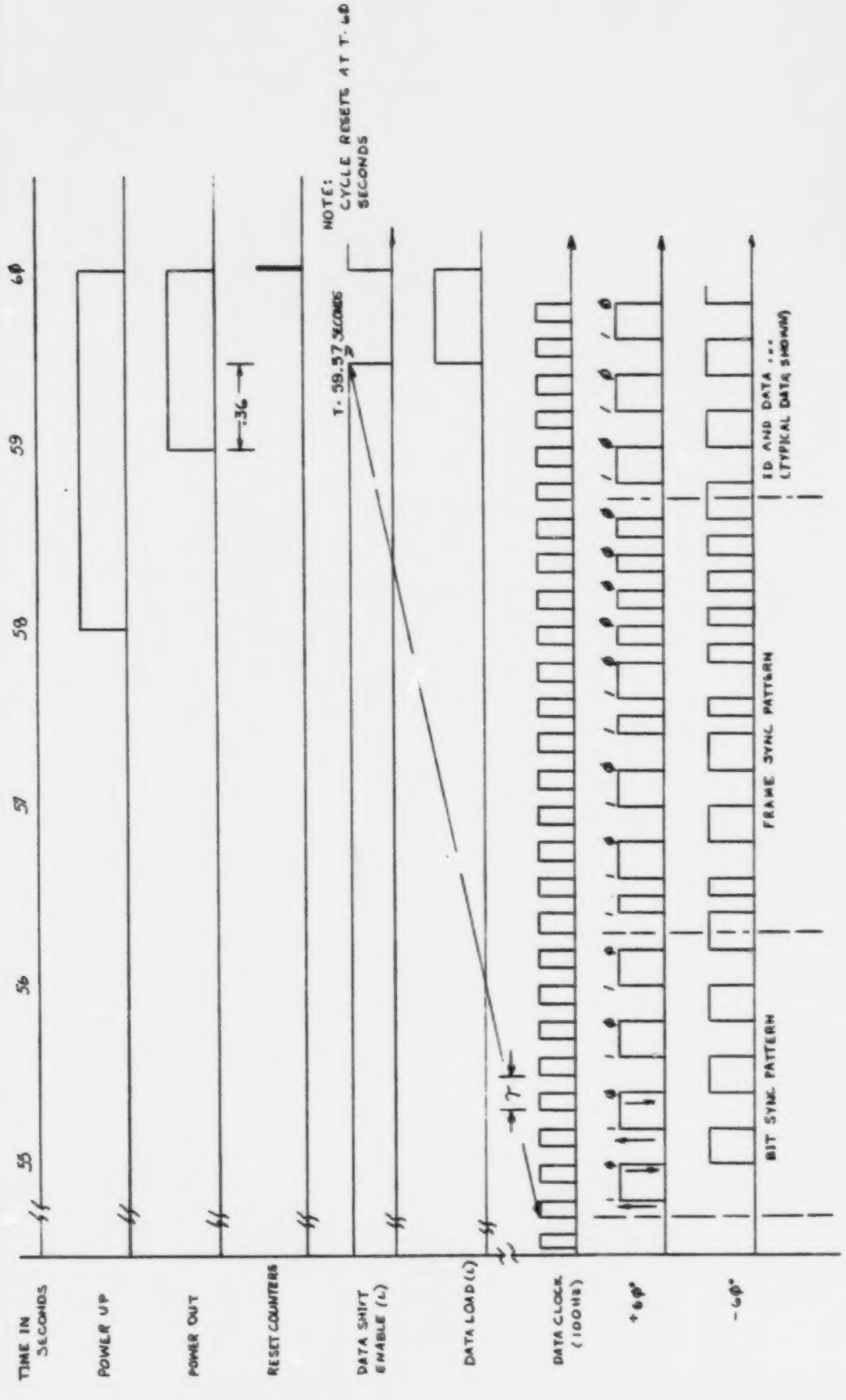

Figure 3. Timing diagram.

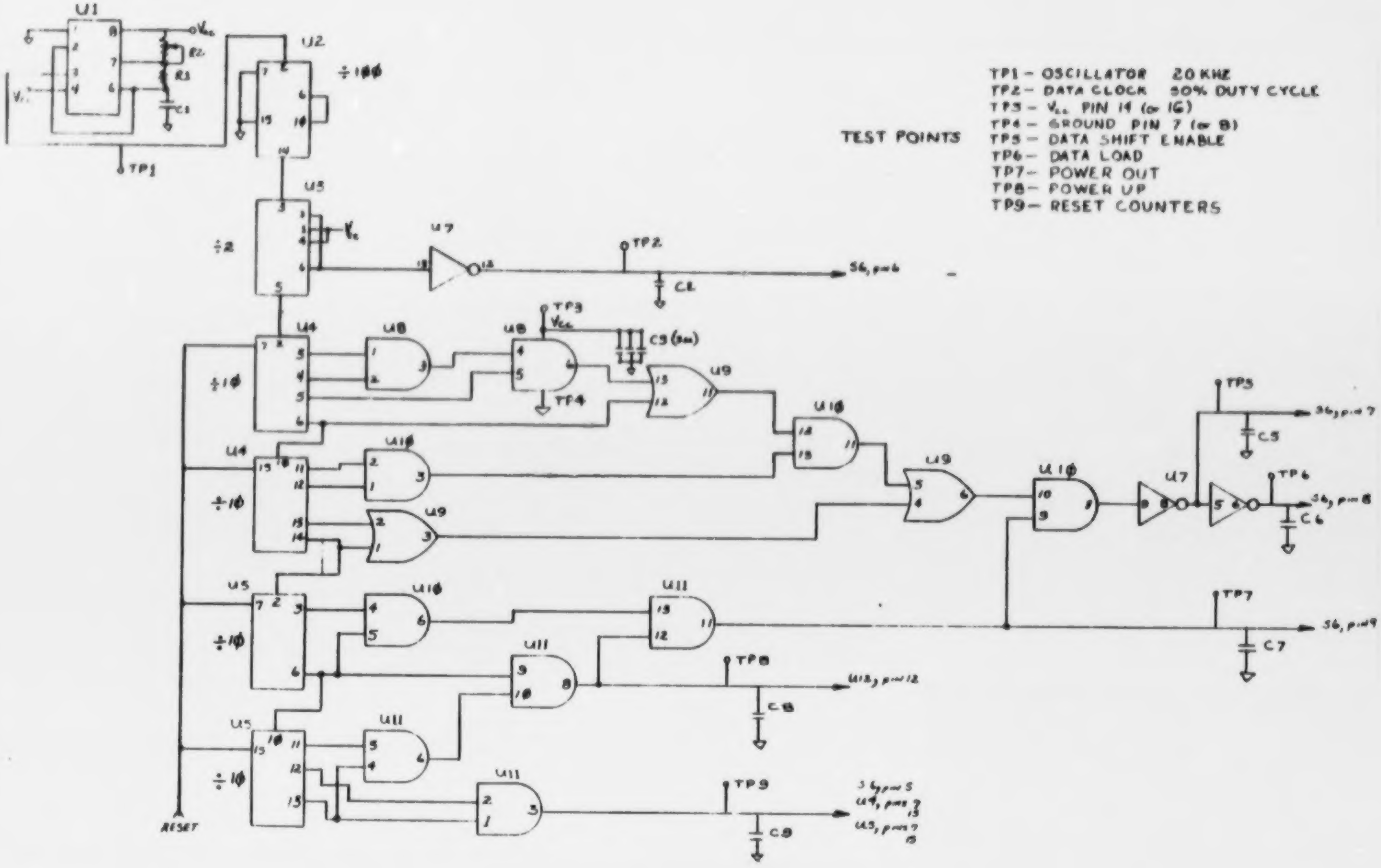

Figure 4. Timing generation circuitry.

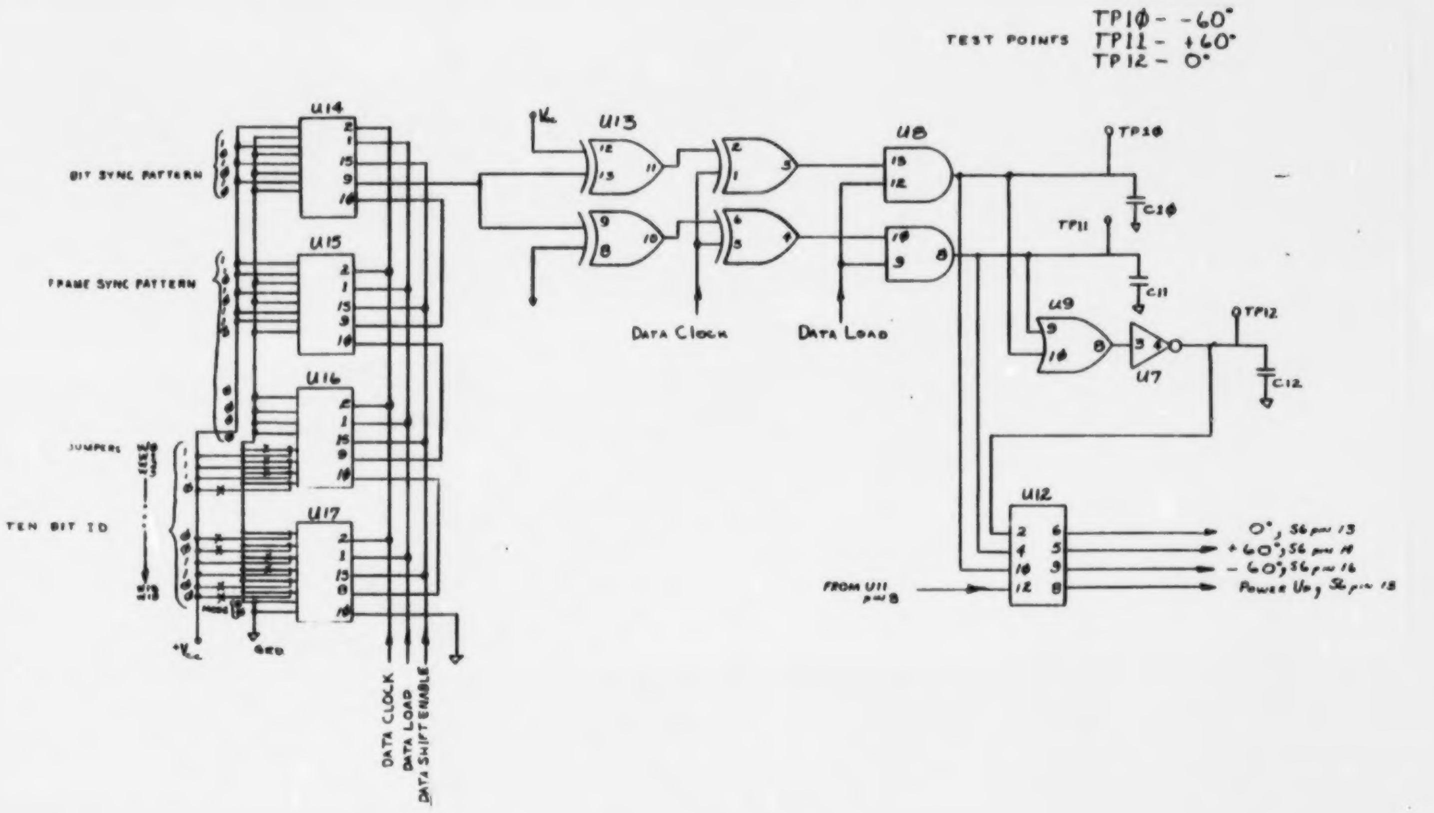

Figure 5. Data encoding circuitry.

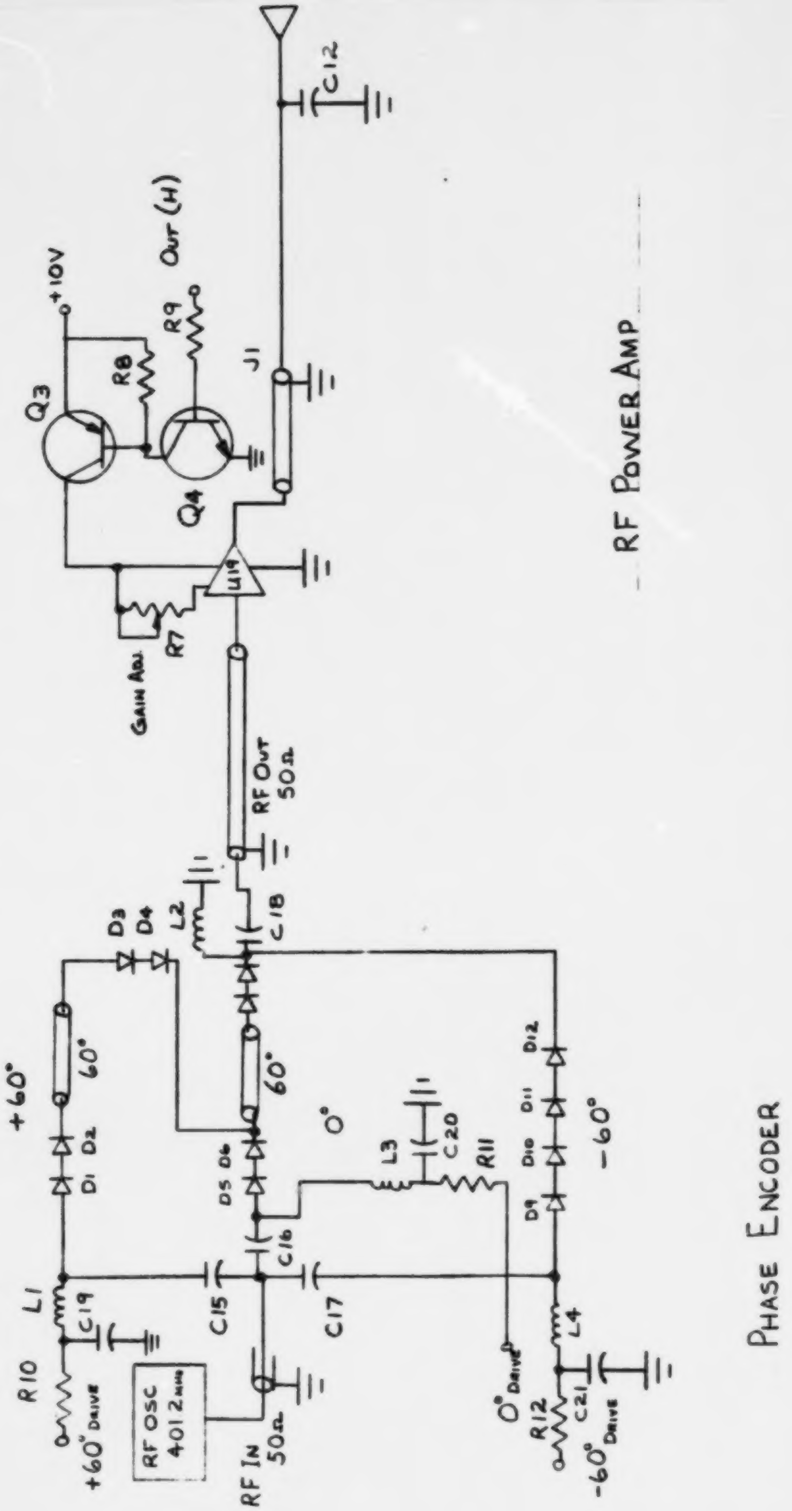

Figure 6. Phase encoder and rf power amplifier circuits.

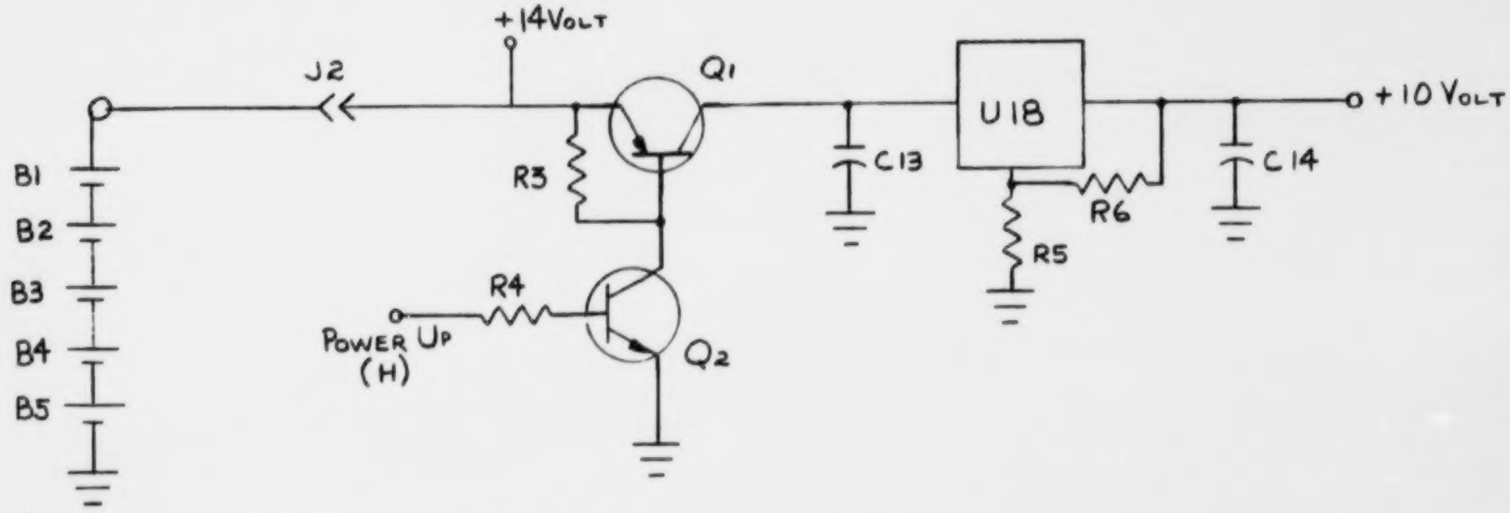

Figure 7. Regulated DC power supply.

RADAR TRACKING

C. Raymond Dickson

National Oceanic and Atmospheric Administration, Idaho Falls, Idaho

BRIEF HISTORY OF TETROON TRACKING

Tetroon tracking was designed to solve atmospheric transport problems. In the 1950's we were following tetroons with double theodolites to obtain trajectories. This supported the radioactive plume studies at the National Reactor Testing Station (now INERL) at Idaho Falls, ID. In the late 1950's we began doing diffusion studies that went out to many kilometers. A means of following a tetroon to determine the centerline of the plume had to be found. Because of the little success we had had with double theodolities, we tried to work with an AN/APS-3 radar taken from a Navy torpedo bomber. We first tried to skin track by putting x-band corner reflectors on the tetroon. This did not work very well because of the low power of this type of radar (this was a 1948 vintage radar).

We realized that it was necessary to develop an inexpensive radar transponder that could be followed to a range of 15 to 20 mi. In 1961 we obtained an M-33 radar, and with the help of Mr. Earl Pound we developed a system with the capability of automatically tracking transponders to a range of 60 mi. The M-33 radar had a 1° beam width with a range of 100,000 yards. The characteristics of this system were reported at a 1961 radar conference in Kansas City.

TYPES OF RADARS USED FOR TETROON TRACKING

We have used many types of radars. One, the SCR-584, has an x- and s-band and a 4° conical scan. We were able to track transponders with it, but its accuracy was not the best. Another type is the BSPS-1 Bendix Coast Guard, which has a 1.6° conical scan. We were able to follow both tetroons and ocean buoys with it. We tracked tetroons with the AN/MPS-19 s-band radar, which belonged to NASA and had a scan of 3°. Still another type is the

AMPQ-12 s-band with a 2.4° conical scan. We have also followed balloons without transponders from an FPS-16 at Wallops Island; and again with transponders on the WSR-57, a National Weather Service (NWS) radar. The NWS radars were not designed to track tetroons and do not give a very accurate height indication because of the large amount of scanning required to find the height from the signal. We used three different WSR-57 radars to follow transponders out to 200 mi. We were able to successfully track tetroons with the Plessey WF3 automatic tracking radar used on the Isle of Wight in the British Isles. Other types of radars we have used are the FAA 2-MW radars in the 1,340-mHz band, used in the Air Traffic Control Radar Beacon System, and the radar developed for the Air Force B-52 bombing runs, manufactured by Reeves.

Many types of radars are on the market. The versatility of tracking tetroons with and without transponders can be seen. The M-33 radar is the one we have used, developed, and modified. We now have five semimobile M-33's in operation. These have a narrow beam width and we can track the transponders automatically.

When using a transponder on a tetroon it is advantageous to put the radar as high as possible in order to follow the tetroon near the ground and below radar height. Using this method the only signal you will see is the electronic signal from the transponder. During skin tracking, the radar is put as low as possible so that it looks upward and ground clutter is minimized.

At present day prices the tetroon-transponder system, based on the study we completed in Tennessee in September 1978, costs approximately $125 per flight. In the past 20 years we have released nearly 2,000 tetroons, many with transponders. We have completed studies in many different parts of the country using radar to follow trajectories. These include studies in Cincinnati, Ohio, Columbus, Ohio, Wallops Island, Virginia, Salt Lake City, Utah, Atlantic City, New Jersey, New York City, the Isle of Wight in Great Britain, Oklahoma City, Oklahoma, Haswell, Colorado, Knoxville, Tennessee, Clarksville, Tennessee, four diffusion tests in Los Angeles, California; the Southwest Energy Study in Southern Utah; and many tests in Idaho Falls, Idaho.

Figure 1 shows the effect of the earth's curvature on the line-of-sight distance required for radar tracking. The earth's curvature determines the distance any tetroon at a given height can be tracked by ground-based radar. Tetroons at low altitude above ground (1,500-3,000 ft) can be tracked only short distances. For example, if a balloon is flown at 1,500 ft, the best range you can get is 52 statute miles because of the earth's curvature, provided there is no interference from terrain features. If the balloon is 3,000 ft in the air, it can be followed for 74 statute miles.

Another problem we have encountered in following tetroons and using them as tracers is the oscillation. The balloons follow a constant density surface rather than a constant height. Figures 2, 3, and 4 show the up and down movements of a balloon. In the morning with a class E or F stability condition (very stable), the balloon has very little oscillation--the height of constant density surfaces changes very little and the balloon remains at a constant height. As heating takes place, thermal mixing occurs and oscillations result. By midafternoon the oscillations may carry the tetroon through the complete mixing layer. Figures 5 and 6 show nighttime and early morning oscillation of tetroons in the west coast marine environment. If you compare these with smoke coming from a stack, you will see looping type plumes and coning type plumes. The motion of the balloons compares with that of the plumes and because the pollutants will follow the same kind of motion, the tetroons should be very good tracers.

Under stagnation conditions we have followed tetroons for as long as 72 hr. During the STATE Project we followed some for 16½ hr (out to 330 km). An interesting thing about transponders is that because they can each be tuned to a different frequency, several can be released simultaneously and each can be tracked separately.

Figure 7 is a computer listing of radar data. We plot the map and the trajectory and compute the statistics from the radar data. A printout from the system gives us an x, y, and z position and in varying terrain gives the altitude above ground. Range and bearing from the radar site are also given. We measure u, v, and w, rotate it, and get the along stream, cross stream, and w components, then run the correlations and auto-correlations of all of these components. This is a standard printout of the radar system.

Last year we began development of a portable radar to use on the STATE Project. Although it wasn't completed, we took it to Tennessee and it worked satisfactorily. It is 12 ft long and has computer-controlled automatic levelers and a self-erecting system for the antenna structure. The antenna structure can be removed in a few minutes and stored while the radar is being moved. The radar is equipped with its own power source, air conditioning, heating, and a complete communications system for communicating with the control base. There are some problems with a mobile system when you are using more than one radar and leap-frogging for many miles; locations must be picked out in advance, and permission obtained from landowners to set up radars on their property.

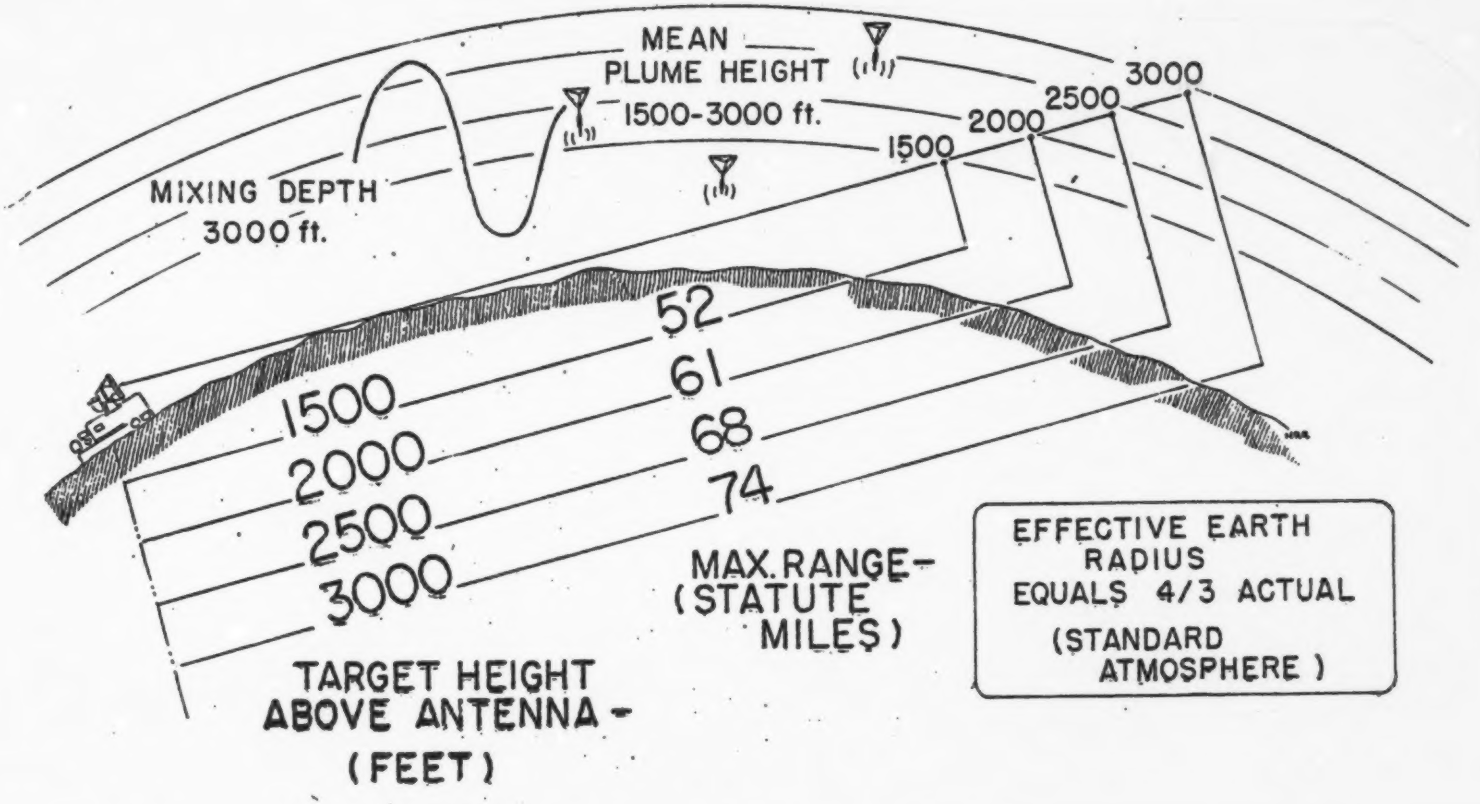

Figure 1. Earth curvature limitation to radar range.

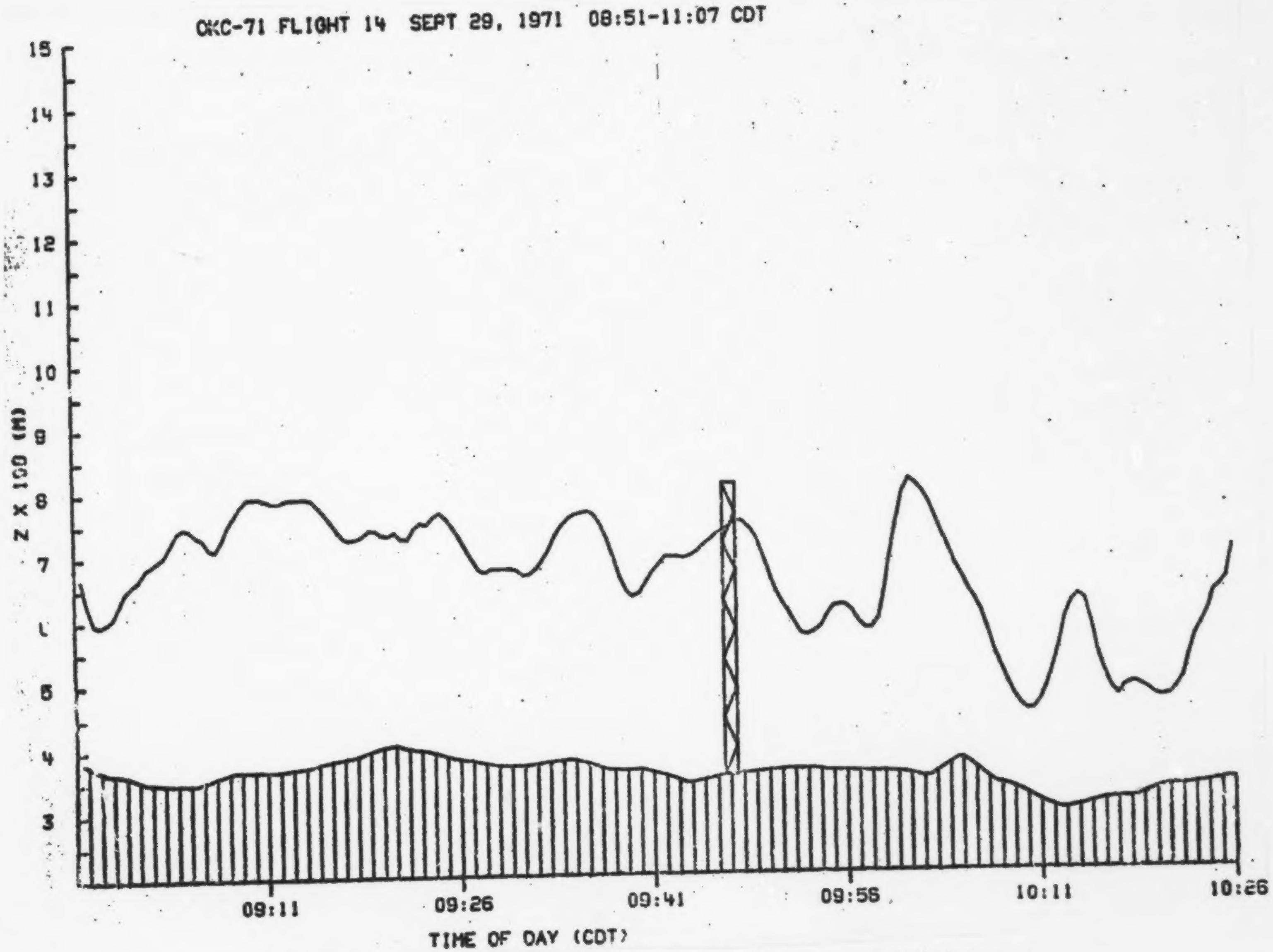

Figure 2. Altitude oscillations of a tetroon in a stable (early morning) air mass.

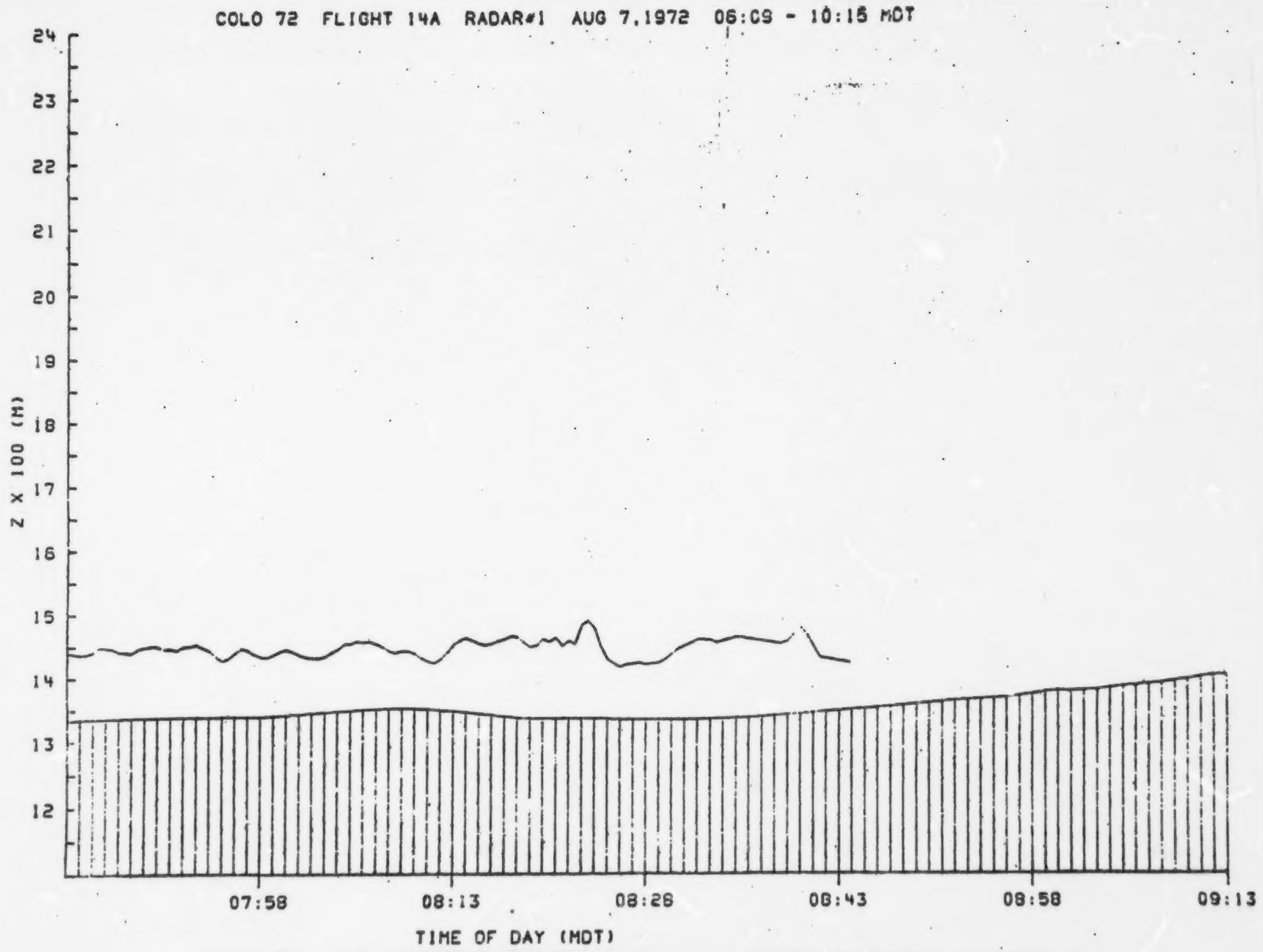

Figure 3. Altitude oscillations of a tetroon as convection begins.

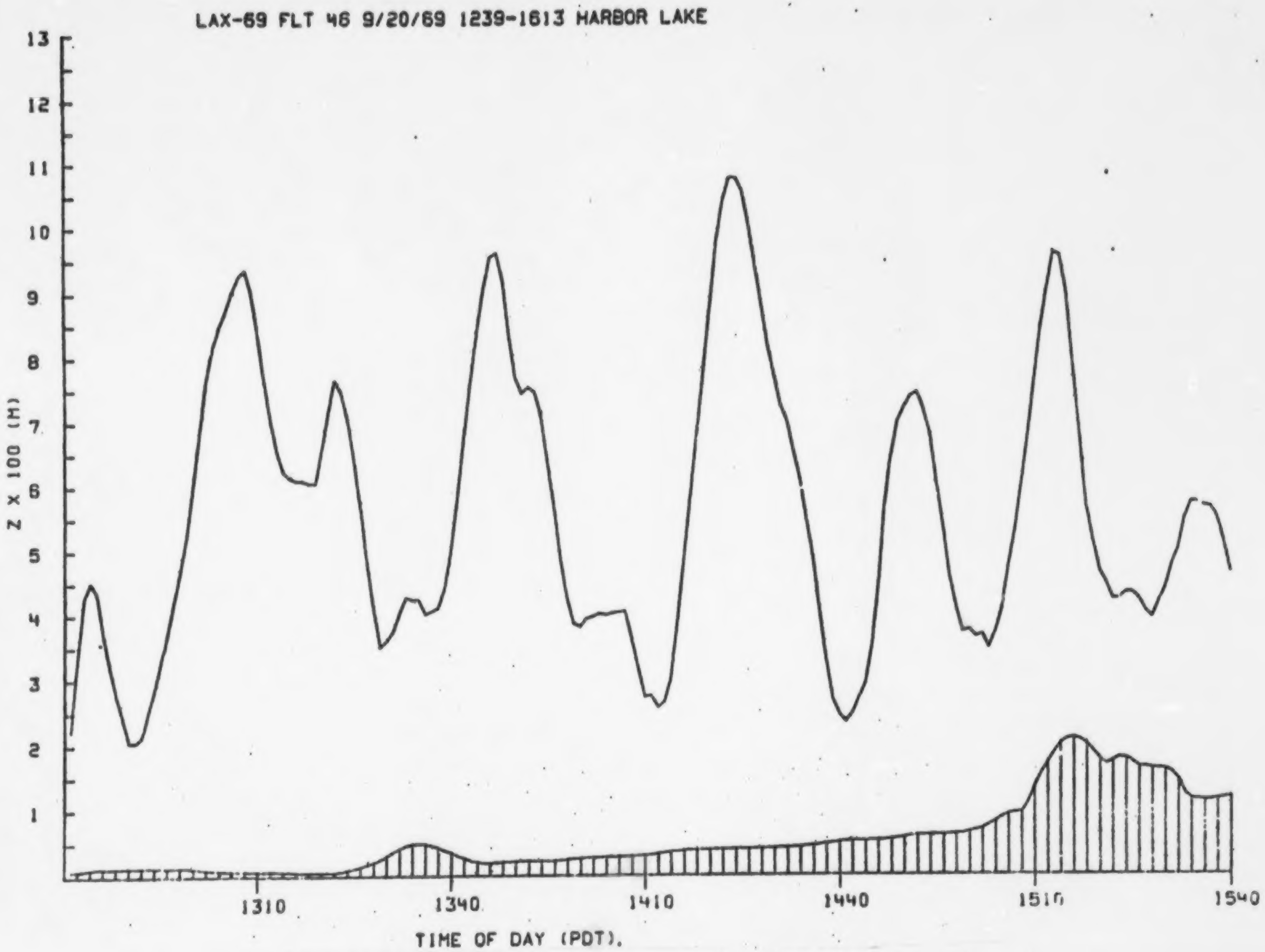

Figure 4. Altitude oscillations of a tetroon during well-developed convection.

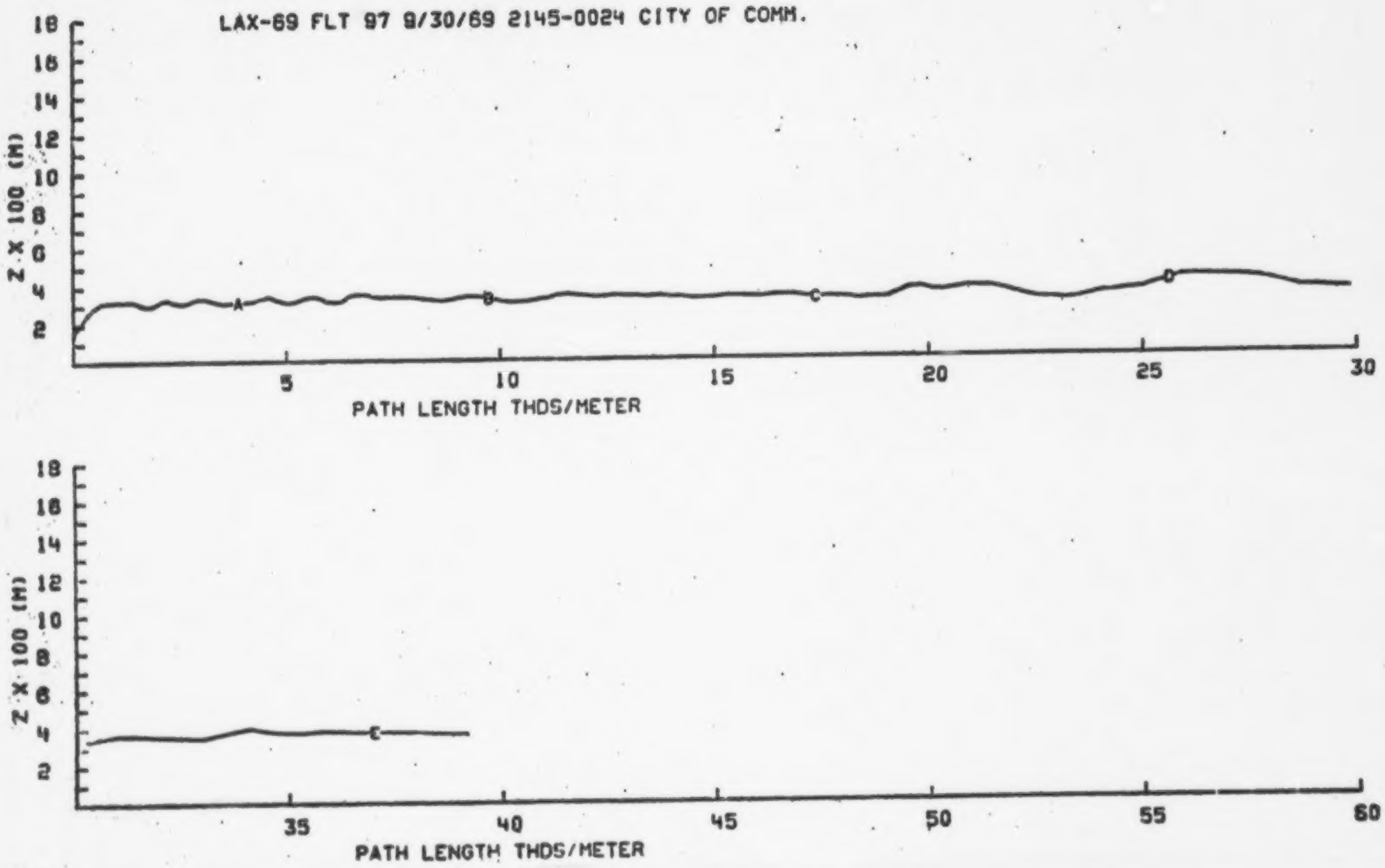

Figure 5. A tetroon flight in a nighttime west coast maritime air mass showing a minimum of altitude change.

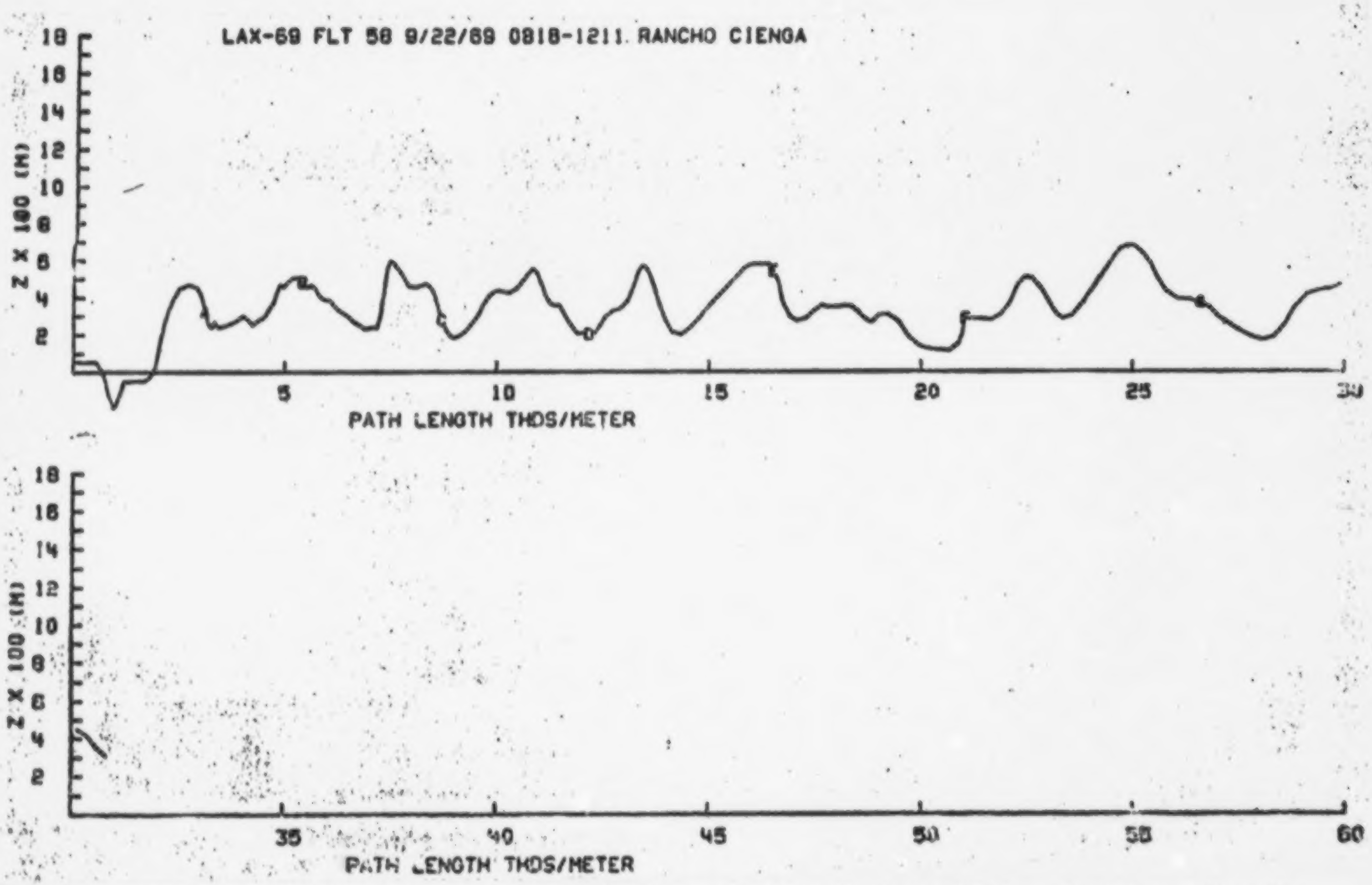

Figure 6. A tetroon flight in a west coast air mass during the morning hours. Vertical oscillations extend through the entire layer below the maritime invasion.

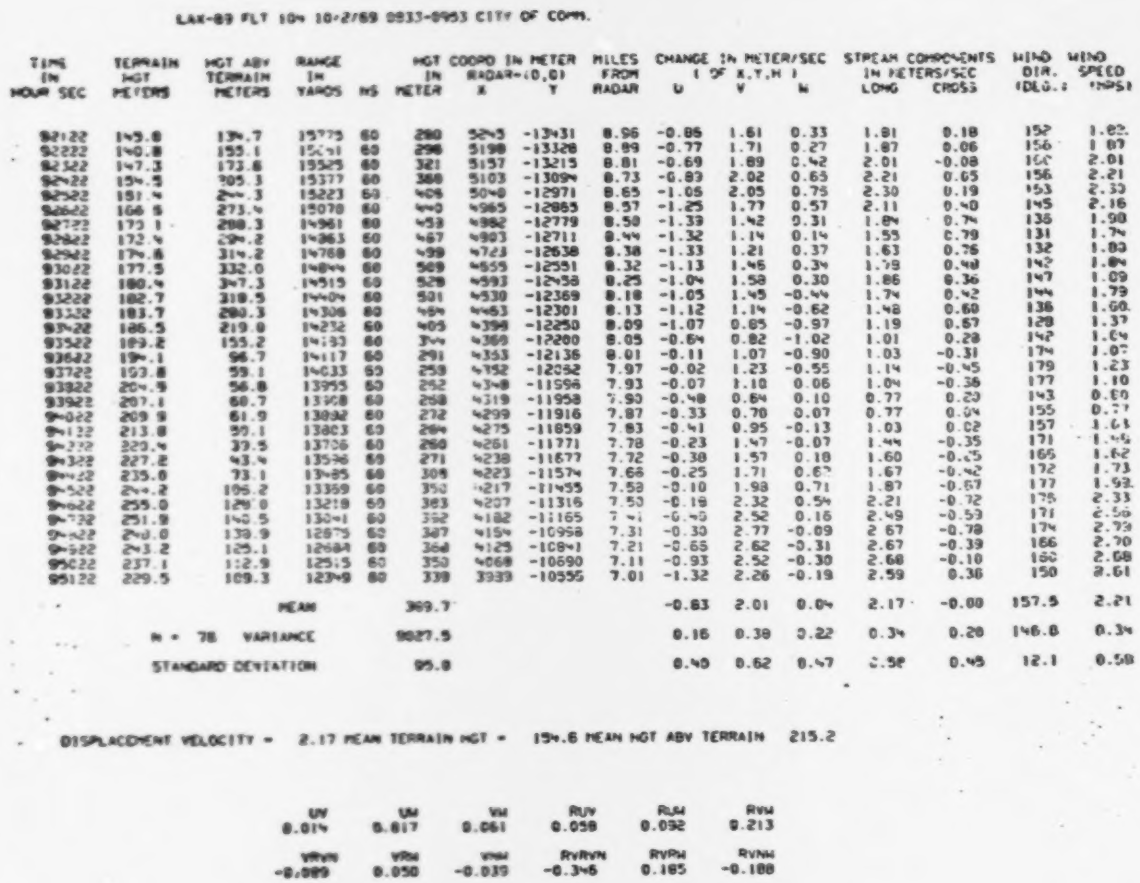

```
                LAX-69 FLT 104 10/2/69 0933-0953 CITY OF COMM.

  TIME     TERRAIN    HGT ABV    RANGE        HGT COORD IN METER  MILES  CHANGE IN METER/SEC   STREAM COMPONENTS  WIND   WIND
   IN        HGT      TERRAIN     IN           IN   RADAR=(0,0)    FROM    ( OF X,Y,H )         IN METERS/SEC     DIR.  SPEED
 HOUR SEC   METERS     METERS    YARDS  NS  METER    X       Y     RADAR    U      V      W      LONG   CROSS    (DEG.)  (MPS)

  92122     145.8      134.7     15775  60   280   5245  -13431   8.96  -0.85   1.61   0.33    1.81    0.18     152    1.82
  92222     140.8      155.1     15641  60   296   5198  -13328   8.89  -0.77   1.71   0.27    1.87    0.06     156    1.87
  92322     147.3      173.6     15525  60   321   5157  -13215   8.81  -0.69   1.89   0.42    2.01   -0.08     160    2.01
  92422     154.5      205.3     15377  60   360   5103  -13094   8.73  -0.83   2.02   0.65    2.21    0.65     156    2.21
  92522     151.4      254.3     15223  60   406   5040  -12971   8.65  -1.05   2.05   0.75    2.30    0.19     153    2.33
  92622     166.5      273.4     15070  60   440   4965  -12865   8.57  -1.25   1.77   0.57    2.11    0.40     145    2.16
  92722     173.1      280.3     14961  60   453   4882  -12779   8.50  -1.33   1.42   0.31    1.84    0.74     136    1.90
  92822     172.4      294.2     14863  60   467   4803  -12711   8.44  -1.32   1.14   0.14    1.55    0.79     131    1.74
  92922     174.6      314.2     14768  60   489   4723  -12638   8.38  -1.33   1.21   0.37    1.63    0.76     132    1.83
  93022     177.5      332.0     14644  60   509   4655  -12551   8.32  -1.13   1.46   0.34    1.79    0.40     142    1.84
  93122     180.4      347.3     14515  60   528   4593  -12458   8.25  -1.04   1.58   0.30    1.86    0.36     147    1.89
  93222     182.7      318.5     14404  60   501   4530  -12369   8.18  -1.05   1.45  -0.44    1.74    0.42     144    1.79
  93322     183.7      280.3     14306  60   464   4463  -12301   8.13  -1.12   1.14  -0.62    1.48    0.60     136    1.60
  93422     186.5      219.0     14232  60   405   4398  -12250   8.09  -1.07   0.85  -0.97    1.19    0.67     128    1.37
  93522     189.2      155.2     14193  60   344   4369  -12200   8.05  -0.64   0.82  -1.02    1.01    0.28     142    1.04
  93622     194.1       96.7     14117  60   291   4353  -12136   8.01  -0.11   1.07  -0.90    1.03   -0.31     174    1.07
  93722     199.8       59.1     14033  60   259   4352  -12052   7.97  -0.02   1.23  -0.55    1.14   -0.45     179    1.23
  93822     204.9       56.8     13955  60   262   4348  -11996   7.93  -0.07   1.10   0.06    1.04   -0.36     177    1.10
  93922     207.1       60.7     13908  60   268   4319  -11958   7.90  -0.48   0.64   0.10    0.77    0.20     143    0.80
  94022     209.9       61.9     13892  60   272   4299  -11916   7.87  -0.33   0.70   0.07    0.77    0.04     155    0.77
  94122     213.8       50.1     13803  60   264   4275  -11859   7.83  -0.41   0.95  -0.13    1.03    0.02     157    1.03
  94222     220.4       39.5     13706  60   260   4261  -11771   7.78  -0.23   1.47  -0.07    1.44   -0.35     171    1.46
  94322     227.2       43.4     13596  60   271   4238  -11677   7.72  -0.38   1.57   0.18    1.60   -0.25     166    1.62
  94422     235.0       73.1     13485  60   308   4223  -11574   7.66  -0.25   1.71   0.62    1.67   -0.42     172    1.73
  94522     244.2      106.2     13359  60   350   4217  -11455   7.58  -0.10   1.98   0.71    1.87   -0.67     177    1.93
  94622     255.0      128.0     13219  60   383   4207  -11316   7.50  -0.19   2.32   0.54    2.21   -0.72     175    2.33
  94722     251.9      140.5     13041  60   392   4182  -11165   7.41  -0.45   2.52   0.16    2.49   -0.53     171    2.56
  94822     248.0      138.9     12875  60   387   4154  -10958   7.31  -0.30   2.77  -0.09    2.67   -0.78     174    2.73
  94922     243.2      125.1     12684  60   368   4125  -10841   7.21  -0.65   2.62  -0.31    2.67   -0.39     166    2.70
  95022     237.1      112.9     12515  60   350   4068  -10690   7.11  -0.93   2.52  -0.30    2.68   -0.10     160    2.68
  95122     229.5      109.3     12349  60   339   3939  -10555   7.01  -1.32   2.26  -0.19    2.59    0.38     150    2.61

                           MEAN          369.7                       -0.83   2.01   0.04    2.17   -0.00   157.5    2.21

               N =  78   VARIANCE       9027.5                        0.16   0.38   0.22    0.34    0.20   146.8    0.34

               STANDARD DEVIATION         95.0                        0.40   0.62   0.47    0.58    0.45    12.1    0.58


   DISPLACEMENT VELOCITY =   2.17 MEAN TERRAIN HGT =   194.6 MEAN HGT ABV TERRAIN   215.2


                       UV        UW        VW        RUV       RUW       RVW
                    0.014     0.017     0.061     0.058     0.092     0.213

                     VRVN       VRW       VNW     RVRVN      RVRW      RVNW
                   -0.089     0.050    -0.039    -0.346     0.185    -0.108
```

Figure 7. Computer printout of radar data.

LIGHT-WEIGHT, LOW-COST RADAR, TRANSPONDER SYSTEMS

Earl F. Pound

Utah State University, Logan, Utah

I have worked on transponder systems for weather applications since June of 1960. Most of this work has been for Ray Dickson's group at the Idaho Engineering Laboratory, Idaho Falls, Idaho. All of this work has been on one type of system using a relatively high-power pulsed radar transmitter at X or S bands to beam a signal to the transponder with a reply at 403 MHz. This category of transponder leaves the complexity on the ground, allowing for a light-weight, long-battery-life, low-cost transponder. The relatively high pulse power of the transmitter (50 kW to 2 MW) allows for a simple crystal video receiver in the transponder. The high frequency (X or S band) and the highly directional antenna used to transmit the radar signal, along with control of the transmitter power, allow for angular tracking of the transponder. The slant range is determined by the round-trip delay of the reply.

The transponder receiver consists of an X or S band antenna, a d.c.-biased microwave detector, and a high-gain video amplifier. This portion of the transponder must operate continuously, always ready to receive a signal, which produces most of the battery drain. The use of high-gain bandwidth transistors in this amplifier allows for relatively low battery drain. The rest of the transponder system works in a pulsed mode, drawing power for 1/1000 or less of the time that the transponder is being interrogated; hence, it contributes only modestly to the battery drain while providing a 1-W pulsed reply signal. This pulsed part of the transponder consists of a blocking oscillator to establish a fixed reply pulse width, a pulsed power amplifier, and a self-excited pulsed transmitter. The system operates about 96 hr at room temperature on two 9-V transistor radio batteries, with a total weight of 150 g. Alkaline or mercury type batteries would almost double this time with only a slight increase in total weight. Lithium type batteries would give at least 3 weeks of life even at reduced temperatures. I have made a low drain model for the Wildlife Service that has a battery life of 4 to 5 months and no increase in size or weight.

A conical scan-type radar is used with this transponder for automatic tracking; that is, the transmitted beam from the radar nutates in a small circle around the average direction of the antenna. The amplitude of the target reply compared to the nutating of the antenna gives the error signal for automatic tracking. The amplitude of the transponder reply is constant; hence, at first glance a person would say that this type of automatic tracking would not work. If the transmitted power is controlled either manually or automatically so that the transponder interrogation is turned off and on by the nutating of the antenna, the average effect would be the same as for a passive target and an automatic track would be achieved. If the transmitted power from the radar is higher than needed, an automatic track would still be achieved but the apparent direction of the transponder would be found somewhere on a circle around the true track. This power control is not overly critical for practical applications.

A reflective target gives an error signal for automatic tracking that is proportional to the misalignment of the radar antenna and the target; that is, it is a linear servo system. The transponder, as a target, gives an on-off error signal and thus causes the automatic tracking servo to become nonlinear. Because the transponder is operating close to maximum sensitivity when it is turning on and off, the signal level is close to the background noise level. The noise added to the signal causes a somewhat random triggering of the transponder reply, thereby restoring some of the lost linearity by the proportion of pulses missed.

The transponder will also work with a PPI type radar display with the target appearing as a line on the screen. The true angular position of target is the center of this line.

The transponder will not work with a mono-pulse type radar unless it is made especially for the transponder. A mono-pulse system derives its error signal for automatic tracking from the received signal. The transponder described here replies at 403 MHz; hence, it requires an additional antenna and a receiver to replace the original receiver. This addition would defeat the original tracking system rendering it useless. Personnel at White Sands

Missile Range have modified a Nike Ajax Radar System to receive in a monopulse mode at 1,680 MHz. This system works with a cross band transponder, with X band for the up leg and L band for the down leg. The main reason for cross band operation is that no light-weight, cost-effective X or S band transmitters are available at present.

Another well-known transponder is that used by radiosondes with the GMD 2 or GMD 4 system. This uses a doppler tone ranging system at approximately 82 kHz and, in addition, the GMD 4 has pulsed course ranging in the event the track is not continuous. This transponder system has some advantages and disadvantages compared to the pulsed system. The main advantage of the GMD system is the lower initial cost, which is partially offset by the availability of surplus radars such as the M33. The main disadvantage of the GMD system is that the transponder transmitter must operate continuously. This means that even the best low-drain all-solid-state GMD transponder would take about 100 times as much battery power as the pulsed type.

Consideration has been given to using the existing FAA radar network with transponders attached to tetroons for weather applications. This is probably not cost-effective because of major limitations of the FAA system for this application.

The FAA transponder radar transmits on a frequency of 1,030 MHz with a peak pulse power of from 25 to 3,000 W depending upon the desired range of the station. Even at 3,000 W, which would involve very few stations, this is about 1/100 of the peak radiated power of the M33 radar. A simple crystal video receiver is therefore impractical for the FAA system. A superregenerative receiver (the type used in the GMD transponder) is also impractical because the quenching frequency could not be made high enough to accurately recover the short pulses transmitted by the FAA radar. The only practical transponder receiver would be of the super-heterodyne type, which would be at least an order of magnitude more complex than the crystal-video type.

The FAA transponder system receives on a frequency of 1,090 MHz. The associated transmit-receive switches and low relative performance of the receiver, coupled with the automatic sensitivity time control, require a relatively powerful transponder reply transmitter. The minimum power used for aircraft transponders is 100 W peak power. The balloon-borne transponder must reply with at least 10 W peak to give even marginal performance with this system. This reply is at 1,090 MHz, where a self-excited oscillator is not practical; hence, a transmitter with two stages or more would be required. This means that the transmitter must be about an order of magnitude more complicated than for the 403 MHz transmitter described earlier.

The use of a reflector could be cost-effective when used with the FAA or other radar systems using a PPI type display. The skin track portion of the FAA system transmits a peak pulse power of 2 MW on a frequency of about 1,340 MHz. A corner reflector built into or hung below a tetroon would have good range with this skin track system. The identification problem could be solved by mounting an array of diodes on the corner reflector so that passing a current through the diodes would change the reflectance. This would cause the radar display to scintillate, the code giving identification, temperature, barometric pressure, etc.

Other sensors such as temperature, barometric pressure, humidity, etc., although practical, have not been added to the transponder. Each would require more battery power and add weight and cost to the transponder. The low production levels for transponders has not allowed these additional sensors to be cost-effective compared to conventional radiosondes. The most practical sensor reply technique would be to add additional pulses to the radar reply pulse using pulse separation to return the sensor signal, or to turn off the radar transmitter and allow the transponder to free run at a lower frequency multiplexed to give sensor signals.

MINIATURIZED LASER DOPPLER VELOCIMETER*

David H. Dickson

U.S. Army Atmospheric Sciences Laboratory,
White Sands Missile Range, New Mexico

Abstract

This laser doppler velocimeter (LDV) was designed for a unique application. The operational concept is a Helicopter Remote Wind Sensor (HRWS) to augment a fire control system for attack helicopters. The HRWS will measure wind speed and direction in the aircraft turbulent environment and average winds for several hundred meters.

The HRWS was fabricated for the Atmospheric Sciences Laboratory by Raytheon Company. This system has been successfully operated on a UH-1 aircraft and a comparative ground test. This paper will describe the system, data results, and potential applications.

SYSTEM DESCRIPTION

A CO_2 laser heterodyne system has been constructed and mounted in a pod compatible with an AH-1 or UH-1 helicopter or fixed wing aircraft equipped with standard wing shackles. A block diagram of the system is shown in Figure 1. It can be subdivided into three subsystems: the transmitter, the scanners, and the processor. The transmitter consists of a CO_2 laser and appropriate beam-combining optics for heterodyne operation. Two scanners are employed; one scans in range and the other produces a conical scan. The beam pattern is shown conceptually in Figure 2. The processor includes the detector and its associated biasing network, a frequency tracker and counter.

A 5-W laser transmits a CW beam into an interferometer, which propagates most of the energy into a telescope and the rest to the detector for use as a local oscillator. The telescope expands the beam to 66 mm and provides the ability to change the location of the focus by translating the telescope secondary. A rotating wedge is placed at the telescope output to generate the conical scan. A complete rotation of the cone takes place approximately every 50 ms, while the location of the focus varies from 1 m to 33 m every second.

---

*This paper was prepared for, but not presented, at the Seminar/Workshop.

Energy scattered from naturally occurring atmospheric aerosols is collected by the same telescope, passed through the interferometer onto a mercury cadmium telluride detector. The detector output is processed by a frequency tracker and digital counter producing data proportional to the signal frequency in both analogue and digital format. A new piece of datum is available every 2.8°, approximately every 400 μs. Output data consist of range, angle, and frequency information. For the flight tests, these data were recorded, although for future applications, a microprocessor will be integrated into the system.

DOPPLER THEORY

Operation of a laser doppler velocimeter may be understood with the aid of Figure 3. A laser beam is transmitted through an interferometer that passes most of the energy to the target and diverts a small amount to the detector. The transmitted beam is passed through a telescope to the target, which, in the present case, consists of aerosols naturally suspended in the atmosphere. Some of the transmitted energy is backscattered by the target particles and enters the detector by the path shown. This returning energy has been shifted in frequency by an amount proportional to the component of particle velocity parallel to the direction of propagation V_{11}, according to the Doppler principle. Figure 4 shows the geometry of the laser system and target velocity vector relationship. Only V_{11} contributes to the Doppler shift.

There are two beams falling on the detector at two different frequencies as shown in Figure 5: a reference beam at the optical frequency f_o with a power of a few milliwatts and the smaller power signal beam at the new frequency $f_o + f_d$ where f_d is the Doppler shift frequency. When these beams are superimposed, the combination contains energy at the difference of these frequencies. The difference is the Doppler frequency and is related to the target velocity.

CONICAL SCANNING

A laser Doppler system measures a single velocity component during any measurement interval. The conical scanning technique, developed for microwave radars for measuring the velocity components of a laminar atmosphere,[1] was selected for this application. Data are taken at several points around the periphery of the cone. As can be seen in Figure 6, the angle between the propagation direction and the velocity vector changes as the beam sweeps around the cone. Therefore, a different velocity component is measured at each point, and the velocity vector can be obtained.

If the cone axis is in the z-direction, it can be easily shown that

$$f_d = \frac{-2}{\lambda} \left(V_z \cos \frac{\delta}{2} + V_x \sin \frac{\delta}{2} \cos \omega t + V_y \sin \frac{\delta}{2} \sin wt \right)$$

where:

V_x, V_y, V_z = velocity components

$\frac{\delta}{2}$ = half-angle

ω = conical scan frequency.

Thus, the frequency consists of a DC term and a sinusoidal component. The DC represents the velocity component parallel to the cone axis, while the magnitude and phase of the time varying part permit the calculation of the other two components. Deviation from laminar flow will yield a more complex time variation, but three-dimensional data can be obtained as long as the data approximate a single frequency sinusoidal function.

COMPONENT DESCRIPTION

Calculations indicated that a 5-W laser would provide sufficient power to reliably measure helicopter flow fields, so a previously developed Raytheon Company 5-W air-cooled laser with low weight and size and an extremely high degree of ruggedness and reliability was selected. The features of this laser include an all metal/ceramic laser tube and a stable lightweight laser frame.

The heterodyne optics consist of a combination of beam splitters and polarizing elements that generate the local oscillator and the transmitter beams, and recombine the collected signal with the local oscillator. Measurements of the detector indicate that local oscillator beams of approximately 1 to 2 mW provide the maximum signal-to-noise ratio. The reflectivity of the beam splitters was selected to generate a local oscillator beam of this value; the remainder of the energy is transmitted into a beam expander. Afer collection of the scattered energy by the beam expander, the heterodyne optics combine the local oscillator with the signal and direct this superposition toward the detector.

The beam expander produces an output beam diameter of 66 mm. It is capable of focusing the beam at ranges varying from 1 m to 33 m. Backscatter energy from the telescope elements had to be controlled to avoid difficulties with the detector. The design from these specifications resulted in a Galilean telescope with an input negative singlet lens and an output doublet.

Range scanning is accomplished by translating the input lens of the beam expander. If the input lens were scanned linearly with time, too much time would be spent at closer ranges. Therefore, a nonlinear drive function is electronically generated, which gives an output scan in which range varies approximately linearly with time.

The conical scan is generated by rotating a wedge about the optical axis. The wedge is driven by a motor, whose speed is variable from 0 to 2,300 rpm. The motor speed is adjusted by a potentiometer, and can be displayed on the control panel. As the motor speed decreases below a few hundred revolutions per minute, the laser beam is automatically blocked for safety reasons, preventing propagation into the atmosphere. In addition to measurements of the motor speed, signals are available every 2.8° of rotation to indicate the angular beam position.

The receiver consists of a 10.6-μm detector and the associated bias circuit and amplifiers. The requirements of high quantum efficiency and good frequency response dictated the use of a mercury-cadmium-telluride (HgCdTe) detector. The detector is mounted in a Dewar flask, which holds liquid nitrogen for a period of at least 6 hr. The electronic circuitry of the receiver was designed to minimize loss of signal-to-noise ratio. The function of the bias circuit is to provide a voltage supply to the detector and to provide the proper matching between the receiver preamplifier and the detector. A prime requirement in designing this circuit is to protect the detector from excess voltages or currents that can result from removal of the local oscillator, too high a local oscillator power, or loss of coolant in the detector Dewar.

The frequency tracker is shown in Figure 7. The input band is translated up to a center frequency of f_o by mixing the input with the output of a voltage-controlled oscillator (VCO). The signal is then limited and fed through a frequency discriminator centered near f_o. In tracking operations the discriminator drives an integrator, the output of which drives the VCO. With the tracking loop closed, the sum of the input and VCO frequencies is constant. The input signal is periodically replaced by the output of a crystal oscillator. The readout circuit makes use of measurements made during this calibration interval to automatically correct for drift in the discriminator and integrator.

The frequency counter counts the positive zero crossings of the VCO during a 160-μs period once each angle clock pulse. The sample gate generator provides this accurately timed counter gate, along with a pulse immediately after it, to clock the output storage register.

The sensor is operated from a control panel, as shown in Figure 18, located in the helicopter. All operations on the system are performed from the control panel except filling the detector with liquid nitrogen, which was done during aircraft preflight. The control panel also has a number of diagnostic capabilities that may be used by maintenance personnel.

DATA ANALYSIS

It should be noted that HRWS was designed to measure to a range of approximately 100 ft from the sensor origin (cone Apex). Further, the sensor is a descendant of other conical scanning devices whose domains of measure were considerably less turbulent and less subject to linear shear than that in a helicopter's vicinity. Wind tunnel and other measurement studies demonstrate the complexity of the helicopter flow-field.[2]

For this experimental system, it was cost-effective to locate the entire sensor in a pod compatible with both rotary and fixed-wing aircraft as well as ground-based installations. A pod using the hard points of the AH-1 rocket pod was accordingly built. A picture of the system enclosed within the pod with the pod attached to a UH-1 helicopter is shown in Figures 9, 10, and 11.

Two simplified approaches have been applied in the data analysis: (1) circular scan methods, and (2) point-pair methods. Considering the latter, which is the simplest, any pair of points separated by a sufficient angle can be used to deduce the wind components transverse to, as well as parallel to, the axis halfway between them.

The point-pair method has been applied to derive downwash profiles as running functions of range over a short sequence of range scans.

RESULTS

Measurements were made in hover and at forward flight velocities at altitudes from 1 m to 500 m. Data were successfully obtained throughout all flights and are currently being processed.

A typical data presentation is shown in Figure 12. The helicopter is hovering with its skids 1 m above the terrain. At a range of 7 m, the radial velocity component is shown as the beam is scanned around a cone. A function, approximately sinusoidal, is observed peaking at 180°. The peak velocity is approximately 18 m/s and the mean approximately 6 m/s. Since a 17° cone half-angle is used, this corresponds to a velocity component parallel to the aircraft axis of 6.3 m/s, a vertical component of 23 m/s, and a zero cross component.

Comparison of wind tunnel and flight results are shown in Figures 13, 14, and 15. Figure 13 is a downwash profile taken in a wind tunnel using a scale AH-1 aircraft.[2]

Figures 14 and 15 are the measured downwash profiles from a hovering UH-1H aircraft at 100 ft above ground level and 20 ft above ground level. The 100-ft hover case is clearly out of ground effect and aircraft physical differences account for the slight profile variation. However, the 20-ft hover is in ground effect, which accounts for the magnitude of differences. The general curve slope remains basically the same for all three cases.

COMPARATIVE GROUND TEST

The HRWS was compared with ground-based wind instruments at Biggs Optical Range (BOR). The comparison consisted of aligning the HRWS with an annometer array as shown in Figure 16. A series of measurements were made under several wind and turbulence levels and reduced to 1-min averages.

Typical data are shown in Figures 17, 18, and 19. Figures 17 and 18 are time history plots of average HRWS measurements to a 500-m range compared with averaged annometer data and Laser Crosswind Sensor (LCS) data, respectively. Figure 19 compares a single annometer at a 24-m range with the HRWS focused at the equivalent range. Summarizing tabular data are shown in Figure 20.

The agreement in the cases shown is quite good. Variations are readily attributed to dissimilar instrumentation.

CONCLUSION

A CO_2 laser doppler velocimeter has been successfully miniaturized, flown aboard a helicopter, and compared with other ground-based systems. Data appear to be consistent with wind tunnel measurements and compares very well with ground-based instruments.

A future system will be coupled to a microprocessor to obtain real-time three-dimensional wind vectors as a function of range.

This miniaturized LDV can readily be used as a diagnostic tool for aircraft wind field investigation and as a ground-based wind sensor to probe the first few hundred meters of the atmosphere.

REFERENCES

1. K. A. Browning and R. Wexler. The Determination of Kinematic Properties of a Wind Field Using Doppler Radar. Journal Applied Meteorology, 7, 1, February 1968.

2. Anton J. Landrelre and John C. Bennett, Jr. Investigation of the Airflow of a Hovering Model Helicopter at Rocket Trajectory and Wind Sensor Locations. United Technologies Research Center, Report No. 477-912573-15, July 1977.

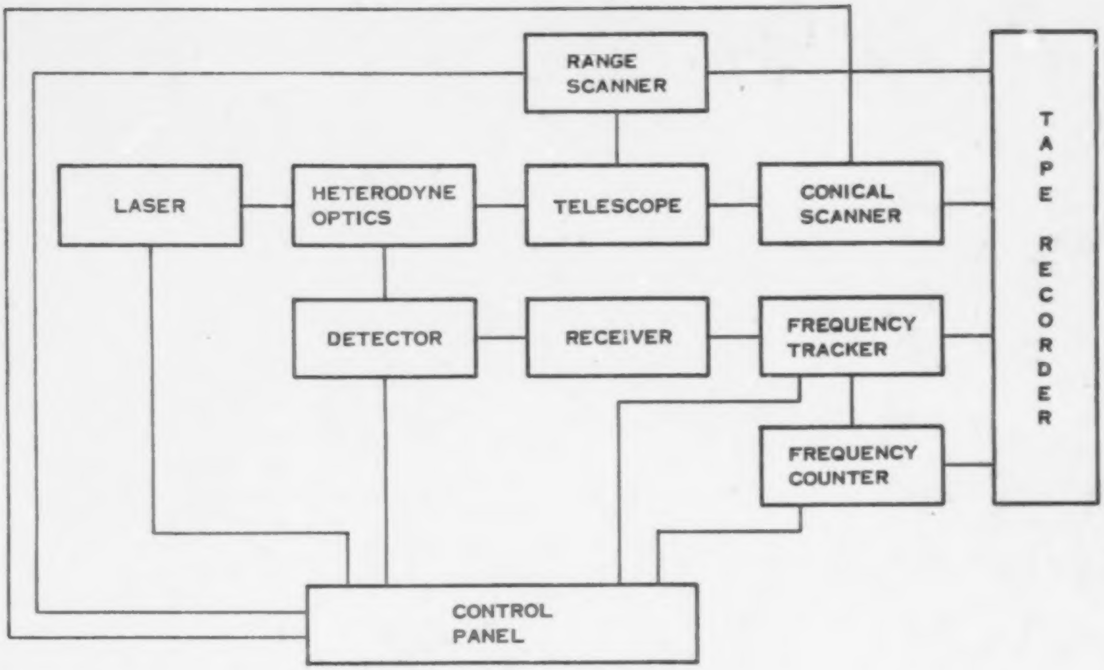

Figure 1. Block diagram HRWS.

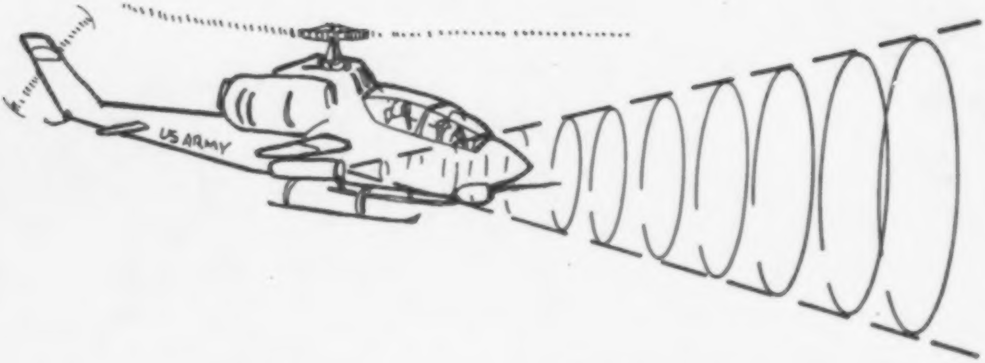

Figure 2. Conical scan configuration on AH-1 Aircraft.

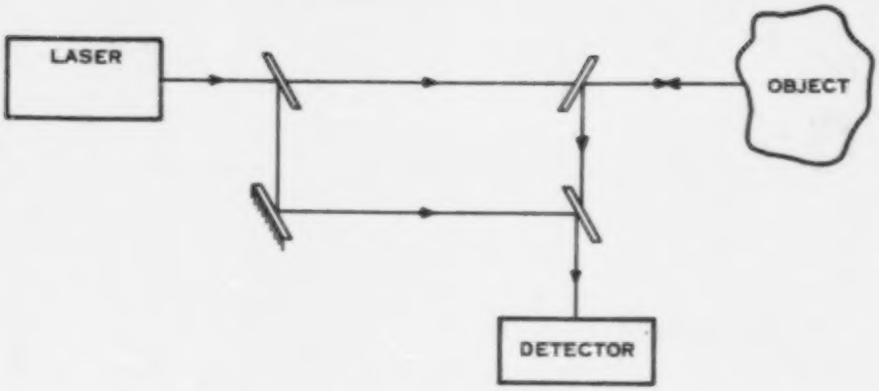

Figure 3. Laser doppler velocimeter transmission and reception.

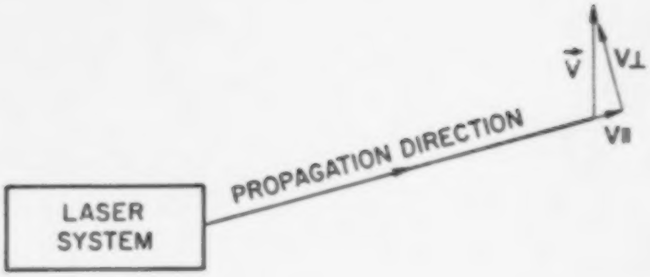

Figure 4. Doppler velocity – measurement geometry.

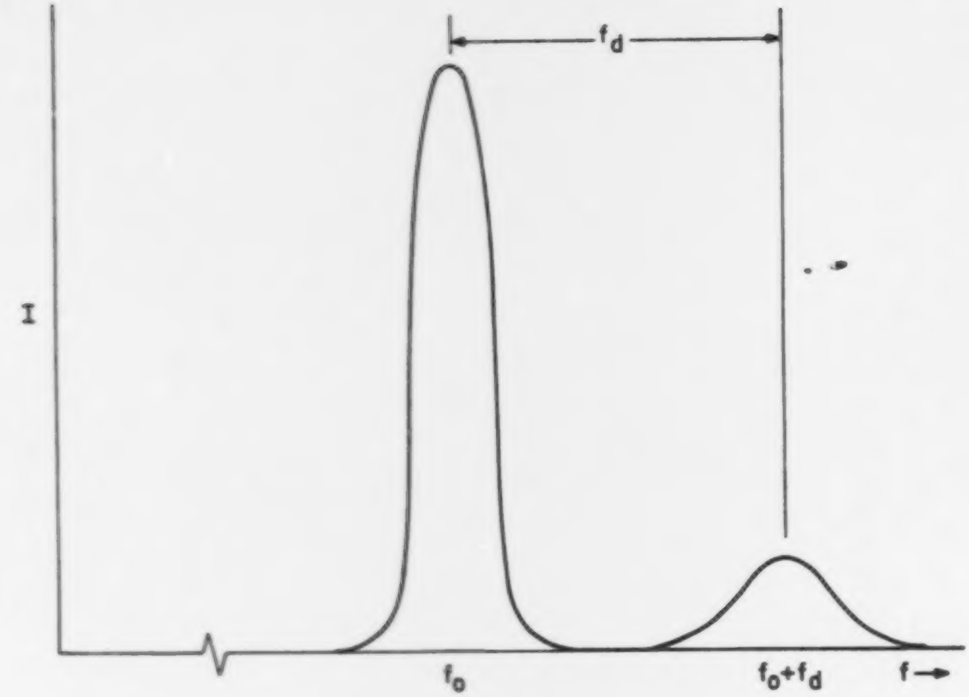

Figure 5. Optical heterodyning.

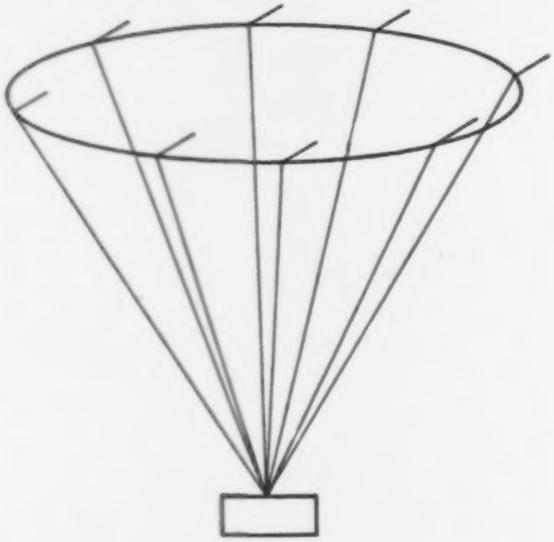

Figure 6. 3-D measurement with conical scan.

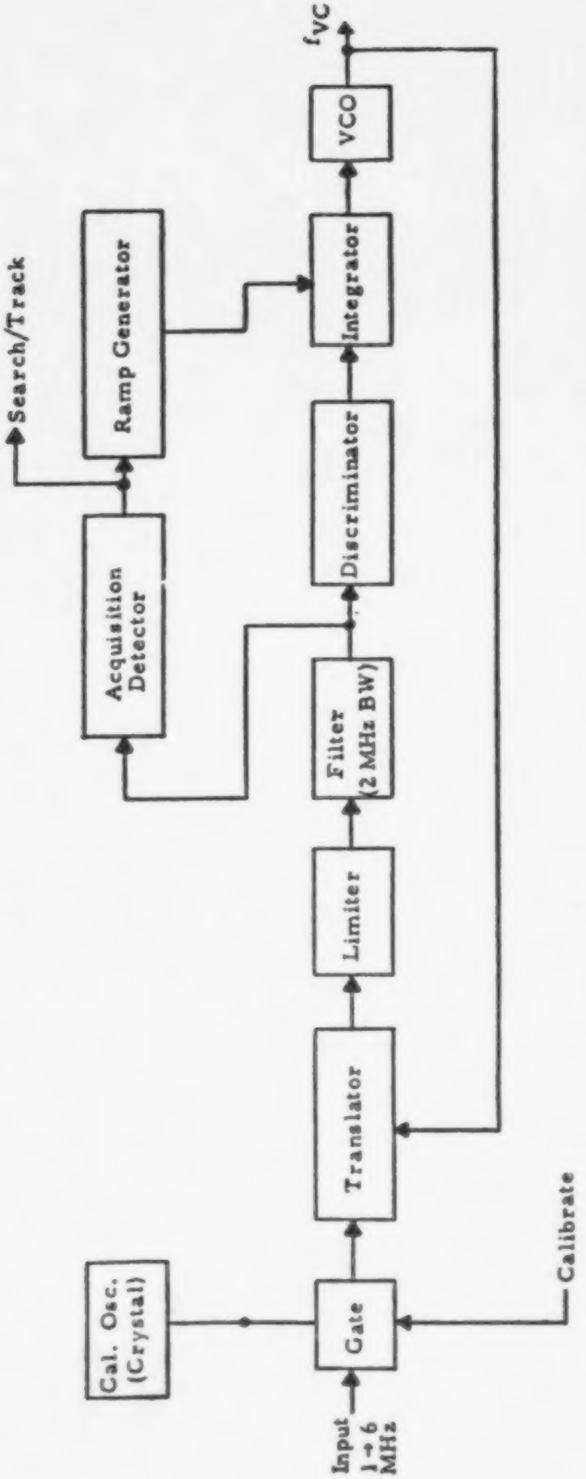

Figure 7. HRWS frequency tracker.

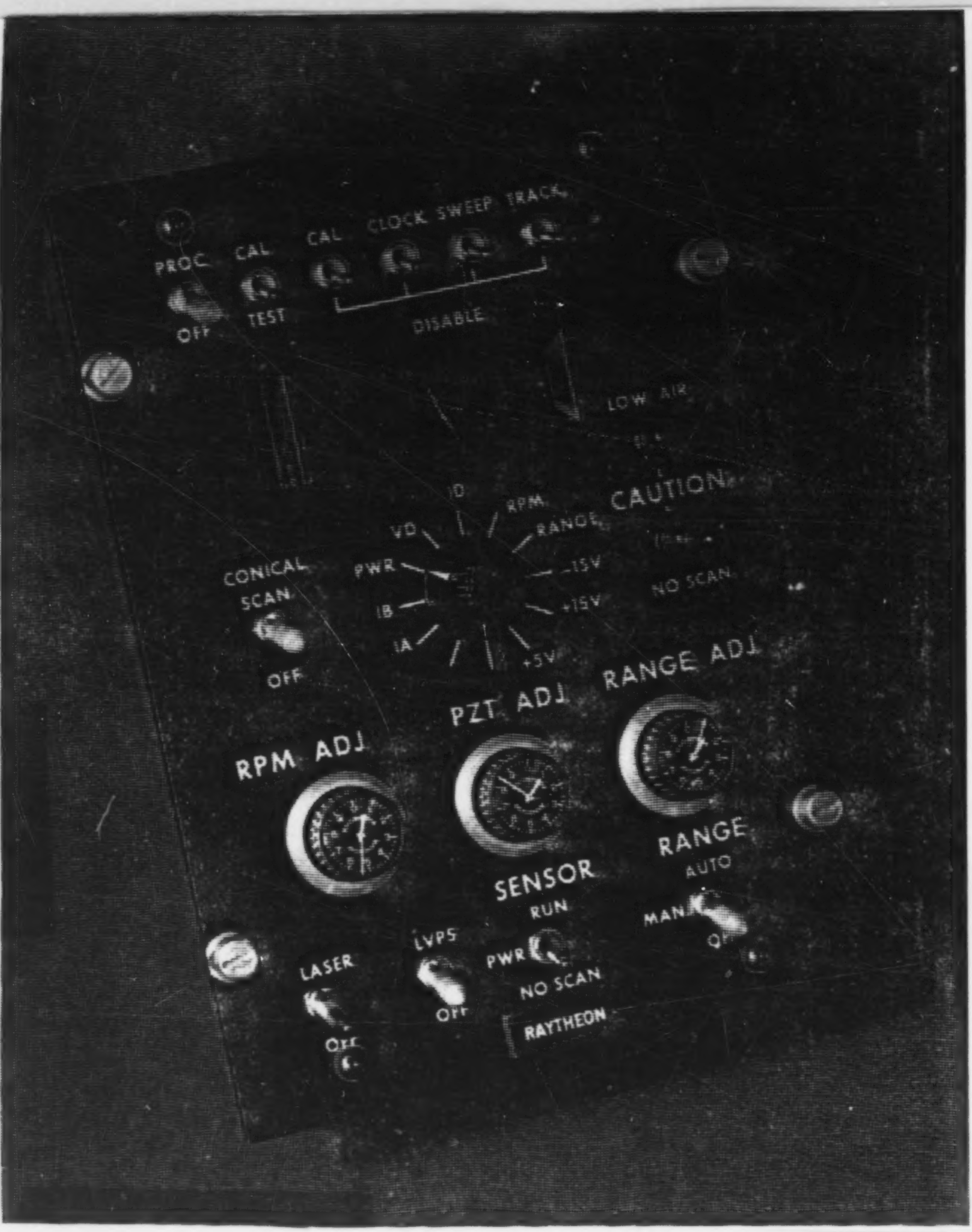

Figure 8. Control panel.

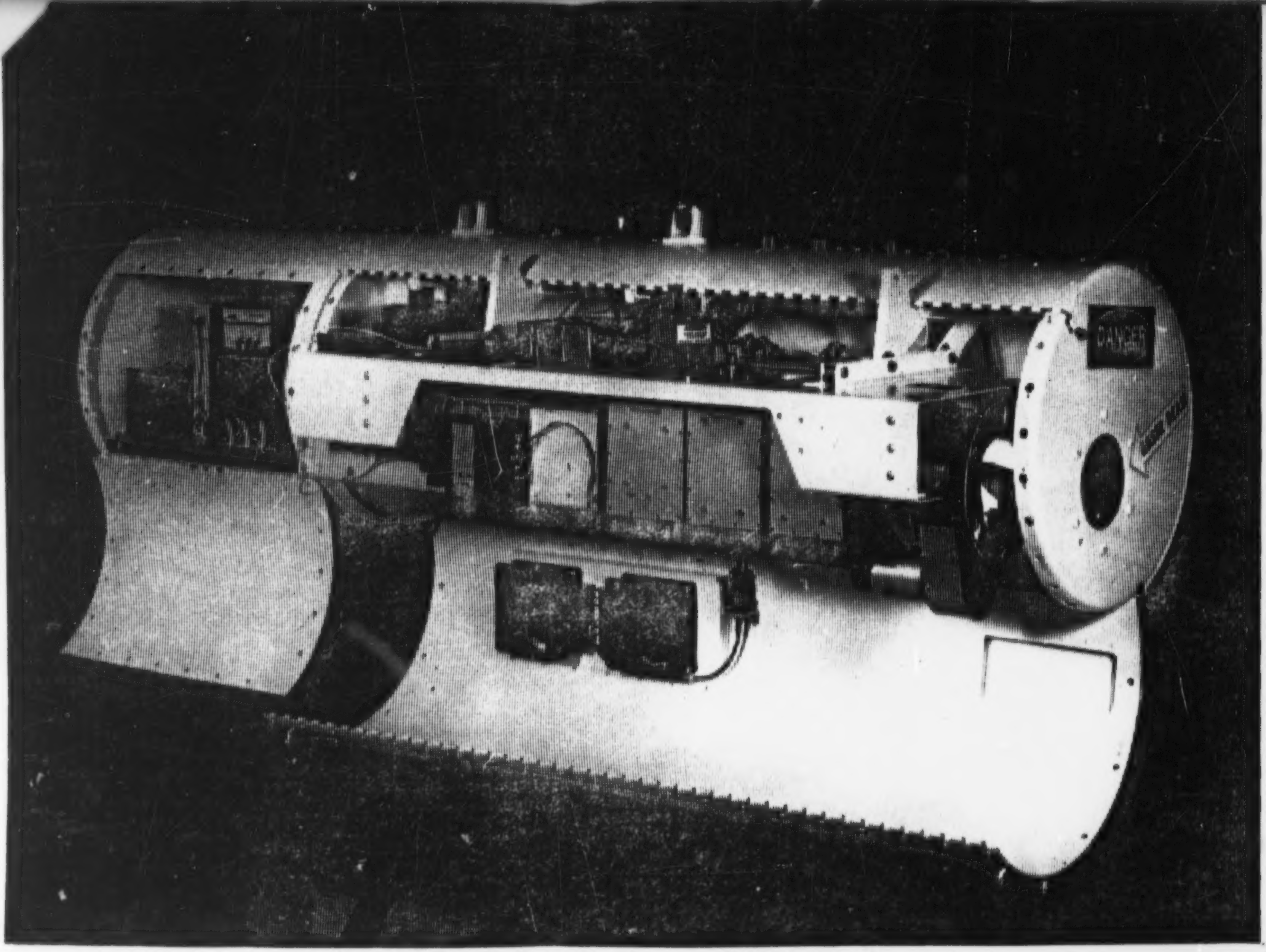

Figure 9. HRWS in pod with access doors open.

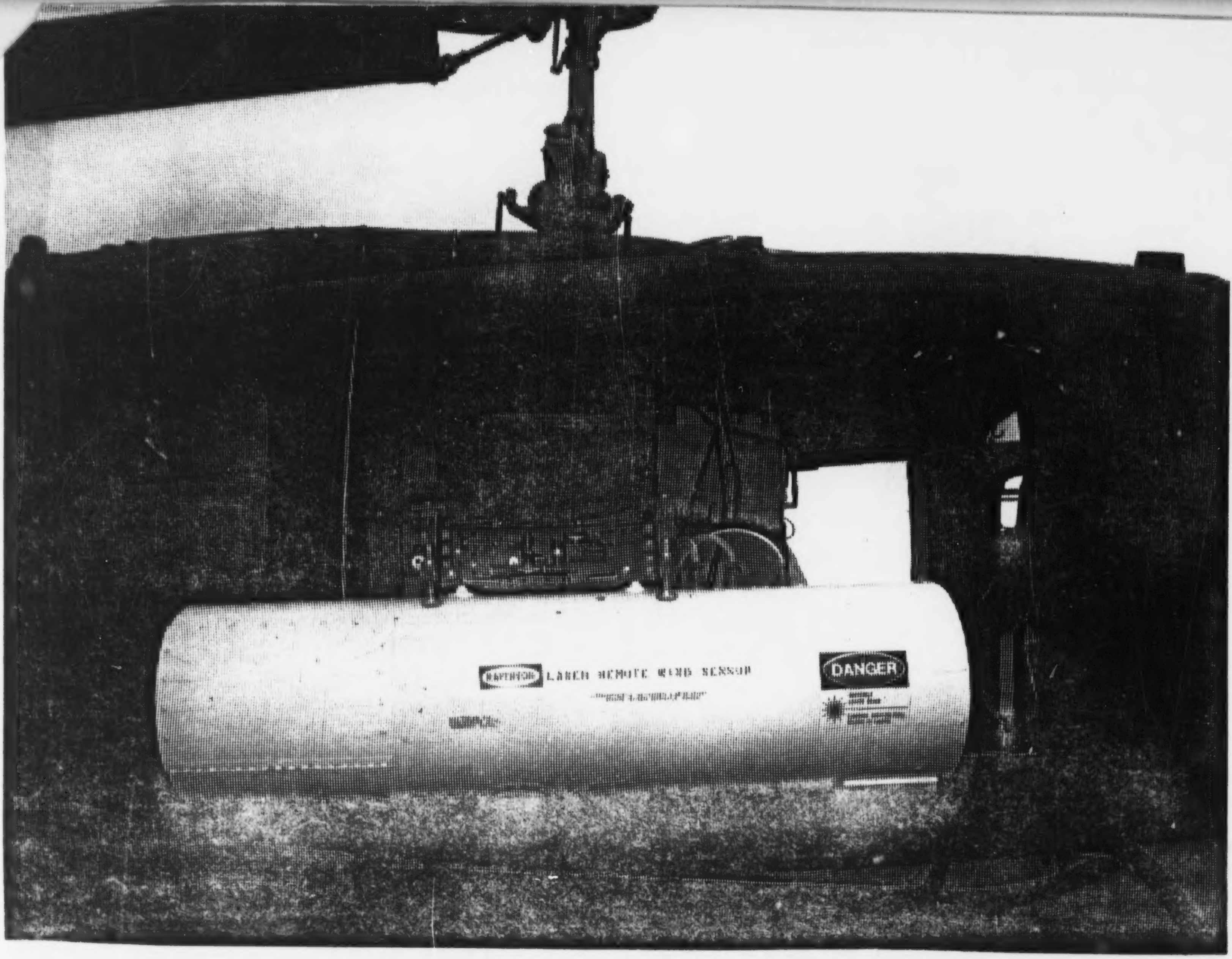

Figure 10. HRWS attached to UH-1H Aircraft.

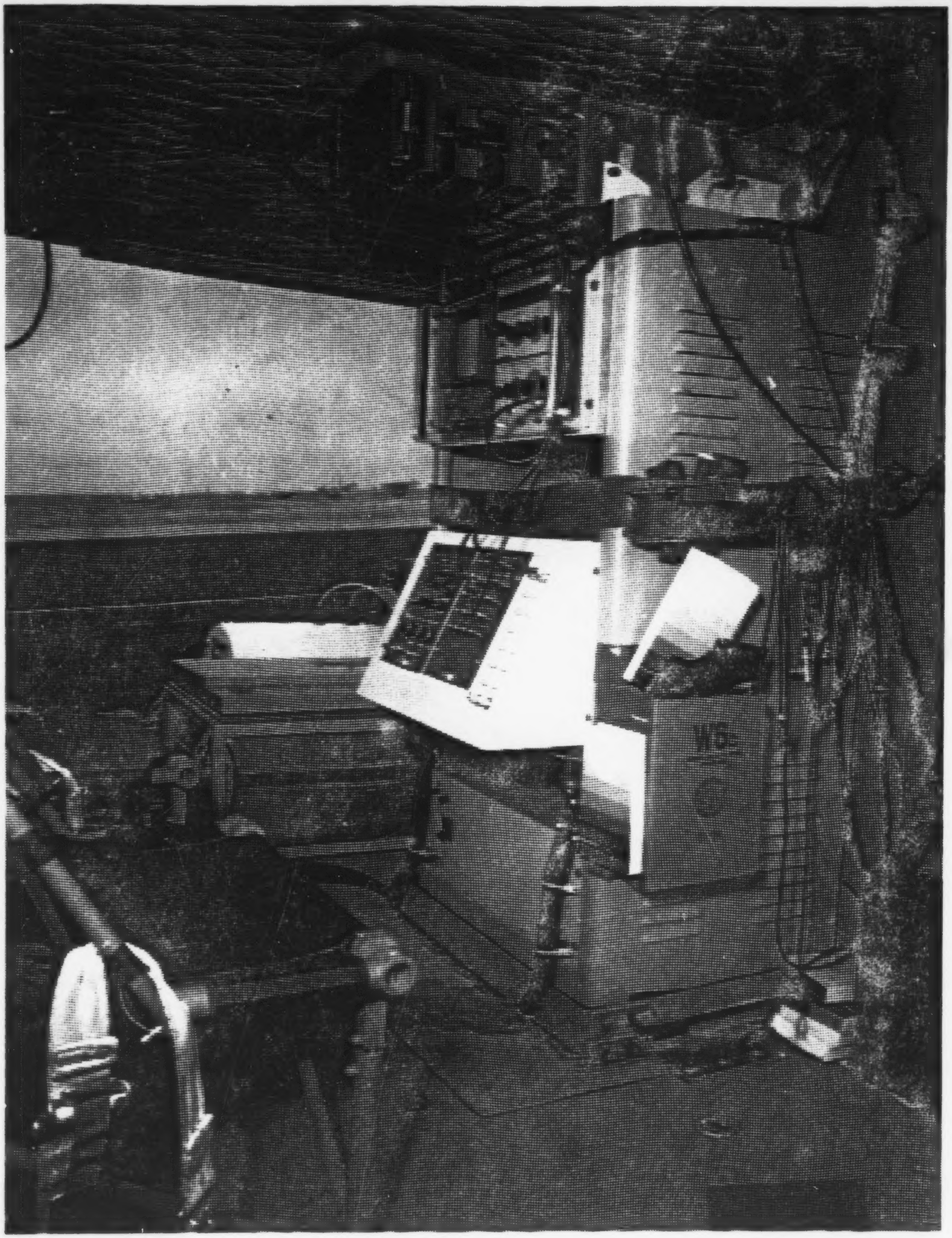

Figure 11. Completed installation of HRWS.

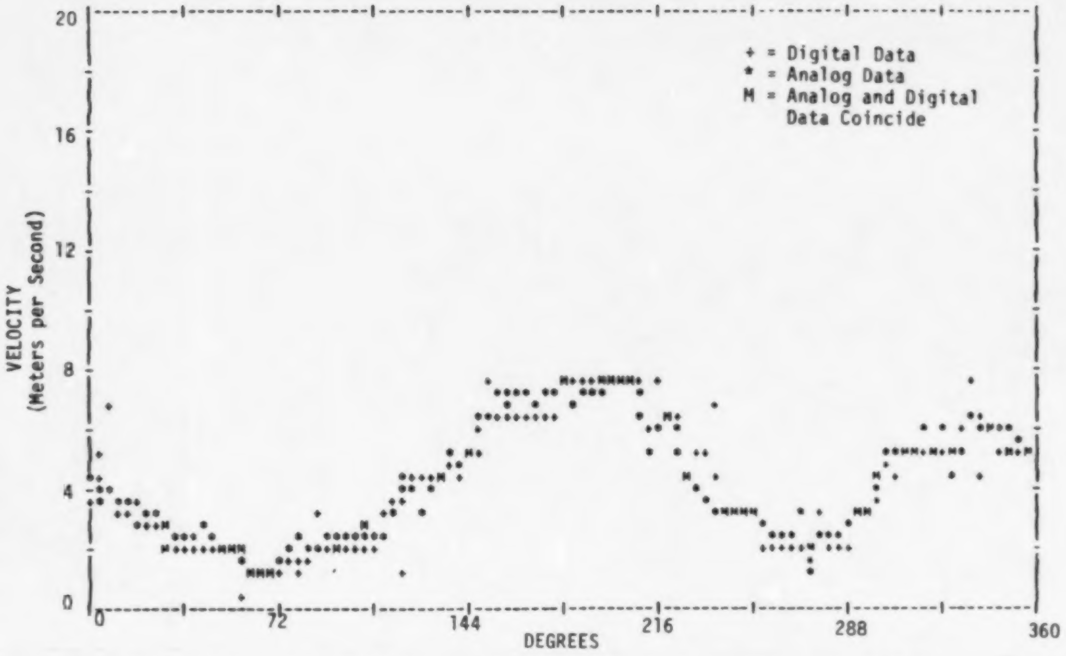

Figure 12. Full scan windfield measurements at 1-meter hover at a range of 7 meters.

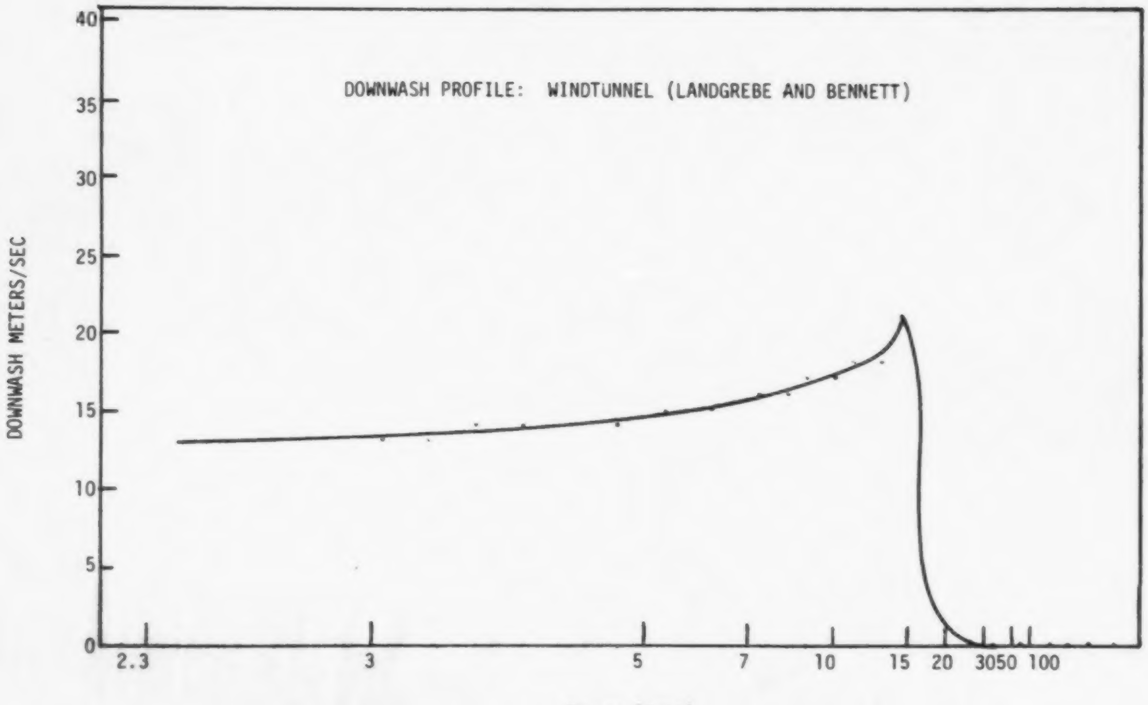

Figure 13. Downwash profile of AH-1 in wind tunnel.

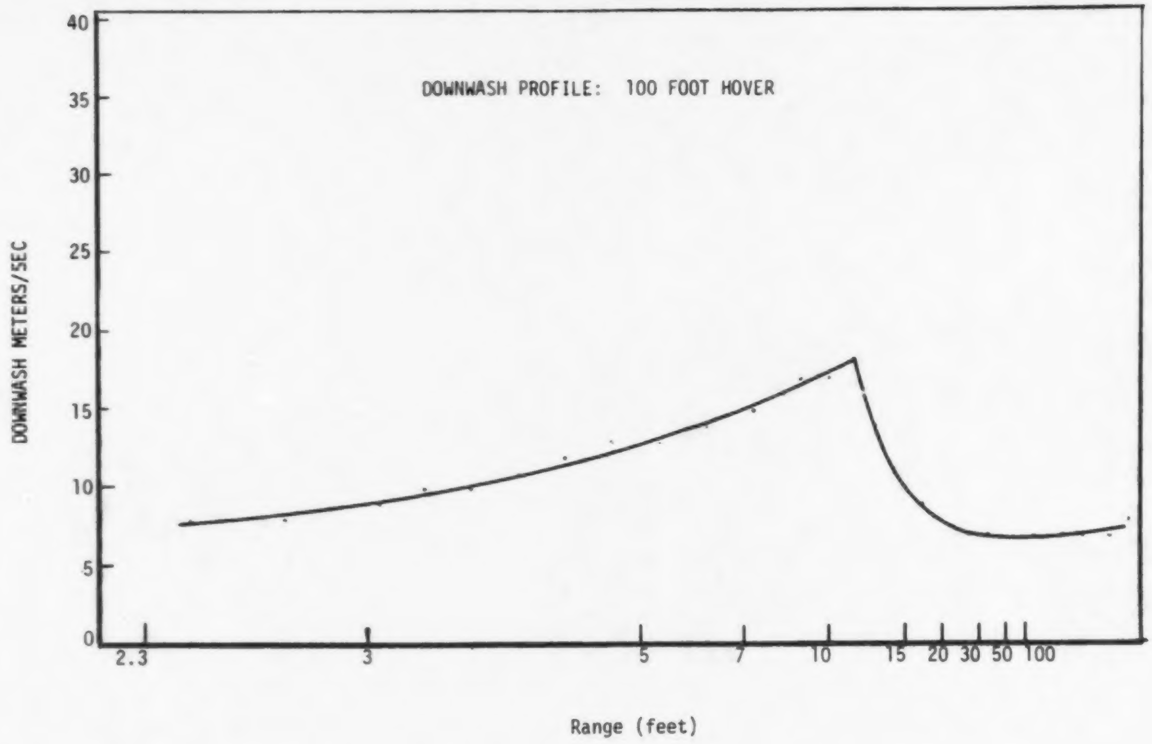

Figure 14. UH-1H downwash profile out of ground effect hover.

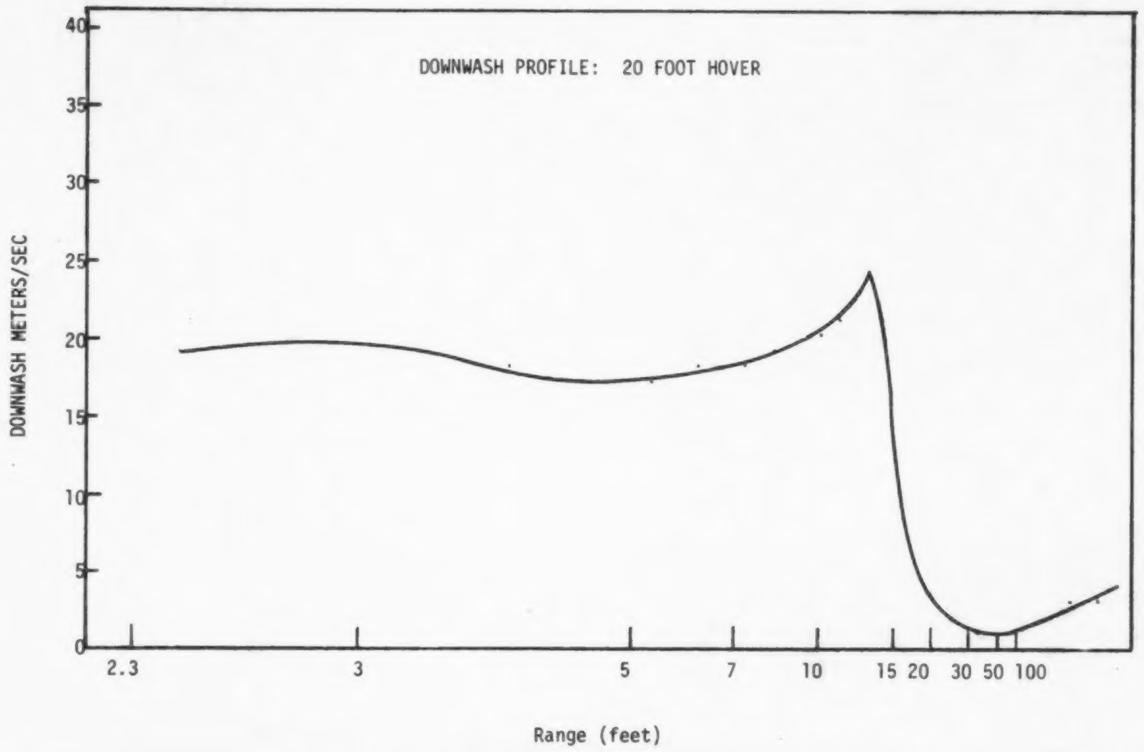

Figure 15. UH-1H downwash profile in ground effect hover.

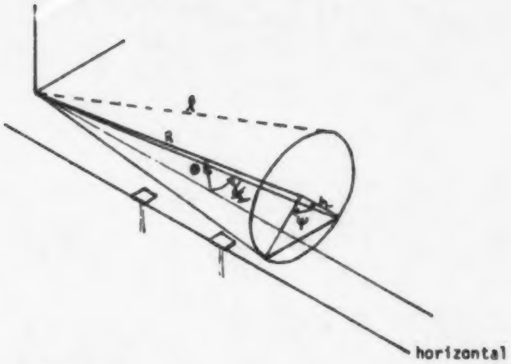

ℓ slant length
R range
w horizontal separation of sampl[illegible]ints = 1/2 ℓ
r radius of conical scan = ℓ sin [illegible]7°
ψ cone angle of separation of sample points = 118°
γ angular separation of sample points = 29°
θ angle of elevation of sensor boresight line = 11°

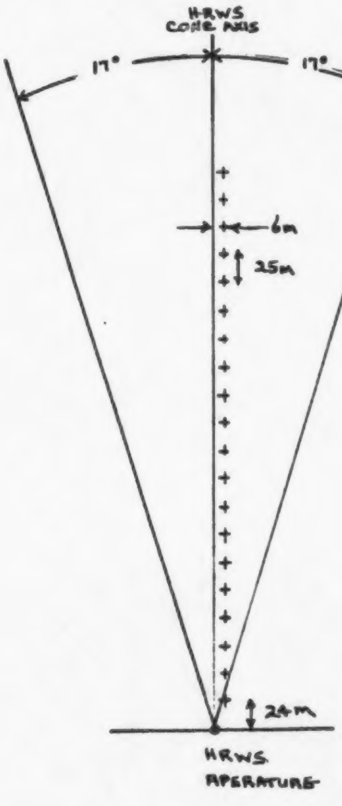

Figure 16. Geometric layout of HRWS on BOR + annometer array and axis of laser crosswind sensor.

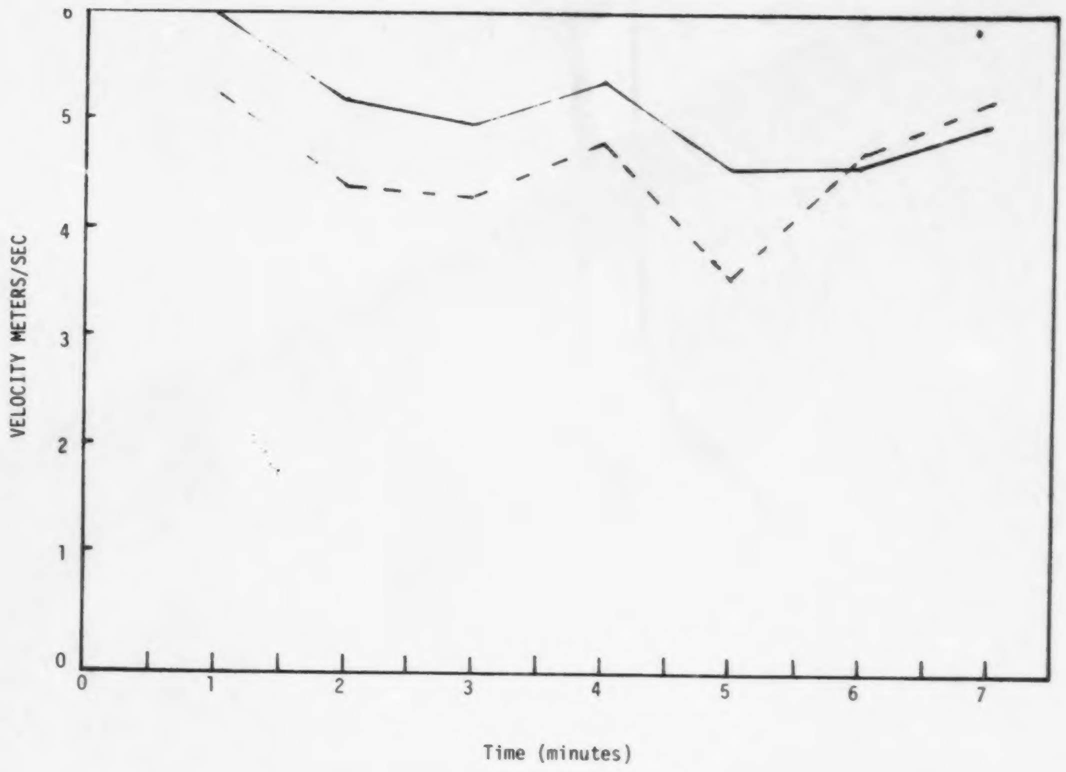

Figure 17. One-minute averages for 500-m range.
—— HRWS data
– – BOR annometer data

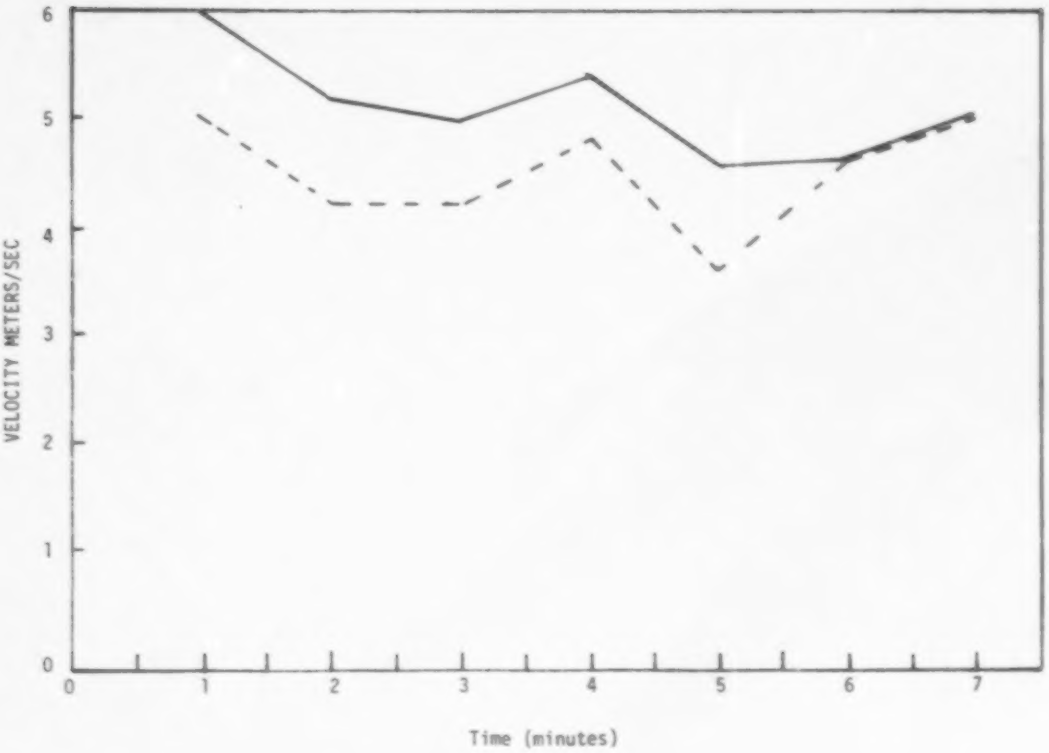

Figure 18. One-minute averages for 500-m range.
—— HRWS data
– – LCS data

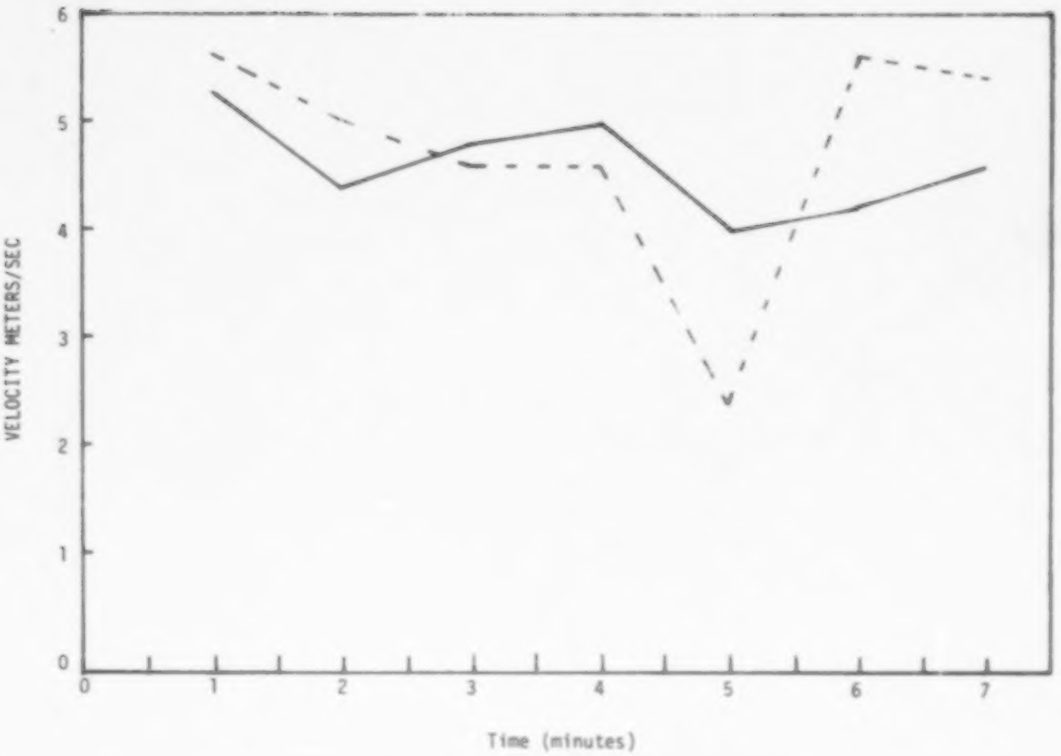

Figure 19. ---- Single annometer at 24 m
——— HRWS focused at 24 m

Elapsed Time	HRWS (m/s)		BOR (m/s)		
(minutes)	Single Focus	500m AV	Single Annometer	Average	LCS
1	5.9	6.0	5.6	5.2	5.0
2	4.4	5.1	4.9	4.4	4.2
3	4.8	4.9	4.6	4.3	4.1
4	5.0	5.4	4.5	4.7	4.7
5	4.0	4.5	2.3	3.4	3.5
6	4.1	4.5	5.5	4.8	4.5
7	4.6	5.0	5.3	5.2	5.0

Figure 20. Tabulated summary of typical HRWS/BOR comparison.

WORKSHOP REPORTS

Preceding page blank

WORKSHOP I

EXPERIMENT DESIGN, MEASUREMENT STRATEGY AND TACTICS, COMMUNICATIONS REQUIREMENTS

Chairman

Roy Evans
Environment Sciences Research
Laboratory

Rapporteur

Cary Eaton
Research Triangle Institute

Participants

Abdul J. Alkezweeny
Kurt Anlauf
Donald L. Blumenthal
Richard Coulter
Rosa de Pena
Cary Eaton
Roy Evans
G. T. Gay
Paul Lioy
Walter A. Lyons
Michael MacCracken
Peter H. McMurray
Leonard Newman
Brynjulf Ottar
Rudolf Pueschel
Joseph Sickles, II
Gary Stensland
George Sverdrup
Gary Tannahill
Frank B. Tatom
Edward Uthe
William M. Vaughan
Scott Wagner
Kenneth T. Whitby
George Wolff

Preceding page blank

EXPERIMENTAL DESIGN, MEASUREMENT STRATEGY AND TACTICS, COMMUNICATIONS REQUIREMENTS

INTRODUCTION

The overall purpose of the Sulfur Transport and Transformation Experiment (STATE) program is to perform measurements to develop and to evaluate regional models of the formation and transport of visibility-reducing aerosols. Models will be used for interpretive or diagnostic purposes and ultimately for predictive purposes to allow States and local agencies to estimate concentrations of these pollutants, considering transboundary transport.

One goal of Project PEPE is the investigation of multiday gas-to-particle conversion chemistry and aerosol formation processes; questions such as the differences in chemical processes when urban or point source plumes are injected into clean air and into dirty air (2-3 days old) should be addressed. The emphasis is on the formation of sulfates and nitrates as opposed to the prediction of the formation of ozone, although ozone may be used as a predictor for the formation of sulfate and nitrate aerosols. Chemical measurements will not emphasize the measurement and speciation of hydrocarbons, although limited sampling and speciation should be performed. Visibility measurements should be a part of the Project PEPE experimental program; some detailed chemical species determination should be performed, probably through X-ray fluorescence (XRF). We would like to differentiate between nitrate species such as nitric acid and ammonium nitrate, but we may be forced to settle for total nitrate.

Another goal of project PEPE is to measure the vertical dispersion and layering of the atmosphere to provide modelers with information to determine the number of layers needed in air quality simulation models. We wish to follow specific air masses for periods of several days to observe the buildup of concentrations in polluted air masses.

The time span of Project PEPE should be mid-July through August of 1980 primarily for logistical reasons. During this period we can expect perhaps two PEPE's, each about 1 week in duration. In the interval between PEPE's, the experimental resources of the project will be devoted to studies of the dispersion and transformation of power plant and urban plumes.

The following mode of operation is envisioned: Certain facilities and equipment must be supplied by the prime contractor for the project, as discussed in the RFP. In addition, the Regional Field Studies Office (RFSO) may elect to fund other governmental and university group participation in the project. It will be the contractor's responsibility to provide some support to and coordination of these groups to produce a coherent program. An RFSO field team will provide final project guidance in the field.

SCENARIO FOR STUDY OF A PEPE

The meteorological forecast data will be monitored to provide as much lead time as possible for planning a PEPE experiment. It is expected that the occurrence of a region of slow-moving air can be anticipated 3 to 4 days in advance, which would then start a "PEPE watch", i.e., notification that an appropriate situation for study may be developing. If the shorter-period (36- or 48-hr) forecasts confirm the previous indications, then the deployment and readiness alerts would be issued for the actual experiment. The criterion for the start of an experiment is that an air parcel will move slowly, or perhaps stagnate, over an area of substantial emissions, with the subsequent motion of that parcel forecast to remain relatively slow (less than 6 ms^{-1}) for at least 36 hr. The definition of the initial parcel is the area of a 100- to 200-km square, or roughly 10 counties.

When the experimental start is set, a tracer release crew would be dispatched to the anticipated center of the (temporary) stagnation area, where they would release the tracer. For at least the first experiment, release would be during the daytime hours of rapid vertical mixing, permitting release at the surface. A tetroon release crew would go to the same point and release a cluster of tetroons--perhaps two triads ballasted to float at 0.4 and 0.8 times the mixing depth. Aircraft completely equipped for mechanism studies would start sampling the parcel by means of spirals, perimeter flights, X-pattern flights, and perhaps other patterns to measure the initial conditions within the parcel. These aircraft would continue to sample the "parcel" at perhaps 6-hr intervals, following the assumed centroid of the parcel wherever it might move for as long as possible. Mobile PIBAL crews would be dispatched in leap-frog fashion to make frequent soundings within the parcel. Horizontal shearing and mixing will change the air in the parcel considerably over the anticipated period of several days that it may be tracked; the definition of the parcel will continue to be an area about the assumed centroid of the initial parcel, to be identified by tetroons when possible and by trajectory calculations otherwise. These measurements in a Lagrangian frame will provide the data for mechanism studies as the pollutants in the parcel age and are reinforced by freshly emitted pollutants along the path followed.

Surface sampling vans would be deployed to perform stationary sampling at locations the parcel is expected to cross over. To the extent possible, these locations would be at existent monitoring stations with ground power available. However, if the driving time to sampling time ratio were to be excessive, one or more mobile vans would continue to make local measurements near the field base. Sequential tracer samplers would have to be deployed well in advance of an experiment; a regional grid would be the most feasible pattern for the samplers. Notification would be provided for start time and sampling duration for each point in the grid.

To provide a very large-scale picture of conditions before and during the Lagrangian measurements, the NASA planes would make regional overflights of roughly 2,500 km total length in flight patterns that might consist of parallel traverses and cross flights. These overflights would start on the day of tracer and tetroon release, or, preferably, on the preceding day, and continue at 12-hr intervals for the duration of the total episode. Flights beginning at approximately noon and midnight would serve to characterize regional distributions near times of maximum mixing and stability, respectively.

Other aircraft would make regional flights within the boundary layer to provide direct compositional measurements. The flights would generally be made over preselected flight paths, which would remain fixed for a number of flights, to provide a temporal sequence in a Eulerian frame. These flights might total 1,000 km in length, and would cover a smaller grid contained within the grid overflown by the NASA planes. While these two grids would probably be fixed for the duration of an episode, they could also be shifted if the continued development of the episode, either by formation or transport, were indicated to be moving outside the initially specified location. The relative sizes of the three regions discussed are shown in Figure I-1.

Since the end of an episode is frequently attended by the development of showers as a new air mass approaches the area, the probability of "dirty" rain is rather high, and an alert to an intensive cloud and rain sampling experiment could be issued because the extent of the polluted air mass feeding into the shower area would be known.

STUDY STRATEGY

The above scenario of a PEPE has the highest priority for the entire duration of the study. However, because the weather sequences during the period chosen for study cannot be preordained, considerable flexibility in the actual conduct of the study is required to maximize the amount of useful information obtained during the study.

Since a PEPE of sufficient predictability and extent may not occur during significant intervals of the study, other kinds of studies will also be performed; studies that can be completed without interfering with possible PEPE experiments. The most frequent type will be plume experiments during which effluent from isolated sources such as power plants or from a source complex such as an urban area will be studied to better characterize the input into PEPE's. These experiments will be conducted in a manner similar to prior plume studies, with spatial scales of the order of 250 km downwind of the source and corresponding durations of up to 24 hr on occasion. The aircraft equipped for mechanism studies will be used primarily, with a number of specific scenarios to be used for individual experiments. As one example, there may be days when plumes from two power plants remain separated horizontally for a long distance, but one plume mixes with the HC- and NO_x-rich air from an urban source. It would be of interest, then, to measure the differential influence of the urban source on sulfate conversion in the two plumes. Other process, or mechanism, studies could be performed, such as opportunistic studies of the pollutant composition of air from recently dissipated clouds, or the role of pre-existent pollutants in conversion processes to enhance data from the multiday Lagrangian measurements, and many others. These experiments would be planned and conducted on a day-by-day basis, with a scenario specified about 12 hr prior to initiation of an experiment, and with active communication with experimental platforms, and feedback to field headquarters during the conduct of each experiment.

FACILITIES AND EQUIPMENT

Study facilities and equipment recommended by the working group are discussed in the following paragraphs. In general, the working group has recommended numbers and general descriptions of equipment that should be used.

In Situ Chemical Measurement Aircraft

The working group recommended that a total of four in situ measurement aircraft should be involved, two of which are envisioned as performing general "Eulerian" frame measurements of the areal extent and concentrations of pollutants within the dirty air mass. These two aircraft will be equipped with instrumentation for criteria air pollutants and other parameters in what we have described as the "base package." Two additional aircraft should be more extensively instrumented to investigate gas-to-particle conversion chemistry and vertical and horizontal dispersion in a "Lagrangian frame," following the marked air parcel as far as logistical considerations will permit.

The base package (to be present in all four aircrafts) should include at least the following parameters:

Altitude (pressure altimeter)
Location (by DME/VOR)
Ozone
B_{scat} (with heated nephelometer)
SO_2 (1 ppb sensitivity)
Temperature
Dewpoint
Turbulence
High-volume samples for particulates
Filter packs for sulfates and SO_2 (BNL system)
Continuous sulfate monitor
Condensation nuclei monitor

This equipment, when possible, should be previously used, field-tested, preferably off-the-shelf devices. An analyzer for NO/NO_2 should be included in the base package if an instrument is available in the summer of 1980 that will provide 0-2 ppb sensitivity. Otherwise, the cost in power and weight requirements may not be justified because the aircraft envisioned in this study will be in the small, light, twin-engine category. The inclusion of a continuous sulfate monitor in the "base package" should also be evaluated, balancing the gain in information against the increased maintenance and calibration requirements. Position location to ±5 miles will be satisfactory for PEPE measurements, although more stringent requirements may be imposed by the urban and power-plant plume studies.

The two "Lagrangian-frame" aircraft should be more extensively instrumented, each one including some or all of the following capabilities:

- Continuous sulfates
- Electrical aerosol analyzer
- Gas grab samples for hydrocarbons
- Perfluorocarbon samples
- Real-time tracer measurements
- Cascade impactor (cut sizes: 0.1 μm, 0.3 μm, 1 μm)
- Filter sampling capability to allow chemical and elemental analyses of particulates
- Radiometers--UV and visible light, upward and downward looking for radiation budgets

The actual inclusion of all of the above equipment at once in each aircraft may not be necessary depending on the objectives of the chemical investigations. Other measurements that would be desirable (but may not be feasible) include aldehydes and formaldehyde; total hydrocarbons by photoionization.

The aircraft should be capable of cruising speeds of at least 150 knots, preferably 200 knots, and should have a flight range of the order of 5 hr or more with a full complement of instrumentation. Aircraft with slower speeds or shorter ranges will probably not be able to traverse the Eulerian frame within reasonable times.

At least one subsidiary or remote base of operations should be prepared for the Lagrangian aircraft to enable them to follow the marked parcels through a multiday path. Since these aircraft will operate more or less continuously after beginning to track a parcel, each aircraft is likely to need two full crews, both pilots and scientific personnel. Remote bases may also be necessary for the Eulerian frame aircraft.

Each aircraft involved in the project must be equipped with a radio link separate from the airways communications frequencies to permit communication with the Mission Control Facility at least once an hour.

Lidar Aircraft

The working group recommends the inclusion of at least two aircraft equipped with lidar type devices for measurement of range-resolved light scattering from aerosols and of total (vertically integrated) concentrations of either SO_2 or O_3. It is assumed that NASA-Langley will fly their Electra equipped with a DIAL system and that one other airborne aerosol lidar, either the EPA-Las Vegas device or the SRI lidar, will be available. NASA will test the DIAL system during the summer of 1979 to determine actual sensitivities of the device for SO_2 and O_3. Measurement of SO_2 would be most valuable to Project PEPE, provided that actual sensitivity for SO_2 is sufficient to quantitate expected ambient levels. Ozone should be measured otherwise. Flights at altitudes of 10,000 ft will be necessary for both lidar aircraft to include the total expected mixing depths; this may or may not require revision of existing instruments.

If at all possible, the Electra should be equipped with in situ instrumentation of O_3, NO, NO_2, SO_2, nephelometer, temperature, dewpoint, and BNL filter pack for sulfates and SO_2. The other lidar aircraft should be fitted with an SO_2-sulfate (BNL) filter pack. Both aircraft should be equipped with transceivers to allow communication with the Mission Control Facility.

Fixed Ground Sampling Networks

EPRI-SURE Network--

Data from the nine Class I sites of the existing EPRI network and six anticipated additional Class I stations should be utilized in this study under a cooperative agreement. The locations of the nine sites are: Montague, MA; Scranton, PA; Indian River, DE; Duncan Falls, OH; Rockport, IN; Giles County, TN; Fort Wayne, IN; Research Triangle Park, NC; and Lewisburg, WV. At least four of these are in the Greater Ohio Valley region. These sites are equipped with O_3, NO, NO_x, and SO_2 gas phase analyzers and an integrating nephelometer. Other samplers collect particulate matter for data analysis of sulfate, nitrate, and acid precipitation. EPRI plans to install Doppler acoustic sounders for determination of winds. The workshop recommends that these be installed as soon as possible and that additional three-wavelength nephelometers and radiometers also be installed. Size-fractionating samplers would also be desirable.

It is recommended that data from the sulfate and nitrate samplers have a time resolution of at least 6 hr during PEPE experiments.

Close coordination between PEPE and EPRI network personnel would be essential.

SURE and MAP3S Precipitation Network--

SURE Class I sites now have colocated precipitation samplers. The Multistate Atmospheric Power Production Pollution Study (MAP3S) system will have similar samplers at approximately eight sites in 1980. Samples are analyzed for sulfate, nitrate, pH, and some metals.

National Air Sampling Network--

The National Air Sampling Network (NASN) has several sites within the study area that measure SO_2, O_3, CO, and total suspended particulate by high-volume sampler. Sulfate analyses are performed on the TSP filters. This information would be useful in determining sulfate buildup.

Inhaled Particulate Monitor Network--

The Inhaled Particulate Monitor Network (IPMN) will have approximately two sites per State. The systems employ dichotomous samplers with particle size cuts at 2.5 and 15 µm.

Ohio River Basin Study--

The Ohio River Basin Study (ORBS) system will consist of three sites. The emphasis of measurements will be on nitrates, nitric acid, and detailed analysis of aerosols. Criteria pollutants will also be monitored.

Tennessee Valley Authority Network--

The Tennessee Valley Authority (TVA) maintains a sampling network around each of its major power generation facilities. Emphasis is on SO_2 measurement although high-volume samples, meteorological data, and some ozone data are also available. Possibly four TVA sites might provide data to define the boundary conditions along the southern edge of the Greater Ohio River Valley.

National Oceanic and Atmospheric Administration Turbidity Network--

Turbidity data from the National Oceanic and Atmospheric Administration (NOAA) system are acquired by use of a pyroheliometer and should be part of the PEPE data base.

National Weather Service Upper Air Soundings

National Weather Service (NWS) releases of rawinsondes are normally made twice per day. It is hoped that the frequency of releases could be increased to four times per day at the following 10 sites: Greensboro, NC; Buffalo, NY; Pittsburgh, PA; Huntington, WV; Nashville, TN; Dayton, OH; Detroit, MI; Salem, IL; Dulles International Airport; and Fort Totten, NY.

Deployable Ground Sampling Systems

Instrumented Vans--

It is hoped that three vans, each equipped with sophisticated instrumentation, will be available for this study. These vans will be in use near urban and industrial centers for plume study, and, upon prediction of a PEPE, can be deployed to preselected sites where electrical power is readily available.

The recommended vans are Bob Stevens' EPA van, Kenneth Whitby's University of Minnesota van, and the General Motors Corporation van.

Each of the vans will be assumed to be equipped with the following analyzers or samplers: SO_2, NO-NO_x, O_3, CO, LBL dichotomous sampler, electrical aerosol analyzer (EAA), optical particle counter (OPC), cascade impactor, heated and unheated nephelometers, and COSPEC, as well as calibration systems and NBS traceable standards.

In addition, it is suggested that the following equipment be installed in one or more of these vans: HNO_3 filter, radiometer, pyrheliometer, 10-m meteorological tower, and continuous sulfate analyzer.

Additional Vehicles--

Automobiles could be equipped to measure ozone (Dasibi) and sulfate (by filter pack). These vehicles could travel highways during a PEPE to provide additional ground coverage of the event.

Tracer Sampling Network--

A tracer sampling network using samplers such as those described by Gilbert Ferber should be included in the project and deployed over the region on a grid determined by the number of samplers that might be available.

Mobile PIBAL

PIBAL releases should be made in both the plume study and in the Lagrangian mode of the PEPE study. Suggested release points during a PEPE would be near tetroons in the Lagrangian air parcel.

Communications Network

Both the Project PEPE field measurements program, and the power plant and urban plume studies between PEPE's, will require good communications between the Mission Control Facility and the individual field units. Communications on a minute-to-minute basis are probably more important for the plume studies than for the PEPE field activities, but communications between all field units and Mission Control at least hourly will be needed for all aspects of the program.

Two methods were suggested by the working group, either of which is probably adequate. Two-way communications via a separate FM network operating at about 165 MHz and an airborne repeater in a dedicated aircraft would provide minute-by-minute communications throughout most of the PEPE area. The repeater aircraft would orbit at an altitude of about 15,000 ft during the entire PEPE and could move with the Lagrangian parcel if necessary. Off-the-shelf equipment such as the Motorola or the GE lines would be satisfactory for this purpose, provided that acquisition was begun about a year in advance of the actual deployment and that adequate resources were budgeted for the contractor to install and maintain the equipment. There is some probability that the Lagrangian parcel would move beyond the range of the repeater at the end of its trajectory.

Radiotelephones provide an alternative means of communication that would operate over a broader geographic area but would provide only intermittent communications between field units and Mission Control. Radiotelephones that are satisfactory for aircraft installation are available either for purchase (e.g., King Radio) or for rent (from Bell); however, lead times for acquisition will probably amount to at least several months, and acquisition should be begun at the beginning of FY80.

High-Altitude Air Force Aerial Photography

The working group recommends that high-altitude aerial photography of the PEPE be obtained from the U.S. Air Force from ongoing U-2 flights. It is thought that this information could be obtained at virtually no cost via a request from EPA to the Air Force. The Las Vegas laboratory already has well-established channels for requesting this assistance from the Air Force.

Mission Control Facility

An operations headquarters must be established at a central location within the PEPE area to coordinate STATE and PEPE field activities. Its functions will include:

1. Forecasting the occurrence of the PEPE and the location of its onset;
2. Acting as field data analysis center;
3. Serving as field laboratory;
4. Maintaining communications with all field units;
5. Assimilating data from satellite imagery to aid in maneuvering field crews.

Chemical Tracer Injection Team(s)

Chemical tracer injection will include SF_6 and up to three perfluorocarbon compounds, provided satisfactory measurement instrumentation is available by summer of 1980. Tracer injection support requirements were assumed to be established by Workshop 2.

Tetroon Tracking

We have assumed tetroon parcel markers will be utilized in Project PEPE, with tetroon release to be accomplished by NOAA. Tracking techniques and requirements were assumed to be established by Workshop 2.

DATA ARCHIVING

The contractor selected for conduct of the study will be responsible for reduction and validation of all data collected as part of the contract and, in addition, will process some data from other experimental platforms. These data will be delivered to the RFSO on magnetic tape in formats to be developed by mutual agreement. Data from other sources, including not only other participants in the experimental studies, but supplementary data such as NWS meteorological data and pollutant monitoring data from existent networks, will need to be included in the total STATE data bank on the PEPE study. A data management system to incorporate all these diverse data sources and to make data available for subsequent analysis should be structured before the data start flowing in. This system should provide format specifications to all participants in the study, and will require good coordination between the STATE data manager and the sources of input data.

Quality Assurance

With the diversity of sampling platforms and methodologies that will be used to provide data during the course of the study, a procedure to ensure the comparability and quality of the collected data is needed. Design of sampling systems and performance of individual instruments can be checked by adherence to good procedures, frequent calibrations, and checking of calibration sources. To provide the final step in a quality assurance program, intercomparisons should be made between complete sampling systems as used in their respective platforms. To accomplish this end, all aircraft should make side-by-side flights at several altitudes under various ambient pollutant conditions, with any given craft making at least one comparison flight a minimum of three times during the study. Selection of an open site, such as a small airport, would permit comparison of aircraft systems with mobile ground systems, which should be made. In turn, comparisons between mobile ground systems and certain of the fixed monitoring stations should be included if the fixed stations are to be used as locations for mobile sampling operations.

MISCELLANEOUS RECOMMENDATIONS

Historical Forecasting of PEPE

A program should be initiated now to review the data and statistical findings from SURE and MAP3S in order to derive a reasonable technique for forecasting the occurrence of a PEPE.

Determine Best Study Window Via Climatological Study

A climatological study should be part of the planning stage for two reasons: (1) to determine the optimum location of tracer injection, and (2) to be a basis for setting the time window for the study. At present, the study is planned to begin in July 1980 and extend for 6 weeks.

Cooperative Study With Canada

The involvement of Canadian air pollution agencies, such as the Federal Atmospheric Environment Services (AES) and the provincial Air Resources Branch (MOE), is welcomed. EPA will establish contact. The suggested study area would be immediately northeast of the Eulerian gridwork proposed in the scenario. Specifically, it would be highly desirable that aircraft (AES) and ground-level support measurement (AES and MOE), including remote sensing and radiosonde releases, be made in the Lake Ontario and Lake Erie regions. This would greatly aid in defining the northern boundary conditions of the Eulerian grid.

EMISSION INVENTORIES

To relate the measurements obtained in the study to pollutant sources, and to provide the requisite input for model development and evaluation, a reasonably accurate and up-to-date emissions inventory for the region of study will be required. The updating and improvement of prior inventories sponsored and performed by EPRI and the MAP3S program should provide a useable inventory of sulfur emissions. Some additional work will be required to compile an inventory of NO_x and other pollutant emissions, with conversion of the EPRI/MAP3S inventory for point sources and updating of NEDS for area source emissions--particularly the mobile source component.

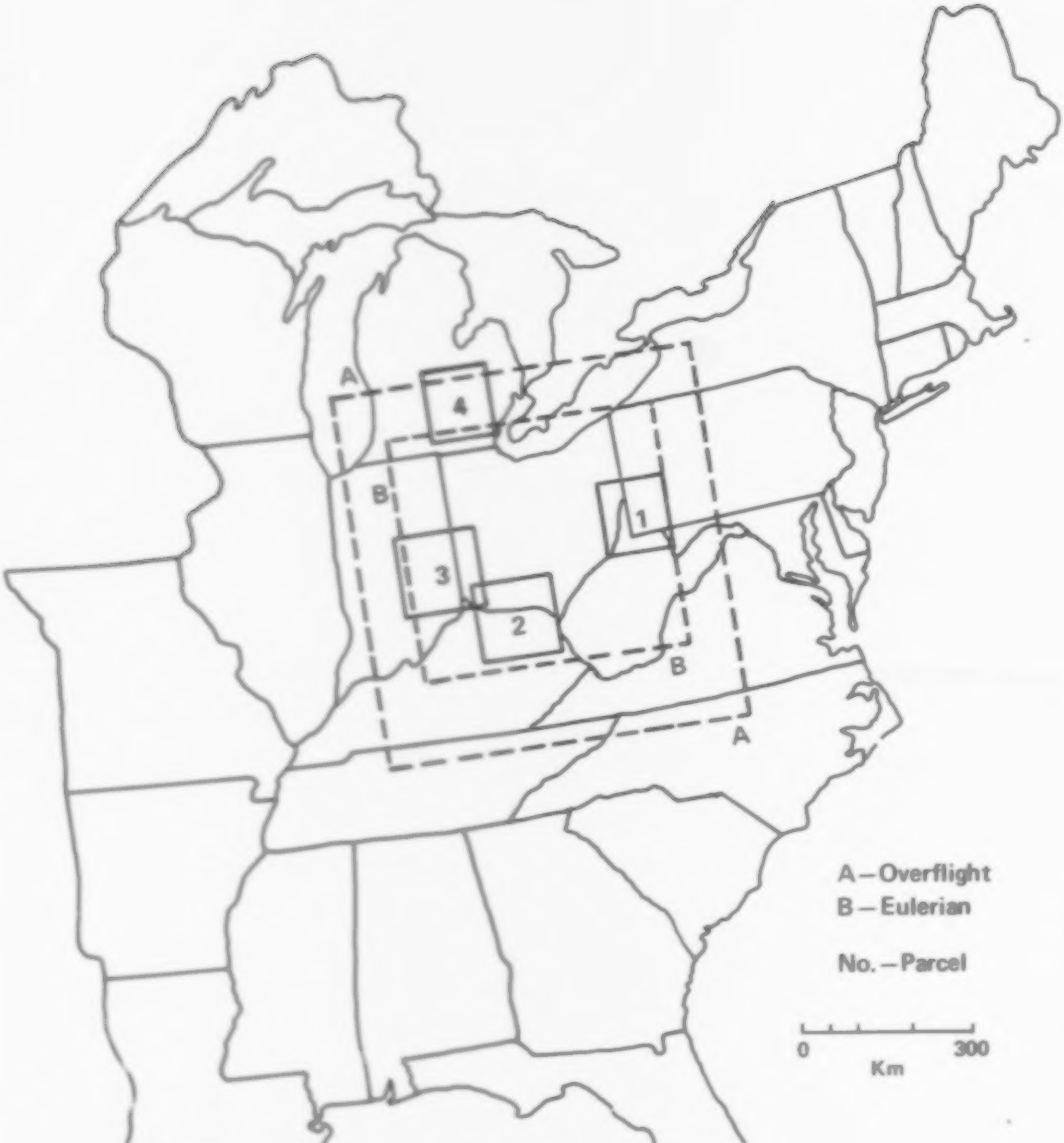

Figure I-1. PEPE scenario.

WORKSHOP II

METEOROLOGY, TRANSPORT, AND MULTIDAY PARCEL TRACKING

Chairman

Harry L. Hamilton, Jr.
Research Triangle Institute

Rapporteur

William King
Research Triangle Institute

Participants

Wendell Ayers

Michael Chan

Jason Ching

John F. Clarke

Walter F. Dabberdt

C. Raymond Dickson

James G. Edinger

Gilbert F. Ferber

Noor Gillani

James G. Haidt

Harry L. Hamilton, Jr.

Rudolf B. Husar

Edwin Keitz

William King

Bryan W. Lambeth

Mei-Kao Liu

Ron Meyers

David Patterson

Earl F. Pound

Perry Samson

Walter J. Saucier

Gene E. Start

Eugene Tong

Fred M. Vukovich

T. L. Waldron

Gerald Watson

Marvin L. Wesely

James J. B. Worth

Bernard Zak

METEOROLOGY, TRANSPORT AND MULTIDAY PARCEL TRACKING

CONCLUSIONS

Meteorologists can provide a 24-hr prediction of the onset of a synoptic situation conducive to the development of a Persistent Elevated Pollution Episode, if it is possible to adequately define the conditions that are sought. (See Recommendation 1.)

Within a developing area of elevated pollution concentrations associated with a high pressure system, a release point can be selected that will provide a high probability that an air parcel marking device will be in that area of elevated pollution concentrations for a multiday period. The residence time in the area will be dependent on the shape of the high pressure system and the speed with which the system moves. With regard to areas of elevated pollution now classified as channeling situations, the residence time of an air parcel track in the area will be limited by the relationship between the alongwind extent of area and the wind speed and on the positions and movement of frontal systems on both the synoptic scale and the mesoscale.

All tracer systems suggested require some development. Accordingly, generic techniques are considered. Two tracer techniques should be used: (a) a technique that will approximate the path of a parcel within the developing area of elevated pollution, and (b) a technique that will provide data for the estimation of dispersion within the developing area of elevated pollution. Technique (a) is conceived as a super pressure balloon(s) of some configuration carrying a suitable device that, with ancillary equipment, will permit position determination. Technique (b) must be a gaseous tracer, probably one of the perfluorocarbons. (See Recommendations 3 through 8.)

RECOMMENDATIONS

1. A study must be made to identify the synoptic situations that give rise to PEPE's in the Ohio Valley. This study should use archived surface and upper air meteorological and air quality data to improve our knowledge of the aerometric conditions associated with identified PEPE's. One task would be to determine the routine meteorological variables that can serve as surrogates for actual pollutant measurements; these surrogates would permit the study to cover a longer historical period and provide a larger data base for the classification of pertinent meteorological situations. In addition, this larger data base would provide data for the determination of the climatological expectancy of a PEPE in the area selected for the future program. At least one recent year of meteorological data for which there are available relatively detailed pollution data (and perhaps previously identified PEPE's) should be reserved as a data set for testing the success of synoptic type classification as the indicator of a developing PEPE. This front-end research effort should provide the following as a minimum:
    a. A classification of the synoptic regimes and wind flow (at the surface and aloft) corresponding to the onset, peaking, decline, and movement of PEPE's.
    b. A set of guidelines for both objective and subjective forecasting of PEPE's and parcel trajectories.
    c. On the basis of historical data and analysis, recommend candidate regions that are most favorable for PEPE experiments and most representative of an urban source complex and/or of a rural industrialized source complex.
2. A study should be undertaken to determine the accuracy of now available forecast trajectories (TDL) relative to trajectories determined from actual data. If these forecast trajectories are a reasonable approximation of the "actual" trajectories, examination of their configuration (speed, curvature) may provide a useful indication of an incipient PEPE situation. This study must use current data because predicted trajectories are not archived.

3. The technique of locating a super pressure balloon that is being used as an air parcel tag by radio direction finding from a chase airplane(s) should be investigated to determine the ease of target acquisition, the flight pattern required for position determination, and the accuracy of position determination with and without visual sighting. A preliminary feasibility investigation should be made to determine equipment development time and costs. This investigation should consider including temperature and pressure data sensing and data transmissions on the homing signal.
4. The existing tetroon-transponder parcel tagging system is proven and operational but to assure the capability of multiday tracking, improved mobility of ground-based radar systems is required. A prototype radar unit with improved mobility has been assembled, but lead time will be required to similarly assemble the additional four available units.
5. The feasibility of using the Loran-C or the Omega navigational aid systems for air parcel tags at 1 km above terrain in the area selected for the proposed study should be investigated empirically. The development of a sufficiently lightweight onboard receiver, data storage system, and data transmitter presents no difficulty, but, as in the case of the radio direction finding system, cost estimates, ease of acquisition of position data from a chase airplane or ground station, and the coverage provided by the navigational aid systems in the area proposed for the PEPE system must be determined.
6. The use of a beacon transmitting to a satellite to provide location data for an air parcel should be studied to determine the possibility of significant weight reduction of the beacon and battery package so that the system would be acceptable from a safety standpoint to the Federal Aviation Administration (FAA). Further, the turnaround time on position data from the satellite ground station must be determined. The costs of this system, including data transmission costs and the lead time required for weight reduction, must be determined.
7. The Sandia LAMP super pressure balloon, if proven as an operating system, should be considered as an air parcel tracer and measurement platform.

8. The gaseous tracer system using perfluorcarbons requires the demonstration of the capability of a sequential sampling system. This is planned for the spring of 1979. This instrument requires laboratory evaluation of sample concentration. Real-time readout (5-min intervals) of perfluorcarbon concentration can be made by another instrument (two-trap) that is suitable for fixed mobile ground operation or airborne operation (if power is available). Fabrication lead time and possibly funding will be required if a sufficient number of the sequential samplers for a ground network of stations is required for the PEPE program.

The Meteorology and Transport and Multiday Parcel Tracking Workshop considered at length the requirements for assimilating tagged parcel location data, gaseous tracer concentration data, low-level wind data, etc., that would furnish feedback essential to continuing operations. The conclusion was reached that a time-shared or dedicated computer would be required.

Without attempting to specify the data input required, the group is adamant that the project must have an onsite weather station with adequate data sources and personnel to provide specialized forecasting services and material necessary for thorough operational briefings as required.

To provide finer time resolution to modellers, the frequency of NWS rawinsonde observations from a selected set of stations in the operational area should be increased to four per day.

Special wind and temperature vs. height (to 2 km) observations for plume studies, and subsynoptic time scale observations for Lagrangian parcel studies will be required to update trajectory forecasts during operations. A multistation mobile network will be required.

WORKSHOP III

MODEL DEVELOPMENT AND VALIDATION--MEASUREMENT NEEDS

Chairman

George M. Hidy
Environmental Research and
Technology, Inc.

Rapporteur

Joseph Sickles, II
Research Triangle
Institute

Participants

Francis Binkowski

Samuel C. Coroniti

Kenneth L. Demerjian

Allen C. Dittenhoefer

Ron Drake

John Eckert

Noor Gillani

Robert G. Lamb

Mei-Kao Liu

Maris Lusis

S. Harvey Melfi

Ron Meyers

David Miller

Brand L. Niemann

Francis Pooler

Joseph Sickles, II

Lowell Smith

Kenneth T. Whitby

William E. Wilson

MODEL DEVELOPMENT AND VALIDATION--MEASUREMENT NEEDS

The overall goal of the PEPE project was stated to be the characterization of transboundary, interstate air pollution involving large-scale regional events. The indicator for such events is elevated particulate sulfate concentration. The scale of the events extends horizontally over 100 to 1,000 km and involves buildup of 2 to 5 days. Using modeling as an interpretation tool, the specific scientific objectives of the study that are relevant to model evaluation were given tentative priorities based on (a) importance to the PEPE modeling, (b) available knowledge, and (c) scientific significance of understanding. Priority one is highest. The topics listed below represent major areas that remain uncertain after preliminary assessment of regional studies conducted to date, including those of the EPRI/SURE, MAP3S, STATE, and the EPA/ITA.

1. Quantification of factors in long-distance transport of pollution such as
    a. The effects of rough terrain in the Appalachians on eastward travel. (1)
    b. Diurnal influences of the boundary layer. (1)
    c. Action of clouds on mixing, conversion chemistry, and removal. (1)
2. Characterization of PEPE air masses
    a. Role of thermodynamic and dynamic properties such as temperature, dew point, mixing, velocity, and sunlight-cloudiness. (1)
    b. Reasons for observed "sharp" changes in concentration buildup and depletion in PEPE's. (2)
    c. The air mass aging character and scale. (2)
    d. Characteristics of plumes at distances on the order of 100 km; the nature of concentration gradient in the PEPE. (3)

3. Sulphur and Nitrogen Budgeting
   a. Requirements for details in chemical conversion such as the particle formation and growth rates, and photochemical vs. other reaction classes. (1)
   b. The location and intensity of emissions. NO_x,HC (1)
      SO_x (2)
   c. The significance of SO_x and NO_x background for regional model initial and boundary conditions. (2)
   d. The role of particle deposition and associated uncertainties in removal of haze. (2)
   e. The role of gas removal, including dry and wet deposition. (3)
4. The merging of regional scale and subgrid scale processes, including their parameterization (2)

For refinement of conceptual modeling of PEPE behavior, three features of long-distance transport require additional study at high priority. These involve questions as to the importance of terrain features, especially the Appalachians, and transport over the mountains. Also, the transport of polluted air during conditions of changing stability at night and day needs additional definition. Virtually nothing is known about the details of vertical mixing and chemical processing by clouds. Additional characterization of the PEPE air masses is needed to improve knowledge for modeling of thermodynamic-dynamic interactions, especially the apparent sharp changes in pollution levels and the definition of "plumes" at great distances.

Fundamental to the evaluation of existing air quality models is the sulfur and nitrogen budgeting in PEPE's. The experimental design should be aimed at improving knowledge in several areas including the chemical conversion rates for gases and particle formation or growth, the location and intensity of SO_x, NO_x, and NMHC emissions. Resolution of major emissions contributing to the PEPE should be hourly if possible. Information on SO_x emissions and methods for obtaining hourly estimates appear to be available, but attention is needed to improve NO_x and NMHC characterization. For improvement of the detailing of chemistry, effort should be made to break down NMHC emissions into reactivity categories. Removal processes for gases appear to be reasonably well defined at present for modeling purposes. However, controversy remains concerning the magnitude and availability of particle removal. This issue needs to be resolved for PEPE, although other programs may already be studying these questions.

MEASUREMENT REQUIREMENTS

The evaluation and refinement of air quality models for interpretation of PEPE behavior will require an elaborate set of measurements. The list of desired parameters is given in Table III-1. These include a range of measurements widely available for air quality and meteorological monitoring as well as measurements that require special instrumentation of a highly experimental nature. Recommended requirements are identified with model verification and evaluation, chemical and aerosol formation processes, and regional scale fluid dynamics. The measurements are assigned priorities for both ground and aircraft observations. By suitable selection of sites, the PEPE project can take advantage of existing meteorological and air quality data collection including that of the NADB/SAROAD system, EPRI's (proposed) Regional Air Quality Study (RAQS), the National Weather Service, and the DOE/DOA/EPRI Precipitation Chemistry networks.

There is concern for the representativeness of observations. Measurements of different spatial and temporal scales may be required. Cell-averaged (Eulerian) data are needed to be compatible with model predictions. Ideal measurements on this scale could be provided by satellite. Although such data may not be available by the time of the proposed study, satellite imagery may provide real-time definitions of the boundary of the polluted air parcels.

Burden measurements of integrated species may be conducted either from the ground or from aircraft. Although these measurements view the atmosphere as a single layer, they will nevertheless provide useful data against which model predictions can be compared. Measurements conducted on different time and spatial scales are necessary for describing subgrid phenomena such as chemistry and fluid dynamics.

Regional (secondary) pollutants such as sulfates and ozone are relatively homogeneously distributed. Thus, a low density sampling network monitoring the routine parameters with the standard averaging times will probably be sufficient for model assessment.

Although the study should capitalize on existing or proposed stations of opportunity, the following additional station locations should be considered:

1. Places most likely for PEPE to pass over.
2. Upwind, within, and downwind of selected urban area.
3. Appalachian mountains (complex terrain).

In addition to the "regular" monitoring stations that provide data for model evaluation, one or two more comprehensive stations are recommended to provide data needed to improve the current understanding of subgrid phenomena. Such parameters as aerosol size distribution, aersol water, hydrocarbons, OH, NH_3, and HNO_3 should be considered.

Airborne measurements, as long as they are not considered to be representative of the ground-level concentrations, will also provide useful input. Their major value will be to provide information on vertical concentration distributions. In addition, flights conducted in conjunction with tracer releases will be used to study all parcel behavior in a Lagrangian framework.

Rawindsondes should be released with increased frequency. Six-hour releases are recommended during the day; whereas three-hour releases may be needed at night when the atmospheric structure is poorly defined. Additional measurements using acoustic radar and/or lidar to determine vertical structure should also be considered at one or two sites.

Modeling Evaluation and Designs

Several models available for application to the PEPE's are summarized in Table III-2. The models are classed as numerical grid schemes, trajectory/plume, or statistical and other. Most of the models have capabilities of dealing with transport, mixing, emission distributions, at least linear oxidation chemistry for sulfur dioxide, and dry deposition. The models that have been used directly for PEPE applications include the DOE/MAP3S series, the Teknekron/Prahm scheme, and the ERT/SURE model.

Although the models could be exercised for design studies, the panel felt that review of the SURE and MAP3S data and other historical aerometric data would be most useful for design of the experiments. These data are becoming available and should be examined by interested investigators in the next several months.

The concept of modularization of models was discussed. In general, the panel believes that such a framework would be helpful for providing a uniform format for investigator's results.

TABLE III-1. DESIRED MEASUREMENTS FOR EVALUATION OF MODELS (PARENTHESES ARE PRIORITY VALUE)

Parameter	Ground	Aircraft	Required for*	Availability monitoring	Comments
SO_2	(1)	(1)	V,C	EPRI/RAQS SAROAD	Need some integral burden
O_3	(1)	(1)	V,C	EPRI/RAQS SAROAD	Need some integral burden
NMHC (including specific breakdown & oxygenates)	(2)	(2)	C		At 1-2 locations; need some information
NO, NO_2	(1)	(1)	V,C	EPRI/RAQS SAROAD	Need some integral burden
PAN	(2)	(2)	C		
HNO_3	(1)	(1)	C		At 1-2 locations
NH_3	(2)	(2)	C		At 1-2 locations
Tracers (gases and tetroons)	(1)	(1)	D,V		
OH	(1)	(1)	C		At 1-2 locations
H_2O_2	(1)	(1)	C		
SO_4	(1)	(1)	V,C	EPRI/RAQS SAROAD	Some continuous desirable
TSP (<15 μm)	(1)	(1)	V	EPRI/RAQS	
RSP (<3 μm)	(1)	(1)	V,C	EPRI/RAQS	
NO_3	(1)	(1)	C,V	EPRI/RAQS	
Carbon	(2)	(2)	C	EPRI/RAQS	Need some information
Organic carbon	(2)	(2)	C	EPRI/RAQS	
Aerosol size distribution	(2)	(2)	C		At 1-2 locations
Light scattering coefficient	(2)	(2)	V,C		

*See footnotes at end of table.

(continued)

TABLE III-1. (continued)

Parameter	Ground	Aircraft	Required for*	Availability monitoring	Comments
Turbidity	(1)	(1)	D,V		Integral vertical aerosol burden
Cloud, water, and chemistry	(1)	(1)	C,D		
Aerosol water	(3)	(3)	C		At 1-2 locations
Precipitation water	(1)	(1)	C	Hydro serv.,EPRI MAP3S, NC-141	
Winds (surface → 3 km)	(1)	(1)	D,V	NWS	Surface and aloft
T	(1)	(1)	D	NWS	Surface and aloft
DP	(1)	(1)	D	NWS	Surface and aloft
Solar radiation	(1)	(1)	D,C	NWS	
Cloudiness	(1)	(1)	D,C	NWS	

*V = Model verification
C = Chemistry
D = Dynamics

TABLE III-2. REGIONAL AIR QUALITY MODELS AVAILABLE FOR DESIGN STUDIES AND EVALUATION

Grid					Trajectory/plume				Statistical/other	
Originator	Winds	Layers	Dimensions	Chemistry	Originator	Layers	Dimensions	Chemistry	Originator	Description
BNL/MAP3S	Diagnostic-Prognostic	3-5	X,Y,Z	Linear Nonlinear Homogeneous	BNL	12	X,Y,Z	Linear & Wet Deposition	ERT	Principle Component Analysis-Statistical Time & Space (Note--Needs data base)
ANL	Interpol	5	X,Y,Z	None	PNL	1-X	X,Y	Linear & Wet Deposition		
ANL/Peters	(Climate only)	?	X,Y,Z	Steady-State Homogeneous	NOAA/ARL	?	X,Y	Linear & Wet Deposition		
SAI	Interpol	3-1/2	X,Y,Z	Linear Nonlinear Homogeneous	ERT/ELSTAR	3+	X,Y,Z	Linear; Nonlinear Homogenous	ANL	Statistic Trajector
ERT/SURE	Interpol	3-5	X,Y,Z	Linear Nonlinear Homogeneous Semi-empirical In O_3, H_2O	SRI. EUROMAP	2	X,Y	Linear & Wet Deposition		
TEKNEKRON/ PRAHM (pseudo-spectral)	Interpol Winds 100M	1-3	X,Y,Z	Linear	LRTAP		X,Y	Linear & Wet Deposition		

WORKSHOP IV, PART 1

INSTRUCTIONS FOR STUDY OF TRANSFORMATION

Chairman

Robert K. Stevens
U.S. Environmental
Protection Agency

Rapporteur

Madhav Ranade
Research Triangle Institute

Participants

Frank Allario

Kurt Anlauf

Dagmar Cronn

Thomas G. Dzubay

Edward Friedman

Lee Langan

Peter H. McMurray

Millán M. Millán

Leonard Newman

Madhav Ranade

Chester W. Spicer

Gary Stensland

Robert K. Stevens

James Tommerdahl

INSTRUMENTATION--TRANSFORMATION MEASUREMENTS

In conjunction with the Seminar on Persistent Elevated Pollution Episodes (PEPE) held at Durham, N.C., on March 19-23, 1979, a workshop on instrumentation needed for measurements under the PEPE program was conducted. The objectives of this workshop were to identify the instruments presently available and to define research tasks (needed to be funded in early FY1980) for developing new instruments by the summer of 1980. In the first part of the workshop, instrumentation for studying transformation in pollutant plumes was considered. The measurement areas focused on during this discussion were:

1. Sulfate speciation and acidity,
2. Nitrates,
3. Formaldehyde and aldehydes,
4. Particulate, and vapor phase organics,
5. Real-time particle size distribution measurements,
6. Halocarbons,
7. Adaptation of instruments to the aircraft platform,
8. Precipitation, and
9. Hydroxyl radical.

SULFATE SPECIATION AND ACIDITY

For the PEPE study, it is desirable to quantitatively monitor sulfur in sulfate form and to know proportions of acid and ammonium sulfate.

Analytical methods presently used for sulfates and total acidity will be sensitive enough for the PEPE measurements. It has been observed at Brookhaven National Laboratory and EPA that size fractionation prior to the collection of the sample is necessary to avoid influence of basic coarse particles in the acidity measurements. It was suggested that separation of particles above 2 μm be effected before sample collection.

The analytical methods available for total acidity include Gran titration, benzaldehyde extraction, and radiolabeled titration. Of these, the radiolabeled titration being developed by EPA/ESRL is the most sensitive and utilizes shorter sampling times.

Recommended collection media for sample collection are Teflon and acid washed quartz filters because these do not produce artifact formation. The filters could be used for nitrates as well as sulfates. If sampling for carbon analysis is achieved on the same filter, quartz could be the filter of choice. If used for sulfate and nitrate measurements alone, the Teflon will be preferable.

Sampling periods of 1/2 to 1 hr at a rate of 500 lpm may be needed to obtain samples for the sulfate, nitrate, and carbon analysis.

Tandem filters for ambient SO_2 measurements are needed as backup for real-time SO_2 and particulate sulfur.

Continuous sulfur measurement by flame photometric detection (FPD) may be used for real-time monitoring of sulfates and SO_2 by the following schemes:

1. Diffusion denuder for SO_2 followed by FPD to differentiate between SO_2 and particulate sulfur;
2. Electrostatic separation of particulate sulfur to differentiate between SO_2 and particulate sulfur;
3. Diffusion denuder including neutralization with NH_3 to present to the flame only $(NH_4)_2\ SO_4$. (This avoids H_2SO_4 losses in the burner block and calibration difficulties.)

The FPD system adaptability to aircraft use is considered marginal at present due to problems associated with pressure changes.

Information regarding particle size dependence of sulfate speciation is desirable in the PEPE. At a minimum, speciation should be determined for two classes--suboptical and optical. Three techniques presently available are the vacuum impactor, micro-orifice impactor, and a diffusion battery with a precutting slit. The vacuum impactor requires a large pump, provides a small sample, and is not well-characterized with respect to losses. The micro-orifice impactor (University of Minnesota) collects particles below 0.1 μm on Teflon substrates suitable for XRF analysis. The performance of this device needs to be documented by further laboratory and field testing. The diffusion battery system can remove particles smaller that 0.1 μm from the sample and has been used in several previous studies. The Tandem Differential Mobility Analyzer (TDMA--University of Minnesota) may also be useful to investigate the hygroscopic nature of the submicron aerosol sample in several size ranges down to 0.01 µm.

NITRATES

The state-of-the-art of nitrate sampling and measurement needs considerable improvement. Samplers used for sulfur measurements may be used. Sampling time should be kept low requiring high flow rates. Negative artifact formation is currently under investigation. Sample stability over several days has been observed; for longer periods, storage in a cold inert atmosphere (such as Argon) is recommended. The Teflon and acid-washed quartz filter would be compatible with nitrate measurement.

The analytical methods include: (a) ion chromatography, (b) formation of nitrobenzene followed by electron capture gas chromatography, and (c) flash vaporization followed by chemiluminescence. Of these, the last method has received limited testing.

NITRIC ACID

Use of tandem filters utilizing nylon or cotton backup filters followed by extraction for GC or IC analysis is recommended for nitric acid measurement. Use of nylon or cotton wool following a filter has been successful in the past. A diffusion denuder for HNO_3 also has the potential to determine HNO_3.

FORMALDEHYDE AND ALDEHYDES

Currently, formaldehyde analysis is conducted after collection in liquid followed by colorimetry. Use of GCMS is required for higher aldehydes. There are no reliable and relatively inexpensive methods presently available.

PARTICULATE AND VAPOR PHASE ORGANICS

Currently, total carbon measurement as well as differentiation between volatile and nonvolatile carbon is practical. Development of a special high-volume sampler is needed for GCMS work. Teflon filter analysis for carbon by nuclear methods (PESA or GRACE) is currently under investigation. A cartridge to collect gaseous organics is being developed by RTI under EPA sponsorship.

It was also expressed by the participants that development of a device to allow total carbon analysis by size is desirable because the organic aerosol may influence the optical properties of the atmosphere significantly.

An inexpensive and real-time nonmethane hydrocarbon monitor (NMHC) is being developed by ESRL/EPA, which may be useful for both ground-level and airborne monitoring. The system will be available for field studies by the summer of 1980.

REAL-TIME PARTICLE SIZE DISTRIBUTION MEASUREMENT

Currently the electrical aerosol analyzer (EAA) coupled with an optical particle counter (OPC) is used for the real-time size distribution measurement. Agreement between the mass data and the estimated means from the volume distribution data from the EAA/OPC system is not always consistent. Causes for this discrepancy may be due to humidity and should be investigated before summer 1980.

HALOCARBONS

During the seminar, perfluorocarbon was proposed as a tracer for air parcel movement. Technology for release and monitoring needs to be refined. Work should begin immediately. Use of state-of-the-art technology to follow urban blobs by using the freons emitted by the major sources was also suggested.

ADAPTATION OF INSTRUMENTS TO THE AIRCRAFT PLATFORMS

From economic considerations, single- and twin-engine airplanes are suited for aircraft measurement. Due to the weight and space limitations of the payload, packaging of the instruments and auxiliary components needs to be examined. A nominal 1,000-lb load capacity and 75 A at 26 V power capacity is expected to be available.

Instruments considered for mounting in the aircraft need to be trimmed, if possible, to allow efficient use of space and load. For example, lightweight and/or d.c. pumps are available that could reduce the weight for several sampling devices. Spares for the instrument complement might be augmented in some cases by using subsystems such as burner-block, and PM tube assemblies as opposed to complete instruments.

The aerosol sample inlets for aircraft need to be developed by summer 1980. State-of-the-art sampling inlets for use on airborne studies are not optimized for aerosol sampling and probably have significant losses of particles <5mm in diameter. Provision of a 15-mm cutoff for the inlets should also be considered to compare with the inhalable particulate matter (IPM) measurements made at ground level.

PRECIPITATION

Sampling in clouds and at ground level was considered to be necessary to study precipitation chemistry associated with PEPE. In airborne measurements, HNO_3 in the cloud water should be considered. A study of the cloud sampling with regard to location (e.g., at an edge or in the middle) and collection efficiency is recommended.

Ground-based samplers are currently available that allow measurement of acidity, SO_4, NO_3, and trace metal analysis. However, questions regarding effects of wind speed and location that may result in size selectivity need to be resolved.

HYDROXYL RADICALS

Hydroxyl radicals may play a role in the SO_2 to sulfate conversion. The resonance fluorescence method developed at Washington State University may be useful. Estimated cost for one measurement is $5,000-$10,000.

SUMMARY

Table IV-1 summarizes the status of instrumentation discussed above.

TABLE IV-1. STATUS OF INSTRUMENTATION FOR PEPE

Parameter	Methods	Response time	Sensitivity	Availability	Ground level	Air-borne
SO_2	Chemiluminescence Tandem filter	1 s 30 min-24 hr	1-5 ppb	Now	x	x
NO_x, O_3	Chemiluminescence photometric	5 s	2 ppb	Now	x	x
NMHC*	GFC/FID†	1 s	30 ppb	Summer 1980‡	x	x
Organics	GC/MS	Collect & analyze	1 ppb	Under development	x	x
HNO_3	(a)Chemiluminescence (b)Sample & collect	(a) 1 s (b) 2.20 min-24 hr	0.1 ppb 0.1 ppb	Now	x	x
H^+	1.Gran titration 2.Radiolabeling	30 min-24 hr 10 min-24 hr	1 $\mu g/m^3$ 1 $\mu g/m^3$	Now	x	x
$SO_4^=$	Sample & collect wet chemistry	30 min	1 $\mu g/m^3$	Now	x	x
S(aerosol)	1.FPD 2.XRF	Real-time 5 min	1 $\mu g/m^3$	Now	x	x
$NO_3^=$	Sample & collect	30 min	1:1 $\mu g/m^3$	Now	x	x
Trace metals	Sample & collect	1-2 hr	1-50 $\mu g/m^3$	Now	x	x
Halocarbons	Semireal time GC/EC	10 min	Picograms	Now	x	x
Hydroxyl radical	Sample & collect	2-24 hr	ppb	Now	x	x

*Nonmethane hydrocarbons.
†Gas filter correlation spectrometry.
‡Only one will be available.

WORKSHOP IV, PART 2

INSTRUMENTATION FOR REMOTE SENSING

Chairman

Frank Allario
Langley Research Center

Rapperteur

Madhav Ranade
Research Triangle
Institute

Participants

L. W. Chaney

Dagmar Cronn

Richard Coulter

John Eckert

Edward Friedman

James G. Haidt

Edwin Keitz

Lee Langan

W. A. McClemy

Millán M. Millán

Earl Pound

Madhav Ranade

Robert K. Stevens

James Tommerdahl

Edward Uthe

INSTRUMENTATION FOR REMOTE SENSING

INTRODUCTION

This Workshop was asked to address two questions:

1. What active airborne remote sensors are available for use in the EPA 1980 Regional Field Studies with respect to the PEPE program?
2. What tasks are required for various sensors to prepare for the 1980 PEPE program?

The Workshop addressed remote sensors other than airborne active remote sensors (e.g., long-path absorption measurements using laser and nonlaser sources) and passive remote sensors because it was agreed that these types of instrumentation may provide significant information on gaseous species in the troposphere, and may provide a wider network of sensors to complement currently planned in situ sensors discussed at the earlier workshop, Instrumentation for Study of Transformation.

The Following agenda was adopted by this Workshop group.

1. An overview discussion was conducted of the role of active/passive remote sensor technology in the PEPE program, with respect to measurements of gases, aerosols, extinction, meteorological parameters, visibility, turbulence, and backscattering.
2. A shopping list of instruments (active/passive) with the potential for application in the 1980 PEPE program was developed based on the following guidelines. The instruments had undergone development, laboratory testing, and sufficient field testing with either calibration testing or correlative measurement testing, which provided reasonable results consistent with expected physical phenomena being measured. Instruments not falling within those guidelines (based upon information available to the attendees) were excluded or identified on the chart.

3. Earth Observation Satellite Systems were not discussed at the Workshop since it appeared that sufficient discussion was generated during the 2-day seminar portion of the meeting to provide an adequate data base for assessing the capability of satellite imagery. However, it was agreed that satellite observations of PEPE's could complement the ground/airborne measuring network in identifying regional boundaries of PEPE and to provide information (in conjunction with meteorological data) on the early formation of regional haze.

The available active remote sensors are summarized in Table IV-2 and have been categorized according to fixed wavelength lidar systems, tunable wavelength lidar systems, or acoustical sounding techniques. Table IV-3 summarizes passive remote sensing technology, and instruments have been categorized according to nondispersive and dispersive correlation radiometers, interferometers, infrared heterodyne spectrometers, and spectroradiometers. Table IV-4 summarizes long-path laser monitoring systems using retroreflectors to provide total integrated burden measurements along a 1-km horizontal path, or a 200-ft vertical path deploying retroreflectors on high vertical structures. A 20-m long-path airborne system has also been included to provide areal coverage of gaseous species such as CO, N_2O, and NH_3.

ROLE OF REMOTE SENSORS IN PEPE PROGRAMS

Two types of remote sensors were considered by the Workshop: (1) active remote sensors in which the sources of radiation are electromagnetic (UV/VIS/IR) and acoustical soundings; and (2) passive remote sensors in which natural sources of radiation are utilized including upwelling thermal radiation, solar-reflected radiation, and direct solar/sky emissions. Platforms considered were high-flying (>20,000 ft) and low-flying (<20,000 ft) aircraft and mobile and stationary ground-based measurements. An extensive topic of discussion involved the role remote sensors can play in providing complementary and independent measurements of gases, aerosols, meteorological parameters, visibility, turbulence, and optical backscatter. Four major roles were identified for the PEPE program.

1. Airborne remote sensors could provide positioning data to other instrumentation (i.e., in situ) for the purpose of obtaining

detailed measurements in localized areas within the large haze region. Remote sensors can provide positioning data to other instruments, which can obtain localized measurements with potentially higher sensitivity and specificity, smaller spatial resolution and basic characteristics of aerosols (i.e., concentration, size distribution, chemical composition). Remote sensing from high-altitude, fast aircraft could provide early information on the formation of regional episodes and define the boundaries, areal extent, tracking information, vertical layering of aerosols, and SO_2, and O_3 concentrations in the regional haze.

2. Airborne remote sensors could serve as the primary instrument technology for assessing characteristics of isolated plumes including structure of the plume, dispersion, degree of Gaussian fit, gaseous SO_2 and O_3 concentrations, and boundary layer structure. These measurements would be conducted from low-altitude, low-speed aircraft and from ground-based stationary and mobile platforms to perform plume characterization studies. For both these applications, on-line data processing of remote sensor data would be required to provide operational data for other instruments.
3. Airborne remote sensors could provide information on the correlation between aerosol concentrations in the regional haze and the concentration of gaseous constituents such as SO_2 and O_3. At present the correlation between aerosol loading and the concentration of SO_2 and O_3 in regional haze episodes is not well understood. Remote sensors could be utilized in a unique operational basis (large areal extent) to provide data for improved understanding of the correlation for a particular episode. Further, active remote sensors from airborne platforms can provide measurements of the location and width of the vertical mixing layer, and potentially provide data to understand the composition of relative "clear" areas within the regional haze.
4. By comparing and complementing remote sensing data with data obtained from the complete measurement network in PEPE, retrospective data analysis can be performed to improve understanding of

chemical transformations, transport, and chemical processes in the regional haze.

The Workshop participants agreed that remote sensors represent cost-effective sensors for providing an extensive data base for regional haze studies by providing large areal coverage, vertical layering, and integrated burden measurements with high potential in model validation studies particularly in the area of transport. The following unique capabilities of remote sensors for the PEPE program were identified.

- Capability to perform daytime/nighttime plume characterization.
- Characterization of vertical structure in plumes and extensive air masses.
- Rapid characterization of plume dispersion.
- Identification of boundary layer behavior over various terrain characteristics.
- Capability to detect invisible plumes.
- Capability to identify aerosol/gaseous distribution along regional haze boundaries with on-line information.
- Provide parameters for model validation and transport processes above the surface.
- Provide measurements of SO_2 and NO_2 transboundary fluxes.
- Provide total burden measurements for boundaries and areal extent of regional haze.

ATMOSPHERIC PARAMETERS MEASURABLE WITH REMOTE SENSORS

The spectrum of atmospheric parameters that can be measured with remote sensors was discussed. Included were gases and aerosols, optical backscattering, meteorological parameters, extinction, visibility, and turbulence.

Gases and Aerosols

The Workshop group identified the capability to measure simultaneously aerosols and SO_2 and aerosols and O_3 with the potential to measure the three species simultaneously with further development of existing DIAL systems. Total burden measurements of O_3 from aircraft platforms represent valuable input parameters to regional modeling. Other species that are measurable with remote sensors include NO_2, CO, NH_3, H_2O, N_2O, CH_4, CO_2.

Optical Backscattering

Optical backscattering capability can be obtained with a variety of active lidar systems, with multiwavelength capability in some cases (see Table IV-2). The High Spectral Resolution Lidar (HSRL) has the unique capability of distinguishing optical backscattering from aerosols and molecules through a unique combination of high resolution Fabry-Perot Filters. This instrument can obtain the vertical and horizontal distribution of the atmospheric optical extinction coefficient, the aerosol-to-molecule scattering ratio, and the aerosol backscattering phase function from aircraft platforms, and can complement the interpretation of multiple wavelength lidar instruments for the characterization of atmospheric contaminant mass loading, size distribution, and composition.

Meteorological Parameters

Remote sensors are capable of measuring meteorological parameters including temperature, winds, water vapor, atmospheric turbulence, height of mixing layer, and clouds. Remote sensors with potential for meteorological applications are tabulated in Table IV-2. Consideration of measurements of meteorological parameters should include both active lidar techniques and acoustical radar measurements.

Visibility

A primary objective of the PEPE program is to improve understanding of visibility in regional haze. Due to the complexity of the visibility problem, the participants did not agree on the capability of current active remote sensors to provide detailed understanding of the visibility problem. However, it was agreed that the multiple wavelength capability of remote sensors should provide a data matrix that, in conjunction with other information, could improve current understanding of the definition of visibility. The potential for application of active lidar techniques to improve understanding of visibility should be further investigated and is recommended as a near-term task.

Summary of Remote Sensing Instrumentation Charts

Although detailed information of remote sensors is given in Tables IV-2, IV-3, and IV-4, this section will provide an overview of the charts. Fourteen fixed wavelength lidar systems were identified, with 12 related to optical backscattering measurements and 2 related to measuring gaseous species--the O_3 instrument is currently operational and the NH_3 instrument may be operational with minor modifications. Of the 14 fixed laser systems, the 2 gaseous species measurements utilize aircraft platforms; the 12 optical scattering instruments are divided into 4 aircraft systems, 5 mobile ground platforms, and 3 stationary platforms. Three tunable wavelength lidar systems were identified, one measuring optical backscattering and two measuring aerosol and gaseous species (O_3, SO_2, H_2O, NO_2). One aircraft instrument with tunable wavelength capability will be operational from an aircraft system and will be capable of simultaneously measuring aerosols and O_3 or aerosols and SO_2.

Of the 11 passive remote sensors identified, only 2 were operational from an aircraft system, namely the aircraft MAPS instrument (CO) and the multispectral observation of pollutants (MOPS) for measuring SO_2, O_3, and NO_2. However, some passive remote sensors (e.g., COSPEC) might have the capability of aircraft deployment with further development, and should be identified as near-term tasks for the 1980 PEPE study. Three of the passive remote sensors are deployable in ground-based mobile vans, and six operate from stationary platforms. A recommendation of the Working Group was that a survey be made to identify those passive remote sensors that, with minor modification, might be used in the airborne mode to provide additional capability to active remote sensor technology for measurement of gaseous species.

Three long-path laser absorption techniques were identified by the Workshop group; one was an operational aircraft system and the remaining two were long-path ground systems. The latter two systems have been extensively tested over horizontal path lengths of 1 km and are currently planned for testing with a retroreflector located approximately 200 ft up a high tower, thereby providing the capability to complement ground-based in situ measurements with vertical burden measurements.

TABLE IV-2a. ACTIVE REMOTE SENSORS (FIXED WAVELENGTH—OPTICAL SENSORS)

Category and instrument	Species	Spectral range µm	Transmitting laser	Receiver telescope diameter (cm)	Viewing mode	Platform	Current status	Field application	Organization/ contact	Remarks
Fixed Wavelength										
High Spectral Resolution Lidar (HSRL)	Aerosol extinction	0.4-0.45	N_2-pumped dye	36	Atmospheric backscatter	A/C	System assembly for 8/79 flight (CV-990)	Regional aerosol extinction profiles	NASA/LaRC (E. V. Browell) + University of Wisconsin (S. Shipley)	Ground-based vertical measurements to 3 km—complete
Laser Absorption Spectrometer	O_3, NH_3	9-12 (discretely tunable)	CO_2 Waveguide laser	15	Reflected ground (molecular absorption)	A/C	Operational	Total burden	JPL (E. T. Menzies)	Field testing in SEV-UP studies
Mark IX	Aerosols	0.700	Ruby	15	Atmospheric backscatter	Mobile van	Operational	Plume studies	SRI (E. Uthe)	Real time data processing and display
Mark V	Aerosols	1.060	Nd:YAG	15	Atmospheric backscatter	Fixed station	Operational	Aerosols	SRI (E. Uthe)	Real time data processing and display
Mark XI	Aerosols	0.530 and 1.06	Nd:YAG	35	Atmospheric backscatter	Aircraft (Queenaire)	Operational	Aerosols	SRI/EPRI(1) (E. Uthe)	Scheduled to fly in 1979
Multi-Wavelength Infrared Lidar	Aerosols	1.06, 1.6, 3.5, 10.6	Nd:YAG and CO_2	40	Atmospheric backscatter	Transportable system	1.06 and 10.6 µm operational	Aerosols	SRI (E. Uthe)	Complete capability requires further development
Mark VIII	Aerosols	0.700	Ruby	15	Atmospheric backscatter	Mobile van	Unknown	Aerosols	EPA(2) (Ching)	--
Lidar	Aerosols	0.700	Ruby	--	Atmospheric backscatter	Mobile van	Unknown	Plume opacity measurements	EPA(3) (Conner)	Used for plume opacity studies
Lidar	Aerosols	0.700	Ruby	20	Atmospheric backscatter	Mobile van	Operational	Plume opacity measurements	EPA/NEIC(4) (Dybdahl)	Plume opacity
Airborne Lidar System III	Aerosols	0.53 and 1.06 simultaneous	Nd:YAG	35	Atmospheric backscatter	Small twin-engine A/C	Operational	Point source/urban plumes	EPA/Las Vegas (Joe Eckert)	Resolution element 30′—vertical 30′—horizontal
Airborne Ozone Sensor	Ozone	9.5	TEA CO_2 laser	25	Downlooking earth reflected	Large twin-engine A/C	Prototype constructed schedules tests 5/79	Total burden ozone	EPA/Las Vegas (Joe Eckert)	Sensitive to ambient O_3 levels
Van-Mounted Lidar System	Tropospheric Aerosols	0.35, 0.693, 10.6 microwave	Ruby, CO_2	≈80	Atomospheric backscatter	Stationary	Operational (ruby, microwave)	Met. parameters Plume studies	NOAA/Boulder (V. Derr)	Molecular and spherical particle discrimination through polarization
Doppler Laser Velocimeter	Aerosols	10	Cu vapor	≈25	Atmospheric backscatter	Stationary	Operational	Atmospheric turbulence Wind speed Plume turbulence	NOAA/Boulder (V. Derr)	Met. parameters
Airborne Laser Doppler Velocimeter	Aerosols	10	Cu vapor	≈25	Atmospheric backscatter	Aircraft/ side viewing	Operational	Plume turbulence	NOAA/Boulder (V. Derr)	Plume turbulence measurements

TABLE IV-2b. ACTIVE REMOTE SENSORS (TUNABLE WAVELENGTH—OPTICAL SENSORS)

Category and instrument	Species	Spectral range µm	Transmitting laser	Receiver telescope diameter (cm)	Viewing mode	Platform	Current status	Field application	Organization/ contact	Remarks
A/C Dial system	SO_2, O_3, NO_2, H_2O, aerosols, temperature, pressure	0.28-0.9	Nd:YAG pumped dye	36	DIAL upward/ downward viewing	A/C	System assembly for 8/79 flight	Regional study of O_3, SO_2, aerosols, trop H_2O profiles	NASA/LaRC (E. V. Browell)	Field demonstration in NASA SEV-UPS Program
DIAL system	SO_2, O_3	0.28-0.35	Nd:YAG pumped dye	50	DIAL	Mobile	Available for testing 1/80	Gaseous atmospheric species	SRI/EPRI(5) (Hawley)	--
Airborne Lidar System II	Aerosols	0.59	Flashlamp pumped dye laser	30	Atmospheric backscatter	Small twin-engine aircraft	Operational	Dimensions/location of point source plumes	EPA/Las Vegas (J. Eckert)	Real time display Resolution element 150 ft.—vertical 150 ft.—horizontal

TABLE IV-2c. ACTIVE REMOTE SENSORS (ACOUSTIC RADAR)

Category and instrument	Measured variable	Organization/ contact	Remarks
RASS	Temperature, winds aloft	SRI (Franhal)	Operational
Angle of arrival	Winds aloft	SRI (Russell)	Possibly available summer 1980
Sodor network	Mixing depth	SRI (Uthe-Russell)	Backscatter sounder Possibly available summer 1980

TABLE IV-3. PASSIVE REMOTE SENSORS

Category and instruments	Species	Spectral coverage µm	Field of view (degrees)	Vertical resolution (km)	Viewing mode	Platform	Current status	Organization/contact	Remarks
Non-Dispersive Gas Filter Correlation Techniques									
A/C Maps	CO, CH_4	4.52-4.8	7.5	<5 km	Thermal IR	A/C	A/C operational	NASA LaRC (H. Reichle)	Measured dispersion of urban plumes outward from Chicago
Fourier Transform Spectrometer	CO, CH_4, CO_2, N_2O, H_2O, SO_2, NO, . . .	2.0-16.0	--	Integrated burden	Direct solar	Mobile van	Operational	EPA-RTP (W. Hergett)	Horizontal range ≈1 km depending upon source intensity
Interferometry									
HSI	Spectrally scanning	1.0-14.0	2	Integrated burden	Direct solar	Balloon/gnd-based	Operational	JPL (B. Farmer)	Stratospheric balloon flights successful
IR Interferometer	Spectrally scanning	2.0-14.0	12	Integrated burden	Aurora's and night glow	Mobile van	Operational	Utah State University (A. Steed)	Nighttime measurements possible
Dispersive Correlation Technique									
COSPEC (passive)	SO_2, NO_2	0.3-0.5	N/A	Integrated burden	Vertical upward viewing	Mobile van possible A/C	Operational & tested in 22 countries	Barringer Res. Inc. & Contractors	Plume dispersion studies (400 km range) Plume model verification SO_2, NO_2 transboundary mass fluxes
COSPEC (active)	SO_2, NO_2	0.3-0.5	N/A	Integrated burden	Line of sight to source	Stationary	Operational & tested	Barringer Res. Inc. & Contractors	1-6 km range
Infrared Heterodyne Spectrometers									
IHR	O_3, NH_3	9-12 (discrete steps)	0.25 mr	<5	Direct solar	Stationary gnd	Operational	NASA LaRC (J. M. Hoell)	Currently performing NH_3 measurements
LHS	Continuous spectral coverage	7.5-13.0	0.25 mr	<5	Direct solar	Stationary gnd	Operational	NASA LaRC (F. Allario)	Laboratory engineering model
Spectroradiometers									
Sun Photometer	Aerosols, water vapor	UV, VIS, Near IR	--	Integrated burden	Direct solar	Stationary	Operational	SRI(Uthe)	Automatic tracking and digital recording
Automatic Telephotometer	Visibility	Visible	--	Integrated burden	Direct solar	Stationary	Operational	SRI-EPRI (Uthe)	TV microcomputer system for evaluating contrast reductions
Multispectral observation of of pollutants (MOPS)	SO_2, O_3, NO_2	(0.30-0.60)	Multispectral imaging	Total burden (1 ppm—m)	Direct solar & nadir	A/C	Operational	JPL	Plume studies of SO_2

TABLE IV-4. LONG PATH LASER MONITORING SYSTEMS

Category and instrument	Species	Spectral range μm	Transmitting laser	Receiver telescope diameter (cm)	Viewing mode	Platform	Current status	Field applications	Organization contact
Tunable Wavelength									
Differential Absorption Pollution Sensor	N_2O, CO, NH_3	0.45-0.60 7.5-13.0	Tunable diode lasers	6	Laser absorption in 20 meter path	A/C	Operational	Regional study of tropospheric budgets & dynamics	NASA-LaRC (F. Allario)
Infrared Laser Atmospheric Monitoring System (ILAMS)	O_3	9-12 (discretely tunable)	CO_2 laser	10	Retroreflector (½-km path length)	Mobile van	Operational test study 8/79	Long path—horizontal & vertical	EPA-RTP (W. McClenney)
Diode Laser Monitoring System	N_2O, CO, NH_3	0.45-0.60 7.5-13.0	Tunable diode lasers	10	Retroreflector (½-km)	Mobile van	Operational	Long path—horizontal & vertical	EPA-RTP (W. McClenney)